The Untargeted Kinome: Building Chemical Capacities and Bridges in Cancer Research

Maria Dolores Beltrán Molina

2016

Supervised by Professor Nicholas C. O. Tomkinson

Department of Pure and Applied Chemistry

A thesis submitted to the University of Strathclyde in part fulfilment of regulations for the degree of Doctor of Philosophy in Chemistry.

Declaration

This thesis is the result of the author's original research. It has been composed by the author and has not previously been submitted for examination which has led to the award of a degree.

Signed: Date

Thesis supervision

This thesis was undertaken at the University of Strathclyde (Glasgow, United Kingdom) and at the Spanish National Cancer Research Centre (CNIO, Madrid, Spain), under the supervision of Prof. Nicholas Tomkinson and Dr. Carmen Blanco-Aparicio.

Signed: Date:

Abstract

This thesis describes our efforts to design and synthesize selective probes for the PIM kinases (PIM-1, PIM-2, and PIM-3), because of their important role in cancer. During the course of the investigation we also examined the splicing kinases CLK1, CLK3, CLK4, DYRK1, DYRK2, SRPK1, and SRPK2.

In *Chapter 2*, SAR and molecular modelling studies were carried out using a known benzothienopyrimidinone PIM inhibitor[1](*J. Med. Chem.*, 2009, **52**, 6621-6636). A series of analogues were synthesized providing low nanomolar activities towards the PIM kinases but showing little selectivity between the isoforms. Within these studies on PIM selectivity, the discovery of potential CLK4 chemical probes was made, which led to the first CLK4 X-ray crystal structure with a compound bound within the ATP binding site.

Chapter 3 describes the discovery of a new series of compounds containing a phenyl pyrimidinone core which showed excellent activity against the PIM kinases. The scaffold offered potential for multiple points of diversity and applications in future programmes. A one-pot strategy for the synthesis of the phenyl pyrimidinone core is also described.

Chapter 4 presents the discovery of a benzothienodiazepine scaffold. Through SAR studies, molecular modeling, and biological evaluation, potential PIM-1 and PIM-3 selective probes with good selectivity as well as low nanomolar activities are discussed. An X-ray crystal structure of PIM-1 with one of our analogues is also described, confirming that the compound is bound in the PIM-1 ATP binding pocket.

Chapter 5 describes the biological evaluation carried out with the potential PIM-1 and PIM-3 selective probes. Solubility, permeability, *in vitro* and *in vivo* assays are detailed, providing low nanomolar activities as well as excellent selectivity towards a wide panel of kinases. Selected probes are further being characterized. On validation, our aim is to make these probes available to the biological community in order to dissect the fundamental biology of these important receptors.

Acknowledgements

First of all, I would like to thank Prof. Nicholas Tomkinson for giving me the opportunity to undertake a PhD within his research group. His advice and encouragement has helped me so much through this experience.

I would also like to thank Dr. Heulyn Jones, Stuart Davidson, and Carla Alamillo for encouraging me and giving me advice with this thesis.

My PhD has been an incredible experience thanks to my research laboratory, especially to the gorgeous Camille, who has been my PhD sister and we have supported each other throughout these three years, but also, to, Andrei, Carla, Marianna, Stuart, Mike, Tom, Justyna, Julian, Natalie, Aymeric, Tyne, Kevin, Jim, Stefano, Jade and Liam.

Also, massive thanks to Dr. Leila Alexander, Dr. Clara Redondo, and Prof. Stefan Knapp at the SGC for our collaboration, their hard work and support, and because this work has been possible thanks to them. Very important to mention Steven Kay, who carried out an excellent work for this project, that has very much added value to the quality of this thesis.

Another massive thanks to the high quality professionals at the CNIO in Madrid, who have helped me so much with all the biology related to this thesis, especially Carmen, Maribel, Manuel y Jose Antonio.

To the University of Strathclyde technicians who kept running the university smoothly and make our everyday work easy.

And finally, I would really like to thank my family, and Craig, who have always supported me, as well as my friends, Patricia, Patricia, Andrea, Sara, Marta, Laia, Mireia, Maria, Pedro, Iván, Xavi, Pau, Aina, Catiana, Ana, Salva, Andy, Alex, Silvia, Mubina, Cesar, Edu, and Clara.

Table of contents

Abbreviations

ADME: Absortion, distribution, metabolism, and excretion

ADP: Adenosine ditriphosphate

AG: Gibbs free energy

ATP: Adenosine triphosphate

AUC: Area under curve

AUC: Area under curve

BAD: Bcl-2-associated death promoter

Bcl-2: B-cell lymphoma 2

BrettPhos: 2-(Dicyclohexylphosphino)3,6-dimethoxy-2′,4′,6′-triisopropyl-1,1′-biphenyl

c-ABL: Abelson murine leukemia viral oncogene

CDK: Cyclin-dependent kinases

cKIT: Mast/stem cell growth factor receptor

Cl: Drug body clearance

CLK4: CDC-like protein kinase 4

C_{max}: Maximum concentration

cMYC: V-myc avian myelocytomatosis viral oncogene homolog

CNIO: Centro nacional de investigaciones oncológicas

DCM: Dichloromethane

DMF: N,N-Dimethylformamide

DMSO: Dimethylsulphoxide

DSF: Differential scanning fluorimetry

DYRK: Dual-specificity tyrosine-(Y)-phosphorylation regulated kinase

EGFR: Epidermial growth factor receptor

ERK1: Extracellular signal-regulated kinases

F: Drug bioavailability

FBS: Fetal bovine serum

FDA: Food and drug administration

FLt3: FMS-like tyrosine kinase 3

GM-CSF: Granulocyte macrophage colony stimulating factor

GPCRs: G-protein coupled receptors

Haspin: Haploid germ cell–specific nuclear protein kinase

Hepes: 4-(2-Hydroxyethyl)-1-piperazineethanesulfonic acid

HSP: Heat shock proteins

HTS: High throughput screening

IC_{50}: Half maximal inhibitory concentration

IFNγ: Human gamma interferon-γ

IR: Infrared spectroscopy

IRAK: Interleukin-1 receptor-associated kinase

ITC: Isothermal titration calorimetry

ITC: Isothermal tritation calorimetry

IV: Drug intravenous administration

IV: Intravenous administration

JAK: Janus kinase

K562: Leukemia cancer cell line

KDR: Kinase insert domain receptor

LCMS: Liquid chromatography–mass spectrometry

LRRK2: Leucine-rich repeat kinase 2

MeOH: Methanol

MMLV: Moloney murine leukemia virus

MMP: Matrix metalloproteinases

Mpt: Melting point

NF-κB: Nuclear factor kappa-light-chain-enhancer of activated B cells

NMR: Nuclear magnetic resonance

Pampa: Parallel artificial membrane permeability assay

PBS: Phospate-buffered saline

$Pd(OAc)_2$: Palladium(II) acetate

$Pd(Ph_3)_2Cl_2$: Palladium(II)bis(triphenylphosphine) dichloride

Pd_2dba_3: Tris(dibenzylideneacetone)dipalladium(0)

PDB: Protein data bank

PDGFR: Platelet-derived growth factor receptors

PI: Percentage of inhibition

PIM: Proviral integration site for moloney murine leukemia virus

PKA: Protein kinase A

P-loop: Phosphate-binding loop

PO: Drug oral adiminstration

PO: Oral administration

POC: Proof of concept

POC: Proof of concept study

PPP: Public private partnership

PRKX: Protein kinase, X-linked

R&D: Research and development

RNA: Ribonucleic acid

RuPhos: 2-Dicyclohexylphosphino-2′,6′-diisopropoxybiphenyl

SAR: Structure activity relationship

SOCS: Suppressor of cytokine signalling proteins

SR protein: Serine/arginine-rich domain protein

SRPK: Serine-arginine protein kinase

STAT: Signal transducer and activator of transcription

TNFα: Tumor necrosis factor alpha

TrKC: Tropomyosin receptor kinase C

V_d: Volume of distribution of a drug

VEGFR: Vascular endothelial growth factor receptor

S/N: Signal to noise ratio

S/B: Signal to background ratio

1. Introduction

1.1. The need for a change within drug discovery

There is a clear concern in the scientific community regarding the current drug discovery process. This process can be divided into seven different steps: target validation, assay development, probe optimization, lead optimization, pre-clinical development, clinical trials and FDA (Food and Drug Administration) approval. This is a lengthy process that can take up to 20 years. Increased investment in research and development (R&D) (up to USA $50 billion per year at present)[2] over the last thirty years has not improved the rate of drug discovery success. The number of drugs approved each year remains constant despite the improvements in technology.[3] The various explanations for the lack of success include the increasing regulatory requirements, the reduction of therapeutic opportunities and the operational efficacies of individual organisations. However, in the past decade, many scientists have also publicly expressed that this lack of success has to do with the poor understanding of human biology, disease mechanism and target validation before the drug discovery process is initiated.[4] In these early stages, biologists perform assays in both living cells and animal models of the disease to demonstrate that the target studied is relevant to the disease. This lengthy and laborious process often occurs without full understanding of the mechanism of action on the target of interest, which can lead to failure during clinical trials, where higher costs are incurred.

There is an agreement that failures would decrease with better "proof of concept" studies of validated pioneer drugs.[5] Chemical biology and structural biology offer techniques for linking together elements from all stages of the drug discovery process. Small molecules could be used as tools to understand the initial stages of the drug discovery process. To address this need, public-private partnerships are becoming more commonplace between academia and industry to obtain more information on the 'proof of concept' whilst sharing the cost and expertise. This may lead to a reduction in the attrition rate during clinical trials and therefore reduce the high costs of new research.[6]

1.2. The need for open-access chemical biology

Over the past few years, industry has relied on the advancement of technology such as structure-based drug design, high-throughput screening, molecular modeling and numerous advances with *in vitro* and *in vivo* biological assays. Nevertheless, this is not reflected in the number of drugs failing clinical programmes, despite their excellent pre-clinical data. For example, only 27 drugs were approved by the FDA in 2013 compared to the 30 drugs approved in 1960.[7] Recent examples include the matrix metalloproteinases inhibitors (MMPs).[8,9] These failures have encouraged industry and academia to provide an alternative strategy to address unmet medical needs. It is believed that open-access chemical biology would be of great use if academia focussed their attention to open-access target validation instead of concentrating on the commercial potential of any discovery, whilst industrial partners provide the resources, experience and expertise.[10]

Amongst the multiple types of interactions between industry and academia, an open consortium model in the form of a public-private partnership (PPP) seems to be the most adequate for this cause (Figure 1).[11]

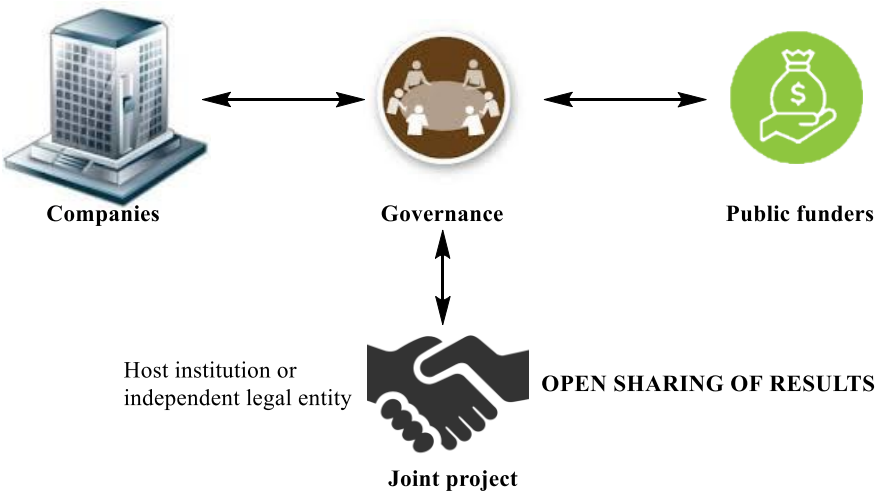

Figure 1: *The open consortium model in a form of public-private partnership.*

In this open consortium, partners work together to answer a scientific question or hypothesis. Projects are funded collectively and the research activities are carried out in different institutions. The results are shared openly between the consortium members and made rapidly available for the scientific community.

This model of collaboration has become very popular. Many companies and universities are now involved, including GlaxoSmithKline (Brentford, UK), Merck (Whitehouse Station, NJ, USA), Novartis (Basel, Switzerland), the Karolinska Institutet (Stockholm, Sweden), the University of Oxford (UK), the Structural Genomics Consortium (UK), the University of Toronto (Canada), and more recently, the University of Strathclyde (UK).

1.3. A PPP to unlock the untargeted kinome

The University of Strathclyde has become a member of a new open-consortium that aims to achieve one common goal: to unlock the human kinome.

Protein kinases are the second most common targets in drug discovery after G-protein coupled receptors (GPCRs). GPCRs, also known as seven trans-membrane domain receptors are a superfamily of proteins localized in the membrane of eukaryotic cells and are involved in a large variety of cellular processes, mainly by transmitting specific signals for each extracellular stimulus through the phospholipid bilayer membrane. Due to their importance in many cellular functions, they provide a wide range of opportunities as therapeutic targets in areas including cancer, obesity, central nervous system disorders and cardiac dysfunctions.[12]

Protein kinases are also very interesting targets because they play important roles in most of the cellular signaling pathways. Their popularity as drug targets has increased in recent years since studies have revealed that kinases represent the most frequently mutated proteins in tumors. There are many drug discovery efforts that already target protein kinases for many diseases such as cancer, fibrosis and asthma, amongst others. So far, twenty seven small-molecule kinase inhibitors have been approved for cancer treatment, specifically targeting the kinases c-Abl, PDGFR, EGFR and VEGFR families, and cKit.[13] Despite the highly selective kinase inhibitor lepatinib, also known as Tyverb®, most kinase inhibitors offer low selectivity profiles and target multiple kinases, leading to a poor 52% attrition rate for kinase inhibitors in phase I clinical trials. Addressing this issue is of great importance as it is directly related to the fact that only 25% of the 518 known human protein kinases are fully characterized. The rest have unknown functions.[14]

The fact that 75% of the function of the human kinome remains unknown suggests that the generation of new drug discovery efforts is driven by the accessibility to clinical ‘proof of concept’ (POC) of the protein kinase of interest. The lack of biological studies on 75% of the

human kinases leaves only 25% of the kinases as potential targets. This fact is reflected in the publication landscape, *e.g*, a recent review showed 20 protein kinases receiving over 15,000 citations in PubMed.[14] The most commonly studied protein kinases are p38α, SRC, EGFR, PKA, ErK1, KDR, ABL, CDK1, KIT and FMS for which POC studies are available, but little is known about the rest of the kinome. Furthermore, surveys have shown that amongst the compounds already being investigated in the initial phases of clinical trials, most of the compounds target a reduced number of kinases for which approved drugs are already available, suggesting that 'POC' is the main motivation for target selection.[14]

It is believed that chemical probes will be essential for the generation of new drug discovery efforts by providing biological evidence of the mechanism of the disease and understanding of the human kinome.[11] Currently there are few drug candidates that could be considered chemical probes following Frye's chemical probe criteria[15] (Table I), but the existing chemical probe arsenal is both small and inadequate for the task.[11]

Table I*: Examples of existing high-quality kinase chemical probes.*[11]

Chemical probe	Target kinase	Inhibition mechanism
CGI1746	BTK	ATP competitive
SGX523	MET	ATP competitive
LRRK2-IN-1	LRRK2	ATP competitive
GSK334470	PDK1	ATP competitive
Selumetinib	MEK	Allosteric
GW2580	cFMS	ATP competitive
JNK-IN-8	JNK	Covalent
GNF-5	ABL	Allosteric
KH-CB19	CLK1/CLK4	ATP competitive
ML167	CLK4	ATP competitive
NIH CLK/DYRK	CLK/DYRK	ATP competitive
Ruxolitinib	JAK2	ATP competitive
Tofacitinib	JAK3	ATP competitive
Lapatinic	EGFR/ERBB2	ATP competitive
Afatinib	EGFR/ERBB2	Covalent
Bl2536	PLK1	ATP competitive
GSK461364	PLK1	ATP competitive
MK5108	AuroraA	ATP competitive
VX-745	$p38_{\alpha/\beta}$	ATP competitive
Skepinone-L	$p38_{\alpha/\beta}$	ATP competitive
MLN-120B	IKK_{β}	ATP competitive
GDC-0879	BRAF	ATP competitive

Other drug targets such as GPCRs or nuclear receptors are also in need of chemical probes. However, protein kinases have become a priority since they are common targets for cancer therapy. Cancer remains a highly unmet medical need, and many potential cancer targets remain undrugged. More information on protein kinases will accelerate the process of understanding and provision of treatments for such diseases.

1.4. Protein kinases: mode of action and topology

The human kinome has been widely studied because of its role in many cellular pathways such as proliferation and signal transduction, which contribute to tumor cell growth and survival.[16,17]

A protein kinase is a protein that modifies the activity of another protein by chemically adding a phosphate group to this protein through its catalytic site in a process known as phosphorylation. Phosphorylation occurs in many cellular processes such as cell cycle, growth, apoptosis and signal transduction.[18] It occurs on the side chains of the amino acids, serine, threonine and tyrosine. The amino acid side chains contain a hydroxyl functional group which is phosphorylated by ATP, generating ADP and the phosphorylated protein. The phosphorylation process either activates or deactivates the protein target depending on the biological function (Figure 2).

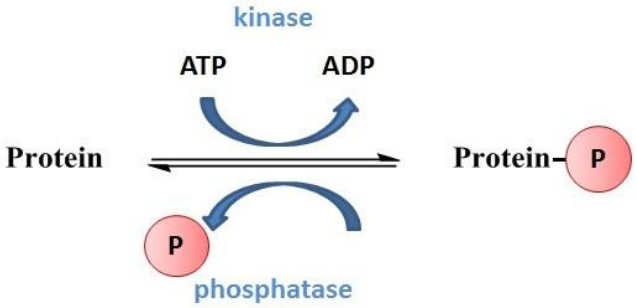

Figure 2: *Protein kinase mode of action.*

Protein kinases have been shown to be the most frequently mutated proteins in tumors, making them an attractive target in drug discovery.[19] Despite being mostly investigated in cancer, deregulation of kinase function has been implicated in many other disorders, such as immunological, neurological, metabolic and infectious diseases.

Very often, drug discovery efforts focus on the optimization of small molecule kinase inhibitors that bind in or around the nucleotide binding cleft, preventing ATP from binding, and therefore altering the biological response. Thus, understanding the structural basis of protein kinases is crucial to develop high quality, potent and selective kinase inhibitors.

Protein kinases have been investigated in depth and their structure is well defined. The tertiary structure is normally the native conformation of kinases and can be divided into two different lobes, the small N-terminal lobe, which is normally constituted by an antiparallel, 5-stranded, β-sheet and one prominent α-helix, and the C-terminal lobe which is mainly α-helical (Figure 3). A deep cleft is generated between these two lobes and forms the ATP binding site (or orthosteric site).

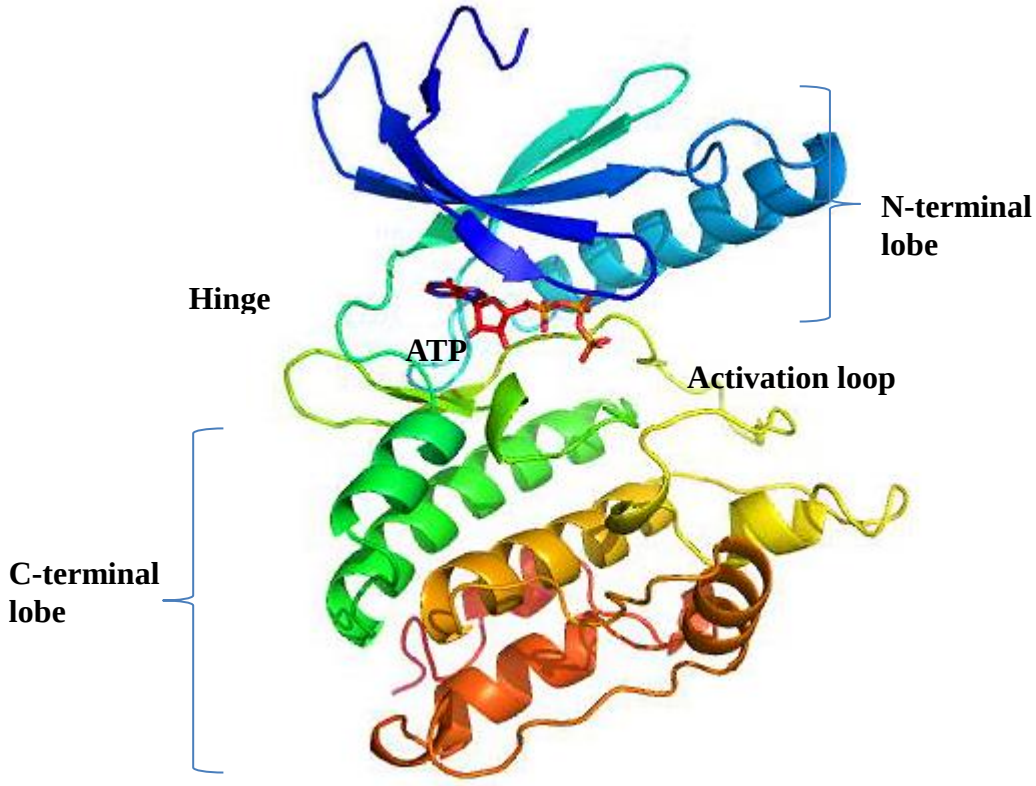

***Figure 3**: General kinase topology.*

The opening and closing of the kinase domain is controlled by the activation loop which produces changes in orientation between the N-lobe and the C-lobe that are required for the binding of substrates, catalysis, and the release of products. The activation loop in the C-lobe is generally formed by 20 different amino acids with a conserved amino acid triad: aspartate, phenylalanine and glycine (DFG), key for coordinating ATP for catalysis.[20] The orientation of

the activation loop when the ATP binds within the catalytic pocket is known as the open conformation, or 'DFG in', this conformation allows the necessary residues to carry out the phosphate transfer. When the activation loop is flipped 'out' relative to its conformation in the active state, the conformation is known as 'DFG out'.

The ATP binding site is highly conserved across the majority of kinases. A molecule of ATP will bind to the hinge *via* sequential hydrogen bonds between the adenine ring and the amide NH and carbonyl groups of the peptide backbone (Figure 4).[21] Magnesium cofactors are essential for the binding of the phosphate unit as they mask the negative charges on the functional group and assist the overall catalysis of the phosphorylation process.

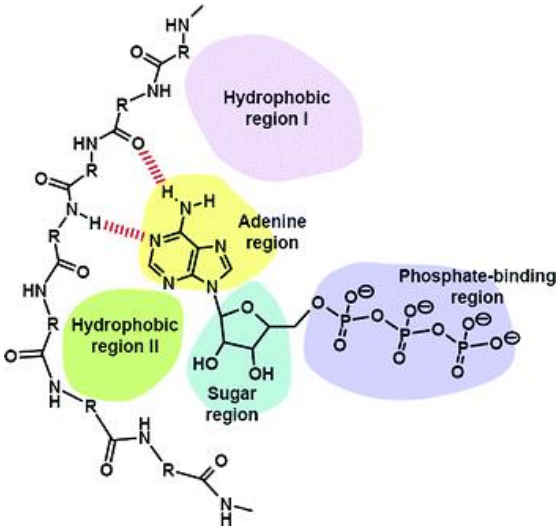

Figure 4: *Generic kinase ATP binding site.*

The majority of kinase inhibitors bind in the ATP binding site, thereby preventing ATP from binding. However, the large number of crystal structures available in the PDB have revealed different binding poses where small molecules can be recognized around the catalytic pocket. These binding modes have classified the inhibitors into four different groups, type I, type II, type III, and type IV, depending on whether the compound binds in an ATP mimetic manner, through the 'DFG in' conformation (type I), or *via* the 'DFG out' conformation (type II), or binding to an allosteric pocket (type III and type IV).[22]

Although the majority of crystal structures revealed type I inhibitors, defining, measuring and building inhibitor selectivity becomes a real challenge due to the conserved catalytic site across the human kinome. On the other hand, adjacent areas not occupied by ATP show more variability, particularly the interior hydrophobic pocket and the solvent-exposed specificity

surface (Figure 4, hydrophobic region II). The 'DFG out' conformation state of protein kinases is currently being the most studied.[23] The activation loop generates a less conserved cavity around the ATP pocket where small changes to a kinase inhibitor can provide high selectivity, as with the type II BCR-Abl inhibitor, imatinib.[21] Thus, designing inhibitors that target these areas (type II) or allosteric pockets (type III and IV) can provide better selectivities ideal for the development of new drugs or chemical tools for biological research.[24]

1.5. Selective chemical probes for PIM kinase isoforms

1.5.1. Biological background

PIM kinases are cytoplasmic serine/threonine oncogenic protein kinases belonging to the CAMK (calmodulin-dependent protein kinase-related) group.[25] The PIM family is made up of three different isoforms; PIM-1, PIM-2, and PIM-3. PIM-1 was identified by cloning retroviral integration sites in MMLV-induced lymphomas.[26] More than 50% of T-cell lymphomas show integration near the PIM locus leading to increased levels of PIM-1 mRNA. PIM-1 was found to be overexpressed in hematopoietic cells.[27]

MMLV proviral insertion cloning in c-myc transgenic mice lacking PIM-1 led to the identification of PIM-2 through its compensatory activation. PIM-2 is ubiquitously expressed with high levels in brain and lymphoid cells, and like PIM-1, PIM-2 also potently synergizes in c-myc induced lymphomagenesis. MMLV proviral insertion cloning in c-myc transgenic mice lacking PIM-1 and PIM-2 led to the identification of PIM-3 in response to PIM-1 and PIM-2 loss,[28] and the isoform was shown to be ubiquitously expressed with highest levels in kidney, breast and brain.[29, 30] The isoforms have high degrees of similarity; PIM-1 and PIM-3 are 70% identical at the amino acid level, while PIM-1 and PIM-2 share 60% homology.

PIM kinases do not have a regulatory domain and are constitutively active when expressed. They are regulated at the transcription and translational levels, through the JAK/STAT pathway, whereas most other kinases are mainly regulated *via* phosphorylation. Their activity is regulated mainly by protein stability, for example, through ubiquitination and proteasomal degradation. Binding to HSP90 stabilizes PIM protein levels (Figure 5) whereas binding to HSP70 results in degradation.[31]

Figure 5 represents the PIM regulation cascade through the JAK/STAT pathway. The STAT factors (STAT5, STAT3) are signal transducers and activators of transcription, which are activated by many cytokines such as interleukins EGF, IFN-γ, GM-CSF, Prolactin, TNFα and phosphorylated by JAK1/2/3 or NF-κB. Activation of STATs leads to their dimerization and nuclear translocation. In the nucleus, STAT3 and STAT5 bind directly to the PIM gene thus regulating gene expression.[31]

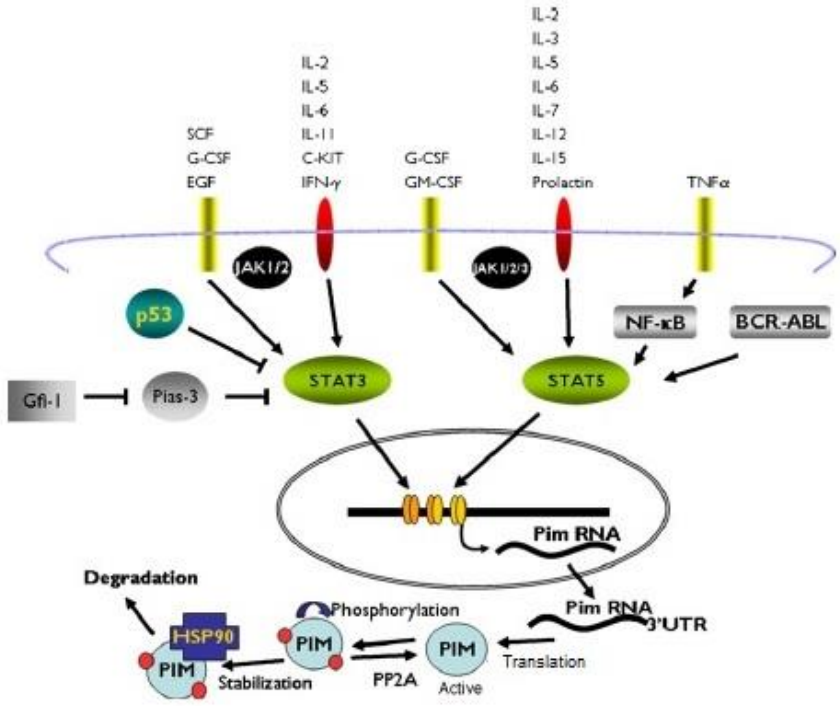

***Figure 5**: The JAK/STAT signalling pathway.*[31]

PIM kinases mediate their physiological effects through phosphorylation of a large number of cellular substrates. Figure 6 represents the activity of PIM kinases after their activation through the JAK/STAT pathway. PIM kinases phosphorylate proteins such as Histone H3 that are necessary for the MYC-dependent transcriptional activation and oncogenic transformation.[32] C-MYC is a gene that codes for transcription factors and it has been shown that a mutated version of c-myc is present in many cancers. PIM also phosphorylates the BAD protein which is a pro-apoptotic member of the Bcl-2 family that is involved in initiating apoptosis (programmed cell death). Phosphorylation of the BAD protein allows binding to the 14-3-3 scaffold protein, which prevents the unphosphorylated BAD protein from binding to ani-apoptotic Bcl-2 family of proteins to counteract their pro-survival actions.[33] In the inflammatory response, PIM phosphorylates SOCS (*S*uppressor *o*f *C*ytokine *S*ignaling)

proteins which are a family of genes involved in inhibiting the JAK-STAT signaling pathway.[34] The cell cycle (events that lead to the division and duplication of cells) is mainly regulated by CDK proteins such as p21 or p27 or phosphatases cdc5a/c (cell division cycle phosphatases). PIM kinases phosphorylate these substrates promoting tumorigenesis and subsequent cell proliferation.[35] Finally, PIM phosphorylates the protein 4E-BP1 which is involved in the cap-dependent protein translation, leading to the activation of protein synthesis.[36] Therefore PIM kinases are intimately involved in transcription, cell survival, inflammation, cell cycle progression and translation.

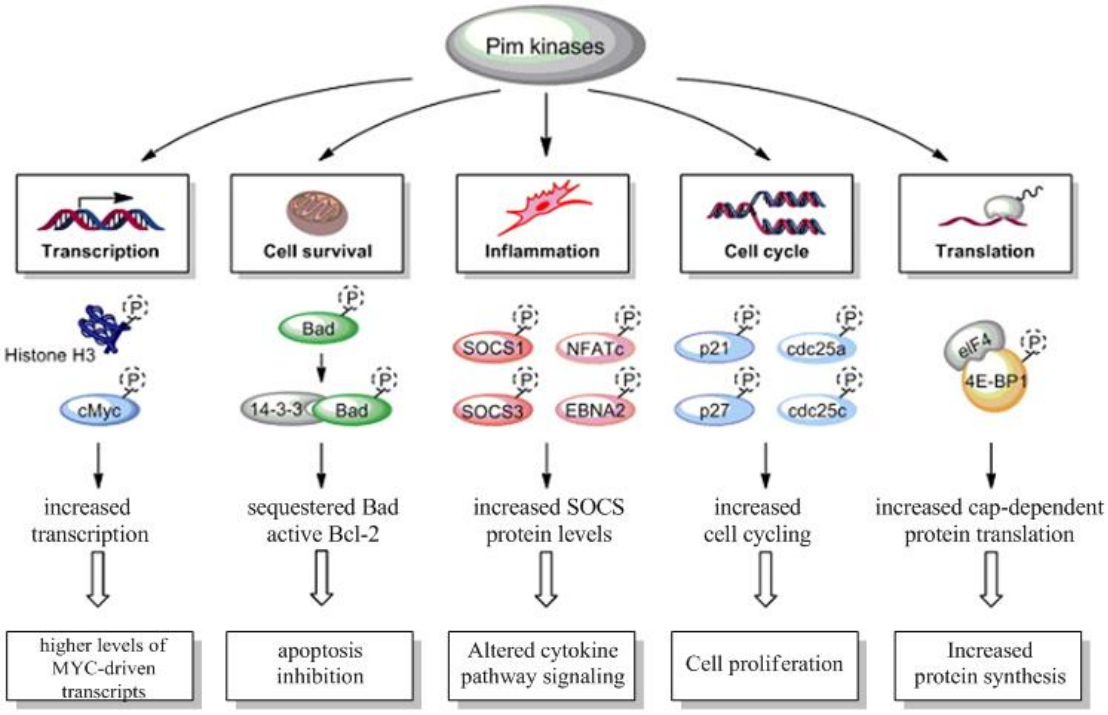

Figure 6: *PIM kinase targets and their roles in inflammation and cancer.*

The main observation that has been determined about the PIM kinase family is that they have a very broad range of cellular substrates related to many cell survival processes. This fact demonstrates the potential for the involvement of PIM kinases in cancer. PIM kinases are weak oncogenes therefore they are considered as proto-oncogenes due to the multiple pathways they are involved in, making them very attractive in drug discovery. A high level of interest and investigation has arisen regarding this family over the past decade, specifically in the generation of inhibitors to understand biological function.

1.5.2. PIM kinase competitor landscape

Due to their important role in inflammation and cancer, PIM kinase inhibitors have been extensively investigated during the past twenty years. At the start of the project, there have been fourteen patents published that indicate PIM kinases as primary targets showing high affinities to the three isoforms PIM-1, PIM-2, PIM-3.[37] It is also important to note that although all the inhibitors published have extremely good binding affinities for the PIM family, there are not yet any inhibitors that selectively target individual isoforms.

In 2004, researchers from Vertex Pharmaceuticals reported the triazolopyridazine **1** as a potent PIM-1 inhibitor with low IC_{50} values and additional cross-reactivity with GSK-3 and CDK-2 protein kinases (Figure 7).[38]

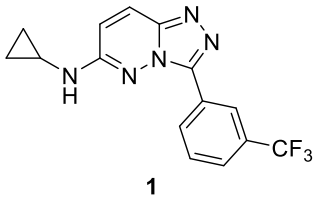

1

PIM-1(K_i):18 nM
GSK-3 (IC_{50}): < 2 nM

Vertex Pharmaceuticals, Inc.

Figure 7: *PIM kinase inhibitor reported by Vertex Pharmaceuticals, Inc.*

In 2008, researchers at SuperGen published a bicyclic heteroaromatic imidazopyridazine **2**, which was shown to be potent for the three isoforms of the PIM family (Figure 8).[39] Imidazopyridazine **2**, also known as SGI-1776, was tested against 353 kinases and had some cross reactivity with kinase Flt3, haspin and Cε. Imidazopyridazine **2** was the first compound to advance to phase I trials, becoming the first-stage investigational drug specifically for PIM kinases.

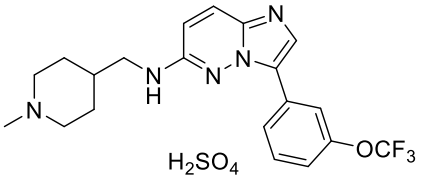

2

IC_{50} PIM-1: 6.7 nM
IC_{50} PIM-2: 363 nM
IC_{50} PIM-3: 69 nM

SuperGen, Inc.

Figure 8: *PIM kinase inhibitor reported by SuperGen, Inc.*

Around the same time, Centro de Investigaciones Oncologicas published another imidazopyridazine compound with improved IC_{50} values (PIM-1: 6 nM, PIM-2: 62 nM) but exhibiting cross reactivity with kinases such as CDK-2 and GSK-3. Many other groups have subsequently described imidazopyridazines as PIM inhibitors.[40,41,42]

Other pharmaceutical companies such as Exelixis and Abbott Laboratories have recently (2009) reported PIM kinase inhibitors using pyrimidinone scaffolds (**3** and **4**) with good IC_{50} values for the three isoforms (Figure 9).[39]

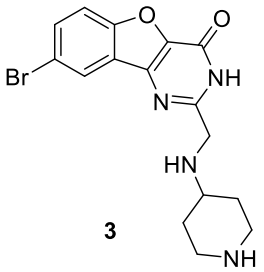

3

IC_{50} PIM < 10 nM

Exelixis, Inc.

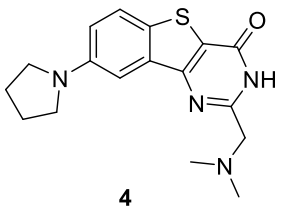

4

K_i PIM-1: 4 nM
K_i PIM-2: 5 nM

Abbot Laboratories

Figure 9: *PIM inhibitors reported by Exelixis, Inc. and Abbott Laboratories.*

More recently, AstraZeneca published a novel benzylidene-1,3-thiazolidine-2,4-dione **5** (Figure 10), which was shown to be an extremely potent pan-PIM inhibitor, demonstrating efficacy in preclinical models of acute myeloid leukemia.[43,44]

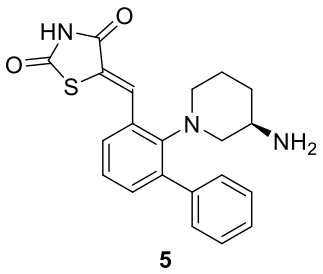

5

IC_{50} PIM-1: 3 nM
IC_{50} PIM-2:15 nM
IC_{50} PIM-3: 9 nM

***Figure 10**: Recent pan-PIM inhibitor reported by AstraZeneca.*

In summary, over the past decade PIM kinases have been extensively investigated for the treatment of inflammation and cancer. Since 2009, many groups have published compounds that behave as PIM inhibitors.[45,46,47] To our knowledge, none of the compounds published to date show any considerable selectivity across the three isoforms of the family, and still do not meet the criteria for them to be considered useful chemical probes.

1.6. Designing chemical probes for PIM kinases

1.6.1. Early medicinal chemistry

In 2010, Frye defined a chemical probe as a chemical tool for biologists that should meet the following criteria: 1) it has to be selective against close-family-member biological targets; 2) it needs to provide sufficient mechanistic data versus its intended target to be able to interpret the mechanism of action through cell-based assays; 3) it needs to have sufficient chemical and physical property data to use it in *in vitro* and cell-based assays with the interpretation of the results attributed to its intact structure; 4) it needs to prove at least one hypothesis of the role of its target in a cell's response to its environment; 5) it needs to be readily available to the scientific community.[15]

Following these requirements, this project started with an extensive literature search on all the inhibitors published for the PIM kinase family to date, analyzing their physicochemical properties, their synthetic tractability and their selectivity profile. The chosen starting point was inhibitor **4** published by Abbott Laboratories in 2009, because of its good selectivity profile, good physicochemical properties and the accessibility of the chemistry (Figure 9).[1]

The Abbott compound **4** has a benzothienopyrimidone core with substituents on positions 2 and 8. Benzothiophenes are important heterocycles used as either biologically active molecules or luminescent components in organic materials. One of the most important drugs based on a benzothiophene core is Raloxifene (**6**, Figure 11), used in the treatment of osteoporosis in postmenopausal women.[48]

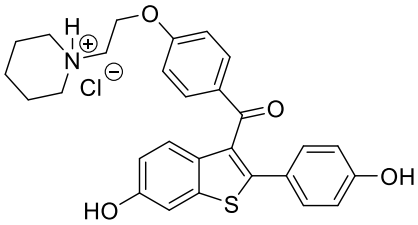

6

Figure 11: *Raloxifene.*

1.6.2. High-throughput screening

Compound **7** (Figure 12) was identified as a hit through high-throughput screening (HTS) and showed 63 nM and 160 nM activities against PIM-1 and PIM-2 respectively, although it also inhibited other kinases such as CLK4 (K_i = 90 nM) and Pbk (K_i = 316 nM).[1]

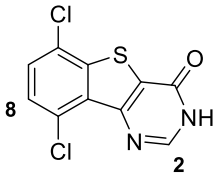

7

Figure 12: *Initial hit discovered by Abbott Laboratories. Positions 8 and 2 of the benzothienopyrimidinone ring are also detailed.*

An X-Ray crystal structure of compound **7** – PIM-1 crystal structure (PDB: 3JYA) confirmed that **7** binds to the ATP binding pocket (Figure 13). The compound is situated so that the carbonyl group is facing the pocket surrounded by Lys-67, Glu-89, Phe-49 and the chlorine at position 6 is interacting with the hydrophobic area generated by the Pro-123 residue adjacent to the hinge region.

The crystal structure also showed that position 2 of the benzothienopyrimidone core points towards the solvent-accessible region which is surrounded by the amino-acid residues Asp-128, Val-126, Asp-131, Glu-171, and Asp-172. This identified enough space to accommodate

a variety of substituents that could form hydrogen bond interactions with the residues and increase the potency and improve physicochemical properties of the probe. Position 8 is facing the hinge region where there is also space to accommodate substituents, allowing the chance to perform a SAR study around that position.

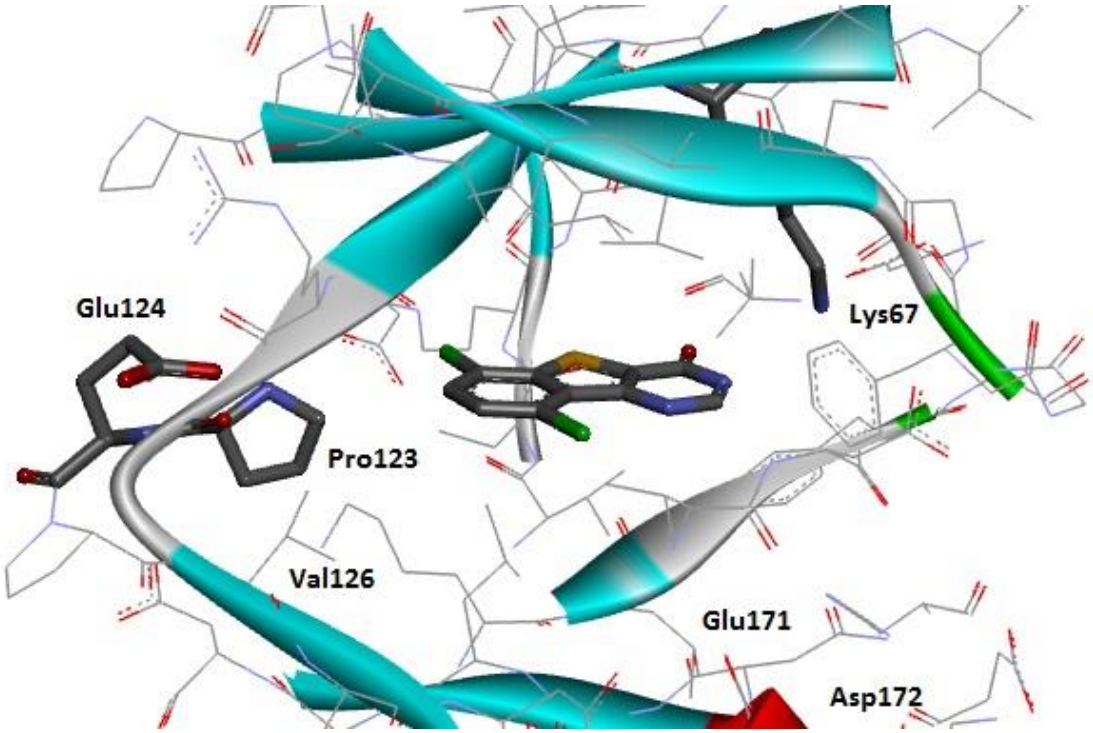

Figure 13: *X-ray crystal structure (PDB: 3JYA) of **7** bound to PIM-1 kinase.*

Information on the kinase structure could also be gathered from its X-ray crystal structure. It showed that PIM kinases (also PIM-2, PDB: 2IWI)[49] have an atypical hinge region characterized by an insertion of one additional residue, Pro-123, that allows formation of only one hydrogen bond with ATP mimetic/competitive inhibitors. This characteristic ensures high selectivity towards PIM kinase inhibition over the rest of the human kinome.

1.6.3. Structure Activity Relationship (SAR) studies

Researchers in Abbott Laboratories performed extensive SAR studies using **7** as a starting point, and reported potent inhibitors targeting the three isoforms of PIM kinases simultaneously (see Figure 10). Two of their best inhibitors, **8** and **9** are shown below (Figure 14):

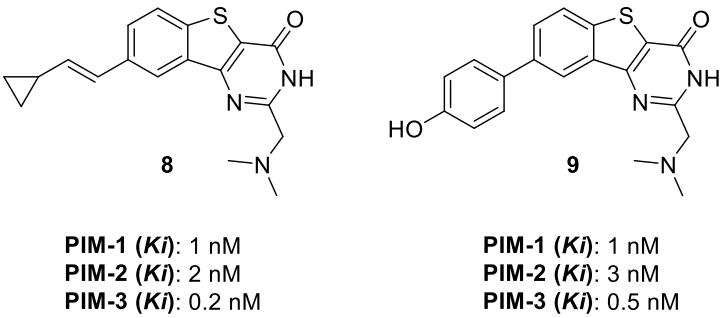

Figure 14: *Abbott compounds that target the three PIM isoforms simultaneously.*

Because PIM-1, PIM-2 and PIM-3 are all implicated in tumorigenesis, it has been proposed that inhibiting the three isoforms simultaneously may improve cancer therapy efficacy. Therefore, many of the inhibitors published in the area target all three isoforms.[50, 51] However, Abbott laboratories published compounds **10**, **11** and **12** (Figure 15) which showed good selectivity between PIM-1 and PIM-2, which suggested that the scaffold might be suitable to design PIM probes.

Although the potency for these compounds against PIM-3 has not been published, we regarded it as a good starting point to design our probes for each of the three PIM isoforms.

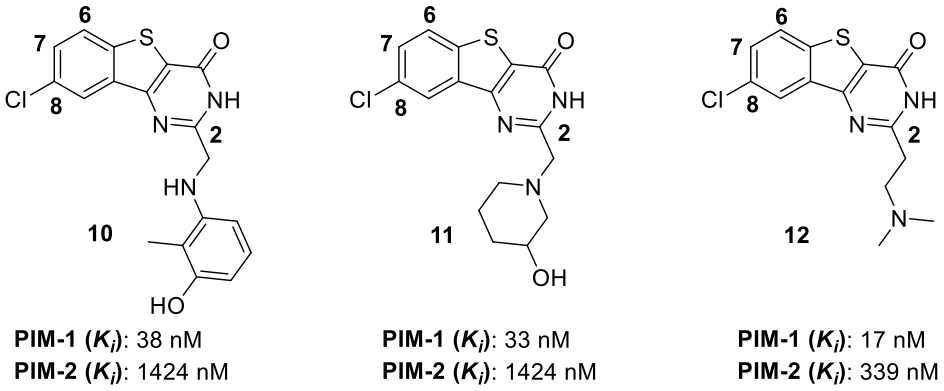

Figure 15: *Inhibitors that showed good selectivity within the family.*

1.6.4. The PIM-1 and PIM-2 crystal structures

The key to the development of successful probes is to analyze the crystal structures that have been published. PIM-1 has proven to be the easiest to crystallize, whereas there is only one PIM-2 crystal structure available in the protein data bank (PDB). To date, there are no PIM-3 crystal structures available. The crystal structures provide information about the nature of the

ATP pocket. Furthermore, superimposition of PIM-1 and PIM-2 together with studying the amino acid sequence can also determine the differences between the isoforms. A PIM-3 virtual model could potentially be constructed by molecular modeling studies if further studies were to be required.

The X-ray crystal structure of PIM-1 – Compound **8** (PDB: 3JXW, Figure 16) showed a key interaction between the carbonyl group of **8** and Lys-67 (2.56 Å). Position 2 showed enough space to expand towards an unexplored region. Key residues that could be targeted in this region include Asp-172, Glu-171, Asp-128, and Asp-186, which could form hydrogen bonding interactions with a compound, stabilizing the binding and therefore increasing the potency.

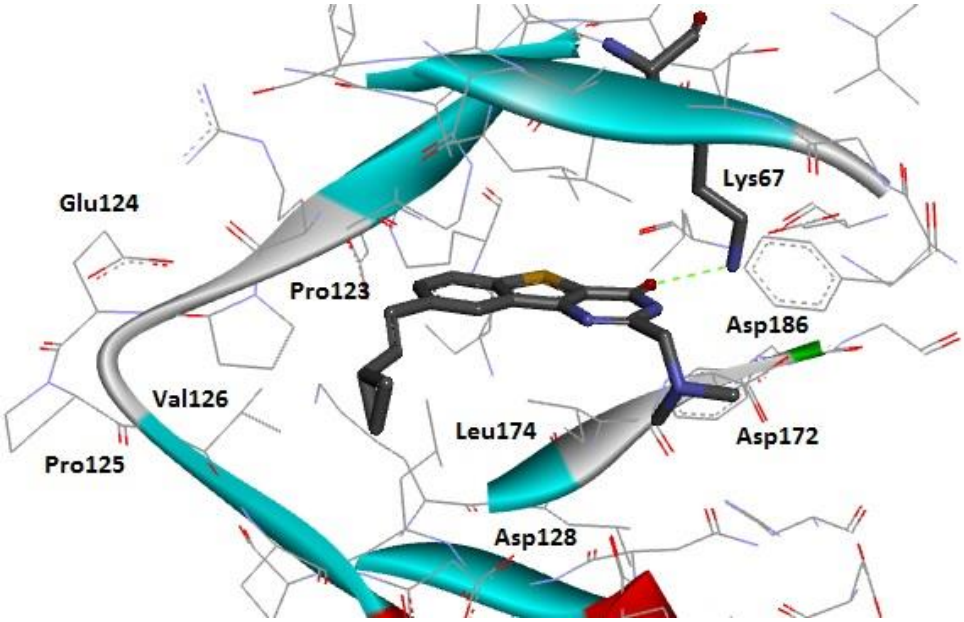

Figure 16: *X-ray crystal structure of PIM-1 – Compound **8**. Hydrogen bond interactions between the amide and Lys67 are represented by a green dotted line.*

Position 8, which is pointing towards the hinge region, does not appear to have any key hydrogen bonding interaction, indicating that part of the compound's potency is due to hydrophobic interactions within that pocket through the lipophilic residues Ile-104, Pro-125, Val-126 and Glu-124. As well as position 8, positions 6 and 7, which are also facing the hinge region, have not yet been studied and there is potential space for expanding towards it with small hydrophobic substituents.

Analysis of the crystal structure showed a unique feature within the PIM kinases. The PIM kinases contain a proline residue (PIM-1: Pro-123, shown in Figure 16) in their hinge region

which eliminates a key hydrogen-bond-donating hinge interaction with ATP and canonical kinase inhibitors. This feature leaves the glutamic acid within the hinge region (PIM-1: Glu-124) as the only possible residue for interaction of PIM inhibitors with the hinge region.

The crystal structure also indicated that the PIM kinases contain another proline residue (PIM-1: Pro-125) at the end of the hinge region which provides a larger hydrophobic pocket for PIM kinase inhibitors. A variety of hydrophobic substituents could possibly fit in this pocket, leading to an increase of potency for the probe. Non-PIM kinases do not have a proline at this position and generally contain an H-donor amino acid.[52]

The polar surface (surface sum over all polar atoms, primarily oxygen and nitrogen, also including their attached hydrogens) of the complex between PIM-1 and **8** (Figure 17), shows how the compound is docked in the binding site. The polar surface shows the hydrophobicity of the hinge region, where the cyclopropane ring fits and the dimethylamine moiety is situated so that it has polar interactions with the residues in proximity to position 2.

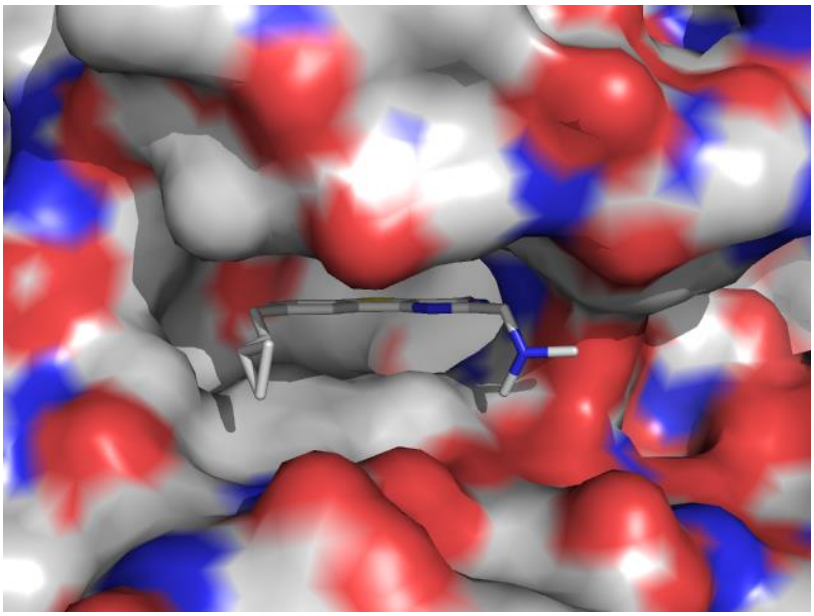

Figure 17: *Polar surface of PIM-1 – Compound* ***8*** *in the binding pocket.*

Since the PIM kinases share 60-70% of their amino acid sequence, it would be expected that the ATP pockets share similar topology. The amino acid sequence reported by Brault (Figure 18) showed that within the hinge region, PIM-1 and PIM-3 share a glutamic acid whereas PIM-2 contains a leucine, which could be a good interaction to target in order to increase

potency and/or selectivity. Additionally, PIM-1 and PIM-3 share a serine at position 43 (position refers to PIM-1 crystal structure) whereas PIM-2 contains a lysine.

Figure 18: *Amino acid sequence for PIM-1, PIM-2 and PIM-3. The kinase domain is shown in grey. The amino acids involved in the ATP binding site are shown in orange.*

PIM-3 and PIM-2 have been found to be very difficult to crystallize. A single crystal structure of PIM-2 with a ruthenium complex (PDB: 2IWI) has been reported by the Structural Genomics Consortium (SGC).[49] The reported PIM-2 X-ray crystal structure had important parts of the isoform missing due to the challenges involved with the crystallization of the protein (Figure 19). The main backbone of the *N*-terminal region of the PIM-2 kinase has a considerable number of amino acids missing, highlighted in Figure 19. In addition, some amino acids within the ATP binding pocket are not fully resolved. For example, the lysine residue which was shown to be key for interaction with the Abbott scaffold does not have its side chain present. In addition, other amino acids are absent.

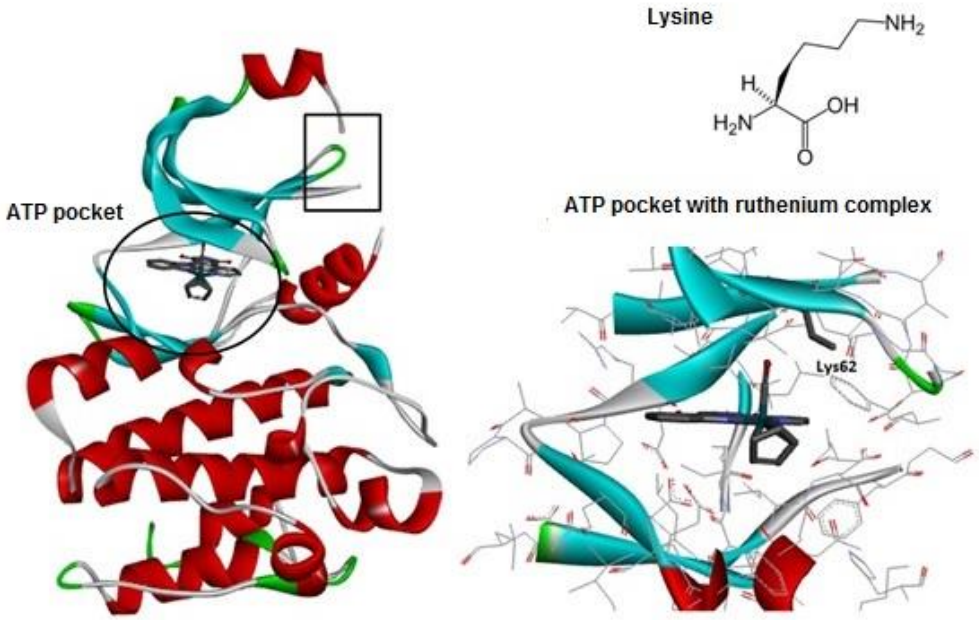

Figure 19: *PIM-2 X-ray crystal structure. On the left hand side some visible parts of the protein are missing. On the right hand side, the ATP binding pocket needs to be repaired. Lys62 has the side chain missing.*

Nevertheless, the PIM-2 crystal structure still provides useful information about the topology of these isoforms and a repaired structure of PIM-2 can be constructed through molecular modelling for further studies. The crystal structures of PIM-1 and PIM-2 confirm that the few non-conserved residues at the ATP binding pocket point their side chains away from the binding site, creating pockets of very similar topology. Despite these similarities, it has been previously discussed in this report that inhibitors can still provide good isoform selectivity. The mechanisms leading to this selectivity or the reasons for differences in selectivity remain unclear.

The information gathered through the literature search, together with the crystal structures constitute a starting point for the development of selective probes for the PIM isoforms. It was envisaged that an initial SAR study using the Abbott scaffold would be performed and the results will provide guidance for future modification of the scaffold to increase potency and selectivity.

1.7. Biological evaluation of the Abbott compound

1.7.1. Kinase selectivity assays

Selection of the Abbott compound as an initial starting point was reinforced by the biological data reported in their publication.[1] Abbott laboratories performed a kinase assay to assess the selectivity of their reported compounds against the kinases that usually showed cross-reactivity with PIM kinases. The initial hit, **7**, and their most potent compound **9** were tested against a panel of human kinases (Table II).

Table II: *Kinase selectivity for compounds **7** and **9**. The inhibition constant values were calculated using the Cheng-Prusoff equation:*

$$K_i = IC_{50} / (1 + ([ATP/Km])$$

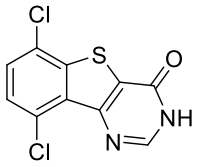

7

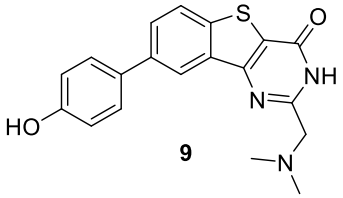

9

Protein kinase	7 (K_i, μM)	9 (K_i, μM)
PIM-1	0.1310	0.0007
PIM-2	0.1642	0.0021
PIM-3	0.0110	0.0004
BTK	0.6365	> 1
CDK2	> 1	> 1
CLK4	0.0896	> 1
EMK	> 1	> 1
IGF1R	0.9909	> 1
IRAK4	> 1	> 1
MSK1	0.7850	> 1
Map4k4	0.8124	> 1
p70S6K	0.7734	> 1
PBK	0.3161	> 1
PKA	> 1	> 1
PRKX	0.5847	> 1
Syk	0.3514	> 1
Src	> 1	> 1
TrkC	0.8283	> 1

The initial hit **7** showed some potency against the PIM kinases as well as an affinity for other kinases such as CLK4, PBK or Syk with activities between 0.3–1 μM and K_i > 1 μM against CDK2, IRAK4, PKA and Src. Overall, the compound gave a promising selectivity profile for an initial hit compound that could be further optimized. It is believed that this selectivity is related to the chlorine on the benzothiophene ring. The chlorine occupies the hydrophobic pocket adjacent to the hinge region generated by the proline amino acid, present in PIM kinases. Other non-PIM kinases contain a hydrogen-bond donor from the backbone amide at this position creating a polarity clash with the chlorine group and generating a further selectivity towards non-PIM kinases.

It is important to mention that amongst the kinase panel, CLK4 is a splicing protein kinase that usually shows the highest cross-reactivity with PIM kinase inhibitors as they share similar amino acids sequences at their ATP binding pockets. Therefore, designing selective inhibitors for PIM kinases over CLK4 has proved challenging.

After optimization, compound **9** was screened against the same panel of kinases and its selectivity was greatly improved compared to that of **7**, exhibiting no activity towards the reported human kinases, even when tested at a high concentration (10 μM), and low nanomolar activities for PIM-1, PIM-2, and PIM-3, of 7 nM, 21 nM, and 14 nM, respectively, were observed.

1.7.2. Cell based assays of Abbott PIM inhibitor

Abbott laboratories also reported cell based assays on their most potent compounds. Compound **9** was tested in a leukemia cancer cell line (K562) that overexpresses PIM kinases, to investigate its antiproliferative activity. K562 cell have also been shown to be resistant to PIM-1 inhibition,[42] suggesting that pan-PIM inhibitors such as **9** should still show some antiproliferative activity due to PIM-2/PIM-3 inhibition. Compound **9** showed an EC_{50} of 1.7 μM in K562 (Table III), a low activity but encouraging as some inhibition could be observed. Other compounds such as **13**, **14**, and **15**, inhibited proliferation with sub micro molar EC_{50} values of 300 nM, 700 nM, and 400 nM, respectively. These compounds were also tested in another human cancer leukemia cell line MV4-100. The compounds showed a lower antiproliferative activity compared to leukemia cell line K562, but the result was encouraging as some inhibition could still be observed.

Table III: *Anti-proliferative activities for compounds **9**, **13**, **14** and **15** in both K562 and MV4-100 cancer cell lines.*

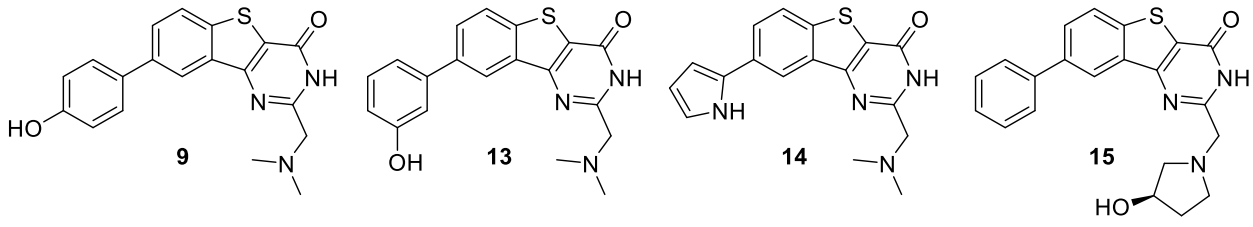

Cell line	9	13	14	15
K562 (EC_{50}, μM)	1.7	0.3	0.7	0.4
MV4-100 (EC_{50}, μM)	2.4	1.4	1.9	5.6

Additional cellular assays were performed to analyze whether the cytotoxicity seen in the cell lines was due to the inhibition of PIM kinases. As previously mentioned (section 1.5.1), BAD protein is a downstream target of the PIM isoforms and is phosphorylated by PIM kinases at Ser112 and Ser136. The phosphorylation of BAD kinase in the presence or absence of PIM kinases was also reported by Abbott Laboratories. Compound **9** was tested in K562 cell lines to analyze the inhibition of the phosphorylation of BAD protein at Ser112. The outcome was very encouraging as an EC_{50} of 0.5 μM was observed, reinforcing the hypothesis that benzothienopyrimidinone compounds exert cytotoxicity on the cancer cell lines *via* PIM kinase inhibition.[1]

1.7.3. Pharmacokinetics and ADME data for compound 9

The pharmacokinetics and ADME (absortion, distribution, metabolism, and excretion) properties of compound **9** were studied and are shown in Table IV and Table V.[1]

Table IV: *Pharmacokinetic properties for compound **9**.*

IV				PO			
AUC (μmol·h/L)	**Cl (L/h/kg)**	**V_d (L/Kg)**	**$t_{1/2}$ (h)**	**AUC (μmol·h/L)**	**C_{max} (μM)**	**T_{max} (h)**	**F (%)**
1.1	7.8	2.5	2.1	2.8	0.52	0.3	76

Table V: *ADME properties for compound* ***9.***

mouse liver microsomes ($t_{1/2}$, min)	human liver microsomes ($t_{1/2}$, min)	CYP (2C9, 2D6, 3A4) (IC_{50}, μM)	Pampa (pH 7.4, % transported)	protein binding in 10% human plasma (% bound)	protein binding in 100% human plasma (% bound)
48	> 60	> 20	17.4	68	92

The compound was dosed into a CD-1 mouse (multipurpose research animal model that can be used in such fields as toxicology, aging and oncology) by both intravenous (IV) and oral (PO) administration. The compound showed excellent data. In pharmacokinetics, AUC, area under curve, which represents the total drug exposure integrated over time, is a parameter used to calculate drug body clearance (Cl), and describes how quickly drugs are eliminated. The Cl observed for compound **9** was 7.8 L/h/Kg. The volume of distribution of a drug, Vd, represents the amount of drug that it is distributed in the body tissue than blood plasma, and compound **9** showed a good value of 23.5 L/Kg. Compound **9** also showed bioavailability (a measurement of the rate and extent to which a drug reaches at the site of action) of 76% when oral dosing was seen, coupled with a half-life of 2.1 h when administered intravenously and 0.3 h when administered orally. The Abbott laboratories also reported the ADME data for compound **9** (Table V). The compound also showed extremely good ADME data. No binding to CYP (cytochrome P450) enzyme was observed (>20 μM), good permeability using parallel artificial membrane permeability assay (Pampa) criteria, enough protein binding and a long half-life in both human and mouse liver microsomes of over 60 minutes and 48 minutes, respectively.

Overall, the accessibility of the chemistry, the good physicochemical properties and the observations in cell-based assays encouraged us to use the Abbott compound as our initial scaffold for the development of chemical probes for the PIM kinases.

1.8. Biological evaluation of the chemical probes

The compounds synthesized during the project were evaluated in a variety of biological assays to analyze their potency, selectivity and quality as chemical probes. Even though the data will be presented together according to each chemical series, it is important to clarify that the primary assay used to follow the SAR study was the Differential Scanning Fluorimetry

(DSF) assay, which was provided by our collaborators at the Structural Genomics Consortium. Other assays, such as kinetic assays, cellular assays and solubility/permeability assays presented during this thesis were carried out by myself towards the end of the project during a three-month placement at the Spanish National Cancer Research Centre (CNIO) in Madrid, Spain. However, a second batch of compounds which was synthesized during the final months of my PhD, was sent to the CNIO and tested by our collaborators in order to obtain biochemical data for every final compound to provide a higher quality thesis and for publication purposes.

Isothermal tritration calorimetry (ITC) data will also be presented, and was carried out by Dr. Clara Redondo at the SGC at the end of the project for publication purposes.

1.8.1. Differential scanning fluorimetry (DSF) assay

DSF is an inexpensive biological assay that identifies low-molecular-weight ligands that bind and stabilize proteins.[53] The assay measures the temperature at which a protein unfolds *via* an increase in the fluorescence of a dye.

The stability of a protein is related to its Gibbs free energy of unfolding, ΔG_u, which is temperature dependent.[54] The stability of a protein decreases with increasing temperature. When temperature increases, ΔG_u decreases and becomes zero at the equilibrium where the concentration of folded and unfolded protein is equal. This temperature where ΔG_u becomes zero is referred to as the melting temperature (T_m).

When a low-molecular-weight ligand binds to a protein it causes a conformational change in the protein, therefore resulting in a thermal stability change of the protein. The free energy contribution of ligand binding results in an increase in ΔG_u, which causes an increase in T_m. Potent inhibitors stabilize the protein in its folded conformation thereby increasing T_m. Shifting of the melting temperature serves as an indicator of a protein-ligand binding strength.

DSF is best performed using a dye. The most common dye is SYPRO Orange® which is strongly quenched by water and binds to hydrophobic surfaces of the protein. When a protein is folded, hydrophobic surfaces of the protein are hidden inside and do not activate the dye. As the protein unfolds with an increase of temperature, the hydrophobic surfaces get exposed to the dye. Therefore, a protein stability curve and melting temperature data can be determined by changing the temperature and monitoring fluorescence (Figure 20).

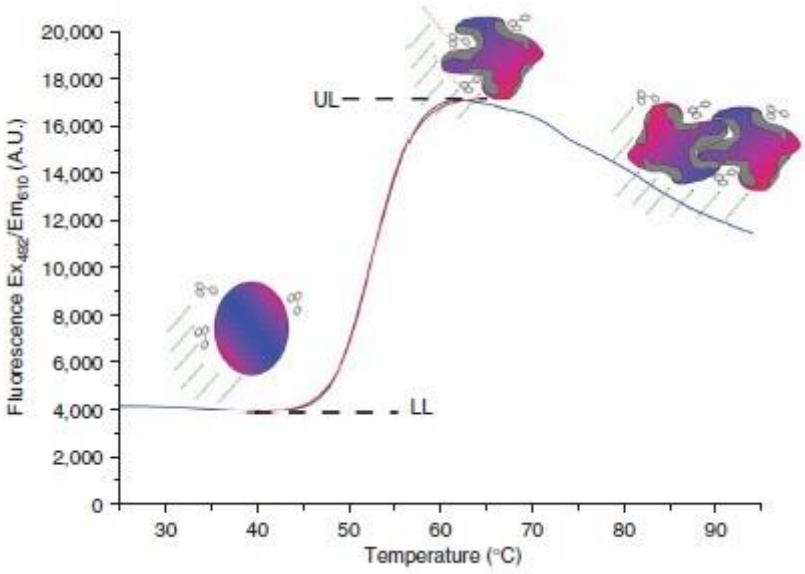

***Figure 20**: Typical DSF assay recording (fluorescence vs temperature) of a protein in the presence of a SYPRO Orange dye (symbolised as a three aromatic-ringed molecule). The lower level (LL) and upper level (UL) are also depicted in the figure.*

The result of the assay is a differential of temperatures, ΔT_m, of the unfolded protein stabilized by the ligand and the melting temperature of the native protein. The higher the ΔT_m, the stronger the affinity of a ligand to the protein. When drawing conclusions from the results, care must be taken as competing effects can mask or promote ligand binding. The technique is therefore generally only used for initial characterization within SAR studies.

1.8.2. Biochemical evaluation: ADP Hunter

A biochemical assay is an assay used to determine how well compounds bind to targets (*e.g.* kinase) or inhibit enzyme activities.

Most biochemical kinase assays measure the ATP consumed. During the reaction, the kinase uses ATP to phosphorylate the kinase substrate, generating the universal co-product ADP and the phosphorylated substrate. It is important to note that depending on the nature of the kinase, the kinase can also auto-phosphorylate and the assay directly measures the addition of a phosphate group to the protein kinase. PIM kinases however do not show auto-phosphorylation and there is a need of a PIM specific substrate, which is common for the three isoforms (PIM-1, PIM-2, and PIM-3).

When a potent ATP competitive inhibitor is added, the generation of ADP should decrease because the inhibitor is blocking the phosphorylation of the substrate by the kinase, as shown in Figure 21.

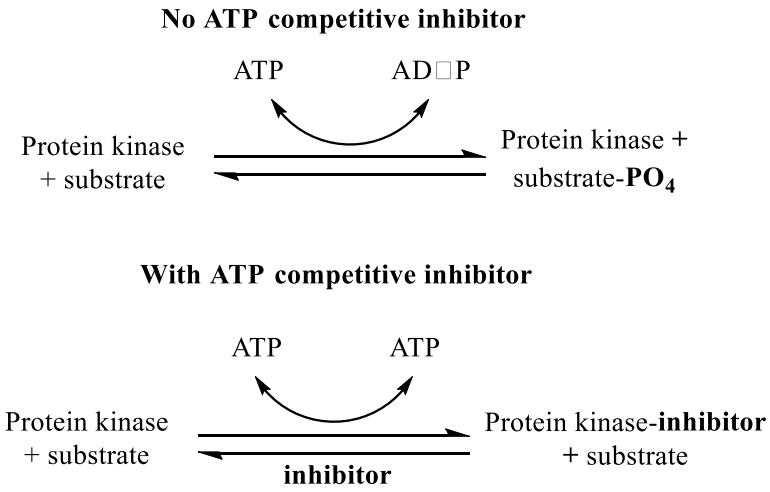

Figure 21: *General mechanism for ATP/inhibitor.*

There are numerous biochemical assays available to analyze the activity of enzymes involved in the transfer of a phosphate group from ATP to a substrate. Some of the common assays require the use of antibodies to detect the generation of the phosphorylated substrate, which are often unavailable or not adequate for the kinase assay conditions. However, HTS kinase assays ideally require kinase platform assays that have a broad applicability to kinases and substrates within drug discovery. A common and robust assay for this purpose is the ADP Hunter assay from DiscoverX, and it was used to measure the inhibition of our candidates against PIM-1, PIM-2, and PIM-3 at the CNIO.

1.8.2.1 Quality assessment of biochemical assays

In a biochemical assay, there are a few important values that determine the quality of the assay.

In a HTS assay, a large number of compounds are tested, and hits are labelled as being "active" or "inactive" against the studied target. It is of extreme importance to measure the effectiveness of the assay before the data is further analyzed, so that any compound is discarded with confidence.

In 1990, the most common factors that determined the quality of an assay were the signal to noise ratio (S/N) that compares the level of the signal to the standard deviation of the background, and the signal to background ratio (S/B) that compared the level of signal compared to level of background. However, these factors are no longer taken into account as they do not consider the variability in the sample, background measurements or signal dynamic range. The Z-factor is today the most common interpretation to determine if an assay has been successful, and it was introduced as a robust measurement of quality that takes into account the difference between positive and negative controls and the variability between the samples. The Z' factor is reported in every biochemical assay and it is measured and defined as shown in Table VI.[55] It is defined in terms of four parameters, the means and the standard deviations of the positive and negative controls. Another important interpretation is the assay window, which is calculated using the signal assay divided by the background and this factor should always be numerically greater than 2 to be able to accurately interpret the data.

Table VI: *Z-factor equation and interpretation.*

Z-factor	Interpretation
1	Ideal. Z' factor never exceeds 1
0.5 < x <1.0	Great assay
0 < x < 0.5	Marginal assay
0	Too much overlap between positive and negative controls

$$Z' = 1 - \left| \frac{3\sigma_+ + 3\sigma_-}{\mu_+ - \mu_-} \right|$$

In summary, a Z-factor of 0.5–1.0 indicates a good quality assay, and is required to correctly interpret the outcome of the assay. For Z-factor values under 0.5, the assay must be repeated and the data discarded.

There are currently many robust kinase biochemical assays that have been developed for HTS and the most common ones use ADP detection because it can be applied to a wide variety of kinases. The three most commonly used ADP detection assays are Transcreener® ADP by BellBrook Labs which analyzes direct immunodetection of ADP using antibodies that selectively recognize ADP. ADP Quest™/ADP Hunter™ by DiscoverX where the ADP is used to drive a cascade of detection enzymes that ultimately produce a fluorescent signal.

Finally, ADP Glo™ by Promega, which is an enzyme-coupled detection assay that analyzes the residual ATP first depleted and then the conversion of ADP to ATP using luciferase detection. As previously mentioned, an ADP Hunter assay was used to carry out the PIM kinetic evaluation, and all Z-factor values as well as the assay window obtained were within the acceptable range and the assay values were therefore of a quality to draw conclusions.

1.8.2.2 ADP Hunter assay principle

This PIM biochemical assay is a very reliable and commonly used assay that analyzes the accumulation of ADP, the product from a transfer of a phosphate group from ATP to the PIM substrate. ADP Hunter is specifically designed for HTS of kinase inhibitors and is compatible with many proteins and protein substrates. The principle of the assay can be explained in two different steps (Figure 22).

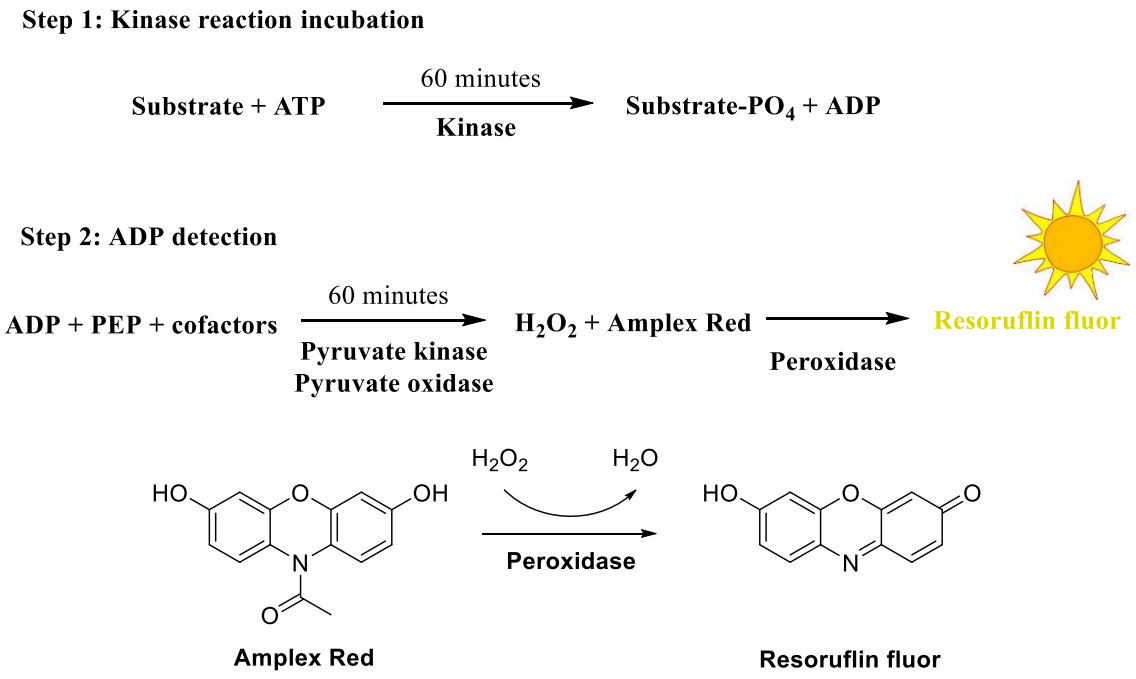

Figure 22: *Schematic principle of ADP Hunter assay.*

Step I of the assay involves the incubation of the ATP, protein kinase and the substrate for 60 minutes at 30 °C. During this time, the kinase catalyzes the phosphorylation of a specific substrate using ATP, which results in the generation of ADP.

Step II of the assay involves the detection of ADP using a solution containing pyruvate kinase and pyruvate oxidase, to generate hydrogen peroxide, and Amplex Red. Amplex Red, is then transformed to Resoruflin fluor, a red fluorescent compound (Figure 22) which has an absorption and fluorescence emission maxima of 563 nm and 587 nm.

Using this principle, the activity of an ATP competitive inhibitor can be measured. A potent inhibitor will block the ATP binding pocket of the kinase thus inhibiting phosphorylation and subsequently, the production of ADP. This will have a knock-on effect on the concentration of Resoruflin fluor, which is used to indirectly measure the inhibitor activity.

1.8.2.3 Detecting the interference with the ADP Hunter detection system

Kinase inhibitors very often show cross-reactivity with other kinases, and that is expected, since the kinome domain and especially the binding pocket are highly conserved within protein kinases. The ADP Hunter assay stop solution contains other kinases and cofactors that are needed to carry out the experiment. However, it is important to determine that the inhibitor being examined is specific to the intended kinase and is not showing any affinity towards the other kinases involved in the ADP Hunter detection system. A third parallel biochemical assay is carried out (Figure 23) in order to analyze that inhibitors are not interfering with the detection system.

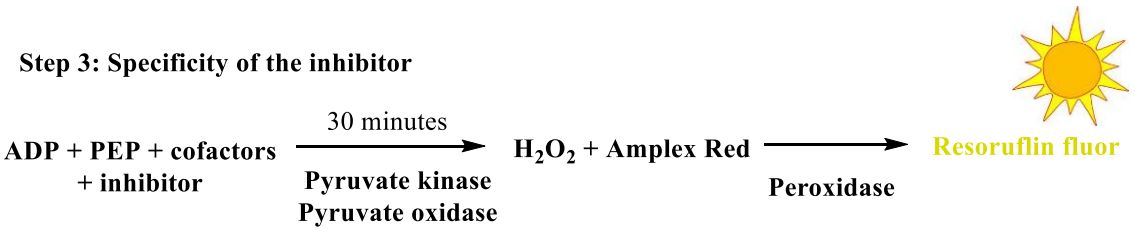

Figure 23: *ADP Hunter step 3 to analyse the specificity of the inhibitor.*

In Step III, a known concentration of ADP, together with the inhibitor, and the corresponding ADP Hunter kit is used, the assay is carried out, and the Resoruflin detected using the ADP Hunter system. No variation in the amount of Resoruflin would indicate that the inhibitor is not interacting with the ADP Hunter detection system.

1.8.2.4 The outcome of the assay –half maximal inhibitory concentration (IC_{50})

Biochemical reactions involving a single substrate are often assumed to follow the best-known model of enzyme activity, the Michaelis-Menten kinetics.[56] The model is named after Leonor Michaelis and Maud Menten and an example is shown in Figure 24.

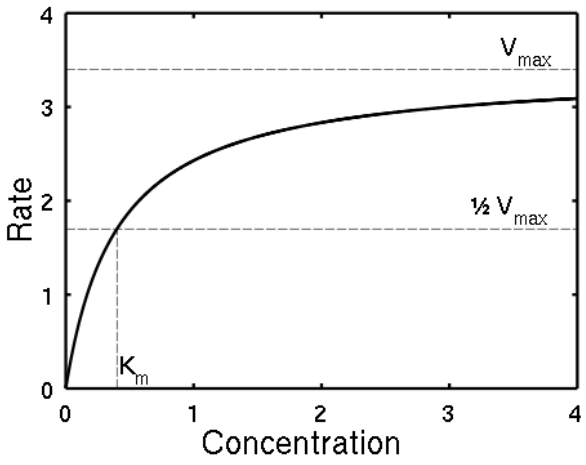

$$v = d[P]/dt = V_{max}[S]/K_m + [S]$$

***Figure 24**: Example of the Michaelis-Menten model where K_m is 0.4 and V_{max} 3.4.*

The Michaelis-Menten model allows a plot of the reaction velocity (v) to be drawn as a function of the substrate concentration [S] for an enzyme that obeys the Michaelis-Menten kinetics. As represented in Figure 24, the Michaelis constant, K_m, is equivalent to the concentration of substrate at which the reaction takes places at half of its maximum rate. Because K_m is an inverse measure of the substrate's affinity for the enzyme, a small K_m represents a higher affinity for the substrate.

Potent and selective adenosine triphosphate (ATP) mimetic inhibitors are often very challenging because the inhibitor competes with ATP which is a natural substrate of the human body, leading to poor potencies and selectivities.

Our collaborators at the SGC calculated the PIM isoforms' affinity for ATP, and the values obtained were PIM-1 (K_m): 10 µM, PIM-2 (K_m): 1.5 µM, and PIM-3 (K_m): 22 µM. The PIM-2 isoform has a higher affinity for ATP compared to PIM-1 and PIM-3 which explains the

conserved selectivity observed for PIM-1 and PIM-3 over PIM-2 and suggests that PIM-2 might be the most difficult isoform to inhibit through an ATP mimetic inhibitor.

When a competitive inhibitor is added to block the phosphorylation of substrate, the concentration of compound required to block a particular response (in this case, the ATP catalysis) is measured. The term IC_{50} is introduced as a measure to express how much of a particular drug/inhibitor is required to inhibit half of the biological response.

The IC_{50} is generally calculated from a dose-response curve (Figure 25). A dose-response curve can be used to plot the data obtained in many types of experiments. The X axis plots concentration of a hormone or a drug whereas the Y axis can plot any biological response. X generally values the logarithm of concentrations of a drug, whereas Y generally corresponds to enzyme activity.

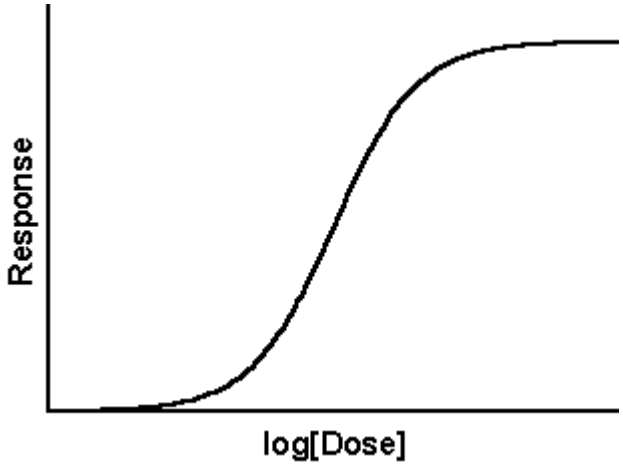

***Figure 25**: Example of a dose-response curve.*

Dose-response curves are used in enzymatic assays to assess the potency of an inhibitor against a biological target. The curves are used to measure the concept of inhibitor concentration (IC_{50}) or the effective concentration (EC_{50}).

The inhibitor constant values (*Ki*) are calculated from the Cheng-Prusoff equation (Figure 26).

$$K_i = IC_{50} / (1 + ([ATP/Km])$$

***Figure 26**: The Cheng-Prusoff equation.*

The IC_{50} is generally defined when carrying out a biochemical assay, whereas the concept of EC_{50} is used in cellular assays and represents the concentration of a drug that induces a response halfway between the maximum response and the baseline.

1.8.3. Cell culture assay: pBAD assay

After biochemical evaluation, the most active PIM-1 inhibitors were further characterized in an *in vitro* assay that detected phosphorylation of BAD protein by PIM-1. As described in section 1.5.1, PIM kinases phosphorylate many cellular substrates, leading to cell survival amongst other outcomes. PIM, as well as PI3K, ERK, AKT, and p90RSK, have been shown to phosphorylate BAD at Ser112. Phosphorylated BAD then binds to the protein 14-3-3 which is taken into the cytoplasm leading to cell survival. Phosphorylation of BAD prevents from binding to Bcl family of proteins, which is needed for apoptosis (Figure 27).

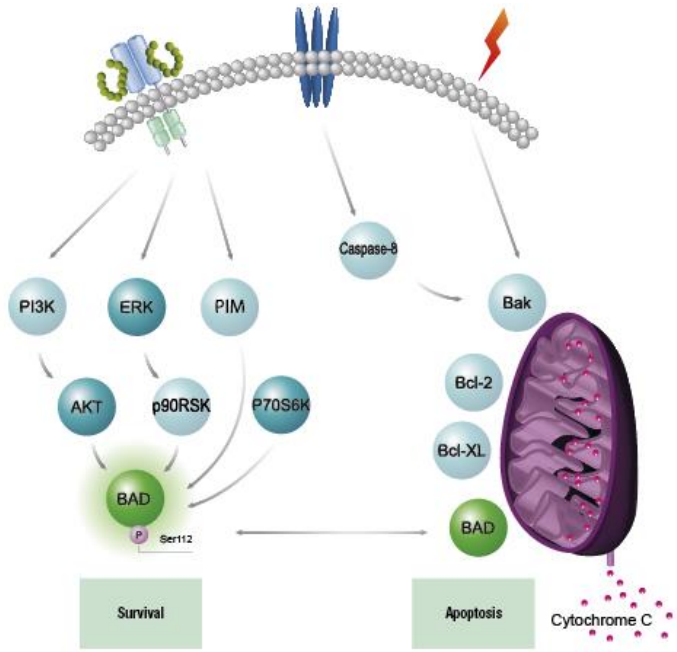

***Figure 27**: BAD phosphorylation cascade leading to apoptosis.*

Within the cellular assay, we can examine how potent our compounds are by determining the inhibition of the phosphorylation at Ser112 of BAD protein using cells that overexpress the PIM-1 isoform. The assay is performed in 0.1% fetal bovine serum (FBS). At this low serum concentration, only PIM protein, which is constitutively more active in cells, phosphorylates BAD at Ser112.

The inhibition of BAD phosphorylation can be studied using an in-cell ELISA protocol and the principle of the assay is shown in Figure 28.

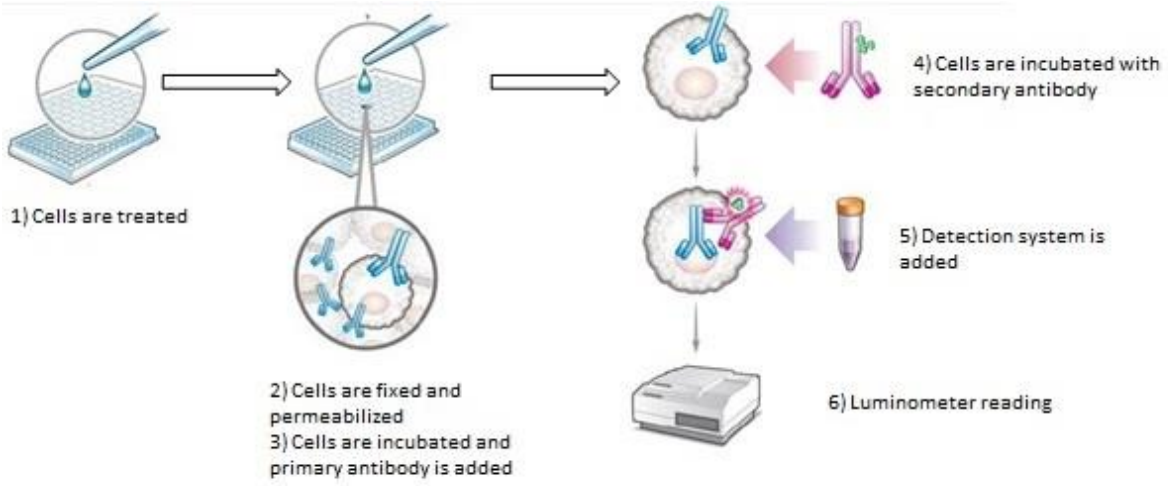

***Figure 28**: Mechanism of pBAD phosphorylation assay.*

The general experimental procedure can be described in six different steps. The first step of the assay corresponds to the growth and counting of cells followed by incubation in the presence of the inhibitors for a period of 3–4 hours. In the second step, the cells are fixed and permeabilized in a 96 well-plate and a primary antibody (specific for BAD phosphorylation) is added. The cells are incubated for 24 hours at 37 °C and immediately washed to add the secondary anti-rabbit antibody. The final step corresponds to the development of the signal, where supersignal ELISA luminol is added and the luminescence is measured using VICTOR luminometer from PerkinElmer. In summary, an effective PIM kinase inhibitor will inhibit the phosphorylation of BAD and the primary antibody will not bind due to the absence of the epitope.

1.8.4. Solubility and permeability of a compound

It has been reported that 39% of drug discovery projects that reached clinical trials failed due to the poor ADME properties that the drug presented.[57, 58] The ADME properties influence the pharmacological activity of a compound as a drug. Solubility and permeability are two extremely important parameters to take into account before any compound is further optimized. Very often, potent compounds do not show cellular activity due to poor aqueous

solubility or permeability. To conclude our study, the permeability and solubility of the most promising candidates was evaluated using a kinetic aqueous solubility assay and a Pampa assay.

1.8.4.1 Kinetic aqueous solubility assay

Solubility is defined as the amount of substance that passes into solution to achieve a saturated solution at constant temperature and pressure. Very often, drug candidates show poor water solubility, leading to poor oral bioavailability and, therefore, to variability in clinical response. The solubility of a compound depends on the structure, specifically hydrogen bond donors, hydrogen bond acceptors, or aromatic rings, amongst others. For *in vivo* studies, poor solubility will make dose formulation difficult, particularly for intravenous dosing, presenting problems for reliable determination of pharmacokinetic or pharmacodynamic parameters and potentially resulting in adverse events. Therefore, it is very important to identify the solubility of a chemical series before any further optimization is carried out, to maximize success in *in vivo* assays.

The optimal solubility for a drug discovery candidate should be around 60 µg/mL in order to ensure efficacy in bioassays, formulation for *in vivo* dosing, and intestinal absorption.[59]

The general way of measuring the aqueous solubility of a drug candidate is *via* LC-MS/MS. The drug candidate is initially prepared at a 10 mM stock and dilutions to 0.5 µM, 1 µM, 5 µM, 10 µM, 50 µM, and 100 µM are prepared in PBS and incubated at room temperature for 90 minutes. The samples are filtered using a vacuum manifold to eliminate any insoluble particles. 50 µL from each well was transferred to a 96-well plate and diluted with 150 µL of acetonitrile/0.1% formic acid. The plate is shaken and 5 µL of each sample injected to the LC-MS/MS and the samples are analyzed. The peak area per concentration is measured and the maximum saturation concentration can be determined.

An example of the outcome of the assay is presented in Figure 29. Rapamycin, a poor water soluble investigational immunosuppressive drug, is used as a control compound to determine the quality of the assay. For each compound, the solubility is quantified through individual standard peak calibration at a known concentration.

Rapamycin			
Final Concentration(µM)	**Conc (µg/ml)**	**cps**	**Rt**
0.5	0.468	$1.32E^{+02}$	3.93
1	0.936	$4.22E^{+02}$	3.90
5	4.68	**$3.74E^{+03}$**	3.90
10	9.36	$3.96E^{+03}$	3.95
50	46.8	$5.05E^{+03}$	3.94
100	93.6	$5.07E^{+03}$	3.95

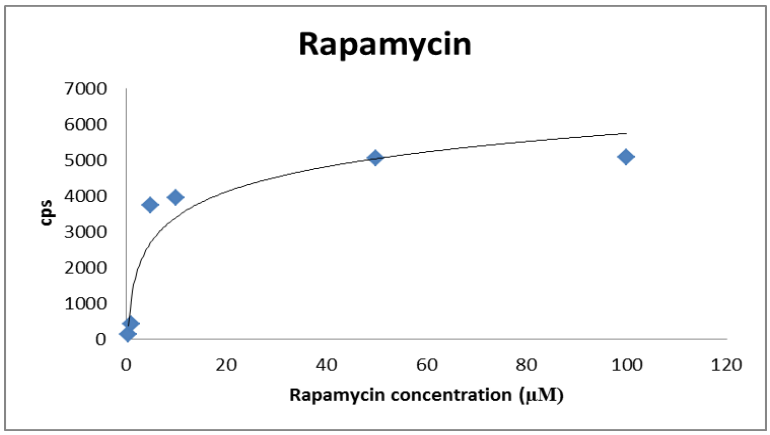

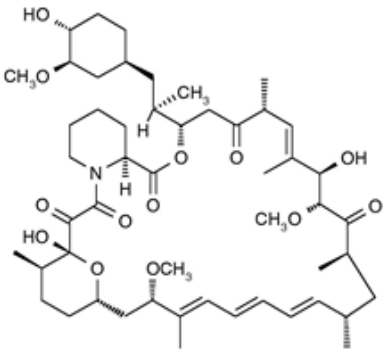

***Figure 29**: Rapamycin aqueous solubility data.*

The outcome of the assay is a plot where Y (counts per second, peak area) is represented against X (compound concentration). The peak area is proportional to the concentration, therefore a straight line should be seen for a soluble compound at 100 µM. In the case of Rapamycin, a straight line is observed for 0.5 µM to 5 µM, however, the solution shows saturation after 5 µM, indicating the poor aqueous solubility of Rapamycin (maximum aqueous solubility concentration: 5 µM).

1.8.4.2 Parallel artificial membrane permeability assay

Drugs are generally absorbed through the intestine, therefore, the permeability of a compound is also a very important property that needs to be taken into account when optimizing a drug candidate. The two most common assays for the determination of a drug's permeability in ADME screenings are the parallel artificial membrane permeability assay (Pampa),[60] that measures a compound's ability to passively permeate across an artificial lipid membrane, and

the cell-based permeability assay (Caco-2),[61] that measures the sum of passive and active permeability using a cell monolayer.

Although both assays are used by pharmaceutical industries, Pampa is becoming very popular due to its reduced costs and fast assay preparation. Many variants of the experiment have been developed since it was first developed, and the most commonly used is the newly improved Pampa assay from BD Genetest™.

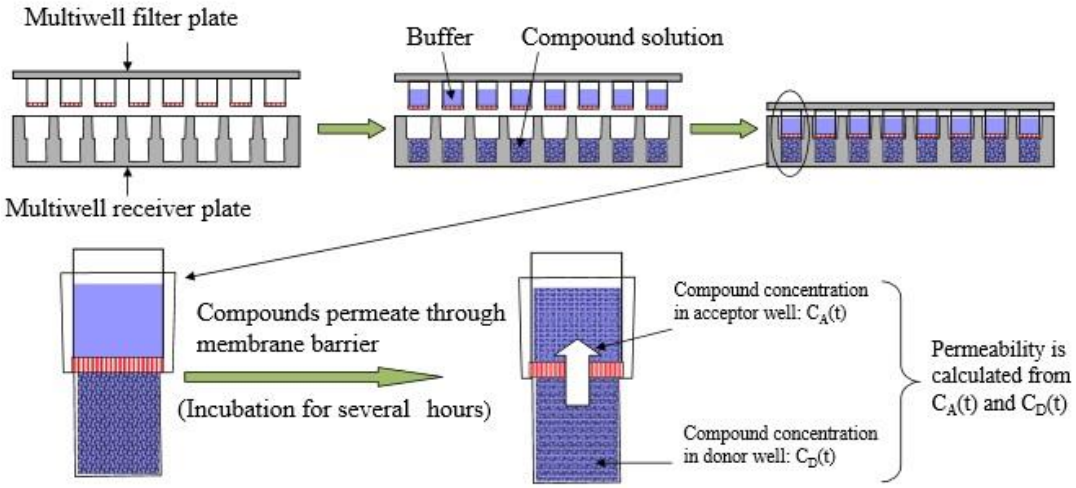

***Figure 30**: Pampa experimental set-up from BD Genetest™.*

In 2008, BD Genetest™ reported a new version of Pampa (Figure 30). The assay requires BD Genetest™ well-plates (Figure 31) that are a combined plate containing a multiwall filter plate and a multiwall receiver plate, divided by an artificial membrane using a lipid-oil-lipid tri-layer structure. The drug candidate is placed, at a concentration where its solubility has been previously studied, in the receiver plate and the filter plate is filled up with phosphate-buffered saline (PBS). The plate is incubated for 5 hours and the compounds are allowed to permeate through the membrane barrier to create an equal concentration through the well-plate. The permeability is calculated by HPLC using both concentrations in the acceptor well and in the donor well.

For the most potent/selective PIM isoform chemical probes, solubility and permeability assays were carried out to analyze these important properties before the compounds are further optimized or further evaluated.

***Figure 31**: Example of PAMPA BD Genetest™ well-plates.*

1.9. Conclusions

Chemical probes are urgently needed to dissect the fundamental biology of many important receptors. PIM kinases have become very interesting targets in cancer drug discovery since they have been shown to be implicated in many cellular processes. Although many pan-PIM inhibitors have been published in the past twenty years, there is a need to provide the scientific community with selective PIM isoform inhibitors as tools to understand the mechanism of PIM kinases in the human body.

Understanding the PIM kinases structure and biological function was the starting point of this PhD project. The information extracted from the literature constitutes the basis for the development of chemical probes for the PIM isoforms.

As previously mentioned, in discussion with with our collaborators at the SGC, the benzothienopyrimidinone scaffold published by Abbott Laboratories was selected as our starting point. Through molecular modelling studies, candidates will be synthesized *via* a well-defined and accessible synthetic route and the SAR study will be guided using DSF data.

The ΔT_m data was key during the course of the project as it will was as a tool to assess the affinity of our compounds to the different isoforms. As well as obtaining ΔT_m on PIM kinases, other kinases of interest such as CLK1, CLK3, CLK4, DYRK1A, DYRK2A, SRPK1, and SRPK2 were also be evaluated using DSF as they very often show cross-reactivity with PIM. Therefore, selectivity over these kinases is of great importance.

Designing selective chemical probes for each isoform of PIM represents the ultimate goal, but previous PIM inhibitors revealed that PIM-1 selectivity is often observed, whereas PIM-2 and PIM-3 selectivity is difficult to accomplish, thus, we elected to initiate our studies by focusing our research on PIM-1 chemical probes.

2. Benzothienopyrimidinones as chemical probes for PIM kinases

2.1. Designing derivatives of compound 9

Our initial aim was to synthesize analogues of the Abbott compound **9** (Figure 32) to establish the collaboration with the SGC.

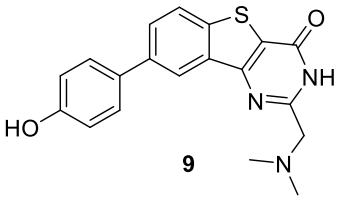

9

PIM-1 (*Ki*): 1 nM
PIM-2 (*Ki*): 3 nM
PIM-3 (*Ki*): 0.5 nM

***Figure 32**: Abbott compound **9**.*

From the examination of the Abbott analogues previously described, it was observed that some compounds did show selectivity within the family (Figure 15, page 16). The Abbot analogues were synthesized using the sequence outlined in Scheme I. The initial SAR studies were performed by varying the amine at position 2 of the benzothienopyrimidinone scaffold. It was proposed that subsequent variation at position 8 *via* cross-coupling reactions with the most active compounds may also prove to be a useful direction of research.

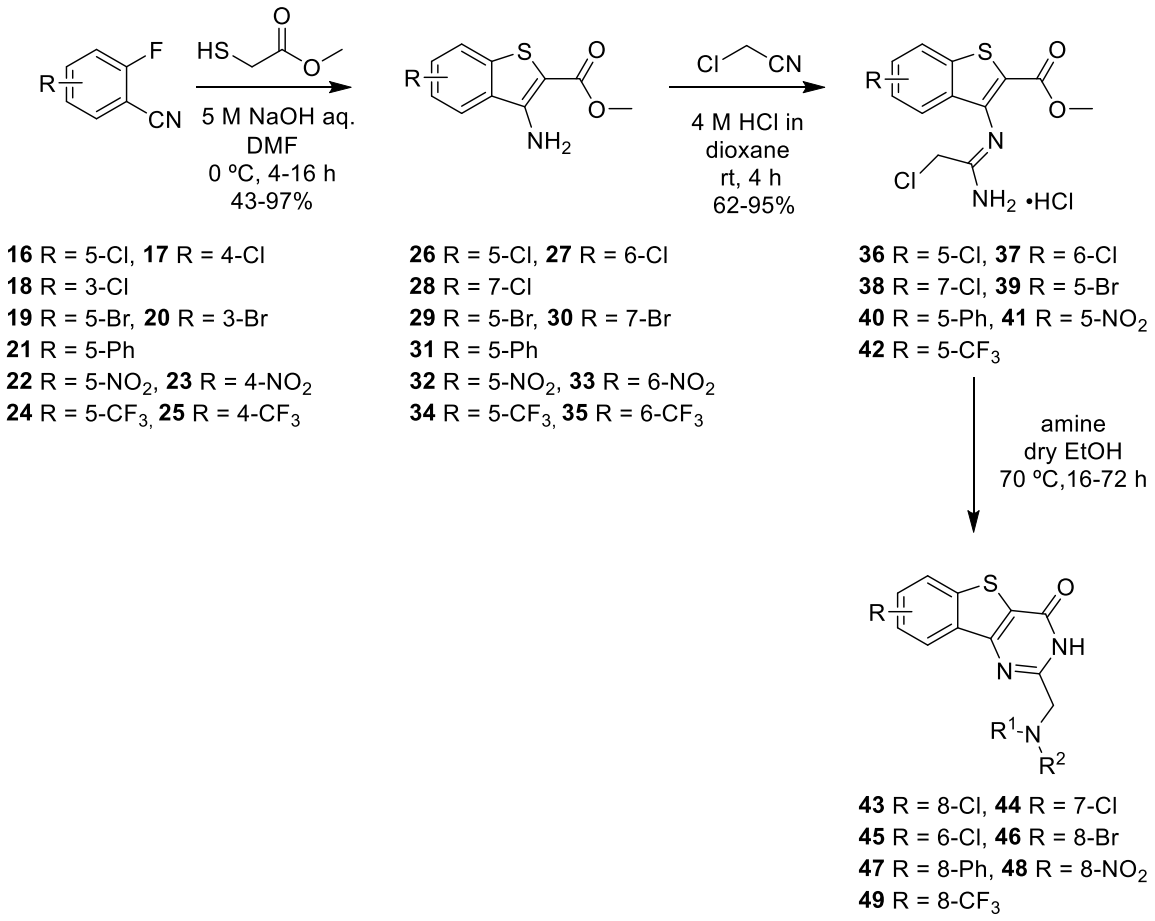

16 R = 5-Cl, **17** R = 4-Cl
18 R = 3-Cl
19 R = 5-Br, **20** R = 3-Br
21 R = 5-Ph
22 R = 5-NO_2, **23** R = 4-NO_2
24 R = 5-CF_3, **25** R = 4-CF_3

26 R = 5-Cl, **27** R = 6-Cl
28 R = 7-Cl
29 R = 5-Br, **30** R = 7-Br
31 R = 5-Ph
32 R = 5-NO_2, **33** R = 6-NO_2
34 R = 5-CF_3, **35** R = 6-CF_3

36 R = 5-Cl, **37** R = 6-Cl
38 R = 7-Cl, **39** R = 5-Br
40 R = 5-Ph, **41** R = 5-NO_2
42 R = 5-CF_3

43 R = 8-Cl, **44** R = 7-Cl
45 R = 6-Cl, **46** R = 8-Br
47 R = 8-Ph, **48** R = 8-NO_2
49 R = 8-CF_3

Scheme I*: *General synthetic route for the synthesis of the benzothienopyrimidinone analogues.

The synthetic procedure developed by Abbott Laboratories started with a nucleophilic aromatic substitution of the aryl fluorides **16**–**25** with 2-mercaptoacetate to give an intermediate that cyclizes to form the benzothienoamino esters **26**–**35** (43-97%). The primary amine was then reacted with 2-chloroacetonitrile to give compounds **36**–**42** as the hydrochloride salts (62-95%). The last step of the synthetic route involved an intramolecular cyclization followed by a nucleophilic substitution of the chloride by a primary or secondary amine to afford derivatives **43**–**49**. The final compounds derived from intereidiates **33** and **35** were not studied due to the project coming to an end.

2.1.1. New methodology developed for the synthesis of 3-Aminobenzo[*b*]thiophene scaffolds

The first step of the synthetic route used for the generation of the benzothienopyrimidinone scaffold involved a nucleophilic aromatic substitution of the aryl fluoride using methyl thioglycolate followed by cyclization to form the benzothienoamino ester, the mechanism for this transformation is detailed in Figure 33.

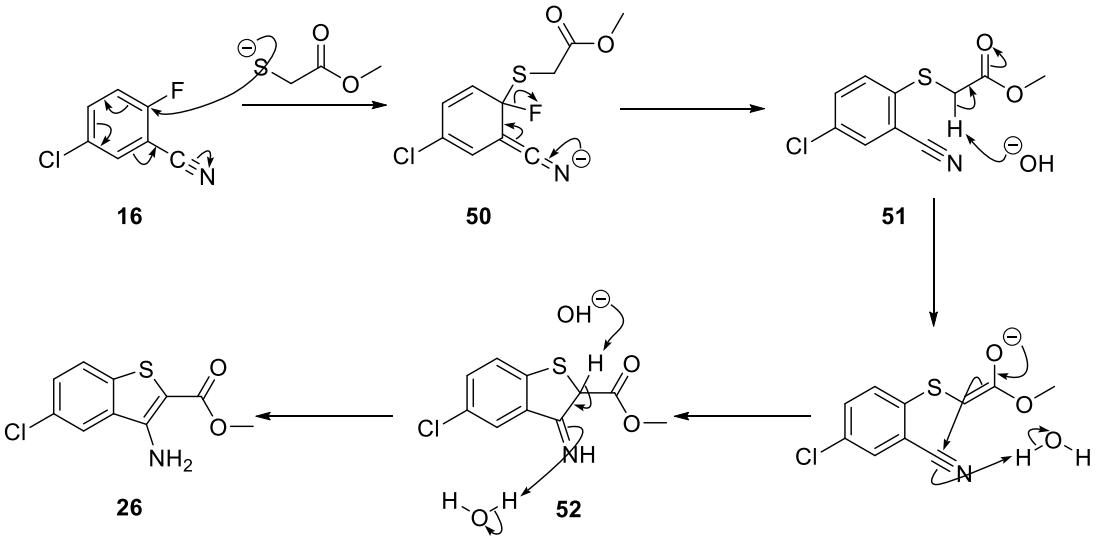

***Figure 33**: Reaction mechanism for the formation of compound **26**.*

Nucleophilic addition to **16** leads to intermediate **50**, which aromatizes to form nitrile derivative **51**. Deprotonation with sodium hydroxide leads to an enolate which attacks the electrophilic nitrile group to form intermediate **52**. Finally, the compound aromatizes to give analogue **26** in 94% yield.

Benzothiophenes are naturally occurring heterocycles found in petroleum deposits such as lignite. Benzothiophenes are also present in many bioactive molecules and natural products. They were found in more complex glycosides isolated from the roots of *E. girjissii*,[62] but more recently have found application in drug discovery, being present as part of an estrogen receptor modulator, Zileuton, an inhibitor of 5-lipoxygenase and leukotriene biosynthesis used for the treatment of asthma, [63] the antifungal agent Sertaconazole, which inhibits the synthesis of ergosterol,[64] and Raloxifene, previously described in Chapter 1.

Due to their increasing importance within drug discovery, it was proposed that a new approach for the synthesis of substituted benzothiophenes would be of great interest to the medicinal chemistry community.

The main research focus of Professor Bagley from the University of Sussex has been the development of microwave-assisted syntheses of nitrogen-containing heterocycles for drug discovery applications. Recently, his group has discovered a new approach to the synthesis of substituted benzothiophenes (Scheme II) using microwave irradiation for 11–35 minutes at high temperature to give the products in good isolated yields.

Together with Bagley, we had the opportunity to apply this new approach to the synthesis of **26**–**35** and publish an alternative synthetic route for the generation of benzothiophenes with considerably decreased reaction times and high yields.[65] The scope of this new microwave-assisted synthesis is summarized in Table VII.

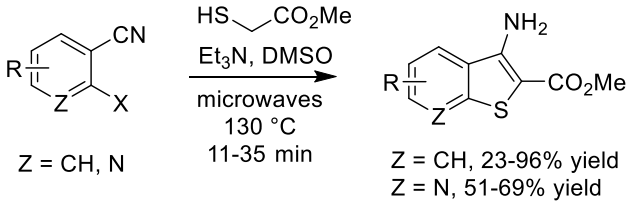

***Scheme II**: Bagley's microwave-assisted reaction conditions.*

Table VII: *Microwave-assisted reaction scope*.[65]

Entry	Substrate	R	X	Z	Time /min	Product	Yield%[a]
1	**16**	5-Cl	F	CH	11	**26**	92
2	**19**	5-Br	F	CH	11	**29**	96
3[b]	**21**	5-Ph	F	CH	15	**31**	85
4	**22**	5-NO_2	F	CH	11	**32**	94
5	**24**	5-CF_3	F	CH	20	**34**	88
6	**23**	4-NO_2	F	CH	35	**33** (R = 6-NO_2)	67
7	**25**	4-CF_3	F	CH	18	**35** (R = 6-CF_3)	81
8	**53**	H	F	CH	15	**59**	65
9	**54**	H	Br	CH	15	**60**	23
10	**55**	H	I	CH	15	**61**	47
11	**56**	H	F	N	15	**62**	66
12	**57**	H	Cl	N	15	**63**	69
13	**58**	H	Br	N	15	**64**	51

[a]Isolated yield of products after reaction according to Scheme X, cooling in a stream of compressed air and pouring the reaction mixture into iced-cold water. [b]Product was isolated by aqueous work up, followed by purification by column chromatography on silica gel.

By switching the base from sodium hydroxide (Scheme I) to triethylamine, and using microwave assisted heating the corresponding benzothiophenes **26**, **29**, **31**, **32**, **34**, **33** and **35** were prepared in high yields. For example, stirring at 0 °C in NaOH aq/DMF for 4 hours gave **26**, **29**, and **32** in 90%, 91%, and 97%, respectively. Using microwave irradiation at 100 °C for 11 minutes gave the same products in 92%, 96%, and 94% yields, respectively, after pouring the reaction mixture into ice-water and collecting the product by filtration. Changing the substituent around the aromatic ring did not seem to affect the transformation, *e.g*, **35** (entry 7) was obtained in 81% yield using microwave-assisted conditions and 78% yield using the Abbott method. Electron-donating functional groups such as phenyl (**31**, entry 6) also gave high yields (85%) using microwave-assisted methods, and only a moderate yield (43%) using the Abbott method.

The reaction seemed most effective when using aryl-fluorides as starting materials (entries 8, 9, and 10), but can also accommodate bromides, chlorides, and iodides with reduced efficiencies. For pyridine based systems (entries 11, 12, and 13) the reaction proceeded in good yield regardless of the aryl-halide used, and we were able to obtain **62**, **63** and **64** in 66%, 69%, and 51%, respectively. In most cases, the reaction proceeded with high yields at

reduced times (11-35 min), and proved comparable to the previously described method in Scheme I and other available methods.[66]

Along with our contribution, this transformation was applied to the synthesis of known kinase inhibitor scaffold, the thieno[2,3-*b*]pyridine core motif of LIMK1 inhibitors,[67] the benzo[4,5]thieno[3,2-*e*][1,4]diazepin-5(2*H*)-one scaffold of MK2 inhibitors[68, 69] and a benzo[4,5]thieno[3,2-*d*]pyrimidin-4-one inhibitor of the PIM kinases shown in Figure 34.

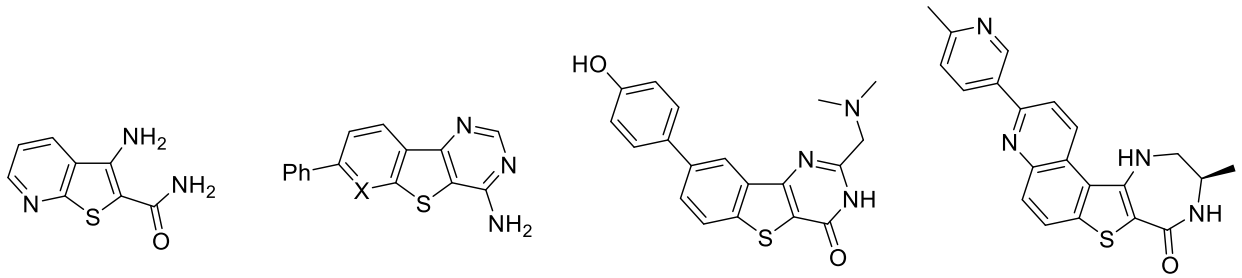

***Figure 34**: Kinase inhibitors containing benzothiophenes synthesized using Bagley's method.*

In conclusion, a novel procedure for the synthesis of benzothiophenes was developed. The reaction was simple, easy to carry out and proceeded with high yields at reduced reaction times. The reaction can be applied to a wide variety of substrates. Given the speed, efficiency and reliability of this method, and its ability to incorporate a wide range of functionalities, this approach is likely to find application in providing chemical tools, rapidly, reliably and efficiently, for advancing studies in chemical biology, as well as to access targets for medicinal chemistry.

2.2. Aliphatic amines as substituents at position 2

Following the described synthetic procedure in Scheme I, compounds **43a**–**43k** were synthesized (Figure 35), using commercially available 5-chloro-2-fluorobenzonitrile **16** as the starting material. The yields presented correspond to the reaction of **36** with the corresponding amine in dry EtOH to afford **43a**–**43k**. The chlorine at position 8 was maintained and modifications on the right hand side of the scaffold were made using commercially available aliphatic amines. The compounds mainly contained hydrogen bond donor functional groups to promote hydrogen bond interactions between the aliphatic amines and the acidic residues of

the receptor, however, other hydrophobic amines were also used to assess the hydrophobicity of the area. The chlorine was maintained as previous work from Abbott Laboratories showed that PIM-1 over PIM-2 selectivity was achieved when the chlorine was present at position 8.

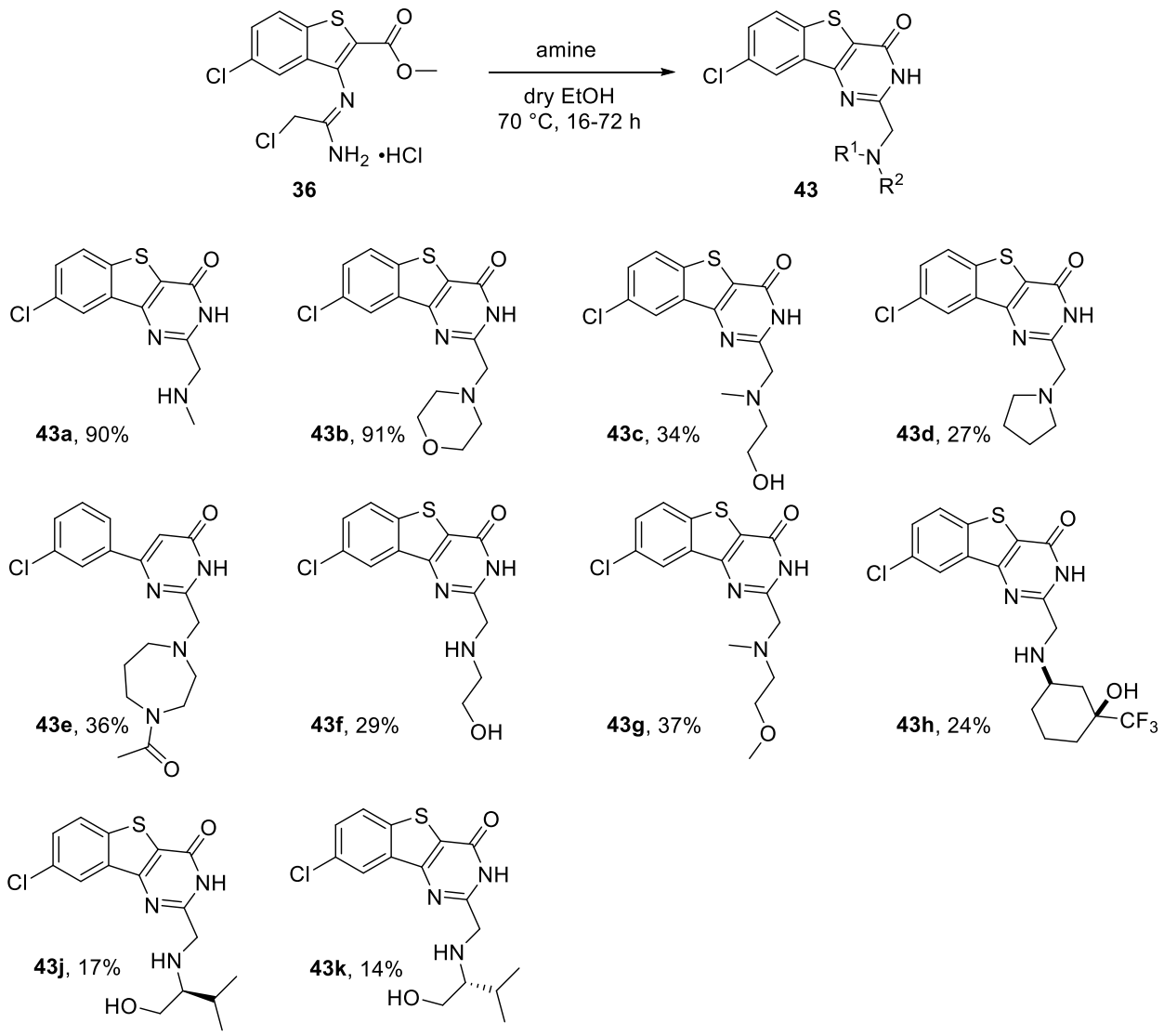

***Figure 35**: Yields and compound structures for **43a–43k**.*

Compounds **43a**–**43k** were sent to the SGC for initial biological assessment using a DSF assay (detailed in Section 1.8.1, Appendix 8.4). The compounds were evaluated against PIM-1, PIM-2, and PIM-3, as well as CLK, SRPK and DYRK kinases, which often show cross-reactivity, therefore, selectivity over these kinases was of great importance to the project.

The DSF data on compounds **43a**–**43k** is summarized in Table VIII.

Table VIII: *DSF results for compounds **43a**–**43k**.*

Compound	PIM-1 (ΔTm, °C)	PIM-2 (ΔTm, °C)	PIM-3 (ΔTm, °C)	CLK4 (ΔTm, °C)	CLK1 (ΔTm, °C)	CLK3 (ΔTm, °C)	DYRK1A (ΔTm, °C)	DYRK2A (ΔTm, °C)	SRPK1 (ΔTm, °C)	SRPK2 (ΔTm, °C)
43a	6.4	4.1	7.1	4.7	3.4	0.5	3.0	2.2	0.0	1.0
43b	2.2	1.1	1.9	7.8	4.9	1.4	3.5	0.7	0.0	0.6
43c	5.4	3.0	6.0	9.5	7.8	1.7	4.5	2.0	0.0	0.2
43d	5.3	2.6	4.5	4.0	2.4	0.2	1.5	0.9	0.0	0.8
43e	3.9	1.7	4.4	6.9	4.9	0.8	3.1	1.0	0.0	0.1
43f	4.4	2.5	4.4	4.6	2.9	0.3	1.9	1.4	0.0	0.6
43g	4.3	2.2	5.2	6.3	4.2	0.4	2.8	0.7	0.0	0.2
43h	6.9	3.1	5.3	6.1	3.8	0.5	3.7	1.2	0.0	0.3
43j	6.4	2.8	5.4	7.8	5.5	0.9	6.1	1.5	0.0	0.4
43k	6.2	0.0	5.0	8.5	5.0	0.0	6.1	1.2	0.1	0.0

The DSF results on the first set of compounds proved very encouraging. The compounds showed a high degree of selectivity especially over CLK3, DYRK2, SRPK1, and SRPK2, which was very promising for our purpose. Furthermore, the selectivity for PIM-1 and PIM-3 over PIM-2 was conserved throughout this set of compounds.

Compound **43a** exhibited a high ΔT_m value of 6.4 °C against PIM-1, selectivity over PIM-2 (ΔT_m of 4.1 °C), excellent selectivity over CLK1 and CLK3 kinases, (ΔT_m < 3.5 °C), DYRK kinases (ΔT_m < 3.0 °C), and ΔT_m of 0 °C for SRPK1 and 1°C for SRPK2. The compound also showed good stabilization against PIM-3, and CLK4 with ΔT_m of 7.1 °C and 4.7 °C, respectively. This was not surprising as PIM-3 shares a similar amino acid sequence with PIM-1 and CLK4.

The rest of the series showed similar binding affinities to compound **43a**. It was observed that compounds containing hydroxyl groups such as **43c**, **43h**, **43j** and **43k** provided more affinity towards PIM-1 and PIM-3, with ΔT_m of 5.4 °C, 6.9 °C, 6.4 °C, and 6.2 °C against PIM-1 respectively. This affinity did not seem to be affected by the chirality of the amino alcohol (**43j**, and **43k**) which showed similar ΔT_m. However, although these compounds showed a high selectivity over PIM-2, CLK1, CLK3, DYRK2, and SRPK kinases with ΔT_m < 4 °C, the selectivity towards CLK4, CLK1, and DYRK2 rapidly decreased, suggesting that these receptors also contain hydrogen bond acceptor residues that are able to interact with the potential probe.

Furthermore, to our surprise, **43b**, **43c**, **43j**, and **43k**, showed high affinities towards CLK4, with a ΔT_m of 7.8 °C, 9.5 °C, 7.8 °C, and 8.5 °C, the highest ΔT_m values observed within this series, suggesting really high affinity towards this receptor. The selectivity observed for **43c**, **43j**, and **43k** is not desirable, as they also show high affinities towards PIM-1, PIM-3, CLK1, and DYRK1, with ΔT_m between 5–7 °C, probably due to interactions with the hydroxyl group and the receptor. Compound **43b,** which contains a morpholine group, showed a good potency towards CLK4 with a ΔT_m of 7.8 °C, a minor stabilization towards CLK1, with a ΔT_m of 4.9 °C, but an excellent selectivity over PIM kinases, DYRK kinases, SRPK kinases, and CLK3.

Compounds **43b**, and **43c**, have been taken for further biological characterization at the SGC against CLK4, as they are currently investigating CLK4 probes. Attempts to obtain a crystal structure of **43b**, or **43c** with CLK4 were unsuccessful. However, the compounds are being taken into biological evaluation in cell-based assays.

In summary, compounds containing aliphatic amines posessing hydroxyl groups around the solvent exposed area show the highest affinity/stabilization. However, the selectivity decreases considerably towards the other kinases. At this stage it was proposed that hydrophobic substituents such as aniline derivatives should be studied to assess the hydrophobicity of the area around position 2.

2.2.1. Biochemical evaluation of 43a–43k

Following biological protocol 8.1.1, **43a**–**43k** were tested at two different concentrations (10 µM, and 1µM) against PIM-1, PIM-2, and PIM-3 with a view to subsequently estabilishing full dose-response curves of the most biologically active compounds. The preliminary data obtained for **43a**-**43k** is presented below (Table IX).

Table IX: *Data on* the *percentage of inhibition for* ***43a–43k***.

Compound	PIM-1 (10 µM)	PIM-1 (1 µM)	PIM-2 (10 µM)	PIM-2 (1 µM)	PIM-3 (10 µM)	PIM-3 (1 µM)
43a	99	87	93	53	95	68
43c	96	67	84	33	89	35
43e	92	40	73	7	79	20
43f	96	61	81	28	88	38
43g	97	68	83	23	90	39
43h	99	84	87	45	94	50
43j	96	65	84	31	87	30
43k	94	64	76	18	86	35

As expected, the compounds showed a higher percentage of inhibition (PI) at 10 µM than at 1 µM. The activity for PIM-1, PIM-2, and PIM-3, was consistent with the DSF assay, and the compounds showed more activity towards PIM-1 than PIM-2 and PIM-3 at 1 µM. For example, at 1 µM concentration, the compounds show a PI higher than 50% for PIM-1, but under 50% in the case of PIM-2 and PIM-3. Even though this preliminary assay serves only as an indication (as only single point experiments were carried out) preference for PIM-1 inhibition over PIM-2 and PIM-3 was observed within this series of compounds. Compounds **43b** and **43d** were not tested in this assay as not enough compound was available to carry out the biological assay.

From this preliminary data, a cut off was established to determine which compounds were progressed for dose-response evaluation against PIM-1, PIM-2, and PIM-3. Compounds showing activities over 70% at 10 µM for PIM-1 were examined in a dose-response curve against each isoform.

Compounds **43a**–**43k**, which showed activities above 70% at 10 µM, were further evaluated and the IC_{50} data is presented in Table X.

Table X: *IC_{50} data obtained for compounds **43a**–**43k**.*

Compound	PIM-1 IC_{50} (nM)	PIM-2 IC_{50} (nM)	PIM-3 IC_{50} (nM)
43a	94	363	130
43c	288	1640	338
43e	495	2540	1830
43f	303	1070	344
43g	345	2240	338
43h	91	642	731
43j	344	2440	447
43k	366	2770	190

The biochemical data obtained for this first set of compounds was very encouraging: high potencies were observed and the results were consistent with the DSF data. The compounds showed selectivity for PIM-1 and PIM-3 over PIM-2. Compounds **43a**, and **43h**, represent the most active compounds against PIM-1, with IC_{50} values of 94 nM and 91 nM, and ΔT_m values of 6.4 °C and 6.9 °C, respectively, suggesting that a melting temperature of around 6–7 °C translates to a potency of approximately 90–100 nM, in the case of the PIM-1 isoform. Both assays also correlated throughout the series, the IC_{50} value increases if the ΔT_m decreases. For example, **43e**, **43f** and **43g**, showed similar ΔT_m values of 3.9 °C, 4.4 °C, and 4.3 °C for PIM-1 respectively, and the IC_{50} observed ranged within 300–500 nM activities, suggesting that the DSF data provided a reliable indication of PIM-1 estabilization.

The IC_{50} values measured for PIM-3 were noticeably lower than those for PIM-1 for examples that possessed similar ΔT_m values, *e.g.*, **43a** showed an ΔT_m of 7.1 °C for PIM-3 and an IC_{50} value of 130 nM for PIM-3, whereas for compound **43a**, an ΔT_m of 6.4 °C translates to an IC_{50} of 94 nM for PIM-1. This fact could be due to the stability of the isoforms used in the experiments, due to the life time of the protein itself, or the poor solubility of the compounds when carrying out the experiments. For PIM-2, the DSF assay and IC_{50} also correlated as low values are observed in both cases.

2.3. Aromatic amines as substituents on position 2

Using the DSF data obtained for compounds **43a**–**43k**, and to further expand the SAR study around position 2, a second set of compounds (**43l**–**43u**, Figure 36) was synthesized. Compounds **43l**–**43u** were designed using a variety of commercial aniline derivates to assess

the topology of the area, the dimensions, and the tolerance of hydrophobicity. The anilines were selected so as to contain acidic groups, halogens, and basic groups to provide a solid SAR in order to understand the PIM-1, PIM-2, and PIM-3 active sites. The chlorine group at position 8 was maintained throughout.

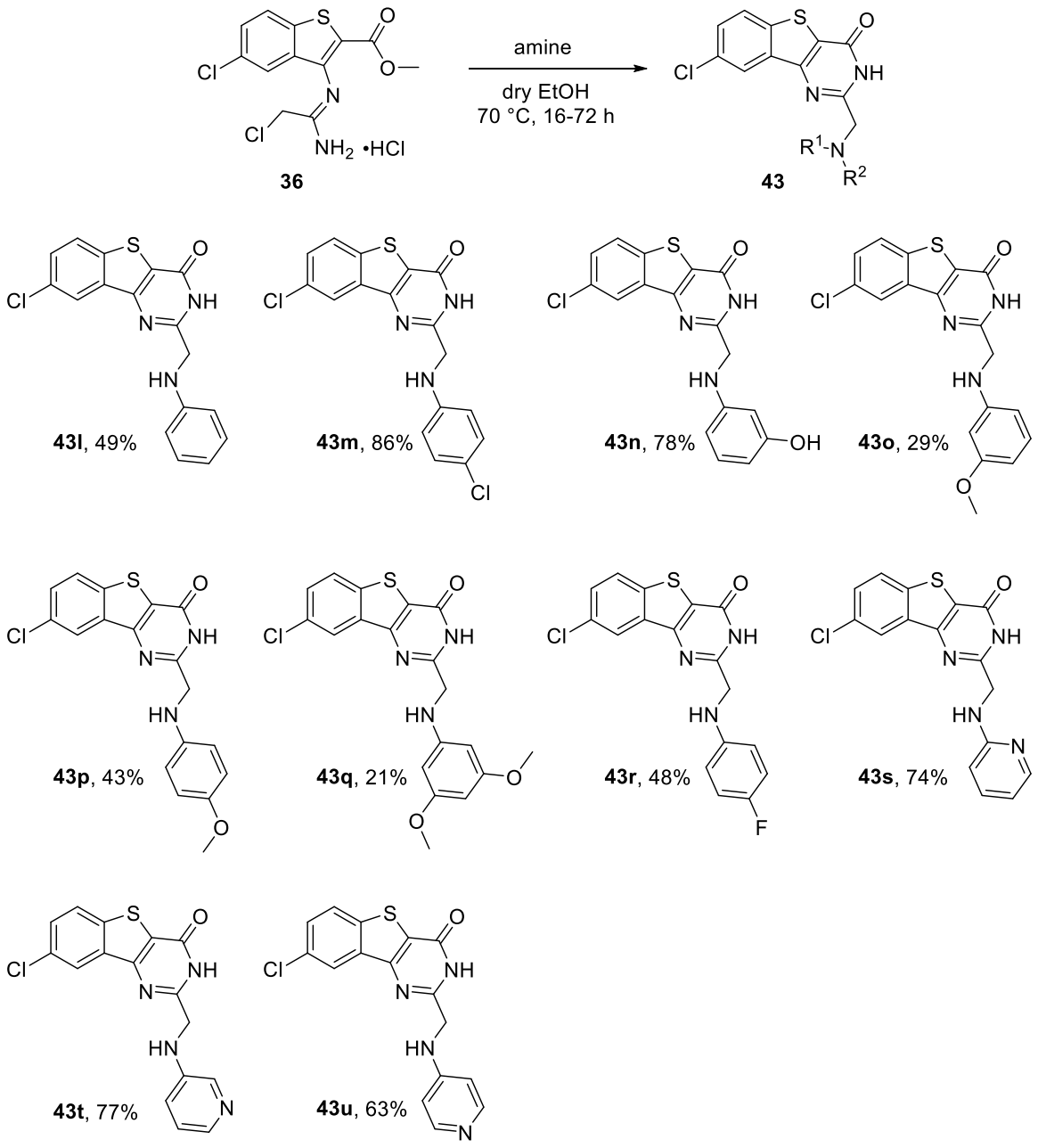

Figure 36: *Yields obtained for compounds* ***43l–43u***.

Compounds **43l**–**43u** represented a good starting point to continue assessing the topology of the solvent exposed area around the right hand side of the benzothienopyrimidinone. The different amines used would provide more information about the SAR to potentially increase the potency/selectivity within the isoforms. The DSF data on compounds **43l**–**43u** are summarized in Table XI.

Table XI: *DSF results for compounds **43l**–**43u**.*

Compound	PIM-1 (ΔT_m, °C)	PIM-2 (ΔT_m, °C)	PIM-3 (ΔT_m, °C)	CLK4 (ΔT_m, °C)	CLK1 (ΔT_m, °C)	CLK3 (ΔT_m, °C)	DYRK1A (ΔT_m, °C)	DYRK2A (ΔT_m, °C)	SRPK1 (ΔT_m, °C)	SRPK2 (ΔT_m, °C)
43l	1.9	0.5	0.1	7.0	4.1	0.9	2.4	0.6	0.0	0.7
43m	2.5	1.5	0.1	4.6	3.7	1.5	2.1	1.2	0.3	0.9
43n	6.7	3.6	8.8	9.2	7.5	2.2	4..1	1.2	2.3	0.1
43o	5.0	3.1	5.7	5.4	3.5	0.5	2.4	1.9	0.0	0.3
43p	1.1	0.4	1.8	3.2	2.3	0.7	0.8	0.9	0.0	0.0
43q	1.7	1.1	2.3	3.8	4.0	1.2	2.1	0.7	0.2	0.7
43r	1.6	0.5	0.0	5.4	3.0	0.6	2.1	0.7	0.0	0.8
43s	7.7	5.4	7.4	6.6	4.3	0.2	2.3	1.7	0.0	0.4
43t	7.1	4.8	7.9	6.6	4.9	0.7	3.2	2.5	0.0	0.4
43u	7.6	4.6	7.0	6.1	2.8	0.0	1.0	0.5	0.0	0.2

The DSF data obtained on the second set of compounds **43l**–**43u** were very encouraging. The selectivity against the SRPK family, CLK3, and the DYRK family was maintained and good PIM-1 and PIM-3 affinities were observed. The aniline derivative, **43l**, decreased the affinity within the PIM kinases, however, the CLK4 affinity was maintained, providing excellent CLK4 selectivity, with a ΔT_m of 7.0 °C and a ΔT_m < 4.0 °C against the rest of the kinases. Aniline derivatives containing halogens or methoxy groups such as **43m**, **43p**, **43q**, and **43r** were not tolerated as the affinity against PIM kinases was decreased to a ΔT_m < 2.5 °C. Compound **43n**, derived from 3-hydroxyaniline, showed extremely good affinities towards PIM-1, PIM-3, CLK1, and CLK4, with a ΔT_m of 6.7 °C, 8.8 °C, 7.5 °C, and 9.2 °C, respectively. Again, it is believed that this potency is due to the hydroxyl group forming hydrogen bond interactions between the potential probe and the receptor. Interestingly, **43o**, which is the methylated analogue of **43n**, still showed affinity towards PIM kinases with a ΔT_m of 5.0 °C, and 5.7 °C against PIM-1, and PIM-3, but decreasing the ΔT_m by 2.0 °C if comparing it to **43n**, highlighting the importance of the hydrogen bond donor for PIM kinases affinity.

Molecular modelling studies suggested that the use of aminopyridine derivatives at position 2 would improve the potency against PIM-1 by forming hydrogen bonding interactions with either Glu-171 or Asp-128 (PIM-1 amino acid reference) around the pocket. Furthermore, we wanted to explore if changing the hydroxyl group for a hydrogen bond acceptor could keep the potency whilst changing the selectivity. This theory encouraged us to synthesize analogues **43s**, **43t**, and **43u**. These studies proved useful as the ΔT_m for PIM-1 was considerably increased to 7.7°C (**43s**), 7.1 °C (**43t**), and 7.6 °C (**43u**), the highest ΔT_m values observed against the PIM-1 isoform. However, the compounds also showed high affinity for PIM-2 (**43s**: 5.4 °C, **43t**: 4.8 °C, **43u**: 4.6 °C) and PIM-3 (**43s**: 7.4 °C, **43t**: 7.9 °C, **43u**: 7.0 °C) as well as the CLK4 isoform, and the CLK1 isoform, suggesting that these compounds are likely to provide high activity towards the PIM isoforms together with a poor selectivity.

From the data presented, it was believed that a change in the scaffold was needed to alter the selectivity observed within the kinases. Although the data obtained at this point provided an encouraging piece of SAR that resulted in an increase of PIM affinity, the selectivity between PIM kinases and CLK4 remained low. It was believed that position 8 of the scaffold should be investigated to assess if selectivity could be achieved through exploring this area of the receptor.

2.3.1. Biological evaluation of 43l-43u

As described in section 8.1.1, the preliminary data at two concentrations (10 μM, and 1 μM) against the three isoforms is shown in Table XII for compounds **43l-43u**.

Table XII: *Data on the percentage of inhibition for compounds **43l**–**43u**.*

Compound	PIM-1 (10 µM)	PIM-1 (1 µM)	PIM-2 (10 µM)	PIM-2 (1 µM)	PIM-3 (10 µM)	PIM-3 (1 µM)
43l	69	13	55	12	48	2
43m	8	2	11	2	6	-3
43n	91	94	40	35	58	56
43o	66	11	29	2	14	-7
43p	17	-3	3	-2	17	4
43q	27	13	3	6	14	3
43r	32	15	8	-2	13	6
43s	99	90	94	66	96	67
43t	98	89	92	50	93	56
43u	97	94	70	42	66	50

Consistent with DSF data obtained in this series, **43m**, **43p**, **43q**, and **43r** little activity against the three isoforms at both concentrations. Surprisingly, **43n** showed higher affinity for PIM-1 than PIM-3, whereas the DSF assay suggested a higher PIM-3 activity. As it inhibited PIM-1 above 70%, we believed the compound should be tested in a dose-response manner to obtain IC_{50} data to provide a solid conclusion to this matter. As expected, the aminopyridine derivatives **43s**, **43t** and **43u** targeted the three isoforms at both concentrations with high percentage of inhibition, PIs higher than 50% even at 1 µM for PIM-1, PIM-2, and PIM-3, suggesting possible low nanomolar pan-PIM inhibitors.

Following the cut off, **43n**, **43s**, **43t** and **43u** were further analyzed in a dose-response experiment and IC_{50} values against PIM-1, PIM-2, and PIM-3 were obtained (Table XIII).

Table XIII: *IC_{50} data for compounds **43n**, **43s**, **43t**, and **43u**.*

Compound	PIM-1 IC_{50} (nM)	PIM-2 IC_{50} (nM)	PIM-3 IC_{50} (nM)
43n	33	2860	66
43s	53	345	467
43t	32	725	187
43u	41	472	487

The IC_{50} data results were encouraging as very low nanomolar activities were observed, and consistency was mostly seen with the DSF data specially for the PIM-1 isoform (Table XI). Compound **43n** showed extremely good potencies against PIM-1 (33 nM) and PIM-3 (66 nM) over PIM-2 (2860 nM), however, as observed in Table XI, this compound did not show

selectivity against the other kinases, probably due to hydrogen bonding interactions between the phenol and the receptor. In fact, this compound showed good potencies against CLK4 and a crystal structure of this compound with CLK4 was obtained and is detailed in section 2.4. We were very pleased to observe the low nanomolar activity obtained for **43s**, **43t**, and **43u**, which were designed from previous molecular modelling studies. These three results showed that the position of the pyridine ring did not affect the potency/selectivity. These two compounds were somewhat selective for PIM-1 (**43s**: 53 nM, **43t**: 32 nM, **43u**: 41 nM), when compared to PIM-2 (**43s**: 345 nM, **43t**: 725 nM, **43u**: 472 nM) and PIM-3 (**43s**: 467 nM, **43t**: 187 nM, **43u**: 487 nM), which showed similar potencies. Due to the poor selectivity offered by these ligands over CLK4 (ΔT_m: 6–7 °C) as well as within the PIM isoforms, the amino pyridine derivatives were not considered for further analysis within this scaffold.

Nevertheless, we were very pleased to observe the increase in potencies for PIM-1 as compared to our first series DSF and biochemical data, with IC_{50} values of 30–41 nM, as compared to the first set of compounds, where the highest PIM-1 IC_{50} was 90 nM (**43a**). We believed that the next step within the SAR study should be to explore position 8 of the benzothienopyrimidinone core, which was proposed to be facing towards the hydrophobic hinge region, and should provide us with further information to gain selectivity between the PIM-1, PIM-2, and PIM-3 isoforms.

2.4. Crystal structure of 43n with CLK4

2.4.1. The importance of CLK4 protein kinase

CLK4 is a splicing kinase belonging to the Cdc2-like kinases (CLK's). The importance of these protein kinases is rising because of their relevant roles in gene splicing.[70, 71] Briefly, alternative gene splicing is the post-translational modification in charge of protein diversity. It occurs in eukaryotes and prior to mRNA translation and it determines the inclusion of a gene code in the mRNA that gives rise to multiple protein isoforms. The process of mRNA splicing is extremely complex, and many diseases are caused by errors in RNA splicing or its regulation. A common example is the Alzheimer's disease.[72]

CLK kinases are becoming relevant targets in the treatment of gene splicing diseases. A major downstream target of these kinases are the family of serine and arginine-rich (SR) proteins. The SR proteins are known to be implicated in the selection and control of splicing sites.[73]

Little is known about CLK4 kinase, in fact, only 30 references can be found in Scifinder when entering the concept "CLK4" (searched on June 2015). Due to their important role in gene splicing, they are becoming very interesting targets in drug discovery, and CLK4 chemical probes are essential to dissect the fundamental biology of these targets, and generate "proof of concept" (POC) data on gene splicing targets.

2.4.2. The crystal structure

The study on PIM selectivity led us to the discovery of several compounds which have the potential to be starting points for the development of CLK4 chemical probes. Our collaborators are currently investigating the design and synthesis of CLK4 probes,[74] and have used some of our data for their studies.

Compounds **43b**, **43c**, **43l** and **43n** (Figure 37) showed ΔT_m values of 7.8 °C, 9.5 °C, 7.8 °C, and 9.2 °C, against CLK4 respectively. These compounds have not only shown the highest ΔT_m observed to date, but they have also shown great selectivity over the other kinases examined, especially, compounds **43b**, and **43l**.

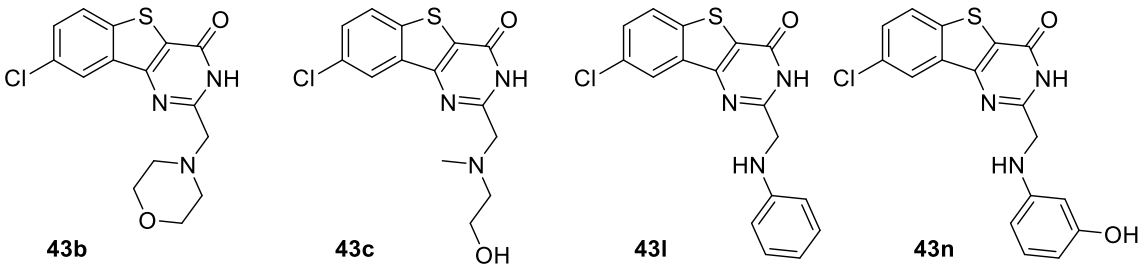

	IC$_{50}$ (nM)			DSF assay (ΔT_m, °C)									
Compound	**PIM-1**	**PIM-2**	**PIM-3**	**PIM-1**	**PIM-2**	**PIM-3**	**CLK4**	**CLK1**	**CLK3**	**DYRK1A**	**DYRK2A**	**SRPK1**	**SRPK2**
43b[a]				2.2	1.1	1.9	7.8	4.9	1.4	3.5	0.7	0.0	0.6
43c	288	1640	338	5.4	3.0	6.0	9.5	7.8	1.7	4.5	2.0	0.0	0.2
43l[a]				1.9	0.5	0.1	7.0	4.1	0.9	2.4	0.6	0.0	0.7
43n	33	22860	66	6.7	3.6	8.8	9.2	7.5	2.2	4..1	1.2	2.3	0.1

[a]No IC50 obtained.

Figure 37: *CLK4 hit compounds and biological data.*

The SGC have been trying to crystallize CLK4 with **43b**, **43c**, **43l**, and **43n**, and, after optimizing the crystallization procedure a crystal of CLK4 with **43n** was successfully

prepared which diffracted at 2.4 Å, becoming the first ever CLK4 crystal structure to be obtained (Figure 38).

***Figure 38**: Crystal structure of CLK4 with compound **43n**.*

The compound binds in the ATP binding pocket in a similar manner as observed for PIM-1 and PIM-2. The main hydrogen bond interaction is the one observed between the pyrimidinone ring of the compound and the lysine residue, which is conserved in CLK4, CLK1, PIM-1, PIM-2, and PIM-3. A snapshot of the electron density of compound **43n** in the binding pocket was taken (Figure 39) and shows that the chlorine is facing the hydrophobic area around the hinge region and the phenol is pointing towards the solvent exposed region. The CLK4 kinase contains two leucine residues in place of the PIM kinase proline residues, suggesting that CLK4, like PIM kinases, is more likely to tolerate hydrophobic than polar substituents around the hinge region.

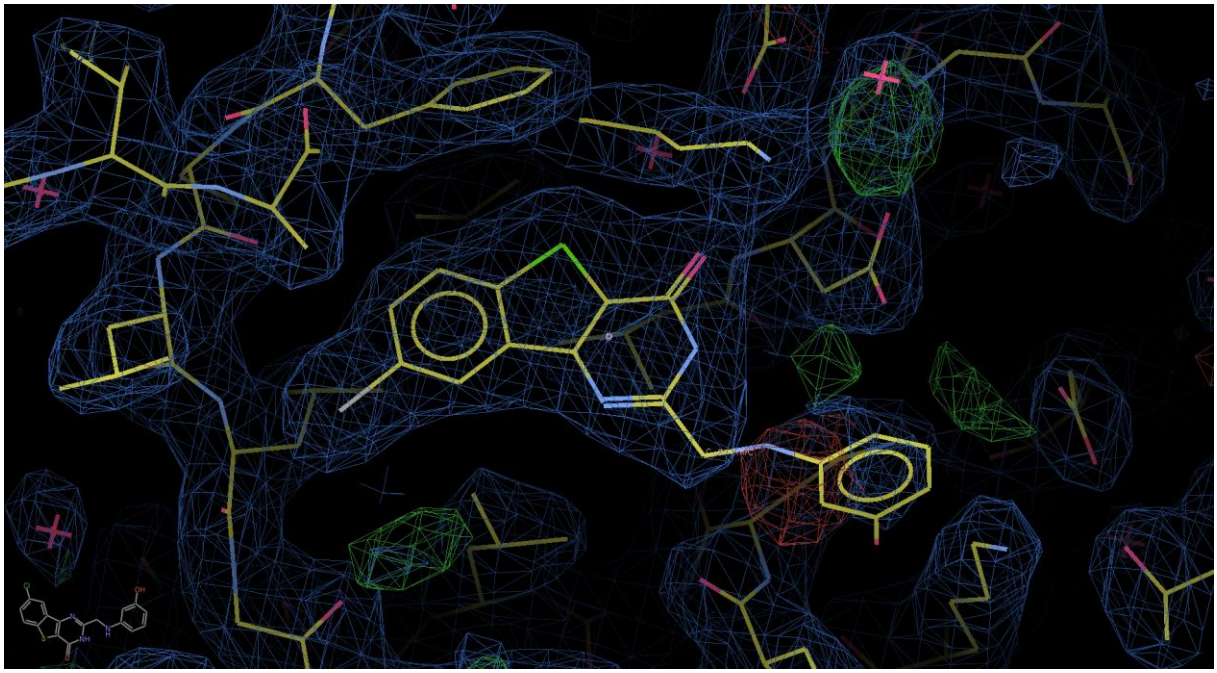

***Figure 39**: Snapshot of crystal structure of CLK4 and compound **43n** in the ATP binding pocket.*

In summary, CLK4 probes are also urgently needed and our collaborators will be carrying out additional studies on the CLK4 compounds prepared. The crystal structure constitutes a great tool for us to investigate the selectivity using molecular modeling studies and in order to optimize PIM isoform selectivity. It is believed that the binding pose is the same pose as the one observed when docking **43n** with PIM kinases. The topology of CLK4 around the solvent exposed area is very similar to the PIM kinases, highlighting the challenge of achieving PIM selectivity over CLK isoforms.

2.5. SAR studies on position 8

The previous data, as well as literature research on PIM kinases, suggested that a small SAR study on position 8 would be appropriate to investigate possible selectivity within the isoforms.

Researchers at Exelixis reported a benzofuropyrimidinone **69** as another class of PIM inhibitor.[75] In their article, they performed some SAR studies on position 8 of the scaffold (Figure 40).

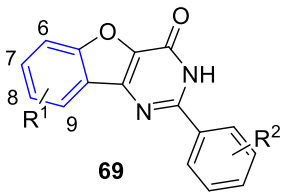

69

Compound	R^1	R^2	Kinase inhibitory activity IC_{50} (nM)			
			PIM-1	**PIM-2**	**PIM-3**	**CLK2**
70	8-Br	2-Cl	17	781	18	231
71	H	2-Cl	5000	5000	5000	5000
72	8-Cl	2-Cl	28	858	30	371
73	8-OMe	2-Cl	61	1451	31	312
74	8-OH	2-Cl	232	3755	106	1288
75	8-CN	2-Cl	281	3429	204	5000
76	8-Ph	2-Cl	3963	5000	88	5000
77	8-OCF_3	2-Cl	293	5000	286	5000
78	8-CF_3	2-Cl	23	2330	102	5000

Figure 40: *SAR studies on the benofuropyrimidinone core reported by Exelixis.*

The Exelixis scaffold **69** binds to the catalytic site of the protein in the same way as benzothienopyrimidinone **8** (PDB: 4ALV). Analysis of the SAR studies on the scaffold revealed that a trifluoromethyl group **78** on position 8 provided PIM-1 potency, a moderate selectivity over PIM-3, and high selectivity over PIM-2 and CLK2.

The data reported by Exelixis encouraged us to synthesize analogues of the initial benzothienopyrimidinone scaffold changing the chlorine at position 8 to a trifluoromethyl group. As well as introducing a trifluoromethyl group, other functional groups such as bromine, phenyl, or nitro, were also examined to establish the difference in activity/selectivity.

Using the synthetic procedures described in Scheme I, **46a**–**49a**, **49b**, **48t**, **48n**, **45l**, **45b**, **44l**, and **44b** were prepared using combinations of the most active amines from sections 2.1 and 2.2. The structures of this new series, and yields for the final step, are summarized in Figure 41.

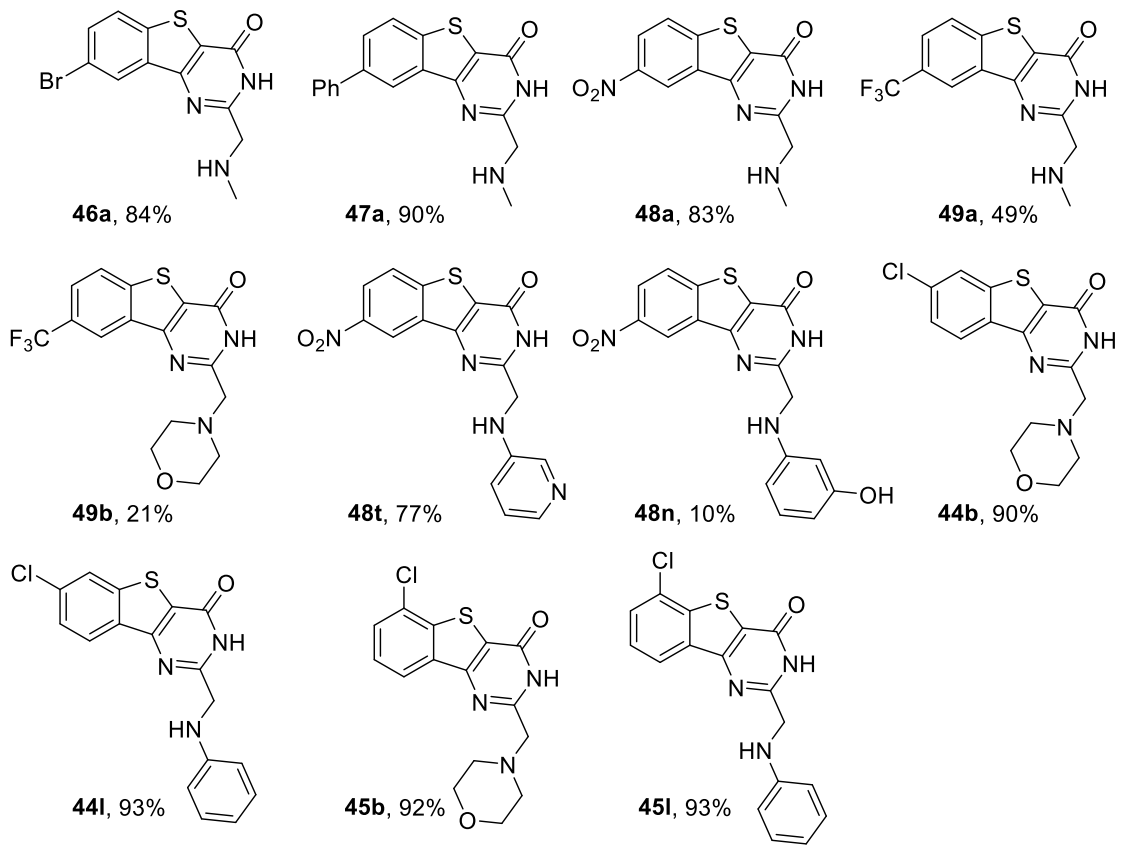

***Figure 41**: Analogues **46a**–**49a**, **49b**, **48t**, **48n**, **44b**, **44l**, **45b**, and **45l** for SAR study.*

Compounds **46a**, **47a** and **48a** were designed as derivatives of **43a** to assess the size of the area facing the hinge region for each PIM isoform. To synthesize analogue **47a**, a Suzuki-Miyaura coupling reaction was performed prior to the nucleophilic aromatic substitution to introduce the phenyl group in position 8 (Scheme III).

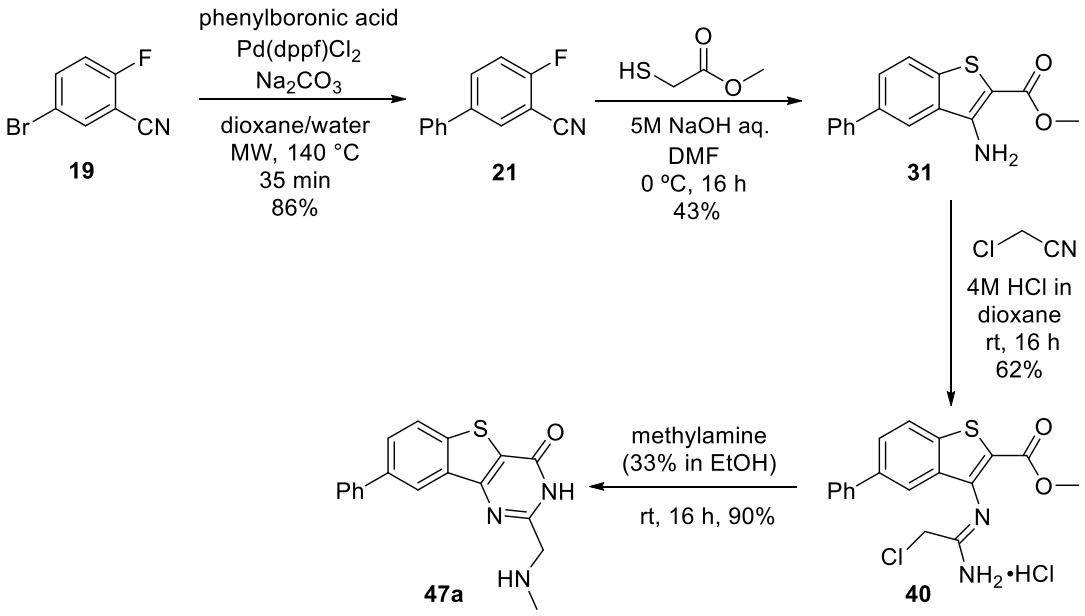

***Scheme III**: Synthetic procedure for the synthesis of **47a**.*

The synthetic sequence commenced with a Suzuki-Miyaura reaction using commercially available fluorobenzonitrile **19** and phenylboronic acid to afford **21** in 86% yield. Compound **31** was prepared using the conditions described previously (Scheme I). The loss of electron-withdrawing group when changing to a phenyl instead of a chlorine substituent slowed the nucleophilic aromatic substitution but we were able to isolate **31** in 43% yield. Next, **31** was reacted with chloroacetonitrile in 4M HCl in dioxane to afford **40** in a 62% yield. The characterization of **40** proved challenging as we were unable to obtain a high quality ^{1}H NMR spectrum for this compound. **40** proved either insoluble or decomposed in each NMR solvent examined. Liquid chromatography-mass spectrometry (LCMS) showed the correct mass for the compound, therefore, the compound was taken as such to the next step reacting it with methylamine (33% in EtOH) to afford **47a** in a 90% yield, thus confirming the proposed identity of **40**.

Within this series, **48n** and **48t** were designed following molecular modeling studies. PIM-1 docking with a library of compounds containing nitro groups at position 8 showed that the nitro group could possibly form hydrogen bonding interactions with the Glu124 within the PIM-1 hinge region, augmenting any PIM-1 selectivity. Therefore, **48n** and **48t** were synthesized to establish if an increase in PIM-1 selectivity was observed.

Furthermore, **44b**, **44l**, **45b**, and **45l**, were designed as derivatives of **43b** and **43l**, which had initially shown CLK4 activity and not PIM activity. A change of the chlorine position around

the aromatic ring would give an indication if position 8 was required for potency/selectivity towards CLK4.

The DSF data for compounds **46a**–**49a**, **49b**, **48t**, **48n**, **45l**, **45b**, **44l**, and **44b** are presented in Table XIV:

Table XIV: *DSF data for compounds **46a**–**49a**, **49b**, **48t**, **48n**, **44b**, **44l**, **45b**, **45l**.*

Compound	PIM-1 (ΔT_m, °C)	PIM-2 (ΔT_m, °C)	PIM-3 (ΔT_m, °C)	CLK4 (ΔT_m, °C)	CLK1 (ΔT_m, °C)	CLK3 (ΔT_m, °C)	DYRK1A (ΔT_m, °C)	DYRK2 (ΔT_m, °C)	SRPK1 (ΔT_m, °C)	SRPK2 (ΔT_m, °C)
46a	6.4	4.1	8.0	4.7	3.4	0.5	3.0	2.2	0.0	1.0
47a	6.4	4.4	11.5	4.4	3.5	0.6	3.1	2.4	0.1	0.4
48a	6.9	6.8	4.4	0.8	1.2	0.0	2.0	3.9	0.2	0.0
49a	4.7	3.7	5.9	0.5	0.7	0.0	0.5	0.9	0.1	0.0
49b	2.5	0.9	1.1	1.9	0.5	0.1	0.5	0.2	0.0	0.1
48t	4.6	3.1	4.1	1.6	0.7	0.0	0.8	0.3	0.0	0.2
48n	2.2	1.3	2.8	1.5	1.4	0.5	2.4	0.1	0.9	0.8
44b	3.7	0.2	2.9	2.3	1.2	0.0	1.0	0.7	0.0	0.0
44l	6.2	1.7	5.0	3.8	3.6	0.0	2.8	0.8	0.8	0.3
45b	3.9	0.4	4.9	2.0	2.0	0.0	2.4	2.2	0.0	0.0
45l	7.6	3.9	9.1	4.0	4.0	0.0	4.8	2.1	0.6	0.2

Overall, the compounds showed a considerable decrease in CLK4 activity, whilst maintaining the selectivity over CLK1, CLK3, DYRK family, and the SRPK family.

As was expected, **46a**–**48a** kept PIM-1 affinity with a ΔT_m of 6.4–6.9 °C, similar to the ΔT_m observed for analogue **43a** (ΔT_m = 6.4 °C for PIM-1). Interestingly, the ΔT_m for PIM-2 did not seem to be affected by the size of the functional group and PIM-3 showed a higher affinity for larger hydrophobic groups. For example, **46a** and **47a** had increased ΔT_m values of 8.0 °C and 11.5 °C, the highest values observed to date, suggesting that the cavity facing the PIM-3 hinge region was bigger such that larger hydrophobic groups could be optimal for achieving PIM-3 selectivity.

Interestingly, introducing a trifluoromethyl group, in compound **49a**, somewhat reduced the stability of PIM-1 to a ΔT_m of 4.7 °C, considerably lower than the chlorine analogue **43a** (ΔT_m of 6.7 °C). PIM-2 and PIM-3 did not seem to be affected by changing the chlorine for a trifluoromethyl group.

Compounds **48n** and **48t** are analogues of **43n** and **43t**, which contain a nitro group, selected to potentiate hydrogen bonding interactions with the glutamic acid residue present in PIM-1 and PIM-3. Unfortunately, the affinity of these compounds decreased considerably by 2–3 °C

when changing from a chlorine substituent to a nitro group. For example, **43n** showed a ΔT_m of 6.6 °C against PIM-1, whereas **48n** showed a decreased ΔT_m of 2.2 °C. This compound did not present PIM-2 activity and a similar decrease was observed with the PIM-3 isoform, suggesting that polar groups are not tolerated. Furthermore, later studies showed that backbone N-H trajectory of Glu124 is not optimal for the hydrogen bonding, explaining the results obtained.

An overlay of the PIM-1 and PIM-2 kinases (Figure 42) from our collaborators at the SGC confirmed that the glutamic acid (E124L, shown in Figure 42) is interacting with the arginine from the hinge region, showing how both glutamic acid and arginine residues (present in both PIM-1 and PIM-3) are pointing outside the ATP pocket, generating an even more hydrophobic hinge region.

Another key factor was that, in both isoforms, the phosphate binding loop (P-loop) folds into the ATP pocket making the suitable aromatic interactions between the phenylalanine (F49) and the inhibitor. This strongly suggested that the activity observed in PIM kinases was related to the P-loop conformation rather than hydrogen bonding interactions and that a change in the binding and conformation was needed to further assess selectivity between PIM-1, PIM-2, and PIM-3.

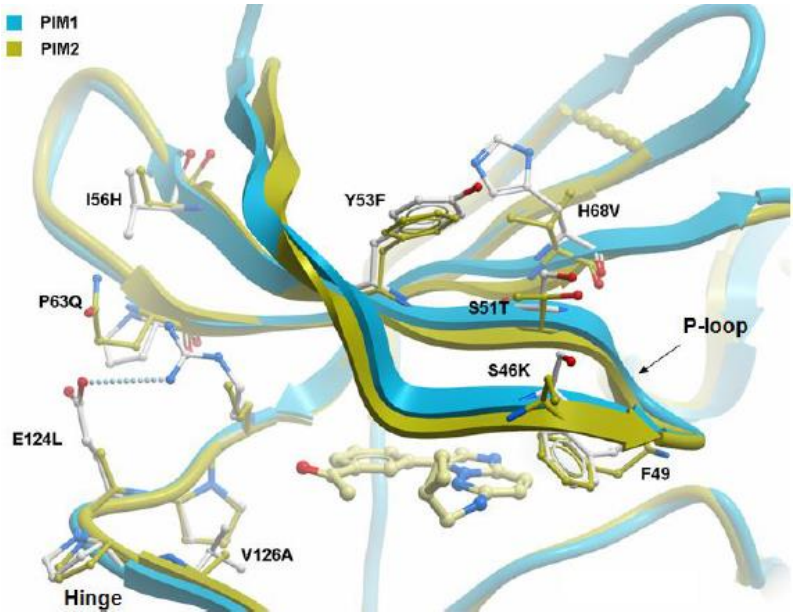

Figure 42: *Ribbon diagram of PIM-1 and PIM-2 (P-loop and hinge regions) PDB: 2C3I and 2IWI. The hydrogen bonding interaction between E124L and arginine is shown by a dotted line. The phenylalanine F49 shows the aromatic interactions between the aromatic ring and the inhibitor.*

Finally, within this series, compounds **44b**, **44l**, **45b**, and **45l** are analogues of **43b** and **43l**, where the chlorine has been moved to positions 7 (**44l** and **44b**) and 6 (**45b** and **45l**) of the aromatic ring. These analogues were synthesized to analyze the effect on CLK4 selectivity and assess if PIM potency varied when moving the chlorine around the aromatic ring. Surprisingly, the four compounds reduced CLK4 affinity, from a ΔT_m of 7–8 °C for compounds **43b** and **43l**, to a ΔT_m of 2–4 °C for compounds **44b**, **44l**, **45b**, and **45l**. Also, the aniline analogues increased the PIM potency, especially **45l**, with a ΔT_m of 7.6 °C and 9.1 °C against PIM-1 and PIM-3, respectively. **44l** also had a ΔT_m value for PIM-1 (6.2 °C), whilst maintaining low activity against PIM-2 and PIM-3. This increase in apparent potency could be due to a slight change in the binding pose when changing the chlorine position, allowing for an aromatic interaction between the aniline and the phenylalanine to take place (F49, Figure 44). We were very interested in this change of selectivity and potency for both PIM-3 and CLK4, and molecular modelling studies using **43l** and **45l** were performed on both kinases to understand the change in affinities when moving the chlorine around the aromatic ring.

Compounds **43l** and **45l** were docked first against a virtual model of PIM-3 providing a series of interesting results (Figures 43, and 44).

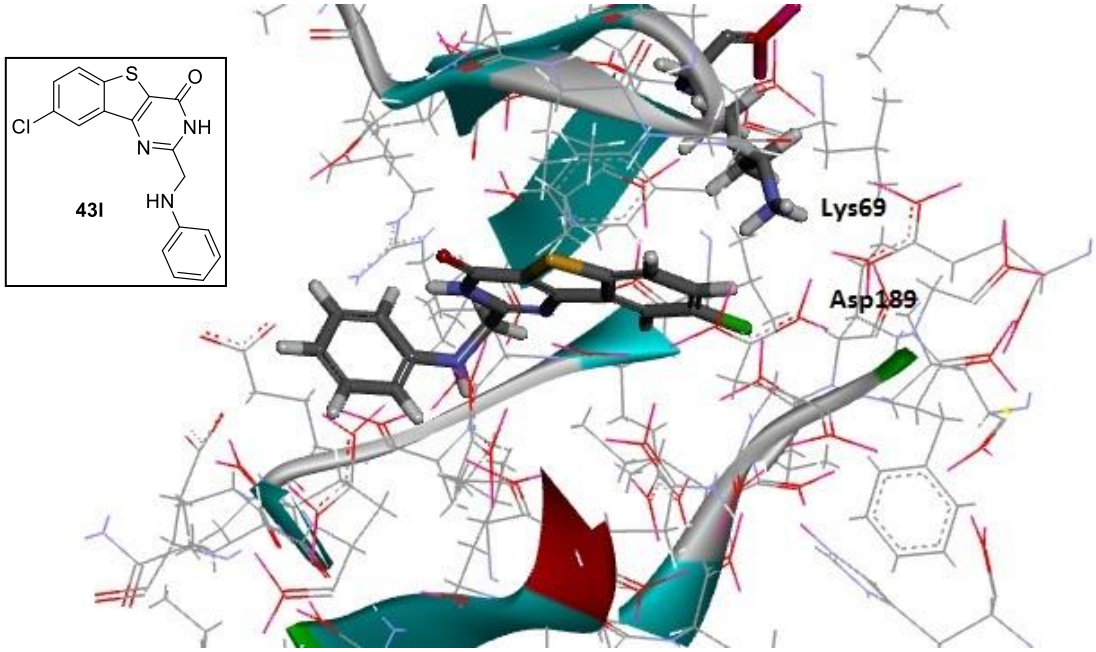

***Figure 43**: Virtual docking of **43l**–PIM-3 ATP binding site.*

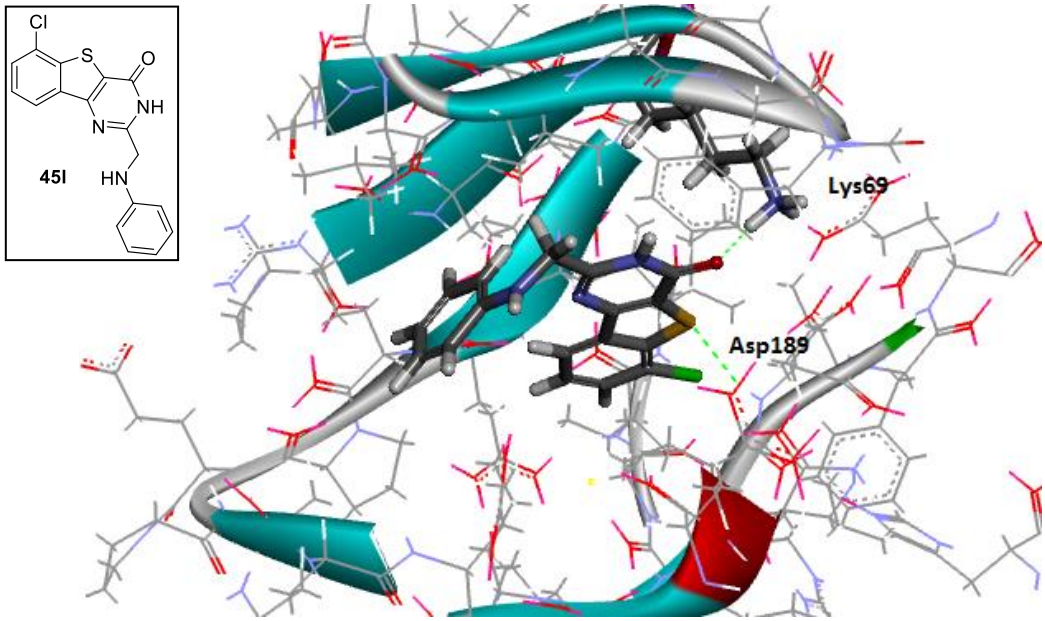

***Figure 44**: Virtual docking of **45l**–PIM-3 ATP binding site.*

In both compounds, a different binding pose was observed than seen for compound **9** (PDB: 3JXW). The cavity of PIM-3 appeared to be slightly closed around the hinge region area, which prevented both compounds from forming the main interaction with Lys69. Compound **43l** flipped in the active site (Figure 43) and no hydrogen-bonding interactions were observed, which can explain the low affinity observed between **43l** and PIM-3 (ΔT_m of 0.1 °C). On the other hand, **45l** fits in the active site of PIM-3 in a manner that allowed the system to keep the interaction between the amide functional group and Lys69 (Figure 44) as well as provide an extra interaction between the thiophene ring and Asp189, potentially explaining the high affinity observed (ΔT_m of 9.1 °C).

When **43l** and **45l** were docked in the CLK4 active site, a similar behaviour was observed.

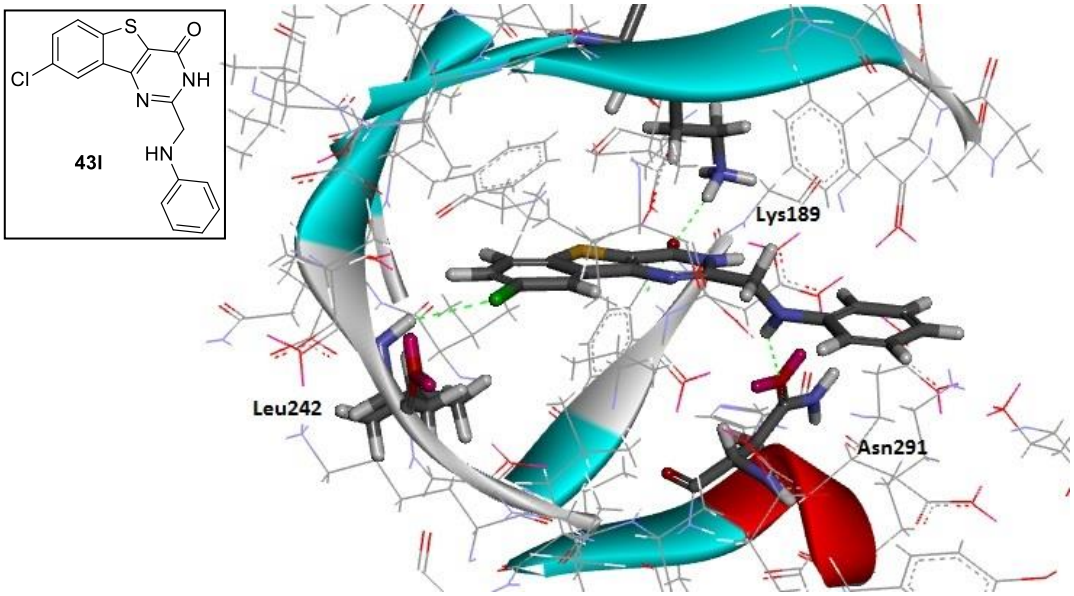

***Figure 45**: Virtual docking of **43l** and CLK4 ATP binding site.*

43l bound within the ATP binding pocket of CLK4 (Figure 45) in a manner previously observed with the original Abbott compound (Figure 16). Three possible interactions may be observed between the receptor and the probe. The chloride is in close proximity with Leu242 from the hinge region, the amide maintained the interaction with the Lys189 and finally, the secondary amine from the arylamine side chain could form another hydrogen bonding interaction with Asn291. The apparently highly favoured binding between CLK4 and **43l** could provide a good explanation for the high affinity observed in the DSF assay (ΔT_m of 7.0 °C) (Table XI).

When **45l** bound within the ATP binding pocket of CLK4 (Figure 46), two hydrogen bonding interactions are observed. The aniline maintained the interaction with Asn291, however, the chlorine lost the interaction with the hinge region, and the amide formed a weak hydrogen bonding interaction with Asp323 instead of Lys189. The looseness of the hydrogen bonding interaction could be an explanation for the decreased potency between **45l** and CLK4 (ΔT_m of 4.0 °C).

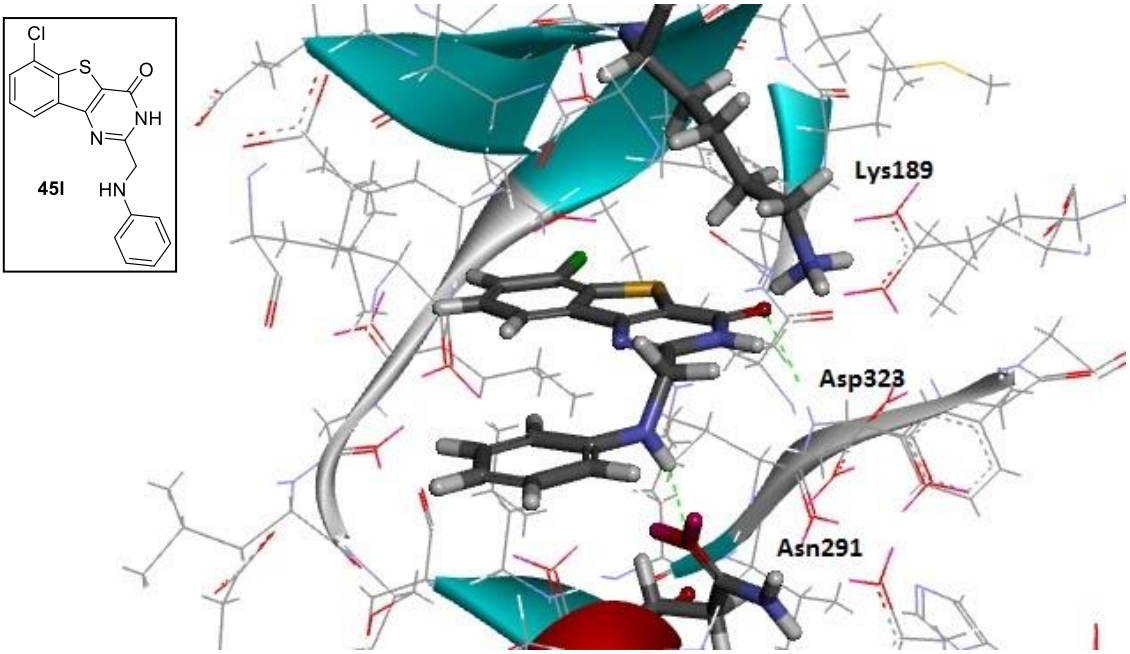

***Figure 46**: Virtual docking of **45l** and CLK4.*

In the case of the morpholine analogues **44b** and **45b**, moving the chlorine around the aromatic ring did not change the affinities for the PIM kinases, as low PIM activity was observed. Compound **45b** showed a ΔT_m of 3.9 °C, 0.4 °C, 4.9 °C, and 2.0 °C (against PIM-1, PIM-2, PIM-3, and CLK4) and compound **44b** showed a ΔT_m values of 3.7 °C, 0.2 °C, 2.9 °C, and 2.3 °C respectively, suggesting that the morpholine group was not tolerated within the PIM ATP pocket. The affinity for CLK4 was also reduced by 6 °C when compared to the original morpholine CLK4 hit **43b** (CLK4 ΔT_m of 7.8 °C), which correlates to what was previously detailed for compound **45l** in Figure 46 and Figure 48, confirming that the chlorine at position 8 of the benzothienopyrimidinone core was key for CLK4 activity.

As was performed for the previous set of compounds, the candidates were further analyzed in a biochemical assay to assess their potencies against PIM-1, PIM-2, and PIM-3.

2.5.1. Biochemical evaluation of 46a–49a, 49b, 48t, 48n, 45l, 45b, 44l, and 44b

Following the biochemical procedure detailed in section 8.1.1, the compounds were tested at 10 µM and 1µM against PIM-1, PIM-2, and PIM-3. The PI obtained for these compounds is presented in Table XV.

Table XV: *Percentage of inhibition obtained for compounds* ***46a–49a***, ***49b***, ***48t***, ***48n***, ***45l***, ***45b***, ***44l***, *and* ***44b***.[a]

Compound	PIM-1 (10 µM)	PIM-1 (1 µM)	PIM-2 (10 µM)	PIM-2 (1 µM)	PIM-3 (10 µM)	PIM-3 (1 µM)
46a	100	93	97	71	97	79
47a	99	90	99	70	100	96
49a	99	83	95	56.	92	55
49b	75	18	38	15	28	-7
48n	97	75	88	47	85	31
48t	80	28	18	-4	53	5
45b	22	6	7	-5	6	4
45l	70	39	55	20	68	34
44l	22	6	7	-5	6	4
44b	32	15	8	-2	13	6

[a] Compound **48a** not tested

The preliminary biochemical assay carried out provided similar information to the DSF assay. As expected, **46a** was the most active compound for PIM-1, PIM-2, and PIM-3, with a PI higher than 70% at 1 µM. Compound **49a** displayed remarkable activity for the three isoforms, suggesting a pan-PIM inhibitor. Unfortunately, **48a** could not be tested at the CNIO as not enough compound was available to carry out the biochemical assay. Compounds **49a** and **48t** showed discrepancies between the DSF assay and biochemical assay, therefore, IC_{50} values were obtained to provide a solid conclusion about the activity against the PIM isoforms. For compounds **45b**, **45l**, **44b** and **44l**, the DSF assay and percentage of inhibition correlated well. Compounds **45b**, **44b**, and **44l**, showed a 22–32% inhibition for PIM-1 at 10 µM, and no activity at 1 µM, as well as having no activity for PIM-2 and PIM-3. **45l** showed a ΔT_m of 7.6 °C and 9.1 °C against PIM-1 and PIM-3, as well as a high 70% percentage of inhibition at 10 µM. Compound **48t** showed reduced affinity for the isoforms compared to its chlorine analogue **43n** (high PIs observed for the three isoforms at 10 µM and 1 µM, Table XII). **48t** showed PI of 80% and 28% for PIM-1 at 10 µM and 1µM, and low PI against PIM-2 and PIM-3, suggesting some possible selectivity towards PIM-1 compared to **43n**.

Following the cut-off values established at the CNIO, **46a**, **49a**, **49b**, **48o**, **48u**, and **45l**, were further evaluated and IC_{50} values were obtained for the three isoforms. The IC_{50} data are shown in Table XVI.

Table XVI: *IC_{50} data obtained for compounds* **46a**, **49a**, **49b**, **48n**, **48t**, and **45l**.

Compound	PIM-1 IC_{50} (nM)	PIM-2 IC_{50} (nM)	PIM-3 IC_{50} (nM)
46a	42	222	43
47a	65	129	5
49a	112	632	186
49b	3250	>50000	6290
48n	232	977	647
48t	2610	>50000	729
45l	184	2230	64

The IC_{50} data obtained supported the initial DSF data and PI. Compound **46a**, containing a bromine substituent, showed in fact, lower nanomolar values, compared to the corresponding chlorine analogue **43a**, against the three isoforms. **46a** displayed very encouraging values for PIM-1 (42 nM), PIM-2 (222 nM), and PIM-3 (43 nM), which also correlated with the DSF assay. Changing the bromine for the phenyl group displayed more remarkable results. **47a** showed IC_{50} values of 65 nM for PIM-1, 129 nM for PIM-2, and 5 nM for PIM-3, the lowest PIM-3 value observed to date. The compound's IC_{50} correlated with the DSF data too, i.e., the PIM-3 isoform showed a ΔT_m value of 11.5 °C and an IC_{50} of 5.2 nM. Despite the compound showing excellent potencies for the PIM isoform, the phenyl substituent was not studied further as it did not provide selectivity within the isoforms.

A decrease in potency for **49a** was seen compared to **43a** for PIM-1, PIM-2, and PIM-3. It appeared that changing the chlorine for a trifluoromethyl group (**49a**) was favourable as the PIM potency was maintained to low nanomolar activities (112 nM, 632 nM, and 186 nM for PIM-1, PIM-2, and PIM-3) but the selectivity observed in the DSF assay increased compared to its analogue **43a**. For example, **49a** showed a ΔT_m of 0.5 °C against CLK4, whereas **43a** showed a ΔT_m of 4.7 °C against CLK4, suggesting that a trifluoromethyl group could be a good funtionality to obtain PIM selectivity over CLK4.

As previously seen with other analogues, morpholine substituents at position 2 were not tolerated, **49b** showed little activity against the PIM kinases.

Furthermore, changing the chlorine at position 8 for a nitro group was not favourable. Compound **48n** provided some activity against PIM kinases with IC_{50} values of 232 nM for PIM-1, 977 nM for PIM-2, and 647 nM for PIM-3, however, these activities were considerably lower than the chlorine analogue **43n**, which provided a low IC_{50} of 33 nM for

PIM-1, no activity for PIM-2, and 66 nM for PIM-3. The same change of activity was observed for compound **48t** which presented little PIM activity.

Finally, we were very pleased to observe a change of potency/selectivity for compound **45l**. The previous analogue **43l**, provided strong binding affinities against CLK4 with a ΔT_m of 7.0 °C, whereas no activity was observed for PIM kinases. Moving the chlorine to position 6 of the aromatic ring switched the activity between kinases, providing a ΔT_m of 3.9 °C for CLK4, and increasing PIM-1 and PIM-3 activity to 184 nM and 64 nM respectively, as well as generating high selectivity over PIM-2. This data is consistent with the DSF data, and the molecular modelling studies, and constitutes the first understanding of PIM kinase *vs* CLK4 selectivity observed to date.

2.6. Conclusions

In conclusion, DSF and biochemical data gathered provided a strong SAR study and an excellent starting point to understand methods for obtaining selectivity within the PIM isoforms.

The benzothienopyrimidinone scaffold showed extremely high selectivities over SRPK kinases, DYRK kinases, CLK1, and CLK3, with CLK4 being the protein kinase that showed the highest cross-reactivity with PIM kinases in our assays. From the biological data, we established that the hinge region facing the aromatic ring of the benzothienopyrimidinone scaffold may be a useful cavity to address the CLK4 selectivity. This was seen in the data obtained for compounds **43l** and **45l** (Figure 47). Compound **43l** did not show significant PIM-inhibitory activity in the DSF assay or the biochemical assay; however, it showed a clear affinity for CLK4, with a ΔT_m of 7.0 °C. This affinity decreased when the chloride was moved to position 6 of the aromatic ring (**45l**), with the CLK4 ΔT_m dropping to 4.0 °C, but PIM activity increased to low nanomolar IC_{50} for PIM-1 and PIM-3.

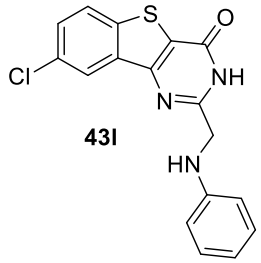

43l

IC_{50} data: Not determine, no significant PIM-inhibitory activity

Compound	PIM-1 (ΔT_m, °C)	PIM-2 (ΔT_m, °C)	PIM-3 (ΔT_m, °C)	CLK4 (ΔT_m, °C)	CLK1 (ΔT_m, °C)	CLK3 (ΔT_m, °C)	DYRK1 (ΔT_m, °C)	DYRK2 (ΔT_m, °C)	SRPK1 (ΔT_m, °C)	SRPK2 (ΔT_m, °C)
43l	1.9	0.5	0.05	7.0	4.0	0.9	2.4	0.7	0	0.7

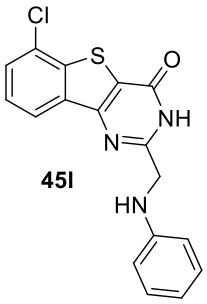

45l

PIM-1 (IC_{50}): 184 nM; **PIM-2 (IC_{50})**: No activity; **PIM-3 (IC_{50})**: 64 nM

Compound	PIM-1 (ΔT_m, °C)	PIM-2 (ΔT_m, °C)	PIM-3 (ΔT_m, °C)	CLK4 (ΔT_m, °C)	CLK1 (ΔT_m, °C)	CLK3 (ΔT_m, °C)	DYRK1 (ΔT_m, °C)	DYRK2 (ΔT_m, °C)	SRPK1 (ΔT_m, °C)	SRPK2 (ΔT_m, °C)
45l	7.6	3.9	9.1	4.0	4.0	0	4.8	2.1	0.6	0.2

***Figure 47**: Summary of DSF data and kinetic data for **43l** and **45l**.*

A potential explanation for the change in selectivity was provided through molecular modelling studies, where a different binding pose was observed which provided additional understanding for methods to achieve PIM selectivity over CLK4. Furthermore, from the SAR study we discovered four CLK4 hits that are currently being investigated at the SGC as potential CLK4 chemical probes (Figure 37), and the first crystal structure of CLK4 with **43n** was obtained (Figure 38).

Regarding the PIM isoforms, the selectivity of PIM-1 and PIM-3 over PIM-2 was consistent throughout the benzothienopyrimidinone series, in both DSF and biochemical assays, with excepcion of **47a** which showed a 13-fold selectivity for PIM-3 over PIM-1.

Although the selectivity seen is yet not fully understood, recent studies from our collaborators at the SGC showed that PIM-2 kinase demonstrates different ligand binding behaviour compared to PIM-1 and PIM-3, suggesting that PIM-2 might be more challenging to target. PIM-1 or PIM-3 considerable selectivity was not observed to date, some compounds though (**43u** nd **47a**) showed some promising selectivity but still required further optimization. At this stage, we believed that modifying the benzothienopyrimidinone scaffold by adding shape or changing the binding pose could be the next method to try and address selectivity between PIM-1 and PIM-3. This theory was studied in Chapter 3 and Chapter 4.

A novel process for the synthesis of substituted benzothiophenes was developed with the ability to incorporate different functional groups.[65] The method is likely to find applications in providing easy access to common medicinal chemistry scaffolds for future drug discovery projects.

The Abbot compound **9** served as a useful starting point to investigate the PIM isoforms. Through molecular modelling studies, DSF data, percentage of inhibition as well as biochemical assays we established a strong SAR within the PIM and CLK4 binding pockets. The SAR study gave us good information to continue searhing for selective chemical probes for the PIM isoforms.

3. Phenyl pyrimidinones as potential chemical probes for PIM kinase isoforms

3.1. Discovery of the phenyl pyrimidinone scaffold

The results obtained on the benzothienopyrimidinone series suggested that slight modifications to the original Abbot scaffold would be needed to change the binding and alter the potency/selectivity of our analogues.

Through molecular modelling studies, a novel phenyl pyrimidinone scaffold (Figure 48), was proposed as an alternative to address PIM potency/selectivity. The central thiophene ring from the original Abbot scaffold was removed to analyze whether the heterocycle was needed for potency. The new scaffold retained the pyrimidinone ring to allow formation of a hydrogen bond interaction between the amide and Lys67, as well as allowing functionalization on both the phenyl and the pyrimidinone ring to carry out a SAR study to optimize potency/selectivity.

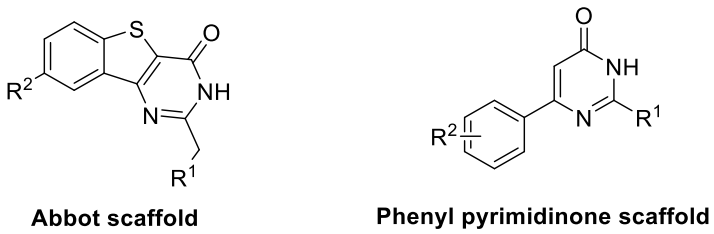

***Figure 48**: Abbot and phenyl pyrimidinone scaffolds.*

To pursue this theory, a virtual library was designed using the most interesting derivatives from the benzothienopyridiminone series in Chapter 2. For example, compound **79**, which is the phenyl pyrimidinone analogue of **43n**, was designed and docked in both PIM-1 and PIM-2 (Figure 49 and Figure 50). Interestingly, a change in the binding pose within the active site was suggested for this new scaffold, and new hydrogen bonding interactions were formed between the virtual probe and the receptor.

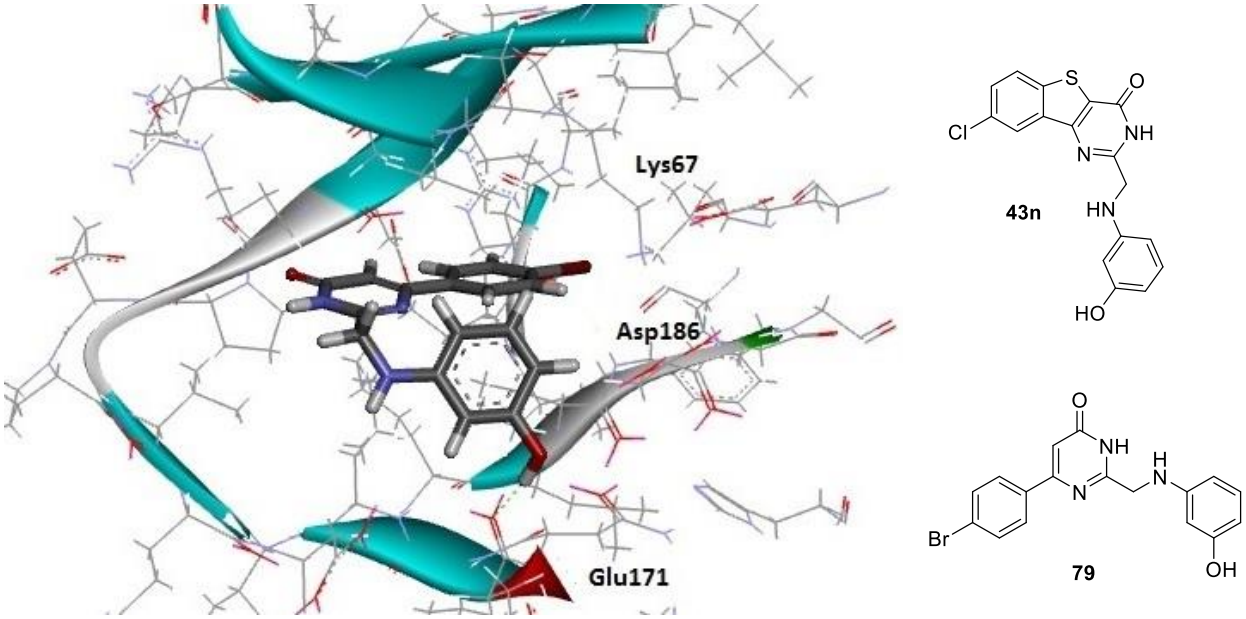

***Figure 49**: Compound **79**–PIM-1 docking pose.*

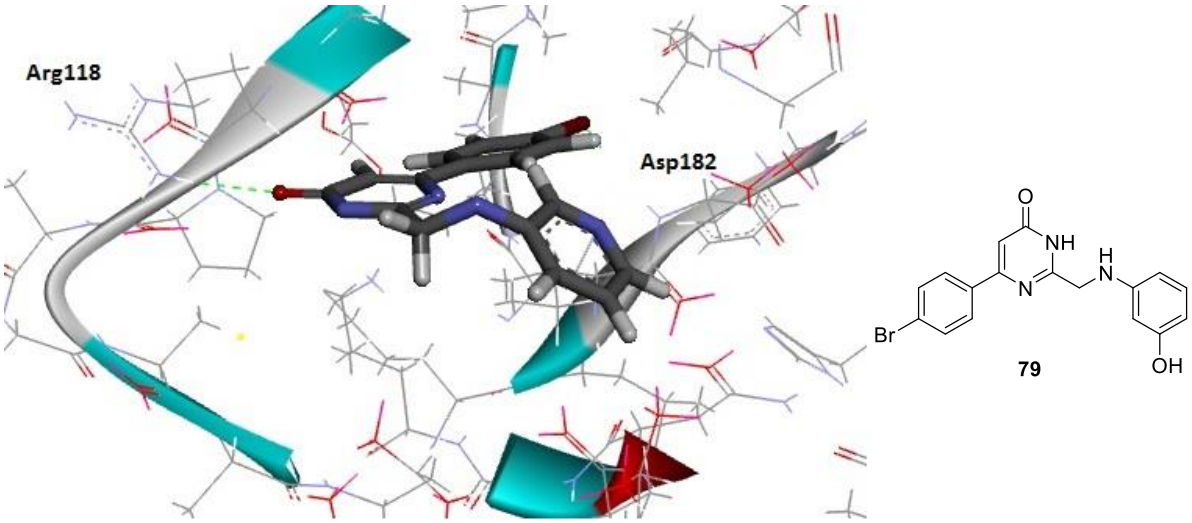

***Figure 50**: Compound **79**–PIM-2 docking.*

Figure 49 shows compound **79** docked in the PIM-1 isoform active site. The modelling studies suggested the compound had flipped inside the active site, with the pyrimidinone ring facing the hinge region, and one hydrogen bonding interactions forming between the phenol group with Glu171 (green dotted lines). The same binding was observed within the PIM-2 isoform, Figure 50, where the pyrimidinone ring formed a hydrogen bonding interaction with Arg118, as observed in PIM-1. Similar binding poses were observed throughout the molecular

modelling studies, and we believed that changing the binding pose could be a way to analyze the effect on the PIM potency or the probe selectivity over CLK4.

3.2. Synthetic approach for the synthesis of final compounds

The results obtained from the modelling studies encouraged us to synthesize analogues containing the new phenyl pyrimidinone scaffold. Since the project was centred on the generation of a small library of compounds to create SAR data, the general synthetic pathway that was adopted had to be designed to facilitate this purpose. With this in mind, a chemical route was proposed using well-established synthetic methods[76, 77] to permit the simple and efficient synthesis of intermediates and final compounds (Scheme IV).

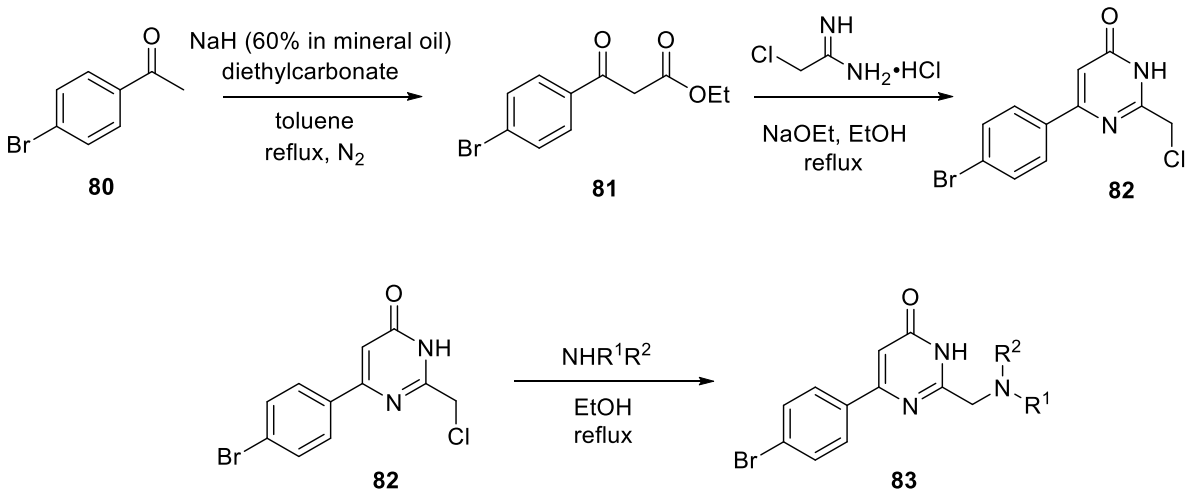

***Scheme IV**: Proposed synthetic route for the synthesis of **83**.*

Commercial 4-bromoacetophenone **80** could be deprotonated and reacted with diethylcarbonate to form **81**.[76] Intermediate **81** could then react with chloroacetamidine hydrochloride to provide **82**, an excellent precursor for our proposed analogues. **82** could then undergo a S_N2 reaction with the amines of interest to provide analogues of **83**.

Reaction of the anion derived from 4-bromoacetophenone with diethyl carbonate proceeded smoothly to deliver **81** as a colourless oil (72%). Disappointedly, refluxing **81** with chloroacetamidine proved unsuccessful, presumably due to polymerization of chloroacetamidine under the reaction conditions and further optimization of this reaction was needed. After multiple attempts, intermediate **81** was reacted with chloroacetamidine

hydrochloride salt in the presence of sodium ethoxide in ethanol at 0 °C for 16 hours to afford **82** in 16% yield. It proved important that the chloroacetamidine was added portion-wise during the first 30 minutes of the reaction to stop polymerization. **82** could then react with a variety of amines using dry EtOH under refluxing conditions to afford analogues **83**.

While the optimization for analogue **82** was ongoing, we decided to pursue the synthesis of **86** and **87** (Scheme V) which resulted from the reaction of **81** and **85** with cyclopropylcarboxamidine hydrochloride to give intermidiates **86** and **87** in good yields (72% and 53%, respectively). These analogues allowed further functionalization at the 3- and 4-position of the phenyl ring which provided a starting point for the generation of SAR around the phenyl pyrimidinone ring.

Benzamidine hydrochloride was also reacted with **81** to give intermediate **88** in good yield (82%). The poor solubility of **88**, as well as the corresponding final compounds, led to multiple difficulties during purification and characterization. For example, we were not able to obtain a good quality ^{13}C NMR for **88** due to the compound precipitating from solution in the NMR tube in multiple solvents, even at high temperatures, therefore, position 3 (using **85** as the precursor) of the phenyl ring was not investigated in conjunction with benzamidine hydrochloride.

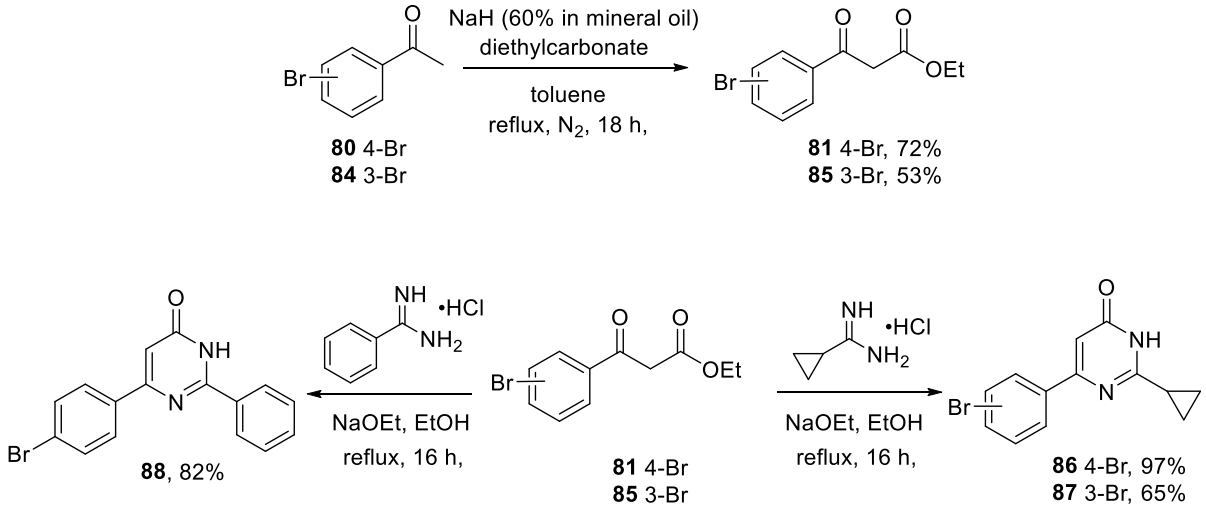

***Scheme V**: Synthetic procedure for the generation of intermidiates **86**, **87** and **88**.*

A Buchwald-Hartwig amination was used as the final step of the synthesis. This coupling process is extensively employed in medicinal chemistry as a robust method for the formation

of Ar-N bonds.[78] The specific reactions for our compounds required the use of BrettPhos palladacycle (combination of a Pd catalyst and bulky ligand), a bulky ligand (BrettPhos), and a base (Na^{t}OBu), to enable the coupling of intermediates **86** and **87** with a primary amine derivative. However, these conditions proved unsuccessful when changing to a secondary amine, and further optimization was required. Following Buchwald's published conditions,[78, 79] we were finally able to couple a secondary amine when changing to the RuPhos precatalyst, together with RuPhos ligand (Scheme VI).

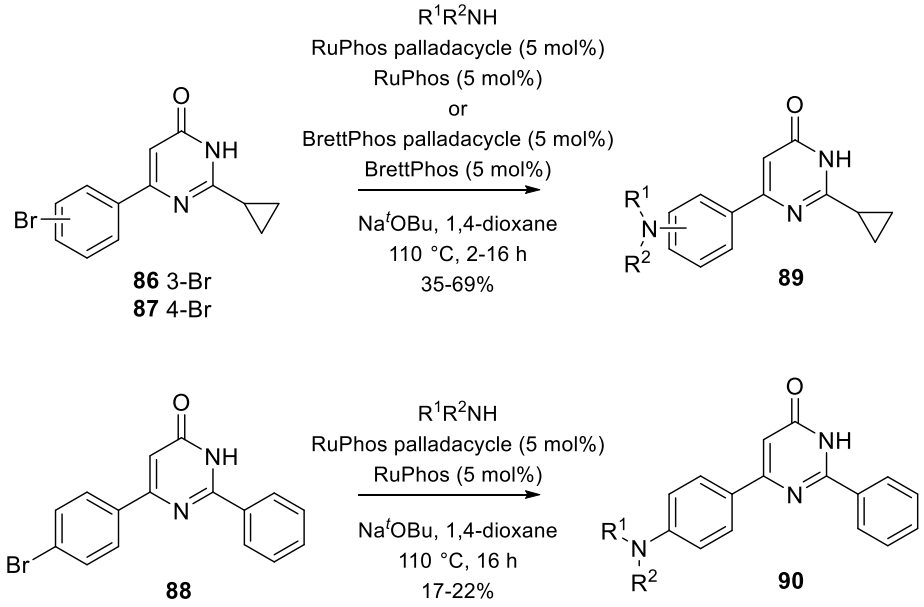

***Scheme VI**: Buchwald-Hartwig coupling conditions for the synthesis of final compounds.*

The above 3-step chemical synthesis appeared ideal for performing SAR studies. Well established and robust reactions were used to synthesize the key intermediates. Ideal features of a standard SAR synthesis were also employed, as the route facilitated the possibility of forming large amounts of intermediates **86**, **87** or **88**. with the potential for late stage diversification *via* palladium catalyzed cross-coupling reactions. These would theoretically enable the incorporation of a wide range of different functional groups into the pyrimidone scaffold. Compounds **91**–**96** (Figure 51) were synthesized using this synthetic route. Yields corresponding to the Buchwald-Hartwig coupling transformation are detailed in the Figure.

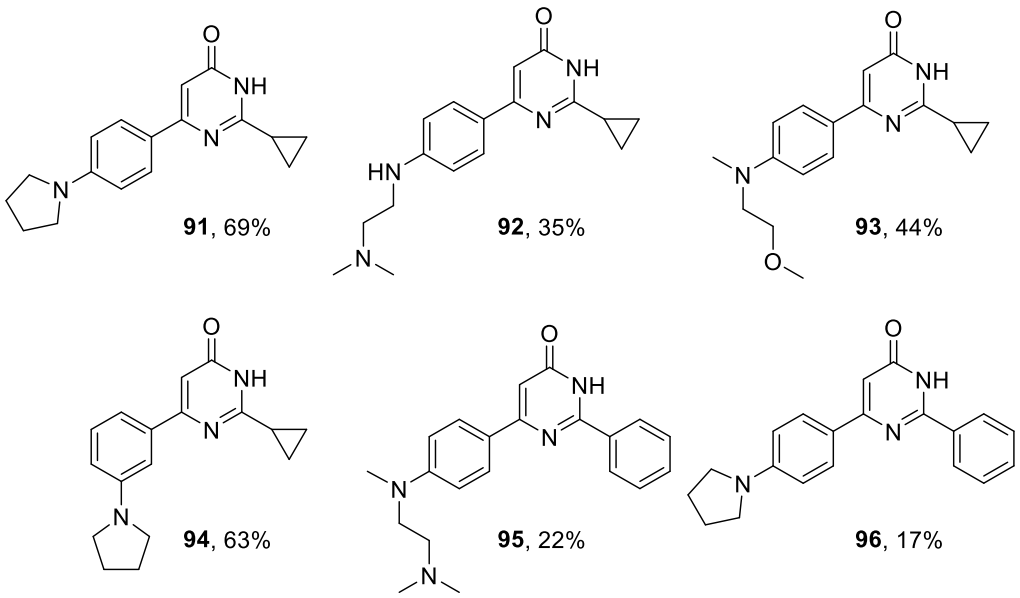

***Figure 51**: Phenyl pyrimidinone analogues **91**–**96**.*

Finally, the synthetic procedure for the synthesis of **82** (Scheme IV) was optimized and provided us with sufficient material to further react **82** with a variety of amines *via* a S_N2 process to provide analogues **97–101** (Figure 52).

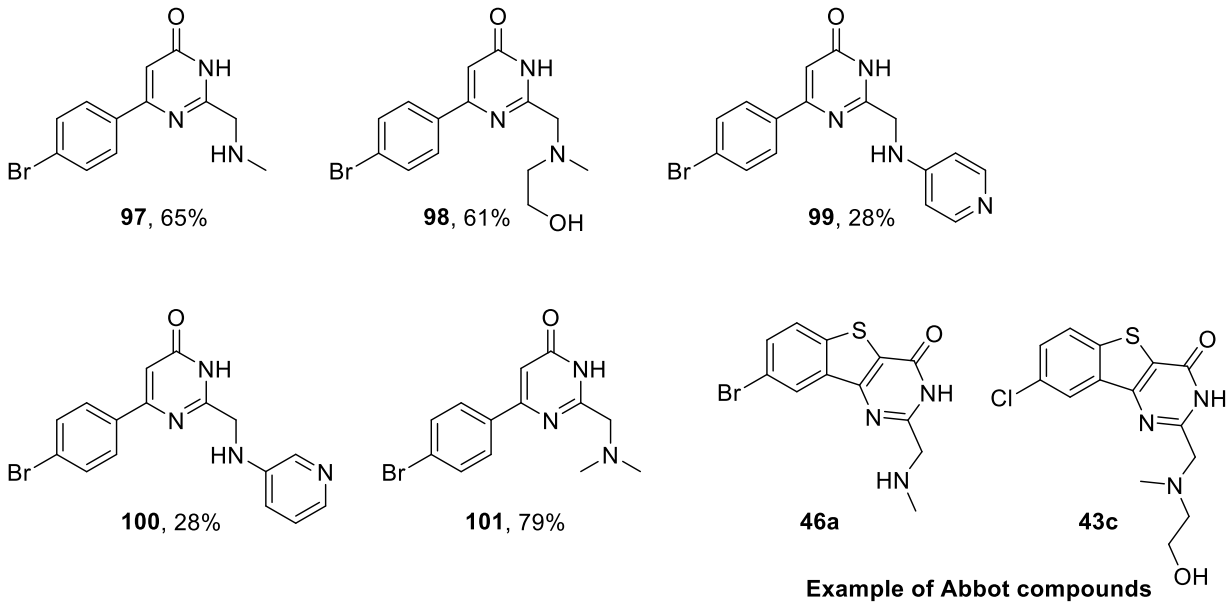

***Figure 52**: Phenyl pyrimidinones **97–101**.*

From the data obtained from compounds **46a**, **43c**, **43t** and **43u**, which are analogues within the benzothienopyrimidinone series, we were encouraged to synthesize **97**, **98**, **99** and **100** (Figure 52) to be able to directly compare the effect caused by the removal of the central thiophene ring. Analogue **101**, which was synthesized using dimethylamine (33% in EtOH), was also studied. Within this SAR study, the bromine on the aryl ring was maintained. There are two reasons for this; bromoacetophenone, which was used as the starting material for the synthesis of analogues **91**–**96**, is an inexpensive and commercially available compound and the reaction with diethylcarbonate proceeded in high yield (72%). Furthermore, little changes in affinity were observed when changing the chlorine for a bromine in the previous series. For the bromine analogue **46a**, PIM-3 displayed a higher ΔT_m value (8.0 °C), providing a potential source of selectivity for PIM-3 over PIM-1 and PIM-2 (Figure 53).

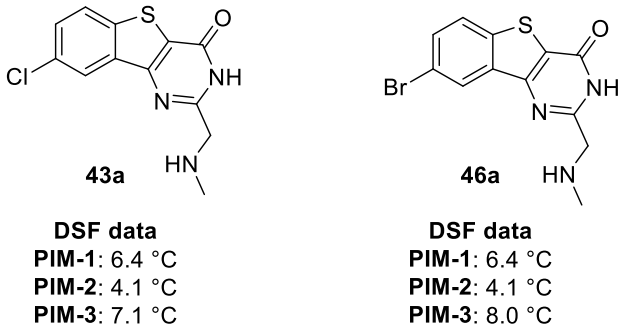

***Figure 53**: DSF data obtained for **43a** and **46a**.*

3.3. Biological evaluation of 91–101

3.3.1. DSF assay on compounds 91–101

Following the procedure that we adopted for the benzothienopyrimidinone series, the phenyl pyrimidinone analogues **91**–**101** were tested in a DSF assay against the PIM kinases, the DYRK kinases, the SRPK kinases, as well as, CLK1, CLK3 and CLK4. The data obtained is presented in Table XVII:

Table XVII: *DSF data results for compounds **86–101**.*

Compound	PIM-1 (ΔT_m, °C)	PIM-2 (ΔT_m, °C)	PIM-3 (ΔT_m, °C)	CLK4 (ΔT_m, °C)	CLK1 (ΔT_m, °C)	CLK3 (ΔT_m, °C)	DYRK1 (ΔT_m, °C)	DYRK2 (ΔT_m, °C)	SRPK1 (ΔT_m, °C)	SRPK2 (ΔT_m, °C)
86	1.5	0.0	4.0	0.5	0.4	0.0	0.5	0.1	0.0	0.0
87	2.8	1.3	11.5	5.9	3.0	0.1	1.7	0.9	0.0	0.0
88	0.0	0.4	0.2	0.3	0.0	0.0	0.7	0.0	0.0	0.0
91	0.0	0.0	2.9	0.2	0.1	0.1	0.0	0.0	0.0	0.0
92	0.0	0.0	4.4	0.2	0.2	0.1	0.1	0.0	0.0	0.0
93	0.5	0.0	1.0	0.8	0.5	0.3	0.1	0.0	0.1	0.0
94	0.5	0.2	0.2	0.4	0.3	0.0	0.4	0.1	0.0	0.0
95	0.1	0.0	2.9	0.6	0.9	0.2	0.1	0.4	0.8	0.2
96	0.0	0.0	4.5	0.4	0.3	0.0	0.0	0.0	0.0	0.0
97	1.8	1.4	0.4	0.6	0.1	0.0	0.5	0.0	0.7	0.0
98	2.9	0.0	2.0	0.2	0.3	0.0	0.3	0.0	0.0	0.0
99	5.1	3.3	0.1	0.8	0.0	0.0	0.2	0.0	0.0	0.0
100	3.9	2.1	2.5	0.5	0.0	0.0	0.0	0.0	0.2	0.1
101	3.8	0.5	3.5	0.0	0.3	0.6	0.1	0.0	0.0	0.0

From the DSF data, it was observed that compounds **91**–**96** exhibited little to no affinity for the kinases examined apart from compound **92** and **96**, which showed moderate ΔT_m values for the PIM-3 isoform (**92**: 4.4 °C, **96**: 4.5 °C) and a good selectivity profile for PIM-3 over PIM-1 and PIM-2 as well as for the other family of kinases analyzed. However, the DSF assay data corresponding to the PIM-3 isoform had been variable throughout previous SAR studies and no solid conclusion could be drawn. Kinetic data would provide a solid value for the activity of **92** and **96** against PIM-3.

The three intermediates **86**, **87** and **88**, were also included in the DSF assay. **88** did not show any affinity for each kinase examined, suggesting that the phenyl ring on the right hand side was not tolerated. Interestingly, both intermediates **86**, and **87** showed ΔT_m values of 4.0 °C and 11.5 °C for the PIM-3 isoform, the highest ΔT_m observed to date. The intermediates **86** and **87** also showed a high degree of selectivity for PIM-3 over PIM-1, PIM-2, CLK4, as well as, the DYRK family, and SRPK family. However, it is important to underline that small molecules such as **86** and **87** can often bind to other sites of the receptor, that are not the catalytic site, leading to misunderstandings within the DSF data. Nevertheless, we were intrigued by this data, and we decided to generate a small SAR study around **87** to attempt to optimize the PIM-3 affinity observed. This study was carried out by Steven Kay, a final year student from the University of Strathclyde, and is detailed in section 3.4.

The analogues synthesized from **82** provided very encouraging data. It was suggested through molecular modelling studies that these analogues were not binding *via* the binding pose observed for the Abbot analogues, where the pyrimidinone ring was forming the main hydrogen bonding interaction with Lys67 (PIM-1 reference) or Lys62 (PIM-2 reference). It was believed, that a change in the binding pose could alter the selectivity/affinity between the PIM isoforms or the selectivity over the CLK4 isoform. We were very pleased to observe that **97**, **98**, **99**, **100** and **101**, showed, no CLK4 affinity with low ΔT_m values (0–0.6 °C), as well as no affinity towards CLK1, CLK3, SRPK family, and DYRK family. Considering that the aim of this part of the PhD research was to increase the selectivity for PIM kinases over CLK4, it was remarkable to see that within a small SAR study we were able to prepare analogues that showed little affinity for the CLK4 kinase. Within the PIM kinases, **97** exhibited little affinity with ΔT_m values of 1.8 °C, 1.4 °C, and 0.4 °C, against PIM-1, PIM-2, and PIM-3. However, when changing from methyl amine (**97**) to dimethyl amine (**101**), the PIM-1 affinity increased to 3.8 °C, the PIM-2 affinity decreased to 0.5 °C, and the PIM-3 affinity increased to 3.5 °C.

Compound **98**, which is a derivative of **43c**, lost affinity when removing the thiophene ring. **43c** provided ΔT_m values of 5.4 °C (PIM-1), 3.0 °C (PIM-2), 6.0 °C (PIM-3), and 9.5 °C (CLK4), whereas the phenyl pyrimidinone analogue **98** showed little affinity with ΔT_m values of 2.9 °C, 0°C, 2 °C, and 0.2 °C against PIM-1, PIM-2, PIM-3, and CLK4, respectively, suggesting that removal of the thiophene ring provided lower potencies for the PIM isoforms.

Compounds **99** and **100** displayed the most interesting results within this series. Compound **100** exhibited a moderate ΔT_m value of 3.9 °C for the PIM-1 isoform, with little affinity for the rest of the kinases, however, **99**, which is the analogue of **43u** provided great selectivity for PIM-1 over PIM-3 and CLK4, with ΔT_m values of 5.1 °C, 3.3 °C, 0.1 °C, 0.8 °C against PIM-1, PIM-2, PIM-3 and CLK4, resulting in a difference of 4.3–5 °C between the PIM-1 isoform *versus* the PIM-3/CLK4 isoforms. The benzothienopyrimidinone analogue **43u** showed ΔT_m values of 7.6 °C (PIM-1), 4.6 °C (PIM-2), 7.0 °C (PIM-3), 6.1 °C (CLK4), with little selectivity observed between PIM-1, PIM-3 and CLK4.

In summary, we were very happy with the results obtained from the phenyl pyrimidinone series. Compounds **91**–**96** exhibited little to no affinity towards the PIM kinases, as well as the rest of the kinase studied, presumably due to either the lack of hydrogen-bonding interactions between the receptor and the analogue, or the compound not binding through the predicted pose from the molecular modelling studies. However, it was observed that by

modifying the binding pose, improvements regarding the selectivity over CLK4 were observed, as little CLK4 affinity was seen throughout this series. Furthermore, compound **99**, despite exhibiting a lower affinity towards PIM-1 (ΔT_m of 5.1 °C) compared to its benzothienopyrimidinone analogue **43u** (ΔT_m of 7.6 °C), had a much higher selectivity over CLK4, with ΔT_m values of 0.8 °C for **99** and 6.1 °C for **43u**, according to the DSF assay. At this stage, further support for our findings were needed from biochemical evaluation of these compounds.

3.3.2. Biochemical evaluation of 91–101

The phenyl pyrimidinone analogues **91**–**101** were further evaluated against PIM-1, PIM-2, and PIM-3. The same protocol (8.1.1) was applied as for the benzothienopyrimidinone series, whereby the PI at two different concentrations (10 µM, and 1 µM) against PIM-1, PIM-2, and PIM-3 was obtained. The data from this assay is presented in Table XVIII.

Table XVIII: *Data on percentage of inhibition for compounds **91**–**101** and **87**.*

Compound	PIM-1 (10 µM)	PIM-1 (1 µM)	PIM-2 (10 µM)	PIM-2 (1 µM)	PIM-3 (10 µM)	PIM-3 (1 µM)
87	52	15	32	5	18	4
91	-4	-10	-1	-2	4	3
92	-3	5	9	8	-12	-1
94	53	27	40	3	63	46
95	4	-1	3	-1	9	-3
96	2	2	8	8	-1	6
98	57	19	27	10	29	6
99	96	65	83	45	94	55
100	91	42	64	22	76	19
101	94	55	53	11	72	14

The PI data displayed some discrepancies with the DSF assay. Intermediates **86** and **88** were not tested due to the lack of material when carrying out the biochemical assay. **87** showed ΔT_m values of 2.8 °C (PIM-1), 1.3 °C (PIM-2), and 11.5 °C (PIM-3), and PI data of 52%, 32%, and 18% at 10 µM for PIM-1, PIM-2, and PIM-3 isoforms. It was surprising to see the inactivity against PIM-3, even though the DSF data showed a high value of 11.5 °C. However, a small molecule such as **87** could bind to another site of the receptor during the

DSF assay leading to high ΔT_m values. The percentage of inhibition data confirmed however, that the compound did not bind in the catalytic site of PIM-3, as no activity was observed.

For compounds **91**, **92**, **95**, and **96**, the PI data indicated little activity against the three PIM isoforms, correlating well to the suggested affinities by the DSF assay. Interestingly, for **99**, **100**, and **101**, the PI data showed higher activities than observed for the DSF data. Regarding the PIM-1 isoform, **99** and **100** correlation between both assays was acceptable, with PI data of 96% (10 µM dose) and 65% (1 µM dose) for the PIM-1 isoform for **99**, and 91% (10 µM dose) and 42% (1 µM dose) for **100**. The PIM-2 and PIM-3 isoforms, however, showed some discrepancies between assays. Compound **99** showed high activities for both PIM-2 and PIM-3 (83% at 10 µM for PIM-2 and 94% at 10 µM for PIM-3) whereas the DSF data showed little affinity with ΔT_m values of 3.3 °C (PIM-2) and 0.1 °C (PIM-3). Similar behaviour was observed for compound **100** regarding the PIM-2 and PIM-3 data, the PI data showed higher activities than the affinities suggested by the DSF assay, with PI values of 64% (10 µM, PIM-2 isoform) and 76% (10 µM, PIM-3 isoform) and DSF values of 2.1 °C and 2.5 °C, respectively. The discrepancies observed between both assays for these compounds are not understood at this stage. It was believed that full IC_{50} curve would provide a better understanding of the activity of these compounds against the three isoforms. Compounds **99**, **100**, and **101**, which showed higher percentage of inhibition of > 70% against the PIM-1 isoform were tested in a dose-response experiment against the three isoforms, the data is presented in Table XIX.

Table XIX*: IC_{50} data obtained for **99**, **100**, and **101**.*

Compound	PIM-1 IC_{50} (nM)	PIM-2 IC_{50} (nM)	PIM-3 IC_{50} (nM)
99	331	815	374
100	1160	9240	3100
101	488	9370	2520

Compound **99** exhibited encouraging potencies against PIM-1 (331 nM), PIM-2 (815 nM) and PIM-3 (374 nM). The DSF, PI and IC_{50} data correlated with regard to selectivity/potency for the PIM-1 isoform. The PI data observed for **99** showed 96% inhibition at 10 µM but a drop to 65% inhibition was observed at 1 µM which is translated to the IC_{50} data where a potency of 331 nM was observed. The PIM-2 data also correlated well between the three assays, with a ΔT_m value of 3.3 °C, PI values of 85% (10 µM) and 45% (1 µM) and a IC_{50} value of 815

nM. However, for the PIM-3 isoform, the DSF data showed a ΔT_m value of 0.1 °C, whereas PI data and IC_{50} data suggested potencies of 374 nM. Nevertheless, the DSF is only used as an indication of protein stabilization and care should be taken when interpreting the results.

It was believed, that the 4-aminopyridine derivative (which allows potential hydrogen bonding interactions between the pyridine and the receptor) would behave in a very similar fashion to the PIM-1 and PIM-3 isoforms. However, the benzothienopyrimidinone analogue **43u**, showed IC_{50} values of 41 nM and 487 nM against PIM-1 and PIM-3 respectively, whereas the phenyl pyrimidinone analogue **99** showed values of 331 nM and 374 nM against PIM-1 and PIM-3, displaying a lower potency for PIM-1 and little selectivity between the two isoforms. The differences observed between selectivity/potency observed could be associated to the different binding pose that these series of compounds might present within the PIM kinases.

For compound **100**, much lower relative activity was observed, with IC_{50} values of 1.2 µM for PIM-1, 9.2 µM for PIM-2, and 3.1 µM for PIM-3. This trend is supported by both the PI and DSF assay. For example, the PI assay showed percentages of inhibition lower than 50% for PIM-1, PIM-2 and PIM-3, at 1 µM concentration (42%, 22%, and 19%, respectively). The loss of potency when changing from the 4-aminopyridine to the 3-aminopyridine is not fully understood within this series. However, a possible explanation could be that the 3-aminopyridine ligand is not placed in a suitable orientation within the PIM active site to form potential hydrogen-bonding interactions, leading to a loss of activity.

Finally, **101** showed IC_{50} values of 488 nM (PIM-1), 9.4 µM (PIM-2) and 2.5 µM (PIM-3) which correlated with both the PI and DSF data. Although the potency for this compound was not ideal, we were very pleased to observe a 5-fold selectivity for PIM-1 over PIM-3, and a 19-fold selectivity for PIM-1 over PIM-2. We were interested in understanding the binding of this analogue within the PIM-1 active site. Attempts at crystallizing **101** with PIM-1 have not been successful, but our collaborators are currently optimizing the crystallisation conditions and we hope to obtain crystals in the future.

In summary, although the initial target compounds (**91**–**96**) did provide low PIM potency, optimization of the synthetic route provided **97**–**101**, which had excellent selectivity against the CLK kinases, the DYRK kinases, and the SRPK kinases, and provided reasonable potencies towards PIM-1 and PIM-3 with IC_{50} values between 300–500 nM. We were excited to see that the novel scaffold had the potential to be used in medicinal chemistry programs, as

high/moderate inhibitory activity was observed with the PIM-1 and PIM-3 kinases. Furthermore, the scaffold showed remarkable selectivity over CLK4, which was the aim of this project, and we were able to achieve after a small SAR study.

The DSF results obtained for **87** were intriguing, and it is important to mention that kinetic assays were not available to us when we first obtained the DSF results for **87**, and so at that time, we decided to further explore this data by carrying out a small SAR study, which was conducted by undergraduate dissertation student, Steven Kay.

3.4. Design and synthesis of analogues of 87

Compound **87** showed ΔT_m values of 2.8 °C (PIM-1), 1.3 °C (PIM-2) and 11.5 °C (PIM-3), suggesting selectivity towards the PIM-3 isoform (Figure 54). Furthermore, **87** also displayed encouraging potential selectivity over CLK4 (ΔT_m: 5.9 °C), CLK1 (ΔT_m: 3.0 °C), as well as CLK3, the DYRK family and the SRPK kinases, with no affinity observed (Figure 54). As previously mentioned, the DSF data for compound **87** could be a particularly unreliable indication of potency, as the compound could be binding to other sites of the receptor due to its small size. This was indeed confirmed, later on, *via* kinetic assays that showed the compound's inactivity within the PIM isoforms (Table XVIII). Nevertheless, the biochemical data was not obtained until the last month of this project, and in fact, very encouraging results were obtained within this SAR study.

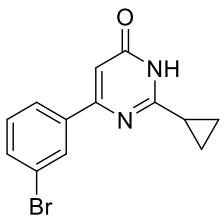

87

Compound	PIM-1 (ΔT_m, °C)	PIM-2 (ΔT_m, °C)	PIM-3 (ΔT_m, °C)	CLK4 (ΔT_m, °C)	CLK1 (ΔT_m, °C)	CLK3 (ΔT_m, °C)	DYRK1 (ΔT_m, °C)	DYRK2 (ΔT_m, °C)	SRPK1 (ΔT_m, °C)	SRPK2 (ΔT_m, °C)
87	2.8	1.3	11.5	5.9	3	0.1	1.7	0.9	0.1	0

***Figure 54**: DSF data for compound **87**.*

The SAR studies performed on this project were achieved by following the iterative cycle identified in Figure 55. The process involved initially implementing computational methods to perform molecular modelling studies. During the course of this side-project, the PIM-3 virtual model was not yet constructed; therefore, the crystal structure of PIM-1 was used together with a virtual library of analogues of **87**. Chemical diversity was added to this intermediate to assess the topology of PIM-1 active site. Potential intermolecular interactions (hydrogen bonding, hydrophobic) between the molecules and the amino acid residues within the protein were then assessed, to determine potential target molecules for synthesis.

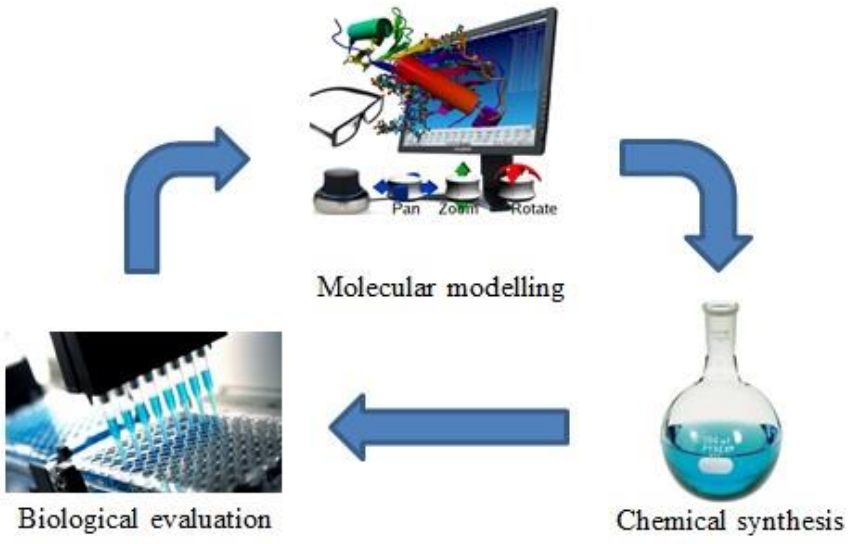

Figure 55: *Diagram depicting the cycle for SAR development.*

An initial set of target molecules were identified from the molecular modelling studies, prior to synthesis and biological evaluation in the DSF assay. As a starting point we generated 50 virtual compounds based around the phenyl pyrimidinone scaffold. All 50 molecules were individually analyzed through molecular modelling studies. The compounds were energy minimized and docked in the PIM-1 active site, to facilitate predictions of the binding mode and potential interactions formed between each molecule and the PIM-1 protein. This virtual screening led to a small library of compounds (Figure 56), with different functionality on the aryl ring.

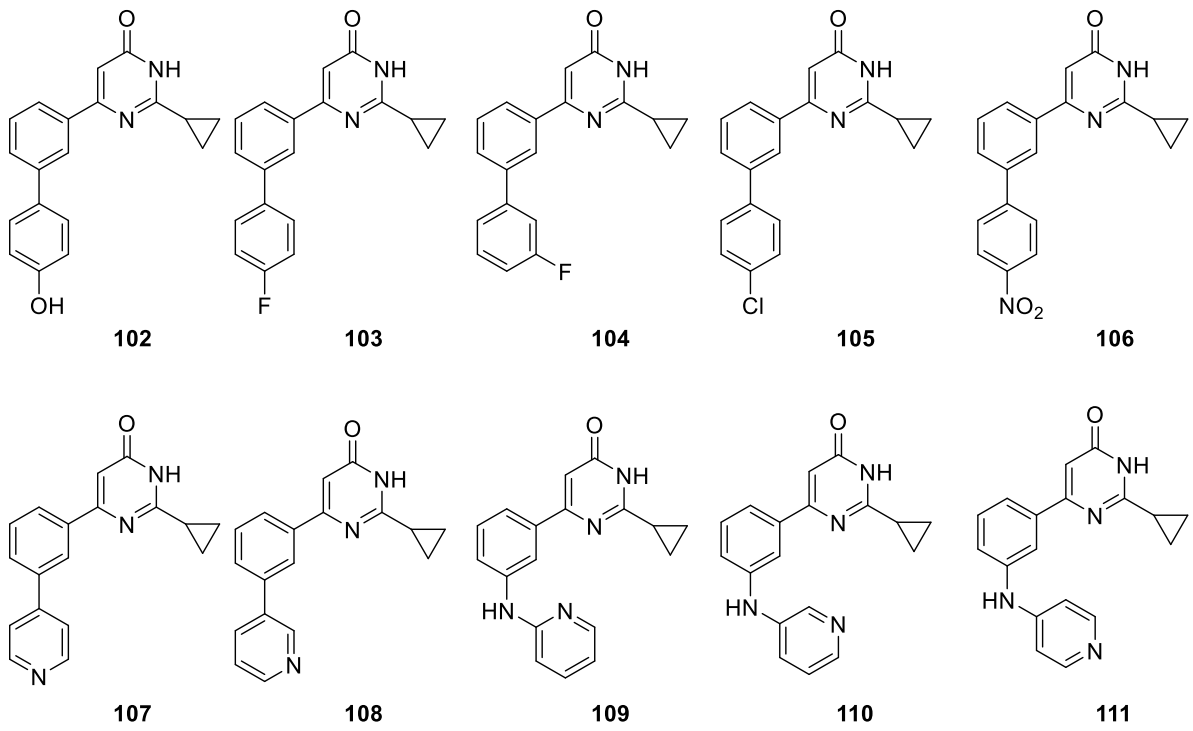

***Figure 56**: Compounds **102**–**111**.*

Details of the synthetic route adopted for the generation of **102**–**111** are detailed in Scheme VII. Preparation of large amounts of intermediate **87** was required and it was carried out using the general procedure shown previously (Scheme V). Functionalization of **87** was achieved by using Suzuki-Miyaura conditions (Path A), which afforded compounds **102**–**108** in high yields, or Buchwald-Hartwig conditions (Path B), which provided analogues **109**–**111**.

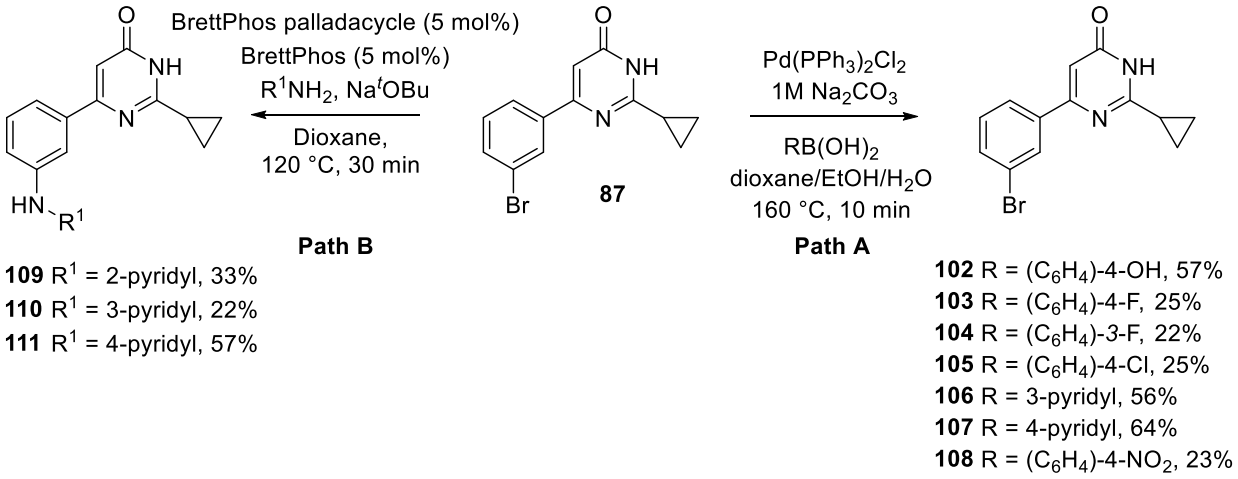

***Scheme VII**: General conditions for the synthesis of **102**–**111**.*

The compounds synthesized were chosen from careful analysis of the molecular modelling data obtained. Through these molecular modelling studies, it was seen that the scaffold containing the cyclopropyl ring was imitating the binding pose as observed for the benzothienopyrimidinone scaffold. All compounds chosen showed the main interaction with the Lys67 and Asp186 from the PIM-1 receptor. An example of molecule **104** docked in the PIM-1 active site is shown in Figure 57.

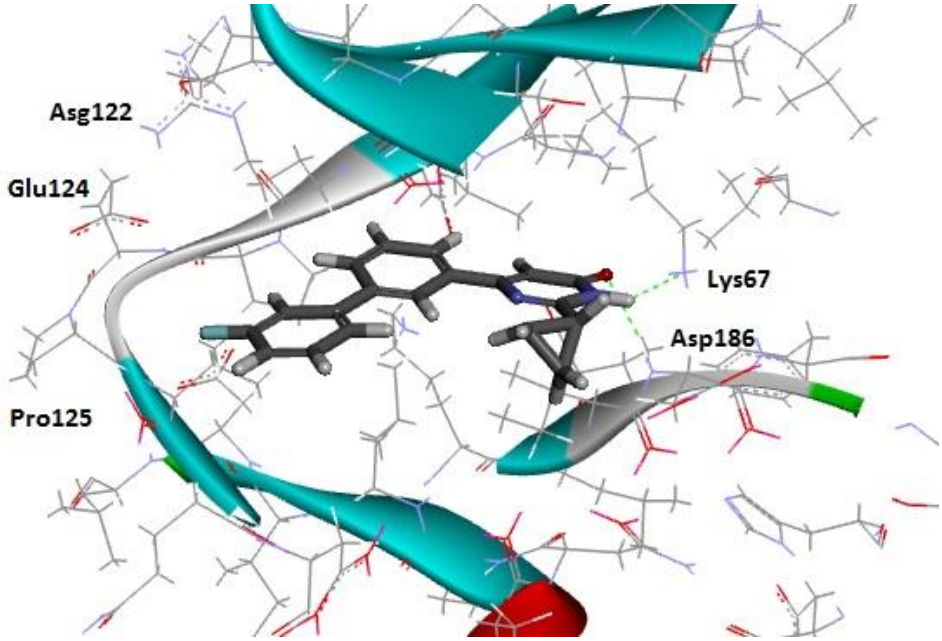

***Figure 57**: Virtual screening of **104** docked in PIM-1 active site.*

3.4.1. DSF assay results for compounds 102–111

Compounds **102**–**108** showed some promising initial results for the series within the DSF assay (Table XX), and allowed some early conclusions to be drawn. The standout observation was that the halogen derivatives (**103–105**), showed little to no affinity, against the three isoforms PIM-1, PIM-2 and PIM-3. The lack of affinity observed for the halogen derivatives could be due to the lack of interactions formed with the receptor, or because they do not adequately occupy the chemical space of the active site.

Table XX: *DSF assay data for compounds **102–108**.*

Compound	PIM-1 (ΔT_m, °C)	PIM-2 (ΔT_m, °C)	PIM-3 (ΔT_m, °C)	CLK4 (ΔT_m, °C)	CLK1 (ΔT_m, °C)	CLK3 (ΔT_m, °C)	DYRK1A (ΔT_m, °C)	DYRK2A (ΔT_m, °C)	SRPK1 (ΔT_m, °C)	SRPK2 (ΔT_m, °C)
102	5.7	0.0	6.4	3.2	2.8	0.0	1.7	2.5	0.2	0.0
103	1.9	0.0	2.6	0.2	0.4	0.0	0.2	0.0	0.0	0.0
104	1.1	0.6	2.5	0.0	0.4	0.0	0.0	0.0	0.0	0.0
105	0.8	1.6	1.3	0.0	0.4	0.0	0.0	0.0	0.0	0.0
106	0.0	0.3	0.4	0.3	0.4	0.0	0.1	0.1	0.0	0.0
107	4.3	1.4	5.0	1.6	2.0	0.0	0.5	0.9	0.0	0.0
108	4.5	0.7	5.1	4.4	2.8	0.0	2.1	1.9	0.0	0.0

Compound **102** exhibited the highest value within this series. The compound showed moderate affinity towards PIM-1 (ΔT_m: 5.7 °C) and PIM-3 (ΔT_m: 6.4 °C) but excellent apparent selectivity over the PIM-2 isoform (ΔT_m: 0 °C) as well as CLK4 (ΔT_m: 3.2 °C), CLK1 (ΔT_m: 2.8 °C) and CLK3, the DYRK and the SRPK kinases, which displayed little to no activity. A possible explanation for this affinity could be due to the development of a potential interaction, between the phenol group and a hydrogen bond acceptor within the protein.

Compounds **105** and **106** also showed lack of affinity with ΔT_m values of 0–1.6 °C for all the kinases examined. This apparent inactivity could be due to the compound not fitting within the PIM-1 active site in the way that the molecular modelling studies predicted.

Compounds **107** and **108**, containing pyridyl substituents also showed moderate affinities towards PIM-1 and PIM-3. Both compounds showed similar behaviour within the PIM kinases, with ΔT_m values of 4.3–4.5 °C for PIM-1, 0.7–1.4 °C for PIM-2, and 5.0–5.1°C for PIM-3. The 4-pyridyl substituent **108** also showed some cross-reactivity with the CLK4 isoform (ΔT_m value of 4.4 °C). Nevertheless, it is important to highlight that, overall, excellent selectivity was displayed over the CLK kinases, DYRK kinases and the SRPK kinases, within this series. Furthermore, we were very encouraged by these results as a preference for PIM-3 over PIM-1 affinity was observed, which constituted the aim for this final year project.

Finally, the DSF assay results obtained for the amino pyridine derivatives **109**–**111** are presented in Table XXI.

Table XXI: *DSF assay results for compounds **109**, **110** and **111**.*

Compound	PIM-1 (ΔTm, ºC)	PIM-2 (ΔT_m, ºC)	PIM-3 (ΔT_m, ºC)	CLK4 (ΔT_m, ºC)	CLK1 (ΔT_m, ºC)	CLK3 (ΔT_m, ºC)	DYRK1A (ΔT_m, ºC)	DYRK2A (ΔT_m, ºC)	SRPK1 (ΔT_m, ºC)	SRPK2 (ΔT_m, ºC)
109	4.5	0.5	4.9	2.3	2.7	0.9	5.6	2.6	0.1	0.0
110	3.1	0.1	2.2	0.7	0.5	0.0	1.8	0.8	0.0	0.0
111	3.4	0.0	4.8	1.0	1.7	0.0	0.0	0.8	0.0	0.0

Compounds **109** and **111** also showed a preference for PIM-3 over PIM-1 and PIM-2. The Buchwald-Hartwig conditions used for the synthesis of these analogues are detailed in Scheme VII.

Compound **109** displayed a ΔT_m value of 4.5 °C for the PIM-1 isoform, little affinity for the PIM-2 isoform (0.5 °C), and a ΔT_m value of 4.9 °C for the PIM-3 isoform. The compound showed moderate selectivity over the CLK kinases with ΔT_m values between 0.9–2.7 °C for CLK4, CLK1, and CLK3, a higher affinity for DYRK1A (ΔT_m: 5.6 °C), and good selectivity over the SRPK kinases. Compound **110**, which contains a 3-aminopyridyl moiety, displayed lower affinities. A possible explanation is that the 3-pyridyl group was not oriented within the PIM-1 active site in such a way to be able to form potential hydrogen-bonding interactions, leading to a lower affinity. Compound **111** displayed good selectivity for PIM-3 (ΔT_m: 4.8 °C) over PIM-1 (ΔT_m: 3.4 °C), as well as an excellent selectivity over PIM-2, the CLK kinases, and the SRPK kinases. The degree of selectivity observed towards PIM-3 for **111** was very encouraging, and biochemical data would be key to drawing a solid conclusion on the PIM-3 activity/selectivity.

3.4.2. Biochemical evaluation of 102–108

The PI data for compounds **102**–**108** against PIM-1, PIM-2, and PIM-3 was obtained as well as the IC_{50} values for the most active compounds. Each compound was dosed in each isoform at 10 µM and 1 µM concentration, and the percentage of inhibition was calculated. The results obtained for compounds **102**–**108** in this assay are detailed in Table XXII.

Table XXII: *IC_{50} and PI data for compounds **102**–**108**.*

Compound	PIM-1 (IC_{50}, nM)	PIM-1 (10 µM)	PIM-1 (1 µM)	PIM-2 (IC_{50}, nM)	PIM-2 (10 µM)	PIM-2 (1 µM)	PIM-3 (IC_{50}, nM)	PIM-3 (10 µM)	PIM-3 (1 µM)
102		57	14		48	10		60	5
103		18	-7		7	5		22	7
104		16	12		6	-11		37	5
105		7	2		5	10		17	-5
107	1030	88	64	>50000	59	24	5450	80	45
108	1060	83	44	>50000	31	8	680	82	42

The PI data for compound **102** is an example for why any conclusions drawn from initial DSF data should be taken with caution. Compound **102** exhibited the highest PIM-1 and PIM-3 ΔT_m values: 5.7 °C for PIM-1 and 6.4 °C for PIM-3. However, when tested in a kinetic assay, the actual PI was moderate for the PIM-1 isoform at a 10 µM dose (57%) as well as at 1 µM dose (14%). A similar trend was observed for the PI values of PIM-2 at both 10 µM (48%) and 1 µM (10%), and for the PIM-3 isoform, which showed 60% inhibition at 10 µM and 5% at 1µM. This data showed that **102**, containing the 4-hydroxyphenyl substituent, did not show significant activity or selectivity within the PIM kinases, and therefore was not be further analyzed.

The DSF data correlated well with the PI data for compounds **103**–**105**. Compounds **103**, **104** and **105** showed little to no affinity within the DSF assay, presumably due to the lack of hydrogen bonding interactions between the aryl ring and the PIM receptor. Confirmation was achieved by the PI data, which displayed poor percentages of inhibition at both 10 µM and 1 µM doses. These data suggested that halogen substituted phenyl groups were not tolerated within that area of the receptor.

Finally, the pyridyl substituents, **107** and **108**, showed encouraging data. Both compounds displayed similar trends, with strong-moderate activity for PIM-1 and PIM-3 in the PI assay and poor activity for PIM-3. Both compounds were active, with similar values for PIM-1 at 10 µM (88% for **107**, 86% for **108**) and 1 µM (64% for **107**, and 44% for **108**) which correlated with the final IC_{50} values obtained for **107** (1.03 µM) and **108** (1.06 µM). Similar behaviour was observed for **107** and **108** in PIM-2, both compounds showed little to no activity for PIM-2 which correlated with the observed IC_{50} values (**107**: 50 µM, **108**: 50 µM). Finally, for the PIM-3 isoform, the compounds showed lower activity (**107**: 5.45 µM, **108**: 680 nM). Nevertheless, the PIM-1 IC_{50} values for molecules **107** and **108** were both approximately 1

μM, which, for an initial SAR study on a novel scaffold, was a respectable value, with the potential for future optimization.

Finally, compounds **106**, **109**, **110** and **111** were also tested in a biochemical assay. These compounds were part of a second batch that was directly tested in a dose-response experiment (Table XXIII) against PIM-1, PIM-2, and PIM-3. For these reason, PI data was not obtained.

Table XXIII: *IC_{50} values for **106**, **109**, **110** and **111**.*

Compounds	PIM-1 (IC_{50}, nM)	PIM-2 (IC_{50}, nM)	PIM-3 (IC_{50}, nM)
106	730	>25000	>50000
109	210	>25000	70
110	730	>25000	660
111	1200	>25000	120

The first conclusion drawn from the data in Table XXIII was that the selectivity for PIM-1 against PIM-2, was maintained (**106**, **109**–**111**, PIM-2 IC_{50} = >25 μM). The initial aim of the project was to design and synthesize compounds using the new scaffold **87** that could be further optimized as future PIM chemical probes. Within this second set of compounds, we had already achieved very promising IC_{50} values. The data for compound **106** provided IC_{50} values for PIM-2 and PIM-3 of >25 μM and >50 μM, respectively, both indicating weak binding affinity for these two isoforms. The selectivity for PIM-1 was confirmed by the PIM-1 IC_{50} value (0.73 μM), showing that ligand **106** has a very encouraging selectivity profile for PIM-1 over PIM-2 and PIM-3. This suggested the formation of an additional interaction between the nitro group and the PIM-1 isoform (that is not taking place in both PIM-2 and PIM-3) resulting in an increased activity with this isoform.

Surprisingly, some very interesting data was obtained for compounds containing an aminopyridyl functionality (**109**–**111**). All three compounds showed selectivity for PIM-1 and PIM-3 over PIM-2 but also, the compounds displayed very good potency for PIM-3 over PIM-1, with low nanomolar IC_{50} values. For example, **109** (containing the 2-amino pyridinyl substituent) improved the PIM-3 potency to an IC_{50} value of 70 nM (PIM-3), showing some low-moderate selectivity over PIM-1 (IC_{50}: 210 nM) and excellent selectivity over PIM-2 (IC_{50}: > 25000 nM). Compound **110** (pyridine-3-ylamino) displayed minor selectivity towards PIM-3. The IC_{50} data observed for PIM-1 and PIM-3 was very similar (PIM-1 IC_{50}: 730 nM, PIM-3 IC_{50}: 660 nM) suggesting that the pyridine-3-ylamino substituent was able to form

hydrogen bonding interactions with both isoforms, therefore, decreasing the selectivity. Finally, the most promising candidate within this series was **111** as it exhibited a 10-fold selectivity for PIM-3 (0.12 μM) over PIM-1 (1.20 μM). Attempts at obtaining a crystal structure of **111** in PIM-3 were not successful to date. However, this is currently ongoing and if successful, will constitute an excellent basis for further optimization within this series.

In conclusion, it is known that chemical probes or potential kinase inhibitors are generally reported with low nanomolar IC_{50} values. High activities are rarely achieved with initial compounds and generally require extensive and time-consuming SAR studies that allow an understanding of the binding between the scaffold and the receptor, which allows for optimization of the potency. In our case, within two rounds of SAR studies (**102**–**111**) on this project, multiple analogues with nM potency were designed with moderate to high selectivity, which is an extremely promising start for a novel scaffold, with a great potential for further optimization.

3.5. One-pot synthesis of intermediate 87

One-pot synthesis is normally referred to as a strategy to improve the efficiency of a chemical transformation where a reactant is subjected to multiple chemical reactions in a single reactor. This strategy is extremely desirable as it avoids multiple purifications and reduces the time involved for each transfomation, as well as constituting a more economical process.[80, 81]

The phenyl pyrimidinone scaffold showed excellent biological results towards the PIM kinases with the potential for multiple points of diversity, suggesting that the scaffold had the potential to be further studied in future programmes. The synthetic procedure for the synthesis of intermediate **87** involved a very simple and high yielding two step procedure that allowed the formation of **87** in large quantities for further functionalization.

With this in mind, it was proposed that the synthesis of **87** could be achieved *via* a one-pot synthesis strategy, preparing the HCl salt of cyclopropylcarboxamidine **113** *in-situ*, with subsequent addition of intermediate **85** to the same reaction mixture (Scheme VIII). Previous work developed in our group confirmed that reaction of the amidine HCl salt **113** with intermediate **85** was successful, so the primary objective was to study if *in situ* formation of **113** was possible. A literature search revealed some precedent for the formation of amidines using NH_4Cl and NaOEt with a wide variety of nitriles.[82, 83]

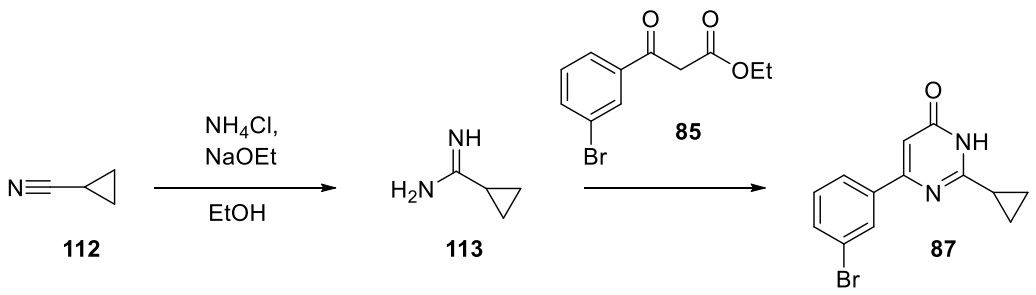

***Scheme VIII**: Proposed one-pot synthesis of **87**.*

The solvent chosen for this transformation was ethanol as previous work in the group (Scheme V) showed that formation of **87** was achieved in high yields (65%) using this solvent. We also believed that the use of a microwave reactor would result in reduced reaction times and costs. In order to convert the thermal process into a microwave procedure, we initially studied the formation of **87** using microwave irradiation before the one-pot procedure was studied further.

3.5.1. Microwave-assisted conditions for the preparation of 87

Intermediate **87** was isolated in 65% yield after refluxing the reaction mixture in ethanol for 36 hours (Scheme IX). A small study of the reaction conditions was carried out to assess the possibility of forming **87** using a microwave reactor.

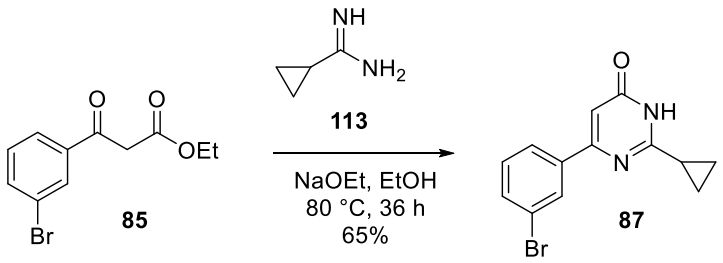

***Scheme IX**: Thermal conditions for the synthesis of **87**.*

After a short optimization of the reaction conditions (Table XXIV) we were able to isolate **87** in 40% yield using microwave assisted conditions with 1 equivalent of commercially available **113**, EtOH (0.4 M), after 60 minutes at 100 °C. The thermal conditions provided a

higher yield (65%) for this transformation. However, the microwave conditions allowed the use of increased temperature and pressure, resulting in shorter reaction times (60 minutes).

Table XXIV: *Study of the microwave assisted synthesis of **87**.*

Test reaction	113 (mmol)	85 (mmol)	NaOEt (mmol)	EtOH (M)	Temp (° C)	Time (min)	Yield (%)
1	0.37	0.37	0.77	0.4	140	30	25
2	0.37	0.37	0.77	0.4	100	60	39
3	0.37	0.74	0.77	0.4	100	60	40

The drawback of this reaction procedure was the formation of additional unidentifiable side products which reduced the isolated yield to 39–40% (entry 2/3) compared to the thermal conditions (65%). It was believed that the reaction conditions could be improved with additional studies. However, this optimization was carried out in order to apply this transformation to the one-pot synthesis strategy of intermediate **87**.

The next step to allow a one-pot procedure of **87** was the development of conditions for the formation of **113** *in situ*. To achieve this, both thermal and microwave conditions were examined.

3.5.2. Study of the generation of 113 *in situ*

Previous work in the group for the generation of **113** using thermal conditions proved unsuccessful (Table XXV). An initial approach was adopted using ammonium chloride, together with sodium ethoxide in EtOH to obtain **113** (Scheme X). A literature search[82] revealed limited evidence that this was possible using the cyclopropyl derivative so a stoichiometric mixture of reagents was used in the initial reaction, to assess feasibility. As discussed previously, EtOH was used as a solvent in order to adapt this procedure to the one-pot strategy.

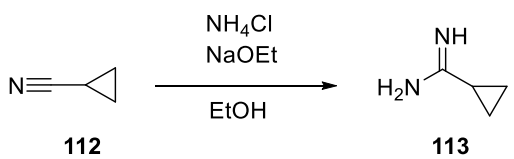

112 **113**

***Scheme X**: Propose synthesis of **113**.*

Table XXV: *Conditions towards the synthesis of **113**.*

Entry	112 (mmol)	NH_4Cl (mmol)	NaOEt (mmol)	Solvent	Temp (° C)	Time (min)	Notes
1	0.37	0.37	-	EtOH	100	60	No reaction
2	0.37	-	0.37	EtOH	100	60	No reaction
3	0.37	0.37	0.37	EtOH	100	60	No reaction

None of the attempted conditions (Table XXV) for the proposed route resulted in **113** by ^{1}H NMR analysis after work-up. An additional study was carried out using other sources of NH_3 such as NH_4OH (33% aqueous solution) or NH_3 in an organic solvent (EtOH or MeOH), this study is summarized in Table XXVI.

Table XXVI: *Optimization studies on the synthesis of **113**.*

Entry	Reagent	NH_3 source	Conditions	Time	Temperature	Outcome
1	**112**	NH_4OH (0.5 M)	Thermal	16 h	rt	No reaction
2	**112**	NH_4OH (0.5 M)	Thermal	16 h	100 °C	No reaction
3	**112**	NH_4OH (0.5 M)	Microwave	3 h	120 °C	46%
4	**112**	NH_4OH (0.5 M)	Microwave	5 h	120 °C	45%
5	**112**	2 M NH_3 in EtOH (0.5 M)	Microwave	3 h	80 °C	No reaction
6	**112**	2 M NH_3 in MeOH (0.5 M)	Microwave	3 h	80 °C	No reaction
7	**112**	7 M NH_3 in MeOH (0.5 M)	Microwave	3 h	80 °C	No reaction

The first source of NH_3 used was NH_3 in H_2O (NH_4OH 33% aqueous solution). We were aware that using H_2O as a solvent could be an inconvenience to our one-pot strategy. However, understanding the reaction and formation of **113** was a priority and conditions could be optimized after becoming familiar with the transformation. Using NH_4OH under thermal conditions (entries 1 and 2, Table XXVI) proved unsuccessful. However, heating NH_4OH for 3 hours at 120 °C in the microwave followed by subsequent solvent evaporation under reduced pressure, afforded **113** in 46% yield, as a white solid, without the need for further purification. Increasing the reaction time to 5 hours (entry 5) did not increase the isolated yield further (45%).

Using 2 M NH_3 in EtOH (entry 5) or 2 M NH_3 in MeOH (entry 6) also proved unsuccessful, as was using 7 M NH_3 in MeOH (entry 7). Attempts at trying to optimize the reaction conditions further using NH_4OH are currently ongoing in the group.

We were encouraged by these results as formation of **113** *in situ* was possible after a short optimization of the reaction. It is important to note that this successful reaction of NH_4OH with reagent **112** to provide **113** represents an inconvenience to our one-pot strategy. The use of EtOH as the solvent for the one-pot procedure would be desirable. However, we thought that we should investigate whether the formation of **87** could be achieved using H_2O instead of EtOH as the reaction medium (Scheme XI). Using H_2O could be beneficial to couple the amidine formation detailed in Table XXVI (entry 3) to the cyclocondensation with intermediate **85**.

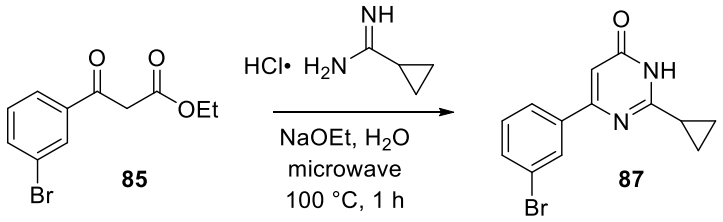

***Scheme XI**: Proposed reaction for the formation of **87** using H_2O as solvent.*

LCMS data of the attempted formation of **87** in H_2O indicated the presence of **87** together with unreacted starting material. When using EtOH, **87** precipitated from the reaction mixture and we are able to obtain this compound by filtration in high yield without further purification. When H_2O was used, no precipitation of the desired product was observed. Nevertheless, it is important to point out that the formation of **87** was observed by LCMS when using H_2O as the solvent. If required, potential optimization of the reaction in H_2O could be carried out.

3.5.3. Future work

Our efforts to develop a one-pot procedure for the synthesis of **87** are still ongoing in the group (Scheme XII).

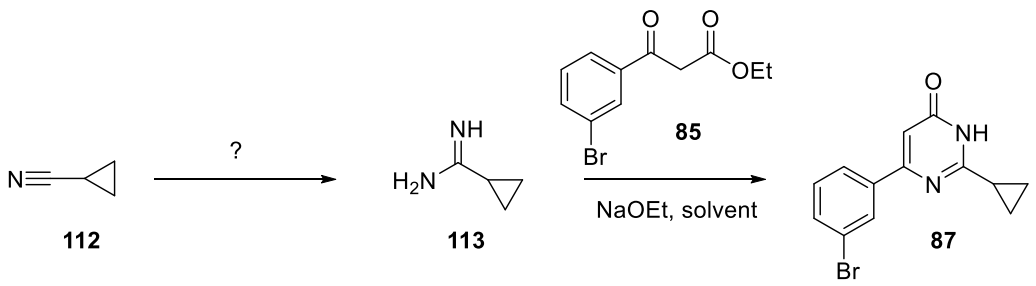

***Scheme XII**: General conditions for the one-pot synthesis of **87**.*

We have already established conditions for the formation of **87** by reacting **113** and **85** under thermal or microwave assisted conditions (Scheme XIII). In order to develop a one-pot strategy, optimization of the formation of **113** in EtOH is still needed. However, other solvent mixtures such as H_2O/EtOH, dioxane, dioxane/H_2O, amongst others, might also be taken into consideration if a change of solvent is required.

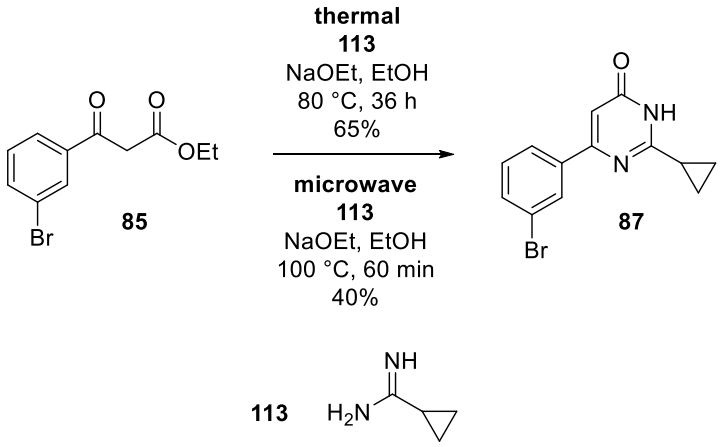

***Scheme XIII**: Thermal and microwave conditions for the synthesis of **87**.*

Regarding the formation of the amidine **113**, some studies have been carried out with little success to date. Formation of **113** was observed when using NH_4OH (Table XXVI, entry 3), however, the use of H_2O in the one-pot synthesis is not desirable and further optimization is required. We believe that the formation of **113** *in situ* will be achieved with further studies, for example, Caron et al. published an alternative approach for the synthesis of amidines *via* formation of 2,2,2-trifluoroethyl or trichloroethyl imidates as intermidiates (Scheme XIV). In

their procedure, longer reaction times as well as low temperatures were required for the formation of both the imidate and the amidine.

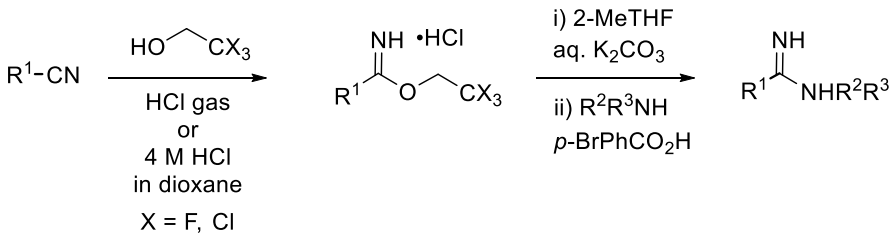

***Scheme XIV**: Synthesis of amidines published by Caron et al.*[84]

This approach will be the next step within our laboratory to potentially develop the synthesis of **113**. Furthermore, alternative methods for the synthesis of amidines using NH_3 (gas) and HCl (gas) have also been described,[85, 86] and provide alternative directions of research if further development is needed. Finally, it is our aim to design conditions that will apply to a wide variety of nitriles, which will subsequently provide an efficient synthesis of intermediates and therefore, analogues, with the potential of further functionalization.

3.6. Conclusions

The initial aims of examining the phenyl pyrimidinone scaffold were to analyze whether the thiophene ring was required for PIM potency, but also, if removing the thiophene ring could improve the selectivity for PIM over the CLK4 isoform. A novel scaffold was designed, containing the important pyrimidinone ring, which was required for PIM potency. A new series of compounds (**91**–**111**) was then designed, performing SAR studies, which were driven by molecular modelling, chemical synthesis and biological evaluation.

Furthermore, the three-step chemical route that was established enabled the formation of final compounds, with the potential for late stage diversification. Following the development of the chemistry, a SAR study was performed and compounds **91**–**111** were prepared.

The small SAR study provided excellent results. The new scaffold showed a decreased affinity for the PIM isoforms compared to the benzothienopyrimidinone series. However, the DSF assay suggested there was excellent selectivity over CLK kinases, SRPK kinases and

DYRK kinases, but most importantly, over the CLK4 kinase. Furthermore, the scaffold showed a preference for the PIM-3 isoform over the PIM-1 and PIM-2 isoforms for compounds **109** and **111**, which as a starting point, was encouraging for the development of PIM-3 chemical probes.

Despite the decreased potencies observed within this scaffold, we were able to obtain low nanomolar values for PIM-1 and PIM-3. For example, **109** (Figure 58) showed an IC_{50} of 210 nM for PIM-1, > 25 µM for PIM-2, and 70 nM for PIM-3. Furthermore, the compound showed a good selectivity profile in the DSF assay, with only a low affinity for CLK4 (ΔT_m: 2.3 °C) and moderate affininty for DYRK1A (ΔT_m: 5.6 °C). We believe that the increase in potency might be due to the aminopyridine moiety forming hydrogen-bonding interactions with the receptor. A crystal structure of **109** in PIM-1 or PIM-3 would be able to provide further information, and attempts at crystallizing **109** in either the PIM-1 or PIM-3 isoforms are currently ongoing.

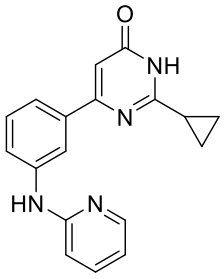

109

***Figure 58**: Structure of compound **109**.*

Finally, the low nanomolar activities observed towards the PIM kinases suggested that the new phenyl pyrimidinone scaffold has the potential to be further studied in future medicinal chemistry programmes. It is important to note that with a three-step synthetic procedure we prepared a series of final compounds showing nanomolar inhibitory activities against a series of significant kinase targets.

A one-pot reaction was examined for the generation of **87**, by formation of the primary amidine derivative **113** *in situ*, followed by reaction with intermediate **85** (Scheme XV). The step involving the reaction between the cyclopropanecarboxamidine hydrochloride **113** and intermediate **85** was optimized using either thermal (65% yield, Scheme XIII) or microwave conditions (40%, Scheme XIII).

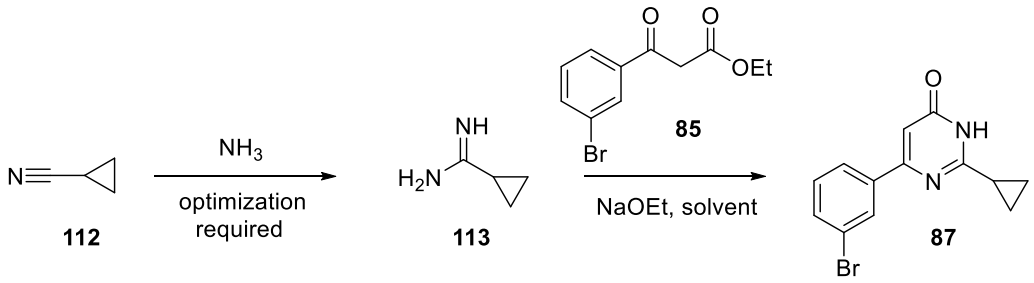

***Scheme XV**: General conditions for the one-pot synthesis of **87**.*

Attempts at preparing the cyclopropanecarboxamidine **113** as the HCl salt has been unsuccessful, but a 46% yield was obtained for **113** when using NH_4OH (33% solution, Table XXVI). The use of ethanol as the reaction solvent in the one-pot strategy would be highly desirable; therefore the generation of **113** *in situ* will be further studied. This transformation constitutes a priority, and further studies are currently undergoing within the group.

In summary, we believe that this new scaffold has the potential to find applications within medicinal chemistry. The scaffold provided excellent selectivity against the CLK kinases, DYRK kinases and SRPK kinases (on the basis of the DSF assay), as well as giving low nanomolar activity for the PIM-3 and PIM-1 isoforms. The crystal structure of one of these analogues in PIM-1 or PIM-3 will provide a better understanding of the behaviour of these analogues, and these results might prompt further SAR studies using this new scaffold.

The work developed within this series is very encouraging, and the results obtained to date constitute a promising start for this new scaffold, with a high potential for further functionalization. Future work within the group will assess directions on how best to move this project forward.

4. Benzothienodiazepines as chemical probes for PIM kinases

4.1. Discovery, design and synthesis of the new scaffold

Selectivity across the PIM isoforms as well as selectivity over the CLK4 kinase still remained a challenge to our project. It was observed through previous series that PIM-1 and PIM-3 potency was achievable as well as the selectivity over PIM-2, and that removal of the thiophene ring provided PIM selectivity over CLK4. However, full understanding of the differences between the PIM-1 and the PIM-3 isoforms to obtain selectivity had not been achieved.

These challenges led us to apply further modifications to the initial benzothienopyrimidinone scaffold to analyze the changes in potency and selectivity.

Recently, the SGC discovered an inhibitor of MAPK7 containing a seven-membered ring motif (Figure 59) that showed extraordinarily good potencies.[87] Our collaboration with the SGC motivated us to change the benzothienopyrimidinone core and introduce a seven-membered ring in order to analyze the effect of shape on binding within the three isoforms.

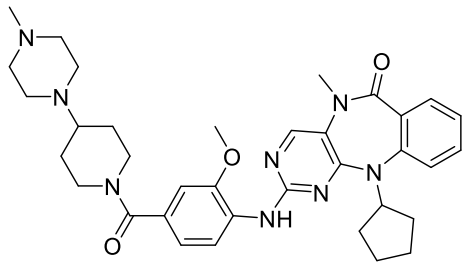

Figure 59*: Seven-membered ring MAPK7 inhibitor published by SGC.*

The new scaffold, a benzothienodiazepine ring (Figure 60), incorporates a seven-membered ring instead of the pyrimidinone ring seen in the previous scaffold. The amide moiety is maintained (which forms a hydrogen bonding interaction with the lysine) required for PIM potency. As an initial approach, a virtual library was designed in order to analyze the binding pose of this new scaffold within the PIM-1 isoform.

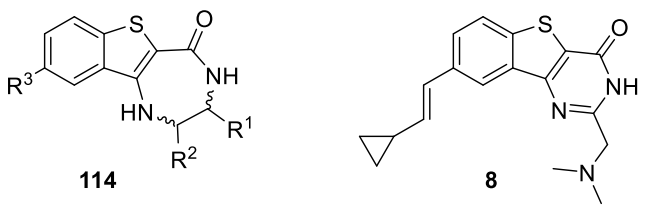

***Figure 60**: The new benzothienodiazepine scaffold **114** and the benzothienopyrimidinone compound **8**.*

From molecular modelling studies, it was observed that the new scaffold was imitating the binding observed for compound **8** (Figure 16 from Chapter 1, page 17). The compound was bound so that the R^3 group was facing the hinge region and the main interaction observed was between the amide from the diazepine ring and the Lys67 residue.

An extensive literature search showed that this chemotype, a five membered ring fused to a lactam, had been previously reported in other medicinal chemistry programs[88, 89] for the design and synthesis of Mitogen activated protein kinase-activated protein kinase 2 (MK2) inhibitors. More recently, a MK2 inhibitor based on a benzothienodiazepine scaffold[68, 69] (Figure 61) was discovered. Anderson *et al.* published **115** as an MK2 inhibitor with low nanomolar activity against MK2 and CDK2 (40 nM, and 12 nM, respectively) as well as good cellular data when analyzing the suppression of TNFα production in the U937 cell line, which is correlated with MK2 inhibition (IC_{50}: 700 nM).[67,68]

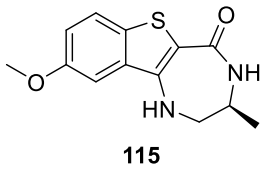

115

MK2 (IC_{50}): 40 nM
CDK2 (IC_{50}): 12 nM
U937 TNF_{∞} release (IC_{50}): 700 nM

***Figure 61**: Compound structure and kinetic data of **115**.*

Since the benzothienodiazepine scaffold offered low nanomolar activities against protein kinases as well as good cellular based data, we were encouraged to carry out a SAR study based on data obtained from the initial benzothienopyrimidinone scaffold introduced in Chapter 2.

4.2. Design and synthesis of the benzothienodiazepine scaffold

4.2.1. Initial SAR study: synthesis and evaluation of 117 and 118

Scheme XVI represents the synthetic route that was adopted for the synthesis of our seven-membered ring analogues **117** and **118**. The initial step of the synthesis involved an aromatic nucleophilic substitution of the benzonitrile **24** to afford the primary amine **34** in 96% yield. A Sandmeyer reaction then introduced a bromine to afford **116** in 64% yield. Buchwald-Hartwig coupling of **116** using Pd_2dba_3 and XantPhos, in dry DMF provided analogues **117** in moderate yields. The reaction was optimized when changing to amino alcohol derivatives, providing higher yields using dry toluene at 70 °C for 16 hours to afford analogues **118** in better yields.

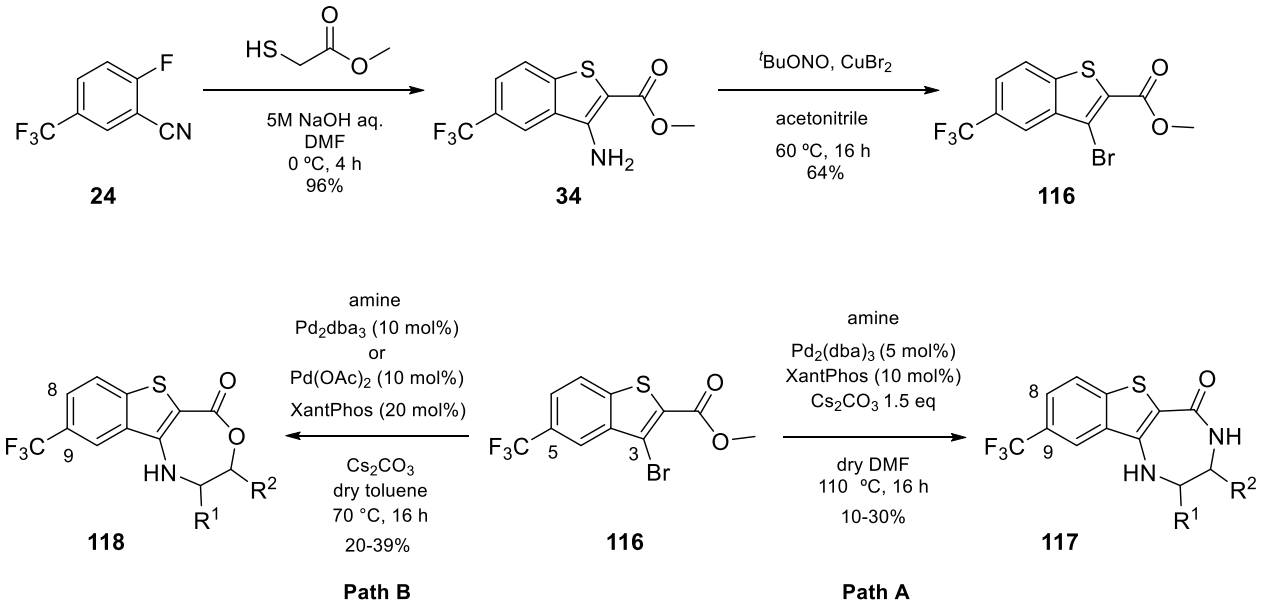

***Scheme XVI**: General conditions for the synthesis of derivatives **117** and **118**. Key positions within the scaffolds are also detailed.*

The trifluoromethyl group at position 5 in **116** proved to be key for the efficacy of the Buchwald-Hartwig coupling on **116**. Initial attempts to synthesize the desired final compounds using a chlorine at position 5 proved unsuccessful (presumably due to competitive oxidative addition into the C-Cl bond). The chlorine at position 5 could also undergo Buchwald-Hartwig couplings resulting in decreased yields. Furthermore, from previous data obtained (Figure 62), it was observed that the chlorine substituent provided little selectivity

within the isoforms as well as over the CLK4 isoform. The trifluoromethyl group substituent **49a**, on the other hand, showed slightly lower affinities for PIM-1 and PIM-3 but a much higher selectivity over CLK4 in the DSF assay, with a ΔT_m value of 0.5 °C for the CLK4 isoform, compared to the chlorine analogue **43a** (ΔT_m value of 4.7 °C). In order to avoid the cross-reactivity at position 5 of intermediate **116** during the Buchwald-Hartwig coupling and increase the selectivity over the CLK4 isoform, a trifluoromethyl group was introduced while the synthetic approach for the synthesis of the analogues containing the chlorine substituent was being optimized.

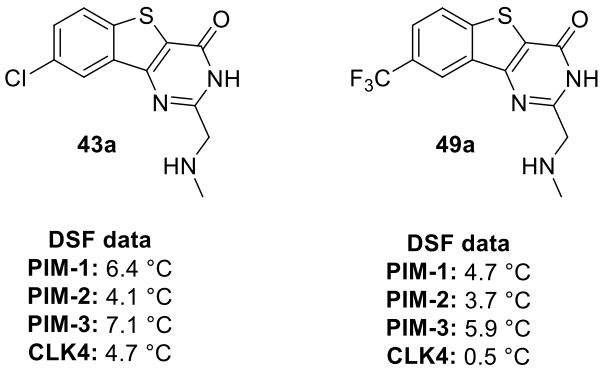

***Figure 62**: DSF data obtained for compounds **43a** and **49a**.*

Following the synthetic procedure detailed in Scheme XVI we undertook a SAR study within this series and we prepared compounds **119**–**126** (Figure 63). The yields for the final step, which corresponds to the Buchwald-Hartwig coupling followed by intramolecular cyclization are also presented (Scheme XVI, Path A and Path B).

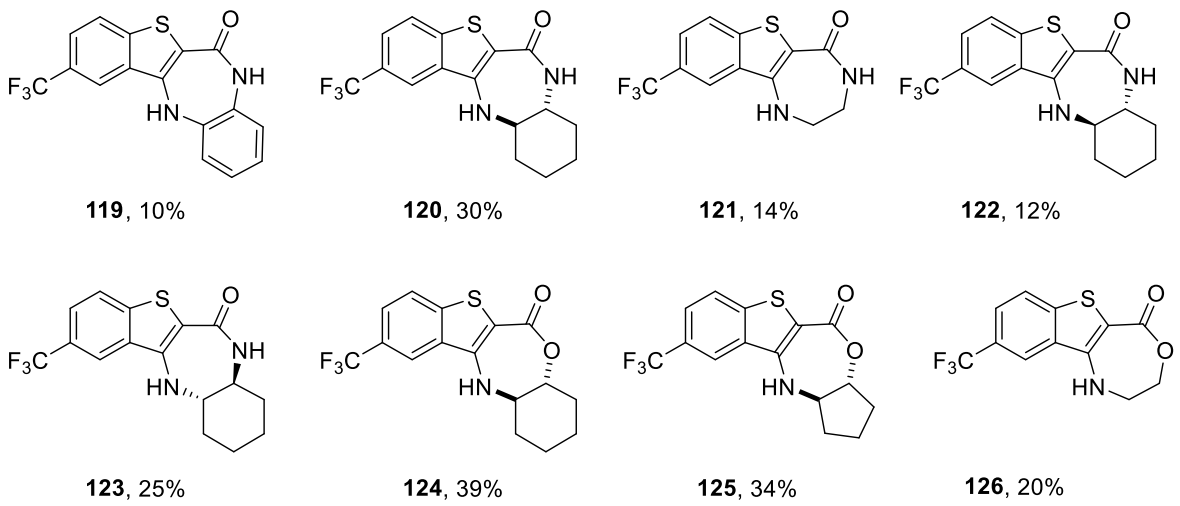

***Figure 63**: Compound structure for analogues **119**–**126** containing a trifluoromethyl group at position 9 of the benzothienodiazepine.*

Within the first SAR study, our priority was to analyze the need of having the amide moiety for PIM potency. To do so, commercially available 1,2-diaminobenzene, *trans*-1,2-diaminocyclohexane and ethylenediamine were used to prepare analogues **119**, **120** and **121**. In addition, **122** and **123**, which are the constituent enantiomers of **120**, were also synthesized to analyze any difference in activity. The amide moiety was changed to an ester when switching from the diamine substituent to an amino alcohol derivative. Commercially available ethanolamine was used for the synthesis of **126**. However, the amino alcohol precursors of compounds **124** and **125** were synthesized using the conditions presented in Scheme XVII.

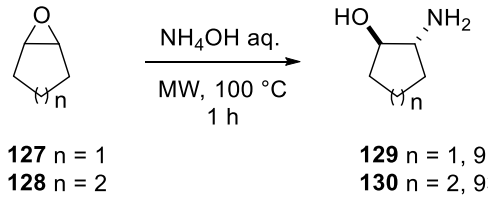

***Scheme XVII:** Conditions for the preparation of the amino alcohol precursors **129** and **130**.*

Ring opening of the epoxides **127** or **128** using ammonium hydroxide *via* an S_N2 type process afforded the amino alcohol derivatives **129** and **130** in 91% and 93% respectively, as racemic mixtures, which were used in the synthesis of analogues **124** and **125**.

The first set of compounds, **119**–**126**, was analyzed in the DSF assay, which gave very encouraging results (Table XXVII).

Table XXVII: *DSF data obtained for compounds **119**–**126**.*

Compound	PIM-1 (ΔT_m, °C)	PIM-2 (ΔT_m, °C)	PIM-3 (ΔT_m, °C)	CLK4 (ΔT_m, °C)	CLK1 (ΔT_m, °C)	CLK3 (ΔT_m, °C)	DYRK1A (ΔT_m, °C)	DYRK2 (ΔT_m, °C)	SRPK1 (ΔT_m, °C)	SRPK2 (ΔT_m, °C)
119	0.0	0.0	0.2	0.0	0.0	0.0	0.0	0.0	0.0	0.0
120	7.2	3.0	5.7	2.8	2.8	0.4	1.4	2.6	0.0	0.0
121	6.2	3.7	4.8	3.4	3.2	0.7	2.7	2.3	0.1	0.0
122	6.5	2.6	4.9	2.2	2.0	0.0	0.6	2.1	0.0	0.2
123	6.6	2.2	N/A	2.8	3.3	0.5	1.0	2.4	0.0	0.2
124	3.8	1.2	3.5	1.0	1.0	0.0	0.3	0.4	0.0	0.0
125	4.3	1.6	2.3	1.6	1.1	0.0	0.8	0.3	0.3	0.0
126	4.6	2.8	4.2	2.0	1.3	0.0	1.2	0.8	0.0	0.0

From this data, it was observed that the 1,2-diaminobenzene derivative **119** was not tolerated as no activity was observed for any of the protein kinases analyzed. Interestingly, compound **120** provided very good results. First of all, a high selectivity over the CLK3 isoform, the DYRK family and the SRPK family was observed. Furthermore, the DSF data values showed a ΔT_m of 7.2 °C for PIM-1, great selectivity over PIM-2 (ΔT_m of 3.0 °C), moderate selectivity over the PIM-3 isoform (ΔT_m of 5.7 °C) but a high selectivity over CLK4 and CLK1, with ΔT_m values of 2.8 °C for both kinases. For the corresponding enantiomers **122** and **123**, the data observed was very similar to the racemic analogue **120**. The PIM-1 potency decreased slightly for both enantiomers, but this could be due to the error associated with the DSF assay. Biochemical assay would provide a solid conclusion to the PIM-1 potency for analogue **120**. The degree of selectivity over PIM-2 and PIM-3 was maintained in both cases and in the same ratio to their racemic mixture. Compounds **122** and **123** showed ΔT_m values of 6.5 °C and 6.6 °C for the PIM-1 isoform, 2.6 °C and 2.2 °C for the PIM-2 isoform, and 4.9 °C (**122**) for the PIM-3 isoform. The data for **123** in the PIM-3 isoform was not obtained as not enough compound was available at the time of the assay.

Compound **121**, which keeps the amide moiety but does not contain the cyclohexane ring, reduced the PIM-1 activity to a ΔT_m value of 6.2 °C whilst maintaining the low activity observed for the remaining kinases, except PIM-3, which was also reduced to a ΔT_m value of 4.8 °C.

Interestingly, within this SAR, were the results obtained for **124**–**126**. It was observed that there was a loss of potency when changing the amide functional group to an ester derivative. For example, **124** which contains an ester group, reduced the PIM-1 ΔT_m to 3.8 °C compared to its analogue **120** (ΔT_m of 7.2 °C for PIM-1), suggesting that the amide from the diazepine ring was required for PIM potency and was probably forming a hydrogen bond interaction with the aspartic acid from the PIM-1 isoform. The same behaviour was observed for PIM-2 and PIM-3, where little activity was observed for **124** (ΔT_m of 1.2 °C and 3.5 °C for PIM-2 and PIM-3, respectively).

This phenomenon was also seen in **126**, the ester analogue of **121**, which had a reduced PIM potency with ΔT_m of 4.6 °C, 2.8 °C, and 4.2 °C for PIM-1, PIM-2 and PIM-3. Finally, the size of the cyclohexane ring did not seem to affect the PIM potency/selectivity as compared to its 5-membered ring analogue **125**. Compound **125**, which contains a five-membered ring cycloalkane, showed ΔT_m of 4.3 °C, 1.6 °C, and 2.3 °C for PIM-1, PIM-2 and PIM-3, similar to the DSF data obtained for the six-membered ring cycloalkane **124**, suggesting there was enough space to accommodate large substituents around that area of the receptor.

In summary, the compounds made in the first SAR study gave very encouraging results, showing excellent selectivity over CLK, DYRK, and SRPK kinases. Within the PIM isoforms, **120**, **122** and **123** gave the best results, highlighting the need for the amide motif within the diazepine ring for PIM potency. Compounds **120**, **122** and **123** showed good selectivity over PIM-2 and a moderate selectivity for PIM-1 over PIM-3.

While the first set of compounds was being analyzed in the DSF assay, a second set of compounds was prepared (Figure 64). A series of amino alcohols were used for the synthesis of further analogues. Compounds **131**–**137** (Figure 41) were synthesized using the route outlined in Scheme VII and were designed in order to assess whether the secondary amine from the diazepine ring was required for PIM potency. Other compounds from this study, **133**–**137**, were prepared from commercially available amino alcohols such as valinol (both enantiomers, **134** and **135**), and phenylalaninol (both enantiomers, **136** and **137**) to further investigate the topology of the area surrounding the right hand side of the molecule.

The yields shown in Figure 64 correspond to the Buchwald-Hartwig coupling followed by intramolecular cyclisation (Scheme XVI, Path B) required for the synthesis of the final compounds. The reaction proceeded in higher yields for secondary amines giving compounds **131**, **132** and **133** in 44%, 45% and 63% respectively, and giving only moderate yields when

using primary amines. Other analogues containing amino alcohols such as D/L-tyrosinol, serinol, and D/L-alaninol were also of great interest within this study. However, the Buchwald-Hartwig coupling proved unsuccessful. We believe the acidic proton from the hydroxyl group on tyrosinol and serinol was leading to competitive reaction pathways.

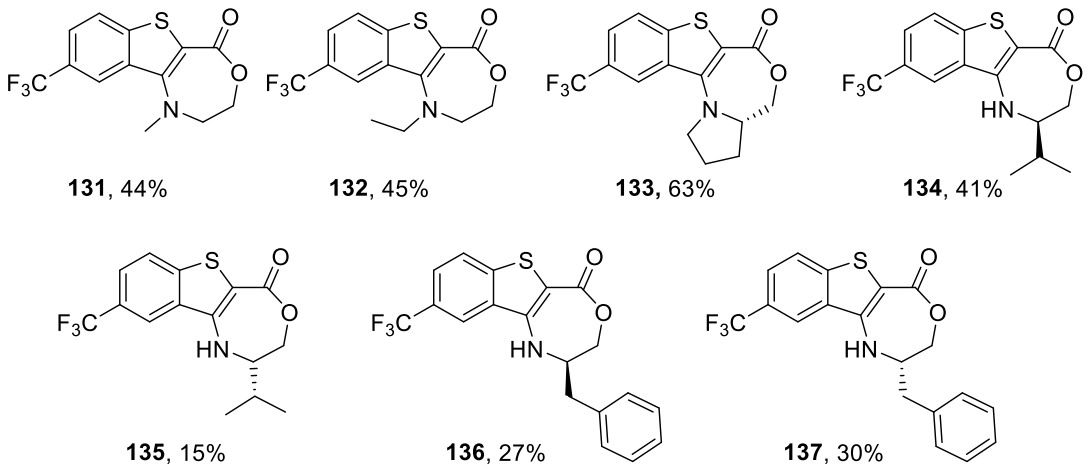

***Figure 64**: Analogues **131**–**137** synthesized using commercial amino alcohols.*

The second set of compounds prepared was tested in the DSF assay (Table XXVIII).

Table XXVIII: *DSF data obtained for compounds **131**–**137**.*

Compound	PIM-1 (ΔT_m, °C)	PIM-2 (ΔT_m, °C)	PIM-3 (ΔT_m, °C)	CLK4 (ΔTm, °C)	CLK1 (ΔTm, °C)	CLK3 (ΔTm, °C)	DYRK1A (ΔTm, °C)	DYRK2 (ΔTm, °C)	SRPK1 (ΔTm, °C)	SRPK2 (ΔTm, °C)
131	1.8	1.2	1.4	1.3	1.2	0.1	0.0	0.5	0.0	0.0
132	1.6	1.6	1.7	0.9	0.7	0.0	0.0	0.4	0.0	0.0
133	1.5	1.0	0.0	0.7	0.4	0.0	0.0	0.5	0.0	0.0
134	7.4	2.9	6.5	4.7	5.0	1.7	3.3	1.4	0.0	0.2
135	5.9	3.6	4.2	2.3	1.7	0.2	2.6	0.5	0.0	0.2
136	2.9	1.2	2.2	1.7	0.7	0.1	0.5	0.0	0.0	0.0
137	3.1	1.5	2.3	1.5	1.5	0.2	0.7	0.0	0.0	0.0

As was expected, the compounds derived from amino alcohols showed lower PIM affinities than the diamines (Table XXVII). Compounds **131**, **132** and **133** showed little activities against the PIM kinases but also lower activity compared to the non-methylated analogue **126**, suggesting that the presence of a secondary amine was required from PIM potency. For example, **131**, which was prepared using *N*-methylethanolamine, had a decreased ΔT_m value for PIM-1 of 1.8 °C, compared to **126**, which had a ΔT_m value of 4.6 °C.

Interestingly, compound **134** provided a high ΔT_m value of 7.4 °C for PIM-1 and 6.5 °C for PIM-3, good selectivity over PIM-2 (ΔT_m: 2.9 °C), a promising selectivity over CLK4 and CLK3 (ΔT_m values of 4.7 °C and 5.0 °C, respectively) and excellent selectivity against the DYRK family and the SRPK family. The corresponding enantiomer of **134**, compound **135**, was less tolerated and decreased the PIM affinity by 2 °C for each kinase isoform, providing ΔT_m values of 5.9 °C, 3.6 °C and 4.2 °C respectively.

The analogues derived from phenylalaninol, **136** and **137**, showed low PIM affinities, suggesting that there was not enough space within the ATP binding site to accommodate such large substituents.

From the data observed for compound **134**, we were very interested in analogue **139** (Scheme XVIII). We were aware that the amide moiety provided higher potencies towards PIM-1, therefore we believed that analogue **139** would provide a higher potency as well as selectivity towards the PIM-1 isoform.

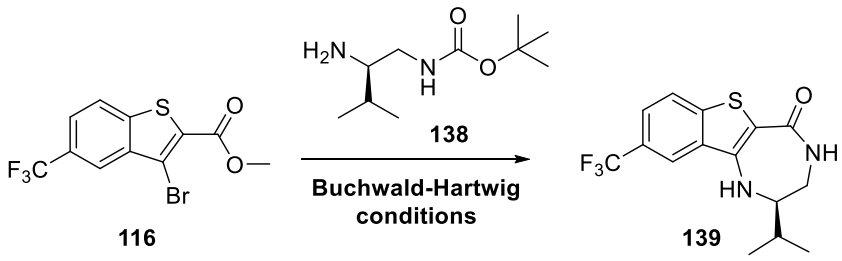

***Scheme XVIII**: Compound structure and synthetic approach for analogue **139**.*

To synthesize compound **139**, the non-commercial Boc-protected amine precursor **138** had to be synthesized. The diamine (**142**, Scheme XIX) needed for the synthesis of **138** was not commercially available, unfortunately, our efforts to synthesize **142** proved unsuccessful and are summarized in Scheme XIX.

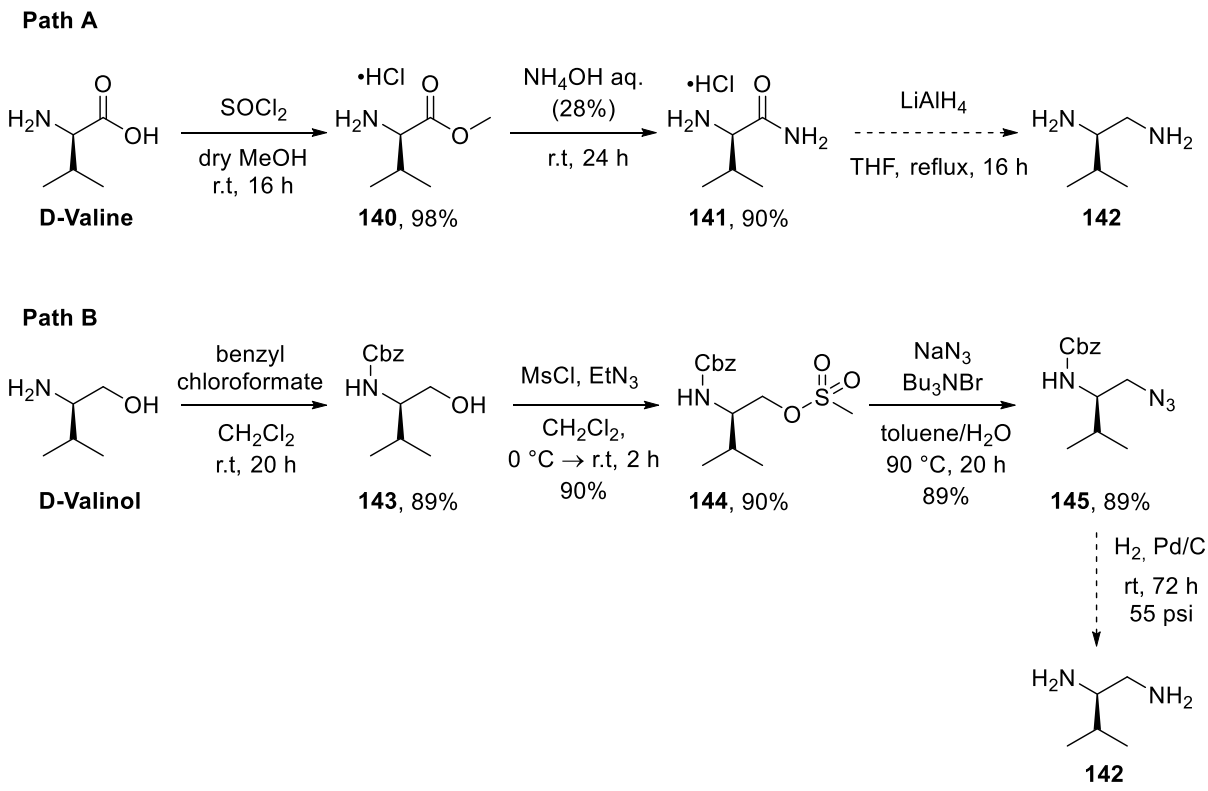

***Scheme XIX**: General conditions (Path A, Path B) used for the synthesis of the diamine **142**.*

Our initial approach to the synthesis of **142** used the general conditions detailed in Scheme XIX (Path A), previously reported by Ager and Malkov.[90, 91] The synthetic procedure started with the esterification of commercially available D-valine to afford compound **140** in 98% yield. Compound **140** was treated with ammonium hydroxide (28% aqueous solution) to afford **141** in 90%. At this point of the synthesis, reduction of **141** to give the diamine using $LiAlH_4$ proved unsuccessful. Even though Prof. Malkov's research group were able to obtain the diamine in 63%,[91] we were unable to isolate a satisfactory quantity of the clean diamine. After multiple attempts varying the reaction conditions, we believed that the amine was either evaporating during the solvent removal under reduced pressure and/or was coordinating to the aluminium therefore reducing the yield observed for the reaction.

Alternative conditions have also been reported for the synthesis of amine **142** (Scheme XIX, Path B).[92] The general procedure uses commercially available D-valinol as the starting material. The primary amine was protected using benzyl chloroformate to afford **143** in 89%. Treatment of **143** with methanesulfonyl chloride activated the primary alcohol and we were able to obtain **144** in high yield (90%). The displacement of sulfonates by azide ion can be used as an indirect conversion of an alcohol to an amine. The azide is commonly reduced to a

primary amine using either Staudinger conditions or hydrogenation. In our case, treatment of **144** with sodium azide afforded **145** in excellent yield. Using a Parr hydrogenator with Palladium on carbon (10 wt. %) reduced the azide and the protected amine to the corresponding diamine. Following their conditions, we carried out a trial reaction using a small quantity of **145** and the presence of **142** within the reaction mixture was observed by ^{1}H NMR spectroscopy. At this time, the Parr hydrogenator broke towards the end of the PhD project, and we were unable to synthesize sufficient diamine **142** to complete the synthesis of **139**.

In summary, the new scaffold provided excellent results. We were excited with the data presented, the selectivity over the CLK1 and CLK3 isoforms, DYRK family and the SRPK family was maintained, but also, the CLK4 selectivity was considerably lower than that observed for the previous series presented in Chapter 2 and 3. Furthermore, PIM potency was observed, as well as PIM-1 over PIM-3 selectivity, and excellent selectivity over PIM-2.

4.2.2. Crystal structure of 121 with the PIM-1 isoform

These results encouraged us to attempt to crystallize **120**, **121**, **122** and **134** with the PIM-1 protein. A crystal structure of PIM-1 with a benzothienodiazepine analogue would provide us with an excellent tool to optimize the analogues and to further understand the binding of these compounds within the PIM-1 active site. Attempts at crystallizing **120**, **122** and **134** have been unsuccessful to date. However, one of the crystals of PIM-1 with **121** diffracted at 1.8 Å and our collaborators at the SGC were able to obtain a crystal structure of **121** in the PIM-1 active site (Protocol 8.6, Figure 65).

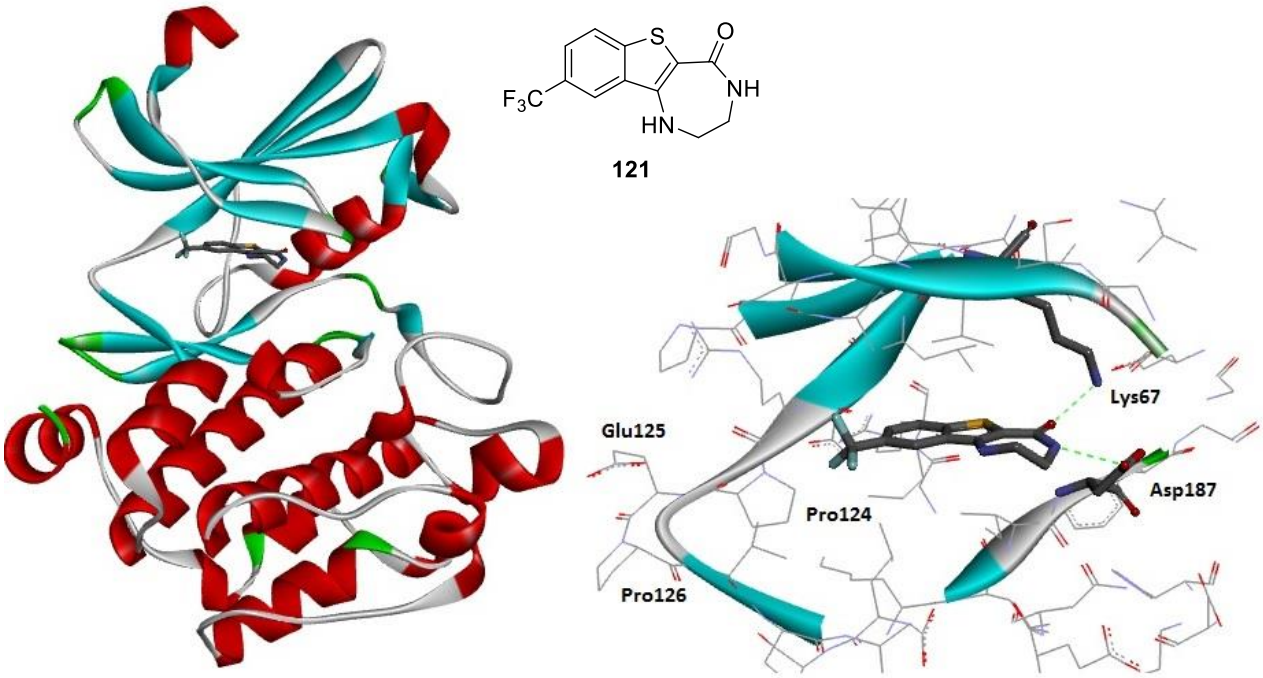

***Figure 65**: Crystal structure of **121**–PIM-1(left). PIM-1 active site–**121** crystal structure (right). Hydrogen bonding interactions are shown with green dotted lines.*

The crystal structure confirmed that the compound **121** was bound in the ATP binding pocket. Two hydrogen bonding interactions were formed between **121** and the receptor. The importance of the amide functionality within the diazepine ring is highlighted by the observation of an interaction between the carbonyl group and the Lys67, as well as a second interaction between the N-H and the Asp187. The crystal structure showed that the trifluoromethyl group at position 9 was facing the hydrophobic hinge region, and that there was enough space to accommodate other substituents to further optimize the PIM potency/selectivity. There was also space next to the diazepine ring, which is facing the solvent exposed area, which could fit the cyclohexane ring present in compounds **120**, **122** and **13**, explaining the high potencies observed for these analogues. To ensure this, docking of **123** using this crystal structure confirmed that analogue **123** imitates the binding observed for **121**, with two hydrogen bonding interactions with Lys67 and Asp186, and the cyclohexane ring fitting in the area surrounded by the amino acids Glu171 and Asn172, shown in Figure 66.

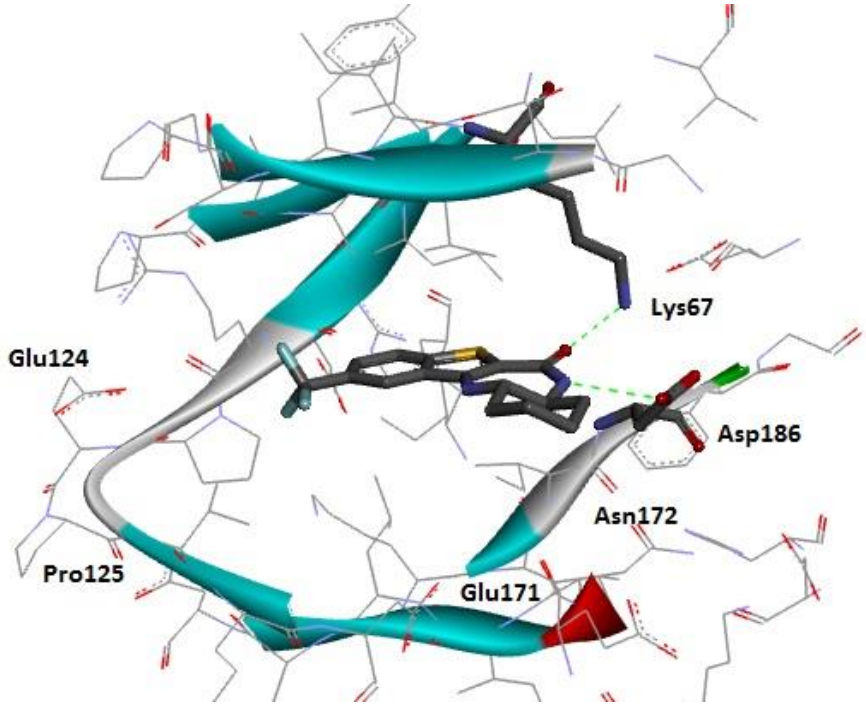

***Figure 66**: Docking study of **123**–PIM-1 active site.*

This crystal structure constituted an excellent tool to continue our SAR study within this series. It provided us with a better understanding of the binding pose of our compounds within the PIM active site, and provided us with additional direction on how to further optimize these compounds as chemical probes.

4.2.3. Biochemical evaluation of 119–126

4.2.3.1 Percentage of inhibition assay of 119–126

The compounds prepared were tested in a biochemical assay against PIM-1, PIM-2, and PIM-3 following protocol 8.1.1. The percentage inhibition obtained for these compounds at 10 µM and 1 µM is presented in Table XXIX.

Table XXIX: *PI data for compounds **119**–**126***

Compound	PIM-1 (10 µM)	PIM-1 (1 µM)	PIM-2 (10 µM)	PIM-2 (1 µM)	PIM-3 (10 µM)	PIM-3 (1 µM)
119	8	-10	1	-6	-7	1
120	97	94	70	42	66	50
121	70	15	24	2	46	2
122	99	97	76	54	69	54
123	100	96	75	46	76	55
124	82	61	35	11	17	5
125	61	66	24	23	16	19
126	96	64	88	20	83	19

The PI data again correlated with the DSF data presented in Table XXIX. Compound **119** showed no activity against the three PIM isoforms. Racemic compound **120**, as well as individual enantiomers **122** and **123**, showed higher potencies for the PIM-1 isoform, with PI data greater than 94% at 1 µM concentration suggesting that these compounds were likely to show low nanomolar activity for PIM-1. We were excited to confirm the selectivity for PIM-1 over PIM-2 and PIM-3. The three analogues showed similar potencies for PIM-2 and PIM-3, and considerably higher for the PIM-1 isoform. Compounds **120**, **122** and **123** showed activities over 70% at 10 µM but 42–55% at 1 µM concentration for both PIM-2 and PIM-3 isoforms. This data was very significant as PIM-1 selectivity and potency was observed over PIM-2 and PIM-3. The degree of selectivity towards PIM-1 as well as the potency for these compounds would be confirmed with IC_{50} data.

Interestingly, **121**, which was crystallized with PIM-1, did not show a high affinity for PIM-1 as was suggested in the DSF data (ΔT_m values of 6.2 °C, 3.7 °C, and 4.8 °C against PIM-1, PIM-2, and PIM-3, respectively). The PI data for this compound showed little activity within this assay, with PI at 10 µM and 1 µM of 70% and 15% for PIM-1, 24% and 2% for PIM-2, and 46% and 2% for PIM-3. At this stage, to ensure that the activity of the compound was fully understood, IC_{50} curves were obtained for **121** in the three isoforms to provide a solid conclusion to the activity of **121**.

Finally, compounds **124**, **125** and **126**, which contain an ester moiety, had decreased PIM potencies for the three isoforms. Compound **124** showed moderate activity for PIM-1, with PI data of 82% and 61% at 10 µM and 1 µM, but little activity was observed for PIM-2 and PIM-3. A similar behaviour was observed for the five-membered ring cycloalkane **125** which had slightly decreased PIM potency of 61% and 66% at 10 µM and 1 µM and again showed

no activity for PIM-2 and PIM-3. Finally, **126** showed good activity for the three isoforms at 10 µM (96%, 88%, 83%, respectively) but only moderate activity when testing at 1 µM (64%, 20%, 19%), suggesting that this compound would show good potencies against the three isoforms but probably within the micromolar activity region.

4.2.3.2 IC_{50} data on compounds 120–126

Following the General Procedure 8.1.5, the compounds with PI data > 70% at 10 µM for the PIM-1 isoform were further analyzed and IC_{50} data obtained for the three isoforms.

The data obtained for compounds **120**–**126** is presented in Table XXX.

Table XXX: *IC_{50} data for compounds **120**–**126**.*

Compound	PIM-1 (IC_{50}, nM)	PIM-2 (IC_{50}, nM)	PIM-3 (IC_{50}, nM)
120	30	6900	103
121	3840	>50000	4530
122	66	4540	201
123	76	3790	589
124	412	>50000	267
125	1580	>50000	527
126	324	1590	696

The IC_{50} data obtained was very encouraging and confirmed the selectivity for PIM-1 and PIM-3 over PIM-2, as IC_{50} values between 1.6–50 µM were observed for all compounds tested against PIM-2. For the PIM-1 isoform, the cyclohexane derivatives **120**, **122** and **123** provided the best results with IC_{50} values of 30 nM, 66 nM and 76 nM, excellent selectivity over PIM-2 and a good selectivity over PIM-3 (IC_{50}: 103 nM, 201 nM, 589 nM, for **120**, **122**, and **123**). Although the selectivity for PIM-1 over PIM-3 was not yet ideal, these compounds still provided really high potencies against PIM-1, as well as a remarkable selectivity over the other kinases analyzed within the DSF assay, but more importantly over CLK4, which had proven to show the highest cross-reactivity with the PIM isoforms.

To our surprise, **121** which was co-crystallized with the PIM-1 isoform, showed rather modest activity against the three isoforms with IC_{50} values of 3.8 µM for PIM-1, 50 µM for PIM-2, and 4.5 µM for PIM-3. These results correlate well with the observed PI data, although the DSF data suggested that higher potency might have been expected in the biochemical assay.

Finally, **124** and **126** provided good potencies against PIM-1, with IC_{50} values of 412 nM and 324, and similar IC_{50} values were obtained for the PIM-3 isoform (267 nM and 696 nM). Compound **125**, which contains a five-membered ring cycloalkane instead of the cyclohexane in **124**, showed slightly greater PIM-3 inhibitory activity over PIM-1 (by 3 fold) with IC_{50} values of 1580 nM (PIM-1), > 50000 nM (PIM-2) and 527 nM (PIM-3), a phenomenon which would be taken into account when addressing PIM-3 over PIM-1 selectivity.

4.2.3.3 Percentage of inhibition data for compounds 131–137

The second set of compounds was also analyzed in the percentage of inhibition assay, followed by the generation of IC_{50} curves. The data obtained is presented for both the PI data and IC_{50} (where appropriate) in Table XXXI.

Table XXXI: *IC_{50} and PI data obtained for **131**–**137**.*

Compound	PIM-1 (10 µM)	PIM-1 (1 µM)	PIM-1 (IC_{50}, nM)	PIM-2 (10 µM)	PIM-2 (1 µM)	PIM-2 (IC_{50}, nM)	PIM-3 (10 µM)	PIM-3 (1 µM)	PIM-3 (IC_{50}, nM)
131	51	18		32	9		23	2	
132	45	15		47	18		30	3	
133	99	85	98	90	34	4530	76	30	143
134	99	92	44	67	23	>50000	45	44	175
135	88	57	451	68	40	>50000	31	14	1940
136	73	37	1870	37	10	>50000	19	3	6920
137	60	29		32	10		21	-1	

As expected from the DSF assay results, **131** and **132** had little activity against the three isoforms, with PI data lower than 50% for PIM-1, PIM-2 and PIM-3 even at 10 µM concentrations, therefore, IC_{50} data were not obtained for these compounds.

Unexpectedly, **133**, which showed low affinity in the DSF assay (Table XXXII), provided excellent results within the biochemical evaluation. The PI data showed 99% at 10 µM and 85% at 1 µM for PIM-1, with an excellent IC_{50} value of 98 nM. For PIM-2, the results correlated with the DSF assay, giving PI values of 90% at 10 µM and 34% at 1 µM, with an IC_{50} value of 4.5 µM, and finally, an IC_{50} value of 143 nM for PIM-3. Again, this poor correlation between the DSF assay and PI data for **133** would be further analyzed and the

biochemical assay is currently being repeated for publication purposes to ensure the activity of this compound is fully understood.

Table XXXII: *DSF data obtained for compound **133***

Compound	PIM-1 (ΔT_m, °C)	PIM-2 (ΔT_m, °C)	PIM-3 (ΔT_m, °C)	CLK4 (ΔTm, °C)	CLK1 (ΔTm, °C)	CLK3 (ΔTm, °C)	DYRK1A (ΔTm, °C)	DYRK2 (ΔTm, °C)	SRPK1 (ΔTm, °C)	SRPK2 (ΔTm, °C)
133	1.5	1	0	0.7	0.4	0	0	0.5	0	0

Finally, the phenylalaninol derivatives showed similar activities to those suggested by DSF assay. Inclusion of a phenyalaninol moiety was not tolerated, as poor activity was observed within the three isoforms. Compound **136** showed IC_{50} values of 1.9 µM for PIM-1, >50 µM for PIM-2, and 6.9 µM for PIM-3, therefore, phenylalaninol derivatives were discarded from future optimization studies.

In conclusion, these data were very encouraging with regard to our project aim. Higher selectivities were seen for compounds **119**–**126** over the CLK family, DYRK family, and SRPK family. Furthermore, racemic **120**, as well as the individual enantiomers **122** and **123**, provided low nanomolar activity for PIM-1, excellent selectivity over PIM-2, and moderate selectivity over PIM-3 (Figure 67).

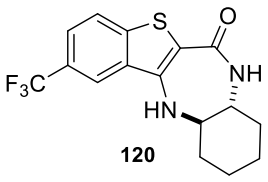

120

PIM-1 (IC_{50}): 30 nM
PIM-2 (IC_{50}): 6.9 µM
PIM-3 (IC_{50}): 103 nM

Compound	PIM-1 (ΔT_m, °C)	PIM-2 (ΔT_m, °C)	PIM-3 (ΔT_m, °C)	CLK4 (ΔTm, °C)	CLK1 (ΔTm, °C)	CLK3 (ΔTm, °C)	DYRK1A (ΔTm, °C)	DYRK2 (ΔTm, °C)	SRPK1 (ΔTm, °C)	SRPK2 (ΔTm, °C)
120	7.2	3	5.7	2.8	2.8	0.4	1.4	2.6	0	0

***Figure 67**: DSF data and biochemical data obtained for **120**.*

The 1,2-cyclohexanediamine derivatives showed the best results within the previous SAR study. To continue with our efforts to design PIM isoform selective chemical probes, 1,2-

cyclohexanediamine derivatives were targeted with various functionalization on the aryl ring. We hoped that modifications on the left hand side of the molecule, which is facing the hinge region, together with further molecular modelling studies using the crystal structure obtained, would provide us with further understanding of the PIM isoforms and an alternative approach to achieve PIM-1 *vs* PIM-3 selectivity.

4.3. Design and synthesis of analogues of 120

Our attempts to find an optimal synthetic route for the synthesis of analogue **149** containing a chlorine instead of a trifluoromethyl group were successful (Scheme XX). The chlorine provided excellent PIM potency in the benzothienopyrimidinone series (compound **43a**, Figure 68). Therefore, the synthesis of **149** was our priority to evaluate how the chlorine would fit within this new series of compounds.

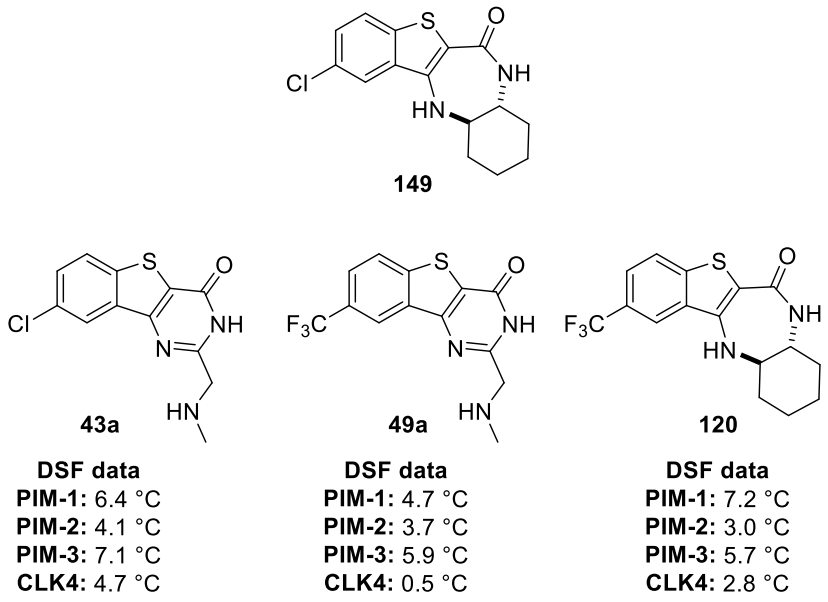

***Figure 68**: Compound structure and DSF data for analogues **43a**, **49a**, and **120**.*

Compounds **149**, **150** and **151** were synthesized following the synthetic route detailed in Scheme XX. The first step was common with our previous synthetic routes, allowing us to obtain **26**, **27** and **28** in 94%, 90% and 89% yields respectively. The Sandmeyer conditions were modified so that an iodine could be introduced instead of a bromine to promote a

selective oxidative addition into the C-I bond instead of the C-Cl bond, allowing the formation of analogues **146**, **147**, **148** in excellent yields.

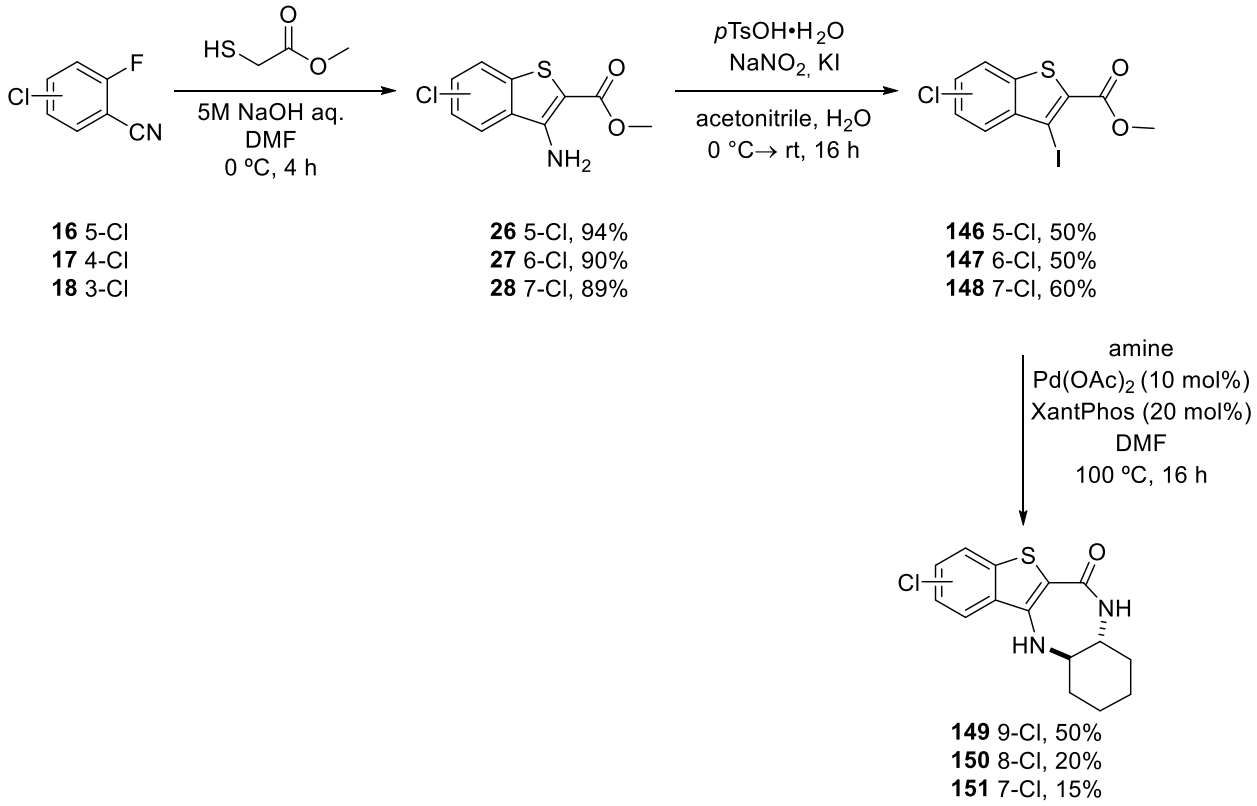

***Scheme XX**: General conditions for the synthesis of **149**, **150**, and **151**.*

From a medicinal chemistry SAR study, the synthesis of the bromine analogues of **149**, **150**, and **151** would be ideal in order to analyze the ideal halogen size required for an optimal fit in the PIM active site. However, after multiple attempts, we were only able to obtain compound **153**, which contains the bromide in position 7 of the aromatic ring, in 32% yield (Scheme XXI). Analogues containing the bromide in positions 8 and 9 showed competitive oxidative additions into the C-Br bond during the Buchwald-Hartwig step, leading to multiple co-products and challenging purifications.

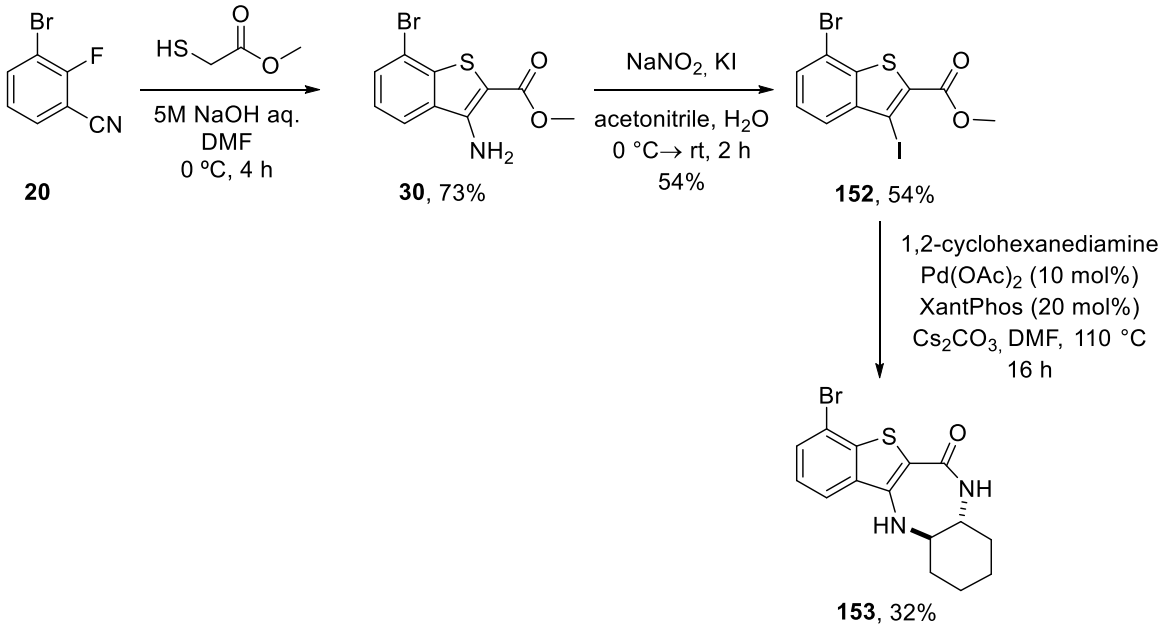

***Scheme XXI**: Synthetic procedure for the synthesis of **153**.*

Further analysis of the molecular modelling of **120** within the PIM active site suggested that there was enough space around the trifluoromethyl group to accommodate additional substituents. We were interested in generating a small library derived from **120** containing a range of functional groups that could provide us with information about the polarity of this region of the active site. To do so, a change in the synthetic procedure was required. The proposed starting material in Scheme XXII, 5-trifluoromethyl-2-fluorobenzonitrile, was reducing the accessibility of the chemistry around the hinge region. At the same time, the nucleophilic aromatic substitution required an electron withdrawing group in the starting fluorobenzonitrile. A new proposed synthetic route was developed using 5-nitro-2-fluorobenzonitrile (**22**) or 4-nitro-2-fluorobenzonitrile (**23**) as the starting materials, depending which position of the phenyl ring was studied. The nitro group could then be reduced to an amino group which could undergo a number of different transformations for the synthesis of new analogues (Scheme XXII).

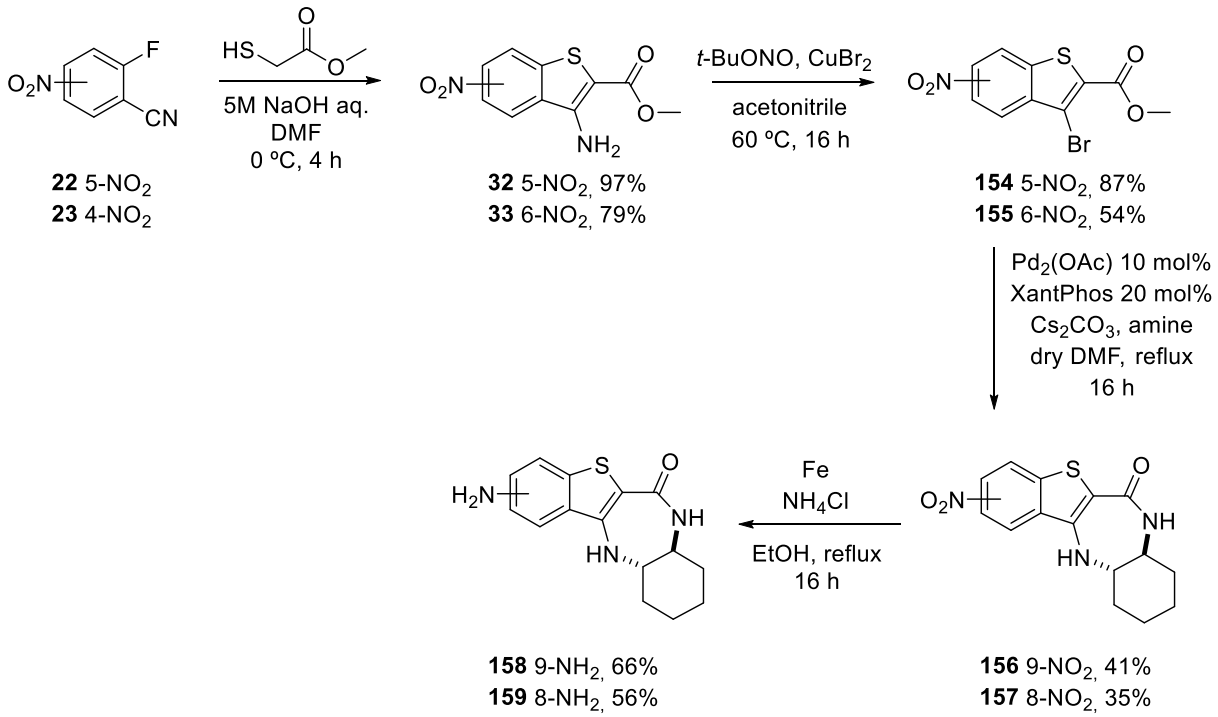

22 5-NO_2
23 4-NO_2

32 5-NO_2, 97%
33 6-NO_2, 79%

154 5-NO_2, 87%
155 6-NO_2, 54%

158 9-NH_2, 66%
159 8-NH_2, 56%

156 9-NO_2, 41%
157 8-NO_2, 35%

***Scheme XXII**: Synthetic procedure for the synthesis of analogues **156–159**.*

The initial two steps of the synthesis were identical to the route described in Scheme XVI. The commercial starting material, fluorobenzonitrile, underwent the nucleophilic aromatic substitution and cyclization reaction followed by a Sandmeyer transformation to provide the intermediates **154** and **155** in excellent yields. For both isomers, the Buchwald-Hartwig coupling proceeded in moderate yields (41% for **156** and 35% for **157**), but we were able to obtain enough material of **156** and **157** to continue the synthesis.

The reduction of the nitro group to the primary amine was initially carried out using hydrogenation conditions and palladium on carbon as catalyst. However, reduction of the amide from the diazepine ring was also observed (**160**, Scheme XXIII) by LCMS. An alternative approach using iron and ammonium chloride in reluxing EtOH proved to be highly successful in selectively reducing the nitro group. These conditions afforded **159** and **158** in excellent yields (56% and 66%, Scheme XXII).

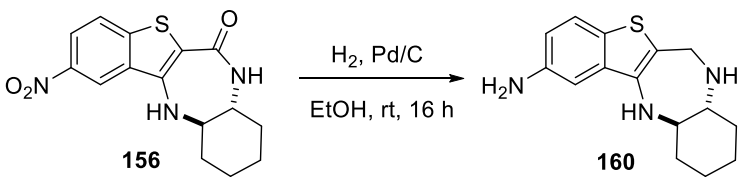

***Scheme XXIII**: Hydrogenation conditions for the reduction of **156**.*

Finally, within this SAR study, we wanted to further functionalize analogue **158**. Molecular modelling studies suggested that position 8 could not accommodate large substituents due to the reduced space around that area of the catalytic site, however, the area around position 9 could fit a wide variety of substituents. As a starting point, we decided to synthesize **161** and **162** using acetyl chloride, which afforded **161** in 30% yield, and isovaleryl chloride to afford compound **162** in 36%.

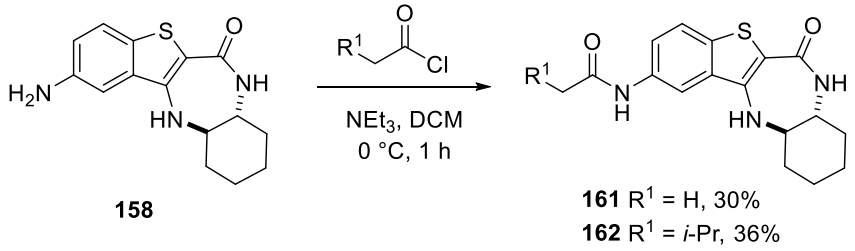

***Scheme XXIV**: Synthetic approach for the synthesis of **161** and **162**.*

To complete the third set of compounds from this SAR study, we wanted to synthesize analogues **164** and **165**, containing the trifluoromethyl group in positions 8 and 7 of the phenyl ring (Scheme XXV). The same synthetic approach was used to synthesize analogue **164**. However, due to time restraints, we were unable to obtain analogue **165**.

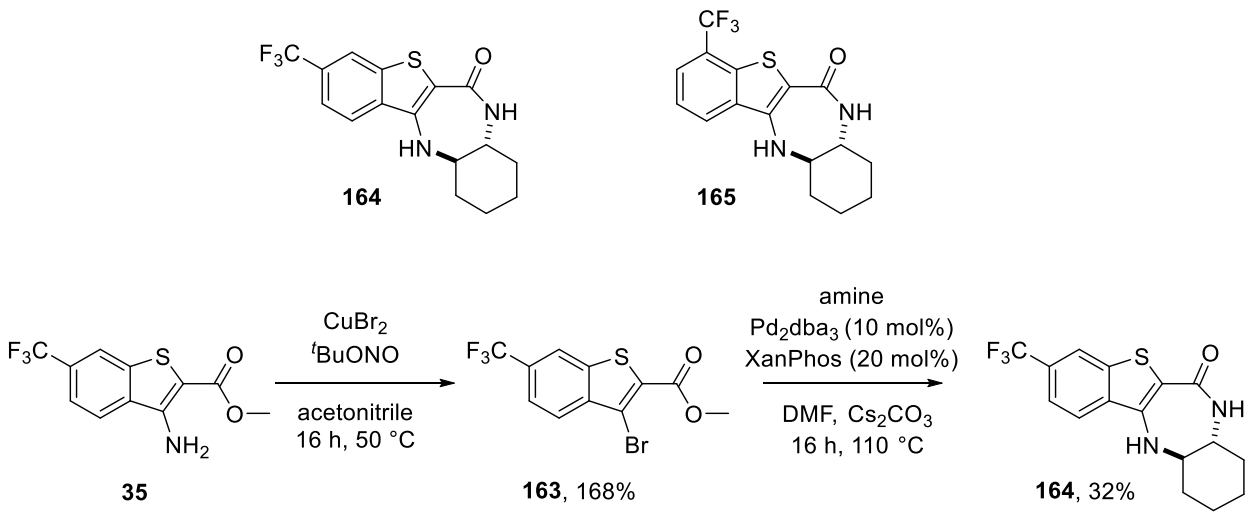

***Scheme XXV**: Compound structures of **164** and **165** (top).*
*Synthetic procedure for the synthesis of **164** (bottom).*

4.3.1. DSF assay of compounds 149, 150–153, 156–159, 161–164

The third set of compounds generated within the previous SAR study (Figure 69), was tested in the DSF assay (Table XXXIII). The yields corresponding to the final step for each compound are also presented.

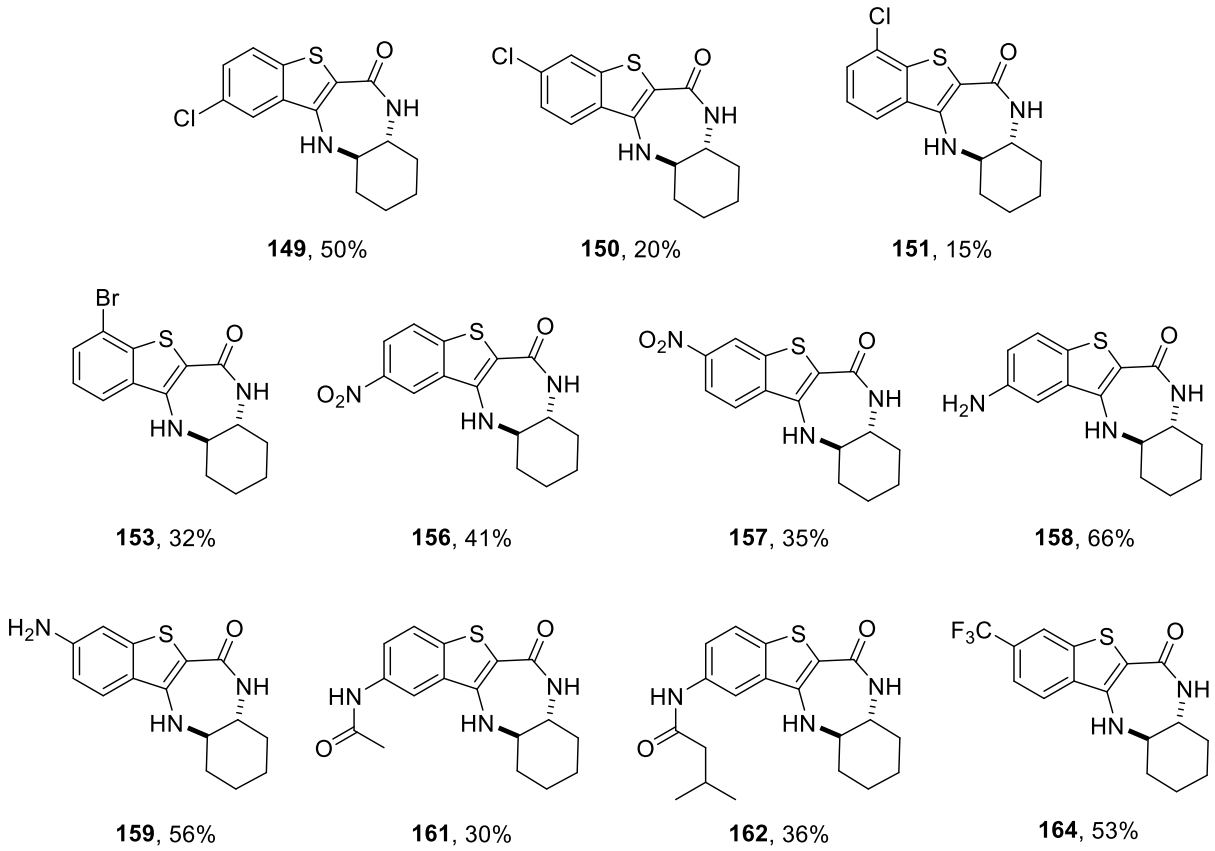

***Figure 69**: Compound structures and yields of **149, 150–153, 156–159, 161–164**.*

Table XXXIII*: DSF data for compounds **149**, **150–153**, **156–159**, **161–164**.*

Compound	PIM-1 (ΔT_m, °C)	PIM-2 (ΔT_m, °C)	PIM-3 (ΔT_m, °C)	CLK4 (ΔT_m, °C)	CLK1 (ΔT_m, °C)	CLK3 (ΔT_m, °C)	DYRK1A (ΔT_m, °C)	DYRK2 (ΔT_m, °C)	SRPK1 (ΔT_m, °C)	SRPK2 (ΔT_m, °C)
149	9.2	1.2	7.7	9.8	8.0	7.9	7.8	5.7	0.0	0.2
150	5.8	2.1	4.7	3.5	0.9	1.2	2.3	2.7	0.1	0.0
151	4.6	3.3	4.6	1.9	2.2	0.3	2.0	2.3	0.1	0.0
153	4.8	2.1	4.8	1.7	1.3	0.3	1.9	2.4	0.2	0.2
156	4.7	2.2	4.4	4.0	4.9	1.0	2.4	3.5	0.0	0.1
157	4.9	0.0	4.3	3.0	2.7	2.8	0.9	3.0	0.0	0.0
158	3.5	0.5	2.3	3.4	2.6	0.6	2.7	1.6	0.0	0.0
159	2.6	0.8	3.7	1.1	0.7	0.2	0.6	1.4	0.0	0.0
161	3.7	0.2	5.4	4.2	3.1	1.4	2.4	5.9	0.0	0.1
162	3.5	0.3	6.1	4.9	0.9	0.2	2.4	6.2	1.6	0.5
164	5.9	0.6	2.6	1.2	0.5	0.0	0.4	0.6	0.0	0.1

The results from the DSF assay were very interesting. As expected, the chlorine analogue **149** showed increased affinity for the PIM kinases, ΔT_m of 9.2 °C, 1.2 °C, and 7.7 °C, the highest

values observed to date. However, this substituent decreased the selectivity considerably over the other kinases. Compound **149** showed a ΔT_m of 9.8 °C, 8.0 °C, 7.9 °C and 7.8 °C for CLK4, CLK1, CLK3 and DYRK1 respectively. In addition, DYRK2 showed a moderate affinity with a ΔT_m value of 5.7 °C and for SRPK1 and SRPK2 a ΔT_m of 0 °C was obtained. Even though the affinity for the PIM kinases had increased considerably, the chlorine in position 9 was not studied further due to the poor selectivity offered over the CLK and DYRK kinases.

When the chlorine atom was moved to position 8 (**150**), the PIM affinity slightly decreased to values of 5.8 °C, 2.1 °C and 4.7 °C for the three isoforms, however, the selectivity over the other kinases increased, *e.g.*, CLK4 showed a reduced ΔT_m of 3.5 °C, CLK1 of 0.9 °C and CLK3 of 1.2 °C. Little affinity was observed towards the DYRK family and the SRPK family. Very similar data was observed for compounds **151** and **153**, which contain the chloride and bromide in position 7 of the phenyl ring. The PIM potency was maintained with ΔT_m of 4.7–4.8 °C for PIM-1, 2.1–3.3 °C for PIM-2, and 4.6–4.8 °C for PIM-3. The ΔT_m for CLK4 decreased slightly to 1.7–1.9 °C but the rest of the kinases seem were not affected by moving the halogen around the phenyl ring.

The compounds containing nitro groups (**156**, and **157**) had decreased affinities towards the PIM isoforms for both positions of the aryl ring (ΔT_m of 4.7 °C and 4.9 °C for PIM-1, 2.2°C and 0 °C for PIM-2, and 4.4 °C and 4.3 °C for PIM-3), providing selectivity over the PIM-2 isoform but not selectivity between PIM-1 and PIM-3 or CLK4 and CLK1. The aniline analogues **158** and **159** showed similar behaviour, with decreased affinities for the PIM isoforms as well as the other family of kinases, suggesting that polar groups were not well tolerated around this area and that hydrophobic substituents should be considered in a subsequent SAR study.

Interestingly, when adding larger substituents such as in the case of amide analogues **161** and **162**, a change of selectivity was observed. The compounds showed higher affinities for PIM-3 over PIM-1 and PIM-2. Compound **161** showed ΔT_m values of 3.7 °C, 0.2 °C, and 5.4 °C for PIM-1, PIM-2, and PIM-3, whereas **162** showed a higher selectivity for PIM-3 over PIM-1 with ΔT_m values of 3.5 °C, 0.3 °C, and 6.1 °C against PIM-1, PIM-2, and PIM-3, respectively. We were very excited with the data obtained, as this degree of selectivity for PIM-3 had not been observed to date, therefore this data constituted an important breakthrough within our project.

Finally, moving the trifluoromethyl group to position 8 of the phenyl ring reduced the PIM potency but we were able to obtain significant selectivity over the CLK, DYRK and SRPK kinases. Compound **164** showed ΔT_m values of 5.9 °C, 0.6 °C, and 2.6 °C for PIM-1, PIM-2, and PIM-3. Although the PIM-1 affinity observed was not optimal, the compound provided promising selectivity for PIM-1 over PIM-2 and PIM-3 and will be analyzed carefully in the biochemical assay.

4.3.2. Biochemical evaluation of **149**, **150–153**, **156–159**, and **161–164**

Compounds **149**, **150**–**153**, **156**–**159**, and **161**–**164** were further analyzed in the PI and biochemical assays; the data is presented in Tables XXXIV and XXXV. Compounds **150**, **151** and **153**, which were synthesized towards the end of the project, were part of a final batch of compounds sent to the CNIO, were directly tested against PIM-1, PIM-2, and PIM-3 in a dose-response experiment (Table XXXV).

Table XXXIV: *PI data and biochemical data of compounds **149**, **156–159**, **161**, **162**, and **164**.*

Compound	PIM-1 (IC_{50}, nM)	PIM-1 (10 µM)	PIM-1 (1 µM)	PIM-2 (IC_{50}, nM)	PIM-2 (10 µM)	PIM-2 (1 µM)	PIM-3 (IC_{50}, nM)	PIM-3 (10 µM)	PIM-3 (1 µM)
149	26	100	93	406	84	39	258	95	78
156	564	92	60	13800	57	12	610	76	23
157	1270	84	54	>50000	32	10	>50000	50	22
158	1410	85	27	9890	58	13	59	71	17
159	1170	86	45	16600	72	24	365	80	30
161	1540	82	31	23700	58	7	55	93	55
162	1950	76	16	12700	49	9	83	95	59
164		52	18		13	-6		18	-2

Table XXXV: *IC_{50} data for compound **150**, **151** and **153**.*

Compound	PIM-1 (nM)	PIM-2 (nM)	PIM-3 (nM)
150	1460	>10000	878
151	1810	>10000	412
153	579	>10000	372

As expected, compound **149** containing a chlorine atom gave excellent PI data with inhibitions over 80% at 10 µM for the three isoforms. **149** gave high potencies in the dose-

response experiment, especially for PIM-1, with IC_{50} values of 26 nM, 406 nM, and 258 nM for PIM-1, PIM-2, and PIM-3, respectively. Despite the high potencies observed for **149**, the compound showed a low selectivity profile against the CLK family and DYRK family in the DSF assay. For this reason, analogues containing the chlorine substituent at position 9 were discarded from further analysis.

Interestingly, when the chlorine was moved to positions 8 or 7 (**150** and **151**), loss of activity for PIM-1 and PIM-2 was seen whereas some activity for PIM-3 was observed. For example, **150** showed an IC_{50} value of 878 nM for PIM-3, 1.46 µM for PIM-1 and 10 µM for PIM-2, showing some PIM-3 over PIM-1 selectivity. The selectivity towards PIM-3 increased when the chlorine was moved to position 7, *e.g.* compound **151**, and we obtained IC_{50} values of 1.81 µM for PIM-1, 10 µM for PIM-2, and 412 nM for PIM-3. However, if the chlorine was changed for a bromine, *e.g.* compound **153**, the compound's activity for PIM-1 increased to an IC_{50} value of 579 nM whereas, the activity for PIM-2 was not affected (IC_{50}: 10 µM), and the PIM-3 activity was maintained (IC_{50}: 372 nM). This set of data was really interesting, as we were able to observe the first PIM-3 over PIM-1 selectivity within the benzothienodiazepine series.

Compound **156**, which contained a nitro group instead of a chlorine atom, showed moderate activity in the preliminary PI assay. For the PIM-1 isoform, 92% inhibition was observed at 10 µM and 60% at 1 µM, suggesting a moderate activity for **156**, which was then confirmed through IC_{50} value of 564 nM. For PIM-2, we were expecting a low activity, as the PI data showed low percentages of inhibition of 57% (10 µM) and 12% (1 µM) which was confirmed indeed *via* IC_{50} data (13.8 µM). Finally, PIM-3 showed slightly lower PI data compared to PIM-1 (76% at 10 µM, and 23% at 1 µM) which correlated to the IC_{50} value observed (610 nM). When moving the nitro substituent to position 8 (**157**) substantial loss of activity was observed, giving IC_{50} values of 12.7 µM, > 50 µM, and > 50 µM for PIM-1, PIM-2, and PIM-3, respectively. This data indicated that the nitro group was not well tolerated within this region of the PIM active site, whether it be in position 8 or 9.

To our surprise, reduction of the nitro to a primary amine led to some really interesting results. For compounds **158** and **159**, the PI data (and DSF data) indicated similar behaviour against the three isoforms, with inhibitions at 10 µM of 85–86% for PIM-1, 58–72% for PIM-2, and 71–80% for PIM-3, suggesting that **158** and **159** would show similar potencies for PIM-1, PIM-2 and PIM-3. However, we were very excited by their corresponding dose-response experiments: compound **158** showed an IC_{50} value of 59 nM for the PIM-3 isoform, little

activity for the PIM-2 isoform (IC_{50}: 10 μM), and moderate activity for the PIM-1 isoform (IC_{50}: 1.4 μM), becoming the first compound to date to show good PIM-3 selectivity over PIM-1. When the amino group was moved to position 8 (**159**), the activity for PIM-3 decreased slightly, showing an IC_{50} of 365 nM, but maintaining the selectivity over PIM-2 (IC_{50}: 16.6 μM) and PIM-1 (IC_{50}: 1.2 μM). This data, together with the data observed for compound **158**, strongly suggested that PIM-3 selectivity could be further studied through an SAR study on position 8 of the benzothienodiazepine, and this data would be taken into account for further PIM-3 studies.

Acylation of the primary amine in structures **158** and **159**, using acyl chlorides afforded compounds **161** and **162** which also provided extremely good potencies and selectivity for PIM-3 over PIM-1 and PIM-2, as was previously suggested in the DSF assay. Both compounds showed higher activities in the PI data for PIM-3, **161** showed 93% inhibition at 10 μM, and 55% at 1 μM, suggesting low nanomolar activity for this isoform. For PIM-1, the activity decreased to 82% and 31% at 10 μM and 1 μM respectively, and PIM-2 showed little activity with PI data of 58% at 10 μM and 7% at 1 μM. The IC_{50} correlated with the PI data with values of 1.5 μM, 23.7 μM, and 55 nM for PIM-1, PIM-2, and PIM-3, respectively, providing excellent activity for the PIM-3 isoform and excellent selectivity for PIM-3 over PIM-1 (28-fold selectivity) and PIM-2 (429-fold selective).

Encouragingly, **162** gave similar PI data and IC_{50} data to **161**. The PIM-1 PI data showed lower activity than that observed for compound **161**, with inhibition of 76% and 16% (10 μM, and 1 μM) for PIM-1, 49% and 9% (10 μM, and 1 μM) for PIM-2, and 95% and 59% (10 μM, and 1 μM) for PIM-3, showing a higher activity for the PIM-3 isoform. The IC_{50} data correlated well and we obtained activities of 1.95 μM for PIM-1, 12.7 μM for PIM-2, and 83 nM for PIM-3, a potential PIM-3 probe providing 24-fold selectivity for PIM-3 over PIM-1.

Finally, the inclusion of a trifluoromethyl group at position 8 of the benzothienodiazepine scaffold (compound **164**) was not well tolerated. Even though the DSF data suggested moderate activity for the PIM-1 isoform (ΔT_m value of 5.9 °C), the PI data showed percentage inhibition lower than 55% at 10 μM for the three isoforms. For this reason, the compound was not further studied.

In summary, maintaining the cyclohexane ring of the scaffold and carrying out a small SAR study on the aryl ring provided very exciting and significant results to our project. High PIM-1 over PIM-3 selectivity was not observed, however, we were able to obtain PIM-3

selectivity by introducing polar groups such as primary amines (**158** and **159**) or aliphatic amides (**161** and **162**) (Figure 70).

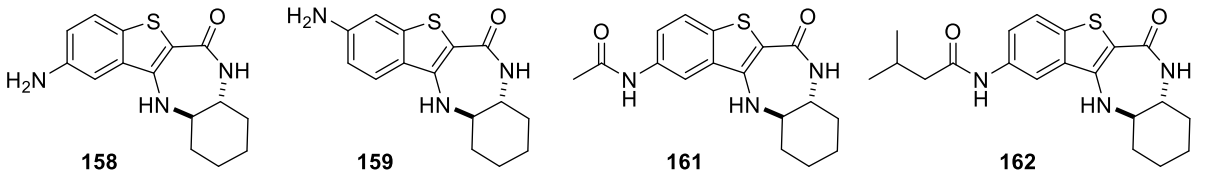

158
IC_{50} data
PIM-1: 1.4 μM
PIM-2: 10 μM
PIM-3: 59 nM

159
IC_{50} data
PIM-1: 1.2 μM
PIM-2: 16.6 μM
PIM-3: 365 nM

161
IC_{50} data
PIM-1: 1.5 μM
PIM-2: 23.7 μM
PIM-3: 55 nM

162
IC_{50} data
PIM-1: 2 μM
PIM-2: 12.7 μM
PIM-3: 83 nM

Compound	PIM-1 (ΔT_m, °C)	PIM-2 (ΔT_m, °C)	PIM-3 (ΔT_m, °C)	CLK4 (ΔT_m, °C)	CLK1 (ΔT_m, °C)	CLK3 (ΔT_m, °C)	DYRK1A (ΔT_m, °C)	DYRK2 (ΔT_m, °C)	SRPK1 (ΔT_m, °C)	SRPK2 (ΔT_m, °C)
158	3.5	0.5	2.3	3.4	2.6	0.6	2.7	1.6	0	0
159	2.6	0.8	3.7	1.1	0.7	0.2	0.6	1.4	0	0
161	3.7	0.2	5.4	4.2	3.1	1.4	2.4	5.9	0	0.1
162	3.5	0.3	6.1	4.9	0.9	0.2	2.4	6.2	1.6	0.5

***Figure 70**: IC_{50} data and DSF data of PIM-3 selective compounds **158**, **159**, **161** and **162**.*

Even though it was observed from the data obtained for compounds **158**, **159**, **161** and **162**, that PIM-3 over PIM-1 selectivity could be achieved through carrying out studies at position 8 of the aryl ring, the PIM-3 potency decreased slightly, suggesting that there might be little space around that area of the receptor to accommodate different substituents. For this reason, our next direction of research was focused mainly on position 9, which provided better potencies against the PIM-3 isoform.

In terms of the selectivity of these compounds over the other kinases analyzed during the DSF assay, the data showed some discrepancies so a solid conclusion was not taken from this data. Compounds **158** and **159** showed little affinity against PIM-3 with ΔT_m values of 2.3 °C and 3.7 °C against PIM-3, respectively, whereas the compounds showed low nanomolar potencies in the biochemical assay. The compounds showed selectivity over the CLK, DYRK and SRPK kinases. However, for a solid conclusion on the selectivity, future potential PIM-3 probes would be tested in a common biochemical kinase profiling assay. Such an assay uses a large panel of kinases with a broad coverage of the human kinome, and will provide us with solid data on the selectivity of a potential drug candidate or chemical probe. For compounds

161 and **162**, the DSF data correlated better with the biochemical assay, as we were able to see some selectivity for PIM-3 over PIM-1 in the DSF assay. Compounds **161** and **162** also showed stabilization of CLK4 and DYRK2 with ΔT_m values of 4.2 °C and 5.9 °C for **161** and 4.9 °C and 6.2 °C for **162**. Even though the cross-reactivity with CLK4 and DYRK2 was not ideal, we decided to carry on studying this type of analogue in the hope of further increasing the potency and selectivity towards the PIM-3 isoform.

As a starting point, molecular modelling studies were carried out with **158**, **161** and **162** using the PIM-1 crystal structure, as well as a PIM-3 virtual model built by our collaborators at the SGC.

4.3.3. Docking studies of 162 in the PIM-1 and PIM-3 active sites

Interestingly, docking studies showed a different binding pose for compounds **161** and **162**, which may explain the reasons for the selectivity observed for PIM-3 over PIM-1. For example, **162** was docked in the PIM-1 active site (Figure 71) and due to the lack of space around the hinge region when adding large substituents (such as isovaleryl) compound **162** flipped in the PIM-1 active site, losing the key hydrogen-bond interaction with Lys67. The compound fitted in the PIM-1 active site and the carbonyl group facing the hinge region with the amide substituent facing towards the solvent-exposed area, thus allowing no key interactions between the receptor and the probe, reducing the potency against the PIM-1 isoform.

When **162** was docked in the PIM-3 active site (Figure 72), the compound also fliped within the active site and the binding pose changed compared to the traditional pose observed for **8** (Figure 16). However, the compound was able to fit within the active site so that it maintained the important interaction with Lys67, which may explain the high activities observed for the PIM-3 isoform.

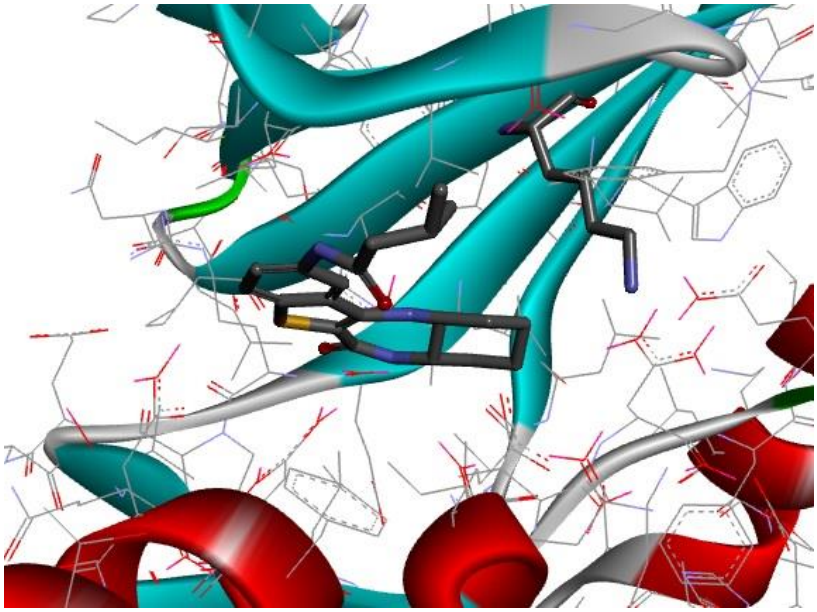

***Figure 71**: Compound **162**–PIM-1 active site docking studies.*

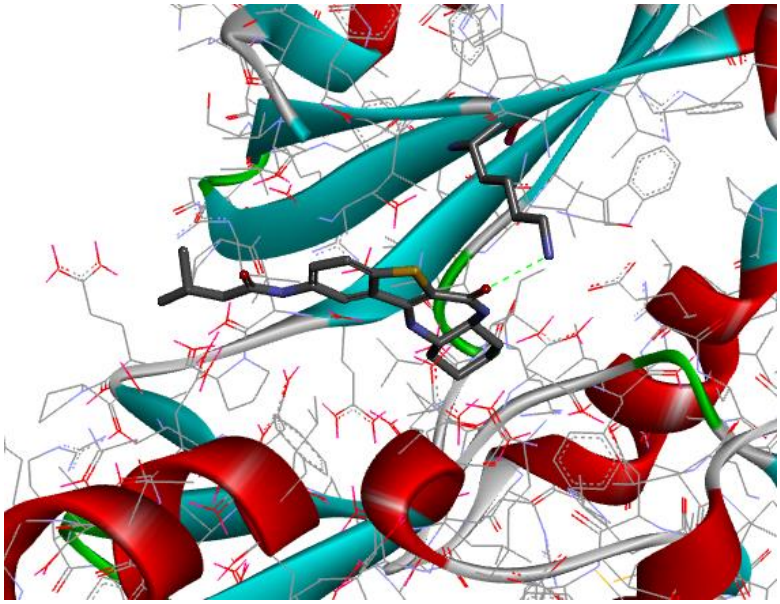

***Figure 72**: Compound **162**–PIM-3 active site docking studies.*

The docking studies previously described served as a useful tool to explain the differences in potency observed for PIM-1 and PIM-3 with compound **162**. We were aware that caution should be taken when interpretating this data as we were working from a virtual model. A PIM-3 crystal structure with **158**, **161**, and **162**, would be ideal in helping to fully understand the binding pose of these compounds. However, attempts at crystallizing **158**, **161** and **162**

proved unsuccessful, although our collaborators are currently optimizing the crystallization conditions.

Nevertheless, these interesting results encouraged us to carry out a SAR study which focused on varying the amides from position 9 to further increase the PIM-3 potency and selectivity over the PIM-2 and PIM-1 isoforms.

4.4. Further optimization of the potential PIM-3 probes

To continue exploring for potential PIM-3 inhibition, candidates shown in Figure 70 were prepared for a small SAR study using the conditions outlined in Scheme XXII and Scheme XXIII, where the nature of the acyl chloride was varied to provide us with a broad understanding of the topology of the pocket within the PIM-3 active site (Figure 73).

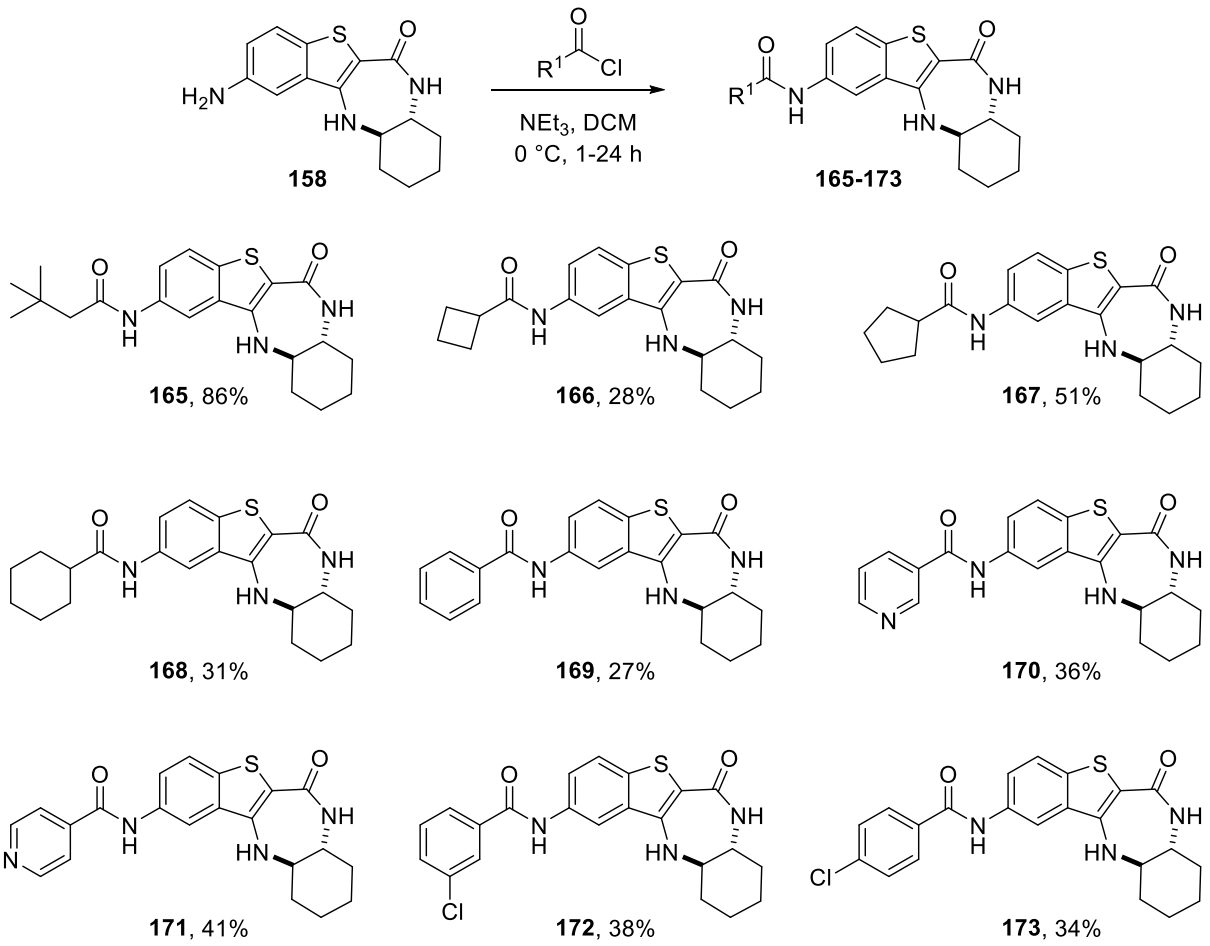

***Figure 73**: Compound structure and yields of **165**–**173**.*

This small SAR study comprised of compounds **166**–**168** which are derivatives of **162** and were designed to investigate how small changes in the amide group affected the PIM-3 activity/selectivity. Compound **165** contained a *tert*-butyl group instead of the isopropyl group present in **162** and it was prepared to study how subtle differences in the steric requirements of this area would affect the potency/selectivity. In addition, the cyclohexane was changed for a phenyl substituent (**169**) and the products from pyridinyl acyl chlorides andchlorophenyl substituents were also investigated (compounds **170**–**173**).

Compounds **165**–**173** were examined in a DSF assay and the results obtained are detailed in Table XXXVI.

Table XXXVI: *DSF data obtained for compounds **165**–**173**.*

Compound	PIM-1 (ΔT_m, °C)	PIM-2 (ΔT_m, °C)	PIM-3 (ΔT_m, °C)	CLK4 (ΔTm, °C)	CLK1 (ΔTm, °C)	CLK3 (ΔTm, °C)	DYRK1A (ΔTm, °C)	DYRK2 (ΔTm, °C)	SRPK1 (ΔTm, °C)	SRPK2 (ΔTm, °C)
165	1.7	2.4	3.9	3.3	0.4	0.0	1.0	4.9	0.5	0.3
166	2.6	1.9	5.3	2.6	2.5	0.1	1.5	5.6	1.1	0.4
167	0.1	1.0	0.6	0.2	0.1	0.0	-0.2	0.1	0.4	0.1
168	2.3	1.7	4.3	2.5	-1.2	0.1	1.3	4.4	1.9	0.7
169	4.9	4.9	5.5	4.1	2.6	1.6	3.0	5.4	9.8	3.5
170	4.5	2.5	5.2	5.5	4.0	2.7	3.0	5.8	3.7	1.3
171	4.0	1.3	4.4	5.9	5.6	3.3	2.2	6.0	5.0	1.5
172	4.3	2.6	4.2	4.7	1.7	1.3	3.0	3.7	7.6	3.4
173	0.7	0.6	0.7	0.6	0.7	0.2	0.4	0.9	2.0	0.6

The DSF assay results were very encouraging as poor activities were observed for the kinases studied within the assay, apart for the PIM-3 isoform. Furthermore, these results also showed selectivity towards the PIM-3 isoform over the PIM-1 and the PIM-2 isoforms, which was the aim of this study.

Due to the poor correlation between the DSF assay and the biochemical assay that has been observed for some previous compounds within these series, the DSF data results will be discussed together with the biochemical data obtained, presented in Table XXXVII.

Table XXXVII: *IC_{50} data obtained for compounds **165**–**173**.*

Compound	IC_{50} data			Selectivity (fold)	
	PIM-1 (nM)	PIM-2 (nM)	PIM-3 (nM)	PIM-3 over PIM-1	PIM-3 over PIM-2
165	>10000	>10000	487	21	21
166	2730	>10000	171	16	58
167	>10000	>10000	>10000	1	1
168	5960	>10000	516	12	19
169	1780	>10000	391	5	26
170	410	>10000	233	2	43
171	655	>10000	376	2	27
172	4920	>10000	1360	4	7
173	>10000	>10000	>10000	1	1

From the DSF data, changing the isopropyl group (**162**) for a tert-butyl group (**165**) decreased PIM-3 affinity, although the selectivity for PIM-3 over PIM-1 and PIM-2 was maintained. The compound showed ΔT_m values of 1.7 °C, 2.4 °C, and 3.9 °C, for PIM-1, PIM-2, and PIM-3, respectively. Compound **165** also showed a moderate selectivity over DYRK2, which gave a ΔT_m of 4.9 °C, and excellent selectivity towards the CLK, SRPK and DYRK1A kinases. The biochemical data for this compound was very encouraging; **165** showed a 21-fold selectivity for PIM-3 over both PIM-1 and PIM-2, with IC_{50} values of 10 µM for PIM-1, 10 µM for PIM-2, and 487 nM for PIM-3. Compound **166**, which contains a cyclobutyl substituent also showed good PIM-3 selectivity (16-fold selectivity for PIM-1 and 58-fold for PIM-2), with IC_{50} values of 2.73 µM for PIM-1, 10 µM for PIM-2, and 171 nM for PIM-3. Compound **166** showed a higher activity for PIM-3 compared to **165** which correlated well with the DSF assay. The compound showed ΔT_m values of 2.6 °C, 1.9 °C, and 5.3 °C, for PIM-1, PIM-2, and PIM-3, respectively, a higher affinity for DYRK2 (ΔT_m: 5.6 °C) and good selectivity towards CLK kinases, DYRK1A and SRPK kinases.

When the cycloalkane ring was larger such as for compound **167**, no activity was observed. For compound **167**, the DSF assay showed little affinity for the PIM isoforms as well as the CLK, DYRK or SRPK kinases, with ΔT_m values of`0.1 °C, 1.0 °C, and 0.6 °C, for PIM-1, PIM-2, and PIM-3 respectively. The IC_{50} data for this compound correlated well with the DSF assay results as next to no activity was observed with IC_{50} values of 10 µM for the three isoforms. For the analogue containing the cyclohexyl substituent, **168**, the affinity increased towards PIM-3, with ΔT_m values of 2.3 °C, 1.7 °C, and 4.3 °C for PIM-1, PIM-2 and PIM-3, respectively. For this compound (**168**), the selectivity observed was also encouraging, the

affinity for DYRK2 decreased (ΔT_m: 4.4 °C), and no CLK cross-reactivity was observed, as well as no affinity with the SRPK family. The selectivity for PIM-3 was confirmed in the biochemical data with IC_{50} values of 5.96 µM for PIM-1, 10 µM for PIM-2, and 0.52 µM for PIM-3.

Interestingly, the benzoyl analogue **169** increased the PIM affinity as well as the DYRK2 and SRPK1 affinities. The compound displayed a low selectivity profile within the DSF assay with ΔT_m values of 4.9 °C for PIM-1, 4.9 °C for PIM-2, 5.5 °C for PIM-3, 4.1 °C for CLK4 and 9.8 °C for SRPK1 (the highest SRPK1 value observed to date). It is important to note that this compound still showed selectivity for PIM-3 over PIM-1, and despite the poor selectivity within the DSF assay, the IC_{50} values were very encouraging: IC_{50} values of 1.78 µM for PIM-1), excellent selectivity over PIM-2 (IC_{50}: 10 µM, 26-fold selectivity), and 391 nM for PIM-3.

The compound containing pyridine substituents provided higher PIM potency but decreased the selectivity within the isoforms. This behaviour was expected as previous analogues from the benzothienopyrimidinone series (**43t**, and **43u**), showed increased PIM potency but decreased selectivity within the isoforms due to the pyridine forming hydrogen-bonding interactions with the receptor. The DSF assay data for these compounds (**170** and **171**) showed poor selectivity within the kinases studied with ΔT_m values of 4.5 °C and 4.0 °C for PIM-1, 2.5 °C and 1.3 °C for PIM-2, 5.2 °C and 4.4 °C for PIM-3, as well as a poor selectivity over CLK4 (ΔT_m of 5.5 °C for **170**, and 5.9 °C for **171**) and DYRK2 (ΔT_m of 5.8 °C for **170**, and 6.0 °C for **171**). Within the biochemical assay results, **170** showed an IC_{50} value of 410 nM for PIM-1, 10µM for PIM-2, and 391 nM for PIM-3. Similar to **170**, compound **171** showed an IC_{50} value of 655 nM for PIM-1, 10µM for PIM-2, and 376 nM for PIM-3. Both compounds provided the two highest IC_{50} values for PIM-1 within this series, and as the selectivity between the PIM-1 and PIM-3 isoforms was poor, these pyridine-based compounds were discarded from further selectivity studies.

Finally, it was observed that chlorobenzoyl substituents such as **172** and **173** resulted in lower activities, presumably due to the lack of space within the PIM active site, especially so for compound **173**. Compound **173** showed no affinity within the DSF assay as well as next to no activity within the biochemical assay, with IC_{50} values of > 10 µM for the three isoforms. The DSF assay for compound **172** showed a higher affinity with ΔT_m values of 4.3 °C for PIM-1, 2.6 °C for PIM-2, 4.2 °C for PIM-3, 4.7 °C for CLK4 and 7.6 °C for SRPK1, however, the biochemical data for this compound showed poor activities, although the compound

maintained the selectivity towards PIM-3, with IC_{50} values of 4.92 µM for PIM-1, 10 µM for PIM-2, and 1.36 µM for PIM-3.

4.5. Conclusions

The new benzothienodiazepine scaffold provided unexpected and very encouraging results. Introducing shape change into the scaffold increased the PIM-1 and PIM-3 potency as well as increasing the selectivity over the CLK, the SRPK and the DYRK kinases, but most importantly, the selectivity over the CLK4 receptor (suggested by DSF assay data). Furthermore, the scaffold also showed excellent selectivity against the PIM-2 isoform, which is fundamental for the development of PIM-1 or PIM-3 chemical probes.

From these SAR studies, we gathered important information on how to achieve PIM-1 or PIM-3 selectivity. For example, introducing small hydrophobic substituents such as the trifluoromethyl group in position 9 of the benzothienodiazepine scaffold provides PIM-1 over PIM-3 and PIM-2 selectivity (compounds **120**, **122** and **123**, Figure 74). Furthermore, these compounds provided selectivity over the CLK, DYRK and SRPK kinases within the DSF assay (Table XXXVIII) with ΔT_m values of 2.2–2.8 °C for CLK4, 2–3.3 °C for CLK1, 2.1–2.6 °C for DYRK2, and 0 °C for CLK3, DYRK1A, and the SRPK family.

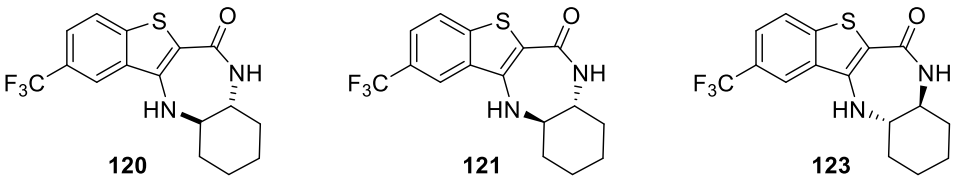

***Figure 74**: PIM-1 selective compounds **120**, **121** and **123**.*

Table XXVIII: *DSF data of compounds **120**, **121**, and **123**.*

Compound	PIM-1 (ΔT_m, °C)	PIM-2 (ΔT_m, °C)	PIM-3 (ΔT_m, °C)	CLK4 (ΔTm, °C)	CLK1 (ΔTm, °C)	CLK3 (ΔTm, °C)	DYRK1A (ΔTm, °C)	DYRK2 (ΔTm, °C)	SRPK1 (ΔTm, °C)	SRPK2 (ΔTm, °C)
120	7.2	3.0	5.7	2.8	2.8	0.4	1.4	2.6	0.0	0.0
121	6.5	2.6	4.9	2.2	2.0	0.0	0.6	2.1	0.0	0.2
123	6.6	2.2	N/A	2.8	3.3	0.5	1.0	2.4	0.0	0.2

The SAR study also showed the importance of both the amide within the diazepine ring and the secondary amine. It was observed that changing the amide moiety for an ester (**124** and **126**) decreased the PIM potency as shown in Figure 75. Compound **120** showed an activity of 30 nM for PIM-1 whereas **124** had decreased activity of 412 nM, presumably due to the loss of hydrogen bonding formation between the N-H from the amide and the Asp186 from the PIM-1 isoform. Furthermore, methylation of the secondary amine such as in compound **131** also decreased the potency towards the PIM kinases. Analogue **126** showed an IC_{50} value of 324 nM for PIM-1, however, methylation of the secondary amine (**131**) showed complete loss of activity.

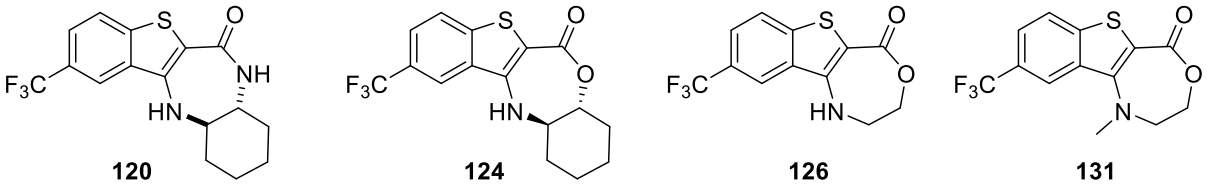

PIM-1 (IC_{50}): 30 nM
PIM-2 (IC_{50}): 6.9 μM
PIM-3 (IC_{50}): 103 nM

PIM-1 (IC_{50}): 412 nM
PIM-2 (IC_{50}): 50 μM
PIM-3 (IC_{50}): 267 nM

PIM-1 (IC_{50}): 324 nM
PIM-2 (IC_{50}): 1.6 μM
PIM-3 (IC_{50}): 696 nM

no activity

***Figure 75**: IC_{50} data and compound structures of **120**, **124**, **126**, and **131**.*

Interestingly, further analysis of analogue **158** led to the discovery of potential PIM-3 selective probes. Position 9 of the benzothienodiazepine scaffold suggested the possibility of achieving selectivity for PIM-3 over the PIM-1 and PIM-2 isoforms. Introducing polar groups at position 9 led to compounds **158**, **161** and **162** (Figure 76), which showed excellent PIM-3 potency as well as good selectivity over PIM-1 and PIM-2.

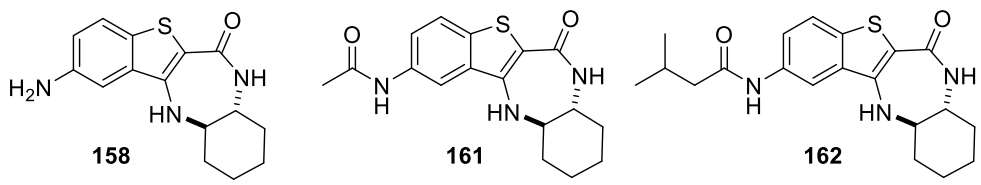

158	**161**	**162**
IC_{50} data	**IC_{50} data**	**IC_{50} data**
PIM-1: 1.4 μM	**PIM-1:** 1.5 μM	**PIM-1:** 2 μM
PIM-2: 10 μM	**PIM-2:** 23.7 μM	**PIM-2:** 12.7 μM
PIM-3: 59 nM	**PIM-3:** 55 nM	**PIM-3:** 83 nM

***Figure 76**: PIM-3 selective analogues **158**, **161** and **162**.*

The data obtained for **158**, **161**, and **162** led us to carry out a final SAR study to try to improve the PIM-3 selectivity/potency by varying the amide substituent at position 9 of the scaffold. Molecular modelling studies were performed and as an outcome, **165**–**173** were prepared. This final set of compounds represented a breakthrough for our project. Within this SAR study we were able to maintain the PIM-3 selectivity over PIM-1 and PIM-2, We were very pleased to see that our efforts at understanding the differences between the PIM isoforms finally led us to two different directions of research resulting in the ability to switch potency and selectivity between the PIM-1 and the PIM-3 isoforms.

Furthermore, some PIM-3 over PIM-1 selectivity was observed when studying position 8 of the benzothienodiazepine scaffold. This position was not further studied examined this project. However, it could be an additional direction of research for the development of PIM-3 chemical probes.

Regarding the PIM-2 isoform, potency and selectivity towards this isoform was not observed during this study. Nevertheless, PIM-2 chemical probes are also a priority and will be our next direction of research together with the optimization of PIM-1 and PIM-3 chemical probes.

5. Additional biological studies

Our efforts to discover potential PIM probes prompted further biological evaluation on promising candidates. The extensive SAR study that has been presented within this thesis provided some excellent results and some potential PIM-1 and PIM-3 chemical probes. However, in order to determine whether one of the potential compounds might be a valid chemical probe, further biological characterization was required. To conclude the work described within this thesis, additional biological data obtained for the most interesting compounds is presented. These assays were carried out at various institutions and provided information that highlighted the potential of these compounds as selective probes.

5.1. Cellular assay data

Some of the candidates previously presented displayed very good activities towards the PIM isoforms. Cellular activity was an important feature to consider when optimizing and developing a good quality chemical probe. At the Centro Nacional de Investiaciones Oncológicas (CNIO), the assay to measure the inhibition of the phosphorylation of BAD protein by PIM-1 was well-established (pBAD assay, described in Section 8.2). Therefore, as part of my three-month placement, the cytotoxicity of the compounds and the inhibition of the phosphorylation of BAD protein by PIM-1 by our compounds was analyzed.

Because PIM-1 is believed to be the protein kinase responsible for the phosphorylation of the BAD protein, candidates that showed low nanomolar potencies for the PIM-1 isoform were studied. We selected compounds from the benzothienopyrimidinone series (Chapter 2), and the phenyl pyrimidinone series (Chapter 3) (Figure 77). Compounds **43a**, **43h**, **43n**, **43s**, **43u**, **46a**, **47a** and **99** showed low nano molar potencies for PIM-1 with IC_{50} values between 32–94 nM. Compound **99** proved to be the most active PIM-1 compound from the phenyl pyrimidinone series at the time of the cell-based assay study. We were also interested in studying the behaviour of the new phenyl pyrimidinone scaffold in cells, therefore, **99** was also included in the assay.

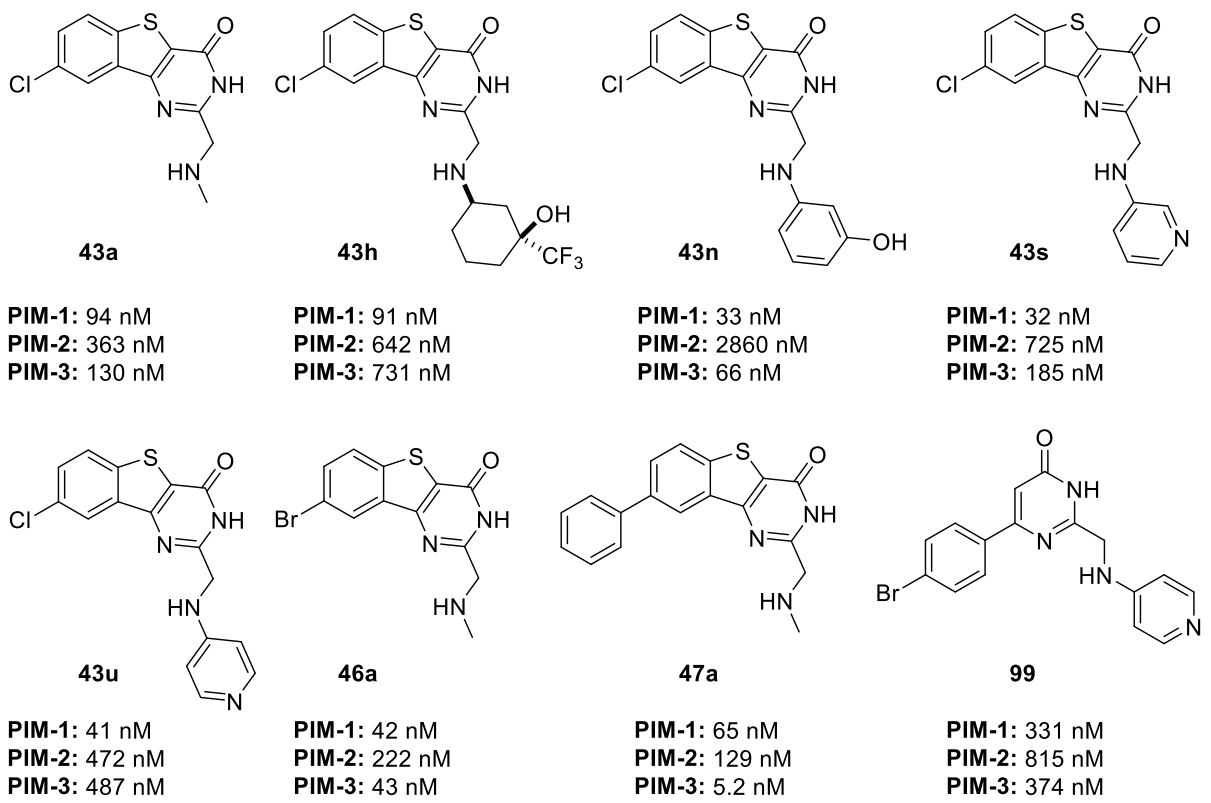

***Figure 77**: IC_{50} data for compounds **43a**, **43h**, **43n**, **43s**, **43u**, **46a**, **47a** and **99**.*

The data obtained from the pBAD assay is shown in Table XXXIX. The assay was carried out using the Protocol 8.2 and the corresponding EC_{50} values were calculated.

Table XXXIX: *pBAD assay results.*

Compound	EC_{50} (µM)
43a	1.14
43h	>10
43n	0.31
43s	>10
43u	1.98
46a	0.63
47a	0.42
99	>10
13937702	0.01

The CNIO control compound (**13937702**) is a confidential CNIO compound that displayed remarkable activity in the pBAD assay. In order to assess whether the assay was reproducible

and the values obtained were acceptable, a control compound was always included and with a reproducible value within assays. In our case, **13937702** displayed an EC_{50} (0.01 µM) which is an acceptable value previously observed within the CNIO. Therefore, the assay was considered satisfactory. The data proved very encouraging. The compounds containing a methyl amine functionality showed excellent data as good activity was observed for the three compounds **43a** (1.14 µM), **46a** (0.63 µM), and **47a** (0.42 µM). Compound **43h** did not display activity in cells (EC_{50}: > 10 µM). Even though the compound showed very good PIM-1 activity in the previous biochemical assays (IC_{50}: 91 nM), the loss of activity in a cell-based assay could be due to poor solubility or permeability of the compound. Compound **43n**, containing the 4-hydroxyaniline, also showed very good potencies for PIM-1 (33 nM), and PIM-3 (66 nM), and we were very pleased to observe an EC_{50} of 310 nM within the cellular assay. The amino pyridine derivatives displayed poor activity (EC_{50} **43s**: > 10 µM; **43u**: 1.98 µM), which could be due to the poor permeability of these compounds.

Unfortunately, compound **99**, the only analogue representing the phenyl pyrimidinone series, showed no activity (EC_{50}: > 10 µM). This loss of activity could be associated to the compound's poor biochemical activity (IC_{50}: 331 nM). Previous work with cell based assays at the CNIO revealed that very potent compounds, with low nano molar IC_{50} values (1–100 nM), were required in order to observe good activity in a cell-based environment. Therefore, it is believed that more potent analogues containing the phenyl pyrimidinone scaffold, such as **109**, **110** or **111**, might have the potential to show better data in a cellular environment.

The most interesting candidates from the benzothienodiazepine series were also evaluated (Figure 78). These analogues, **120–123**, **133–134**, and **149**, displayed little to no activity for PIM-2, and excellent potencies for PIM-1 and PIM-3, with a slight selectivity towards the PIM-1 isoform. Compound **149**, was the most active compound for PIM-1 (IC_{50}: 26 nM), but also showed good potencies for PIM-2 (IC_{50}: 406 nM) and PIM-3 (IC_{50}: 258 nM).

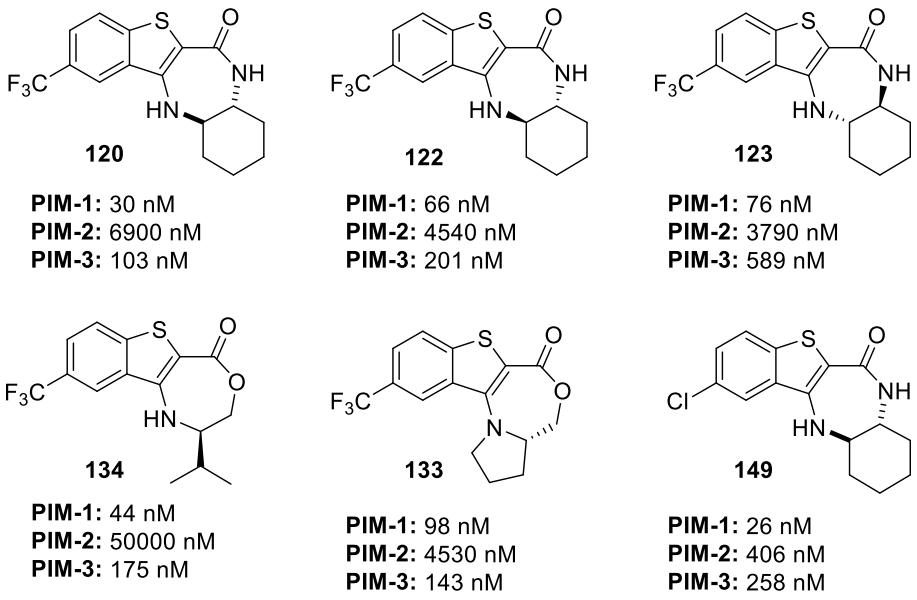

***Figure 78**: Compound structure and IC_{50} data of **120–123**, **133–134**, and **149**.*

We were very pleased to see the data obtained for the benzothienodiazepine series. All compounds displayed lower EC_{50} values than for **43a**, **43h**, **43n**, **43s**, **43u**, **46a**, **47a** and **100**, reinforcing the fact that the analogues were responsible for the inhibition of the phosphorylation of BAD by the PIM-1 isoform. The data obtained for the pBAD assay is presented in Table XL.

Table XL: *pBAD EC_{50} data for compounds **120–123**, **133–134**, and **149**.*

Compound	EC_{50} (µM)
120	0.12
122	>10
123	0.20
134	0.81
133	0.53
149	0.24
13937702	0.01

The control (**13937702**, CNIO reference) provided a satisfactory value, EC_{50} of 0.01 µM, therefore, the values obtained for these analogues were considered acceptable. Overall, the compounds displayed an EC_{50} < 1 µM, except compound **122** which did not show any activity (EC_{50} > 10 µM). We believed that the compound had to be tested again as both the racemic

mixture **120** and the enantiomer **123** provided similar results with EC_{50} values of 0.12 μM for **120** and 0.20 μM for **123**. The outcome of the assay for compound **120** is represented in Figure 79. As previously mentioned, the data was obtained by plotting the Log[compound concentration, μM] *vs* the percentage of inhibition. It was observed that both duplicates satisfactorily correlated and a curve with the expected shape was then obtained, indicating the success of the assay. The exact EC_{50} value for each inhibitor was calculated using Activitybase and GraphPad softwares.

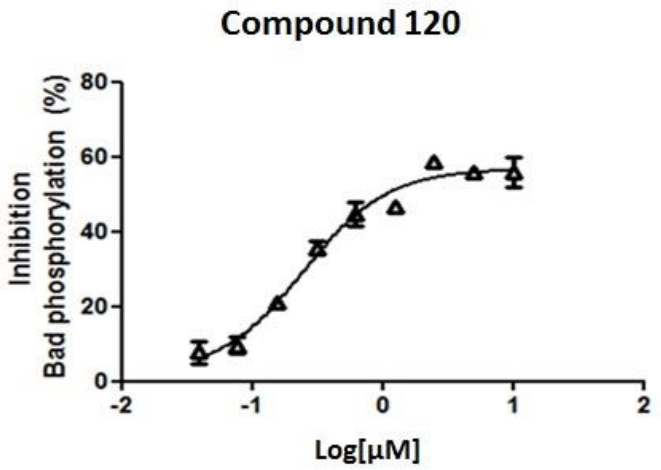

***Figure 79**: pBAD assay curve for compound **120**.*

Compounds **134** and **133**, containing the ester moiety, also showed good potencies with EC_{50} values of 0.81 μM for **134** (Figure 80), and 0.53 μM for **133**. The slightly loss of activity seen in the cellular assay regarding **134** and **133** was related to the permeability and solubility of the compounds, which will be discussed in more detailed later on. Nevertheless, we were very pleased to observe that the analogues were still able to show inhibition of a cellular mechanism. Finally, **149**, containing the chlorine atom at position 9 instead of a trifluoromethyl group, also provided very encouraging data (EC_{50}: 0.24 μM, Figure 81).

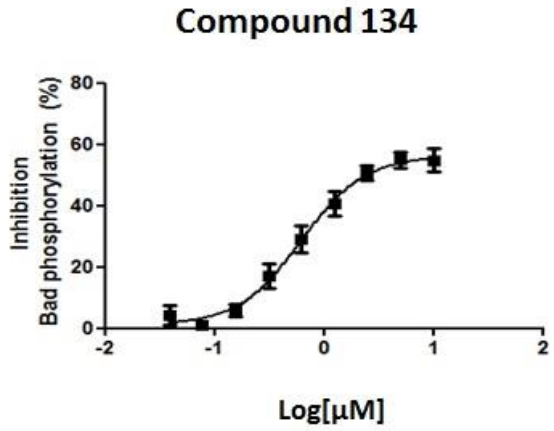

***Figure 80**: EC_{50} curve for compound **134**.*

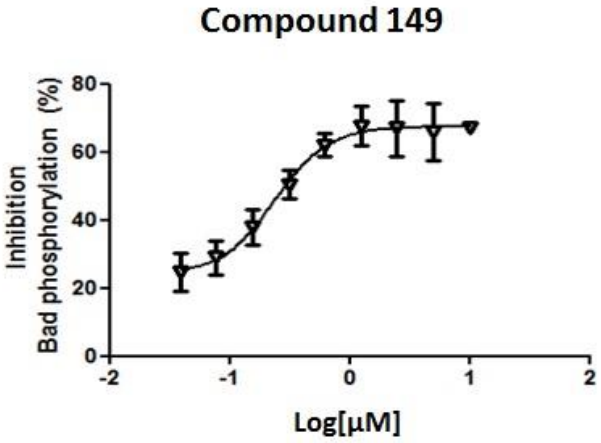

***Figure 81**: EC_{50} curve for compound **149**.*

The cellular data obtained for these analogues was remarkable which was very important for the design of chemical probes. The high potencies observed for PIM-1 in the biochemical assay correlated with cell based assays and we were able to obtain EC_{50} values in the nanomolar range. We were aware that the selectivity towards PIM-1 was not optimal, but we also believe that further optimization could be carried out to achieve further PIM-1 selectivity to design a PIM-1 chemical probe.

To continue characterizing the PIM-1 selective compounds previously presented, a small study of the permeability and solubility, together with some PIM-3 selective candidates was carried out. The solubility and permeability of the analogues were two important properties to consider when designing a good quality chemical probe or a drug candidate. For a chemical probe design, these represented important studies to analyze whether the compounds were

entering the cells. However, when designing a drug, these two properties become extremely important and are directly related to the pharmacokinetics of the drug (ADME properties). We believed that understanding these properties within our analogues could prove useful for future design and optimization studies.

5.2. Analysis of the permeability and solubility

Following the protocol described in sections 8.3.1 and 8.3.2, the solubility and permeability of the compounds were analyzed. The data obtained for each compound is summarized in Table XLI. The permeability was measured using the Pampa procedure from BD Genetest™ (detailed in section 8.3.2). In this table, the maximum concentration in aqueous solubility obtained for every compound is also shown, as well as the cellular activity obtained for the PIM-1 candidates (Figure 82).

Finally, the permeability and solubility of compounds **158**, **159**, and **16** (Figure 82) was also analyzed. To date, cellular assays to assess the inhibition of the PIM-3 isoform have not been available to our project. However, we thought that information on the permeability and solubility of the PIM-3 selective compounds would be useful if future cell based assays are carried out with these compounds.

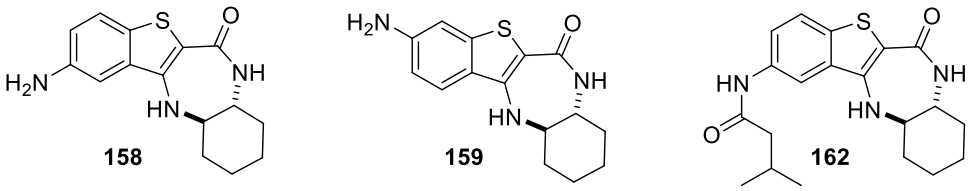

PIM-1: 1410 nM
PIM-2: 9890 nM
PIM-3: 59 nM

PIM-1: 1170 nM
PIM-2: 16600 nM
PIM-3: 365 nM

PIM-1: 1950 nM
PIM-2: 12700 nM
PIM-3: 83 nM

Figure 82**: PIM-3 selective compounds **158**, **159** and **162

Table XLI: *Permeability and solubility data of compounds **43n**, **43u**, **120**, **122**, **124**, **134**, **133**, **149**, **158**, **159**, and **162**.*

Compound	PERMEABILITY PAMPA (x 10^{-6} cm/s)	SOLUBILITY (max concentration aqueous solubility, µM)	P-BAD assay EC_{50} (µM)	Target
43n	3.02	5	0.31	PIM-1
43u	0.00	100	>10	
120	0.84	100	0.12	
122	3.69	10	>10	
124*	1.46	50	N/A	
134	2.48	5	0.81	
133	0.80	50	0.53	
149	4.23	10	0.24	
158*	1.56	50	N/A	PIM-3
159*	0.65	100	N/A	
162*	1.14	100	N/A	

*Cellular data not obtained for **124**, **158**, **159**, and **162**.

Before the permeability of the compound was analyzed, the maximum aqueous solubility concentration was first determined for each compound. The concentrations at which each compound showed the highest aqueous solubility were then used to carry out the PAMPA assay. Following the BD Genetest™ criteria,[93] for the determination of the permeability of a drug candidate, a compound would be considered to have low permeability if the value obtained was lower than 1.5 x 10^{-6} cm/s, while a value higher than 1.5 x 10^{-6} cm/s would indicate a highly permeable compound.

From the data in Table XLI, the lack of potency observed in the cellular assay for the PIM-1 candidates can be explained by the permeability and solubility data. Compound **43n** showed an EC_{50} value of 0.31 µM, as well as a great permeability (3.02 x 10^{-6} cm/s), and a moderate aqueous solubility (5 µM). The poor cell activity observed for compound **43u** may be understood if looking at the permeability data (0.0 x 10^{-6} cm/s), suggesting that the compound might not be entering the cells and therefore no activity was measured.

We were very encouraged by compound **120**, which showed a moderate to good permeability (0.84 x 10^{-6} cm/s), a good aqueous solubility (100 µM), as well as an excellent cellular value (0.12 µM).

The data obtained for the corresponding enantiomer **122** proved surprising. Despite the compound not displaying any activity within the cellular assay, **122** showed encouraging permeability values (3.69 x 10^{-6} cm/s) as well as good aqueous solubility (10 µM). This data suggested that the compound should be re-tested in the pBAD assay.

We were interested to analyze the difference in properties between **120** and **124**, containing the amide moiety (**120**) and the ester group (**124**). Compound **124** increased the permeability of the compound with a value of 1.46 x 10^{-6} cm/s, but slightly decreasing the solubility to a maximum concentration of 50 µM. The changes observed could be explained when comparing the polarity between the ester group and the amide. The higher polarity of the amide group facilitates the aqueous solubility but induces lower cell permeability.

Compound **134** showed a good permeability value (2.4 x 10^{-6} cm/s), but a low aqueous solubility (5 µM). The outcome of the kinetic aqueous solubility assay is shown in Figure 83. Following the General Protocol 8.3, dilutions of 0.5 µM, 1 µM, 5 µM, 10 µM, 50 µM, and 100 µM of the studied compound were obtained in a 96-well plate. 50 µL from each well was transferred to a 96-well plate and diluted with 150 µL of acetonitrile/0.1% formic acid. For each compound, the solubility was quantified through individual standard peak area calibration at a known concentration. For example, the outcome of the assay for compound **134** is represented in Figure 83. The table represents the initial concentration, the final concentration of injection, the peak area (Cps), and the retention time (Rt) during the LC-MS method.

Concentracion (µM)	Conc (µg/ml)	Cps	Rt
0.5	0.1646	3570	3.23
1	0.3293	7837	3.23
5	1.6467	40118	3.21
10	3.2934	63876	3.21
50	16.467	16883	3.21
100	32.934	13499	3.21

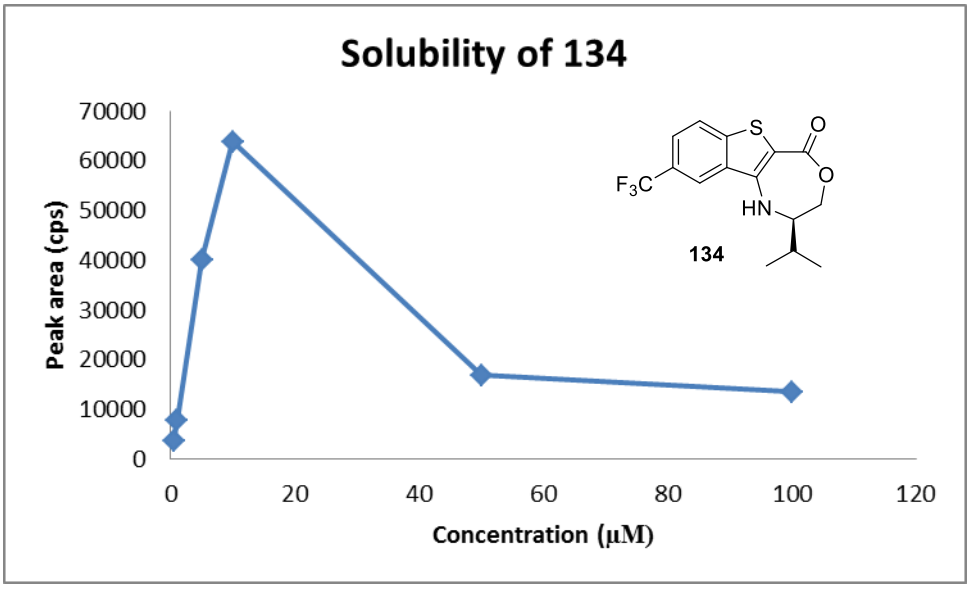

***Figure 83**: Aqueous solubility assay for compound **134**.*

The peak area is proportional to the concentration. Therefore, a straight line should be observed in the plot for a compound that is water soluble at 100 µM. Following this principle, we were able to quantify the maximum aqueous solubility of our analogues. In the case of **134**, saturation was observed after reaching a concentration of 5 µM, indicating that the approximate maximum aqueous solubility for **134** corresponds to a concentration of 5 µM. Nevertheless, **134** still displayed good cellular activity with an EC_{50} value of 0.81 µM.

Finally, **133** and **149** displayed good EC_{50} values of 0.53 µM and 0.24 µM respectively, as well as good solubility and permeability data. The permeability obtained was moderate for **133** with a value of 0.8 x 10^{-6} cm/s and excellent for **149** (4.23 x 10^{-6} cm/s), with good solubility for both **133** (50 µM) and **149** (10 µM).

Regarding the potential PIM-3 selective compounds **158**, **159**, and **162**, the data proved very encouraging as excellent solubility was displayed for **158** (50 µM), **159** (100 µM), and **162** (100 µM, Figure 84). The data obtained for compound **162** is shown in Figure 84, where a straight line is observed, indicating that the compound is water soluble to a concentration of 100 µM. Regarding permeability, **158** proved to be highly permeable (1.56 x 10^{-6} cm/s), whereas **159** had decreased permeability of 0.65 x 10^{-6} cm/s, and **162** proved to be close to the highly permeable limit with a value of 1.14 x 10^{-6} cm/s.

Concentracion (µM)	Conc (µg/ml)	Cps	Rt
0.5	0.1436	1713	2.79
1	0.2873	2413	2.77
5	1.4369	11108	2.77
10	2.8738	22849	2.77
50	14.369	87870	2.76
100	28.738	192100	2.78

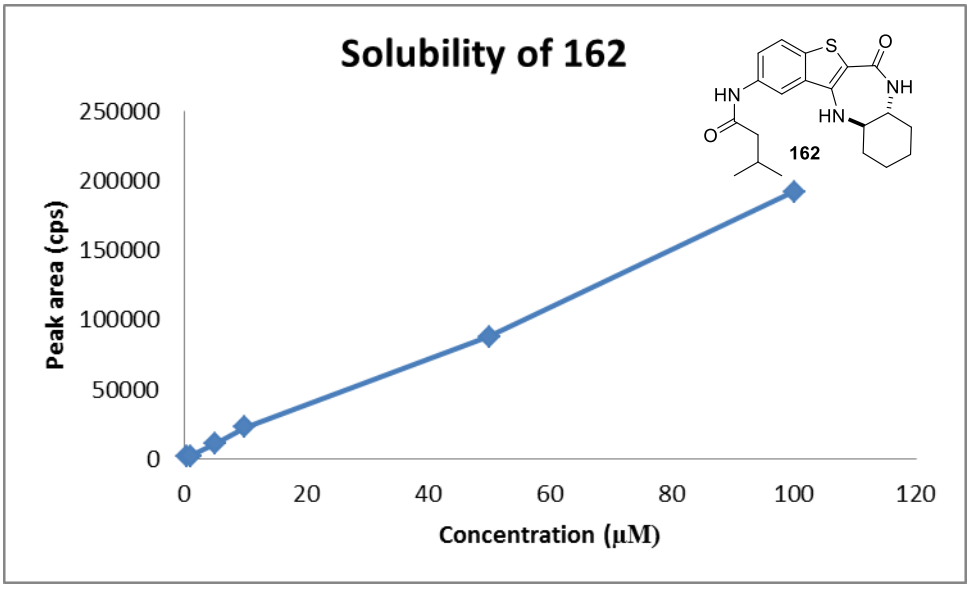

***Figure 84**: Solubility assay data for compound **162**.*

In summary, we have shown that the designed analogues display good cellular activity, as well as encouraging permeability and solubility data which takes us a step forward for the design of chemical probes for the PIM isoforms.

We are aware that additional biological assays, such as PIM-3 cell based assays, are required, however, we are currently working to find an appropriate assay that will give us cellular activity for the PIM-3 selective candidates. In the meantime, other biological data has been obtained to support our efforts to identify chemical probes.

5.3. Other biological studies

5.3.1. Study of the selectivity against Haspin and FLt_3

Within the CNIO, the measurement of the activity against Haspin and FLt_3 kinases is also studied when designing PIM inhibitors. Both Haspin and FLt_3 have previously shown cross-reactivity with the PIM kinases,[94, 95] Therefore, achieving selectivity over both Haspin and FLt_3 was also required for a good quality chemical probe design. To provide additional data for the selectivity of our analogues, compounds **120** and **134** (representing the PIM-1 selective candidates) as well as **158** and **162** (PIM-3 candidates) were studied against both protein kinases.

The FLt_3 kinase assay was carried out using the ADP Hunter technique, and the data obtained is shown in Table XLII. For the study of the Haspin activity, ADP Glo technique was used,[96] and the data obtained is also shown in Table XLII.

Table XLII: *Study of the activity against Flt_3 and Haspin.*

Compound	FLt_3 (ADP Hunter, IC_{50}, µM)	Haspin (ADP Glo, IC_{50}, µM)
120	>50	80.0
134	>50	12.5
158	>50	22.0
162	>50	53.0

The data obtained showed remarkable selectivity for these analogues against both FLt_3 and Haspin protein kinases. The analogues showed a low activity against FLt_3 with IC_{50} values of > 50 µM as well as little activity against Haspin with IC_{50} values of 80 µM (**120**), 12.5 µM (**134**), 22 µM (**158**), and 53 µM (**162**).

This data serves as an encouragement to carry on with the optimization of these candidates. At this stage, a full kinase screening profile would prove very useful to assess the real selectivity of these analogues against an expanded list of human kinases. Unfortunately, due

to the elevated cost of this type of assay, it was our priority to confirm the degree of selectivity observed within our candidates. To do so, alternative kinetic assays were carried out with the most interesting candidates to confirm the potency and selectivity that was previously observed.

5.4. PIM-3 selective candidate

From the data obtained for compounds **158**, **159**, **161** and **162**, we selected **162** as a PIM-3 selective candidate due to its good selectivity over PIM-1 and PIM-2, the excellent solubility and permeability data, and the remarkable selectivity observed against Haspin and FLt_3 (Figure 85). Unfortunately, we thought that **158**, and **161**, did not show the required PIM-1 selectivity and further optimization would be required before any compounds are tested in a kinome scan.

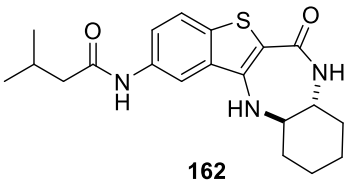

162

Compound	PIM-1 (IC_{50}, nM)	PIM-2 (IC_{50}, nM)	PIM-3 (IC_{50}, nM)	FLt_3 (IC_{50}, nM)	Haspin (IC_{50}, nM)
162	1950	12700	83	50000	53000

Permeability (cm/S)	Solubility (µM)
1.14×10^{6}	100

***Figure 85**: Biological data obtained for **162**.*

To confirm the selectivity observed towards the PIM-3 isoform before any other assays were carried out for **162**, the compound was sent to Eurofins Scientific, a worldwide laboratory testing service. Compound **162** was tested using the ADP Glo technique against both PIM-1 and PIM-3, and an IC_{50} value was obtained for both protein kinases. At this stage, due to the elevated costs of the assay, **162** was not tested against the PIM-2 isoform due to the high selectivity observed (IC_{50}, PIM-2 = 12700 nM). The dose response curves for PIM-1 and PIM-3, together with the IC_{50} values, obtained from the assay are shown in Figure 86.

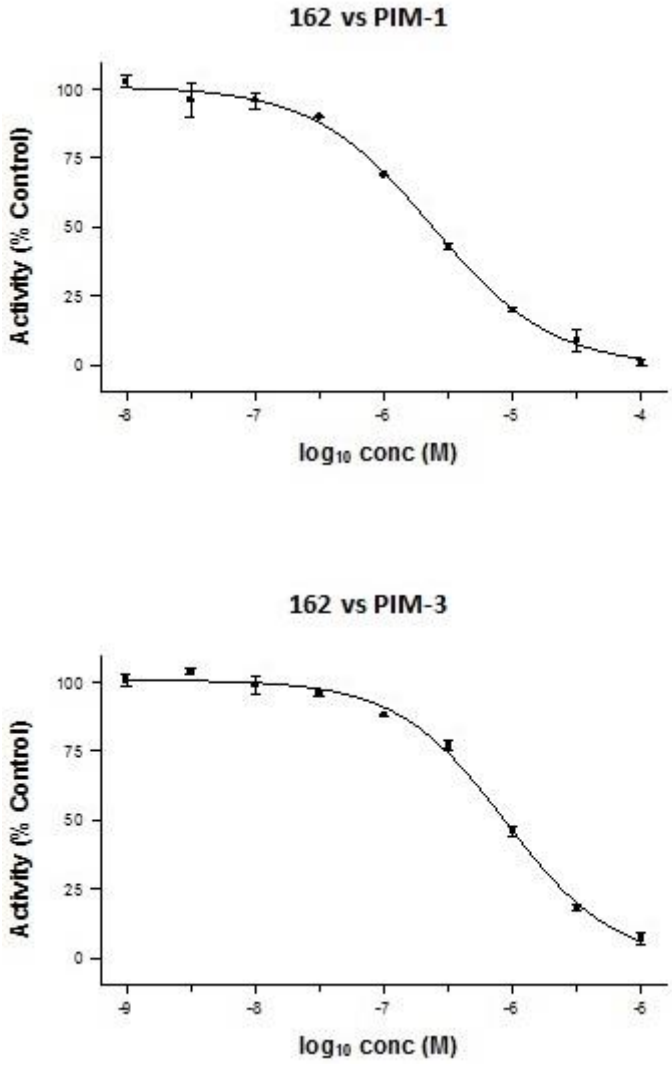

Compound	PIM-1 (IC_{50}, nM)	PIM-3 (IC_{50}, nM)
162	2366	873

***Figure 86**: Dose-Response curves and IC_{50} values for **162** with PIM-1 (top), and **162** with PIM-3 (bottom).*

The data obtained from Eurofins Scientific was surprising as different IC_{50} values were observed for the PIM-1 and the PIM-3 isoforms than the values observed when using the previous assay. An IC_{50} value of 2366 nM was obtained for PIM-1, which correlated with the data obtained at the CNIO (IC_{50}, ADP Hunter technique: 1950 nM) and 873 nM for the PIM-3 isoform, considerably higher than the observed using the ADP Hunter technique at the CNIO (IC_{50} = 83 nM). Despite the differences between the data, it was still encouraging to observe

that the compound maintained selectivity towards the PIM-3 isoform over the PIM-1 isoform (2.7-fold selectivity).

The differences observed between both assays were unexpected and a third assay was therefore needed in order to draw a more solid conclusion. Our collaborators at the SGC agreed to carry out the isothermal titration calorimetry (ITC)[97] assay with compound **162** against PIM-1, PIM-2 and PIM-3.

5.4.1. ITC data of compound 162

Isothermal titration calorimetry is a technique that analyzes biomolecular interactions. The assay measures the heat generated or absorbed when molecules interact. This type of assay can be applied to the study of multiple interactions such as protein-small molecule, enzyme-inhibitor and protein-DNA interactions, amongst others. The outcome of the assay is, therefore, a binding constant, K_D, which correlates with both IC_{50} and EC_{50}.

Following the protocol detailed in Section 8.5, compound **162** was first tested with the PIM-3 isoform and the results are shown in Figure 87.

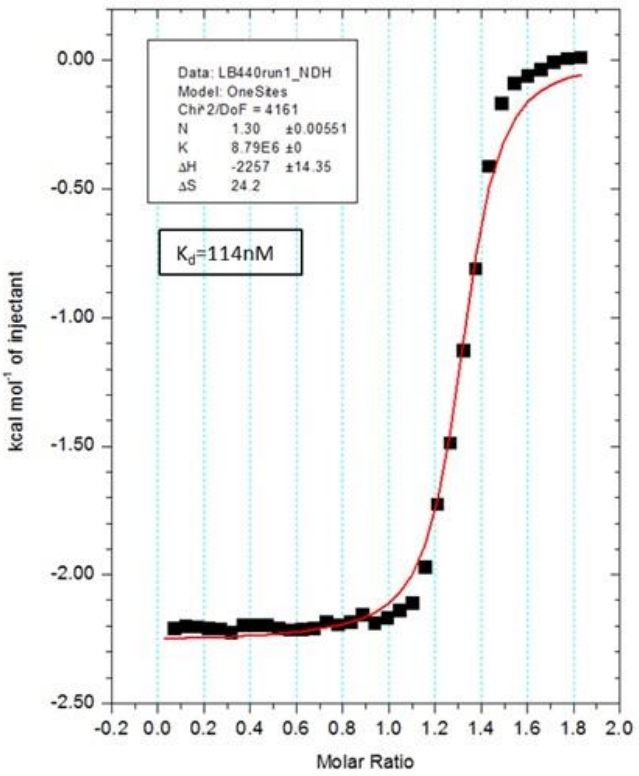

***Figure 87**: ITC data obtained for **162** and PIM-3.*

A K_D constant of 114 nM was obtained for **162** against the PIM-3 isoform. This data was very encouraging as it correlated with the previous IC_{50} data from the CNIO (IC_{50}: 88 nM), suggesting low nanomolar potencies for **162**, whereas the Eurofin data provided an IC_{50} of 873 nM for the PIM-3 isoform.

The ITC data for **162** in PIM-1 and PIM-2 is currently ongoing. The proteins are currently being expressed and therefore the ITC data in PIM-1 and PIM-2 have not yet been generated, and will not be presented within this thesis.

Other compounds within the same series such as **158** (Figure 88), also showed PIM-3 selectivity, and were also included in the ITC assay to determine if similar values were obtained between the two assays. Unfortunately, this compound precipitated when carrying out the experiment at 25 °C, and an accurate value could not be obtained. The assay was also carried out at 15 °C to avoid precipitation of the compound, but the heat produced by the binding was too weak to obtain a constant value.

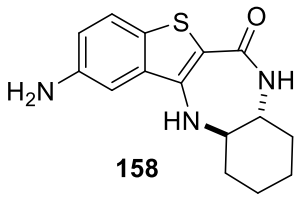

158

PIM-1: 1410 nM
PIM-2: 9890 nM
PIM-3: 59 nM

***Figure 88**: Compound structure and IC_{50} data of **158**.*

Our collaborators at the SGC are currently expressing more PIM-3 protein to carry out the ITC assay with other PIM-3 selective compounds. This data will provide the opportunity to compare whether the IC_{50} values from the CNIO and the ITC correlate and we can draw a solid conclusion on the potency/selectivity of these potential candidates.

6. Conclusions

PIM kinases are a family of serine/threonine kinases that have become relevant targets due to their important role in inflammation and cancer. PIM kinase inhibitors have been extensively investigated in past years. However, most of the inhibitors that have been published in the literature target the three isoforms simultaneously. Little is known about the mechanism of these important receptors separately. Therefore, it was our aim to provide the scientific community with chemical probes for the PIM isoforms. Chemical probes are considered to be urgently needed in order to dissect the fundamental biology of relevant receptors. Designing selective probes will provide researchers with the tools for POC studies of relevant targets, and will promote new drug discovery areas, as well as giving a solid understanding of the mechanism of the target studied before any process is initiated, which will subsequently maximise the success of the research programme.

The conserved catalytic domain in protein kinases makes these receptors very challenging to target selectively. Furthermore, PIM kinase isoforms (PIM-1, PIM-2, and PIM-3) share 60-70% of their amino acid sequence, which added difficulty when designing PIM isoform selective probes. Nevertheless, it was our aim to study the various differences between the isoforms and apply these studies to the design of selective probes.

Through molecular modelling studies, chemical synthesis and biological evaluation, three different chemical series have been studied and excellent results have been generated.

6.1. The benzothienopyrimidinone series

The project started through extensive molecular modelling studies to analyze the differences between the three PIM isoforms. To do so, the benzothienopyrimidinone compound published by Abbot Laboratories[1] was selected and served as a starting point for the design and synthesis of the chemical probes.

An initial SAR study of the Abbot compound led to compounds **43a**, **43h** and **43u** (Figure 89), which provided very interesting candidates with high potencies for the PIM kinases despite low selectivity. Examples of potent compounds are **43a**, **43h** and **43u**, where cellular data and permeability/solubility data was also obtained. Despite the poor selectivity observed for these compounds within the PIM isoforms as well as CLK4, they served as useful tools for

the understanding of the topology of the PIM kinases catalytic site. From this SAR study, it was observed that hydrogen bond donors/acceptors around the 2-position of the benzothienopyrimidinone core (such as methylamine, trifluorocyclohexanol, or 4-aminoyridine) increased the potency for the PIM kinases but decreased the selectivity within the isoforms. These compounds offered good PIM-1 potencies (IC_{50}: 41–94 nM), and moderate PIM-2 and PIM-3 selectivity with PIM-2 IC_{50} values of 363 nM (**43a**), 642 nM (**43h**), and 472 nM (**43u**), and PIM-3 IC_{50} values of 130 nM (**43a**), 731 nM (**43h**), and 487 nM (**43u**). Furthermore, the compounds showed promising selectivity over the CLK1 isoform, the CLK3 isoform, the DYRK and the SRPK families, but potentially high cross-reactivity with the CLK4 protein kinase with ΔT_m values of 4.7–6.6 °C.

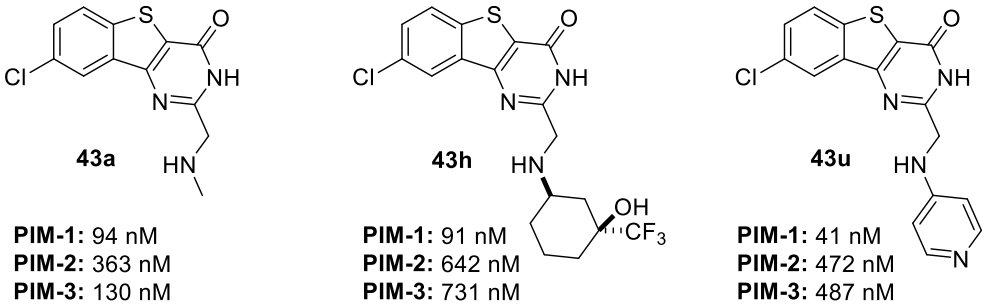

Compound	PIM-1 (ΔTm, ºC)	PIM-2 (ΔTm, ºC)	PIM-3 (ΔTm, ºC)	CLK4 (ΔTm, ºC)	CLK1 (ΔTm, ºC)	CLK3 (ΔTm, ºC)	DYRK1A (ΔTm, ºC)	DYRK2A (ΔTm, ºC)	SRPK1 (ΔTm, ºC)	SRPK2 (ΔTm, ºC)
43a	7.4	4.1	7.1	4.7	3.4	0.5	3.0	2.2	0.0	1.0
43h	6.9	3.1	5.3	6.1	3.8	0.5	3.7	1.2	0.0	0.3
43u	7.1	4.8	7.9	6.6	4.9	0.7	3.2	2.5	0.0	0.4

***Figure 89**: Compound structure, DSF and IC_{50} data for **43a**, **43h**, and **43u**.*

This data led us to consider other areas of SAR study using this scaffold. Molecular modelling studies revealed that the PIM kinases contained a very uncommon hydrophobic hinge region. A small SAR study was carried out to gather information about the hinge region, and revealed that the PIM kinases happily accommodate large and hydrophobic substituents around the 8-position, such as the phenyl ring in **47a** and the trifluoromethyl group in **49a** (Figure 90). The DSF data revealed a slight preference for the PIM-3 isoform over PIM-1 and PIM-2, which correlated with the kinetic assay. High potencies were observed when using the phenyl substituent **47a** with IC_{50} of 65 nM (PIM-1), 129 nM (PIM-2) and 5.2 nM (PIM-3), or the trifluoromethyl group, **49a**, with IC_{50} of 112 nM (PIM-1), 632 nM (PIM-2) and 186 nM

(PIM-3). Furthermore, this SAR study revealed that moving the chlorine around the aromatic ring was also favourable. High PIM-inhibitory potency was also observed even when using hydrophobic substituents such as aniline (**45l**, Figure 90) with IC_{50} values of 184 nM for PIM-1, excellent selectivity over PIM-2 (2230 nM), and 64 nM for the PIM-3 isoform. This study provided further information about the topology of the hinge region of the PIM kinases, and it increased the selectivity over the CLK family, DYRK family and SRPK family. Understanding the differences between the isoforms, however, still remains a challenge.

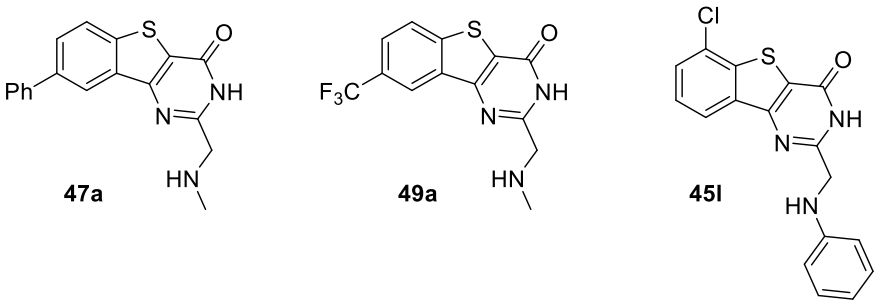

Compound	PIM-1 (ΔTm, °C)	PIM-2 (ΔTm, °C)	PIM-3 (ΔTm, °C)	CLK4 (ΔTm, °C)	CLK1 (ΔTm, °C)	CLK3 (ΔTm, °C)	DYRK1A (ΔTm, °C)	DYRK2A (ΔTm, °C)	SRPK1 (ΔTm, °C)	SRPK2 (ΔTm, °C)
47a	6.4	4.4	11.5	4.4	3.5	0.6	3.1	2.4	0.1	0.4
49a	4.7	3.7	5.9	0.5	0.7	0.0	0.5	0.9	0.1	0.0
45l	7.6	3.9	9.1	4.0	4.0	0.0	4.8	2.1	0.6	0.2

Compound	PIM-1 IC_{50} (nM)	PIM-2 IC_{50} (nM)	PIM-3 IC_{50} (nM)
47a	65	129	5.2
49a	112	632	186
45l	184	2230	64

***Figure 90**: Compound structure, DSF data and IC_{50} data for **47a**, **49a** and **45l**.*

The information gathered from this initial SAR study led to a modification of the benzothienopyrimidinone scaffold and two further chemical series were designed, a phenylpyrimidinone series (Chapter 3) and a benzothienodiazepine series (Chapter 4).

The SAR study carried out within the benzothienopyrimidinone series also led to the discovery of potential CLK4 chemical probes (Figure 91). As mentioned in section 2.4, CLK4 protein kinase is becoming very relevant due to its implication in alternative gene splicing diseases such as the Alzheimer's disease.[72] Compounds **43b**, **43c**, **43l**, and **43n** provided excellent ΔT_m values for the CLK4 kinases and good selectivity, especially for compounds

43b and **43l**. Compound **43n** provided poor selectivity, an IC_{50} of 33 nM was observed for PIM-1 and 66 nM for PIM-3, as well as high ΔT_m values for CLK1 (7.5 °C) and DYRK1A (4.1 °C). However, our collaborators' interest in the CLK protein kinases led to the acquisition of the first CLK4 crystal structure together with compound **43n** (Figure 92). Attempts at crystallizing **43b**, **43c** and **43l** have been unsuccessful to date.

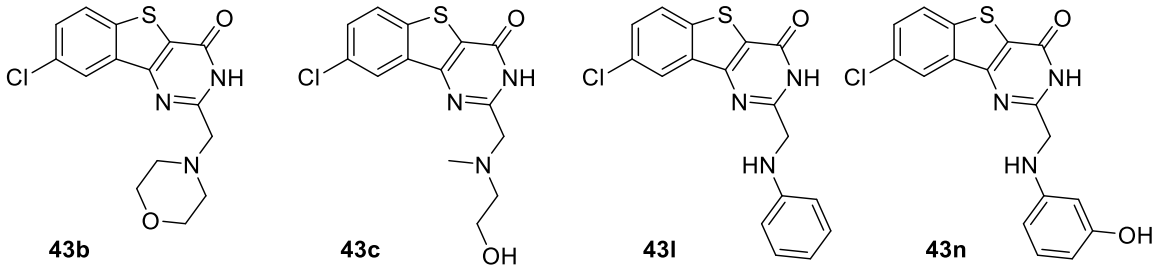

	IC_{50} (nM)			DSF assay (ΔT_m, °C)									
Compound	**PIM-1**	**PIM-2**	**PIM-3**	**PIM-1**	**PIM-2**	**PIM-3**	**CLK4**	**CLK1**	**CLK3**	**DYRK1A**	**DYRK2A**	**SRPK1**	**SRPK2**
43b	No PIM activity			2.2	1.1	1.9	7.8	4.9	1.4	3.5	0.7	0.0	0.6
43c				5.4	3.0	6.0	9.5	7.8	1.7	4.5	2.0	0.0	0.2
43l				1.9	0.5	0.1	7.0	4.1	0.9	2.4	0.6	0.0	0.7
43n	33	22860	66	6.7	3.6	8.8	9.2	7.5	2.2	4..1	1.2	2.3	0.1

Figure 91: *CLK4 hit compounds and DSF biological data.*

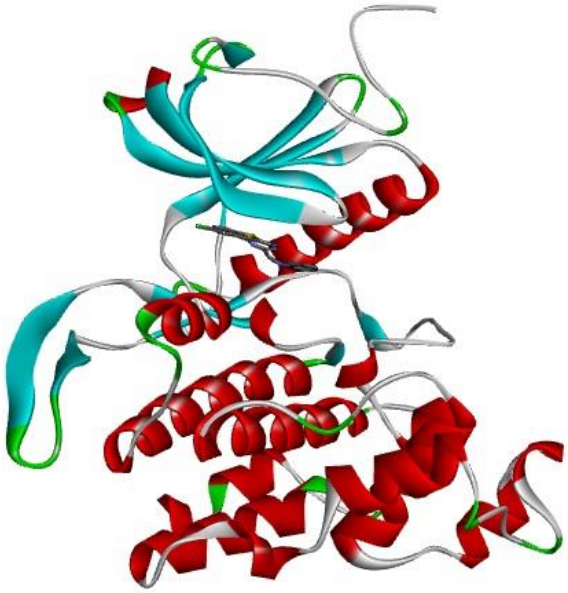

Figure 92*: Crystal structure of CLK4 with compound* ***43n****.*

This crystal structure served as an excellent tool to further understand the cross reactivity between the CLK4 isoform and the PIM kinases, and enhanced the potential of the benzothienopyrimidinone series as potential CLK4 chemical probes.

Finally, the benzothienopyrimidinone series also allowed us to develop novel methodology for their synthesis in collaboration with Prof. Mark Bagley. A new methodology for the synthesis of nitrogen containing heterocycles (such as the benzothiophenes described) was proposed (Scheme XXVI). The reaction proved simple to carry out and proceeded in high yields. The reaction's ability to incorporate various functionalities is likely to find applications within the drug discovery community due to the increasing use of benzothiophenes as kinase inhibitor scaffolds.

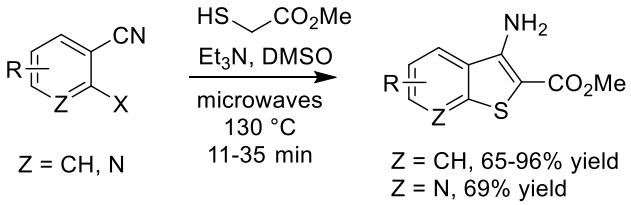

***Scheme XXVI**: Microwave-assisted reaction conditions.*

6.2. Phenylpyrimidinone series

The SAR studies from the benzothienopyrimidinone series provided important information about the nature of the PIM isoforms. It was shown that the most important interaction between the receptor and the compound was the one made by the amide moiety within the pyrimidinone ring and the Lys67 (PIM-1 reference), as seen in Figure 93.

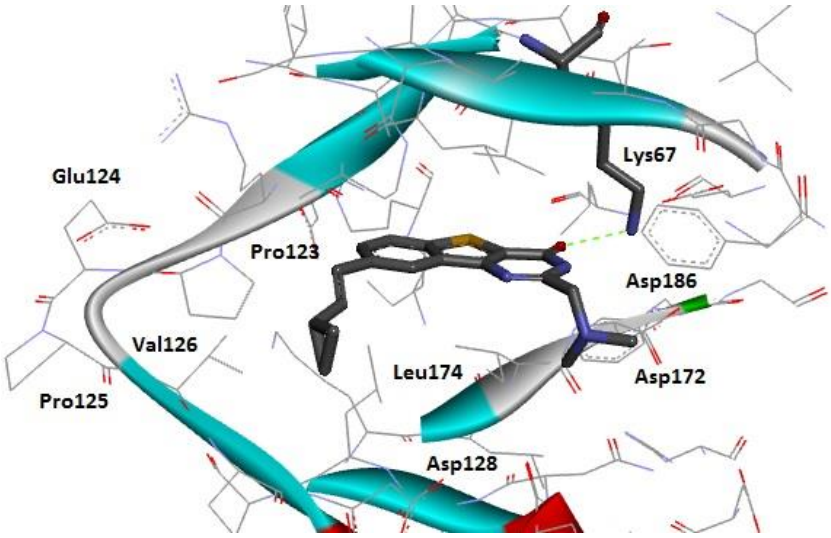

Figure 93: *X-ray crystal structure of PIM-1 – Compound **8**. Hydrogen bond interactions between the amide and Lys67 are represented by a black dotted line. PDB: 3JXW*

It was also observed that despite the high potencies, the selectivity between the PIM isoforms when using the benzothienopyrimidinone scaffold was poor, and that modifications on the scaffold would be needed to analyze possible changes in the binding pocket. As an initial option, we kept the pyrimidinone moiety (to maintain the interaction with Lys67) and removed thiophene ring which led to the generation of the second chemical series, a phenyl pyrimidinone scaffold (Figure 94).

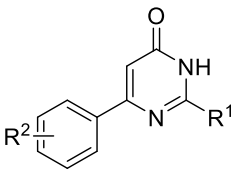

Figure 94*: Phenyl pyrimidinone moiety.*

A virtual library was designed and molecular modelling studies surprisingly identified an alternative binding pose for the phenyl pyrimidinone moiety in the PIM-1 isoform (Figure 95). This data prompted the study of the phenyl pyrimidinone series as a potential scaffold for the design and synthesis of PIM chemical probes.

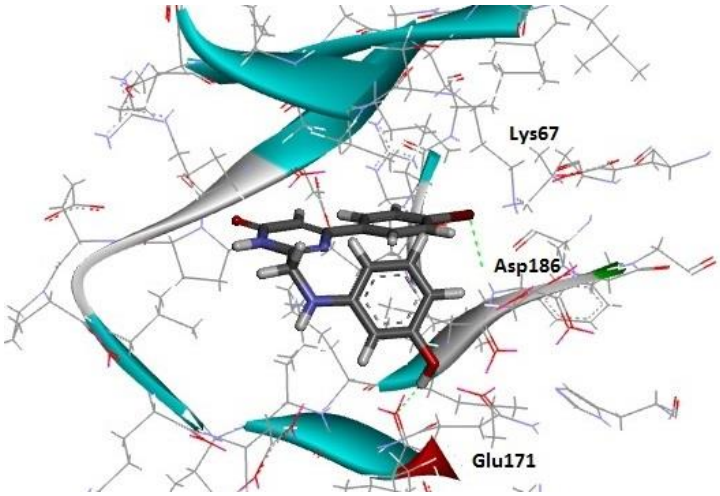

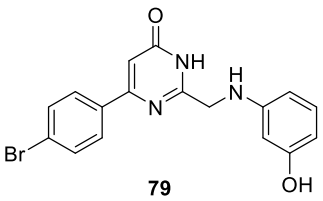

***Figure 95**: Compound **79**–PIM-1 docking. Green dotted lines represent the hydrogen bonding interactions.*

A chemical route was designed using well-established synthetic methods to permit a simple and efficient synthesis of intermediates and final compounds. After carrying out a small SAR study, we we were able to design derivatives with nanomolar potencies against the PIM kinases as well as selectivity within the isoforms (Figure 96).

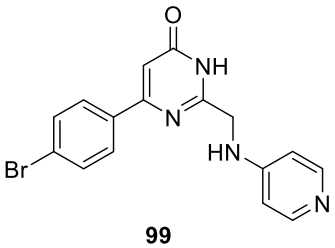

PIM-1: 331 nM
PIM-2: 815 nM
PIM-3: 374 nM

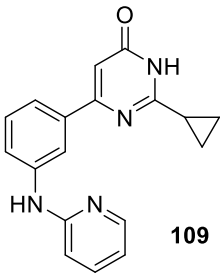

PIM-1: 210 nM
PIM-2: 25000 nM
PIM-3: 70 nM

Compound	PIM-1 (ΔTm, °C)	PIM-2 (ΔT_m, °C)	PIM-3 (ΔT_m, °C)	CLK4 (ΔT_m, °C)	CLK1 (ΔT_m, °C)	CLK3 (ΔT_m, °C)	DYRK1A (ΔT_m, °C)	DYRK2A (ΔT_m, °C)	SRPK1 (ΔT_m, °C)	SRPK2 (ΔT_m, °C)
99	5.1	3.3	0.1	0.8	0.0	0.0	0.2	0.0	0.0	0.0
109	4.5	0.5	4.9	2.3	2.7	0.9	5.6	2.6	0.1	0.0

***Figure 96**: Compound structure, IC_{50} data and DSF data for **99** and **109**.*

For example, compound **99** provided good potency towards the PIM kinases with IC_{50} values of 331 nM for PIM-1, 815 nM for PIM-2, and 374 nM for PIM-3, as well as an excellent selectivity within the DSF assay against additional kinases. It is important to highlight the lack of activity observed for CLK4 (ΔT_m: 0.8 °C). This selectivity had proved very challenging to achieve due to cross-reactivity between PIM kinases and CLK4. The reason for the selectivity observed for **99** is not yet understood and it is believed that a crystal structure showing the binding pose of **99** will provide further information on this matter.

Compound **109** showed high potencies as well as encouraging selectivity for PIM-3 over PIM-1 and PIM-2, with IC_{50} values of 210 nM (PIM-1), 25000 nM (PIM-2) and 70 nM (PIM-3), providing the first compound to show PIM-3 selectivity over PIM-1. The compound also showed good selectivity over CLK4, CLK1, CLK3 and the SRPK kinases, despite some activity for DYRK1A (ΔT_m: 5.6 °C).

The work developed within this series has shown significant results. Within a small SAR study we have designed a new promising scaffold with high potential for further functionalization. The chemical route is simple and allowed the synthesis of final candidates in a three-step procedure. The candidates have shown low potencies against the PIM kinases and encouraging selectivity over CLK, DYRK and SRPK kinases. We believe that this new chemical scaffold is likely to find application in the medicinal chemistry community as a potential scaffold for kinase inhibitors or as a chemical probe.

6.3. Benzothienodiazepine series

As a second alternative to the modification of the original Abbot scaffold, and knowing the hydrophobicity of the PIM kinase active site, a seven-membered ring was introduced, generating a third chemical series, the benzothienodiazepine series (Figure 97). This series kept the amide moiety, which forms an important interaction with the receptor providing PIM potency.

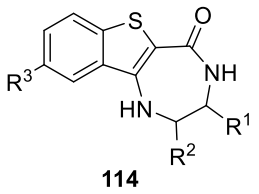

114

***Figure 97**: The new benzothienodiazepine scaffold.*

Excellent results were obtained from the SAR study carried out using this new scaffold. Additional information about the topology of the PIM kinases was gathered and, using the same scaffold, we were able to achieve selectivity for PIM-1 over PIM-2 and PIM-3, as well as selectivity for PIM-3 over PIM-1 and PIM-2. Unfortunately, PIM-2 selective candidates have not been observed within this work. A crystal structure of PIM-1 with the diazepine candidate **121** was obtained and confirmed that the compound was bound in the PIM-1 active site and that the amide moiety was interacting with Lys67 *via* a hydrogen bonding interaction. This crystal structure of PIM-1 with **121** was extremely helpful for the design of the candidates that resulted from this study (Figure 98).

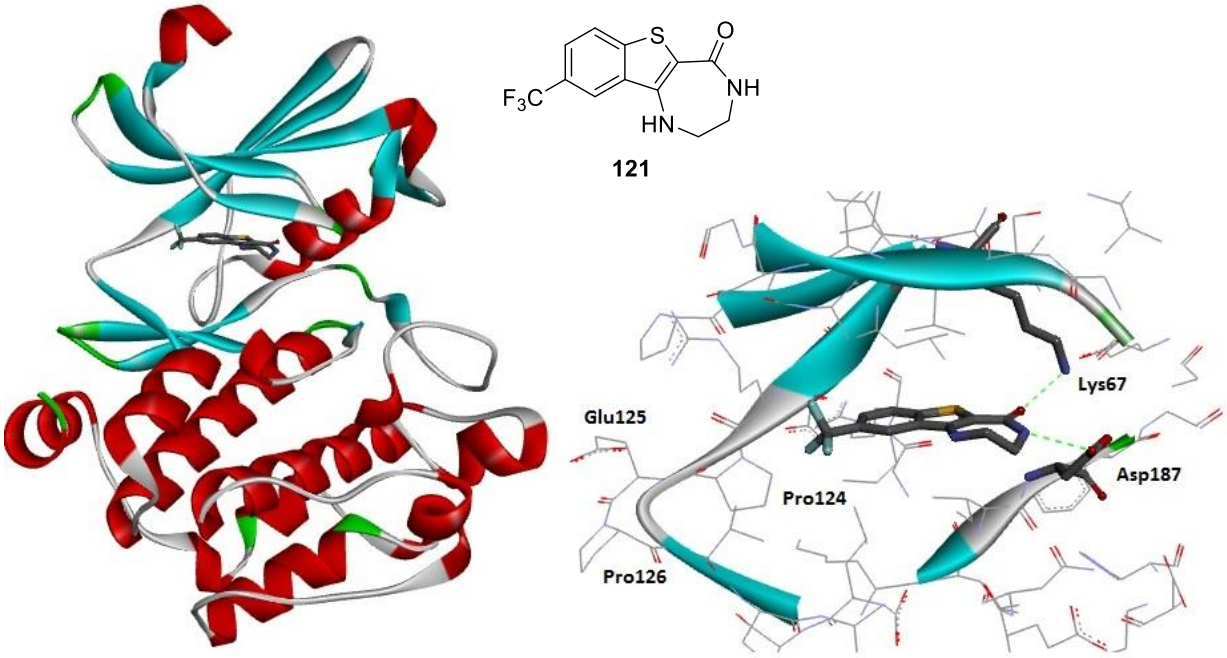

***Figure 98**: Crystal structure of **121**–PIM-1(left). PIM-1 active site–**121** crystal structure (right). Hydrogen bonding interactions are shown with green dotted lines.*

The SAR studies also revealed that the 1,2-cyclohexanediamine substituent on the right hand side of the scaffold provided the best potency, but other substituents such as D-valinol, or L-prolinol could also provide PIM-1 selectivity. Furthermore, position 9 of the benzothienodiazepine ring turned out to be key when looking for selectivity between PIM-1 and PIM-3. For example, from the SAR studies, it was observed that small hydrophobic substituents in position 9 were best to obtain PIM-1 selectivity over PIM-2 and PIM-3 (Figure 99). Substituents such as the trifluoromethyl group (**120**, **134**, **133**) or chlorine (**149**) provided high PIM-1 potency as well as a moderate selectivity towards the PIM-3 isoform, which was a very challenging selectivity to achieve.

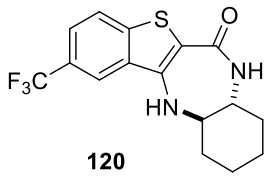

120

PIM-1: 30 nM
PIM-2: 6900 nM
PIM-3: 103 nM

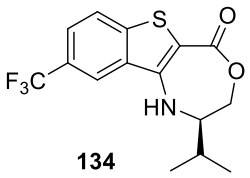

134

PIM-1: 44 nM
PIM-2: 50000 nM
PIM-3: 175 nM

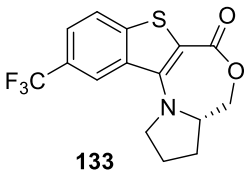

133

PIM-1: 98 nM
PIM-2: 4530 nM
PIM-3: 143 nM

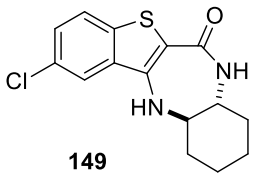

149

PIM-1: 26 nM
PIM-2: 406 nM
PIM-3: 258 nM

Compound	PIM-1 (ΔTm, °C)	PIM-2 (ΔT_m, °C)	PIM-3 (ΔT_m, °C)	CLK4 (ΔT_m, °C)	CLK1 (ΔT_m, °C)	CLK3 (ΔT_m, °C)	DYRK1A (ΔT_m, °C)	DYRK2A (ΔT_m, °C)	SRPK1 (ΔT_m, °C)	SRPK2 (ΔT_m, °C)
120	7.2	3.0	5.7	2.8	2.8	0.4	1.4	2.6	0.0	0.0
134	7.4	2.9	6.5	4.7	5.0	1.7	3.3	1.4	0.0	0.2
133	1.5	1.0	0.0	0.7	0.4	0.0	0.0	0.5	0.0	0.0
149	9.2	1.2	7.7	9.8	8.0	7.9	7.8	5.7	0.0	0.2

***Figure 99**: Compound structure, DSF data and IC_{50} values for **120**, **134**, **133**, and **149**.*

For all compounds, except **133**, the IC_{50} values correlated with the DSF data. It is not yet understood why poor affinity was observed for **133** in the DSF assay compared to the IC_{50} data. Nevertheless, **120**, **134**, and **149** showed excellent selectivity for PIM-1 over PIM-2, and moderate selectivity for PIM-1 over PIM-3. The compound containing the chlorine substituent, **149**, showed good PIM potencies but very low selectivity within the DSF assay, where the compound also showed high affinities for CLK4 (ΔT_m: 9.8 °C), CLK1 (ΔT_m: 8.0 °C), CLK3 (ΔT_m: 7.9 °C), and DYRK1A (ΔT_m: 5.7 °C).

Although the selectivity for PIM-1 over PIM-2 is excellent, further optimization regarding the selectivity for PIM-1 over PIM-3 would be required for a good quality PIM-1 chemical probe. Even though this selectivity was not desirable, the compounds were taken for additional

biological studies in cells. The inhibition of the phosphorylation of the BAD protein by PIM-1 was studied (Protocol 8.2) and our compounds offered excellent EC_{50} values (Table XLIII): **120** (EC_{50}: 0.12 µM), **134** (EC_{50}: 0.81 µM), **133** (EC_{50}: 0.53 µM), and **149** (EC_{50}: 0.4 µM).

Table XLIII*: pBAD assay results for compounds **120**, **134**, **133** and **149**.*

Compound	EC_{50} (µM)
120	0.12
134	0.81
133	0.53
149	0.24

This data proved to be very encouraging, and it highlighted the potential of these compounds to become selective probes. Furthermore, these compounds also offered good solubility as well as permeability, which are important attributes when designing a drug candidate or a selective probe.

Finally, it was observed that achieving PIM-3 selectivity over PIM-1 and PIM-2 was possible when studying the aryl ring of the scaffold and after a short SAR study, we discovered potential PIM-3 candidates, including **158** and **162**, with good solubility and permeability data (Figure 100).

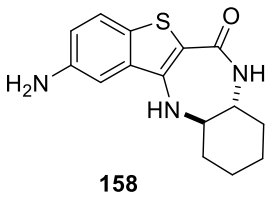

158

PIM-1: 1410 nM
PIM-2: 9890 nM
PIM-3: 59 nM

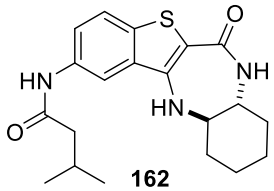

162

PIM-1: 1950 nM
PIM-2: 12700 nM
PIM-3: 83 nM

Compound	PIM-1 (ΔTm, ºC)	PIM-2 (ΔTm, ºC)	PIM-3 (ΔTm, ºC)	CLK4 (ΔTm, ºC)	CLK1 (ΔTm, ºC)	CLK3 (ΔTm, ºC)	DYRK1A (ΔTm, ºC)	DYRK2A (ΔTm, ºC)	SRPK1 (ΔTm, ºC)	SRPK2 (ΔTm, ºC)
158	3.5	0.5	2.3	3.4	2.6	0.6	2.7	1.6	0.0	0.0
162	3.5	0.3	6.1	4.9	0.9	0.2	2.4	6.2	1.6	0.5

Compound	PERMEABILITY PAMPA (x 10^{-6} cm/s)	SOLUBILITY (max concentration aqueous solubility, µM)
158	1.56	50
162	1.14	100

***Figure 100**: PIM-3 selective compounds **158**, and **162**.*

The compounds offered good selectivity within the DSF data. The IC_{50} data and the DSF data had previously shown some discrepancies for the PIM-3 isoform, which are not yet understood. However, **158** offered an excellent selectivity profile over the CLK family, DYRK family, and the SRPK family, whereas **162** showed some cross-reactivity with DYRK2 (ΔT_m: 6.2 °C), and CLK4 (ΔT_m: 4.9 °C). We are currently studying the selectivity/potency observed for **158** and **162** using the ITC assay and other kinetic assay services before the compounds are taken for further studies, such as a kinome scan, or a PIM-3 cellular assay. From the data gathered, a solid conclusion about the potential of these compounds as PIM-3 chemical probes will be drawn and they will then be taken for further evaluation.

In conclusion, designing selective chemical probes for the PIM isoforms has proven very challenging. The PIM kinases possess an unusually hydrophobic hinge region which can provide selectivity over the rest of human kinome. The very similar topology of the PIM isoforms, however, makes these isoforms very difficult to target separately. Our efforts to understand the differences between the isoforms using molecular modelling studies as well as SAR studies have provided us with useful information and after multiple hypotheses and compound design we were able to design and synthesize potential PIM-3 probes that offer 24-fold selectivity over PIM-1 and 153-fold selectivity over PIM-2 in the case of compound **162**. PIM-1 chemical probes have also been designed although further optimization would be ideal. PIM-2 selectivity has not been achieved to date, through the SAR studies undertaken. It is believed that targeting PIM-2 selectively will be very challenging. PIM-2 selectivity has not been seen to date, neither within this study nor in past PIM scientific publications, to our knowledge. Furthermore, potential CLK4 chemical probes have also been described and the first crystal structure of CLK4 has been reported within this study.

Overall, this study contributes to the discovery of potential chemical probes for human kinases, especially the PIM kinases and the CLK4 kinase, and that the discovery of these probes can provided impact in cancer research and gene splicing diseases, which will be reflected in future science.

7. Experimental

7.1. General Techniques

All temperatures are expressed in °C.

Commercially available solvents and reagents were used without further purification or drying and all reactions performed under an air atmosphere unless otherwise stated. Dry solvents were obtained by standard operating procedure for Innovative Technology Solvent Purification System. All glassware used for air/moisture sensitive reactions was previously dried in the oven at 150 °C for 5–16 hours.

NMR spectra were recorded using a Bruker DPX400, DPX500, AV400 or AVIII600 (with cyroprobe) referenced to tetramethylsilane. Chemical shifts are reported in parts per million (ppm) and coupling constants (*J*) in Hz. The following abbreviations are used for multiplicities: s = singlet; d = doublet; t = triplet; m = multiplet; dd = doublet of doublets; ddd = doublet doublet of doublets. If not specifically stated, the NMR experiments were run at 20 ºC.

IR spectra were recorded from solid samples using a SHIMADZU IRAFFINITY-1 spectrophotometer with a Perkin Elmer Universal ATR (attenuated total reflectance) sampling accessory. Absorption frequencies are reported in wavenumbers (cm^{-1}). Melting points were measured on a Stuart automatic melting point apparatus, SMP40.

Column chromatography was carried out using 200-400 mesh silica gel using an eluent system stated in each experimental section.

Analytical thin layer chromatography was carried out using aluminium-backed plates coated with Merck Kieselgel 60 GF254 that were visualised under UV light (at 254 nm).

LC–MS samples were carried out using Agilent technologies using a gradient of 5–95% acetonitrile/water. GC–MS was performed using an Agilent 7890A GC system, equipped with a 30 m DB5MS column connected to a 5975C inert XL CI MSD with Triple-Axis Detector. High-resolution mass spectra were obtained courtesy of the EPSRC Mass Spectrometry Service at University of Wales, Swansea, U.K. using the ionization methods specified.

7.2. General procedures

7.2.1. General Procedure A for the synthesis of the intermediate 26–35

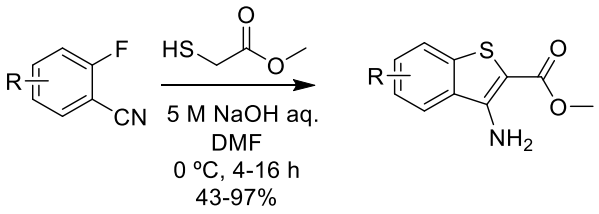

To a cold solution of fluorobenzonitrile in DMF was added dropwise methylthioglycolate. The reaction was stirred at 0 ºC for 30 minutes. Aqueous NaOH solution (5M) was added dropwise at 0 ºC, and the reaction was stirred for 16 hours at room temperature. The reaction was quenched with ice-water and a white solid precipitated. The solid was filtered, washed with petrol (100 mL) to give the desired amino ester. Analogues were purified depending on their solubility.

7.2.2. General Procedure B for the synthesis of the intermediate 36–41

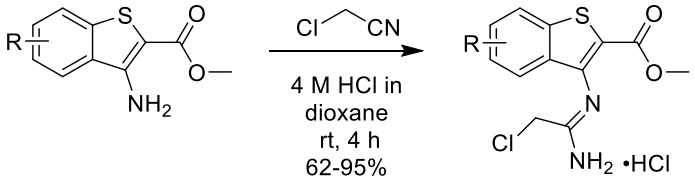

Aminobenzothiophene ester was suspended in a solution of HCl in 1,4-dioxane (4M). The reaction mixture was stirred at room temperature for 20 minutes and chloroacetonitrile was added dropwise. The reaction mixture was stirred at room temperature for 4–16 hours. The suspension was filtered under reduced pressure, washed with petrol (60 mL) and dried under vacuum for 6 hours to give the desired product as the HCl salt. The compound is used without further purification.

7.2.3. General Procedure C for the synthesis of 43a–43u, 46a, 47a, 48a, 49a, 48t, 48n, 44b, 44l, 45b, and 45l

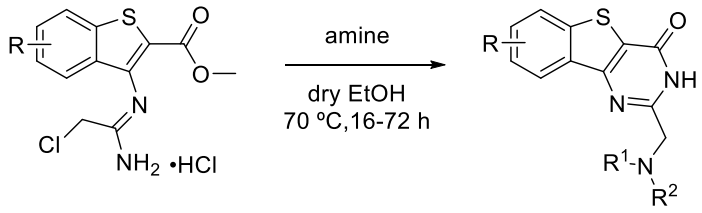

To a solution of intermidiate in dry solvent was added the correspondent amine. The reaction was stirred for 16–64 hours under a nitrogen atmosphere at a specific temperature (rt–80 ºC). Analogues were purified depending on their solubility.

7.2.4. General Procedure D for the synthesis of 86–88

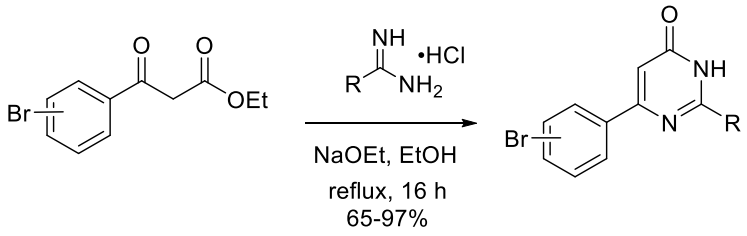

To a solution containing intermediate **81** or **85** in dry EtOH was added the acetamidine and NaOEt. The reaction mixture was stirred at a certain temperature during 16 hours under a nitrogen atmosphere. After cooling to room temperature, the solid was filtered, washed with water and dried to give the desired product. The product was used as such in the following step.

7.2.5. General Procedure E for the synthesis of 91–96

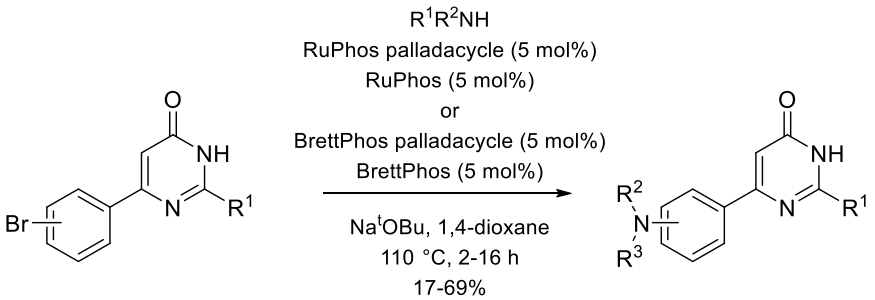

To a microwave vial containing **86**, **87** or **88** was added the corresponding amine, base, palladium source, ligand and dry solvent. The vial was sealed and placed under nitrogen atmosphere and stirred at a 110 ºC for 2–16 hours. The analogues were purified depending on solubility.

7.2.6. General Procedure F for the synthesis of 97–111

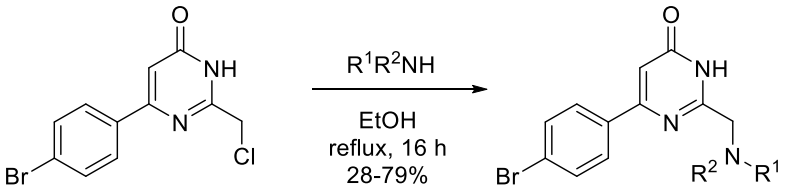

To a solution of **82** in dry solvent was added the corresponding amine. The reaction mixture was stirred for 16 hours at a specific temperature. If needed, the reaction was cooled to room temperature and the solvent evaporated under reduced pressure. The analogues were purified depending on their solubility.

7.2.7. General Procedure G for the synthesis of the intermediate 116 and 163

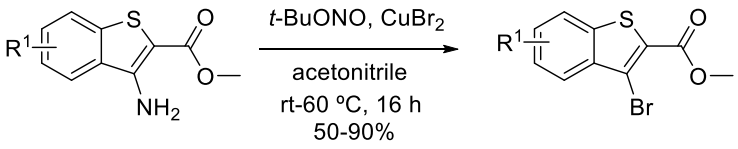

To a solution of the amino ester intermidiate in acetonitrile was added copper (II) bromide and the mixture stirred for 10 minutes. After that time, *t*-butyl nitrite was added dropwise to the solution and the reaction mixture was stirred for 16 hours at a specific temperature (rt–60 ºC). The solvent was evaporated under reduced pressure and the analogues were purified depending on their solubilities.

7.2.8. General Procedure H for the synthesis of the intermediates 146, 147, 148 and 152

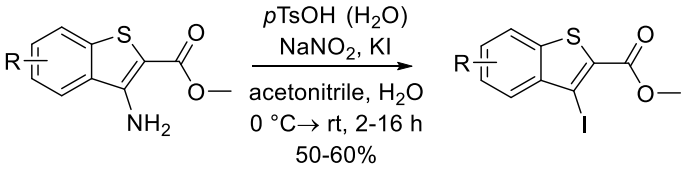

To a solution containing the amino ester intermidiate in acetonitrile was added *p*-toluenesulphonic acid. The resulting suspension was placed at 10–15°C and to this, a solution of $NaNO_2$ and potassium iodide in water was added gradually. The reaction was allowed to warm to room temperature and left stirring for 5 hours. The solvent was evaporated under reduced pressure. Water was added to the crude mixture and the resulting solid was filtered under vacuum. The solid was washed with water and methanol to afford the desired product.

7.2.9. General Procedure I for the synthesis of 119–126, 131–137, 149–151, 153, 156, 157, and 164

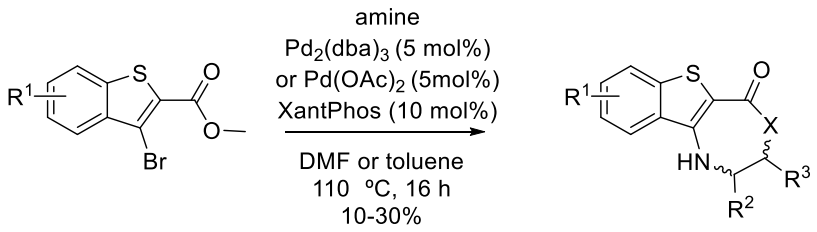

To a microwave vial containing intermidiate was added the corresponding amine, base, palladium source, ligand and dry DMF. The vial was sealed and placed under a nitrogen atmosphere. The reaction mixture was stirred for 24 hours at 110 ºC. Each of the analogues was purified depending on their solubility.

7.2.10. General Procedure J for the synthesis of the amines 129 and 130

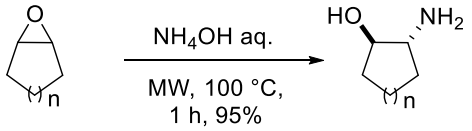

A microwave vial was charged with the epoxide and aqueous ammonia (28–30 %). The vial was sealed and heated to 90 ºC for 30 minutes. The solvent was removed under reduced pressure and the residue dissolved in MeOH. The solution was passed through an SCX cartridge, flushed with MeOH (3 x 10 mL) and then with a solution of NH_3 2 M in MeOH (2 x 10 mL). The NH_3 fractions were concentrated under reduced pressure to give the desired product.

7.2.11. General Procedure K for the synthesis of 158 and 159

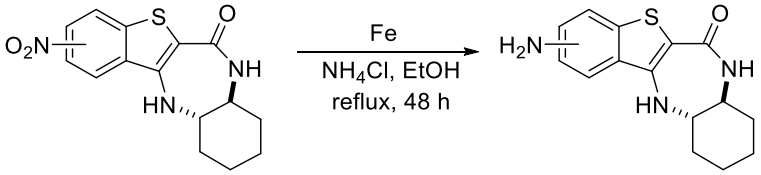

To a solution containing of intermidiate in EtOH was added iron and ammonium chloride. The reaction mixture was refluxed for 48 hours. After that time, the reaction was cooled down to room temperature and the solvent evaporated under reduced pressure. EtOAc was added and the organic fraction was washed with water, brine, dried over magnesium sulphate and concentrated to afford the desired compounds as brown solids.

7.2.12. General Procedure L for the synthesis of 161, 162, 165–173

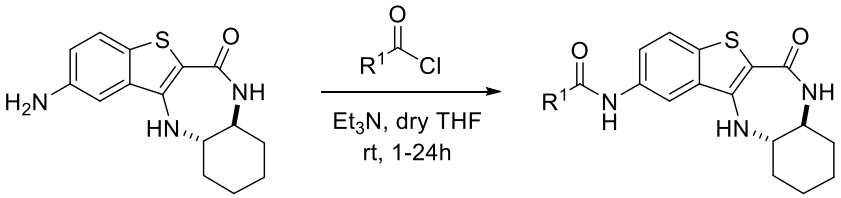

A suspension of **158** and triethylamine in dry THF was placed in an ice-bath and the corresponding acyl chloride was added dropwise to the reaction mixture. The reaction was stirred between 1–16 hours at room temperature. The crude product was purified depending on solubility.

7.3. Compound characterization

4-Fluoro-[1,1'-biphenyl]-3-carbonitrile (21)

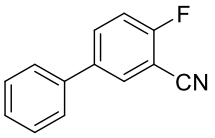

A microwave vial was charged with 5-bromo-2-fluorobenzonitrile (2.4 g, 12 mmol), K_2CO_3 (5 g, 36 mmol), phenylboronic acid (1.5 g, 12.5 mmol) and Pd(dppf)Cl_2 (86 mg, 0.12 mmol), 1,4-dioxane (24 mL) and water (8 mL). The vial was sealed and flushed with N_2. The reaction mixture was irradiated at 140 ºC during 35 minutes. The solution was filtered through celite, flushed with DCM and concentrated *in vacuo*. The residue was purified by flash chromatography using 1:1 petrol/CH_2Cl_2 to afford the title compound **21** as a white solid (2.05 g, 10.3 mmol, 86%). **Mpt** 70–71 ºC; **IR** (ATR)/cm^{-1}: 2987, 2233, 1485; **^{1}H NMR** (500 MHz, DMSO) δ 8.23 (dd, *J* = 5.2, 2.5 Hz, 1H), 8.07 (ddd, *J* = 8.7, 5.2, 2.5 Hz, 1H), 7.74–7.69 (m, 2H), 7.60 (appt, *J* = 9.0 Hz, 1H), 7.51–7.46 (m, 2H), 7.44–7.39 (m, 1H); **^{13}C NMR** (126 MHz, DMSO) δ 161.9 (d, *J* = 255.9 Hz), 137.6 (d, *J* = 2.6 Hz), 137.1, 134.2 (d, *J* = 8.7 Hz), 117.0 (d, *J* = 19.2 Hz), 100.7 (d, *J* = 15.2 Hz), 131.8, 129.1, 128.3, 126.9, 114.0; **LRMS** (ES + APCI) *m/z* 198 $(M+H)^+$.

Methyl 3-amino-5-chlorobenzo[*b*]thiophene-2-carboxylate[1] (26)

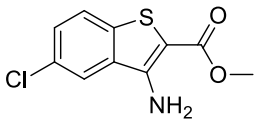

Following General Procedure A, 5-chloro-2-fluorobenzonitrile (3.0 g, 19 mmol), DMF (60 mL), methylthioglycolate (2.1 g, 20 mmol), NaOH aqueous solution (5 M, 6 mL). The reaction mixture was poured into ice-water and the resulting solid collected, washed with water and dried under vacuum to give the title compound **26** as a white solid (4.4 g, 18.2 mmol, 94%). **Mpt** 170–173 ºC; **IR** (ATR)/cm^{-1}: 3477, 3365, 1681, 1278; **^{1}H NMR** (500 MHz, DMSO) δ 8.30 (d, *J* = 2.1 Hz, 1H), 7.88 (d, *J* = 8.6 Hz, 1H), 7.53 (dd, *J* = 8.6, 2.1 Hz, 1H), 7.17 (s, 2H), 3.79 (s, 3H); **^{13}C NMR** (126 MHz, DMSO) δ 164.6, 148.7, 137.3, 132.7,

129.1, 128.4, 125.0, 122.7, 96.2, 51.4; **LRMS** (ES + APCI) *m/z* 242.0 $(M+H)^+$; **HRMS** (ESI, +ve) *m/z*: calc. for $C_{10}H_9{}^{35}ClNO_2S$ 242.0037, found 242.0039 $(M+H)^+$.

Methyl 3-amino-6-chlorobenzo[*b*]thiophene-2-carboxylate (**27)**

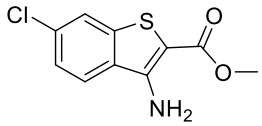

Following General Procedure A, 3-chloro-2-fluorobenzonitrile (3.5 g, 20 mmol), DMF (60 mL), methylthioglycolate (1.9 g, 21 mmol), NaOH aqueous solution (5 M, 7.7 mL). The reaction mixture was poured into ice-water and the resulting solid collected, washed with water and dried under vacuum to give the title compound **27** as a white solid (4.4 g, 17.9 mmol, 90%). **Mpt** 158–159 ºC (lit.,[66] mp 151–152 °C); **IR** (ATR)/cm^{-1}: 3423, 3333, 2945, 1667, 1521; **1H NMR** (400 MHz, DMSO) δ 8.15 (d, *J* = 8.7 Hz, 1H), 8.01 (d, *J* = 1.7 Hz, 1H), 7.45 (dd, *J* = 8.7, 1.7 Hz, 1H), 7.20 (s, 1H), 3.79 (s, 2H); **^{13}C NMR** (101 MHz, DMSO) δ 164.6, 149.1, 140.2, 133.4, 130.2, 124.6, 124.5, 122.7, 95.1, 51.3; **LRMS** (ES + APCI) *m/z* 242.0 $(M+H)^+$; **HRMS** (ESI, +ve) *m/z* calc. for $C_{10}H_9{}^{35}ClNO_2S$ 242.0037, found 242.0039 $(M+H)^+$.

Methyl 3-amino-7-chlorobenzo[*b*]thiophene-2-carboxylate (28)

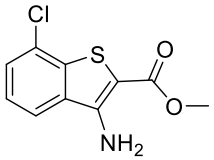

Following General Procedure A, 3-chloro-2-fluorobenzonitrile (3.5 g, 20 mmol), DMF (60 mL), methylthioglycolate (1.9 g, 21 mmol), and NaOH aqueous solution (5 M, 7.7 mL). The reaction mixture was poured into ice-water and the resulting solid collected, washed with water and dried under vacuum to give the title compound **28** as a white solid (4.3 g, 17.7 mmol, 89%). **Mpt** 169–170 ºC decomp.; **IR** (ATR)/cm^{-1}: 3473, 3361, 2956, 1682, 1602; **^{1}H NMR** (400 MHz, DMSO) δ 8.16 (d, *J* = 7.9 Hz, 1H), 7.63 (d, *J* = 7.9 Hz, 1H), 7.45 (appt, *J* = 7.9 Hz, 1H), 7.25 (s, 2H), 3.81 (s, 3H); **^{13}C NMR** (101 MHz, DMSO) δ 164.5, 150.0, 137.6,

133.3, 127.9, 127.0, 125.6, 122.2, 95.2, 51.4; **LRMS** (ES + APCI) *m/z* 242.0 $(M+H)^+$; **HRMS** (ESI, +ve) *m/z* calc. for $C_{10}H_9{}^{35}ClNO_2S$ 242.0037, found 242.0039 $(M+H)^+$.

Methyl 3-amino-5-bromobenzo[*b*]thiophene-2-carboxylate[1] (29)

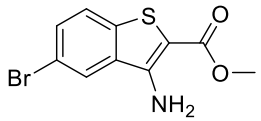

Following General Procedure A, 5-bromo-2-fluorobenzonitrile (2 g, 10.0 mmol), DMF (40 mL), methylthioglycolate (1.2 g, 10.5 mmol), NaOH aqueous solution (5 M, 4.5 mL). The reaction mixture was poured into ice-water and the resulting solid collected, washed with water and dried under vacuum to give the title compound **29** as a white solid (2.6 g, 9.0 mmol, 91%). **Mpt** 170–171 ºC; **IR** (ATR)/cm^{-1}: 3477, 3363, 2954, 1681; **^{1}H NMR** (400 MHz, DMSO) δ 8.46 (d, *J* = 2.1 Hz, 1H), 7.81 (d, *J* = 8.6 Hz, 1H), 7.63 (dd, *J* = 8.6, 2.1 Hz, 1H), 7.21 (s, 2H), 3.79 (s, 3H); **^{13}C NMR** (101 MHz, DMSO) δ 164.5, 148.6, 137.7, 133.2, 131.0, 125.7, 125.2, 117.0, 96.0, 51.4; **LRMS** (ES + APCI) *m/z* 285.9 $(M+H)^+$; **HRMS** (ESI, +ve) *m/z*: calc. for $C_{10}H_9{}^{79}BrNO_2S$ 285.9532, found 285.9535 $(M+H)^+$.

Methyl 3-amino-7-bromobenzo[*b*]thiophene-2-carboxylate (30)

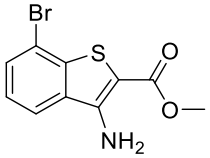

Following General Procedure A, 3-bromo-2-fluorobenzonitrile (2.5 g, 12.5 mmol), DMF (35 mL), methylthioglycolate (1.2 mL, 13.1 mmol), NaOH aqueous solution (5 M, 5.5 mL). The reaction mixture was poured into ice-water and the resulting solid collected, washed with water and dried under vacuum to give the title compound **30** as a white solid (2.6 g, 9.1 mmol, 73%). **Mpt** 144–146 ºC; **IR** (ATR)/cm^{-1}: 3488, 3374, 1656, 1435; **^{1}H NMR** (400 MHz, DMSO) δ 8.21 (dd, *J* = 7.9, 0.9 Hz, 1H), 7.78 (dd, *J* = 7.9, 0.9 Hz, 1H), 7.39 (appt, *J* = 7.9 Hz, 1H), 7.23 (s, 2H), 3.82 (s, 3H); **^{13}C NMR** (101 MHz, DMSO) δ 164.5, 150.2, 140.1, 132.8,

131.1, 125.7, 122.6, 115.8, 95.2, 51.4; **LRMS** (ES + APCI) *m/z* 285.0 $(M+H)^+$; **HRMS** (ESI, +ve) *m/z* calc. for $C_{10}H_9{}^{79}BrNO_2S$ 392.1428, found 392.1427 $(M+H)^+$.

Methyl 3-amino-5-phenylbenzo[*b*]thiophene-2-carboxylate (31)

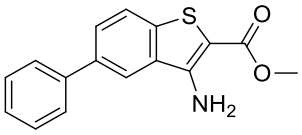

Following General Procedure A, **15** (1.0 g, 5.0 mmol), DMF (20 mL), methylthioglycolate (0.6 g, 5.3 mmol), and NaOH aqueous solution (5 M, 2 mL) were reacted at room temperature for 16 hours. Water (50 mL) and EtOAc (50 mL) were added. The organic fraction was washed with brine (4 x 30 mL), dried using $MgSO_4$, filtered and concentrated *in vacuo*. The residue was purified by flash chromatography using Petrol/EtOAc (8:2) to afford the title compound **31** as a white solid (0.6 g, 2.1 mmol, 43%). **Mpt** 96–97 ºC; **IR** (ATR)/cm^{-1}: 3439, 3338, 2949, 1658; **^{1}H NMR** (400 MHz, DMSO) δ 8.53 (d, *J* = 1.5 Hz, 1H), 7.91 (d, *J* = 8.5 Hz, 1H), 7.84 (dd, *J* = 8.5, 1.5 Hz, 1H), 7.78 (dd, *J* = 8.5, 1.5 Hz, 2H), 7.51 (appt, *J* = 7.5 Hz, 2H), 7.39 (appt, *J* = 7.5 Hz, 1H), 7.25 (s, 2H), 3.80 (s, 3H); **^{13}C NMR** (101 MHz, DMSO) δ 164.8, 149.9, 139.6, 138.0, 136.2, 132.2, 128.9, 127.5, 127.2, 126.7, 123.6, 121.0, 95.1, 51.0; **LRMS** (ES + APCI) *m/z* 284.0 $(M+H)^+$; **HRMS** (ESI, +ve) *m/z*: calc. for $C_{16}H_{14}NO_2S$ 284.0740, found 284.0741 $(M+H)^+$.

Methyl 3-amino-5-nitrobenzo[*b*]thiophene-2-carboxylate (32)

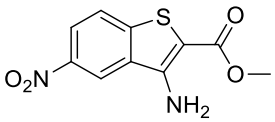

Following General Procedure A, 2-fluoro-5-nitrobenzonitrile (5.0 g, 30 mmol), DMF (80 mL), methylthioglycolate (3.4 g, 32 mmol), NaOH aqueous solution (5 M, 10 mL). The reaction mixture was poured into ice-water and the resulting solid collected, washed with water and dried under vacuum to give the title compound **32** as a red solid (7.5 g, 29 mmol, 97%). **Mpt** > 250 ºC decomp.; **IR** (ATR)/cm^{-1}: 3442, 3095, 2340, 1680; **^{1}H NMR** (400 MHz, DMSO) δ 9.24 (d, *J* = 2.2 Hz, 1H), 8.29 (dd, *J* = 8.9, 2.2 Hz, 1H), 8.12 (d, *J* = 8.9 Hz, 1H),

7.48 (s, 2H), 3.82 (s, 3H); **^{13}C NMR** (101 MHz, DMSO) δ 164.4, 149.8, 145.0, 131.4, 124.4, 122.1, 119.5, 96.8, 51.6, 39.5; **LRMS** (ES + APCI) *m/z* 253.0 $(M+H)^+$; **HRMS** (ESI, +ve) *m/z*: calc. for $C_{10}H_9N_2O_4S$ 253.0278, found 253.0277 $(M+H)^+$.

Methyl 3-amino-6-nitrobenzo[b]thiophene-2-carboxylate (33)

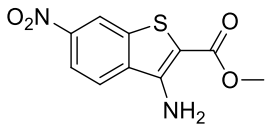

Following General Procedure A, 2-fluoro-4-nitrobenzonitrile (3.0 g, 18.0 mmol), DMF (60 mL), methylthioglycolate (2.0 g, 18.9 mmol), NaOH (5 M, 6 mL). The reaction mixture was poured into ice-water and the resulting solid filtered, washed with water and dried under vacuum to give the title compound **33** as a red solid (3.6 g, 14.2 mmol, 79%). **Mpt** 228–230 ºC (lit.,[66] mp 229–231 °C); **IR** (ATR)/cm^{-1}: 3489, 3367, 1697, 1624; **^{1}H NMR** (400 MHz, DMSO) δ 8.90 (d, *J* = 2.1 Hz, 1H), 8.7 (d, *J* = 8.7 Hz, 1H), 8.19 (dd, *J* = 8.7, 2.1 Hz, 1H), 7.30 (s, 2H), 3.83 (s, 3H); **^{13}C NMR** (101 MHz, DMSO) δ 164.3, 148.3, 146.9, 138.8, 135.6, 124.2, 119.7, 118.5, 99.7, 51.6; **LRMS** (ES + APCI) *m/z* 253.0 $(M+H)^+$; **HRMS** (ESI, +ve) *m/z* calc. for $C_{10}H_9O_4N_2NaS$ 275.0097, found 275.0101 $(M+Na)^+$.

Methyl 3-amino-5-(trifluoromethyl)benzo[*b*]thiophene-2-carboxylate (34)

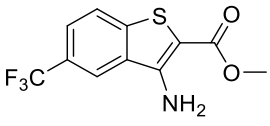

Following General Procedure A, 2-fluoro-5-(trifluoromethyl) benzonitrile (1 g, 5.3 mmol), DMF (15 mL), methylthioglycolate (0.5 g, 5.5 mmol), NaOH aqueous solution (5 M, 2 mL). The reaction mixture was poured into ice-water and the resulting solid collected, washed with water and dried under vacuum to give the title compound **34** as a white solid (1.4 g, 5.0 mmol, 96%). **Mpt** 140–141 ºC; **IR** (ATR)/cm^{-1}: 3468, 3335, 1664; **^{1}H NMR** (400 MHz, $CDCl_3$) δ 7.91–7.89 (m, 1H), 7.81 (d, *J* = 8.5 Hz, 1H), 7.65 (dd, *J* = 8.5, 1.5 Hz, 1H), 5.96 (s, 2H), 3.91 (s, 3H); **^{13}C NMR** (101 MHz, $CDCl_3$) δ 165.0, 147.6, 142.5, 130.5, 126.0 (q, *J* = 32.7 Hz), 123.8 (q, *J* = 272.1 Hz), 123.8–123.6 (m), 123.5, 123.8–123.6 (m), 100.1, 51.23; **LRMS** (ES

+ APCI) *m/z* 276.0 $(M+H)^+$; **HRMS** (EI, +ve) *m/z*: calc. for $C_{11}H_8F_3NO_2S$ 275.0228, found 275.0231 (M^+ •).

Methyl 3-amino-6-(trifluoromethyl)benzo[*b*]thiophene-2-carboxylate (35)

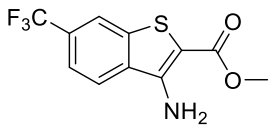

Following General Procedure A, 2-fluoro-4-(trifluoromethyl)benzonitrile (3.0 g, 15.8 mmol), DMF (55 mL), methylthioglycolate (1.8 g, 16.6 mmol), and NaOH aqueous solution (5 M, 6 mL). The reaction mixture was poured into ice-water and the resulting solid collected, washed with water and dried under vacuum to give the title compound **35** as a white solid (3.4 g, 12.3 mmol, 78%). **Mpt** 129–131 ºC (lit.,[66] mp 126–127 °C); **IR** (ATR)/cm^{-1}: 3471, 3344, 2964, 1664; **^{1}H NMR** (400 MHz, DMSO) δ 8.38–8.32 (m, 2H), 7.71 (d, *J* = 8.7 Hz, 1H), 7.27 (s, 2H), 3.81 (s, 3H); **^{13}C NMR** (101 MHz, DMSO) δ 164.5, 148.8, 138.9, 134.1, 128.4 (q, *J* = 32.0 Hz), 124.2 (q, *J* = 272.7 Hz), 124.1, 121.0–120.7 (m), 120.3–120.0 (m), 97.4, 51.5; **LRMS** (ES + APCI) *m/z* 276.0 $(M+H)^+$; **HRMS** (ESI, +ve) *m/z* calc. for $C_{11}H_9F_3NO_2SNa$ 298.0124, found 298.0120 $(M+Na)^+$.

Methyl 3-((1-amino-2-chloroethylidene)amino)-5-chlorobenzo[*b*]thiophene-2-carboxylate hydrochloride[1] (36)

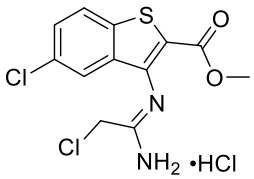

Following General Procedure B, **26** (1.5 g, 6.2 mmol), chloroacetonitrile (0.9 g, 12 mmol) in HCl in dioxane (4M, 30 mL) to afford the title compound **36** as a white solid (2 g, 5.6 mmol, 90%). **Mpt** > 210 ºC decomp.; **IR** (ATR)/cm^{-1}: 3392, 2694, 1712, 1681, 1247; **^{1}H NMR** (400 MHz, MeOD) δ 8.10–8.07 (m, 1H), 7.97 (d, *J* = 2.0 Hz, 1H), 7.66 (dd, *J* = 8.7, 2.0 Hz, 1H), 4.74 (s, 2H), 3.99 (s, 3H); **^{13}C NMR** (101 MHz, MeOD) δ 166.6, 162.0, 139.1, 136.6, 133.8,

130.2, 129.6, 126.3, 122.8, 101.4, 53.6, 40.1; **LRMS** (ESI, +ve) *m/z* 316.9 $(M+H)^+$; **HRMS** (ESI, +ve) *m/z*: calc. for $C_{12}H_{11}{}^{35}Cl_2N_2O_2S$ 316.9914, found 316.9913 $(M+H)^+$.

Methyl 3-((1-amino-2-chloroethylidene)amino)-6-chlorobenzo[*b*]thiophene-2-carboxylate hydrochloride (37)

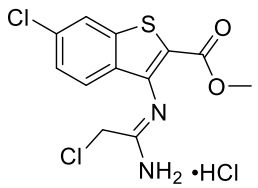

Following general procedure B, **27** (1.5 g, 6.2 mmol), chloroacetonitrile (765 µL, 12.1 mmol) in HCl in dioxane (4 M, 25 mL) to afford the title compound **37** as a white solid (2.1 g, 5.9 mmol, 95%). **Mpt** > 250 ºC decomp.; **IR** (ATR)/cm^{-1}: 3290, 2675 (br), 1682, 1621; **^{1}H NMR** (400 MHz, MeOD) δ 8.15 (d, *J* = 1.8 Hz, 1H), 7.88 (d, *J* = 8.8 Hz, 1H), 7.60 (dd, *J* = 8.8, 1.8 Hz, 1H), 4.74 (s, 2H), 3.97 (s, 3H); **^{13}C NMR** (101 MHz, MeOD) δ 166.6, 162.1, 141.8, 136.1, 133.9, 131.0, 130.3, 128.2, 124.7, 124.3, 53.5, 40.0; **LRMS** (ES + APCI) *m/z* 316.9 $(M+H)^+$; **HRMS** (ESI, +ve) *m/z* calc. for $C_{12}H_{11}{}^{35}Cl_2N_2O_2S$ 336.0568, found 336.0571 $(M+H)^+$.

Methyl 3-((1-amino-2-chloroethylidene)amino)-7-chlorobenzo[*b*]thiophene-2-carboxylate hydrochloride (38)

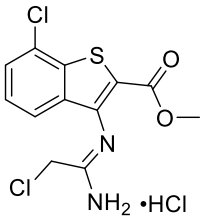

Following general procedure B, **28** (1.5 g, 6.2 mmol), chloroacetonitrile (765 µL, 12.1 mmol) in HCl in dioxane (4 M, 25 mL) to afford the title compound **38** as a white solid (2.0 g, 5.6 mmol, 90%). **Mpt** > 250 ºC decomp.; **IR** (ATR)/cm^{-1}: 3307, 2604, 1679, 1613; **^{1}H NMR** (400 MHz, MeOD) δ 7.88 (dd, *J* = 7.9, 0.8 Hz, 1H), 7.72 (dd, *J* = 7.9, 0.9 Hz, 1H), 7.62 (t, *J* = 7.9 Hz, 1H), 4.74 (s, 2H), 4.00 (s, 3H); **^{13}C NMR** (101 MHz, MeOD) δ 166.6, 162.0, 139.5, 136.9, 131.7, 131.00, 129.6, 129.30, 128.9, 122.4, 53.7, 40.0; **LRMS** (ES + APCI) *m/z* 316.9

$(M+H)^+$; **HRMS** (ESI, +ve) *m/z* calc. for $C_{12}H_{11}{}^{35}Cl_2N_2O_2S$ 336.0568, found 336.0571 $(M+H)^+$.

Methyl 3-((1-amino-2-chloroethylidene)amino)-5-bromobenzo[*b*]thiophene-2-carboxylate hydrochloride (39)

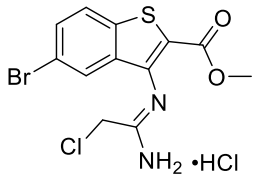

Following general procedure B, **29** (2.8 g, 9.9 mmol), chloroacetonitrile (1.5 g, 19.3 mmol) in HCl in dioxane (4 M, 33 mL) to afford the title compound **39** as a white solid (3.5 g, 9.3 mmol, 94%). **Mpt** > 220–221 ºC decomp.; **IR** (ATR)/cm^{-1}: 3388, 2696, 1712, 1678, 1253; **^{1}H NMR** (400 MHz, MeOD) δ 8.13–8.10 (m, 1H), 8.00 (d, *J* = 8.7 Hz, 1H), 7.77 (dd, *J* = 8.7, 2.0 Hz, 1H), 4.74 (s, 2H), 3.98 (s, 3H); **^{13}C NMR** (101 MHz, MeOD) δ 166.6, 162.0, 139.5, 137.0, 132.8, 132.3, 129.5, 126.4, 126.0, 121.3, 53.6, 40.1; **LRMS** (ESI, +ve) *m/z* 360.9 $(M+H)^+$; **HRMS** (ESI, +ve) *m/z* calc. for $C_{12}H_{11}{}^{35}Cl^{79}BrN_2O_2S$ 360.9408, found 360.9405 $(M+H)^+$.

Methyl 3-((1-amino-2-chloroethylidene)amino)-5-phenylbenzo[b]thiophene-2-carboxylate hydrochloride (40)

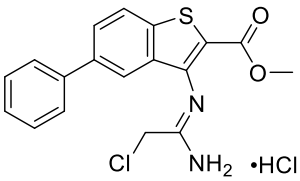

Following general procedure B, **31** (250 mg, 0.9 mmol), chloroacetonitrile (108 μL, 1.72 mmol) in HCl in dioxane (4 M, 4 mL) to afford the title compound **40** as a white solid (220 mg, 0.56 mmol, 62%). **LRMS** (ESI, +ve) *m/z* 359.0 $(M+H)^+$; **HRMS** (ESI, +ve) *m/z* calc. for $C_{18}H_{16}{}^{35}ClN_2O_2S$ 327.0357, found 327.0357 (M-MeOH).

Methyl 3-((1-amino-2-chloroethylidene)amino)-5-nitrobenzo[*b*]thiophene-2-carboxylate hydrochloride (41)

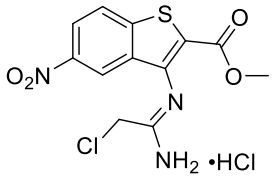

Following General Procedure B, **32** (3.0 g, 12 mmol), chloroacetonitrile (1.8 g, 23.4 mmol) in HCl in dioxane (4 M, 27 mL) to afford the title compound **41** as a white solid (3.4 g, 10.2 mmol, 86%). **Mpt** > 211 ºC decomp.; **IR** (ATR)/cm^{-1}: 3172, 2966, 2596, 1714; **^{1}H NMR** (400 MHz, MeOD) δ 8.85 (d, *J* = 2.1 Hz, 1H), 8.48 (dd, *J* = 8.9, 2.1 Hz, 1H), 8.34 (d, *J* = 8.9 Hz, 1H), 4.80 (s, 2H), 4.03 (s, 3H); **^{13}C NMR** (101 MHz, MeOD) δ 167.0, 161.6, 148.1, 145.7, 135.6, 131.2, 126.2, 126.1, 123.5, 119.2, 53.8, 40.2; **LRMS** (ESI, +ve) *m/z* 328.0 $(M+H)^+$; **HRMS** (ESI, +ve) *m/z* calc. for $C_{12}H_{11}{}^{35}ClN_3O_4S$ 328.0153, found 328.0146 $(M+H)^+$.

Methyl 3-((1-amino-2-chloroethylidene)amino)-5-(trifluoromethyl)benzo[b]thiophene-2-carboxylate hydrochloride (42)

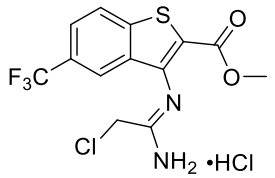

Following General Procedure B, **34** (0.2 g, 0.72 mmol), chloroacetonitrile (0.1 g, 1.4 mmol) in HCl in dioxane (4 M, 4 mL) to afford the title compound **42** as a white solid (0.6 g, 0.67 mmol, 93%). **Mpt** > 197–198 ºC decomp.; **IR** (ATR)/cm^{-1}: 3402, 2952, 1716, 1024, 1072; **^{1}H NMR** (400 MHz, MeOD) δ 8.32–8.26 (m, 2H), 7.91 (dd, *J* = 8.5, 2.0 Hz, 1H), 4.75 (s, 2H), 4.00 (s, 3H); **^{13}C NMR** (101 MHz, MeOD) δ 166.9, 161.9, 143.8, 135.3, 133.0, 126.1, 125.9, 125.8–125.5 (m), 121.0–120.5 (m), 53.7, 49.0, 40.2 (two carbons not reported); **LRMS** (ESI, +ve) *m/z* 351.0 $(M+H)^+$; **HRMS** (ESI, +ve) *m/z* calc. for $C_{13}H_{11}{}^{35}ClF_3N_2O_2S$ 351.0176, found 351.0177 $(M+H)^+$.

Chloro-2-((methylamino)methyl)benzo[4,5]thieno[3,2-*d*]pyrimidin-4(3*H*)-one[1] (43a)

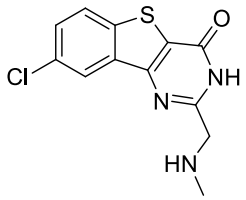

Following General Procedure C, **36** (100 mg, 0.28 mmol) and methylamine 33% in MeOH (7 mL) for 16 hours at room temperature. The solvent was then evaporated under reduced pressure to give a white solid. The solid was dissolved in MeOH/CH_2Cl_2 (1:1, 10 mL) and loaded onto an SCX cartridge (1 g). The cartridge was flushed with MeOH (3 x 5 mL) and then with a solution of NH_3 in MeOH (2 M, 10 mL). The NH_3 in MeOH fractions were evaporated under reduced pressure to give the title compound **43a** as a white solid (71 mg, 0.25 mmol, 90%). **Mpt** 185–186 ºC decomp.; **IR** (ATR)/cm^{-1}: 3439, 1664, 1543; **^{1}H NMR** (400 MHz, DMSO) δ 8.16 (d, *J* = 2.0 Hz, 1H), 8.14 (d, *J* = 8.7 Hz, 1H), 7.64 (dd, *J* = 8.7, 2.0 Hz, 1H), 3.86 (s, 2H), 2.46 (s, 3H); **^{13}C NMR** (101 MHz, DMSO) δ 162.0, 159.6, 152.1, 138.6, 136.1, 130.1, 128.5, 125.7, 122.5, 122.2, 52.8, 34.4; **LRMS** (ES + APCI) *m/z* 280.0 $(M+H)^+$; **HRMS** (ESI, +ve) *m/z* calc. $C_{12}H_{11}{}^{35}ClN_3OS$ 280.0306, found 280.0302 $(M+H)^+$.

8-Chloro-2-(morpholinomethyl)benzo[4,5]thieno[3,2-*d*]pyrimidin-4(3*H*)-one[1] (43b)

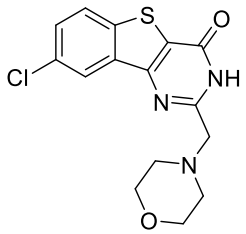

Following General Procedure C, **36** (100 mg, 0.28 mmol), morpholine (96 µL, 1.12 mmol) in EtOH (4 mL) during 16 hours at 80 ºC. The solvent was evaporated under reduced pressure and the residue partially dissolved in 1:1 CH_2Cl_2/MeOH (10 mL). The solution was filtered through an SCX cartridge, flushed with MeOH (3 x 5 mL) and then with a solution of NH_3 in MeOH (2 M, 2 x 5 mL).The NH_3 in MeOH fractions were evaporated under reduced pressure to give the title compound **43b** as a yellow solid (41 mg, 0.12 mmol, 91%). **Mpt** 135–136 ºC decomp.; **IR** (ATR)/cm^{-1}: 2949, 1664, 1572; **^{1}H NMR** (400 MHz, DMSO) δ ppm 12.41 (s,

1H), 8.21 (d, *J* = 8.5 Hz, 1H), 8.17 (d, *J* = 2.4 Hz, 1H), 7.70 (dd, *J* = 8.5, 2.4 Hz, 1H), 3.62–3.60 (m, 4H), 3.58 (s, 2H), 2.56–2.54 (m, 4H); **^{13}C NMR** (100 MHz, DMSO) δ 158.8, 157.3, 151.7, 138.8, 135.6, 130.6, 129.0, 125.9, 123.2, 122.4, 66.2, 60.7, 53.1; **LRMS** (ES + APCI) *m/z* 336.0 $(M+H)^+$; **HRMS** (ESI, +ve) *m/z* calc. $C_{15}H_{15}{}^{35}ClN_3O_2S$ 336.0568, found 336.0572 $(M+H)^+$.

8-Chloro-2-(((2-hydroxyethyl)(methyl)amino)methyl)benzo[4,5]thieno[3,2-*d*]pyrimidin-4(3*H*)-one (43c)

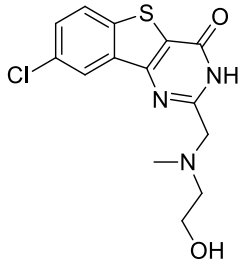

Following General Procedure C, **36** (100 mg, 0.28 mmol), 2-(methylamino)ethanol (135 µL, 1.68 mmol) in EtOH (4 mL) during 24 hours at 90 ºC. The reaction mixture was cooled down to room temperature and a white solid precipitated. The white solid was filtered and washed with MeOH to give the title compound **43c** as a white solid (30 mg, 0.4 mmol, 34%). **Mpt** 121–122 ºC decomp.; **IR** (ATR)/cm^{-1}: 3471, 2819, 1645; **^{1}H NMR** (500 MHz, DMSO) δ 8.20 (d, *J* = 8.7 Hz, 1H), 8.15 (d, *J* = 2.1 Hz, 1H), 7.69 (dd, *J* = 8.7, 2.1 Hz, 1H), 3.69 (s, 2H), 3.53 (t, *J* = 5.5 Hz, 2H), 2.60 (t, *J* = 5.5 Hz, 2H), 2.29 (s, 3H); **^{13}C NMR** (126 MHz, DMSO) δ 158.5, 158.4, 151.8, 139.0, 135.4, 130.6, 129.0, 125.8, 123.0, 122.4, 60.0, 59.4, 58.3, 42.2; **LRMS** (ES + APCI) *m/z* 324.0 $(M+H)^+$; **HRMS** (ESI, +ve) *m/z*: calc. for $C_{14}H_{15}{}^{35}ClN_3O_2S$ 324.0571, found 324.0568 $(M+H)^+$.

8-Chloro-2-(pyrrolidin-1-ylmethyl)benzo[4,5]thieno[3,2-*d*]pyrimidin-4(3*H*)-one (43d)

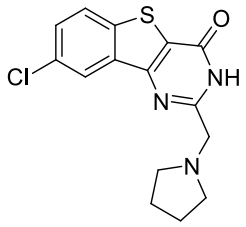

Following General Procedure C, **36** (100 mg, 0.28 mmol), pyrrolidine (93 µL, 1.12 mmol) in EtOH (4 mL) during 48 hours at 90 ºC. The solvent was evaporated under reduced pressure and the residue partially dissolved in CH_2Cl_2/MeOH (1:1, 10 mL). The solution was filtered through an SCX cartridge (1 g), flushed with MeOH (3 x 5 mL) and then with a solution of NH_3 in MeOH (2 M, 2 x 5 mL). The NH_3 in MeOH fractions were evaporated under reduced pressure to give the title compound **43d** as a white solid (24 mg, 0.08 mmol, 27%). **Mpt** 153–154 ºC decomp.; **IR** (ATR)/cm^{-1}: 2966, 2804, 1664, 1572; **^{1}H NMR** (400 MHz, DMSO) δ 8.19 (d, *J* = 8.5 Hz, 1H), 8.15 (d, *J* = 2.5 Hz, 1H), 7.68 (d, *J* = 8.5, 2.5 Hz, 1H), 3.71 (s, 2H) , 2.65–2.62 (m, 4H), 1.75–1.72 (m, 4H); **^{13}C NMR** (101 MHz, DMSO) δ 158.3, 157.9, 151.6, 138.6, 135.4, 130.3, 128.6, 125.4, 122.7, 122.1, 57.3, 53.1, 23.2; **LRMS** (ES + APCI) *m/z* 320.0 $(M+H)^+$; **HRMS** (ESI, +ve) *m/z* calc. $C_{15}H_{15}{}^{35}ClN_3OS$ 320.0619, found 320.0620 $(M+H)^+$.

2-((4-Acetyl-1,4-diazepan-1-yl)methyl)-8-chlorobenzo[4,5]thieno[3,2-*d*]pyrimidin-4(*3H*)-one (43e)

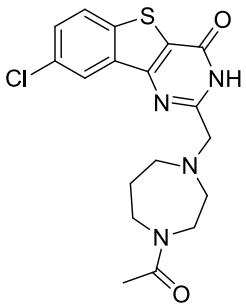

Following General Procedure C, **36** (100 mg, 0.28 mmol), 1-(1,4-diazepan-1-yl)ethanone (221 µL, 1.68 mmol) in EtOH (4 mL) for 24 hours at 50 ºC. The reaction was cooled down to room temperature and a white solid precipitated. The solid was washed with EtOH (20 mL) to

afford the title compound **43e** as a white solid (40 mg, 0.1 mmol, 36%). **Mpt** 130–131 ºC decomp.; **IR** (ATR)/cm^{-1}: 3479, 2987, 1658, 1649; **^{1}H NMR** (400 MHz, DMSO) δ 8.19 (d, *J* = 8.6 Hz, 1H), 8.14 (s, 1H), 8.13 (d, *J* = 2.2 Hz, 1H), 7.68 (dd, *J* = 8.6, 2.2 Hz, 1H), 3.76–3.65 (m, 2H), 3.58–3.41 (m, 4H), 2.89–2.82 (m, 1H), 2.79–2.68 (m, 3H), 2.02–1.98 (m, 3H), 1.87–1.79 (m, 1H), 1.77–1.70 (m, 1H); **^{13}C NMR** (101 MHz, DMSO) δ 170.6, 158.6, 158.2, 152.1, 139.3, 135.5, 131.1, 129.4, 125.8, 123.2, 122.8, 59.0, 55.4–54.9, 54.5–54.1, 48.2–47.3, 44.6–44.0, 27.7–26.8, 21.4; **LRMS** (ES + APCI) *m/z* 391 (M+H); **HRMS** (ESI, +ve) *m/z* calc. $C_{18}H_{20}{}^{35}ClN_4O_2S$ 391.0990, found 391.0992 $(M+H)^+$.

8-Chloro-2-(((2-hydroxyethyl)amino)methyl)benzo[4,5]thieno[3,2-*d*]pyrimidin-4(3*H*)-one (43f)

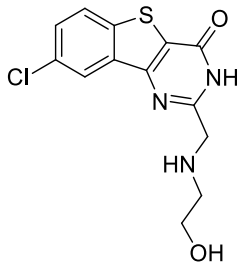

Following General Procedure C, **36** (100 mg, 0.28 mmol), ethanolamine (100 µL, 1.66 mmol) in EtOH (4 mL) at for 24 hours at 90 ºC. The reaction was cooled down to room and a white solid precipitated. The solid was filtered and washed with MeOH (10 mL) to afford the title compound **43f** as a white solid (25 mg, 0.41 mmol, 29%). **Mpt** 161–163 ºC decomp.; **IR** (ATR)/cm^{-1}: 3120 (br), 2864 (br), 1660, 1541; **^{1}H NMR** (500 MHz, DMSO) δ 8.19 (d, *J* = 7.0 Hz, 1H), 8.18 (s, 1H), 7.69 (dd, *J* = 8.6, 2.2 Hz, 1H), 3.83 (s, 2H), 3.50 (t, *J* = 5.5 Hz, 2H), 2.70 (t, *J* = 5.5 Hz, 2H); **^{13}C NMR** (126 MHz, DMSO) δ 160.3, 159.6, 152.4, 139.3, 136.1, 131.0, 129.4, 126.3, 123.0, 122.9, 60.6, 51.7, 51.3; **LRMS** (ES + APCI) *m/z* 310.0 $(M+H)^+$; **HRMS** (ESI, +ve) *m/z* calc. $C_{13}H_{13}{}^{35}ClN_3O_2S$ 310.0414, found 310.0412 $(M+H)^+$.

8-Chloro-2-(((2-methoxyethyl)(methyl)amino)methyl)benzo[4,5]thieno[3,2-*d*]pyrimidin-4(3*H*)-one (43g)

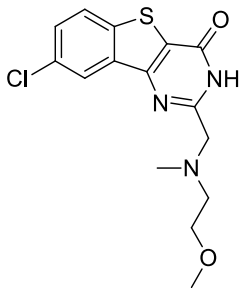

Following General Procedure C, **36** (100 mg, 0.28 mmol), 2-methoxyethyl methyl amine (180 µL, 1.68 mmol) in EtOH (4 mL) for 24 hours at 90 ºC. The solvent was evaporated under reduced pressure and the residue dissolved in DCM/MeOH (1:1, 15 mL). The solution was filtered through an SCX cartridge, flushed with MeOH (3 x 5 mL) and then with a solution of NH_3 in MeOH (2 M, 2 x 5 mL). The MeOH fraction was evaporated under reduced pressure to give the desired product. The residue was purified by reverse phase semi-preparative HPLC to afford the title compound **43g** as a white solid (35 mg, 0.1 mmol, 37%). **Mpt** 140–142 ºC; **IR** (ATR)/cm^{-1}: 2864, 1664, 1589; **^{1}H NMR** (500 MHz, DMSO) δ 8.20 (d, *J* = 8.7 Hz, 1H), 8.19–8.14 (m, 2H), 7.69 (dd, *J* = 8.7, 2.1 Hz, 1H), 3.68 (s, 2H), 3.49 (t, *J* = 5.6 Hz, 2H), 3.25 (s, 3H), 2.72 (t, *J* = 5.6 Hz, 2H), 2.37 (s, 3H); **^{13}C NMR** (101 MHz, DMSO) δ 158.3, 158.2, 151.8, 138.9, 135.5, 130.6, 129.0, 125.8, 122.9, 122.4, 69.9, 59.5, 57.9, 55.8, 42.5; **LRMS** (ES + APCI) *m/z* 338.0 $(M+H)^+$; **HRMS** (ESI, +ve) *m/z*: calc. $C_{15}H_{17}{}^{35}ClN_3O_2S$ 338.0728, found 338.0725 $(M+H)^+$.

8-Chloro-2-((((1*R*,3*S*)-3-hydroxy-3-(trifluoromethyl)cyclohexyl)amino)methyl)benzo[4,5]thieno[3,2-*d*]pyrimidin-4(3*H*)-one (43h)

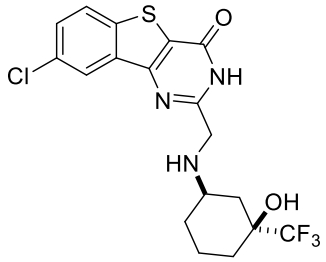

Following General Procedure C, **36** (100 mg, 0.29 mmol), *cis*-3-amino-1-(trifluoromethyl)cyclohexan-1-ol (183 mg, 0.99 mmol) in dry EtOH (5 mL) for 48 hours at 50 ºC. The solvent was evaporated under reduced pressure and the residue purified by reverse phase HPLC to give the title compound **43h** as a white solid (30 mg, 0.07 mmol, 24%). **Mpt** 190–191 ºC decomp.; **IR** (ATR)/cm^{-1}: 3396 (br), 3280, 2775 (br), 1672; **^{1}H NMR** (400 MHz, DMSO) δ 8.23 (d, *J* = 2.0 Hz, 1H), 8.20 (d, *J* = 8.7 Hz, 1H), 7.69 (dd, *J* = 8.7, 2.0 Hz, 1H), 7.63 (br, 3H), 3.84 (d, *J* = 15.9 Hz, 2H), 3.11–3.04 (m, 1H), 1.92–1.81 (m, 2H), 1.81–1.72 (m, 1H), 1.72–1.63 (m, 2H), 1.63–1.43 (m, 3H); **^{13}C NMR** (101 MHz, DMSO) δ 159.4, 158.6, 151.8, 138.9, 135.5, 130.6, 129.0, 125.8, 122.6, 122.5, 51.2, 48.7, 32.1, 30.2, 28.9, 15.4 (2 carbon not observed); **LRMS** (ES + APCI) *m/z* 432.0 $(M+H)^+$; **HRMS** (ESI, +ve) *m/z* calc. $C_{18}H_{18}{}^{35}ClF_3N_3O_2S$ 432.0754, found 432.0755 $(M+H)^+$.

(*S*)-8-Chloro-2-(((1-hydroxy-3-methylbutan-2-yl)amino)methyl)benzo[4,5]thieno[3,2-*d*]pyrimidin-4(3*H*)-one (43j)

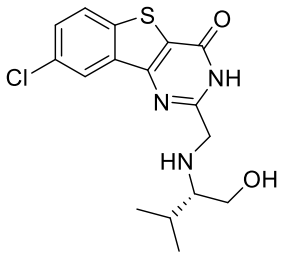

Following General Procedure C, **36** (200 mg, 0.57 mmol), L-valinol (190 μL, 1.71 mmol) in dry EtOH (6.5 mL) for 72 hours at 50 ºC. The solvent was evaporated under reduced pressure and the residue purified by HPLC to give the title compound **43j** as a white solid (35 mg, 0.09, 17%). **Mpt** 191–193 ºC decomp.; **IR** (ATR)/ cm^{-1}: 3421 (br), 3138 (br), 2868, 1651; **^{1}H**

NMR (400 MHz, DMSO) δ 8.20–8.17 (m, 2H), 8.16 (d, *J* = 2.1 Hz, 1H), 7.68 (dd, *J* = 8.7, 2.2 Hz, 1H), 3.93 (d, *J* = 16.1 Hz, 1H), 3.84 (d, *J* = 16.1 Hz, 1H), 3.48 (dd, *J* = 10.8, 4.3 Hz, 1H), 3.33 (dd, *J* = 10.8, 7.2 Hz, 1H), 2.41–2.33 (m, 1H), 1.88–1.74 (m, 1H), 0.91 (d, *J* = 6.9 Hz, 3H), 0.88 (d, *J* = 6.9 Hz, 3H); **^{13}C NMR** (101 MHz, DMSO) δ 163.2, 160.3, 158.4, 151.9, 138.9, 135.4, 130.6, 129.0, 125.8, 122.5, 122.4, 64.1, 60.9, 49.6, 28.6, 18.6; **LRMS** (ES + APCI) *m/z* 352.0 $(M+H)^+$; **HRMS** (ESI, +ve) *m/z* calc. for $C_{16}H_{19}{}^{35}ClN_3O_2S$ 352.0881, found 352.0885 $(M+H)^+$.

(*R*)-8-Chloro-2-(((1-hydroxy-3-methylbutan-2-yl)amino)methyl)benzo[4,5]thieno[3,2-*d*]pyrimidin-4(3*H*)-one (43k)

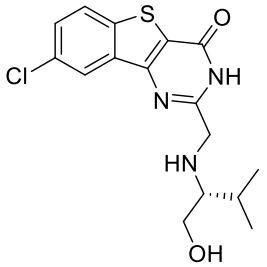

Following General Procedure C, **36** (200 mg, 0.57 mmol), D-valinol (190 μL, 1.71 mmol) in dry EtOH (6.5 mL) for 72 hours at 50 ºC. The solvent was evaporated under reduced pressure and the residue purified by HPLC to give the title compound **43k** as a white solid (30 mg, 0.08, 14%). **Mpt** 189–191 ºC decomp.; **IR** (ATR)/cm^{-1}: 3423 (br), 2968 (br), 1651, 1575; **^{1}H NMR** (400 MHz, DMSO) δ 8.20 (d, *J* = 8.7 Hz, 1H), 8.17 (d, *J* = 2.1 Hz, 1H), 7.69 (dd, *J* = 8.7, 2.1 Hz, 1H), 3.93 (d, *J* = 16.2 Hz, 1H), 3.83 (d, *J* = 16.2 Hz, 1H), 3.48 (dd, *J* = 10.8, 4.3 Hz, 1H), 3.32 (dd, *J* = 10.8, 7.2 Hz, 2H), 2.38–2.35 (m, 1H), 1.85–1.79 (m, 1H), 0.90 (d, *J* = 7.0 Hz, 3H), 0.88 (d, *J* = 7.0 Hz, 3H); **^{13}C NMR** (101 MHz, DMSO) δ 160.5, 158.4, 151.9, 138.9, 135.4, 130.6, 129.0, 125.8, 122.4, 122.4, 64.1, 61.0, 49.6, 28.6, 18.6, 18.6; **LRMS** (ES + APCI) *m/z* 352.0 $(M+H)^+$; **HRMS** (ESI, +ve) *m/z* calc. for $C_{16}H_{19}{}^{35}ClN_3O_2S$ 352.0881, found 352.0885 $(M+H)^+$.

8-Chloro-2-((phenylamino)methyl)benzo[4,5]thieno[3,2-*d*]pyrimidin-4(3*H*)-one[1] (43l)

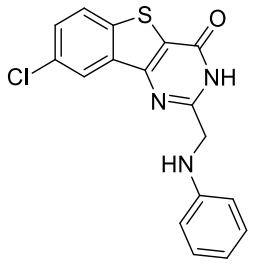

Following General Procedure C, **36** (100 mg, 0.28 mmol), aniline (114 µL, 1.26 mmol) in EtOH (4 mL) for 48 hours at 90 ºC. The reaction was cooled to room temperature and a white solid precipitated. The solid was filtered and washed with 1:1 MeOH/CH_2Cl_2 (10 mL) to afford the title compound **43l** as a white solid (47 mg, 0.14 mmol, 49%). **Mpt** 230–231 ºC decomp.; **IR** (ATR)/cm^{-1}: 3406, 2987, 1662; **^{1}H NMR** (400 MHz, DMSO) δ 12.84 (s, 1H), 8.23 (d, *J* = 2.2 Hz, 1H), 8.20 (d, *J* = 8.7 Hz, 1H), 7.69 (dd, *J* = 8.7, 2.2 Hz, 1H), 7.14–7.06 (m, 2H), 6.70 (dd, *J* = 7.4 Hz, 1.2 Hz, 2H), 6.61–6.59 (m, 1H), 6.14 (t, *J* = 6.0 Hz, 1H), 4.36 (d, *J* = 6.0 Hz, 2H); **^{13}C NMR** (101 MHz, DMSO) δ 158.8, 158.4, 151.8, 147.8, 138.9, 135.4, 130.7, 129.1, 129.0, 125.9, 122.8, 122.6, 116.8, 112.6, 45.9; **LRMS** (ES + APCI) *m/z* 342.0 (M+H); **HRMS** (ESI, +ve) *m/z* calc. $C_{17}H_{13}{}^{35}ClN_3OS$ 342.0462, found 342.0467 $(M+H)^+$.

8-Chloro-2-(((4-chlorophenyl)amino)methyl)benzo[4,5]thieno[3,2-*d*]pyrimidin-4(3*H*)-one (43m)

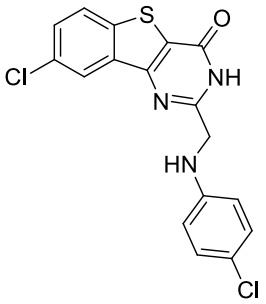

Following General Procedure C, **36** (100 mg, 0.28 mmol), 4-chloroaniline (176 µL, 1.68 mmol) in DMF (5 mL) for 40 hours at 90 ºC. The solvent was evaporated under reduced pressure. MeOH (15 mL) was added and a white solid precipitated. The white solid was filtered under reduced pressure and washed with MeOH (2 x 15 mL). The white solid was

washed with acetone (3 x 15 mL) to afford the title compound **43m** as a white solid (90 mg, 0.23 mmol, 86%). **Mpt** 150–152 ºC; **IR** (ATR)/cm^{-1}: 3400, 2985, 1587; **^{1}H NMR** (400 MHz, DMSO) δ 12.86 (s, 1H), 8.23 (s, 1H), 8.21 (d, *J* = 8.6 Hz, 1H), 7.71 (dd, *J* = 8.6, 2.2 Hz, 1H), 7.17–7.13 (m, 2H), 6.74–6.71 (m, 2H), 6.34 (t, *J* = 6.1 Hz, 1H), 4.36 (d, *J* = 6.1 Hz, 2H); **^{13}C NMR** (101 MHz, DMSO) δ 158.3, 158.3, 151.7, 146.8, 138.9, 135.4, 130.6, 129.1, 128.6, 125.8, 122.8, 122.4, 120.1, 114.0, 45.7; **LRMS** (ES + APCI) *m/z* 376.0 (M+H)$^{+}$; **HRMS** (ESI, +ve) *m/z* calc. for $C_{17}H_{12}{}^{35}Cl_2N_3OS$ 376.0073, found 376.0072 (M+H)$^{+}$.

8-Chloro-2-(((3-hydroxyphenyl)amino)methyl)benzo[4,5]thieno[3,2-*d*]pyrimidin-4(*3H*)-one[1] (43n)

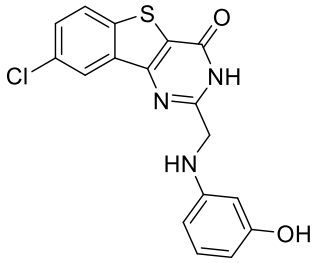

Following General Procedure C, **36** (100 mg, 0.28 mmol), 3-aminophenol (183 mg, 1.68 mmol) in EtOH (4 mL) for 24 hours at 90 ºC. The solvent was evaporated under reduced pressure to give a white/pink solid. The residue was dissolved in DCM/MeOH (1:1, 8 mL). The solution was filtered through an SCX cartridge, flushed with MeOH (3 x 5 mL) and then with a solution of NH_3 in MeOH (2 M, 2 x 5 mL). The MeOH fractions were evaporated under reduced pressure to give the desired product. The white solid was suspended in acetone (10 mL), sonicated for 10 minutes and filtered to afford the title compound **43n** as a white solid (80 mg, 0.22 mmol, 78%). **Mpt** 192–193 ºC decomp.; **IR** (ATR)/cm^{-1}: 3423, 2972, 1662, 1496; **^{1}H NMR** (400 MHz, DMSO) δ 12.79 (s, 1H), 9.02 (s, 1H), 8.25 (d, *J* = 2.2 Hz, 1H), 8.21 (d, *J* = 8.8 Hz, 1H), 7.70 (dd, *J* = 8.7, 2.2 Hz, 1H), 6.86 (t, *J* = 8.0 Hz, 1H), 6.17–6.13 (m, 1H), 6.11 (appt, *J* = 2.1 Hz, 1H), 6.05–5.99 (m, 2H), 4.30 (d, *J* = 5.7 Hz, 2H); **^{13}C NMR** (101 MHz, DMSO) δ 158.8, 158.3, 158.2, 151.7, 149.0, 138.9, 135.4, 130.6, 129.6, 129.1, 125.8, 122.7, 122.5, 104.4, 104.1, 99.7, 46.0; **LRMS** (ES + APCI) *m/z* 358.0 (M+H)$^{+}$; **HRMS** (ESI, +ve) *m/z* calc. $C_{17}H_{13}{}^{35}ClN_3O_2S$ 358.0412, found 358.0415 (M+H)$^{+}$.

8-Chloro-2-(((3-methoxyphenyl)amino)methyl)benzo[4,5]thieno[3,2-*d*]pyrimidin-4(3*H*)-one (43o)

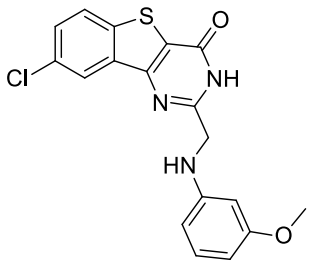

Following General Procedure C, **36** (100 mg, 0.28 mmol), 3-methoxyaniline (108 µL, 1.28 mmol) in EtOH (4 mL) for 24 hours at 90 ºC. A white solid precipitated. The white solid was filtered under reduced pressure and washed with CH_2Cl_2/MeOH (1:1, 10 mL) to afford the title compound **43o** as a white solid (30 mg, 0.08 mmol, 29%). **Mpt** 150–152 ºC decomp.; **IR** (ATR)/cm^{-1}: 3415, 2931 (br), 1660; **^{1}H NMR** (400 MHz, DMSO) δ 8.21 (d, *J* = 2.1 Hz, 1H), 8.16 (d, *J* = 8.7 Hz, 1H), 7.67 (dd, *J* = 8.7, 2.1 Hz, 1H), 6.99 (t, *J* = 8.0 Hz, 1H), 6.33–6.25 (m, 2H), 6.22–6.13 (m, 1H), 4.33 (s, 2H), 3.64 (s, 3H); **^{13}C NMR** (101 MHz, DMSO) δ 160.5, 158.8, 158.5, 151.9, 149.2, 139.1, 135.5, 130.9, 130.0, 129.3, 126.0, 122.9, 122.7, 105.8, 102.6, 98.7, 54.9, 46.0; **LRMS** (ES + APCI) *m/z* 372.0 $(M+H)^+$; **HRMS** (ESI, +ve) *m/z* calc. $C_{18}H_{15}{}^{35}ClN_3O_2S$ 372.0568, found 372.0562 $(M+H)^+$.

8-Chloro-2-(((4-methoxyphenyl)amino)methyl)benzo[4,5]thieno[3,2-*d*]pyrimidin-4(*3H*)-one (43p)

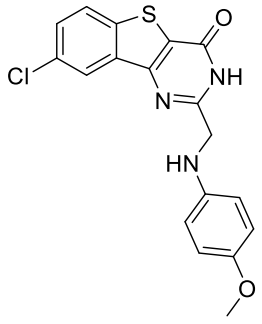

Following General Procedure C, **36** (100 mg, 0.28 mmol) 4-methoxyaniline (206 mg, 1.68 mmol) in EtOH (4 mL) for 24 hours at 90 ºC. The reaction was cooled down to room temperature and an orange solid precipitated. The residue was dissolved in CH_2Cl_2/MeOH

(1:1, 10 mL). The solution was filtered through an SCX cartridge, flushed with MeOH (3 x 5 mL) and then with a solution of NH_3 in MeOH (2 M, 2 x 5 mL). The NH_3 in MeOH fraction was evaporated under reduced pressure to give the title compound **43p** as an orange solid (45 mg, 0.12 mmol, 43%). **Mpt** 205–207 ºC decomp; **IR** (ATR)/cm^{-1}: 1672, 1583, 1512; **^{1}H NMR** (400 MHz, DMSO) δ 12.72 (s, 1H), 8.24 (d, *J* = 2.0 Hz, 1H), 8.20 (d, *J* = 8.6 Hz, 1H), 7.70 (dd, *J* = 8.6, 2.0 Hz, 1H), 6.77–6.70 (m, 2H), 6.69–6.62 (m, 2H), 4.31 (s, 2H), 3.61 (s, 3H); **^{13}C NMR** (101 MHz, DMSO) δ 159.0, 158.3, 151.7, 151.4, 141.8, 138.9, 135.4, 130.7, 129.1, 125.9, 122.7, 122.5, 114.6, 113.8, 55.2, 46.7; **LRMS** (ES + APCI) *m/z* 372.0 $(M+H)^+$; **HRMS** (ESI, +ve) *m/z* calc. $C_{18}H_{15}{}^{35}ClN_3O_2S$ 372.0568, found 372.0571 $(M+H)^+$.

8-Chloro-2-(((3,5-dimethoxyphenyl)amino)methyl)benzo[4,5]thieno[3,2-*d*]pyrimidin-4(3*H*)-one (43q)

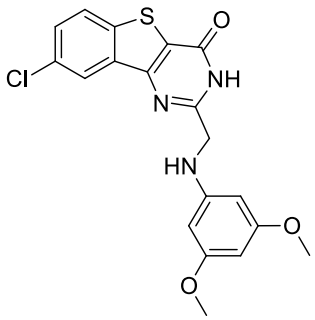

Following General Procedure C, **36** (100 mg, 0.28 mmol), 3,5-dimethoxyaniline (257 mg, 1.68 mmol) in EtOH (4 mL) for 48 hours at 90 ºC. The reaction was cooled down to room temperature and an white solid precipitated. The solid was dissolved in a mixture of CH_2Cl_2/MeOH (1:1, 10 mL) and loaded into an SCX cartridge (1 g). The SCX cartridge was washed with CH_2Cl_2/MeOH (1:1, 10 mL) and the compound was then eluted with NH_3 in MeOH (2 M, 25 mL). The NH_3 in MeOH fraction was evaporated under reduced pressure to give the title compound **43q** as a yellow solid (23 mg, 0.06 mmol, 21%); **Mpt** 170–171 ºC decomp.; **IR** (ATR)/cm^{-1}: 3394, 2930 (br), 1666, 1203; **^{1}H NMR** (400 MHz, DMSO) δ 12.83 (s, 1H), 8.24 (d, *J* = 2.0 Hz, 1H), 8.21 (d, *J* = 8.7 Hz, 1H), 7.70 (dd, *J* = 8.7, 2.0 Hz, 1H), 6.17 (t, *J* = 6.0 Hz, 1H), 5.91 (d, *J* = 2.1 Hz, 2H), 5.78 (appt, *J* = 2.1 Hz, 1H), 4.32 (d, *J* = 6.0 Hz, 2H), 3.64 (s, 6H); **^{13}C NMR** (101 MHz, DMSO) δ 161.1, 158.6, 158.3, 151.7, 149.6, 138.9, 135.4, 130.7, 129.1, 125.8, 122.7, 122.5, 91.5, 89.4, 54.8, 45.9; **LRMS** (ES + APCI) *m/z* 402 $(M+H)^+$; **HRMS** (ESI, +ve) *m/z* calc. $C_{19}H_{17}{}^{35}ClN_3O_3S$ 402.0674, found 402.0674 $(M+H)^+$.

8-Chloro-2-(((4-fluorophenyl)amino)methyl)benzo[4,5]thieno[3,2-*d*]pyrimidin-4(3*H*)-one (43r)

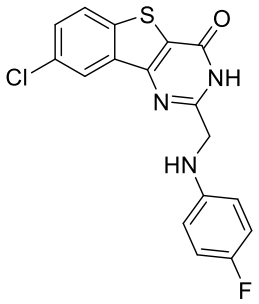

Following general procedure C, **36** (100 mg, 0.28 mmol), 4-fluoroaniline (161µL, 1.68 mmol) in EtOH (4 mL) during 48 hours at 90 ºC. The reaction was cooled down to room temperature and a white solid precipitated. The solid was filtered under reduced pressure and washed with petrol (30 mL) to give the title compound **43r** as a white solid (43 mg, 0.11 mmol, 48%). **Mpt** 170–171 ºC decomp.; **IR** (ATR)/cm^{-1} 3406, 2900, 1662, 1510; **^{1}H NMR** (400 MHz, DMSO) δ 12.80 (s, 1H), 8.22 (d, *J* = 2.0 Hz, 1H), 8.20 (d, *J* = 8.9 Hz, 1H), 7.69 (dd, *J* = 8.9, 2.0 Hz, 1H), 7.01–6.90 (m, 2H), 6.74–6.66 (m, 2H), 6.08 (s, 1H), 4.33 (d, *J* = 5.0 Hz, 2H); **^{13}C NMR** (101 MHz, DMSO) δ 158.6, 153.7, 157.1 (d, *J* = 235.1 Hz), 151.7, 144.5, 138.9, 135.4, 130.6, 129.1, 125.8, 122.8, 122.5, 115.3 (d, *J* = 21.9 Hz), 113.3 (d, *J* = 7.2 Hz), 46.3; **LRMS** (ES + APCI) *m/z* 360 $(M+H)^{+}$.

8-Chloro-2-((pyridin-2-ylamino)methyl)benzo[4,5]thieno[3,2-*d*]pyrimidin-4(*3H*)-one (43s)

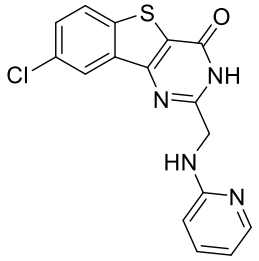

Following General Procedure C, **36** (100 mg, 0.28 mmol), 2-aminopyridine (160 mg, 1.68 mmol) in DMF (4 mL) for 40 hours at 80 ºC. The solvent was evaporated under reduced pressure to give a brown residue. The residue was washed with MeOH (20 mL) and filtered to afford a white solid. The white solid was washed with a solution of 20 % Na_2CO_3 in water (10 mL) and filtered to afford the title compound **43s** as a white solid (70 mg, 0.2 mmol, 74%).

Mpt 174–175 ºC decomp.; **IR** (ATR)/cm^{-1}: 3244, 3118, 1651, 1581, 1024; **^{1}H NMR** (400 MHz, DMSO) δ 8.75 (s, 2H), 8.22 (d, *J* = 8.7 Hz, 1H), 8.17 (d, *J* = 6.0 Hz, 1H), 8.01 (appt, *J* = 7.0 Hz, 1H), 7.73–7.62 (m, 2H), 7.25 (d, *J* = 8.7 Hz, 1H), 6.99 (appt, *J* = 7.0 Hz, 1H), 5.59 (s, 2H).; **^{13}C NMR** (101 MHz, DMSO) δ 158.2, 155.1, 153.0, 142.8, 141.0, 138.8, 135.0, 130.6, 129.2, 126.1, 123.4, 121.6, 115.0, 112.5, 53.4, 1 carbon not observed; **LRMS** (ES + APCI) *m/z* 343.0 (M+H)$^{+}$; **HRMS** (ESI, +ve) *m/z* calc. $C_{16}H_{12}{}^{35}ClN_4OS$ 343.0415, found 343.0417 (M+H)$^{+}$.

8-Chloro-2-((pyridin-3-ylamino)methyl)benzo[4,5]thieno[3,2-*d*]pyrimidin-4(*3H*)-one (43t)

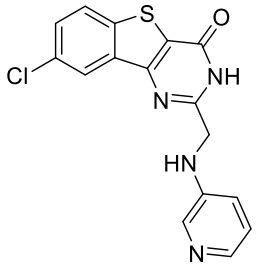

Following General Procedure C, **36** (100 mg, 0.28 mmol), 2-aminopyridine (0.16 g, 1.68 mmol) in DMF (4 mL) during 40 hours at 80 ºC. The solvent was evaporated under reduced pressure to give a brown residue. The residue was washed with MeOH (20 mL) and filtered to obtain a the title compound **43t** as a white solid (75 mg, 0.22 mmol, 78%). **Mpt** 182–184 ºC decomp.; **IR** (ATR)/cm^{-1}: 3367, 2970, 1566; **^{1}H NMR** (400 MHz, DMSO) δ 8.29 (d, *J* = 5.7 Hz, 1H), 8.27–8.25 (m, 1H), 8.23 (d, *J* = 8.7 Hz, 1H), 7.84–7.79 (m, 2H), 7.77–7.72 (m, 1H), 7.70 (dd, *J* = 8.7, 2.2 Hz, 1H), 6.83 (s, 1H), 5.87 (s, 2H); **^{13}C NMR** (126 MHz, DMSO) δ 155.3, 151.2, 148.3, 140.1, 138.7, 135.4, 132.8, 130.4, 129.9, 128.8, 128.0, 127.5, 125.9, 123.4, 121.8, 61.5; **LRMS** (ES + APCI) *m/z* 343.0 (M+H)$^{+}$; **HRMS** (ESI, +ve) *m/z* calc. $C_{16}H_{12}{}^{35}ClN_4OS$ 343.0415, found 343.0416 (M+H)$^{+}$.

8-Chloro-2-((pyridin-4-ylamino)methyl)benzo[4,5]thieno[3,2-*d*]pyrimidin-4(*3H*)-one (43u)

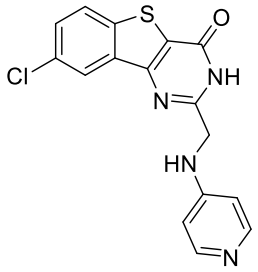

Following General Procedure C, **36** (100 mg, 0.28 mmol), 2-aminopyridine (160 mg, 1.68 mmol) in DMF (4 mL) for 40 hours at 80 ºC. The solvent was evaporated under reduced pressure to give a brown residue. The residue was washed with MeOH (20 mL) and filtered to give a white solid. The white solid was washed with a solution of 20% Na_2CO_3 in water (10 mL) and filtered to title compound **43u** as a white solid (60 mg, 0.17 mmol, 63%). **Mpt** 220–222 ºC decomp.; **IR** (ATR)/cm^{-1}: 3327, 2935, 1598, 1550; **^{1}H NMR** (400 MHz, DMSO) δ 8.23 (d, *J* = 7.4 Hz, 2H), 8.07 (s, 2H), 8.00 (d, *J* = 8.6 Hz, 1H), 7.92 (d, *J* = 2.2 Hz, 1H), 7.51 (dd, *J* = 8.6, 2.2 Hz, 1H), 6.85 (d, *J* = 7.4 Hz, 2H), 5.24 (s, 2H); **^{13}C NMR** (101 MHz, DMSO/benzene) δ 168.3, 162.0, 158.7, 152.6, 144.2, 137.9, 137.2, 129.1, 127.1, 125.3, 122.3, 121.4, 108.8, 62.0; **LRMS** (ES + APCI) *m/z* 343.0 $(M+H)^+$; **HRMS** (ESI, +ve) *m/z* calc. $C_{16}H_{12}{}^{35}ClN_4OS$ 343.0415, found 343.0417 $(M+H)^+$.

8-Bromo-2-((methylamino)methyl)benzo[4,5]thieno[3,2-*d*]pyrimidin-4(3*H*)-one (46a)

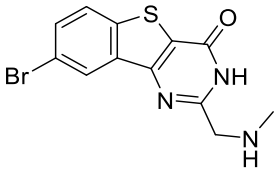

Following General Procedure C, **39** (2 g, 6.2 mmol), methylamine 33% in MeOH (30 mL) for 16 hours at room temperature. The solvent was then evaporated under reduced pressure to give a crude white solid. The solid was dissolved in MeOH/CH_2Cl_2 (1:1, 30 mL) and loaded into an SCX cartridge. The cartridge was flushed with MeOH (3 x 30 mL) and then with a solution of NH_3 in MeOH (2 M, 50 mL). The NH_3 in MeOH fractions were evaporated under reduced pressure to give the title compound **46a** as a white solid (1.7 g, 5.2 mmol, 84%). **Mpt**

> 208 ºC decomp.; **IR** (ATR)/cm^{-1}: 2954, 2530 (br), 1674, 1531.**^{1}H NMR** (400 MHz, DMSO) δ 8.37 (d, *J* = 1.9 Hz, 1H), 8.12 (d, *J* = 8.7 Hz, 1H), 7.78 (dd, *J* = 8.6, 2.1 Hz, 1H), 4.01 (s, 2H), 2.57 (s, 3H); **^{13}C NMR** (101 MHz, DMSO) δ 160.3, 157.0, 153.5, 139.1, 136.0, 131.3, 126.1, 125.4, 122.6, 118.5, 51. 0, 33.9; **LRMS** (ES + APCI) *m/z* 323.9 $(M+H)^+$; **HRMS** (ESI, +ve) *m/z* calc. $C_{12}H_{11}{}^{79}BrN_3OS$ 323.9801, found 323.9804 $(M+H)^+$.

2-((Methylamino)methyl)-8-phenylbenzo[4,5]thieno[3,2-*d*]pyrimidin-4(3*H*)-one (47a)

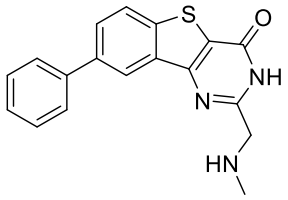

Following General Procedure C, **40** (80 mg, 0.20 mmol), methylamine 33% in MeOH (6 mL) for 16 hours at room temperature. The solvent was then evaporated under reduced pressure to give a crude white solid. The solid was dissolved in $MeOH/CH_2Cl_2$ (1:1, 10 mL) and loaded into an SCX cartridge (1g). The cartridge was flushed with MeOH (3 x 30 mL) and then with a solution of NH_3 in MeOH (2 M, 50 mL). The NH_3 in MeOH fractions were evaporated under reduced pressure to give the title compound **47a** as a white solid (59 mg, 0.18 mmol, 90%). **Mpt** > 220–221 ºC decomp.; **^{1}H NMR** (400 MHz, DMSO) δ 13.24 (s, 1H), 9.42 (s, 1H), 8.62 (s, 1H), 8.29 (d, *J* = 8.5 Hz, 1H), 8.03 (dd, *J* = 8.5, 2.0 Hz, 1H), 7.80 (d, *J* = 7.5 Hz, 2H), 7.57 (t, *J* = 7.5 Hz, 2H), 7.46 (t, *J* = 7.5 Hz, 1H), 4.35 (s, 2H), 2.79 (s, 3H); **^{13}C NMR** (126 MHz, DMSO) δ 160.6, 159.3, 153.1, 139.6, 139.4, 137.4, 135.1, 129.1, 127.7, 127.6, 126.9, 124.4, 121.6, 120.6, 53.0, 34.8; **LRMS** (ES + APCI) *m/z* 322.1 $(M+H)^+$; **HRMS** (ESI, +ve) *m/z* calc. for $C_{19}H_{14}N_3OS$ 322.1009, found 322.1011 $(M+H)^+$.

2-((Methylamino)methyl)-8-nitrobenzo[4,5]thieno[3,2-*d*]pyrimidin-4(3*H*)-one (48a)

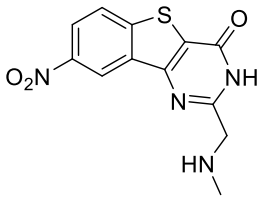

Following General Procedure C, **41** (0.2 g, 0.55 mmol), methylamine 33% in MeOH (8 mL) for 16 hours at room temperature. The solvent was then evaporated under reduced pressure to give a crude white solid. The solid was dissolved in MeOH/CH_2Cl_2 (1:1, 10 mL) and loaded into an SCX cartridge (1g). The cartridge was flushed with MeOH (3 x 10 mL) and then with a solution of NH_3 in MeOH (2 M, 20 mL). The NH_3 in MeOH fractions were evaporated under reduced pressure to give the title compound **48a** as a white solid (0.15 g, 0.46 mmol, 83%). **Mpt** > 221–223 ºC decomp.; **IR** (ATR)/cm^{-1}: 3390, 2964, 1658, 1592; **^{1}H NMR** (400 MHz, DMSO) δ 8.91–8.89 (m, 1H), 8.35–8.32 (m, 2H), 8.20 (s, 1H), 4.02 (s, 2H), 2.60 (s, 3H); **^{13}C NMR** (101 MHz, DMSO) δ 163.6, 159.7, 152.8, 146.0, 145.1, 135.0, 125.1, 123.1, 121.9, 117.9, 52.2, 33.7; **LRMS** (ES + APCI) *m/z* 291.0 $(M+H)^+$; **HRMS** (ESI, +ve) *m/z* calc. for $C_{12}H_{11}N_4O_3S$ 291.0546, found 291.0549 $(M+H)^+$.

2-((Methylamino)methyl)-8-(trifluoromethyl)benzo[4,5]thieno[3,2-*d*]pyrimidin-4(*3H*)-one (49a)

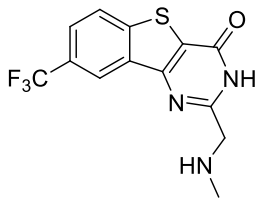

Following General Procedure C, **42** (100 mg, 0.26 mmol), methylamine 33 % in MeOH 6 mL at room temperature for 24 hours. The solvent was evaporated under reduced pressure to give a white solid. The white solid was dissolved in MeOH and loaded into an SCX cartridge (1 g). The SCX cartridge was washed with MeOH (10 mL) and then it was washed with a solution of NH_3 2 M in MeOH (15 mL). The NH_3 in MeOH fractions were evaporated under reduced pressure to afford the title compound **49a** as a white solid (40 mg, 0.13 mmol, 49%). **Mpt**

180–182 ºC decomp.; **IR** (ATR)/cm-$^{-1}$: 3412, 2891, 1660, 1606; **^{1}H NMR** (400 MHz, DMSO) δ 8.66 (s, 1H), 8.49 (d, *J* = 8.6 Hz, 1H), 8.03 (dd, *J* = 8.6, 1.4 Hz, 1H), 4.34 (s, 2H), 2.76 (s, 3H); **^{13}C NMR** (101 MHz, DMSO) δ 157.8, 155.7, 152.9, 151.3, 144.1, 133.8, 126.5 (q, *J* = 32.5 Hz) 125.7, 125.3–125.0 (m), 120.5–120.3 (m), 48.0, 33.1, 1 carbon not reported; **LRMS** (ES + APCI) *m/z* 314.0 $(M+H)^+$; **HRMS** (ESI, +ve) *m/z* calc. $C_{13}H_{11}F_3N_3OS$ 314.0569, found 314.0565 $(M+H)^+$.

2-(Morpholinomethyl)-8-(trifluoromethyl)benzo[4,5]thieno[3,2-*d*]pyrimidin-4(*3H*)-one (49b)

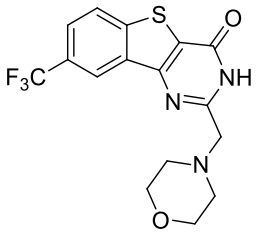

Following General Procedure C, **42** (100 mg, 0.26 mmol), morpholine (140 mg, 1.56 mmol) in EtOH (4 mL) during 16 hours at 80 ºC. The solvent was evaporated under reduced pressure to give a white/yellow solid. The residue was dissolved in MeOH and loaded into an SCX cartridge (1 g). The SCX cartridge was washed with MeOH (10 mL) and with a solution of NH_3 in MeOH (2 M, 15 mL). The NH_3 in MeOH fractions were evaporated under reduced pressure to the title compound **49b** as a white solid (20 mg, 0.05 mmol, 21%). **Mpt** 120–121 ºC decomp.; **IR** (ATR)/cm^{-1}: 2864, 1666, 1321, 1114; **^{1}H NMR** (400 MHz, DMSO) δ 12.63 (s, 1H), 8.40–8.38 (m, 2H), 7.94 (d, *J* = 8.7 Hz, 1H), 3.63–3.59 (m, 4H), 3.58 (s, 2H), 2.58–2.52 (m, 4H); **^{13}C NMR** (101 MHz, DMSO) δ 158.3, 157.3, 152.1, 143.9, 133.9, 126.3 (q, *J* = 32.1 Hz), 125.4, 125.0–124.6 (m), 124.3 (q, *J* = 272.1 Hz), 123.3, 120.0–119.7 (m), 66.1, 60.5, 53.0; **LRMS** (ES + APCI) *m/z* 370.0 $(M+H)^+$; **HRMS** (ESI, +ve) *m/z* calc. $C_{16}H_{15}F_3N_3O_2S$ 370.0832, found 370.0833 $(M+H)^+$.

8-Nitro-2-((pyridin-3-ylamino)methyl)benzo[4,5]thieno[3,2-*d*]pyrimidin-4(3*H*)-one (48t)

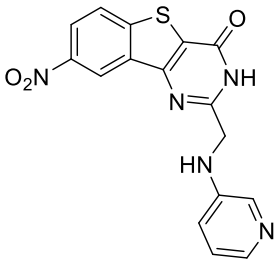

Following General Procedure C, **41** (200 mg, 0.55 mmol), 3-aminopyridine (260 mg, 1.56 mmol) in EtOH (8 mL) during 16 hours at 80 ºC. The solvent was evaporated under reduced pressure to give a yellow solid. The residue was dissolved in MeOH and loaded into an SCX cartridge (1 g). The SCX cartridge was washed with MeOH (10 mL) and with a solution of NH_3 2 M in MeOH (15 mL). The NH_3 in MeOH fractions were evaporated under reduced pressure to afford the title compound **48t** a yellow solid (150 mg, 0.42 mmol, 77%). **Mpt** > 251 ºC decomp.; **IR** (ATR)/cm^{-1}: 3394, 3140, 1658, 1573; **^{1}H NMR** (400 MHz, DMSO) δ 13.66 (s, 1H), 8.59 (d, *J* = 1.5 Hz, 1H), 8.45–8.38 (m, 2H), 8.31–8.27 (m, 1H), 8.27–8.22 (m, 1H), 7.82 (dd, *J* = 8.7, 5.7 Hz, 1H), 7.73 (dd, *J* = 8.7, 1.5 Hz, 1H), 6.80 (s, 2H), 5.81 (s, 2H); **^{13}C NMR** (101 MHz, DMSO) δ 159.0, 155.2, 151.8, 148.4, 146.0, 145.5, 133.9, 132.8, 129.9, 128.1, 127.6, 125.6, 124.5, 122.8, 117.8, 61.0; **LRMS** (ES + APCI) *m/z* 354.0 $(M+H)^+$; **HRMS** (ESI, +ve) *m/z* calc. for $C_{16}H_{13}N_5O_3S$ 354.0655, found 354.0656 $(M+H)^+$.

2-(((3-Hydroxyphenyl)amino)methyl)-8-nitrobenzo[4,5]thieno[3,2-*d*]pyrimidin-4(3*H*)-one (48n)

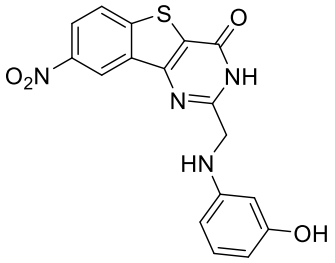

Following General Procedure C, **41** (200 mg, 0.55 mmol), 3-aminophenol (170 mg, 1.56 mmol) in EtOH (8 mL) during 16 hours at 80 ºC. The solvent was evaporated under reduced pressure to give a yellow solid. The residue was dissolved in MeOH and loaded into an SCX cartridge (1 g). The SCX cartridge was washed with MeOH (10 mL) and with a solution of

NH_3 2 M in MeOH (15 mL). The NH_3 in MeOH fractions were evaporated under reduced pressure to afford the title compound **48n** as a white solid (20 mg, 0.05 mmol, 10%). **Mpt** 192–194 ºC decomp.; **IR** (ATR)/cm^{-1}: 2970 (br), 1668, 1580; **^{1}H NMR** (500 MHz, DMSO) δ 12.89 (s, 1H), 9.00 (s, 1H), 8.89 (d, *J* = 1.8 Hz, 1H), 8.41–8.33 (m, 2H), 6.87 (appt, *J* = 8.0 Hz, 1H), 6.17–6.02 (m, 4H), 4.34 (s, 2H); **^{13}C NMR** (126 MHz, DMSO) δ 159.8, 158.2, 152.5, 149.0, 146.2, 145.5, 134.1, 129.6, 125.4, 123.6, 122.7, 118.4, 104.4, 104.1, 99.7, 99.5, 45.9; **LRMS** (ES + APCI) *m/z* 369.0 $(M+H)^+$; **HRMS** (ESI, +ve) *m/z* calc. for $C_{17}H_{13}N_4O_4S$ 369.0652, found 369.0655 $(M+H)^+$.

7-Chloro-2-(morpholinomethyl)benzo[4,5]thieno[3,2-*d*]pyrimidin-4(3*H*)-one (44b)

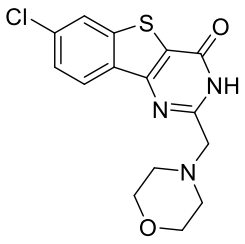

Following General Procedure C, **37** (200 mg, 0.57 mmol), morpholine (245 µL, 2.84 mmol) in EtOH (4 mL) during 48 hours at 50 ºC. The resulting solid was filtered under reduced pressure, washed with EtOH (20 mL) and dried to afford the title compound **44b** as a white solid (172 mg, 0.51 mmol, 90%). **Mpt** > 250 ºC decomp.; **IR** (ATR)/cm^{-1}: 2820 (br), 1658, 1586; **^{1}H NMR** (400 MHz, DMSO) δ 12.61 (s, 1H), 8.36 (d, *J* = 1.9 Hz, 1H), 8.21 (d, *J* = 8.5 Hz, 1H), 7.62 (dd, *J* = 8.5, 1.9 Hz, 1H), 3.62–3.57 (m, 2H), 3.57 (s, 1H), 2.55–2.52 (m, 2H); **^{13}C NMR** (101 MHz, DMSO) δ 158.3, 157.1, 152.0, 141.6, 133.7, 132.9, 126.2, 124.7, 123.6, 122.1, 66.1, 60.5, 53.0; **LRMS** (ES + APCI) *m/z* 336.0 $(M+H)^+$; **HRMS** (ESI, +ve) *m/z* calc. for $C_{15}H_{15}{}^{35}ClN_3O_2S$ 336.0568, found 336.0571 $(M+H)^+$.

7-Chloro-2-((phenylamino)methyl)benzo[4,5]thieno[3,2-*d*]pyrimidin-4(3*H*)-one (44l)

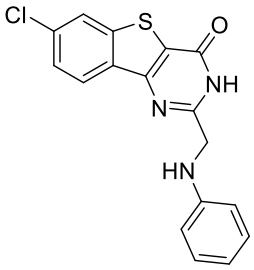

Following General Procedure C, **37** (200 mg, 0.57 mmol), morpholine (245 µL, 2.84 mmol) in EtOH (4 mL) during 48 hours at 50 ºC. The resulting solid was filtered under reduced pressure, washed with EtOH (20 mL) and dried to afford the title compound **44l** as a white solid (181 mg, 0.53 mmol, 93%). **Mpt** > 236–238 ºC; **IR** (ATR)/cm^{-1}: 3409, 2913 (br), 1658, 1591; **^{1}H NMR** (400 MHz, DMSO) δ 12.76 (s, 1H), 8.33 (d, *J* = 1.7 Hz, 1H), 8.22 (d, *J* = 8.5 Hz, 1H), 7.62 (dd, *J* = 8.5, 1.7 Hz, 1H), 7.09 (appt, *J* = 7.9 Hz, 2H), 6.69 (d, *J* = 7.9 Hz, 2H), 6.59 (appt, *J* = 7.9 Hz, 1H), 6.15–6.07 (m, 1H), 4.36 (d, *J* = 5.1 Hz, 2H); **^{13}C NMR** (101 MHz, DMSO) δ 158.9, 158.3, 152.1, 147.8, 141.7, 133.8, 132.8, 128.9, 126.1, 124.7, 123.6, 121.6, 116.8, 112.6, 45.9; **LRMS** (ES + APCI) *m/z* 342.0 $(M+H)^+$; **HRMS** (ESI, +ve) *m/z* calc. for $C_{17}H_{13}{}^{35}ClN_3OS$ 342.0462, found 342.0464 $(M+H)^+$.

6-Chloro-2-(morpholinomethyl)benzo[4,5]thieno[3,2-*d*]pyrimidin-4(3*H*)-one (45b)

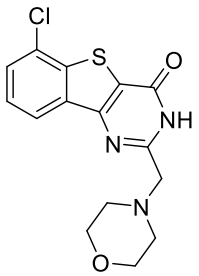

Following General Procedure C, **38** (200 mg, 0.57 mmol), morpholine (245 µL, 2.84 mmol) in EtOH (4 mL) during 48 hours at 50 ºC. The resulting solid was filtered under reduced pressure, washed with EtOH (20 mL) and dried to afford the title compound **45b** as a white solid (175 mg, 0.52 mmol, 92%). **Mpt** > 250 ºC decomp.; **IR** (ATR)/cm^{-1}: 2854 (br), 1667, 1600; **^{1}H NMR** (400 MHz, DMSO) δ 12.70 (s, 1H), 8.21 (dd, *J* = 7.9, 0.8 Hz, 1H), 7.81 (dd, *J* = 7.7, 0.8 Hz, 1H), 7.63 (appt, *J* = 7.8 Hz, 1H), 3.63–3.59 (m, 4H), 3.58 (s, 2H), 2.56–2.52

(m, 4H); **^{13}C NMR** (101 MHz, DMSO) δ 158.3, 157.5, 153.0, 139.0, 135.9, 128.6, 127.5, 127.4, 122.4, 122.1, 66.1, 60.5, 53.0; **LRMS** (ES + APCI) *m/z* 336.0 $(M+H)^+$; **HRMS** (ESI, +ve) *m/z* calc. for $C_{15}H_{15}{}^{35}ClN_3O_2S$ 336.0568, found 336.0570 $(M+H)^+$.

6-Chloro-2-((phenylamino)methyl)benzo[4,5]thieno[3,2-*d*]pyrimidin-4(3*H*)-one (45l)

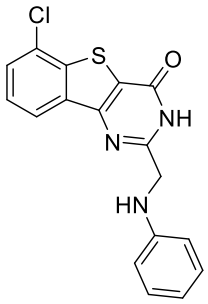

Following General Procedure C, **38** (200 mg, 0.57 mmol), aniline (250 µL, 2.84 mmol) in EtOH (4 mL) during 48 hours at 50 ºC. The resulting solid was filtered under reduced pressure, washed with EtOH (10 mL) and dried to afford the title compound **45l** as a white solid (180 mg, 0.53 mmol, 93%). **Mpt** > 236–238 ºC; **IR** (ATR)/cm^{-1}: 3395, 2816 (br), 1666, 1593; **^{1}H NMR** (400 MHz, DMSO) δ 12.85 (br, 1H), 8.23 (d, *J* = 7.8 Hz, 1H), 7.80 (d, *J* = 7.8 Hz, 1H), 7.64 (appt, *J* = 7.8 Hz, 1H), 7.10 (appt, *J* = 7.5 Hz, 2H), 6.69 (d, *J* = 7.5 Hz, 2H), 6.59 (appt, *J* = 7.5 Hz, 1H), 6.13 (s, 1H), 4.37 (s, 2H); **^{13}C NMR** (101 MHz, DMSO) δ 159.3, 158.3, 153.1, 147.7, 139.0, 135.8, 128.9, 128.6, 127.5, 127.3, 122.4, 121.6, 116.8, 112.6, 46.0; **LRMS** (ES + APCI) *m/z* 342.0 $(M+H)^+$; **HRMS** (ESI, +ve) *m/z* calc. for $C_{17}H_{13}{}^{35}ClN_3OS$ 342.0462, found 342.0465 $(M+H)^+$.

Ethyl 3-(4'-bromophenyl)-3-oxopropanoate (81)

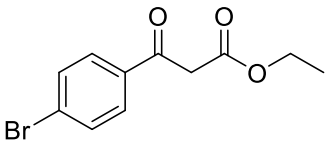

Sodium hydride as a 60% dispersion in mineral oil (1 g, 26 mmol) was placed in a 3-neck flask under nitrogen atmosphere. To the sodium hydride was added dry toluene (40 mL) and diethyl carbonate (7.3 mL, 60 mmol) with stirring. A solution of 4'-bromoacetophenone (2 g,

10 mmol) in dry toluene (15 mL) was added dropwise to the flask. The mixture was stirred at reflux under nitrogen atmosphere for 18 h. After cooling to room temperature, glacial acetic acid (4 mL) was added to the stirring mixture. The mixture is then poured over ice and conc. HCl (2 mL) was added. The aqueous layer was washed with EtOAc. The combined organic fractions were washed with cold H_2O, sat. $NaHCO_3$ (aq), and brine. The solution was dried over $MgSO_4$, filtered and the solvent evaporated under reduced pressure. The crude oil was purified by flash chromatography using 2:8 EtOAc/petrol to obtain the title compound **81** as a dark brown oil (1.95 g, 7.19 mmol, 72%). **IR** (ATR)/cm^{-1}: 1710, 1672, 1593; **^{1}H NMR** of keto tautomer (400 MHz, $CDCl_3$) δ 7.77 (d, *J* = 8.5 Hz, 2H), 7.61 (d, *J* = 8.5 Hz, 2H), 4.18 (q, *J* = 7.2 Hz, 2H), 3.81 (s, 2H), 1.23 (t, *J* = 7.2 Hz, 3H); **^{13}C NMR** (101 MHz, $CDCl_3$) δ 191.5, 167.2, 132.2, 131.8, 130.0, 77.2, 61.6, 46.0, 14.1; **LRMS** (ES + APCI) *m/z* 270.9 $(M+H)^+$; **HRMS** (ESI, +ve) *m/z* calc. $C_{11}H_{12}{}^{79}BrO_3$ 270.9964, found 270.9967 $(M+H)^+$.

6-(4-Bromophenyl)-2-(chloromethyl)pyrimidin-4(3*H*)-one (82)

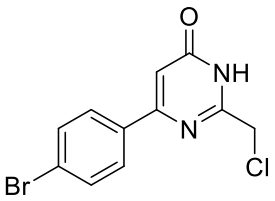

Compound **81** (1.40 g, 5.0 mmol) and EtONa (0.32 g, 4.7 mmol) were dissolved in dry EtOH (7 mL) and chloroacetamidine salt (0.5 g, 3.4 mmol) was added portion-wise. The reaction was stirred at 0 ºC during 1 hour and then at room temperature during 16 hours. The solvent was evaporated under reduced pressure. Purification of the compound by flash chromatography using 1:1 petrol/EtOAc afforded the title compound **82** as a brown solid (165 mg, 0.55 mmol, 16%). **Mpt** > 208 ºC decomp; **IR** (ATR)/cm^{-1}: 2694, 2571, 1658; **^{1}H NMR** (400 MHz, DMSO) δ 12.86 (s, 1H), 8.01 (d, *J* = 8.5 Hz, 2H), 7.69 (d, *J* = 8.5 Hz, 2H), 6.93 (s, 1H), 4.56 (s, 2H); **^{13}C NMR** (101 MHz, DMSO) δ 159.6, 157.6, 135.3, 132.0, 130.7, 129.7, 124.7, 109.0, 43.3; **LRMS** (ES + APCI) *m/z* 298.9 $(M+H)^+$; **HRMS** (ESI, +ve) *m/z* calc. for $C_{11}H_9{}^{79}Br^{35}ClN_2O$ 298.9582, found 298.9581 $(M+H)^+$.

Ethyl 3-(3-bromophenyl)-3-oxopropanoate (85)

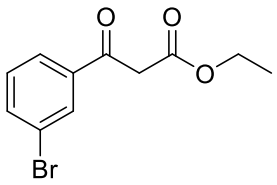

Sodium hydride as a 60% dispersion in mineral oil (2.2 g, 91 mmol) was placed in a 3-neck flask under nitrogen atmosphere. To the sodium hydride was added dry toluene (100 mL) and diethyl carbonate (25 mL, 0.2 mol) with stirring. A solution of 3'-bromoacetophenone (7 g, 35 mmol) in dry toluene (40 mL) was added dropwise to the flask. The mixture was stirred at reflux under nitrogen atmosphere for 18 h. After cooling to room temperature, glacial acetic acid (8 mL) was added to the stirring mixture. The mixture is then poured over ice and conc. HCl (5 mL) was added. The aqueous layer was washed with EtOAc. The combined organic fractions were washed with cold H_2O, sat. $NaHCO_3$ (aq), and brine. The solution was dried over $MgSO_4$, filtered and the solvent evaporated under reduced pressure. The crude oil was purified by flash chromatography using 0.5:9.5 EtOAc/petrol to afford the title compound **85** as a dark brown oil (5.0 g, 18.4 mmol, 53%). **IR** (ATR)/cm^{-1}: 1735, 1689, 1610; **^{1}H NMR** of keto tautomer (400 MHz, $CDCl_3$) δ 8.06 (s, 1H), 7.84 (d, *J* = 7.9 Hz, 1H), 7.7 (d, *J* = 7.9 Hz, 1H), 7.35 (appt, *J* = 7.2 Hz, 1H), 4.20 (q, *J* = 7.2 Hz, 2H), 3.91 (s, 2H), 1.25 (t, *J* = 7.2 Hz, 3H); **^{13}C NMR** (101 MHz, $CDCl_3$) δ 191.2, 167.1, 136.2, 134.0, 131.4, 130.3, 127.4, 124.5, 61.6, 45.9, 14.1; **LRMS** (ES + APCI) *m/z* 270.9 $(M+H)^+$; **HRMS** (ESI, +ve) *m/z* calc. $C_{11}H_{12}{}^{79}BrO_3$ 270.9964, found 270.9968 $(M+H)^+$.

6-(4-Bromophenyl)-2-cyclopropylpyrimidin-4(3*H*)-one (86)

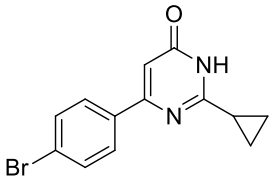

Following general procedure D, **81** (1.00 g, 3.68 mmol), cyclopropanecarboximidamide hydrochloride (443 mg, 3.68 mmol), and NaOEt (525 mg, 7.72 mmol) were dissolved in dry EtOH (25 mL) to give the title compound **86** as a white solid (1.08 g, 3.6 mmol, 97%). **Mpt** >

261 ºC decomp.; **IR** (ATR)/cm^{-1}: 3360, 2831, 1660; **^{1}H NMR (**400 MHz, DMSO) δ 12.69 (s, 1H), 7.93 (d, *J* = 8.6 Hz, 2H), 7.64 (d, *J* = 8.6 Hz, 2H), 6.67 (s, 1H), 2.01–1.91 (m, 1H), 1.17–1.10 (m, 2H), 1.11–1.03 (m, 2H); **^{13}C NMR** (101 MHz, DMSO) δ 164.1, 162.8, 159.4, 135.6, 131.5, 128.8, 123.9, 106.0, 13.5, 9.9; **LRMS** (ES + APCI) *m/z* 291.0 $(M+H)^+$; **HRMS** (ESI, +ve) *m/z* calc. for $C_{13}H_{12}{}^{79}BrN_2O$ 291.0131, found 291.0128 $(M+H)^+$.

6-(3-Bromophenyl)-2-cyclopropylpyrimidin-4(3*H*)-one (87)

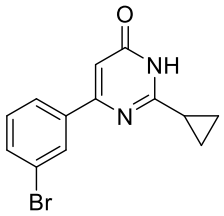

Following General Procedure D, **85** (1.0 g, 3.68 mmol), cyclopropanecarboximidamide hydrochloride (443 mg, 3.68 mmol), and NaOEt (52.5 mg, 7.72 mmol) were dissolvent in dry EtOH (25 mL) to give the title compound **87** as a white solid (0.7 g, 2.40 mmol, 65%). **Mpt** 251–252 ºC decomp.; **IR** (ATR)/cm^{-1}: 2777, 1656, 1595; **^{1}H NMR** (400 MHz, DMSO) δ 12.72 (s, 1H), 8.14 (s, 1H), 7.99 (d, *J* = 7.9 Hz, 1H), 7.66 (d, *J* = 7.9 Hz, 1H), 7.41 (appt, *J* = 7.9 Hz, 1H), 6.71 (s, 1H), 2.03–1.92 (m, 1H), 1.16–1.11 (m, 2H), 1.11–1.04 (m, 2H); **^{13}C NMR** (101 MHz, DMSO) δ 164.1, 162.6, 158.9, 138.8, 132.9, 130.7, 129.3, 125.8, 122.1, 106.7, 13.5, 10.0; **LRMS** (ES + APCI) *m/z* 291.0 $(M+H)^+$; **HRMS** (ESI, +ve) *m/z* calc. for $C_{13}H_{12}{}^{79}BrN_2O$ 291.0128, found 291.0132 $(M+H)^+$.

6-(4-Bromophenyl)-2-phenylpyrimidin-4(3*H*)-one (88)

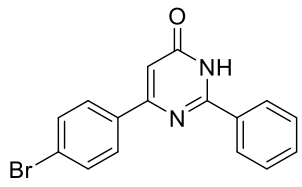

Following General Procedure D, **81** (3.00 g, 11.0 mmol), benzimidamide hydrochloride (1.90 g, 12.0 mmol) and NaOEt (1.12 g, 16.5 mmol) were dissolved in dry EtOH (70 mL). Filtration gave the title compound **88** as a white solid (2.90 g, 8.9 mmol, 82%). **Mpt** > 250

°C; **IR** (ATR)/cm^{-1}: 2777, 1656, 1595; **^{1}H NMR** (400 MHz, DMSO) δ 12.77 (s, 1H), 8.25 (d, *J* = 7.1 Hz, 2H), 8.16–8.10 (m, 2H), 7.73–7.68 (m, 2H), 7.63–7.52 (m, 3H), 6.95 (s, 1H); **LRMS** (ES + APCI) *m/z* 327.0 $(M+H)^+$; **HRMS** (ESI, +ve) *m/z* calc. for $C_{16}H_{12}{}^{79}BrN_2O$ 327.0128, found 327.0127 $(M+H)^+$.

2-Cyclopropyl-6-(4-(pyrrolidin-1-yl)phenyl)pyrimidin-4(3*H*)-one (91)

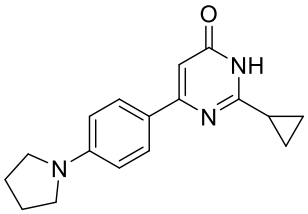

Following General Procedure E, **86** (150 mg, 0.51 mmol), pyrrolidine (51 μL, 0.61 mmol), RuPhos (11.8 mg, 0.025 mmol), RuPhos Palladacycle (20.40 mg, 0.025 mmol), Na^{t}OBu (73 mg, 0.76 mmol) were dissolved in 1,4-dioxane (1.8 mL) and reacted for 16 hours at 110 ºC. The reaction mixture was filtered through celite and the organic solvent evaporated. The white solid was triturated with MeOH and filtered to give the title compound **91** as a white solid (100 mg, 0.51 mmol, 69%). **Mpt** 196–198 ºC decomp.; **IR** (ATR)/cm^{-1}: 3429, 2837, 1645, 1589; **^{1}H NMR** (400 MHz, DMSO) δ 7.82 (d, *J* = 8.9 Hz, 2H), 6.54 (d, *J* = 8.9 Hz, 2H), 6.32 (s, 1H), 3.30–3.22 (m, 4H), 2.02–1.85 (m, 5H), 1.09–1.03 (m, 2H), 0.99–0.92 (m, 2H); **^{13}C NMR** (101 MHz, DMSO) δ 165.2, 164.1, 160.7, 148.9, 127.8, 123.2, 111.2, 101.5, 47.2, 24.9, 14.2, 9.2; **LRMS** (ES + APCI) *m/z* 282.1 $(M+H)^+$; **HRMS** (ESI, +ve) m/z calc. for $C_{17}H_{20}N_3O$ 282.1601, found 282.1600 $(M+H)^+$.

2-Cyclopropyl-6-(4-((2-(dimethylamino)ethyl)amino)phenyl)pyrimidin-4(3*H*)-one (92)

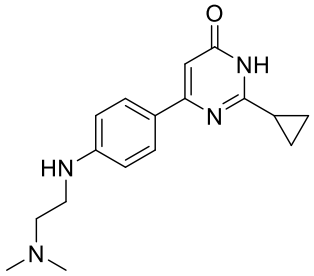

Following General Procedure E, **86** (200 mg, 0.68 mmol), *N*,*N*-dimethylethane-1,2-diamine (89 μL, 0.81 mmol), BrettPhos (18.5 mg, 0.034 mmol), BrettPhos Palladacycle (27.0 mg, 0.034 mmol), Na^{t}OBu (73.0 mg, 0.76 mmol) were dissolved in dry 1,4-dioxane (2 mL) and reacted for 4 hours at 110 ºC. The reaction mixture was filtered through celite and the organic solvent evaporated. The crude mixture was purified by flash chromatography using 9:1 CH_2Cl_2/MeOH to give the title compound **92** as a white solid (70 mg, 0.23 mmol, 35%). **Mpt** 229–231 ºC decomp.; **IR** (ATR)/cm^{-1} 3365, 2968, 1651, 1591; **^{1}H NMR** (400 MHz, DMSO) δ 12.37 (s, 1H), 10.11 (s, 1H), 7.80 (d, *J* = 8.8 Hz, 2H), 6.68 (d, *J* = 8.8 Hz, 2H), 6.41 (s, 1H), 3.53–3.43 (m, 2H), 3.21 (t, *J* = 6.4 Hz, 2H), 2.80 (s, 6H), 1.97–1.89 (m, 1H), 1.13–1.06 (m, 2H), 1.07–0.99 (m, 2H); **^{13}C NMR** (101 MHz, DMSO) δ 163.0, 162.9, 160.8, 149.9, 128.2, 124.2, 111.9, 102.1, 55.1, 42.4, 37.6, 13.4, 9.6; **LRMS** (ES + APCI) *m/z* 299.1 $(M+H)^+$; **HRMS** (ESI, +ve) *m/z* calc. for $C_{17}H_{23}N_4O$ 299.1866, found 299.1866 $(M+H)^+$.

2-Cyclopropyl-6-(4-((2-methoxyethyl)(methyl)amino)phenyl)pyrimidin-4(3*H*)-one (93)

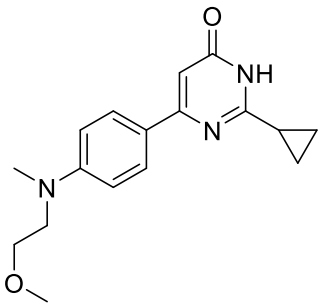

Following General Procedure E, **86** (100 mg, 0.34 mmol), 2-methoxy-N-methylethan-1-amine (121 mg, 1.36 mmol), RuPhos (8 mg, 0.013 mmol), RuPhos Palladacycle (14.0 mg, 0.012 mmol), Na^{t}OBu (66 mg, 0.68 mmol) were dissolved in dry 1,4-dioxane (1.8 mL) and reacted for 2 hours at 110 ºC. The reaction mixture was filtered through celite and the organic solvent evaporated. The crude mixture was purified by flash chromatography using 1:1 petrol/EtOAc to give the title compound **93** as a white solid (45 mg, 0.15 mmol, 44%). **Mpt** 201–202 ºC; **IR** (ATR)/cm^{-1}: 2821 (br), 1658, 1587; **^{1}H NMR** (400 MHz, DMSO) δ 12.36 (s, 1H), 7.82 (d, *J* = 9.1 Hz, 2H), 6.72 (d, *J* = 9.1 Hz, 2H), 6.40 (s, 1H), 3.55 (dd, *J* = 8.6, 3.1 Hz, 2H), 3.48 (dd, *J* = 8.5, 3.1 Hz, 2H), 3.24 (s, 3H), 2.97 (s, 3H), 1.98–1.87 (m, 1H), 1.12–1.08 (m, 2H), 1.06–1.00 (m, 2H); **^{13}C NMR** (101 MHz, DMSO) δ 163.0, 162.9, 160.8, 150.6, 128.0, 123.0,

111.2, 102.0, 69.5, 58.2, 51.0, 38.5, 13.4, 9.6; **LRMS** (ES + APCI) *m/z* 300.1 $(M+H)^+$; **HRMS** (ESI, +ve) *m/z* calc. for $C_{17}H_{22}N_3O_2$ 300.1707, found 300.1705 $(M+H)^+$.

2-Cyclopropyl-6-(3-(pyrrolidin-1-yl)phenyl)pyrimidin-4(3*H*)-one (94)

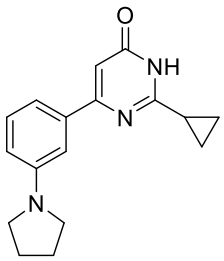

Following General Procedure E, **87** (150.0 mg, 0.51 mmol), pyrrolidine (51 μL, 0.61 mmol), RuPhos (11.8 mg, 0.025 mmol), RuPhos Palladacycle (20.4 mg, 0.025 mmol), and Na^{t}OBu (73.0 mg, 0.76 mmol) were dissolved in 1,4-dioxane (1.8 mL) and reacted for 16 hours at 110 ºC. The reaction mixture was filtered through celite and the organic solvent evaporated. The white solid was triturated with MeOH and filtered to give the title compound **94** as a white solid (90 mg, 0.32 mmol, 63%). **Mpt** 170–172 ºC; **IR** (ATR)/cm^{-1}: 2962, 2823, 1656, 1597; **^{1}H NMR** (400 MHz, DMSO) δ 12.57 (s, 1H), 7.26–7.14 (m, 2H), 7.08 (s, 1H), 6.62 (d, *J* = 7.2 Hz, 1H), 6.56 (s, 1H), 3.29–3.22 (m, 4H), 2.03–1.89 (m, 5H), 1.14–1.08 (m, 2H), 1.09–1.00 (m, 2H); **^{13}C NMR** (101 MHz, DMSO) δ 163.4, 162.9, 161.6, 147.8, 137.1, 129.1, 113.7, 113.6, 109.7, 105.6, 47.3, 24.9, 13.5, 9.8; **LRMS** (ES + APCI) *m/z* 282.1 $(M+H)^+$; **HRMS** (ESI, +ve) *m/z* calc. for $C_{17}H_{20}N_3O$ 282.1601, found 282.1598 $(M+H)^+$.

6-(4-((2-(Dimethylamino)ethyl)(methyl)amino)phenyl)-2-phenylpyrimidin-4(3*H*)-one (95)

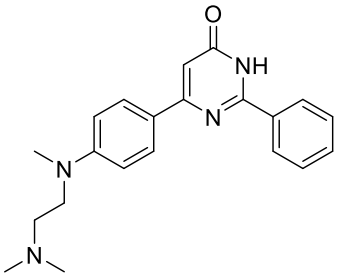

Following General Procedure E, **88** (150.0 mg, 0.51 mmol), N^1,N^1,N^2-trimethylethane-1,2-diamine (99.0 mg, 0.81 mmol), RuPhos (11.8 mg, 0.025 mmol), RuPhos Palladacycle (20.4 mg, 0.025 mmol), and Na^{t}OBu (73.0 mg, 0.76 mmol) were dissolved in 1,4-dioxane (2 mL) and reacted for 16 hours at 110 ºC. The reaction mixture was filtered through celite and the organic solvent evaporated. The crude mixture was purified by flash chromatography using 100% EtOAc to give the title compound **95** as a white solid (35.0 mg, 0.10 mmol, 22%). **Mpt** > 250 ºC; **IR** (ATR)/cm^{-1}: 2939, 2765, 1639, 1600; **^{1}H NMR** (400 MHz, DMSO) δ 8.25 (d, *J* = 7.1 Hz, 2H), 8.03 (d, *J* = 8.5 Hz, 2H), 7.59–7.53 (m, 3H), 6.78 (d, *J* = 8.6 Hz, 2H), 6.69 (s, 1H), 3.55 (t, *J* = 6.7 Hz, 2H), 2.98 (s, 3H), 2.57–2.49 (m, 2H), 2.29 (s, 6H); **^{13}C NMR** (101 MHz, DMSO) δ 172.1, 164.3, 161.0, 156.7, 150.5, 133.2, 131.4, 128.6, 128.3, 127.7, 122.9, 111.3, 102.8, 55.0, 49.0, 44.9, 38.1; **LRMS** (ES + APCI) *m/z* 349.2 $(M+H)^+$; **HRMS** (ESI, +ve) *m/z* calc. for $C_{21}H_{25}N_4O$ 349.2023, found 349.2023 $(M+H)^+$.

2-Phenyl-6-(4-(pyrrolidin-1-yl)phenyl)pyrimidin-4(3*H*)-one (96)

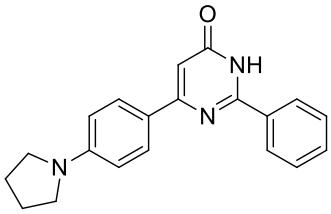

Following General Procedure E, **88** (150.0 mg, 0.51 mmol), pyrrolidine (51 μL, 0.61 mmol), RuPhos (11.8 mg, 0.025 mmol), RuPhos Palladacycle (20.4 mg, 0.025 mmol), and Na^{t}OBu (73.0 mg, 0.76 mmol) were dissolved in 1.4-dioxane (1.8 mL) and reacted for 16 hours at 110 ºC. The reaction mixture was filtered through celite and the organic solvent evaporated. The

crude mixture was purified by flash chromatography using 1:1 petrol/EtOAc to give the title compound **96** as a white solid (25 mg, 0.08 mmol, 17%). **Mpt** 233–234 ºC; **IR** (ATR)/cm^{-1} 2945 (br), 1633, 1591; **^{1}H NMR** (400 MHz, DMSO) δ 12.46 (s, 1H), 8.24 (d, *J* = 7.0 Hz, 2H), 8.03 (d, *J* = 8.9 Hz, 2H), 7.64–7.50 (m, 3H), 6.66 (s, 1H), 6.62 (d, *J* = 8.9 Hz, 2H), 3.34–3.26 (m, 4H), 2.02–1.92 (m, 4H); **LRMS** (ES + APCI) *m/z* 318.1 $(M+H)^+$; **HRMS** (ESI, +ve) *m/z* calc. for $C_{20}H_{20}N_3O$ 318.1601, found 318.1602 $(M+H)^+$.

6-(4-Bromophenyl)-2-((methylamino)methyl)pyrimidin-4(3*H*)-one (97)

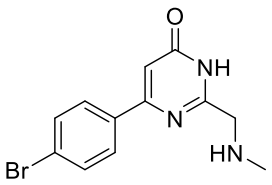

Following general procedure F, **82** (70 mg, 0.23 mmol) and methylamine 33% in MeOH (4 mL) were reacted for 16 hours at room temperature. The solvent was then evaporated under reduced pressure to give a crude white solid. The solid was dissolved in MeOH/CH_2Cl_2 (1:1, 10 mL) and loaded into an SCX cartridge. The cartridge was flushed with MeOH (3 x 5 mL) and then with a solution of NH_3 in MeOH (2 M, 10 mL). The NH_3 in MeOH fractions were evaporated under reduced pressure to give the title compound **97** as a white solid (44 mg, 0.15 mmol, 65%). **Mpt** 61–62 ºC; **IR** (ATR)/cm^{-1}: 3167, 2702, 1660, 1581; **^{1}H NMR** (400 MHz, $CDCl_3$) δ 7.86–7.81 (m, 2H), 7.61–7.56 (m, 2H), 6.72 (s, 1H), 3.86 (s, 3H), 2.52 (s, 2H); **^{13}C NMR** (101 MHz, $CDCl_3$) δ 164.0, 161.8, 160.5, 135.5, 132.1, 125.4, 124.8, 108.1, 53.4, 36.4; **LRMS** (ES + APCI) *m/z* 294.0 $(M+H)^+$; **HRMS** (ESI, +ve) *m/z* calc. for $C_{12}H_{13}{}^{79}BrN_3O$ 294.0237, found 294.0235 $(M+H)^+$.

6-(4-Bromophenyl)-2-(((2-hydroxyethyl)(methyl)amino)methyl)pyrimidin-4(3*H*)-one (98)

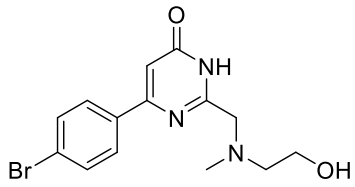

Following general procedure F, **82** (100 mg, 0.33 mmol), and 2-(methylamino)ethan-1-ol (66 μL, 0.86 mmol) in dry EtOH (3 mL) were reacted at 55 ºC during 16 hours. The solvent was evaporated under reduced pressure. The residue was triturated with EtOH (4 mL) and filtered under reduced pressure to afford the title compound **98** as a white solid (68 mg, 0.20 mmol, 61%). **Mpt** > 201 ºC decomp.; **^{1}H NMR** (400 MHz, DMSO) δ 12.06 (s, 1H), 8.00 (d, *J* = 8.6 Hz, 2H), 7.67 (d, *J* = 8.6 Hz, 2H), 6.82 (s, 1H), 4.67 (s, 1H), 3.58 (s, 2H), 3.51 (t, *J* = 5.5 Hz, 2H), 2.57 (t, *J* = 5.5 Hz, 2H), 2.27 (s, 3H); **^{13}C NMR** (101 MHz, DMSO) δ 162.5, 160.3, 159.0, 135.3, 131.6, 128.9, 124.1, 108.0, 59.9, 59.4, 58.3, 42.2; **LRMS** (ES + APCI) *m/z* 338.0 $(M+H)^+$; **HRMS** (ESI, +ve) *m/z* calc. for $C_{14}H_{17}{}^{79}BrN_3O_2$ 338.0499, found 338.0504 $(M+H)^+$.

6-(4-Bromophenyl)-2-((pyridin-4-ylamino)methyl)pyrimidin-4(3*H*)-one (99)

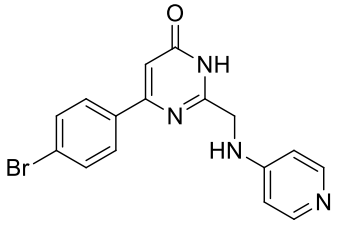

Following general procedure F, **82** (75 mg, 0.25 mmol), 4-aminopyridine (80 mg, 0.85 mmol) in dry DMF (0.5 mL) were reacted at 50 ºC during 72 hours. The solvent was evaporated under reduced pressure. The residue was purified by HPLC to afford the title compound **99** as a white solid (25 mg, 0.07 mmol, 28%). **Mpt** 188–189 ºC; **IR** (ATR)/cm^{-1}: 3334, 3089, 1645, 1583; **^{1}H NMR** (400 MHz, DMSO) δ 8.38 (s, 1H), 8.30 (s, 2H), 8.18 (d, *J* = 6.5 Hz, 2H), 7.81 (d, *J* = 8.4 Hz, 2H), 7.59 (d, *J* = 8.4 Hz, 2H), 6.85 (d, *J* = 6.5 Hz, 2H), 6.54 (s, 1H), 5.21 (s, 2H); **^{13}C NMR** (101 MHz, DMSO) δ 167.5, 164.8, 159.7, 159.1, 144.4, 135.8, 131.7, 128.5, 123.8, 108.9, 106.4, 58.8; **LRMS** (ES + APCI) *m/z* 357.0 $(M+H)^+$; **HMRS** (ESI, +ve) *m/z* calc. for $C_{16}H_{14}{}^{79}BrN_4O$ 357.0334, found 357.0339 $(M+H)^+$.

6-(4-Bromophenyl)-2-((pyridin-3-ylamino)methyl)pyrimidin-4(3*H*)-one (100)

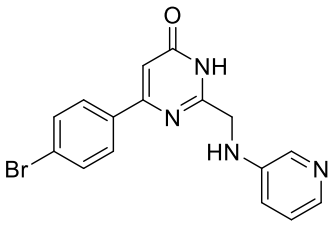

Following general procedure F, **82** (85 mg, 0.29 mmol), 3-aminopyridine (80 mg, 0.86 mmol) in dry DMF (0.6 mL) were reacted at 50 ºC during 72 hours. The solvent was evaporated under reduced pressure. The residue was purified by HPLC to afford the title compound **100** as a white solid (28 mg, 0.08 mmol, 28%). **Mpt** 189–192 ºC; **IR** (ATR)/cm^{-1}: 3358 (br), 3161(br), 1583, 1562; **^{1}H NMR** (500 MHz, DMSO) δ 8.32 (s, 1H), 8.21–8.04 (m, 2H), 7.79 (d, *J* = 8.5 Hz, 2H), 7.72–7.68 (m, 1H), 7.63–7.58 (m, 1H), 7.55 (d, *J* = 8.5 Hz, 2H), 6.62 (s, 2H), 6.18 (s, 1H), 5.39 (s, 2H); **^{13}C NMR** (101 MHz, DMSO) δ 174.1, 173.4, 162.7, 157.8, 148.2, 138.2, 132.2, 131.2, 129.9, 128.0, 127.2, 122.0, 105.4, 65.5; **LRMS** (ES + APCI) *m/z* 357.0 $(M+H)^+$; **HRMS** (ESI, +ve) *m/z* calc. for $C_{16}H_{14}{}^{79}BrN_4O$ 357.0346, found 357.0349 $(M+H)^+$.

6-(4-Bromophenyl)-2-((dimethylamino)methyl)pyrimidin-4(3*H*)-one (101)

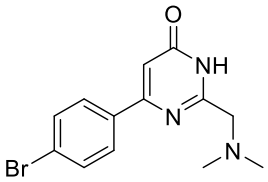

Following general procedure F, **82** (100 mg, 0.33 mmol) and dimethylamine 33% in EtOH (4 mL) were reacted at room temperature during 16 hours. The solvent was evaporated under reduced pressure. The residue was filtered through silica and eluted with 1:9 MeOH/CH_2Cl_2 solution to afford the title compound **101** as a brown solid (80 mg, 0.26 mmol, 79%). **Mpt** 163–164 ºC decomp.; **IR** (ATR)/cm^{-1}: 2825, 1666, 1612; **^{1}H NMR** (400 MHz, $CDCl_3$) δ 12.17 (s, 1H), 8.02–7.98 (m, 2H), 7.70–7.65 (m, 2H), 6.84 (s, 1H), 3.42 (s, 2H), 2.28 (s, 6H); **^{13}C NMR** (101 MHz, $CDCl_3$) δ 162.6, 159.4, 159.0, 135.4, 131.7, 128.9, 124.1, 108.1, 61.2,

45.0; **LRMS** (ES + APCI) *m/z* 308.0 $(M+H)^+$; **HRMS** (ESI, +ve) *m/z* calc. for $C_{13}H_{15}{}^{79}BrN_3O$ 308.0382, found 308.0390 $(M+H)^+$.

Methyl 3-bromo-5-(trifluoromethyl)benzo[*b*]thiophene-2-carboxylate (116)

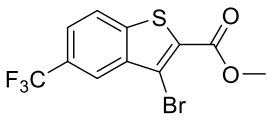

Following General Procedure G, **34** (2.9 g, 10.5 mmol), copper (II) bromide (3.5 g, 15.8 mmol), t-butyl nitrite (1.3 mL, 11.0 mmol) in acetonitrile (40 mL) were stirred for 16 hours at 50 ºC. The solvent was evaporated under reduced pressure and the residue purified by flash chromatography using 9:1 Petrol/DCM to afford the title compound **116** as a white solid (2.3 g, 6.7 mmol, 64%). **Mpt** 118–119 ºC; **IR** (ATR)/cm-$^{-1}$: 1728, 1519, 1224; **^{1}H NMR** (400 MHz, $CDCl_3$) δ 8.26–8.22 (m, 1H), 7.94 (d, *J* = 8.7 Hz, 1H), 7.73 (dd, *J* = 8.7, 2.0 Hz, 1H), 3.99 (s, 3H); **^{13}C NMR** (101 MHz, $CDCl_3$) δ 160.6, 142.1, 137.6, 129.7, 127.0 (q, *J* = 32.2 Hz), 125.2, 124.0 (q, *J* = 272.0 Hz), 124.4–124.1 (m), 121.6–121.2 (m), 114.3, 53.0; **LRMS** (ES + APCI) *m/z* 338.9 $(M+H)^+$; **HRMS** (ESI, +ve) *m/z* calc. for $C_{11}H_7{}^{79}BrF_3O_2S$ 338.9297, found 338.9297 $(M+H)^+$.

2-(Trifluoromethyl)-7,12-dihydro-6*H*-benzo[*b*]benzo[4,5]thieno[3,2-*e*][1,4]diazepin-6-one (119)

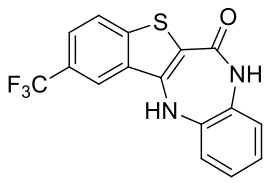

Following General Procedure I, **116** (200 mg, 0.59 mmol), 1,2-diaminobenzene (82 mg, 0.78 mmol), Pd_2dba_3 (27 mg, 0.03 mmol), Xantphos (34 mg, 0.06 mmol), Cs_2CO_3 (566 mg, 1.74 mmol) in DMF (4 mL). Purification by silica chromatography using a gradient CH_2Cl_2/EtOAc (9:1) then CH_2Cl_2/EtOAc (7:3) afforded the desired product **119** as a light brown solid (20 mg, 0.06 mmol, 10%). **Mpt** 183–184 ºC decomp.; **IR** (ATR)/cm^{-1}: 3118, 1687, 1481, 1101; **^{1}H NMR** (400 MHz, DMSO) δ 11.29 (s, 1H), 8.39 (d, *J* = 8.5 Hz, 1H), 8.31 (s, 1H), 7.83 (s, 1H), 7.78 (dd, *J* = 8.5, 1.7 Hz, 1H), 7.16–7.06 (m, 2H), 7.03–6.96 (m, 1H), 6.82 (d, *J* = 7.7

Hz, 1H); **^{13}C NMR** (101 MHz, DMSO) δ 153.2, 141.8, 134.3, 130.6, 128.8, 127.7, 127.0, 127.1 (q, *J* = 272.0 Hz), 125.5 (q, *J* = 32.0 Hz), 124.9, 123.1, 122.0, 121.0, 118.90–118.61 (m), 109.4, 108.2; **LRMS** (ES + APCI) *m/z* 335.0 $(M+H)^+$; **HRMS** (ESI, +ve) *m/z* calc. for $C_{16}H_{10}F_3N_2OS$ 335.0462, found 335.0460 $(M+H)^+$.

2-(Trifluoromethyl)-7,7a,8,9,10,11,11a,12-octahydro-6*H*-benzo[*b*]benzo[4,5]-thieno[3,2-*e*][1,4]diazepin-6-one (120)

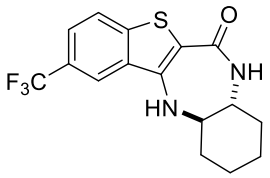

Following General Procedure I, **116** (150 mg, 0.44 mmol), (±)-*trans*-1,2-diaminocyclohexane (57 µL, 0.53 mmol), Xantphos (25 mg, 0.04 mmol), Pd_2dba_3 (20 mg, 0.02 mmol), Cs_2CO_3 (300 mg, 0.90 mmol) in DMF (4.5 mL). Purification by silica chromatography using CH_2Cl_2/EtOAc (8:2) afforded the title compound **120** as a white solid (45 mg, 0.13 mmol, 30%). **Mpt** 109–111 ºC decomp.; **IR** (ATR)/cm^{-1}: 3321, 2924, 1597, 1197, 1166; **^{1}H NMR** (500 MHz, DMSO) δ 8.69 (s, 1H), 8.00 (d, *J* = 8.4 Hz, 1H), 7.69 (dd, *J* = 8.5, 1.3 Hz, 1H), 7.49 (s, 1H), 6.88 (s, 1H), 3.21–3.07 (m, 2H), 2.37–2.29 (m, 1H), 2.19–2.09 (m, 1H), 1.76–1.65 (m, 2H), 1.44–1.17 (m, 4H).; **^{13}C NMR** (126 MHz, DMSO) δ 164.6, 142.5, 140.4, 132.9, 124.8 (q, *J* = 272.0 Hz), 124.4 (q, *J* = 32.0 Hz), 123.8, 122.9–122.6 (m), 120.7–120.3 (m), 106.7, 58.8, 54.5, 31.7, 31.5, 23.4, 23.2.; **LRMS** (ES + APCI) *m/z* 341.0 $(M+H)^+$; **HRMS** (ESI, +ve) *m/z* calc. for $C_{16}H_{16}F_3N_2OS$ 341.0934, found 341.0932 $(M+H)^+$.

9-(Trifluoromethyl)-1,2,3,4-tetrahydro-5*H*-benzo[4,5]thieno[3,2-*e*][1,4]diazepin-5-one (121)

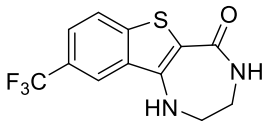

Following General Procedure I, **116** (200 mg, 0.63 mmol), ethylenediamine (55 µL, 0.8 mmol), Xantphos (73 mg, 0.12 mmol), Pd_2dba_3 (58 mg, 0.06 mmol), Cs_2CO_3 (307 mg, 1.41 mmol) in DMF (6.5 mL). The solvent was evaporated under reduced pressure and the residue

purified by HPLC to afford the title compound **121** as a white solid (25 mg, 0.09 mmol, 14%). **Mpt** 159–160 ºC decomp.; **IR** (ATR)/cm^{-1}: 3308, 3024, 1691, 1115; **^{1}H NMR** (400 MHz, DMSO) δ 8.42 (s, 1H), 8.02 (d, *J* = 8.5 Hz, 1H), 7.91 (s, 1H), 7.76 (s, 1H), 7.70 (d, *J* = 8.5 Hz, 1H), 3.57–3.45 (m, 2H), 3.41–3.34 (m, 2H); **^{13}C NMR** (101 MHz, DMSO) δ 165.8, 142.6, 141.2, 133.0, 124.7 (q, *J* = 272.0 Hz), 124.4 (q, *J* = 32.0 Hz), 123.9, 123.0–122.7 (m), 119.9–119.7 (m), 107.1, 46.4, 42.3; **LRMS** (ES + APCI) *m/z* 287.0 $(M+H)^+$; **HRMS** (ESI, +ve) *m/z* calc. for $C_{12}H_{10}F_3NO_2S$ 287.0464, found 287.0464 $(M+H)^+$.

(7a*R*,11a*R*)-2-(Trifluoromethyl)-7,7a,8,9,10,11,11a,12-octahydro-6*H* benzo[*b*]benzo[4,5]thieno[3,2-*e*][1,4]diazepin-6-one (122)

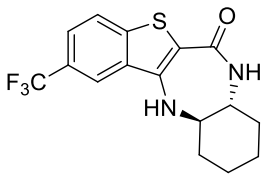

Following General Procedure I, **116** (100 mg, 0.29 mmol), (*R*)-(*R*)-*trans*-1,2–diaminocyclohexane (57 µL, 0.53 mmol), Xantphos (17 mg, 0.03 mmol), Pd_2dba_3 (15 mg, 0.015 mmol), Cs_2CO_3 (200 mg, 0.6 mmol) in DMF (4 mL). Purification by silica chromatography using 8:2 CH_2Cl_2/EtOAc afforded the title compound **122** as a light brown solid (12 mg, 0.04 mmol, 12%). **Mpt** 149–150 ºC decomp.; **IR** (ATR)/cm^{-1}: 3336, 2933, 2858, 1602, 1168; **^{1}H NMR** (400 MHz, DMSO) δ 8.70 (s, 1H), 8.01 (d, *J* = 8.5 Hz, 1H), 7.70 (dd, *J* = 8.5, 1.5 Hz, 1H), 7.49 (s, 1H), 6.88 (s, 1H), 3.21–3.08 (m, 2H), 2.37–2.28 (m, 1H), 2.20–2.08 (m, 1H), 1.78–1.63 (m, 2H), 1.46–1.17 (m, 4H); **^{13}C NMR** (101 MHz, DMSO) δ 164.5, 142.5, 140.4, 132.9, 124.4 (q, *J* = 32.0 Hz), 123.8, 122.9–122.7 (m), 120.5–120.3 (m), 106.7, 58.8, 54.5, 31.7, 31.5, 23.4, 23.2, 1 carbon not observed; **LRMS** (ES + APCI) *m/z* 341.0 $(M+H)^+$; **HRMS** (ESI, +ve) *m/z* calc. for $C_{16}H_{16}F_3N_2OS$ 341.0931, found 341.0930 $(M+H)^+$.

(7a*S*,11a*S*)-2-(Trifluoromethyl)-7,7a,8,9,10,11,11a,12-octahydro-6*H*-benzo[b]benzo[4,5]thieno[3,2-*e*][1,4]diazepin-6-one (123)

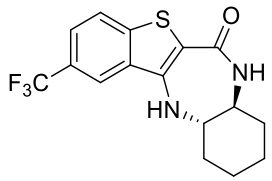

Following General Procedure I, **116** (200 mg, 0.59 mmol), (*S*)-(*S*)-*trans*-1,2–diaminocyclohexane (57 µL, 0.53 mmol), Xantphos (34 mg, 0.06 mmol), $Pd(OAc)_2$ (6.6 mg, 0.03 mmmol), Cs_2CO_3 (307 mg, 0.94 mmol) in DMF (5 mL). Purification by silica chromatography using 8:2 CH_2Cl_2/EtOAc afforded the title compound **123** as a light brown solid (50 mg, 0.15 mmol, 25%). **Mpt** > 147–148 ºC (decomp.); **IR** (ATR)/cm^{-1}: 3334, 2934, 2858, 1602, 1111; **^{1}H NMR** (400 MHz, DMSO) δ 8.69 (s, 1H), 8.00 (d, *J* = 8.4 Hz, 1H), 7.69 (dd, *J* = 8.5, 1.0 Hz, 1H), 7.48 (s, 1H), 6.88 (s, 1H), 3.19–3.07 (m, 2H), 2.37–2.27 (m, 1H), 2.10–2.08 (m, 1H), 1.77–1.61 (m, 2H), 1.45–1.17 (m, 4H); **^{13}C NMR** (101 MHz, DMSO) δ 164.5, 142.5, 140.4, 132.9, 124.8 (q, *J* = 272.0 Hz), 124.4 (q, *J* = 32 Hz), 123.8, 122.9–122.6 (m), 120.6–120.2 (m), 106.7, 58.8, 54.5, 31.7, 31.5, 23.4, 23.2; **LRMS** (ES + APCI) *m/z* 341.0 $(M+H)^+$; **HRMS** (ESI, +ve) *m/z* calc. for $C_{16}H_{16}F_3N_2OS$ 341.0930, found 341.0932 $(M+H)^+$.

10-(Trifluoromethyl)-2,3,4,4a,12,12a-hexahydrobenzo[*b*]benzo[4,5]thieno[3,2-*e*][1,4]oxazepin-6(1*H*)-one (124)

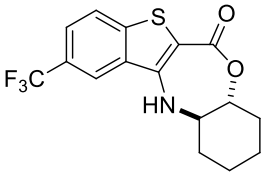

Following General Procedure I, **116** (200 mg, 0.59 mmol), **130** (80 mg, 0.7 mmol), Xantphos (34 mg, 0.06 mmol), $Pd(OAc)_2$ (6.6 mg, 0.03 mmmol), Cs_2CO_3 (307 mg, 0.94 mmol) in dry toluene (5 mL). The solvent was evaporated under reduced pressure and the residue purified by silica chromatography using CH_2Cl_2/Petrol (9:1) afforded the title compound **124** as a light brown solid (79 mg, 0.23 mmol, 39%). **Mpt** > 238 ºC decomp.; **IR** (ATR)/cm^{-1}: 3346, 2933,

2862, 1635, 1572; **^{1}H NMR** (400 MHz, DMSO) δ 8.76 (s, 1H), 8.04 (d, *J* = 8.5 Hz, 1H), 7.78 (dd, *J* = 8.5, 1.4 Hz, 1H), 7.52 (s, 1H), 4.46–4.33 (m, 1H), 3.56–3.47 (m, 1H), 2.42–2.33 (m, 1H), 2.25–2.16 (m, 1H), 1.78–1.65 (m, 2H), 1.53–1.37 (m, 2H), 1.36–1.22 (m, 2H); **^{13}C NMR** (101 MHz, DMSO) δ 164.4, 143.4, 143.2, 132.0, 124.8 (q, *J*= 272.0 Hz), 124.6 (q, *J*= 32.0 Hz), 124.2–124.1 (m), 124.0, 121.2–120.9 (m), 99.3, 77.3, 57.8, 31.7, 31.3, 23.1, 22.5; **LRMS** (ES + APCI) *m/z* 342.0 $(M+H)^+$; **HRMS** (ESI, +ve) *m/z* calc. for $C_{16}H_{15}F_3NO_2S$ 342.0770, found 342.0772 $(M+H)^+$.

9-(Trifluoromethyl)-1,2,3,3*a*,11,11*a*-hexahydro-5*H*-benzo[4,5]thieno[3,2-e]cyclopenta[*b*][1,4]oxazepin-5-one (125)

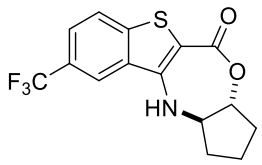

Following General Procedure I, **116** (200 mg, 0.59 mmol), **129** (62 mg, 0.6 mmol), Xantphos (34 mg, 0.06 mmol), $Pd(OAc)_2$ (6.6 mg, 0.03 mmmol), Cs_2CO_3 (307 mg, 0.94 mmol) in dry toluene (5 mL). The solvent was evaporated under reduced pressure and the residue purified by silica chromatography using CH_2Cl_2/Petrol (8.5:1.5) afforded the title compound **125** as a light brown solid (65 mg, 0.20 mmol, 34%). **Mpt** > 230 ºC decomp.; **IR** (ATR)/cm^{-1}: 3354, 2970, 2958, 1628; **^{1}H NMR** (400 MHz, DMSO) δ 8.64 (s, 1H), 8.32 (s, 1H), 8.06 (d, *J* = 8.5 Hz, 1H), 7.79 (d, *J* = 8.5 Hz, 1H), 4.72–4.60 (m, 1H), 3.77–3.63 (m, 1H), 2.41–2.20 (m, 2H), 1.97–1.73 (m, 4H); **^{13}C NMR** (101 MHz, DMSO) δ 164.5, 144.4, 143.6, 132.0, 124.9 (q, *J*= 32.0 Hz), 124.6 (q, *J*= 272.0 Hz), 124.3–124.1 (m), 124.0, 121.1–120.9 (m), 101.4, 82.3, 61.7, 30.3, 29.8, 21.0; **LRMS** (ES + APCI) *m/z* 328.0 $(M+H)^+$; **HRMS** (ESI, +ve) *m/z*: calc. for $C_{15}H_{13}F_3NO_2S$ 328.0614, found 328.0617 $(M+H)^+$.

9-(Trifluoromethyl)-2,3-dihydrobenzo[4,5]thieno[3,2-*e*][1,4]oxazepin-5(1*H*)-one (126)

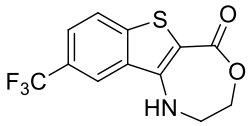

Following general procedure I, **116** (100 mg, 0.29 mmol), ethanolamine (25 µL, 0.35 mmol), Xantphos (17 mg, 0.03 mmol), Pd_2dba_3 (15 mg, 0.015 mmmol), Cs_2CO_3 (200 mg, 0.6 mmol) in dry toluene (4 mL). The solvent was evaporated under reduced pressure and the residue purified by silica chromatography using 3:7 petrol/EtOAc afforded the desired product **126** as a light brown solid (20 mg, 0.07 mmol, 20%). **Mpt** 94–95 ºC decomp.; **IR** (ATR)/cm^{-1}: 3377, 1651, 1573; **^{1}H NMR** (400 MHz, DMSO) δ 8.50 (s, 1H), 8.41 (s, 1H), 8.05 (d, *J* = 8.5 Hz, 1H), 7.79 (dd, *J* = 8.5, 1.5 Hz, 1H), 4.54–4.45 (m, 2H), 3.76–3.68 (m, 2H); **^{13}C NMR** (101 MHz, DMSO) δ 165.6, 144.2, 143.6, 132.0, 124.9 (q, *J* = 32.0 Hz), 124.5 (q, *J* = 272.0 Hz), 124.3–124.1 (m), 124.1, 120.6–120.4 (m), 99.9, 66.9, 45.7; **LRMS** (ES + APCI) *m/z* 288.0 $(M+H)^+$; **HRMS** (ESI, +ve) *m/z* calc. for $C_{12}H_9F_3NO_2S$ 288.0303, found 288.0301 $(M+H)^+$.

2-Aminocyclopentan-1-ol (129)

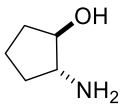

Following General Procedure J, cyclopentenoxide (1.0 g, 11.9 mmol) and ammonium hydroxide 33% solution (20 mL) and the reaction mixture was heated in a Biotage microwave for 50 minutes at 85 ºC. The solvent was evaporated under reduced pressure to obtain the desired amine **129**, as a colourless oil (1.1 g, 10.8 mmol, 91%). **IR** (ATR)/cm^{-1}: 3367 (br), 3351, 2945 (br); **^{1}H NMR** (400 MHz, $CDCl_3$) δ 3.78–3.68 (m, 1H), 3.08–2.93 (m, 1H), 2.07–1.90 (m, 2H), 1.77–1.60 (m, 2H), 1.59–1.46 (m, 1H), 1.36–1.22 (m, 1H); **^{13}C NMR** (101 MHz, $CDCl_3$) δ 80.0, 60.2, 32.6, 32.1, 19.9; **LRMS** *m/z* 102.0 $(M+H)^+$; **HRMS** (ESI, +ve) *m/z*: calc. for $C_5H_{11}NO$ 101.0835, found 101.0835 $(M+H)^+$.

2-Aminocyclohexan-1-ol (130)

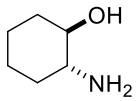

Following General Procedure J, cyclohexenoxide (1.0 g, 10.2 mmol) and ammonium hydroxide 33% solution (20 mL) and the reaction mixture was heated in a Biotage microwave for 50 minutes at 85 ºC. The solvent was evaporated under reduced pressure to obtain the desired amine **130**, as a colourless oil (1.1 g, 9.5 mmol, 93%). **Mpt** 108–110 °C; **IR** ATR)/cm^{-1}: 3346 (br), 3302, 2928 (br); **^{1}H NMR** (400 MHz, $CDCl_3$) δ 3.14–2.98 (m, 1H), 2.60–2.31 (m, 4H), 1.95–1.84 (m, 1H), 1.84–1.75 (m, 1H), 1.69–1.53 (m, 2H), 1.29–1.15 (m, 3H), 1.12–0.97 (m, 1H); **^{13}C NMR** (101 MHz, $CDCl_3$) δ 75.9, 57.1, 34.7, 33.9, 25.1, 24.8; **LRMS** (ES + APCI) *m/z* 116.1 $(M+H)^+$; **HRMS** (ESI, +ve) *m/z* calc. for $C_6H_{14}NO$ 116.1068, found 116.1070 $(M+H)^+$.

1-Methyl-9-(trifluoromethyl)-2,3-dihydrobenzo[4,5]thieno[3,2-*e*][1,4]oxazepin-5(1*H*)-one (131)

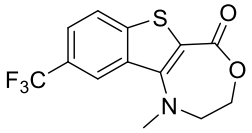

Following general procedure I, **116** (200 mg, 0.59 mmol), *N*-methyl ethanolamine (49 µL, 0.61 mmol), Xantphos (136 mg, 0.23 mmol), Pd_2dba_3 (108 mg, 0.11 mmmol), Cs_2CO_3 (576 mg, 1.7 mmol) in toluene (5.5 mL). The solvent was evaporated under reduced pressure and the residue purified by silica chromatography using 3:7 petrol/EtOAc afforded the title compound **131** as a light brown solid (80 mg, 0.26 mmol, 44%). **Mpt** > 120 ºC decomp.; **IR** (ATR)/cm-^{1}: 2972, 1621, 1470; 1122; **^{1}H NMR** (400 MHz, $CDCl_3$) δ 8.03 (s, 1H), 7.79 (d, *J* = 8.5 Hz, 1H), 7.61 (dd, *J* = 8.5, 1.5 Hz, 1H), 4.64–4.57 (m, 2H), 3.81–3.75 (m, 2H), 3.20 (s, 3H); **^{13}C NMR** (101 MHz, $CDCl_3$) δ 163.0, 147.7, 141.4, 132.7, 123.7–123.5 (m), 123.3, 120.4–120.0 (m), 116.2, 71.4, 51.2, 37.3, 2 carbons not observed, **LRMS** (ES + APCI) *m/z* 302.0 $(M+H)^+$; **HRMS** (ESI, +ve) *m/z*: calc. for $C_{13}H_{11}F_3NO_2S$ 302.0457, found 302.0454 $(M+H)^+$.

1-Ethyl-9-(trifluoromethyl)-2,3-dihydrobenzo[4,5]thieno[3,2-*e*][1,4]oxazepin-5(1*H*)-one (132)

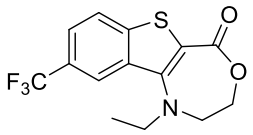

Following general procedure I, **116** (200 mg, 0.59 mmol), *N*-ethyl ethanolamine (69 µL, 0.7 mmol), Xantphos (136 mg, 0.23 mmol), Pd_2dba_3 (108 mg, 0.11 mmmol), Cs_2CO_3 (576 mg, 1.7 mmol) in toluene (5.5 mL). The solvent was evaporated under reduced pressure and the residue purified by silica chromatography using 3:7 petrol/EtOAc afforded the title compound **132** as a brown solid (83 mg, 0.27 mmol, 45%). **Mpt** 126–128 ºC decomp.; **IR** (ATR)/cm^{-1}: 2958, 1608, 1477; 1171; **^{1}H NMR** (400 MHz, DMSO) δ 8.15 (d, *J* = 8.5 Hz, 1H), 8.00 (s, 1H), 7.79 (dd, *J* = 8.5, 1.5 Hz, 1H), 4.66–4.58 (m, 2H), 3.87–3.78 (m, 2H), 3.52 (q, *J* = 7.1 Hz, 2H), 1.10 (t, *J* = 7.1 Hz, 3H); **^{13}C NMR** (101 MHz, DMSO) δ 161.3, 147.0, 140.9, 132.4, 125.3 (q, *J* = 32 Hz), 124.3, 123.4–123.0 (m), 119.3–118.9 (m), 116.2, 72.2, 48.1, 43.3, 12.6, 1 carbon not reported; **LRMS** (ES + APCI) *m/z* 316.0 (M+H); **HRMS** (ESI, +ve) *m/z* calc. for $C_{14}H_{13}F_3NO_2S$ 316.0614, found 316.0613 $(M+H)^+$.

(*S*)-10-(Trifluoromethyl)-2,3,3a,4-tetrahydro-1*H*,6*H*-benzo[4,5]thieno[3,2-e]pyrrolo[2,1-*c*][1,4]oxazepin-6-one (133)

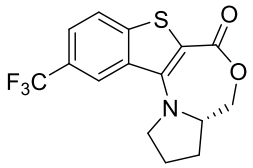

Following general procedure I, **116** (200 mg, 0.59 mmol), L-prolinol (63.5 µL, 0.7 mmol), Xantphos (136 mg, 0.23 mmol), Pd_2dba_3 (108 mg, 0.11 mmmol), Cs_2CO_3 (576 mg, 1.7 mmol) in toluene (5.5 mL). The solvent was evaporated under reduced pressure and the residue purified by silica chromatography using 4:6 petrol/EtOAc afforded the title compound **133** as a white solid (120 mg, 0.37 mmol, 63%). **Mpt** > 234 ºC decomp.; **IR** (ATR)/cm-^{1} 2981, 2872, 1600, 1114; **^{1}H NMR** (400 MHz, DMSO) δ 8.05 (d, *J* = 1.5 Hz, 1H), 7.83 (d, *J* = 8.5 Hz, 1H), 7.63 (dd, *J* = 8.5, 1.5 Hz, 1H), 4.74 (d, *J* = 12.0 Hz, 1H), 4.15–4.08 (m, 1H), 4.06–3.89 (m, 2H), 3.68–3.54 (m, 1H), 2.42–2.27 (m, 1H), 2.12–2.00 (m, 1H), 2.01–1.84 (m, 1H), 1.87–1.69 (m, 1H), **^{13}C NMR** (101 MHz, DMSO) δ 160.6, 148.5, 141.2, 133.0, 123.7–123.5 (m), 123.4,

120.3–120.1 (m), 116.2, 74.2, 58.7, 48.1, 30.1, 22.9, 2 carbons not reported; **LRMS** (ES + APCI) *m/z* 328.0 $(M+H)^+$; **HRMS** (ESI, +ve) *m/z* calc. for $C_{15}H_{13}F_3NO_2S$ 328.0614, found 328.0615 $(M+H)^+$.

(*R*)-2-Isopropyl-9-(trifluoromethyl)-2,3-dihydrobenzo[4,5]thieno[3,2-*e*][1,4]oxazepin-5(1*H*)-one (134)

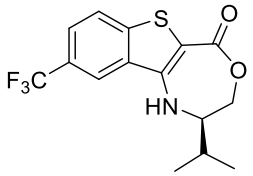

Following general procedure I, **116** (200 mg, 0.59 mmol), L-valinol (67 µL, 0.65 mmol), Xantphos (136 mg, 0.23 mmol), Pd_2dba_3 (108 mg, 0.11 mmmol), Cs_2CO_3 (576 mg, 1.7 mmol) in toluene (5.5 mL). The solvent was evaporated under reduced pressure and the residue was purified by silica chromatography using 100% CH_2Cl_2 to afford the title compound **134** as a white solid (79 mg, 0.24 mmol, 41%). **Mpt** 147–148 ºC; **IR** (ATR)/cm^{-1}: 3400, 2958, 1639, 1571; ^{1}H NMR (400 MHz, DMSO) δ 8.70 (s, 1H), 8.41 (s, 1H), 8.06 (d, *J* = 8.5 Hz, 1H), 7.79 (d, *J* = 9.5 Hz, 1H), 4.55 (dd, *J* = 13.2, 4.8 Hz, 1H), 4.41 (d, *J* = 13.2 Hz, 1H), 3.47 – 3.39 (m, 1H), 2.05–1.88 (m, 1H), 1.02 (d, *J* = 6.7 Hz, 3H), 0.99 (d, *J* = 6.7 Hz, 3H); **^{13}C NMR** (101 MHz, DMSO) δ 165.8, 143.7, 143.2, 132.3, 124.9 (q, *J* = 32.0 Hz), 124.6 (q, *J* = 272.0 Hz), 124.4–124.17 (m), 124.1, 121.0–120.64 (m), 99.1, 67.0, 60.4, 27.5, 19.9, 17.7; **LRMS** (ES + APCI) *m/z* 330.0 $(M+H)^+$; **HRMS** (ESI, +ve) *m/z* calc. for $C_{15}H_{15}F_3NO_2S$ 330.0767, found 330.0770 $(M+H)^+$.

(*S*)-2-Isopropyl-9-(trifluoromethyl)-2,3-dihydrobenzo[4,5]thieno[3,2-*e*][1,4]oxazepin-5(1*H*)-one (135)

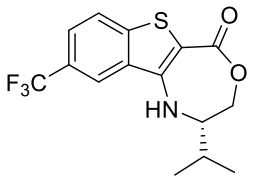

Following general procedure I, **116** (200 mg, 0.59 mmol), D-valinol (67 µL, 0.65 mmol), Xantphos (136 mg, 0.23 mmol), Pd_2dba_3 (108 mg, 0.11 mmmol), Cs_2CO_3 (576 mg, 1.7 mmol) in toluene (5.5 mL). The solvent was evaporated under reduced pressure and the residue purified by silica chromatography using 100% CH_2Cl_2 afforded the title compound **135** as a white solid (30 mg, 0.09 mmol, 15%). **Mpt** 155–157 ºC; **IR** (ATR)/cm^{-1}: 3294 (br), 2970, 1639, 1571, 1151, 1114; **^{1}H NMR** (400 MHz, DMSO) δ 8.69 (s, 1H), 8.37 (s, 1H), 8.04 (d, *J* = 8.5 Hz, 1H), 7.78 (dd, *J* = 8.5, 1.4 Hz, 1H), 4.59–4.49 (m, 1H), 4.47–4.38 (m, 1H), 3.47–3.38 (m, 1H), 1.98 (dh, *J* = 13.3, 6.7 Hz, 1H), 1.02 (d, *J* = 6.7 Hz, 3H), 0.99 (d, *J* = 6.7 Hz, 3H); **^{13}C NMR** (101 MHz, DMSO) δ 165.7, 143.6, 143.1, 132.2, 124.9 (q, *J* = 32.0 Hz), 124.5 (q, *J* = 272.0 Hz), 124.3–124.1 (m), 124.0, 120.6–120.6 (m), 99.1, 67.0, 60.4, 27.5, 19.7, 17.6; **LRMS** (ES + APCI) *m/z* 330.0 $(M+H)^+$; **HRMS** (ESI, +ve) *m/z* calc. for $C_{15}H_{14}F_3NO_2S$ 330.0770, found 330.0770 $(M+H)^+$.

(*R*)-2-Benzyl-9-(trifluoromethyl)-2,3-dihydrobenzo[4,5]thieno[3,2-*e*][1,4]oxazepin-5(1*H*)-one (136)

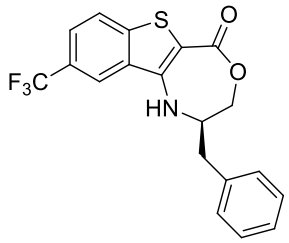

Following general procedure I, **116** (200 mg, 0.59 mmol), D-phenylalaninol (94 mg, 0.61 mmol), Xantphos (136 mg, 0.23 mmol), Pd_2dba_3 (108 mg, 0.11 mmmol), Cs_2CO_3 (576 mg, 1.7 mmol) in toluene (5 mL). The solvent was evaporated under reduced pressure and the residue purified by silica chromatography using 3:7 petrol/CH_2Cl_2 followed by 100 % CH_2Cl_2 afforded the title compound **136** as a light brown solid (60 mg, 0.15 mmol, 27%). **Mpt** 132–134 ºC; **IR** (ATR)/cm^{-1}: 3315, 3059, 1614, 1571, 1112; **^{1}H NMR** (400 MHz, DMSO) δ 8.40–8.33 (m, 2H), 8.06 (s, 1H), 7.87 (dd, *J* = 8.6, 1.5 Hz, 1H), 7.33–7.27 (m, 4H), 7.24–7.16 (m, 1H), 4.99 (t, *J* = 5.5 Hz, 1H), 4.25–4.14 (m, 1H), 3.59–3.45 (m, 2H), 3.00 (dd, *J* = 13.7, 5.5 Hz, 1H), 2.80 (dd, *J* = 13.7, 8.8 Hz, 1H); **^{13}C NMR** (101 MHz, DMSO) δ 159.8, 140.9, 138.8, 137.4, 136.9, 129.2, 128.2, 126.9 (q, *J* = 32.0 Hz), 126.1, 125.0, 124.2 (q, *J* = 272.4 Hz), 123.1–122.9 (m), 120.6–120.2 (m), 106.6, 62.3, 53.7, 36.5; **LRMS** (ES + APCI) *m/z* 378.0 $(M+H)^+$; **HRMS** (ESI, +ve) *m/z* calc. for $C_{19}H_{15}F_3NO_2S$ 378.0770, found 378.0771 $(M+H)^+$.

(*S*)-2-Benzyl-9-(trifluoromethyl)-2,3-dihydrobenzo[4,5]thieno[3,2-*e*][1,4]oxazepin-5(1*H*)-one (137)

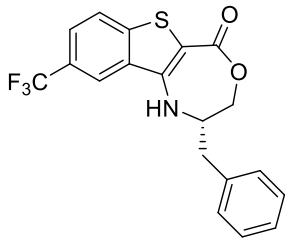

Following general procedure I, **116** (200 mg, 0.59 mmol), L-phenylalaninol (94 mg, 0.61 mmol), Xantphos (136 mg, 0.23 mmol), Pd_2dba_3 (108 mg, 0.11 mmmol), Cs_2CO_3 (576 mg, 1.7 mmol) in dry toluene (5 mL). The solvent was evaporated under reduced pressure and the residue purified by flash chromatography using 3:7 petrol/CH_2Cl_2 followed by 100 % CH_2Cl_2 afforded the title compound **137** as a light brown solid (65 mg, 0.17 mmol, 30%). **Mpt** 135–137 ºC; **IR** (ATR)/cm^{-1}: 3315, 3026, 1616, 1026; **^{1}H NMR** (400 MHz, DMSO) δ 8.59 (s, 1H), 8.43 (s, 1H), 8.08 (d, *J* = 8.5 Hz, 1H), 7.80 (d, *J* = 8.4 Hz, 1H), 7.38–7.22 (m, 5H), 4.43–4.31 (m, 2H), 4.15–3.98 (m, 1H), 2.99 (dd, *J* = 13.5, 6.5 Hz, 1H), 2.90 (dd, *J* = 13.6, 7.9 Hz, 1H); **^{13}C NMR** (101 MHz, DMSO) δ 165.6, 143.7, 143.0, 137.5, 132.2, 129.4, 128.4, 126.5, 124.9 (dd, *J* = 32 Hz), 124.5 (q, *J* = 272.3 Hz), 124.4–124.1 (m), 124.0, 120.8–120.5 (m), 99.6, 67.9, 56.3, 35.5; **LRMS** (ES + APCI) *m/z* 378.0 $(M+H)^+$; **HRMS** (ESI, +ve) *m/z* calc. for $C_{19}H_{15}F_3NO_2S$ 378.0770, found 378.0762 $(M+H)^+$.

Methyl 5-chloro-3-iodobenzo[*b*]thiophene-2-carboxylate (146)

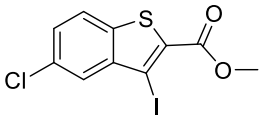

Following General Procedure H, **26** (0.8 g, 3.3 mmol), *p*-toluenesulphonic acid monohydrate (1.9 g, 9.9 mmol) were dissolved in acetonitrile (15 mL), and a solution sodium nitrite (456 mg, 6.6 mmol) and potassium iodide (1.4 g, 8.3 mmol) in water (2.5 mL). The solvent was evaporated under reduced pressure. Water (5 mL) was added and the solid filtered. The yellow solid was washed with water (5 mL) and methanol (5 mL) to afford the title compound **146** as an orange solid (595 mg, 1.6 mmol, 50%). **Mpt** 147–149 ºC; **IR** (ATR)/cm^{-1}: 2948,

1712, 1495; **^{1}H NMR** (400 MHz, DMSO) δ 8.16 (d, *J* = 8.7 Hz, 1H), 7.88 (d, *J* = 2.0 Hz, 1H), 7.65 (dd, *J* = 8.7, 2.0 Hz, 1H), 3.91 (s, 3H); **^{13}C NMR** (101 MHz, DMSO) δ 161.1, 143.0, 138.2, 132.0, 131.5, 128.5, 126.5, 125.3, 89.5, 52.8; **LRMS** (ES + APCI) *m/z* 352.8 $(M+H)^+$; **HRMS** (ESI, +ve) *m/z* calc. for $C_{10}H_7{}^{35}ClIO_2S$ 352.8894, found 352.8892 $(M+H)^+$.

Methyl 6-chloro-3-iodobenzo[*b*]thiophene-2-carboxylate (147)

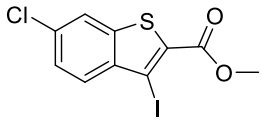

Following General Procedure H, **27** (1.0 g, 4.0 mmol), *p*-toluenesulphonic acid monohydrate (2.3 g, 12.0 mmol) were dissolved in acetonitrile (18 mL), and a solution sodium nitrite (552 mg, 8.0 mmol) and potassium iodide (1.7 g, 10.0 mmol) in water (3 mL). The solvent was evaporated under reduced pressure. Water (10 mL) was added and the solid filtered. The yellow solid was washed with water (10 mL) and methanol (10 mL) to afford the title compound **147** as an orange solid (725 mg, 2.0 mmol, 50%). **Mpt** 147–149 ºC; **IR** (ATR)/cm^{-1}: 2954, 1729, 1498; **^{1}H NMR** (400 MHz, DMSO) δ 8.31 (d, *J* = 2.0 Hz, 1H), 7.91 (d, *J* = 8.8 Hz, 1H), 7.61 (dd, *J* = 8.8, 2.0 Hz, 1H), 3.91 (s, 3H); **^{13}C NMR** (101 MHz, DMSO) δ 161.2, 140.5, 140.5, 133.4, 130.7, 129.0, 127.0, 122.7, 90.3, 52.8; **LRMS** (ES + APCI) *m/z* 352.8 $(M+H)^+$; **HRMS** (ESI, +ve) *m/z* calc. for $C_{10}H_7{}^{35}ClIO_2S$ 352.8894, found 352.8895 $(M+H)^+$.

Methyl 7-chloro-3-iodobenzo[*b*]thiophene-2-carboxylate (148)

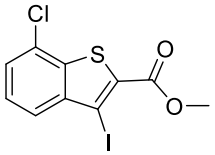

Following General Procedure H, **28** (1.0 g, 4.0 mmol), *p*-toluenesulphonic acid monohydrate (2.3 g, 12.0 mmol) were dissolved in acetonitrile (18 mL), and a solution sodium nitrite (552 mg, 8.0 mmol) and potassium iodide (1.7 g, 10.0 mmol) in water (3 mL). The solvent was evaporated under reduced pressure. Water (10 mL) was added and the solid filtered. The yellow solid was washed with water (10 mL) and methanol (10 mL) to afford the title

compound **148** as an orange solid (870 mg, 2.4 mmol, 60%). **Mpt** 146–148 ºC; **IR** (ATR)/cm^{-1}: 2947, 1710, 1495; **^{1}H NMR** (400 MHz, DMSO) δ 7.88 (d, *J* = 8.0, 1H), 7.74 (d, *J* = 7.9 Hz, 1H), 7.61 (appt, *J* = 7.9 Hz, 1H), 3.92 (s, 3H); **^{13}C NMR** (101 MHz, DMSO) δ 160.9, 142.9, 138.2, 130.6, 127.7, 127.6, 126.8, 126.5, 91.6, 52.9; **LRMS** (ES + APCI) *m/z* 352.8 $(M+H)^+$; **HRMS** (ESI, +ve) *m/z* calc. for $C_{10}H_7{}^{35}ClIO_2S$ 352.8894, found 352.8898 $(M+H)^+$.

2-Chloro-7,7*a*,8,9,10,11,11*a*,12-octahydro-6*H*-benzo[*b*]benzo[4,5]thieno[3,2-*e*][1,4]diazepin-6-one (149)

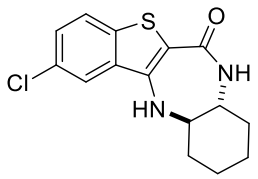

Following General Procedure I, **146** (300 mg, 0.84 mmol), (±)-*trans*-1,2-diaminocyclohexane (132 µL, 1.08 mmol), Xantphos (97 mg, 0.17 mmol), $Pd(OAc)_2$ (20 mg, 0.08 mmol), Cs_2CO_3 (400 mg, 1.26 mmol) in dry DMF (7 mL). Purification by silica chromatography using CH_2Cl_2/EtOAc (7:3) afforded the title compound **149** as a white solid (130 mg, 0.42 mmol, 50%). **Mpt** > 231–233 ºC decomp.; **IR** (ATR)/cm^{-1}: 3385, 2932, 1608 1441; **^{1}H NMR** (400 MHz, DMSO) δ 8.35 (d, *J* = 1.8 Hz, 1H), 7.80 (d, *J* = 8.6 Hz, 1H), 7.49–7.38 (m, 2H), 6.62 (s, 1H), 3.25–2.97 (m, 2H), 2.38–2.17 (m, 1H), 2.24–2.02 (m, 1H), 1.84–1.56 (m, 2H), 1.45–1.14 (m, 4H); **^{13}C NMR** (101 MHz, DMSO) δ 164.6, 139.7, 137.2, 134.3, 128.6, 127.0, 124.4, 122.3, 106.7, 58.8, 54.5, 31.8, 31.5, 23.4, 23.2; **LRMS** (ES + APCI) *m/z* 307.0 $(M+H)^+$; **HRMS** (ESI, +ve) *m/z* calc. for $C_{15}H_{16}{}^{35}ClN_2OS$ 307.0666, found 307.0670 $(M+H)^+$.

3-Chloro-7,7*a*,8,9,10,11,11*a*,12-octahydro-6*H*-benzo[*b*]benzo[4,5]thieno[3,2-*e*][1,4]diazepin-6-one (150)

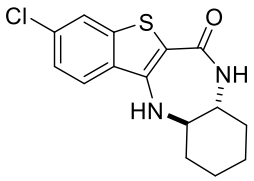

Following General Procedure I, **147** (300 mg, 0.84 mmol), (±)-*trans*-1,2-diaminocyclohexane (132 µL, 1.08 mmol), Xantphos (97 mg, 0.17 mmol), $Pd(OAc)_2$ (20 mg, 0.08 mmol), Cs_2CO_3 (400 mg, 1.26 mmol) in dry DMF (7 mL). Purification by silica chromatography using CH_2Cl_2/EtOAc (7:3) afforded the title compound **150** as a white solid (40 mg, 0.13 mmol, 15%). **Mpt** 193–194 ºC decomp.; **IR** (ATR)/cm^{-1}: 3315, 2945, 1605, 1465; **^{1}H NMR** (400 MHz, DMSO) δ 8.18 (d, *J* = 8.7 Hz, 1H), 7.92 (d, *J* = 1.8 Hz, 1H), 7.41–7.35 (m, 2H), 6.63 (s, 1H), 3.18–3.03 (m, 2H), 2.37–2.23 (m, 1H), 2.18–2.09 (m, 1H), 1.75–1.59 (m, 2H), 1.42–1.17 (m, 4H); **^{13}C NMR** (101 MHz, DMSO) δ 164.7, 140.2, 140.1, 132.2, 131.9, 124.4, 123.8, 122.1, 105.6, 58.7, 54.4, 31.8, 31.5, 23.4, 23.2.; **LRMS** (ES + APCI) *m/z* 307.0 $(M+H)^+$; **HRMS** (ESI, +ve) *m/z* calc. for $C_{15}H_{16}{}^{35}ClN_2OS$ 307.0666, found 307.0668 $(M+H)^+$.

4-Chloro-7,7*a*,8,9,10,11,11*a*,12-octahydro-6*H*-benzo[*b*]benzo[4,5]thieno[3,2-*e*][1,4]diazepin-6-one (151)

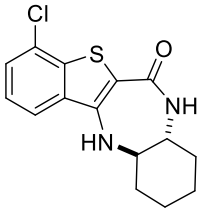

Following General Procedure I, **148** (300 mg, 0.84 mmol), (±)-*trans*-1,2-diaminocyclohexane (132 µL, 1.08 mmol), Xantphos (97 mg, 0.17 mmol), $Pd(OAc)_2$ (20 mg, 0.08 mmol), Cs_2CO_3 (400 mg, 1.26 mmol) in dry DMF (7 mL). Purification by silica chromatography using CH_2Cl_2/EtOAc (7:3) afforded the title compound **151** as a white solid (52 mg, 0.17 mmol, 20%); **Mpt** > 191 ºC; **IR** (ATR)/cm^{-1}: 3398, 3315, 2924, 1600, 1444; **^{1}H NMR** (400 MHz, DMSO) δ 8.18 (d, *J* = 7.6 Hz, 1H), 7.55 (dd, *J* = 7.6, 0.5 Hz, 1H), 7.46 (s, 1H), 7.40 (appt, *J* = 7.9 Hz, 1H), 6.66 (s, 1H), 3.24–3.06 (m, 2H), 2.34–2.26 (m, 1H), 2.17–2.08 (m, 1H), 1.74–1.64 (m, 2H), 1.40–1.19 (m, 4H); **^{13}C NMR** (101 MHz, DMSO) δ 164.6, 140.8, 137.5, 134.8, 126.7, 126.6, 125.1, 121.9, 105.9, 58.7, 54.4, 31.8, 31.4, 23.4, 23.2; **LRMS** (ES + APCI) *m/z*

307 $(M+H)^+$; **HRMS** (ESI, +ve) *m/z* calc. for $C_{15}H_{16}{}^{35}ClN_2OS$ 307.0666, found 307.0670 $(M+H)^+$.

Methyl 7-bromo-3-iodobenzo[*b*]thiophene-2-carboxylate (152)

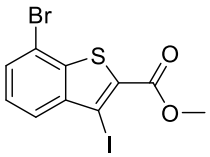

Following general procedure H, *p*-toluenesulphonic acid hydrate (2.20g, 11.58 mmol) in MeCN (20 mL) was added **30** (1.1 g, 3.86 mmol). The resulting suspension of amine was cooled down to 10–15 °C and to this, a solution of sodium nitrite (530 mg, 7.72 mmol) and potassium iodide (1.6 g, 9.65 mmol) in water (3 mL) was added dropwise. The reaction was allowed to warm to room temperature and then stirred for 2 hours. The solvent was evaporated, the crude mixture was triturated with water (20 mL) and the solid filtered under reduced pressure. The product was washed with MeOH (20 mL) dried under vacuum to give a yellow solid (850 mg, 2.1 mmol, 54%). **Mpt** 155–156 ºC; **IR** (ATR)/cm^{-1}: 2947, 1708, 1495; **^{1}H NMR** (400 MHz, DMSO) δ 7.94 (d, *J* = 7.9 Hz, 1H), 7.87 (d, *J* = 7.9 Hz, 1H), 7.54 (appt, *J* = 7.9 Hz, 1H), 3.92 (s, 3H); **^{13}C NMR** (101 MHz, DMSO) δ 161.0, 142.4, 140.6, 130.8, 130.4, 127.8, 127.2, 114.9, 91.8, 52.9; **LRMS** (ES + APCI) *m/z* 395.8 $(M+H)^+$; **HRMS** (ESI, +ve) *m/z* calc. for $C_{10}H_8{}^{79}BrIO_2S$ 396.8389, found 396.8389 $(M+H)^+$.

4-Bromo-7,7*a*,8,9,10,11,11*a*,12-octahydro-6*H*-benzo[*b*]benzo[4,5]thieno[3,2-*e*][1,4]diazepin-6-one (153)

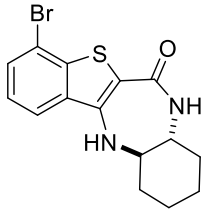

Following General Procedure I, **152** (160 mg, 0.40 mmol), (±)-*trans*-1,2-diaminocyclohexane (53 µL, 0.44 mmol), Xantphos (47 mg, 0.08 mmol), $Pd(OAc)_2$ (9.0 mg, 0.04 mmmol), Cs_2CO_3 (195.5 mg, 0.60 mmol) in DMF (5 mL). Purification by silica chromatography using 1:1 petrol/EtOAc afforded the title compound **153** as a light brown solid (45 mg, 0.15 mmol, 32%). **Mpt** > 198–199 ºC decomp.; **IR** (ATR)/cm^{-1}: 3315, 2924, 1599, 1444; **^{1}H NMR** (400

MHz, DMSO) δ 8.23 (d, *J* = 7.9 Hz, 1H), 7.68 (d, *J* = 7.9 Hz, 1H), 7.46 (s, 1H), 7.32 (appt, *J* = 7.9 Hz, 1H), 6.64 (s, 1H), 3.20–3.03 (m, 2H), 2.36–2.22 (m, 1H), 2.19–2.09 (m, 1H), 1.77–1.60 (m, 2H), 1.40–1.17 (m, 4H); **^{13}C NMR** (101 MHz, DMSO) δ 164.6, 140.9, 139.9, 134.3, 129.8, 125.2, 122.3, 115.5, 105.9, 58.7, 54.4, 31.8, 31.5, 23.4, 23.2; **LRMS** (ES + APCI) *m/z* 351.0 $(M+H)^+$; **HRMS** (ESI, +ve) *m/z* calc. for $C_{15}H_{16}{}^{79}BrN_2OS$ 351.0161, found 351.0166 $(M+H)^+$.

Methyl 3-bromo-5-nitrobenzo[b]thiophene-2-carboxylate (154)

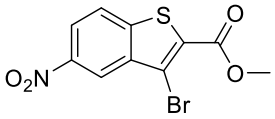

Following General Procedure G, **32** (2.0 g, 8.0 mmol), copper (II) bromide (3.5 g, 15.8 mmol), t-butyl nitrite (1.0 mL, 8.8 mmol) in acetonitrile (35 mL) were stirred for 16 hours at 30 ºC. The solvent was evaporated under reduced pressure. The residue was triturated with MeOH (30 mL), filtered under reduced pressure and washed with cold MeOH to afford the title compound **154** as a white solid (2.2 g, 6.9 mmol, 87%). **Mpt** 212–214 ºC; **IR** (ATR)/cm^{-1}: 2987, 1691, 1514, 1260; **^{1}H NMR** (400 MHz, $CDCl_3$) δ 8.88 (d, *J* = 2.0 Hz, 1H), 8.37 (dd, *J* = 8.9, 2.0 Hz, 1H), 7.99 (d, *J* = 8.9 Hz, 1H), 4.01 (s, 3H); **^{13}C NMR** (101 MHz, $CDCl_3$) δ 161.1, 146.6, 144.8, 139.0, 131.1, 124.0, 122.3, 121.5, 115.8, 53.2; **LRMS** (ES + APCI) *m/z* 315.9 $(M+H)^+$; **HRMS** (ESI, +ve) *m/z* calc. for $C_{10}H_7{}^{79}BrNO_4S$ 315.9274, found 315.9269 $(M+H)^+$.

Methyl 3-bromo-6-nitrobenzo[*b*]thiophene-2-carboxylate (155)

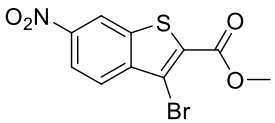

Following General Procedure G, **33** (3.0 g, 12.5 mmol), copper (II) bromide (5.6 g, 24.9 mmol), tert-butyl nitrite (1.8 mL, 14.4 mmol) in acetonitrile (70 mL) were stirred for 16 hours at 50 ºC. The solvent was evaporated under reduced pressure and purified by flash chromatography using 9:1 petrol/CH_2Cl_2 to afford the title compound **155** as a white solid

(2.2 g, 6.9 mmol, 54%). **Mpt** 209–211 ºC; **IR** (ATR)/cm^{-1}: 2953, 1716, 1517; **^{1}H NMR** (500 MHz, DMSO) δ 9.17 (s, 1H), 8.30 (d, *J* = 8.9 Hz, 1H), 8.07 (d, *J* = 8.9 Hz, 1H), 3.93 (s, 3H); **^{13}C NMR** (126 MHz, DMSO) δ 160.4, 146.8, 141.9, 138.5, 133.2, 125.9, 120.8, 120.4, 113.5, 53.2; **LRMS** (ES + APCI) *m/z* 315.9 $(M+H)^+$; **HRMS** (ESI, +ve) *m/z* calc. for $C_{10}H_7{}^{79}BrNO_4S$ 315.9274, found 315.9269 $(M+H)^+$.

2-Nitro-7,7*a*,8,9,10,11,11*a*,12-octahydro-6*H*-benzo[*b*]benzo[4,5]thieno[3,2-*e*][1,4]diazepin-6-one (156)

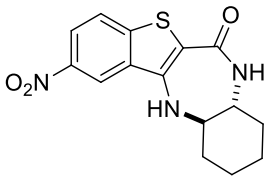

To a solution of **154** (1.00 g, 2.86 mmol) in dry *N*,*N*-dimethylformamide (15 mL) was added p-TsOH·H_2O (59 mg, 0.31 mmol) and the reaction refluxed for 16 hours at 170 ºC. The reaction mixture was cooled down to room temperature and the solvent evaporated under reduced pressure. The red solid was triturated with MeOH and filtered under reduced pressure to give the title compound **156** as a dark red solid (400 mg, 1.26 mmol, 41%). **Mpt** 230–232 ºC; **IR** (ATR)/cm^{-1}: 3331, 2929, 2854, 1606; **^{1}H NMR** (400 MHz, DMSO) δ 9.30 (d, *J* = 2.2 Hz, 1H), 8.20 (dd, *J* = 8.9, 2.2 Hz, 1H), 8.03 (d, *J* = 8.9 Hz, 1H), 7.54 (s, 1H), 7.13 (s, 1H), 3.17–3.12 (m, 2H), 2.42–2.29 (m, 1H), 2.21–2.07 (m, 1H), 1.77–1.63 (m, 2H), 1.48–1.19 (m, 4H); **^{13}C NMR** (101 MHz, DMSO) δ 164.3, 145.3, 144.3, 140.9, 133.1, 123.8, 120.9, 119.3, 107.4, 58.7, 54.4, 31.7, 31.5, 23.4, 23.2; **LRMS** (ES + APCI) *m/z* 318.0 $(M+H)^+$; **HRMS** (ESI, +ve) *m/z* calc. for $C_{15}H_{16}N_3O_3S$ 318.0907, found 318.0905 $(M+H)^+$.

3-Nitro-7,7*a*,8,9,10,11,11*a*,12-octahydro-6*H*-benzo[*b*]benzo[4,5]thieno[3,2-*e*][1,4]diazepin-6-one (157)

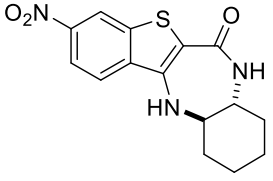

To a solution of **155** (250 mg, 0.72 mmol) in *N*,*N*-dimethylformamide (4 mL) was added *p*-TsOH·H_2O (13.5 mg, 0.07 mmol) and the reaction refluxed for 16 hours at 170 ºC. The reaction mixture was cooled down to room temperature and the solvent evaporated under reduced pressure. The red solid was triturated with MeOH and filtered under reduced pressure to give the title compound **157** as a dark red solid (80 mg, 0.25 mmol, 35%). **Mpt** 222–225 ºC decomp.; **IR** (ATR)/cm^{-1}: 3331, 2935, 1598, 1545; **^{1}H NMR** (400 MHz, DMSO) δ 8.80 (d, *J* = 2.1 Hz, 1H), 8.40 (d, *J* = 9.0 Hz, 1H), 8.15 (dd, *J* = 9.0, 2.2 Hz, 1H), 7.60 (s, 1H), 6.80 (s, 1H), 3.22–3.06 (m, 2H), 2.38–2.21 (m, 1H), 2.24–2.03 (m, 1H), 1.86–1.57 (m, 2H), 1.49–1.07 (m, 4H); **^{13}C NMR** (101 MHz, DMSO) δ 164.3, 146.1, 139.7, 138.7, 137.3, 123.9, 119.0, 117.9, 110.6, 58.8, 54.5, 31.8, 31.5, 23.4, 23.2; **LRMS** (ES + APCI) *m/z* 318.0 $(M+H)^+$; **HRMS** (ESI, +ve) *m/z* calc. for $C_{15}H_{16}N_3O_3S$ 318.0907, found 318.0911 $(M+H)^+$.

2-Amino-7,7a,8,9,10,11,11a,12-octahydro-6*H*-benzo[*b*]benzo[4,5]thieno[3,2-*e*][1,4]diazepin-6-one (158)

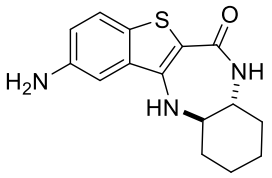

To a solution of **156** (200 mg, 0.63 mmol) in dry EtOH (3 mL) was added ammonium chloride (116 mg, 2.16 mmol) and iron (104 mg, 1.86 mmol). The reaction was heated under reflux conditions for 48 hours. The solvent was evaporated under reduced pressure. The crude solid was dissolved in EtOAc (15 mL) and aqueous solution 10% EDTA (10 mL) were added to the solution. The mixture was stirred for 16 hours. The organic layer was separated, washed with water (10 mL), $NaHCO_3$ sat. (15 mL), brine (15 mL), dried over magnesium sulphate and concentrated under reduced pressure to give the title compound **158** as an orange solid (120 mg, 0.42 mmol, 66%). **Mpt** > 211–212 ºC decomp.; **IR** (ATR)/cm^{-1}: 3298 (br), 2929, 1589, 1552; **^{1}H NMR** (400 MHz, DMSO) δ 7.37 (d, *J* = 8.5 Hz, 1H), 7.20 (s, 1H), 7.14 (d, *J* = 2.0 Hz, 1H), 6.79 (dd, *J* = 8.5, 2.0 Hz, 1H), 6.14 (s, 1H), 5.00 (s, 2H), 3.14–3.08 (m, 2H), 3.08–3.01 (m, 1H), 2.32–2.21 (m, 1H), 1.74–1.61 (m, 2H), 1.38–1.12 (m, 4H); **^{13}C NMR** (101 MHz, DMSO) δ 165.1, 145.3, 140.2, 134.1, 126.6, 122.7, 117.2, 105.5, 105.4, 58.8, 54.5, 32.0, 31.5, 23.5, 23.3; **LRMS** (ES + APCI) *m/z* 288.1 $(M+H)^+$; **HRMS** (ESI, +ve) *m/z* calc. for $C_{15}H_{18}N_3OS$ 288.1165, found 288.1166 $(M+H)^+$.

3-Amino-7,7a,8,9,10,11,11a,12-octahydro-6*H*-benzo[*b*]benzo[4,5]thieno[3,2-*e*][1,4]diazepin-6-one (159)

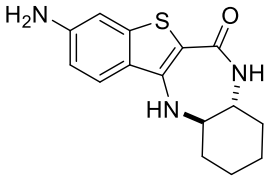

To a solution of **157** (100 mg, 0.31 mmol) in dry EtOH (1.5 mL) was added ammonium chloride (59.0 mg, 1.10 mmol) and iron (52 mg, 0.93 mmol). The reaction was heated under refluxed conditions for 48 hours. The solvent was evaporated under reduced pressure. The crude solid was dissolved in EtOAc (5 mL) and aqueous solution 10% EDTA (10 mL) were added to the solution. The reaction was stirred for 16 hours. The organic layer was separated, washed with water (10 mL) and concentrated under reduced pressure to give the title compound **159** as an orange solid (50 mg, 0.17 mmol, 56%). **Mpt** > 207–209 ºC decomp.; **IR** (ATR)/cm^{-1} 3307 (br), 2929, 1591, 1552; **^{1}H NMR** (400 MHz, DMSO) δ 7.76 (d, *J* = 8.7 Hz, 1H), 6.99 (s, 1H), 6.72 (d, *J* = 8.5 Hz, 1H), 6.59 (d, *J* = 8.6 Hz, 1H), 6.25 (s, 1H), 5.44 (s, 2H), 3.12–2.95 (m, 2H), 2.33–2.19 (m, 1H), 2.09 (s, 1H), 1.75–1.58 (m, 2H), 1.34–1.09 (m, 4H); **^{13}C NMR** (101 MHz, DMSO) δ 165.1, 148.9, 141.4, 140.9, 123.3, 122.9, 112.3, 104.4, 100.1, 58.7, 54.5, 31.9, 31.5, 23.5, 23.3; **LRMS** (ES + APCI) *m/z* 288.1 $(M+H)^+$; **HRMS** (ESI, +ve) *m/z* calc. for $C_{15}H_{18}N_3OS$ 288.1167, found 288.1165 $(M+H)^+$.

***N*-(6-oxo-7,7a,8,9,10,11,11*a*,12-Octahydro-6*H*-benzo[*b*]benzo[4,5]thieno[3,2-*e*][1,4]diazepin-2-yl)acetamide (161)**

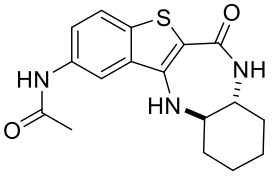

To a solution of **158** (60 mg, 0.20 mmol), triethylamine (28 µL, 0.20 mmol) in dry THF (1.5 mL) at 0 ºC was added dropwise acetyl chloride (14 µL, 0.20 mmol). The reaction was stirred for 1 hour. EtOAc was added to the mixture (5 mL) and sat. sodium bicarbonate (5 mL). The organic layer was collected, washed with water (5mL), brine (5mL), dried over magnesium sulphate and concentrated to give the title compound **161** as a brown solid (20 mg, 0.06 mmol, 30%). **Mpt** > 200–201 ºC decomp.; **IR** (ATR)/cm^{-1}: 3402, 3165 (br), 2924, 1622,

1604, 1556; **^{1}H NMR** (400 MHz, DMSO) δ 9.98 (s, 1H), 8.18 (s, 1H), 7.67 (d, *J* = 8.6 Hz, 1H), 7.48 (dd, *J* = 8.6, 1.6 Hz, 1H), 7.33 (s, 1H), 6.42 (s, 1H), 3.19–3.03 (m, 2H), 2.37–2.24 (m, 1H), 2.16–2.09 (m, 1H), 2.06 (s, 3H), 1.77–1.58 (m, 2H), 1.49–1.15 (m, 4H); **^{13}C NMR** (101 MHz, DMSO) δ 168.1, 164.9, 140.6, 135.1, 133.8, 133.3, 122.6, 121.0, 113.8, 106.2, 58.8, 54.5, 31.9, 31.5, 23.7, 23.5, 23.3; **LRMS** (ES + APCI) *m/z* 330.1 $(M+H)^+$; **HRMS** (ESI, +ve) *m/z*: calc. for $C_{17}H_{20}N_3O_2S$ 330.1271, found 330.1274 $(M+H)^+$.

3-Methyl-*N*-(-6-oxo-7,7a,8,9,10,11,11a,12-octahydro-6*H*-benzo[*b*]benzo[4,5]thieno[3,2-*e*][1,4]diazepin-2-yl)butanamide (162)

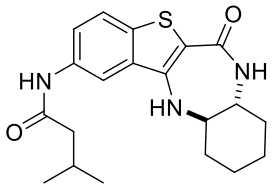

To a solution of **158** (70 mg, 0.24 mmol), trimethylamine (34 μL, 0.26 mmol) in dry THF (1.8 mL) at 0 ºC was added dropwise acetyl chloride (30 μL, 0.24 mmol). The reaction is stirred for an hour. EtOAc is added to the mixture (5 mL) and sat. sodium bicarbonate (5 mL). The organic layers were collected, washed with water (5mL), brine (5mL), dried over magnesium sulphate. The crude product is purified by flash chromatography using 1:1 EtOAc/CH_2Cl_2 to give the title compound **162** as a yellow solid (32 mg, 0.09 mmol, 36%). **Mpt** > 203 ºC decomp.; **IR** (ATR)/cm^{-1}: 3474, 3165 (br), 2932, 1666, 1666, 1493; **^{1}H NMR** (500 MHz, DMSO) δ 9.91 (s, 1H), 8.22 (s, 1H), 7.67 (d, *J* = 8.6 Hz, 1H), 7.50 (dd, *J* = 8.6, 2.0 Hz, 1H), 7.35 (s, 1H), 6.45 (s, 1H), 3.20–3.03 (m, 3H), 2.38–2.26 (m, 1H), 2.21 (d, *J* = 7.1 Hz, 2H), 2.16–2.03 (m, 1H), 1.75–1.61 (m, 2H), 1.43–1.14 (m, 4H), 0.95 (d, *J* = 6.6 Hz, 6H); **^{13}C NMR** (126 MHz, DMSO) δ 170.5, 164.9, 140.6, 135.2, 133.8, 133.4, 122.6, 121.1, 113.7, 106.2, 99.5, 58.8, 54.5, 45.4, 32.0, 31.5, 25.6, 23.5, 22.3; **LRMS** (ES + APCI) *m/z* 372.1 $(M+H)^+$; **HRMS** (ESI, +ve) *m/z* calc. for $C_{20}H_{26}N_3O_2S$ 372.1740, found 372.1741 $(M+H)^+$.

Methyl 3-bromo-6-(trifluoromethyl)benzo[*b*]thiophene-2-carboxylate (163)

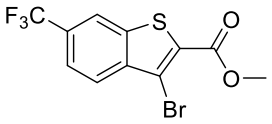

Following General Procedure G, **35** (2.5 g, 9.2 mmol), copper (II) bromide (4.1 g, 18.3 mmol), tert-butyl nitrite (1.2 mL, 9.6 mmol) in acetonitrile (43 mL) were stirred for 16 hours at 50 ºC. The solvent was evaporated under reduced pressure and the residue purified by flash chromatography using 9:1 Petrol/DCM to afford the title compound **163** as a white solid (2.1 g, 6.2 mmol, 68%). **Mpt** 98–99 ºC; **IR** (ATR)/cm^{-1}: 2954, 1722; **^{1}H NMR** (400 MHz, $CDCl_3$) δ 8.14–8.12 (m, 1H), 8.09 (d, *J* = 8.6 Hz, 1H), 7.72 (d, *J* = 8.6, 1H), 4.00 (s, 3H); **^{13}C NMR** (101 MHz, $CDCl_3$) δ 161.4, 141.0, 139.1, 126.2, 130.4 (q, *J* = 32.0 Hz); 124.0 (d, *J* = 272.0 Hz); 122.6–122.2 (m), 120.6–120.3 (m), 114.7, 77.2, 53.0; **LRMS** (ES + APCI) *m/z* 338.9 $(M+H)^+$; **HRMS** (ESI, +ve) *m/z* calc. for $C_{11}H_7{}^{79}BrF_3O_2S$ 338.9297, found 338.9298 $(M+H)^+$.

3-(Trifluoromethyl)-7,7*a*,8,9,10,11,11*a*,12-octahydro-6*H*-benzo[*b*]benzo[4,5]thieno[3,2-*e*][1,4]diazepin-6-one (164)

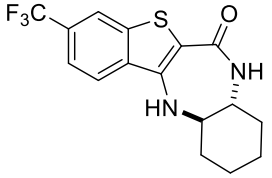

Following General Procedure I, **163** (300 mg, 0.88 mmol), (±)-*trans*-1,2-diaminocyclohexane (158 µL, 0.13 mmol), Xantphos (102 mg, 0.18 mmol), Pd_2dba_3 (81 mg, 0.09 mmol), Cs_2CO_3 (430 mg, 1.32 mmol) in DMF (10 mL). Purification by silica chromatography using CH_2Cl_2/EtOAc (8:2) afforded the title compound **164** as a white solid (50 mg, 0.15 mmol, 32%). **Mpt** > 110–112 ºC decomp.; **IR** (ATR)/cm^{-1}: 3332, 2929 (br), 1600, 1562; **^{1}H NMR** (400 MHz, DMSO) δ 8.39 (d, *J* = 8.6 Hz, 1H), 8.27 (s, 1H), 7.66 (dd, *J* = 8.6, 1.4 Hz, 1H), 7.51 (s, 1H), 6.74 (s, 1H), 3.23–3.08 (m, 2H), 2.37–2.26 (m, 1H), 2.18–2.08 (m, 1H), 1.76–1.63 (m, 2H), 1.45–1.16 (m, 4H); **^{13}C NMR** (101 MHz, DMSO) δ 164.6, 139.9, 138.8, 135.8, 127.2 (q, *J* = 32.0 Hz), 124.4 (q, *J* = 272.0 Hz), 123.8, 120.4–120.1 (m), 119.8–119.4 (m),

108.0, 58.8, 54.5, 31.8, 31.5, 23.40, 23.2; **LRMS** (ES + APCI) *m/z* 341.0 $(M+H)^+$; **HRMS** (ESI, +ve) *m/z* calc. for $C_{16}H_{13}F_3N_2OS$ 341.0937, found 341.0933 $(M+H)^+$.

3,3-Dimethyl-*N*-(6-oxo-7,7*a*,8,9,10,11,11*a*,12-octahydro-6*H*-benzo[*b*]benzo[4,5]thieno[3,2-*e*][1,4]diazepin-2-yl)butanamide (165)

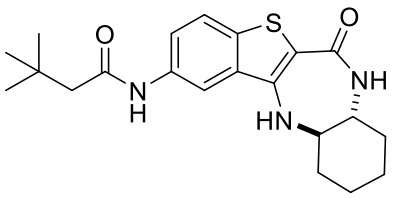

Following General Procedure X, **158** (70 mg, 0.24 mmol), tert-butylacetyl chloride (35 µL, 0.25 mmol), and triehylamine (37 µL, 0.26 mmol) in THF (1.8 mL) for 16 hours at room temperature. The solvent was evaporated under reduced pressure and the crude mixture purified by flash chromatography using 8:2 EtOAc/petrol to afford the title compound **165** as a yellow solid (80 mg, 0.20 mmol, 86%). **Mpt** > 198–199 ºC decomp.; **IR** (ATR)/cm^{-1}: 3300 (br), 2932, 1680, 1599, 1441; **^{1}H NMR** (400 MHz, DMSO) δ 9.86 (s, 1H), 8.20 (s, 1H), 7.67 (d, *J* = 8.6 Hz, 1H), 7.52 (dd, *J* = 8.6, 1.6 Hz, 1H), 7.35 (s, 1H), 6.45 (s, 1H), 3.21–3.01 (m, 2H), 2.38–2.26 (m, 1H), 2.21 (s, 2H), 2.17–2.06 (m, 1H), 1.75–1.62 (m, 2H), 1.40–1.17 (m, 4H), 1.04 (s, 9H); **^{13}C NMR** (101 MHz, DMSO) δ 169.9, 164.9, 140.7, 135.2, 133.8, 133.4, 122.6, 121.1, 113.7, 106.2, 58.8, 54.5, 49.4, 32.0, 31.6, 30.8, 29.7, 23.5, 23.3; **LRMS** (ES + APCI) *m/z* 386.1 $(M+H)^+$; **HRMS** (ESI, +ve) *m/z* calc. for $C_{21}H_{28}N_3O_2S$ 386.1897, found 386.1896 $(M+H)^+$.

_N_-(-6-oxo-7,7_a_,8,9,10,11,11_a_,12-Octahydro-6_H_-benzo[_b_]benzo[4,5]thieno[3,2-_e_][1,4]diazepin-2-yl)cyclobutanecarboxamide (166)

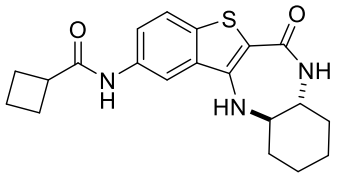

Following General Procedure L, **158** (60 mg, 0.21 mmol), cyclobutanoyl chloride (25 µL, 0.21 mmol), and triehylamine (31 µL, 0.23 mmol) in THF (1.7 mL) for 1 hour at room temperature. EtOAc was added to the mixture (5 mL) and sat. sodium bicarbonate (5 mL). The organic layers were collected, washed with water (2 x 5 mL), brine (2 5 mL), dried over magnesium sulphate. The crude product was purified by flash chromatography using 1:1 EtOAc/petrol to give the title compound **166** as a yellow solid (22 mg, 0.06 mmol, 28%). **Mpt** > 250 ºC decomp.; **IR** (ATR)/cm^{-1}: 3389, 3251, 2932, 1669, 1613, 1435; **^{1}H NMR** (400 MHz, DMSO) δ 9.79 (s, 1H), 8.25 (s, 1H), 7.66 (d, *J* = 8.6 Hz, 1H), 7.49 (dd, *J* = 8.6, 1.6 Hz, 1H), 7.34 (s, 1H), 6.45 (s, 1H), 3.31–3.19 (m, 1H), 3.19–3.02 (m, 2H), 2.38–2.18 (m, 3H), 2.17–2.04 (m, 3H), 2.02–1.87 (m, 1H), 1.88–1.76 (m, 1H), 1.75–1.60 (m, 2H), 1.32–1.16 (m, 4H); **^{13}C NMR** (101 MHz, DMSO) δ 172.7, 164.9, 140.6, 135.2, 133.7, 133.3, 122.6, 121.1, 113.7, 106.1, 58.8, 54.5, 31.9, 31.5, 24.6, 23.5, 23.3, 17.8; **LRMS** (ES + APCI) *m/z* 370.1 $(M+H)^+$; **HRMS** (ESI, +ve) *m/z* calc. for $C_{20}H_{24}N_3O_2S$ 370.1584, found 370.1587 $(M+H)^+$.

_N_-(6-oxo-7,7_a_,8,9,10,11,11_a_,12-octahydro-6_H_-benzo[_b_]benzo[4,5]thieno[3,2-_e_][1,4]diazepin-2-yl)cyclopentanecarboxamide (167)

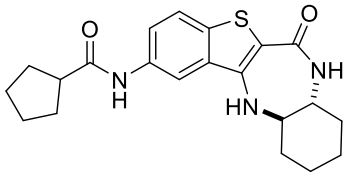

Following General Procedure L, **158** (60 mg, 0.21 mmol), cyclopentanoyl chloride (25 µL, 0.21 mmol), and triehylamine (34 µL, 0.23 mmol) in THF (1.7 mL) for 1 hour at room temperature. EtOAc was added to the mixture (5 mL) and sat. sodium bicarbonate (5 mL). The organic layers were collected, washed with water (5mL), brine (5mL), dried over

magnesium sulphate. The crude product was purified by flash chromatography using 100% EtOAc to give the title compound **167** as a white solid (47 mg, 0.12 mmol, 51%). **Mpt** > 250 ºC decomp.; **IR** (ATR)/cm^{-1}: 3240, 2926, 1666, 1599, 1428; **^{1}H NMR** (400 MHz, DMSO) δ 10.03 (s, 1H), 8.14 (d, *J* = 1.7 Hz, 1H), 8.04 (d, *J* = 8.9 Hz, 1H), 7.43 (dd, *J* = 8.9, 1.9 Hz, 1H), 7.24 (s, 1H), 6.47 (s, 1H), 3.19–3.03 (m, 2H), 2.84–2.73 (m, 1H), 2.33–2.22 (m, 1H), 2.16–2.05 (m, 1H), 1.91–1.80 (m, 2H), 1.79–1.62 (m, 6H), 1.60–1.49 (m, 2H), 1.34–1.17 (m, 4H).; **^{13}C NMR** (101 MHz, DMSO) δ 174.7, 164.9, 140.6, 139.5, 138.8, 128.4, 123.0, 115.7, 111.5, 103.7, 58.7, 54.4, 45.4, 31.9, 31.5, 30.1, 25.6, 23.5, 23.2; **LRMS** (ES + APCI) *m/z* 384.2 (M+H)$^{+}$; **HRMS** (ESI, +ve) *m/z* calc. for $C_{21}H_{26}N_3O_2S$ 384.1740, found 384.1741 (M+H)$^{+}$.

_N_-(-6-oxo-7,7_a_,8,9,10,11,11_a_,12-Octahydro-6_H_-benzo[b]benzo[4,5]thieno[3,2-_e_][1,4]diazepin-2-yl)cyclohexanecarboxamide (168)

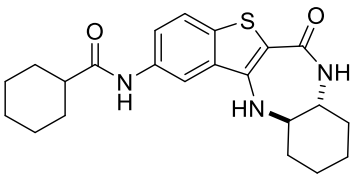

Following General Procedure L, **158** (70 mg, 0.24 mmol), triethylamine (34 μL, 0.26 mmol) in dry THF (2 mL) at 0 ºC was added dropwise cyclohexanoyl chloride (30 μL, 0.23 mmol). The reaction is stirred for 1 hour. EtOAc was added to the mixture (5 mL) and sat. sodium bicarbonate (5 mL). The organic layers were collected, washed with water (5mL), brine (5mL), dried over magnesium sulphate. The crude product was purified by flash chromatography using 1:1 EtOAc/petrol to give the title compound **168** as a yellow solid (30 mg, 0.07 mmol, 31%). **Mpt** > 179 ºC decomp.; **IR** (ATR)/cm^{-1}: 3352, 3142, 2919, 2848, 1680, 1621; **^{1}H NMR** (400 MHz, DMSO) δ 9.84 (s, 1H), 8.28 (s, 1H), 7.66 (d, *J* = 8.5 Hz, 1H), 7.46 (d, *J* = 8.5 Hz, 1H), 7.32 (s, 1H), 6.43 (s, 1H), 3.22–3.01 (m, 2H), 2.41–2.23 (m, 2H), 2.17–2.05 (m, 1H), 1.91–1.60 (m, 7H), 1.55–1.11 (m, 9H); **^{13}C NMR** (101 MHz, DMSO) δ 174.1, 164.9, 140.6, 135.3, 133.6, 133.3, 122.6, 121.0, 113.6, 106.1, 58.8, 54.5, 44.7, 31.9, 31.5, 29.2, 29.2, 25.4, 25.2, 23.5, 23.3; **LRMS** (ES + APCI) *m/z* 398.1 (M+H)$^{+}$; **HMRS** (ESI, +ve) *m/z* calc. for $C_{22}H_{28}N_3O_2S$ 398.1897, found 398.1895 (M+H)$^{+}$.

_N_-(-6-oxo-7,7_a_,8,9,10,11,11_a_,12-Octahydro-6_H_-benzo[_b_]benzo[4,5]thieno[3,2-_e_][1,4]diazepin-2-yl)benzamide (169)

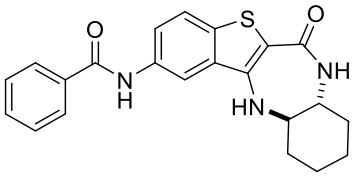

Following General Procedure L, **158** (70 mg, 0.24 mmol), triethylamine (34 μL, 0.26 mmol) in dry THF (2 mL) at 0 ºC was added dropwise benzoyl chloride (29 μL, 0.25 mmol). The reaction was stirred for 3 hours at room temperature. The solvent was evaporated under reduced pressure and the crude product was purified by flash chromatography using 8:2 EtOAc/petrol to give the title compound **169** as a yellow solid (25 mg, 0.06 mmol, 27%). **Mpt** > 179 ºC decomp.; **IR** (ATR)/cm^{-1}: 3251, 2909, 1630; **^{1}H NMR** (400 MHz, DMSO) δ 10.34 (s, 1H), 8.43 (d, *J* = 1.6 Hz, 1H), 8.03–7.96 (m, 2H), 7.74 (d, *J* = 8.6 Hz, 1H), 7.64–7.51 (m, 4H), 7.35 (s, 1H), 6.49 (s, 1H), 3.25–3.00 (m, 2H), 2.41–2.23 (m, 1H), 2.23–2.04 (m, 1H), 1.88–1.53 (m, 2H), 1.35–1.16 (m, 4H); **^{13}C NMR** (101 MHz, DMSO) δ 165.3, 164.9, 140.6, 134.9, 134.6, 134.6, 133.3, 131.6, 128.4, 127.6, 122.6, 122.4, 115.7, 106.1, 58.8, 54.5, 31.9, 31.5, 23.5, 23.3; **LRMS** (ES + APCI) *m/z* 392.1 $(M+H)^+$; **HMRS** (ESI, +ve) *m/z* calc. for $C_{22}H_{22}N_3O_2S$ 392.1428, found 392.1427 $(M+H)^+$.

_N_-(-6-oxo-7,7_a_,8,9,10,11,11_a_,12-Octahydro-6_H_-benzo[_b_]benzo[4,5]thieno[3,2-_e_][1,4]diazepin-2-yl)nicotinamide (170)

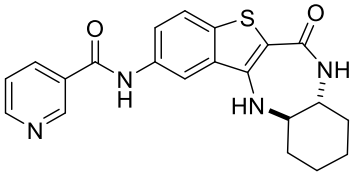

Following General Procedure L, **158** (70 mg, 0.24 mmol), triethylamine (61 μL, 0.44 mmol) in dry THF (2 mL) at 0 ºC was added dropwise isonicotinoyl chloride hydrochloride (40 mg, 0.23 mmol). The reaction was stirred for 24 hours at room temperature. The solvent was evaporated under reduced pressure. The crude product was purified by flash chromatography using 100% EtOAc + 0.1% MeOH to give the title compound **170** as a brown solid (30 mg,

0.10 mmol, 36%). **Mpt** > 219–220 ºC decomp.; **IR** (ATR)/cm^{-1}: 3378, 3222, 2924, 1666, 1589, 1442; **^{1}H NMR** (400 MHz, DMSO) δ 10.58 (s, 1H), 9.18 (d, *J* = 1.8 Hz, 1H), 8.78 (dd, *J* = 4.8, 1.5 Hz, 1H), 8.44 (d, *J* = 1.6 Hz, 1H), 8.39–8.34 (m, 1H), 7.77 (d, *J* = 8.6 Hz, 1H), 7.64 (dd, *J* = 8.6, 1.8 Hz, 1H), 7.60 (dd, *J* = 7.7, 5.0 Hz, 1H), 7.36 (s, 1H), 6.52 (s, 1H), 3.23–3.06 (m, 2H), 2.39–2.27 (m, 1H), 2.19–2.07 (m, 1H), 1.78–1.62 (m, 2H), 1.43–1.15 (m, 4H); **^{13}C NMR** (101 MHz, DMSO) δ 164.8, 163.9, 152.1, 148.6, 140.6, 135.4, 134.8, 134.5, 133.3, 130.2, 123.5, 122.7, 122.3, 115.7, 106.2, 58.8, 54.5, 31.9, 31.5, 23.5, 23.3; **LRMS** (ES + APCI) *m/z* 393.1 (M+H)$^{+}$; **HRMS** (ESI, +ve) *m/z* calc. for $C_{21}H_{21}N_4O_2S$ 393.1380, found 393.1381 (M+H)$^{+}$.

_N_-(-6-oxo-7,7_a_,8,9,10,11,11_a_,12-Octahydro-6_H_-benzo[_b_]benzo[4,5]thieno[3,2-_e_][1,4]diazepin-2-yl)isonicotinamide (171)

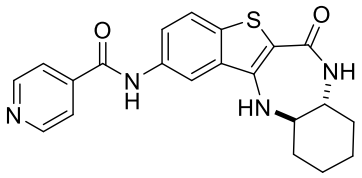

Following General Procedure L, **158** (70 mg, 0.24 mmol), triethylamine (61 μL, 0.44 mmol) in dry THF (2 mL) at 0 ºC was added dropwise isonicotinoyl chloride hydrochloride (40 mg, 0.23 mmol). The reaction was stirred for 24 hours at room temperature. The solvent was evaporated under reduced pressure. The crude product was purified by flash chromatography using 100% EtOAc + 0.1% MeOH to give the title compound **171** as a brown solid (40 mg, 0.10 mmol, 41%). **Mpt >** 205–207 ºC decomp.; **IR** (ATR)/cm^{-1}: 3456 (br), 3238 (br), 2917, 1658, 1613; **^{1}H NMR** (400 MHz, DMSO) δ 10.63 (s, 1H), 8.93–8.68 (m, 2H), 8.43 (s, 1H), 7.95–7.87 (m, 2H), 7.77 (d, *J* = 8.5 Hz, 1H), 7.62 (d, *J* = 8.5 Hz, 1H), 7.37 (s, 1H), 6.54 (s, 1H), 3.21–3.02 (m, 2H), 2.39–2.24 (m, 1H), 2.19–2.05 (m, 1H), 1.77–1.60 (m, 2H), 1.47–1.17 (m, 4H); **^{13}C NMR** (101 MHz, DMSO) δ 164.8, 163.8, 150.3, 141.6, 140.6, 135.0, 134.2, 133.3, 122.8, 122.3, 121.5, 115.9, 106.2, 58.8, 54.5, 31.90, 31.5, 23.5, 23.3; **LRMS** (ES + APCI) *m/z* 393.1 (M+H)$^{+}$; **HRMS** (ESI, +ve) *m/z* calc. for $C_{21}H_{21}N_4O_2S$ 393.1380, found 393.1374 (M+H)$^{+}$.

3-Chloro-*N*-(-6-oxo-7,7*a*,8,9,10,11,11*a*,12-Octahydro-6*H*-benzo[*b*]benzo[4,5]thieno[3,2-*e*][1,4]diazepin-2-yl)benzamide (172)

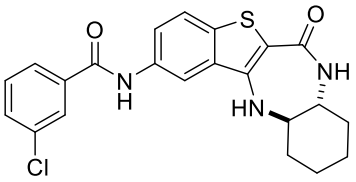

Following General Procedure L, **158** (60 mg, 0.21 mmol), 3-chlorobenzoyl chloride (28 µL, 0.22 mmol), and triehylamine (31 µL, 0.23 mmol) in THF (1.7 mL) for 16 hours at room temperature. CH_2Cl_2 was added to the mixture (5 mL) and sat. sodium bicarbonate (5 mL). The organic layers were collected, washed with water (2 x5 mL), brine (2 x 5mL), dried over magnesium sulphate and concentrated to give the title compound **172** as an orange solid (32 mg, 0.08 mmol, 38%). **Mpt** > 250 ºC decomp.; **IR** (ATR)/cm^{-1}: 3304, 2917, 1658, 1584, 1416; **^{1}H NMR** (400 MHz, DMSO) δ 10.46 (s, 1H), 8.41 (s, 1H), 8.06 (s, 1H), 7.97 (d, *J* = 7.3 Hz, 1H), 7.76 (d, *J* = 8.4 Hz, 1H), 7.72–7.54 (m, 3H), 7.36 (s, 1H), 6.51 (s, 1H), 3.19–3.04 (m, 2H), 2.37–2.27 (m, 1H), 2.21–2.07 (m, 1H), 1.77–1.59 (m, 2H), 1.43–1.17 (m, 4H); **^{13}C NMR** (101 MHz, DMSO) δ 164.9, 163.8, 140.6, 136.6, 134.8, 134.6, 133.3, 133.3, 131.4, 130.5, 127.3, 126.4, 122.7, 122.3, 115.7, 106.2, 58.8, 54.5, 31.9, 31.5, 23.5, 23.3; **LRMS** (ES + APCI) *m/z* 426.1 $(M+H)^+$; **HRMS** (ESI, +ve) *m/z* calc. for $C_{22}H_{21}{}^{35}ClN_3O_2S$ 426.1038, found 426.1035 $(M+H)^+$.

4-Chloro-*N*-(-6-oxo-7,7*a*,8,9,10,11,11a,12-octahydro-6*H*-benzo[*b*]benzo[4,5]thieno[3,2-*e*][1,4]diazepin-2-yl)benzamide (173)

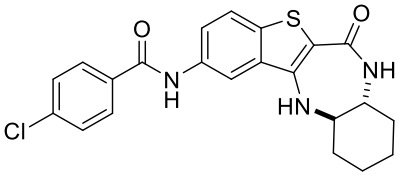

Following General Procedure L, **158** (60 mg, 0.21 mmol), 4-chlorobenzoyl chloride (28 µL, 0.22 mmol), and triehylamine (31 µL, 0.23 mmol) in THF (1.7 mL) for 16 hours at room temperature. CH_2Cl_2 was added to the mixture (5 mL) and sat. sodium bicarbonate (5 mL). The organic layers were collected, washed with water (2 x 5 mL), brine (5 mL), dried over

magnesium sulphate and concentrated to give the title compound **173** as an orange solid (30 mg, 0.07 mmol, 34%). **Mpt** > 250 ºC decomp.; **IR** (ATR)/cm^{-1}: 3328, 2931, 1652, 1589, 1442; **^{1}H NMR** (400 MHz, DMSO) δ 10.50 (s, 1H), 8.43 (d, *J* = 1.7 Hz, 1H), 8.09–8.03 (m, 2H), 7.75 (d, *J* = 8.6 Hz, 1H), 7.69–7.60 (m, 3H), 7.37 (s, 1H), 6.53 (s, 1H), 3.24–3.00 (m, 2H), 2.38–2.26 (m, 1H), 2.18–2.06 (m, 1H), 1.75–1.63 (m, 2H), 1.43–1.16 (m, 4H); **^{13}C NMR** (101 MHz, DMSO) δ 164.9, 164.3, 140.7, 136.5, 134.7, 134.7, 133.3, 129.6, 128.5, 122.6, 122.5, 115.9, 106.0, 58.8, 54.5, 31.9, 31.6, 23.5, 23.3, 1 carbon not reported; **LRMS** (ES + APCI) *m/z* 426.1 $(M+H)^+$; **HRMS** (ESI, +ve) *m/z* calc. for $C_{22}H_{21}{}^{35}ClN_3O_2S$ 426.1038, found 426.1037 $(M+H)^+$.

8. Appendix

8.1. ADP Hunter protocol

For the performance of the biochemical assay, the ADP Hunter assay kit (90-0083L) provided with reagent A (100 mL), reagent B (200 mL), ADP hunter stop solution (50 mL), ADP hunter standard (225 µM, 25 mL), and, ADP Hunter buffer, containing 15 mM Hepes, 20 mM NaCl, 1 mM EGTA, 0.02 %Tween 20, 10 mM $MgCl_2$, 0.1 % bovine gamma globulins at pH 7.4 (250 mL).

Materials that were not provided by the ADP Hunter assay kit are 384-well untreated low-volume polyesterene black plates (Corning 3677), 96-well plate (Nun 249944).

The sealers that were used when centrifuging the assay plates were available from PerkinElmer (600185). The equipment needed for the assay was the automatic robot Biomek FX Dual Span 8 (Beckman-Coulter), the data reader Envision (PerkinElmer), and the centrifuge (Eddpendorf 5810).

PIM-1, PIM-2, and PIM-3 biochemical assay

The biochemical assay to measure PIM-1 activity relies on the ADP Hunter assay kit (DiscoveRx Corp., Cat. # 90-0083L).

The PIM-1 and PIM-2 enzymes used had been expressed and purified at CNIO as a recombinant human protein with a C-terminal histidine tag and were stored at -80 °C. The protein was active and stable. The PIM-3 enzyme was commercially available from Milipore (14-738).

Assay conditions were as indicated by the kit manufacturers with the following adaptations for the kinase activity step. Kinase assay buffer and assay volume were kept as recommended (15 mM, HEPES, pH 7.4, 20 mM NaCl, 1 mM EGTA, 0.02% Tween 20, 10 mM, $MgCl_2$ and 0.1 mg/ml bovine globulins. The plate was incubated for 60 minutes at 30 °C. Commercially avaiable ATP was used (Sigma, 10 mM), the PIM substrate peptide (PIMtide: ARKRRRHPSGPPTA) was also commercially available (10 mM, Bionova). As a positive control for kinase activity inhibition a known CNIO pan-PIM inhibitor was used (ETP-00039010: PIM-1 28.6 nM, PIM-2 78.9 nM, PIM-3 1.50 nM). The concentration of DMSO concentration was 2% during the kinase reaction. The biochemical assay was performed in 384-well plates. The final outcome of the coupled reactions provided by the kit is the release of the fluorescent product Resorufin and has been measured with a multilabel HTS counter

VICTOR V(PerkinElmer) using an excitation filter at 544 nm and an emission filter at 580 nm.

The assay was performed in 384 well plate format with a final volume of 20 µL (ATP+substrate+kinase+inhibitor). The PIM-1 final concentration was 0.036 µg/mL, PIM-2 0.093 µg/mL, and PIM-3 0.120 µg/mL. The ATP and PIMtide final concentrations were 100 µM and 80 µM, respectively, Table I.

Table I: *Final assay concentrations for PIM-1, PIM-2, and PIM-3 SP experiment*

µg/mL	PIM-1	PIM-2	PIM-3
enzyme	0.036	0.093	0.12
ATP	100	100	100
Substrate	80	80	80

8.1.1. Single point experiment on final compounds

As a starting point for the biochemical evaluation of the final compounds that were previously synthesized to inhibit the activity of PIM kinases, a primary screening (single point experiment, SP) at two different concentrations (10 µM, and 1 µM) was carried out against the three PIM isoforms. To carry out the experiment, ATP, PIMtide, ADP Hunter kit, PIM-1, PIM-2, PIM-3, and the inhibitors were prepared.

The first step was the generation of the ATP pool, PIM-1 pool, PIM-2 pool, PIM-3 pool, and the PIMtide pool. The intermediate pools were used as an intermediate solution to obtain the desired final concentrations in the 384 well assay plate. The assay concentrations needed for each PIM isoform are summarized in Table I.

Preparation of the reagents pools:

i) **Preparation of 200 µM ATP pool**: 220 µL of ATP (10 mM) were dispensed in 10.7 mL of ADP Hunter Buffer solution.

ii) **Preparation of 168.4 µM PIMtide pool**: 290 µL of PIMtide (10 mM) were dispensed in 16.7 mL of ADP Hunter Buffer solution.

iii) **Preparation of PIM-1 pool**:
Preparation of PIM-1 intermediate concentration (0.213 µg/mL): 1 µL of PIM-1 (21.3 µg/mL) reagent was dispensed into 99 µL of PIMtide pool.
Preparation of PIM-1 final concentration pool (0.078 µg/mL): 26 µL of PIM-1 (0.213 µg/mL) intermediate concentration pool were dispensed into 7.5 mL of PIMtide pool.

iv) **Preparation of PIM-2 pool**:

Preparation of PIM-2 intermediate concentration (0.07 µg/mL): 3 µL of PIM-2 (0.7 µg/mL) reagent was dispensed into 30 µL of PIMtide pool.

Preparation of PIM-2 final concentration pool (0.195 µg/mL): 20 µL of PIM-2 (0.7 µg/mL) intermediate concentration pool were dispensed into 7.5 mL of PIMtide pool.

v) **Preparation of PIM-3 pool**:

Preparation of PIM-3 intermediate concentration (0.12 µg/mL): 6 µL of PIM-3 reagent was dispensed into 60 µL of PIMtide pool.

Preparation of PIM-3 final concentration pool (0.25 µg/mL): 52.5 µL of PIM-3 intermediate concentration pool were dispensed into 20 mL of PIMtide pool.

8.1.2. Preparation of intermediate daughter plate (enzyme + substrate + inhibitors):

Once the pools are ready and kept in ice, the intermediate daughter plate 1 and 2 were prepared. 28.5 µL of PIM pool was dispensed to all the wells of both intermediate daughter plates. The first column of the well corresponded to the standard ETP-39010 which was diluted using 3-fold serial dilutions starting at 2 µM. Moreover, 1.5 µL of the 73 inhibitors plates (400 µM, and 40 µM) were dispensed using automatic robot to the intermediate daughter plate. Each daughter plate will correspond to one concentration of inhibitors, as shown in Figure 1, and Figure 2. Column 12th of the intermediate plate corresponded to the negative and positive controls, with the positive controls (E-H, containing 2% DMSO in water + pool kinase) and the negative controls containing only substrate pool, no kinase is added. The intermediate daughter plate was sealed, stirred for 30 seconds at 400 rpm, and incubated during 10 minutes at room temperature.

Intermidiate plate 2 (kinase + substrate + inhibitors (20 µM)) (- SP)												
	1	2	3	4	5	6	7	8	9	10	11	12
A	Standard 1 (2 µM) 1/3 serial dilution	Inh (20 µM)	Inh (20 µM)	Inh (20 µM)	Inh (20 µM)	Inh (20 µM)	Inh (20 µM)	Inh (20 µM)	Inh (20 µM)	Inh (20 µM)	Inh (20 µM)	Negative Control DMSO (2 % in water)
B		Inh (20 µM)	Inh (20 µM)	Inh (20 µM)	Inh (20 µM)	Inh (20 µM)	Inh (20 µM)	Inh (20 µM)	Inh (20 µM)	Inh (20 µM)		
C		Inh (20 µM)	Inh (20 µM)	Inh (20 µM)	Inh (20 µM)	Inh (20 µM)	Inh (20 µM)	Inh (20 µM)	Inh (20 µM)	Inh (20 µM)		
D		Inh (20 µM)	Inh (20 µM)	Inh (20 µM)	Inh (20 µM)	Inh (20 µM)	Inh (20 µM)	Inh (20 µM)	Inh (20 µM)	Inh (20 µM)		
E		Inh (20 µM)	Inh (20 µM)	Inh (20 µM)	Inh (20 µM)	Inh (20 µM)	Inh (20 µM)	Inh (20 µM)	Inh (20 µM)	Inh (20 µM)		Positive cntrol DMSO (2 % in water)
F		Inh (20 µM)	Inh (20 µM)	Inh (20 µM)	Inh (20 µM)	Inh (20 µM)	Inh (20 µM)	Inh (20 µM)	Inh (20 µM)	Inh (20 µM)		
G		Inh (20 µM)	Inh (20 µM)	Inh (20 µM)	Inh (20 µM)	Inh (20 µM)	Inh (20 µM)	Inh (20 µM)	Inh (20 µM)	Inh (20 µM)		
H		Inh (20 µM)	Inh (20 µM)	Inh (20 µM)	Inh (20 µM)	Inh (20 µM)	Inh (20 µM)	Inh (20 µM)	Inh (20 µM)	Inh (20 µM)		

Figure 1: *Intermediate daughter plate 1 containing kinase + substrate+ 73 inhibitors for a single point experiment.*

Intermidiate plate 1 (kinase + substrate + inhibitors (2 µM)) (- SP)												
	1	2	3	4	5	6	7	8	9	10	11	12
A	Standard 1 (2 µM) 1/3 serial dilution	Inh (2 µM)	Inh (2 µM)	Inh (2 µM)	Inh (2 µM)	Inh (2 µM)	Inh (2 µM)	Inh (2 µM)	Inh (2 µM)	Inh (2 µM)	Inh (2 µM)	Negative Control DMSO (2 % in water)
B		Inh (2 µM)	Inh (2 µM)	Inh (2 µM)	Inh (2 µM)	Inh (2 µM)	Inh (2 µM)	Inh (2 µM)	Inh (2 µM)	Inh (2 µM)		
C		Inh (2 µM)	Inh (2 µM)	Inh (2 µM)	Inh (2 µM)	Inh (2 µM)	Inh (2 µM)	Inh (2 µM)	Inh (2 µM)	Inh (2 µM)		
D		Inh (2 µM)	Inh (2 µM)	Inh (2 µM)	Inh (2 µM)	Inh (2 µM)	Inh (2 µM)	Inh (2 µM)	Inh (2 µM)	Inh (2 µM)		
E		Inh (2 µM)	Inh (2 µM)	Inh (2 µM)	Inh (2 µM)	Inh (2 µM)	Inh (2 µM)	Inh (2 µM)	Inh (2 µM)	Inh (2 µM)		Positive cntrol DMSO (2 % in water)
F		Inh (2 µM)	Inh (2 µM)	Inh (2 µM)	Inh (2 µM)	Inh (2 µM)	Inh (2 µM)	Inh (2 µM)	Inh (2 µM)	Inh (2 µM)		
G		Inh (2 µM)	Inh (2 µM)	Inh (2 µM)	Inh (2 µM)	Inh (2 µM)	Inh (2 µM)	Inh (2 µM)	Inh (2 µM)	Inh (2 µM)		
H		Inh (2 µM)	Inh (2 µM)	Inh (2 µM)	Inh (2 µM)	Inh (2 µM)	Inh (2 µM)	Inh (2 µM)	Inh (2 µM)	Inh (2 µM)		

Figure 2: *Intermediate daughter plate 2 containing kinase + substrate+ 73 inhibitors for a single point experiment.*

8.1.3. Preparation of the final assay 384 well plate (SP, PIM-1, PIM-2, and PIM-3):

The ATP intermediate plate was prepared dispensing 30 µL of ATP pool to every well from the 96 well plate and stored at 4 °C. The previously described intermediate daughter plates were used to generate the final assay well plate. 10 µL of every well from the intermediate daughter plate 1 were dispensed per duplicated in Z series (per quadrants) to the 384 well plate. 10 µL of every well from the intermediate daughter plate 2 were dispensed per duplicated in Z series (per quadrants). The assay plate was sealed and stirred during 30 seconds at 400 rpm. At this stage, 10 µL of ATP intermediate plate were dispensed to every well from the 384 assay plate. The assay plate was sealed and shaken during 30 seconds at 400 rpm. The reaction plate was incubated during 60 minutes at 30 °C. The reaction 384 assay plate example is shown in Figure 3.

	1	2	3	4	5	6	7	8	9	10	11	12	13	14	15	16	17	18	19	20	21	22	23	24
A	Standard EP39010 (1µM; 1/3 serial dilutions)		Inh (10 µM)		Inh (10 µM)		Inh (10 µM)		Inh (10 µM)		Inh (10 µM)		Inh (10 µM)		Inh (10 µM)		Inh (10 µM)		Inh (10 µM)		Inh (10 µM)		Postive control	
B			Inh 1 (1 µM)		Inh 1 (1 µM)		Inh 1 (1 µM)		Inh 1 (1 µM)		Inh 1 (1 µM)		Inh 1 (1 µM)		Inh 1 (1 µM)		Inh 1 (1 µM)		Inh 1 (1 µM)		Inh 1 (1 µM)			
C			Inh (10 µM)		Inh (10 µM)		Inh (10 µM)		Inh (10 µM)		Inh (10 µM)		Inh (10 µM)		Inh (10 µM)		Inh (10 µM)		Inh (10 µM)		empty wells			
D			Inh 1 (1 µM)		Inh 1 (1 µM)		Inh 1 (1 µM)		Inh 1 (1 µM)		Inh 1 (1 µM)		Inh 1 (1 µM)		Inh 1 (1 µM)		Inh 1 (1 µM)		Inh 1 (1 µM)					
E			Inh (10 µM)		Inh (10 µM)		Inh (10 µM)		Inh (10 µM)		Inh (10 µM)		Inh (10 µM)		Inh (10 µM)		Inh (10 µM)		Inh (10 µM)					
F			Inh 1 (1 µM)		Inh 1 (1 µM)		Inh 1 (1 µM)		Inh 1 (1 µM)		Inh 1 (1 µM)		Inh 1 (1 µM)		Inh 1 (1 µM)		Inh 1 (1 µM)		Inh 1 (1 µM)					
G			Inh (10 µM)		Inh (10 µM)		Inh (10 µM)		Inh (10 µM)		Inh (10 µM)		Inh (10 µM)		Inh (10 µM)		Inh (10 µM)		Inh (10 µM)					
H			Inh 1 (1 µM)		Inh 1 (1 µM)		Inh 1 (1 µM)		Inh 1 (1 µM)		Inh 1 (1 µM)		Inh 1 (1 µM)		Inh 1 (1 µM)		Inh 1 (1 µM)		Inh 1 (1 µM)					
I			Inh (10 µM)		Inh (10 µM)		Inh (10 µM)		Inh (10 µM)		Inh (10 µM)		Inh (10 µM)		Inh (10 µM)		Inh (10 µM)		Inh (10 µM)				Negative control	
J			Inh 1 (1 µM)		Inh 1 (1 µM)		Inh 1 (1 µM)		Inh 1 (1 µM)		Inh 1 (1 µM)		Inh 1 (1 µM)		Inh 1 (1 µM)		Inh 1 (1 µM)		Inh 1 (1 µM)					
K			Inh (10 µM)		Inh (10 µM)		Inh (10 µM)		Inh (10 µM)		Inh (10 µM)		Inh (10 µM)		Inh (10 µM)		Inh (10 µM)		Inh (10 µM)					
L			Inh 1 (1 µM)		Inh 1 (1 µM)		Inh 1 (1 µM)		Inh 1 (1 µM)		Inh 1 (1 µM)		Inh 1 (1 µM)		Inh 1 (1 µM)		Inh 1 (1 µM)		Inh 1 (1 µM)					
M			Inh (10 µM)		Inh (10 µM)		Inh (10 µM)		Inh (10 µM)		Inh (10 µM)		Inh (10 µM)		Inh (10 µM)		Inh (10 µM)		Inh (10 µM)					
N			Inh 1 (1 µM)		Inh 1 (1 µM)		Inh 1 (1 µM)		Inh 1 (1 µM)		Inh 1 (1 µM)		Inh 1 (1 µM)		Inh 1 (1 µM)		Inh 1 (1 µM)		Inh 1 (1 µM)					
O			Inh (10 µM)		Inh (10 µM)		Inh (10 µM)		Inh (10 µM)		Inh (10 µM)		Inh (10 µM)		Inh (10 µM)		Inh (10 µM)		Inh (10 µM)					
P			Inh 1 (1 µM)		Inh 1 (1 µM)		Inh 1 (1 µM)		Inh 1 (1 µM)		Inh 1 (1 µM)		Inh 1 (1 µM)		Inh 1 (1 µM)		Inh 1 (1 µM)		Inh 1 (1 µM)					

Figure 3: *Single point assay plate experiment.*

8.1.4. ADP Hunter detection procedure

After the incubation, 10 µL of Reagent A from ADP Hunter kit were dispensed into every well, followed by 20 µL of Reagent B. The assay plate was sealed and stirred during 30 seconds at 400 rpm and then incubated during 30 minutes at room temperature.

Data analysis

The assay plate was read using EnVision and the RFU data obtained was normalized against the control activity included for each compound (i.e, 100 % PIM1 activity, without compound) and the percentage of inhibition was calculated using the formula shown below:

$$100 - \left[\frac{(\text{sample fluorescence} - \text{low control fluorescence})}{(\text{fluorescence pos. control} - \text{fluorescence neg. control})} \times 100 \right]$$

For a single point experiment at two different concentrations, a percentage of inhibition was obtained at two concentrations, per duplicate per compound. In HTS screening the single point experiment at two concentrations provides enough evidence to discard any non-potent compound before the dose-response curve experiment (DR experiment) was carried out against the more potent inhibitors.

8.1.5. Dose response experiments

The protocol used for the secondary screening (DR curve experiment) corresponds to the same protocol used for single point experiment, described in section 8.1.1–8.1.4.

In a DR experiment, the selected compounds were initially prepared into a 96-well plate starting with 1 mM concentration using a 3-fold serial dilution dissolved in 40% DMSO, as shown in Figure 4.

Inhibitors plate (1 mM, 40% DMSO)												
	1	2	3	4	5	6	7	8	9	10	11	12
A	Standard 1 (40 µM) 1/3 serial dilution	Standard 2 (40 µM) 1/3 serial dilution	Inhibitor 1 (3-fold serial dilutions)									DMSO (40% in water)
B			Inhibitor 2 (3-fold serial dilutions)									
C			Inhibitor 3 (3-fold serial dilutions)									
D			Inhibitor 4 (3-fold serial dilutions)									
E			Inhibitor 5 (3-fold serial dilutions)									
F			Inhibitor 6 (3-fold serial dilutions)									DMSO (40% in water)
G			Inhibitor 7 (3-fold serial dilutions)									
H			Inhibitor 8 (3-fold serial dilutions)									

***Figure 4**: Example of intermediate compound plate containing the standards, inhibitors and controls.*

The inhibitor plates were used to prepare the intermediate daughter plate (Figure 5), using the same experimental procedure as described in 8.1.2. The dispensation was also carried out using the robot Biomek FX Dual Span 8 for better accuracy.

Intermidiate plate (kinase + substrate + inhibitors)												
	1	2	3	4	5	6	7	8	9	10	11	12
A	Standard 1 (2 µM) 1/3 serial dilution	Standard 2 (2 µM) 1/3 serial dilution	Inhibitor 1 (3-fold serial dilutions)									
B			Inhibitor 2 (3-fold serial dilutions)									negative control
C			Inhibitor 3 (3-fold serial dilutions)									
D			Inhibitor 4 (3-fold serial dilutions)									
E			Inhibitor 5 (3-fold serial dilutions)									
F			Inhibitor 6 (3-fold serial dilutions)									positive control
G			Inhibitor 7 (3-fold serial dilutions)									
H			Inhibitor 8 (3-fold serial dilutions)									

***Figure 5**: Intermediate daughter plate*

When the corresponding intermediate daughter plate was prepared, the final assay plate (Figure 6) was generated using the protocol described in section 8.1.3. The intermediate daughter plates containing enzyme, inhibitor, and PIMtide, were dispensed to the final assay plate, per duplicate. Inmediately, the ATP intermediate plate was dispensed into the assay plate, and the reaction was incubated during 60 minutes at 30 °C. The detection system was carried out using protocol 1.3.4.

	DR experiment 384 well plate																							
	1	2	3	4	5	6	7	8	9	10	11	12	13	14	15	16	17	18	19	20	21	22	23	24
A	Standard ETP39010 (1µM; 1/3 serial dilutions)		Standard ETP39010 (1µM; 1/3 serial dilutions)		inh (25 µM)		inh (8,3 µM)		inh (2,7 µM)		inh (0,9 µM)		inh (0,4 µM)		inh (0,1 µM)		inh (0,03 µM)		inh (0,01 µM)		inh (0,004 µM)		Postive control	
B					inh (25 µM)		inh (8,3 µM)		inh (2,7 µM)		inh (0,9 µM)		inh (0,4 µM)		inh (0,1 µM)		inh (0,03 µM)		inh (0,01 µM)		inh (0,004 µM)			
C					inh (25 µM)		inh (8,3 µM)		inh (2,7 µM)		inh (0,9 µM)		inh (0,4 µM)		inh (0,1 µM)		inh (0,03 µM)		inh (0,01 µM)		inh (0,004 µM)			
D					inh (25 µM)		inh (8,3 µM)		inh (2,7 µM)		inh (0,9 µM)		inh (0,4 µM)		inh (0,1 µM)		inh (0,03 µM)		inh (0,01 µM)		inh (0,004 µM)			
E					inh (25 µM)		inh (8,3 µM)		inh (2,7 µM)		inh (0,9 µM)		inh (0,4 µM)		inh (0,1 µM)		inh (0,03 µM)		inh (0,01 µM)		inh (0,004 µM)			
F					inh (25 µM)		inh (8,3 µM)		inh (2,7 µM)		inh (0,9 µM)		inh (0,4 µM)		inh (0,1 µM)		inh (0,03 µM)		inh (0,01 µM)		inh (0,004 µM)			
G					inh (25 µM)		inh (8,3 µM)		inh (2,7 µM)		inh (0,9 µM)		inh (0,4 µM)		inh (0,1 µM)		inh (0,03 µM)		inh (0,01 µM)		inh (0,004 µM)			
H					inh (25 µM)		inh (8,3 µM)		inh (2,7 µM)		inh (0,9 µM)		inh (0,4 µM)		inh (0,1 µM)		inh (0,03 µM)		inh (0,01 µM)		inh (0,004 µM)			
I					inh (25 µM)		inh (8,3 µM)		inh (2,7 µM)		inh (0,9 µM)		inh (0,4 µM)		inh (0,1 µM)		inh (0,03 µM)		inh (0,01 µM)		inh (0,004 µM)		Negative control	
J					inh (25 µM)		inh (8,3 µM)		inh (2,7 µM)		inh (0,9 µM)		inh (0,4 µM)		inh (0,1 µM)		inh (0,03 µM)		inh (0,01 µM)		inh (0,004 µM)			
K					inh (25 µM)		inh (8,3 µM)		inh (2,7 µM)		inh (0,9 µM)		inh (0,4 µM)		inh (0,1 µM)		inh (0,03 µM)		inh (0,01 µM)		inh (0,004 µM)			
L					inh (25 µM)		inh (8,3 µM)		inh (2,7 µM)		inh (0,9 µM)		inh (0,4 µM)		inh (0,1 µM)		inh (0,03 µM)		inh (0,01 µM)		inh (0,004 µM)			
M					inh (25 µM)		inh (8,3 µM)		inh (2,7 µM)		inh (0,9 µM)		inh (0,4 µM)		inh (0,1 µM)		inh (0,03 µM)		inh (0,01 µM)		inh (0,004 µM)			
N					inh (25 µM)		inh (8,3 µM)		inh (2,7 µM)		inh (0,9 µM)		inh (0,4 µM)		inh (0,1 µM)		inh (0,03 µM)		inh (0,01 µM)		inh (0,004 µM)			
O					inh (25 µM)		inh (8,3 µM)		inh (2,7 µM)		inh (0,9 µM)		inh (0,4 µM)		inh (0,1 µM)		inh (0,03 µM)		inh (0,01 µM)		inh (0,004 µM)			
P					inh (25 µM)		inh (8,3 µM)		inh (2,7 µM)		inh (0,9 µM)		inh (0,4 µM)		inh (0,1 µM)		inh (0,03 µM)		inh (0,01 µM)		inh (0,004 µM)			

***Figure 6**: 384 well plate ADP Hunter assay containing 16 inhibitors at nine different concentrations for a dose-response experiment for PIM-1 and PIM-3.*

Data acquisition

The assay plate was read using conditions described in 8.1.4. The IC_{50} value for each inhibitor was calculated using the relative fluorescence units (RFU) data obtained from EnVision lector.

After calculation of % inhibition for each concentration, the values were fitted in a four parameter logistic model or sigmoidal dose-response curve using Activitybase software, and the IC_{50} was obtained.

8.2. pBAD in cell Elisa general protocol

Cell culture

H1299 cells obtained from ATCC were cultivated in Dulbecco's modified Eagle's medium (DMEM, Gibco), supplemented with 10% fetal bovine serum (FBS, Sigma Aldrich), antibiotics and antimycotics in a humidified incubator at 37 °C with 5% CO_2.

Culture conditions and cell line conservation

H1299 cells were grown in DMEM culture medium supplemented with glutamine (Sigma), 10% FBS (Sigma), 40U/mL penicillin, 40 U/mL streptomycin and 1 µg/mL fungizone (Gibco/Invitrogen). The cells were grown in 10 cm diameter plates and splitted when

confluent monolayer of cells was observed under inverted microscope. After passing the cells to a new culture dish, they were incubated at 37 °C with 5 % CO_2 atmosphere for 3-4 days until the plate was confluent again. All work was carried out in a flow-hood (Bio-II-A, Telstar). The cells that were not needed in culture were stored in liquid nitrogen to conserve the cell line. The cells used in the incell ELISA assay were detached from the plate, transfered to a 115 mL conical tube and centrifuge for 1200 rpm. The pellet was diluted in 90 % FCS / 10 % DMSO.

Protocol

20.000 cells/well were seeded in a 96 well plate (Becton Dickinson, 354651) using a multidrop dispenser (Thermo Electron Corporation), to a final volume of 200 µL per well in DMEM/10 % FBS. The cells were allowed to attach for 24 hours at 37 °C with 5% CO_2. The inhibitors were prepared in an intermediate 96 well-plate (Costar 3797) using ½ serial dilutions starting at 1 mM for each inhibitor. 2 µL from each of the wells from the intermediate inhibitors plate (containing the control compound ETP-00047879 from CNIO) were added using the automatic robot Biomek FX Dual Span 8 to the 96 well-plate containing the cells and incubated in 0.1% FBS, during 3.5 hours at 37 °C with 5% CO_2 (Figure 7). The culture medium was aspirated and the cells were washed twice with phosphate buffered saline (PBS, Biowhittaker) and fixed using 5% paraformaldehyde solution for 30 minutes at room temperature. After aspiration of formaldehyde, fixed cells were permebealized using PBS/0.1% Triton X-100 (Roche) with a volume of 100 µL for every well. The permeabilisation solution was aspirated and PBST/0.6% H_2O_2 (100 µL, Sigma) was added to every well and left shaking during 15 minutes at room temperature to block the endogenous peroxidase activity.

	Control	Control	10 µM	5 µM	2,5 µM	1,25 µM	0,625 µM	0,31 µM	0,16 µM	0,078 µM	0,039 µM	Control
A			Inhibitor 1									
B			Inhibitor 1									
C			Inhibitor 2									
D			Inhibitor 2									
E			Inhibitor 3									
F			Inhibitor 3									
G			Inhibitor 4									
H			Inhibitor 4									

***Figure 7**: 96-well plate example in cell ELISA protocol, containing inhibitors, control ETP-00047879, and cells.*

The quenching solution was aspired and the cells were washed twice using PBST (100 µL). The cells were blocked using 5% BSA (Sigma Aldrich) in PBST during 1 hour at room temperature and immediately washed twice with PBST. Primary antibody-pBAD Ser112 (100 µL, 1/1000 in PBST + 2.5% BSA) commercially available from Cell signalling (9291S) was added to every well and the plate was incubated overnight at 4 °C. After incubation, the cells were washed three times with PBST. 30 µL of peroxidase-conjugated anti-rabbit HRP antibody Amersham 3619 (1/2000 in PBST + 2.5% BSA) were added and the cells incubated during one hour at room temperature. The cells were washed three with PBST and twice eith PBS. 100 µL of supersignal ELISA Femto (Pierce) was added and the cells were shaken for two minutes. After that time, the plate was read using Victor (PerkinElmer) and the data collected and fitted into a four parameter logistic model or sigmoidal dose-response curve using Activitybase and GraphPad softwares to obtaine the effective concentration values, EC_{50}, for each inhibitor.

8.3. Kinetic aqueous solubility assay and PAMPA

The kinetic solubility assay was carried out using LC-MS/MS (Agilent 1100 triple quadrupole API2000) and vacuum manifold (186001831, Waters). The materials and reagents needed were 96 well assay plate from Multiscreen HTS Millipore, Nunc™ DeepWell plates from Thermoscientific, 96-well sample collection plate (002481, Waters), PBS, and DMSO (Sigma Aldrich).

The PAMPA assay was carried out using LC-MS/MS (Agilent 1100 coupled to an API2000 triple quadrupole) and mass spectrometry methods are specifically developed for each new compound in order to detect and quantify it in biological samples.

Different methods are available for sample clean up in order to achieve the lowest limit of quantification. FDA guidelines are followed to ensure the quality of the methods developed.

In vitro studies of plasma protein binding by ultrafiltration, as well as degree of partition between red blood cells and plasma are set up for using when necessary. BD Genetest™ plates were used to carry out the PAMPA assay.

8.3.1. General protocol for solubility and PAMPA

Solubility assay

The compounds were initially stored in a 10 mM stock solution in 100% DMSO. Using the stock solution, dilutions were prepared to 0.05 mM, 0.1 mM, 0.5 mM, 1 mM, 5 mM, and 10 mM in Nunc plates (24994, Thermoscientific). 10 µL of each concentration were transferred to Nunc™ DeepWell plates and diluted with 990 µL (1:100 dilution) of PBS, pH 7.4 (2% DMSO final).

The plate was incubated at room temperature during 1.5 hour with vigorous shaking. The assay plate (multiscreen HTS solubility filter plate) was filtered under vacuum (10 mmHg) using Manifold to eliminate any non-soluble particles before LC-MS/MS injection. 50 µL from each well was transferred to a 96-well plate (002481, Waters) and diluted with 150 µL of acetonitrile/0.1% formic acid. The plate was shaken and 5 µL of each sample was injected to the LC-MS/MS (gradient 5–95 acetonitrile/water + 0.1% formic acid) with an eluent flow rate of 5 mL/min. For each compound, its solubility was quantified through individual standard peak area calibration at a known concentration. The control compound generally used is Rapamycin, a poor water soluble investigational immunosuppressive drug.

PAMPA procedure

Using the data from the kinetic aqueous solubility assay, the concentrations at which each compound showed highest solubility are used to carry out the PAMPA assay. 300 µL of each solution prepared in section 9.3.1 (concentration previously selected for every compound depending on solubility) was transferred to every well into the multiwell receiver plate from the BD Genetest™ well plate, and 200 µL of PBS was added to every well from the multiwell donor plate. The plates were mounted and incubated during 5 hours. 100 µL from the each well were transfer to 96 well collection plate (002481, Waters) and analysed by LC-MS/MS ((gradient 5–95 acetonitrile/water + 0.1% formic acid) with an eluent flow rate of 5 mL/min.)

The data was analysed using the formula shown below:

$$P_e = \frac{-\ln[1 - C_A / C_{equilibrium}]}{S * (1/V_D + 1/V_A) * t}$$

Where C_A (t) is the compound concentration in acceptor well at time t, C_D (t) is the compound concentration in donor well at time t, $C_{equilibrium}$ (t) = [C_D (t)*V_D + C_A (t)* V_A]/(V_D+V_A), V_D =

donor well volume (0.3 mL), V_A = acceptor well volume (0.2 mL), A = membrane area (0.3 cm^2), and t is the incubation time.

Using the BD Genetest™ criteria used for the determination of the permeability of a drug candidate. A compound is considered to have low permeability if the value obtained is lower that 1.5 x 10^{-6} cm/s, on the other hand, a higher value than 1.5 x 10^{-6} cm/s would indicate a highly permeable compound.

8.4. Tm-Shift assay

Thermal melting experiments were carried out using a Stratagene Mx3005p Real Time PCR machine (Agilent Technologies). Proteins were buffered in 10 mM HEPES, pH 7.5, 500 mM NaCl and assayed in a 96-well plate at a final concentration of 2 μM in a 20-μl volume. Compounds were added at a final concentration of 12.5 μM (final DMSO concentration was 0.02%). SYPRO Orange (Molecular Probes) was added as a fluorescence probe at a dilution of 1:1,000 (v/v). Excitation and emission filters for the SYPRO-Orange dye were set to 465 nm and 590 nm, respectively. The temperature was raised with a step of 3 °C per minute from 25 °C to 96 °C, and fluorescence readings were taken at each interval. The observed temperature shifts, ΔTm^{obs}, were recorded as the difference between the transition midpoints of sample and reference wells containing protein without ligand in the same plate and determined by non-linear least squares fit. Experiments were performed in triplicate and data were analysed as previously described (Fedorov *et al*., 2012).

8.5. Isothermal Titration Calorimetry (ITC)

Experiments were carried out on a VP-ITC micro-calorimeter (MicroCal™, LLC Northampton, MA). All experiments were performed at 25 °C, while stirring at 286 rpm, in 20 mM HEPES pH 7.5, 200 mM NaCl, 0.5 mM tris (2-carboxyethyl) phosphine (TCEP) [ITC buffer]. PIM3 protein solution was buffer exchanged by dialysis into the ITC buffer. Titration was performed by injecting the protein (300 μM) into a reaction cell containing 2ml of compound solution (30 μM). All injections were performed using an initial injection of 2 μl followed by 34 injections of 8 μl with a duration of 16 sec per injection and a spacing of 240 sec between injections. Integrated heat of the titrations after correction for the heat of dilution were analysed using the MicroCal ORIGIN software package. The first data point was excluded from the analysis. The corrected data were fitted to a single binding site model using

a nonlinear least-square minimization algorithm, and the thermodynamic binding parameters were calculated ($\Delta G = \Delta H - T\Delta S = -RT\ln K_B$, where ΔG, ΔH and ΔS are the changes in free energy, enthalpy and entropy of binding, respectively).

8.6. Crystallization

PIM1 (aa 1-312) was used for co-crystallization with its consensus peptide PIMtide (ARKRRRHPSGPPTA-amide) and selected compounds. Protein was buffer exchanged into 50 mM HEPES, pH 7.5, 300 mM NaCl, 0.5 mM TCEP and concentrated up to 10 mg/ml. The protein was incubated with 1 mM of each ligand at 4 °C, 1 h and set up for crystallization using a mosquito® crystallization robot (TTP Labtech). Coarse screens were typically set up onto Greiner 3-well plates using three different drop ratios of precipitant to protein per condition (100+50 nl, 75+75 nl and 50+100 nl). All crystallizations were carried out using the sitting-drop vapour diffusion method at 4 °C. In order to improve the first crystals obtained with the coarse screens, a specialized screen was designed around the initial crystallization conditions (increasing the volume in the drop ratios of precipitant to protein/condition (100+200 nl, 150+150 nl and 200+100 nl) and finally all co-crystals were obtained using the reservoir solutions containing 10 % PEG3350, 0.1 M bis-tris pH 6.2, 0.1 M potassium thiocyanate and 5% EDO.

8.7. Preparation and characterization of 102-111

General Procedure A: Suzuki-Miyaura cross-coupling

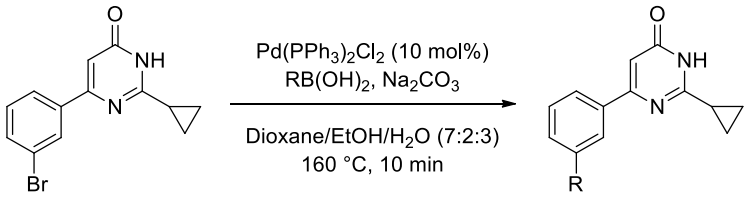

A microwave vial was charged with a mixture of 6-(3-bromophenyl)-2-cyclopropylpyrimidin-4(3*H*)-one (1.0 eq.), $Pd(PPh_3)_2Cl_2$ (0.1 eq.) and the corresponding boronic acid (1.3 eq.) in dioxane/EtOH/H_2O (7:2:3) (0.04 M) and an aqueous solution of sodium carbonate (Na_2CO_3) (1.0 M). The vial was then sealed and placed under an inert atmosphere. The reaction mixture was heated for 10 min in a Biotage microwave reactor at 160 °C. The reaction mixture was allowed to cool to room temperature before being filtered through Celite® to remove any

insoluble Pd species and washed with dichloromethane (DCM), followed by an aqueous work-up. Analogues were purified by different methods depending on their solubility, to afford the desired compound.

General Procedure B: Buchwald-Hartwig amination

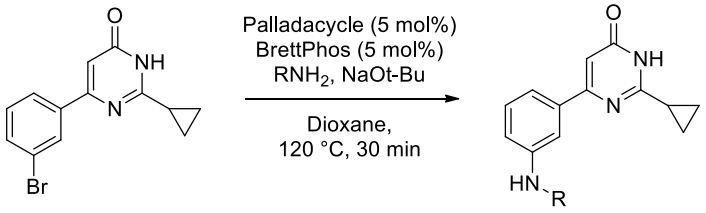

A solution of 6-(3-bromophenyl)-2-cyclopropylpyrimidin-4(3*H*)-one (1.0 eq.), methanesulfonato(2-dicyclohexylphosphino-3,6-dimethoxy-2',4',6'-tri-i-propyl-1,1'- biphenyl) (2'-amino-1,1'-biphenyl-2-yl)palladium(II) (BrettPhos palladacycle) (0.05 eq.), BrettPhos (0.05 eq.), sodium *tert*-butoxide (NaO*t*-Bu) (1.5 eq.) and the corresponding primary amine (1.2 eq.) in 1,4-dioxane (0.2 M) was added to a microwave vial which flushed with N_2 and sealed. The reaction mixture was irradiated for 30 min in a Biotage microwave instrument at 120 °C. The sample was allowed to cool to room temperature before being filtered through Celite® to remove any insoluble Pd species and washed with DCM. The mixture was then concentrated under reduced pressure. Analogues were purified by different methods depending on their solubility, to afford the desired compound.

2-Cyclopropyl-6-(4'-hydroxy-[1,1'-biphenyl]-3-yl)pyrimidin-4(3*H*)-one (102)

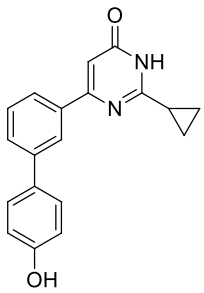

Following General Procedure A, a mixture of intermediate **87** (150 mg, 0.51 mmol), (4-hydroxyphenyl) boronic acid (91 mg, 0.66 mmol), $Pd(PPh_3)_2Cl_2$ (35 mg, 0.05 mmol), 1 M Na_2CO_3 aqueous solution (1.0 mL) and 1,4-dioxane/EtOH/H_2O (7:2:3) (0.04 M, 11.6 mL) was heated to 160 °C for 10 min. The reaction mixture was allowed to cool to room temperature before being filtered through Celite® and the cake was rinsed with DCM (10 mL). Water was

added to the filtrate and the layers were partitioned. The aqueous layer was extracted with DCM (2 × 10 mL) and the combined organic extracts were washed with aq. $NaHCO_3$ (10 mL) and brine (10 mL). The organic extracts were dried over $MgSO_4$ before being filtered and concentrated under reduced pressure. The compound was triturated with methanol (MeOH) (20 mL) to afford the title compound as an off-white solid (90 mg, 0.30 mmol, 57%) **M.pt** 246-248 °C; **IR** (ATR)/cm^{-1} 3201(br), 3062, 2789, 1651, 1602, 1516; **^{1}H NMR** (500 MHz, DMSO-*d_6)* δ (ppm) 12.67 (bs, 1H, CON*H*), 9.58 (bs, 1H, O*H*), 8.12 (s, 1H, Ar*H*), 7.88 (d, *J* 7.5 Hz, 1H, Ar*H*), 7.66 (d, *J* 7.5 Hz, 1H, Ar*H*), 7.56 (d, *J* 8.5 Hz, 2H, 2 × Ar*H*), 7.48 (at, *J* 7.5 Hz, 1H, Ar*H*), 6.87 (d, *J* 8.5 Hz, 2H, 2 × Ar*H*) 6.75 (s, 1H, C=C*H*CONH), 2.04-1.95 (m, 1H, -C*H*), 1.22-1.13 (m, 2H, 2 × C*H*), 1.12-1.04 (m, 2H, 2 × C*H*); **^{13}C NMR** (125 MHz, DMSO-*d_6*) δ (ppm) 163.6, 162.7, 160.6, 157.2, 140.4, 136.9, 130.4, 128.9, 127.8, 124.7, 124.1, 115.6, 105.6, 13.4, 9.8 (4 C missing); **LRMS** (ES + APCI) *m/z*: calc. for $C_{19}H_{16}N_2O_2$ 304.31, found 305.1 $[M+H]^+$; **HMRS** (ESI, +ve) *m/z*: calc. for $C_{19}H_{16}N_2O_2$ 305.1285 $[M+H]^+$, found 305.1286 $[M+H]^+$.

2-Cyclopropyl-6-(4'-fluoro-[1,1'-biphenyl]-3-yl)pyrimidin-4(3*H*)-one (103)

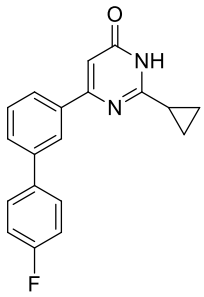

Following General Procedure A, a mixture of intermediate **87** (150 mg, 0.51 mmol), (4-fluorophenyl) boronic acid (92 mg, 0.65 mmol), $Pd(PPh_3)_2Cl_2$ (35 mg, 0.05 mmol), 1M Na_2CO_3 aqueous solution (1.0 mL) and 1,4-dioxane/EtOH/H_2O (7:2:3) (0.04 M, 11.6 mL) was heated to 160 °C for 10 min. The reaction mixture was allowed to cool to room temperature before being filtered through Celite® and the cake was rinsed with DCM (10 mL). Water was added to the filtrate and the layers were partitioned. The aqueous layer was extracted with DCM (2 × 10 mL) and the combined organic extracts were washed with aq. $NaHCO_3$ (10 mL) and brine (10 mL). The organic extracts were dried over $MgSO_4$ before being filtered and concentrated under reduced pressure. Further purification *via* flash column chromatography (dry loading EtOAc/PET 2:1 isocratic) afforded the title compound as an off-white solid (40 mg, 0.13 mmol, 25%) **M.pt** 236-239 °C; **IR** (ATR)/cm^{-1} 3062, 2783, 1666, 1597; **^{1}H NMR** (500 MHz, $CDCl_3$) δ (ppm) 13.78 (bs, 1H, CON*H*), 8.14 (at, *J* 2.2 Hz, 1H, Ar*H*), 7.94 (dt, *J* 8.0, 2.0 Hz, 1H, Ar*H*), 7.64 (dt, *J* 8.0, 2.0 Hz, 1H, Ar*H*), 7.61-7.57 (m, 2H, 2 × Ar*H*) 7.53 (at, *J* 8.0 Hz, 1H, Ar*H*), 7.20-7.15 (m, 2H, 2 × Ar*H*), 6.79 (s, 1H, C=C*H*CONH), 2.10-2.04 (m, 1H, -C*H*), 1.42-1.37 (m, 2H, 2 × C*H*), 1.21-1.16 (m, 2H, 2 × C*H*); **^{13}C NMR** (125 MHz, $CDCl_3$) δ (ppm) 166.2, 164.1, 163.5, 161.4, 140.6, 137.2, 136.8, 129.2, 129.1, 128.7, 128.6, 125.9, 125.7, 115.7, 115.6, 105.6, 14.5, 10.7 (1 C missing); **LRMS** (ES + APCI) *m/z*: calc. for $C_{19}H_{15}FN_2O$ 306.32, found 307.2 $[M+H]^+$; **HMRS** (ESI, +ve) *m/z*: calc. for $C_{19}H_{15}FN_2O$ 307.1241 $[M+H]^+$, found 307.1243 $[M+H]^+$.

2-Cyclopropyl-6-(3'-fluoro-[1,1'-biphenyl]-3-yl)pyrimidin-4(3*H*)-one (104)

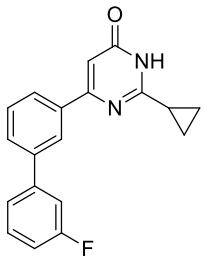

Following General Procedure A, a mixture of intermediate **87** (150 mg, 0.51 mmol), (4-fluorophenyl) boronic acid (92 mg, 0.65 mmol), $Pd(PPh_3)_2Cl_2$ (35 mg, 0.05 mmol), 1M Na_2CO_3 aqueous solution (1.0 mL) and 1,4-dioxane/EtOH/H_2O (7:2:3) (0.04 M, 11.6 mL) was heated to 160 °C for 10 min. The reaction mixture was allowed to cool to room temperature before being filtered through Celite® and the cake was rinsed with DCM (10 mL). Water was added to the filtrate and the layers were partitioned. The aqueous layer was extracted with DCM (2 × 10 mL) and the combined organic extracts were washed with aq. $NaHCO_3$ (10 mL) and brine (10 mL). The organic extracts were dried over $MgSO_4$ before being filtered and concentrated under reduced pressure. Crude product was initially purified *via* flash column chromatography (dry loading EtOAc/PET 2:1 isocratic). Further purification by reverse phase chromatography (H_2O 0.1% HCOOH/MeCN 0.1% HCOOH 95:5 to 0:100) afforded the title compound as an off-white solid (35 mg, 0.11 mmol, 22%) **M.pt** 242-245 °C; **IR** (ATR)/cm^{-1} 3057, 2781, 1656, 1598; **^{1}H NMR** (400 MHz, DMSO-*d_6)* δ (ppm) 12.62 (bs, 1H, CON*H*), 8.23 (at, *J* 1.6 Hz, 1H, Ar*H*), 8.01 (dt, *J* 8.0, 1.6 Hz, 1H, Ar*H*), 7.79 (dt, *J* 7.6, 1.6 Hz, 1H, Ar*H*), 7.65-7.48 (m, 4H, 4 × Ar*H*) 7.22 (td, *J* 8.0, 2.0 Hz, 1H, Ar*H*), 6.83 (s, 1H, C=C*H*CONH), 2.03-1.94 (m, 1H, -C*H*), 1.19-1.13 (m, 2H, 2 × C*H*), 1.10-1.03 (m, 2H, 2 × C*H*); **^{13}C NMR** (101 MHz, DMSO-*d_6*) δ (ppm) 163.7, 161.2, 160.1, 142.0, 138.9 137.1, 130.6, 129.1, 128.5, 126.3, 124.8, 122.7, 114.2, 113.5, 113.3, 106.2 13.3, 9.7 (1 C missing); **LRMS** (ES + APCI) *m/z*: calc. for $C_{19}H_{15}FN_2O$ 306.35, found 307.1 $[M+H]^+$; **HMRS** (ESI, +ve) *m/z*: calc. for $C_{19}H_{15}FN_2O$ 307.1241 $[M+H]^+$, found 307.1243 $[M+H]^+$.

6-(4'-Chloro-[1,1'-biphenyl]-3-yl)-2-cyclopropylpyrimidin-4(3*H*)-one (105)

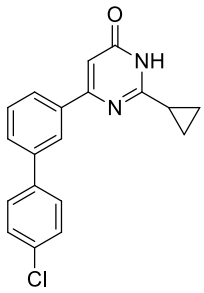

Following General Procedure A, a mixture of intermediate **87** (150 mg, 0.51 mmol), (4-chlorophenyl) boronic acid (104 mg, 0.66 mmol), $Pd(PPh_3)_2Cl_2$ (35 mg, 0.05 mmol), 1M Na_2CO_3 aqueous solution (1.0 mL) and 1,4-dioxane/EtOH/H_2O (7:2:3) (0.04 M, 11.6 mL) was heated to 160 °C for 10 min. The reaction mixture was allowed to cool to room temperature before being filtered through Celite® and the cake was rinsed with DCM (10 mL). Water was added to the filtrate and the layers were partitioned. The aqueous layer was extracted with DCM (2 × 10 mL) and the combined organic extracts were washed with aq. $NaHCO_3$ (10 mL) and brine (10 mL). The organic extracts were dried over $MgSO_4$ before being filtered and concentrated under reduced pressure. The compound was triturated with methanol (20 mL) to afford the title compound as an off-white solid (42 mg, 0.13 mmol, 25%) **M.pt** 247-249 °C; **IR** (ATR)/cm^{-1} 3070, 2779, 1668, 1601, 1478; **^{1}H NMR** (400 MHz, DMSO-*d_6*) δ (ppm) 12.67 (bs, 1H, CON*H*), 8.23 (at, *J* 1.6 Hz, 1H, Ar*H*), 8.00 (dt, *J* 7.6, 1.6 Hz, 1H, Ar*H*), 7.81-7.73 (m, 3H, 3 × Ar*H*), 7.59-7.51 (m, 3H, 3 × Ar*H*) 6.81 (s, 1H, C=C*H*CONH), 2.05-1.95 (m, 1H, -C*H*), 1.21-1.14 (m, 2H, 2 × C*H*), 1.12-1.05 (m, 2H, 2 × C*H*); **^{13}C NMR** (101 MHz, DMSO-*d_6*) δ (ppm) 163.9, 162.8, 160.4, 139.2, 138.6 137.3, 132.6, 129.3, 128.9, 128.6, 128.5, 126.3, 124.9, 106.4 13.5, 9.9 (3 C missing); **LRMS** (ES + APCI) *m/z*: calc. for $C_{19}H_{15}{}^{35}ClN_2O$ 322.79, found 323.3 $[M+H]^+$; **HMRS** (ESI, +ve) *m/z*: calc. for $C_{19}H_{15}{}^{35}ClN_2O$ 323.0946 $[M+H]^+$, found 323.0947 $[M+H]^+$.

2-cyclopropyl-6-(4'-nitro-[1,1'-biphenyl]-3-yl)pyrimidin-4(3*H*)-one (106)

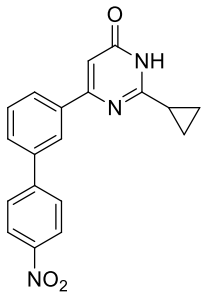

Following General Procedure A, a mixture of intermediate **87** (150 mg, 0.51 mmol), (4-nitrophenyl) boronic acid (111 mg, 0.66 mmol), $Pd(PPh_3)_2Cl_2$ (35 mg, 0.05 mmol), 1M Na_2CO_3 aqueous solution (1.0 mL) and 1,4-dioxane/EtOH/H_2O (7:2:3) (0.04 M, 11.6 mL) was heated to 160 °C for 10 min. The reaction mixture was allowed to cool to room temperature before being filtered through Celite® and the cake was rinsed with DCM (10 mL). The filtrate was concentrated under reduced pressure. Crude product was initially purified *via* flash column chromatography (dry loading EtOAc/PET 2:1 isocratic). Further purification by reverse phase chromatography (H_2O 0.1% HCOOH/MeCN 0.1% HCOOH 95:5 to 0:100) afforded the title compound as an off-white solid (40 mg, 0.12 mmol, 23%) **M.pt** 255-257 °C; **IR** (ATR)/cm^{-1} 3073, 2902, 1662, 1593, 1509, 1478, 1409, 1348; **^{1}H NMR** (400 MHz, DMSO-*d_6)* δ (ppm) 12.69 (bs, 1H, CON*H*), 8.35-8.28 (m, 3H, 3 × Ar*H*), 8.11-8.01 (m, 3H, 3 × Ar*H*), 7.87 (d, *J* 7.6 Hz, 1H, Ar*H*), 7.61 (at, *J* 8.0 Hz, 1H, Ar*H*), 6.85 (s, 1H, C=C*H*CONH), 2.03-1.94 (m, 1H, -C*H*), 1.20-1.13 (m, 2H, 2 × C*H*), 1.11-1.04 (m, 2H, 2 × C*H*); **^{13}C NMR** (101 MHz, DMSO-*d_6*) δ (ppm) 164.0, 162.9, 160.2, 146.8, 146.2 138.2, 137.5, 129.6, 129.1, 128.1, 127.5, 125.5, 124.1, 106.6, 13.6, 10.0 (3 C missing); **LRMS** (ES + APCI) *m/z*: calc. for $C_{18}H_{15}N_3O$ 333.34, found 334.2 $[M+H]^+$; **HMRS** (ESI, +ve) *m/z*: calc. for $C_{19}H_{15}N_3O_3$ 334.1186 $[M+H]^+$, found 334.1188 $[M+H]^+$.

2-cyclopropyl-6-[3-(pyridin-3-yl)phenyl]pyrimidin-4(3*H*)-one (108)

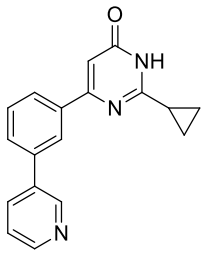

Following General Procedure A, a mixture of intermediate **87** (150 mg, 0.51 mmol), pyridin-3-yl boronic acid (82 mg, 0.66 mmol), $Pd(PPh_3)_2Cl_2$ (35 mg, 0.05 mmol), 1M Na_2CO_3 aqueous solution (1.0 mL) and 1,4-dioxane/EtOH/H_2O (7:2:3) (0.04 M, 11.6 mL) was heated to 160 °C for 10 min. The reaction mixture was allowed to cool to room temperature before being filtered through Celite® and the cake was rinsed with DCM (10 mL). Water was added to the filtrate and the layers were partitioned. The aqueous layer was extracted with DCM (2 × 10 mL) and the combined organic extracts were washed with aq. $NaHCO_3$ (10 mL) and brine (10 mL). The organic extracts were dried over $MgSO_4$ before being filtered and concentrated under reduced pressure. Crude product was initially purified *via* flash column chromatography (dry loading EtOAc/DCM 3:1 isocratic, DCM/MeOH 95:5 isocratic). Further purification by reverse phase chromatography (H_2O 0.1% HCOOH/MeCN 0.1% HCOOH 95:5 to 0:100) afforded the title compound as an off-white solid (83 mg, 0.29 mmol, 56%) **M.pt** 246-248 °C; **IR** (ATR)/cm^{-1} 3062, 2813, 1645, 1597, 1446; **^{1}H NMR** (400 MHz, DMSO-d_6) δ (ppm) 13.19 (bs, 1H, CON*H*), 9.47 (s, 1H, Ar*H*), 9.11 (d, *J* 3.6 Hz, 1H, Ar*H*), 8.77 (at, *J* 1.6 Hz, 1H, Ar*H*), 8.66 (dt, *J* 8.0, 2.0 Hz, 1H, Ar*H*), 8.55 (dt, *J* 8.0, 1.6 Hz, 1H, Ar*H*), 8.32 (dt, *J* 7.6, 1.6 Hz, 1H, Ar*H*), 8.09 (at, *J* 8.0 Hz, 1H, Ar*H*) 8.02 (dd, *J* 8.0, 4.8 Hz, 1H, Ar*H*) 7.34 (s, 1H, C=C*H*CONH), 2.55-2.45 (m, 1H, -C*H*), 1.71-1.65 (m, 2H, 2 × C*H*), 1.61-1.55 (m, 2H, 2 × C*H*); **^{13}C NMR** (101 MHz, DMSO-d_6) δ (ppm) 163.9, 162.9, 160.3, 148.7, 147.8 137.5, 135.2, 134.3, 129.4, 128.7, 126.6, 125.1, 123.8, 106.4, 13.5, 9.9 (2 C missing); **LRMS** (ES + APCI) *m/z*: calc. for $C_{18}H_{15}N_3O$ 289.33, found 290.1 $[M+H]^+$; **HMRS** (ESI, +ve) *m/z*: calc. for $C_{18}H_{15}N_3O$ 290.1288 $[M+H]^+$, found 290.1288 $[M+H]^+$.

2-cyclopropyl-6-[3-(pyridin-4-yl)phenyl]pyrimidin-4(3*H*)-one (107)

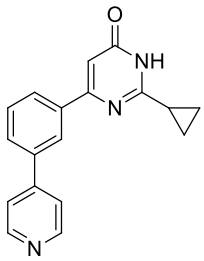

Following General Procedure A, a mixture of intermediate **87** (150 mg, 0.51 mmol), pyridine-4-boronic acid hydrate (93 mg, 0.66 mmol), $Pd(PPh_3)_2Cl_2$ (35 mg, 0.05 mmol), 1M Na_2CO_3 aqueous solution (1.0 mL) and 1,4-dioxane/EtOH/H_2O (7:2:3) (0.04 M, 11.6 mL) was heated to 160 °C for 10 min. The reaction mixture was allowed to cool to room temperature before being filtered through Celite® and the cake was rinsed with DCM (10 mL). The filtrate was concentrated under reduced pressure. Crude product was initially purified *via* flash column chromatography (dry loading EtOAc/DCM 3:1 isocratic, DCM/MeOH 95:5 isocratic) to afford the title compound as an off-white solid (96 mg, 0.33 mmol, 64%) **M.pt** 254-256 °C; **IR** (ATR)/cm^{-1} 3060, 2818, 1647, 1595, 1446; **^{1}H NMR** (400 MHz, DMSO-d_6) δ (ppm) 12.72 (bs, 1H, CON*H*), 8.67 (d, *J* 6.4 Hz, 2H, 2 × Ar*H*), 8.33 (at, *J* 1.6 Hz, 1H, Ar*H*), 8.09 (dt, *J* 7.6, 1.6 Hz, 1H, Ar*H*), 7.89 (dt, *J* 8.0, 2.0 Hz, 1H, Ar*H*), 7.80 (d, *J* 6.4 Hz, 2H, 2 × Ar*H*), 7.61 (at, *J* 8.0 Hz, 1H, Ar*H*), 6.86 (s, 1H, C=C*H*CONH), 2.03-1.94 (m, 1H, -C*H*), 1.20-1.14 (m, 2H, 2 × C*H*), 1.11-1.04 (m, 2H, 2 × C*H*); **^{13}C NMR** (101 MHz, DMSO-d_6) δ (ppm) 163.6, 162.5, 159.8, 149.9, 146.2 137.2, 137.1, 129.2, 128.3, 127.3, 124.7, 121.0, 106.1, 13.2, 9.6 (3 C missing); **LRMS** (ES + APCI) *m/z*: calc. for $C_{18}H_{15}N_3O$ 289.33, found 290.2 $[M+H]^+$; **HMRS** (ESI, +ve) *m/z*: calc. for $C_{18}H_{15}N_3O$ 290.1288 $[M+H]^+$, found 290.1289 $[M+H]^+$.

2-cyclopropyl-6-[3-(pyridin-3-ylamino)phenyl]pyrimidin-4(3*H*)-one (109)

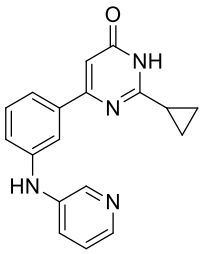

Following General Procedure B, a mixture of intermediate **87** (150 mg, 0.51 mmol), pyridin-3-amine (58 mg, 0.61 mmol), BrettPhos (14 mg, 0.03 mmol), BrettPhos palladacycle (23 mg, 0.03 mmol), NaO*t*-Bu (74 mg, 0.77 mmol) and 1,4-dioxane (0.2 M, 2.6 mL) was heated to 120 °C for 30 min. The reaction mixture was allowed to cool to room temperature before being filtered through Celite®. The cake was rinsed with DCM (10 mL) and the filtrate was concentrated under reduced pressure. Crude product was purified *via* flash column chromatography (dry loading EtOAc/DCM 3:1 isocratic, DCM/MeOH 95:5 isocratic) afforded the title compound as an off-white solid (83 mg, 0.27 mmol, 53%) **M.pt** 250-252 °C; **IR** (ATR)/cm^{-1} 3267, 3010, 2822, 1662, 1601, 1577, 1446; **^{1}H NMR** (400 MHz, DMSO-d_6) δ (ppm) 12.70 (bs, 1H, CON*H*), 8.54 (bs, 1H, N*H*), 8.39 (d, *J* 2.4 Hz, 1H, Ar*H*), 8.06 (dd, *J* 5.2, 1.2 Hz, 1H, Ar*H*), 7.74 (at, *J* 2.0 Hz, 1H, Ar*H*), 7.51 (ddd, *J* 8.0, 2.4, 1.6 Hz, 1H, Ar*H*), 7.45 (d, *J* 8.0 Hz, 1H, Ar*H*), 7.32 (at, *J* 8.0 Hz, 1H, Ar*H*), 7.25 (dd, *J* 8.4, 4.8 Hz, 1H, Ar*H*), 7.19 (dd, *J* 8.0, 1.6 Hz, 1H, Ar*H*), 6.57 (s, 1H, C=C*H*CONH), 2.00-1.92 (m, 1H, -C*H*), 1.14-1.09 (m, 2H, 2 × C*H*), 1.08-1.02 (m, 2H, 2 × C*H*); **^{13}C NMR** (101 MHz, DMSO-d_6) δ (ppm) 163.3, 162.4, 160.2, 142.5, 140.4 139.3, 139.0, 137.2, 129.2, 123.3, 122.2, 118.3, 118.0, 114.9, 105.4, 13.1, 9.4 (1 C missing); **LRMS** (ES + APCI) *m/z*: calc. for $C_{18}H_{16}N_4O$ 304.35, found 305.1 $[M+H]^+$; **HMRS** (ESI, +ve) *m/z*: calc. for $C_{18}H_{16}N_4O$ 305.1397 $[M+H]^+$, found 305.1398 $[M+H]^+$.

2-cyclopropyl-6-(3-(pyridin-4-ylamino)phenyl)pyrimidin-4(3H)-one (111)

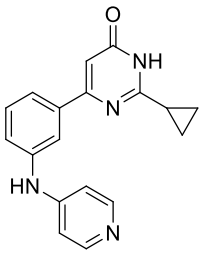

Following General Procedure B, a mixture of intermediate **87** (150 mg, 0.51 mmol), pyridin-3-amine (58 mg, 0.61 mmol), BrettPhos (26 mg, 0.05 mmol), BrettPhos palladacycle (46 mg, 0.05 mmol), NaO*t*-Bu (74 mg, 0.77 mmol) and 1,4-dioxane (0.2 M, 2.6 mL) was heated to 120 °C for 30 min. The reaction mixture was allowed to cool to room temperature before being filtered through Celite®. The cake was rinsed with DCM (10 mL) and the filtrate was concentrated under reduced pressure. Crude product was first purified *via* flash column chromatography (dry loading EtOAc/DCM 3:1 isocratic, DCM/MeOH 95:5 isocratic). Further purification by reverse phase chromatography (H_2O 0.1% HCOOH/MeCN 0.1% HCOOH 95:5 to 0:100) afforded the title compound as an off-white solid (35 mg, 0.11 mmol, 22%) **M.pt** 238-240 °C; **IR** (ATR)/cm^{-1} 3259, 3060, 2826, 1653, 1590, 1504; **^{1}H NMR** (400 MHz, DMSO-d_6) δ (ppm) 9.03 (bs, 1H, CON*H*), 8.33-8.09 (m, 3H, N*H*, 2 × Ar*H*), 7.82 (at, *J* 1.6 Hz, 1H, Ar*H*), 7.62 (d, *J* 7.6 Hz, 1H, Ar*H*), 7.41 (at, *J* 7.6 Hz, 1H, Ar*H*), 7.30 (d, *J* 7.2 Hz, 1H, Ar*H*), 7.02-6.91 (m, 2H, 2 × Ar*H*), 6.61 (s, 1H, C=C*H*CONH), 2.01-1.92 (m, 1H, -C*H*), 1.16-1.10 (m, 2H, 2 × C*H*), 1.09-1.02 (m, 2H, 2 × C*H*); **^{13}C NMR** (101 MHz, DMSO-d_6) δ (ppm) 163.8, 162.8, 160.2, 150.3, 149.4 140.6, 137.7, 129.6, 121.6, 120.9, 118.3, 109.5, 105.6, 13.5, 9.9 (3 C missing); **LRMS** (ES + APCI) *m/z*: calc. for $C_{18}H_{16}N_4O$ 304.35, found 305.1 $[M+H]^+$; **HMRS** (ESI, +ve) *m/z*: calc. for $C_{18}H_{16}N_4O$ 305.1397 $[M+H]^+$, found 305.1394 $[M+H]^+$.

2-cyclopropyl-6-(3-(pyridin-2-ylamino)phenyl)pyrimidin-4(3H)-one (110)

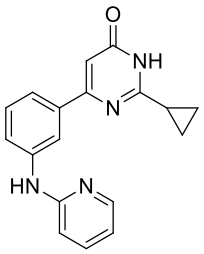

Following General Procedure B, a mixture of intermediate **87** (150 mg, 0.51 mmol), pyridin-3-amine (58 mg, 0.61 mmol), BrettPhos (26 mg, 0.05 mmol), BrettPhos palladacycle (46 mg, 0.05 mmol), NaO*t*-Bu (74 mg, 0.77 mmol) and 1,4-dioxane (0.2 M, 2.6 mL) was heated to 120 °C for 30 min. The reaction mixture was allowed to cool to room temperature before being filtered through Celite®. The cake was rinsed with DCM (10 mL) and the filtrate was concentrated under reduced pressure. Crude product was purified *via* flash column chromatography (dry loading EtOAc/DCM 3:1 isocratic, DCM/MeOH 95:5 isocratic) affording the title compound as an off-white solid (52 mg, 0.17 mmol, 33%) **M.pt** 232-234 °C; **IR** (ATR)/cm^{-1} ; **^{1}H NMR** (400 MHz, DMSO-*d*$_6$) δ (ppm) 12.63 (bs, 1H, CON*H*), 9.13 (bs, 1H, N*H*), 8.28 (at, *J* 2.0 Hz, 1H, Ar*H*), 8.17 (ddd, *J* 4.8, 1.6, 0.8 Hz, 1H, Ar*H*), 7.87 (ddd, *J* 8.4, 2.0, 0.8 Hz, 1H, Ar*H*), 7.58 (ddd, *J* 8.8, 7.2, 2.0 Hz, 1H, Ar*H*), 7.46 (dt, *J* 7.6, 1.6 Hz, 1H, Ar*H*), 7.32 (at, *J* 8.0 Hz, 1H, Ar*H*), 6.85 (dt, *J* 8.4, 1.2 Hz, 1H, Ar*H*) 6.76 (ddd, *J* 7.2, 5.2, 0.8 Hz, 1H, Ar*H*) 6.52 (s, 1H, C=C*H*CONH), 2.02-1.93 (m, 1H, -C*H*), 1.20-1.14 (m, 2H, 2 × C*H*), 1.11-1.04 (m, 2H, 2 × C*H*); **^{13}C NMR** (101 MHz, DMSO-*d*$_6$) δ (ppm) 163.6, 162.8, 161.1, 155.8, 147.2, 141.9, 137.3, 136.8, 128.8, 119.6, 118.7, 116.4, 114.5, 110.8, 105.6, 13.5, 9.8 (1 C missing); **LRMS** (ES + APCI) *m/z*: calc. for $C_{18}H_{16}N_4O$ 304.35, found 305.3 $[M+H]^+$; **HMRS** (ESI, +ve) *m/z*: calc. for $C_{18}H_{16}N_4O$ 305.1397 $[M+H]^+$, found 305.1397 $[M+H]^+$.

8.8. ^{1}H and ^{13}C spectra and LCMS data of final compounds

8-Chloro-2-((methylamino)methyl)benzo[4,5]thieno[3,2-*d*]pyrimidin-4(3*H*)-one (43a)

^{1}H NMR spectrum (400 MHz, DMSO)

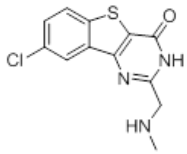

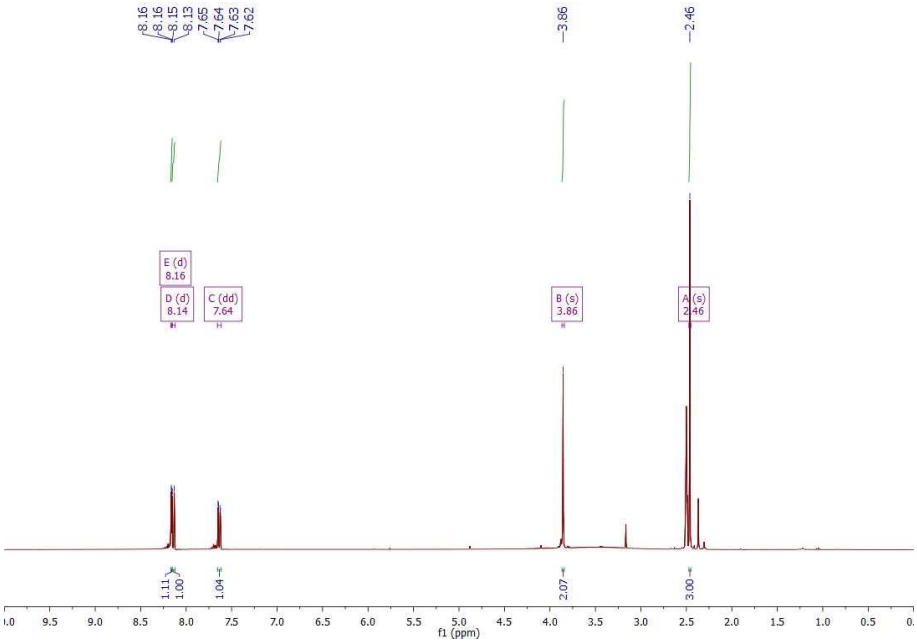

^{13}C NMR spectrum (101 MHz, DMSO)

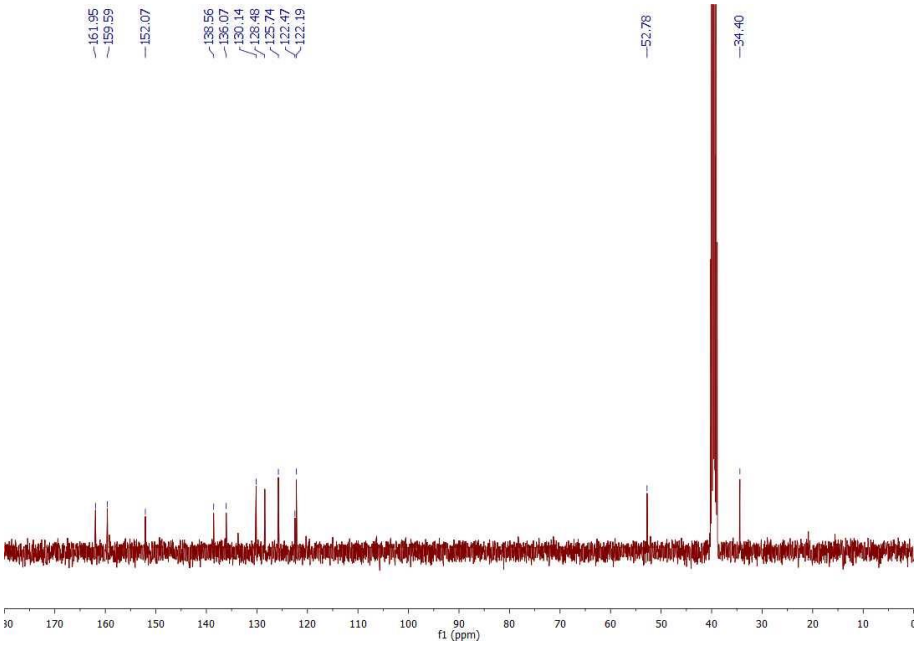

LC-MS (ES + APCI)

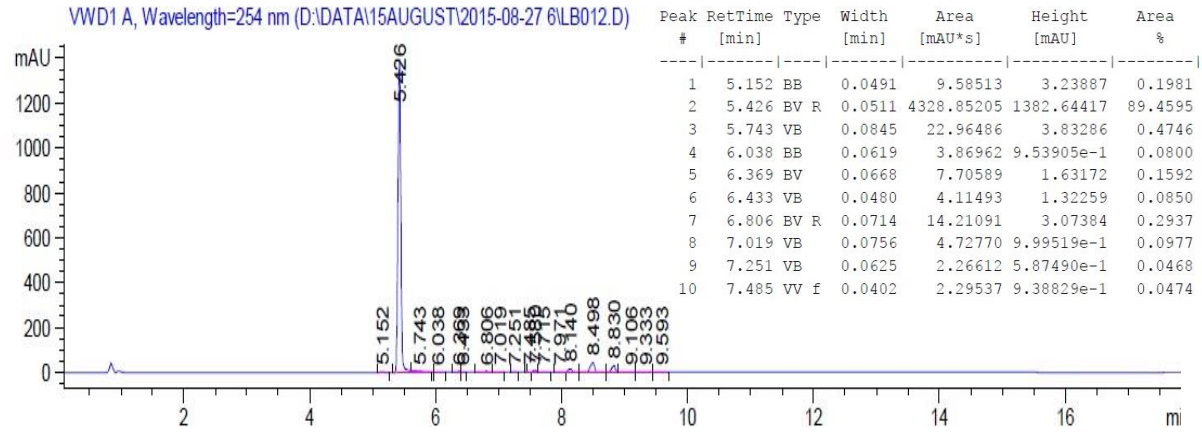

Peak #	RetTime [min]	Type	Width [min]	Area [mAU*s]	Height [mAU]	Area %
1	5.152	BB	0.0491	9.58513	3.23887	0.1981
2	5.426	BV R	0.0511	4328.85205	1382.64417	89.4595
3	5.743	VB	0.0845	22.96486	3.83286	0.4746
4	6.038	BB	0.0619	3.86962	9.53905e-1	0.0800
5	6.369	BV	0.0668	7.70589	1.63172	0.1592
6	6.433	VB	0.0480	4.11493	1.32259	0.0850
7	6.806	BV R	0.0714	14.21091	3.07384	0.2937
8	7.019	VB	0.0756	4.72770	9.99519e-1	0.0977
9	7.251	VB	0.0625	2.26612	5.87490e-1	0.0468
10	7.485	VV f	0.0402	2.29537	9.38829e-1	0.0474

8-Chloro-2-(morpholinomethyl)benzo[4,5]thieno[3,2-*d*]pyrimidin-4(3*H*)-one (43b)

^{1}H NMR spectrum (400 MHz, DMSO)

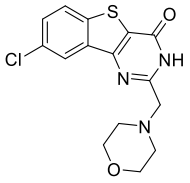

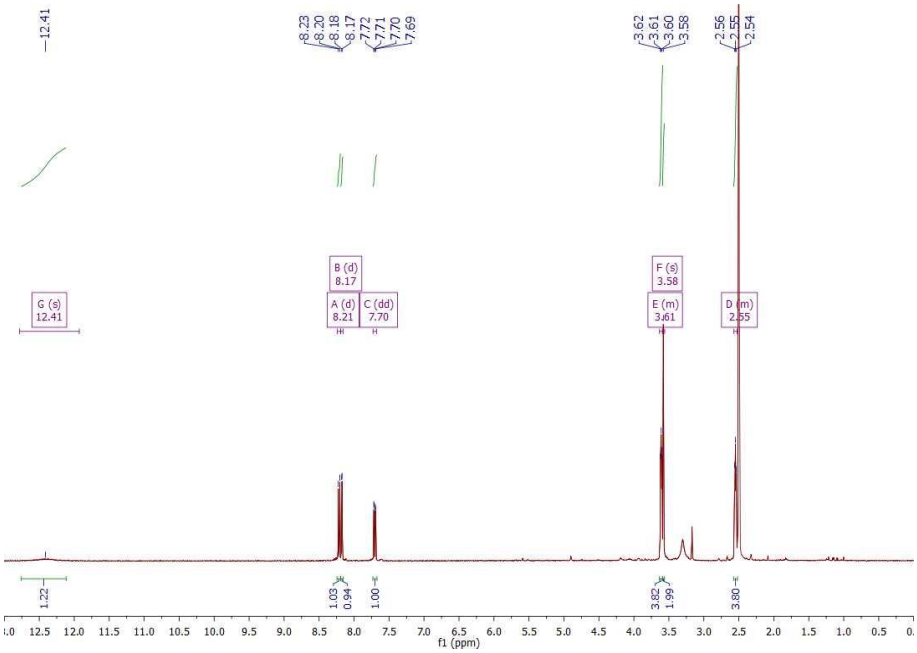

^{13}C NMR spectrum (101 MHz, DMSO)

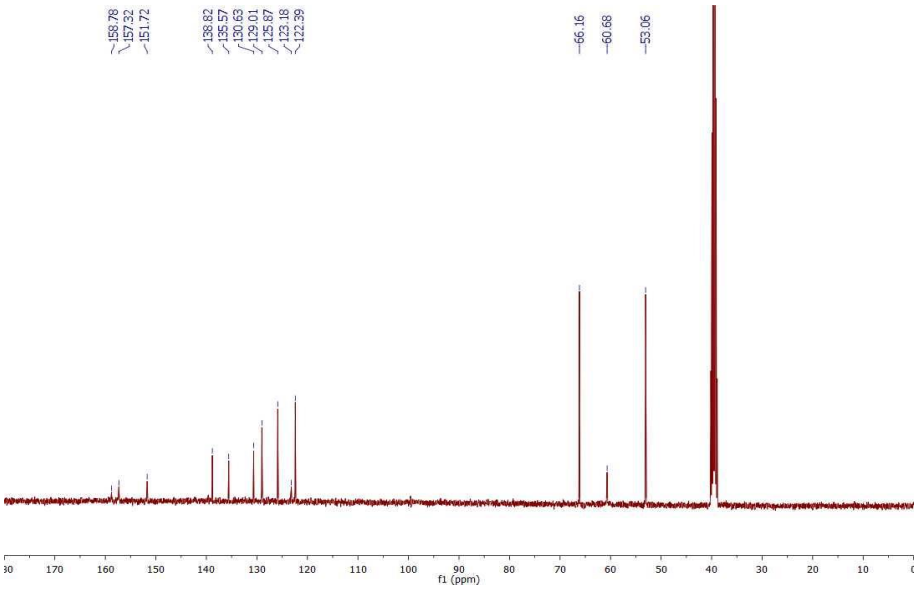

LC-MS (ES + APCI)

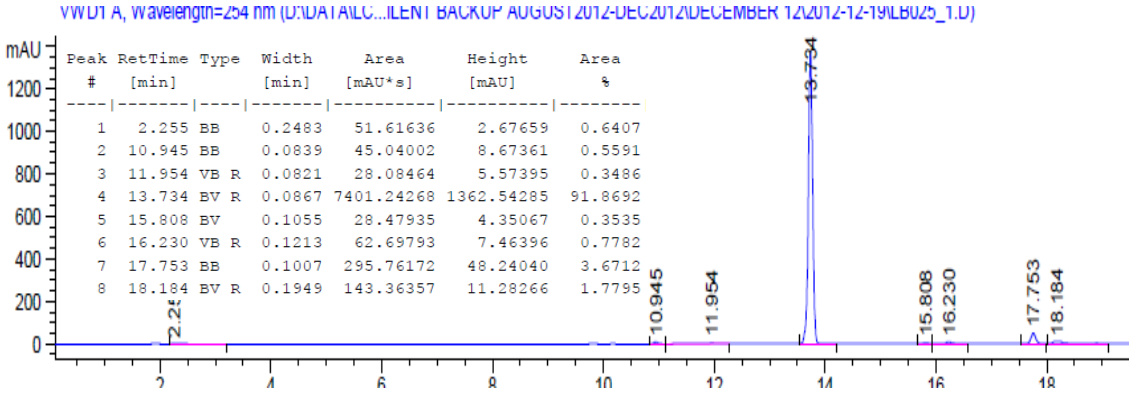

8-Chloro-2-(((2-hydroxyethyl)(methyl)amino)methyl)benzo[4,5]thieno[3,2-*d*]pyrimidin-4(3*H*)-one (43c)

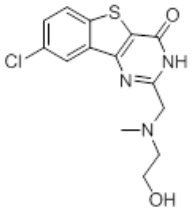

^{1}H NMR spectrum (500 MHz, DMSO)

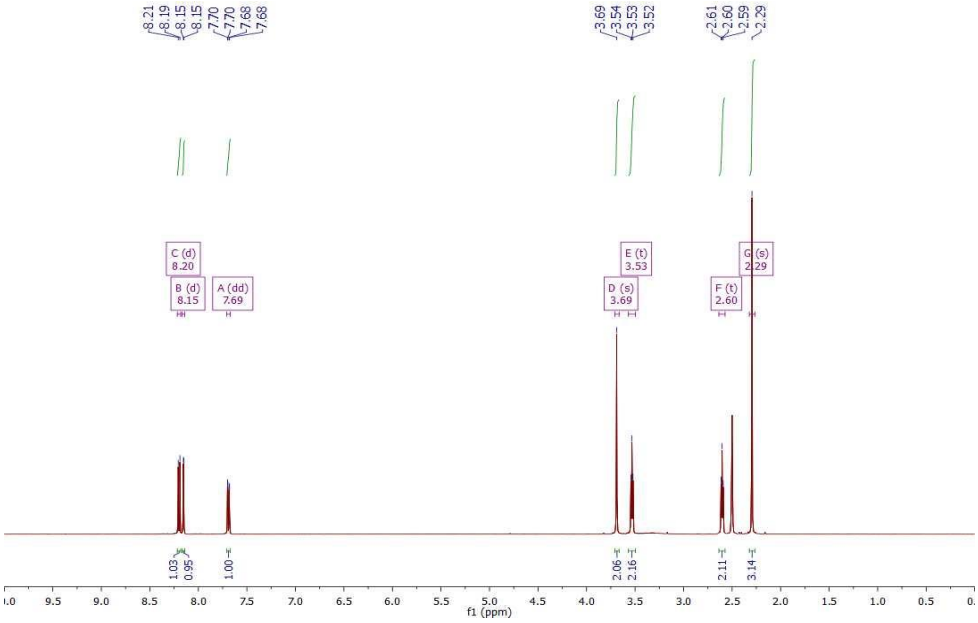

^{13}C NMR spectrum (126 MHz, DMSO)

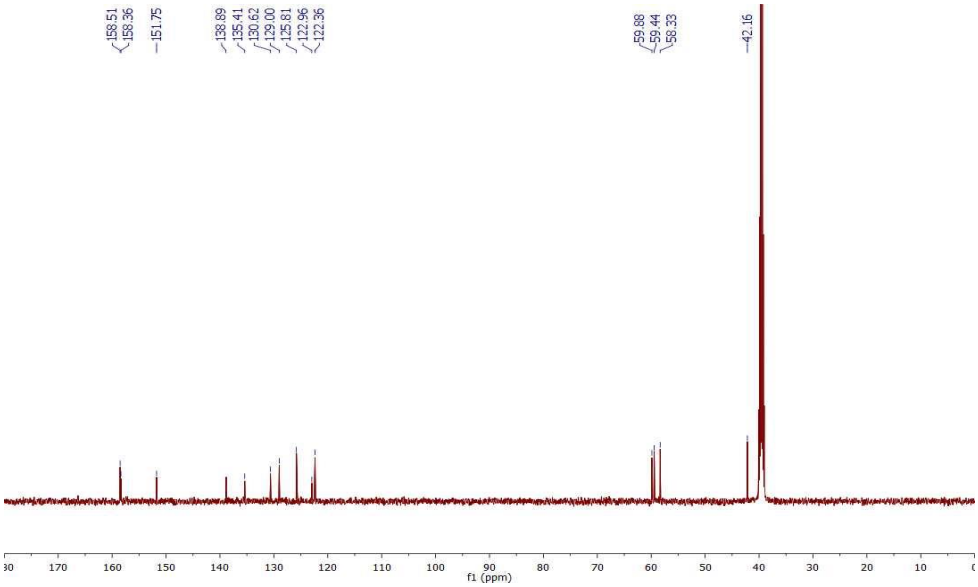

LC-MS (ES + APCI)

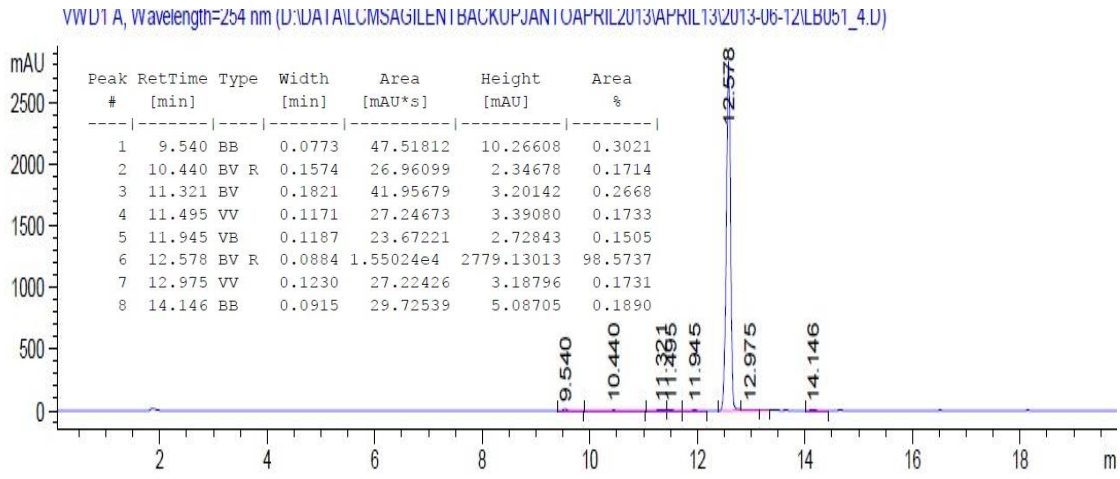

8-Chloro-2-(pyrrolidin-1-ylmethyl)benzo[4,5]thieno[3,2-*d*]pyrimidin-4(3*H*)-one (43d)

^{1}H NMR spectrum (400 MHz, DMSO)

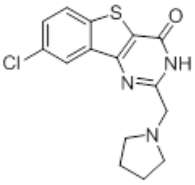

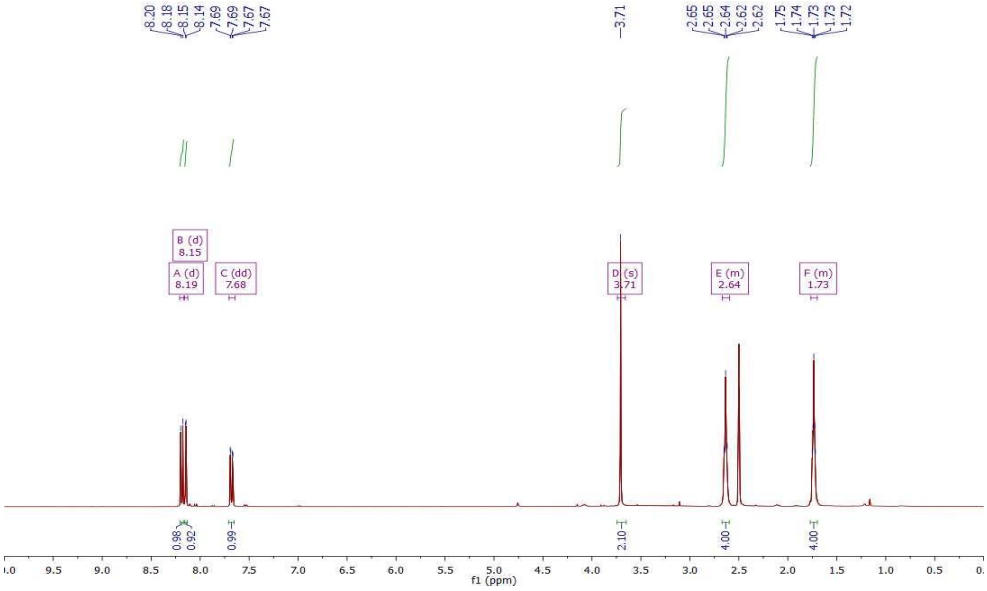

^{13}C NMR spectrum (101 MHz, DMSO)

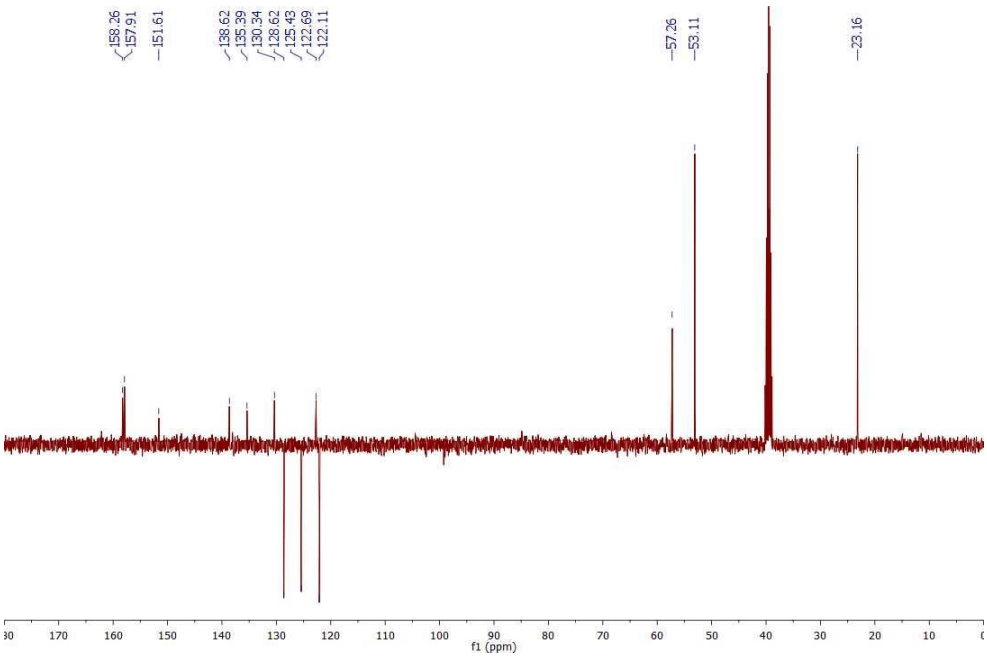

LC-MS (ES + APCI)

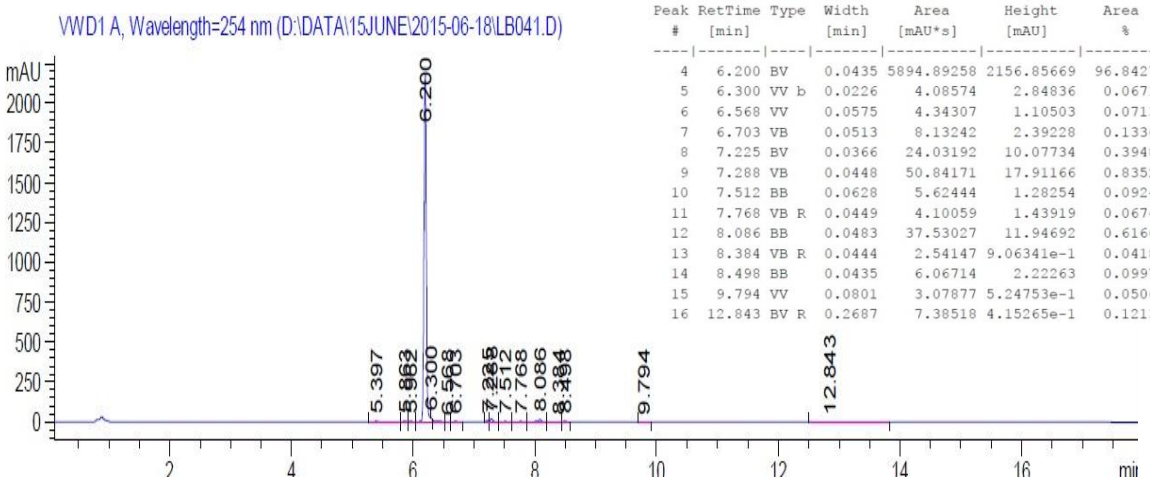

Peak #	RetTime [min]	Type	Width [min]	Area [mAU*s]	Height [mAU]	Area %
4	6.200	BV	0.0435	5894.89258	2156.85669	96.8427
5	6.300	VV b	0.0226	4.08574	2.84836	0.0671
6	6.568	VV	0.0575	4.34307	1.10503	0.0713
7	6.703	VB	0.0513	8.13242	2.39228	0.1336
8	7.225	BV	0.0366	24.03192	10.07734	0.3948
9	7.288	VB	0.0448	50.84171	17.91166	0.8352
10	7.512	BB	0.0628	5.62444	1.28254	0.0924
11	7.768	VB R	0.0449	4.10059	1.43919	0.0674
12	8.086	BB	0.0483	37.53027	11.94692	0.6166
13	8.384	VB R	0.0444	2.54147	9.06341e-1	0.0418
14	8.498	BB	0.0435	6.06714	2.22263	0.0997
15	9.794	VV	0.0801	3.07877	5.24753e-1	0.0506
16	12.843	BV R	0.2687	7.38518	4.15265e-1	0.1213

2-((4-Acetyl-1,4-diazepan-1-yl)methyl)-8-chlorobenzo[4,5]thieno[3,2-*d*]pyrimidin-4(*3H*)-one (43e)

^{1}H NMR spectrum (400 MHz, DMSO)

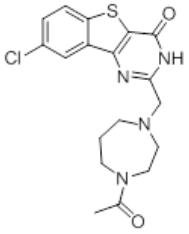

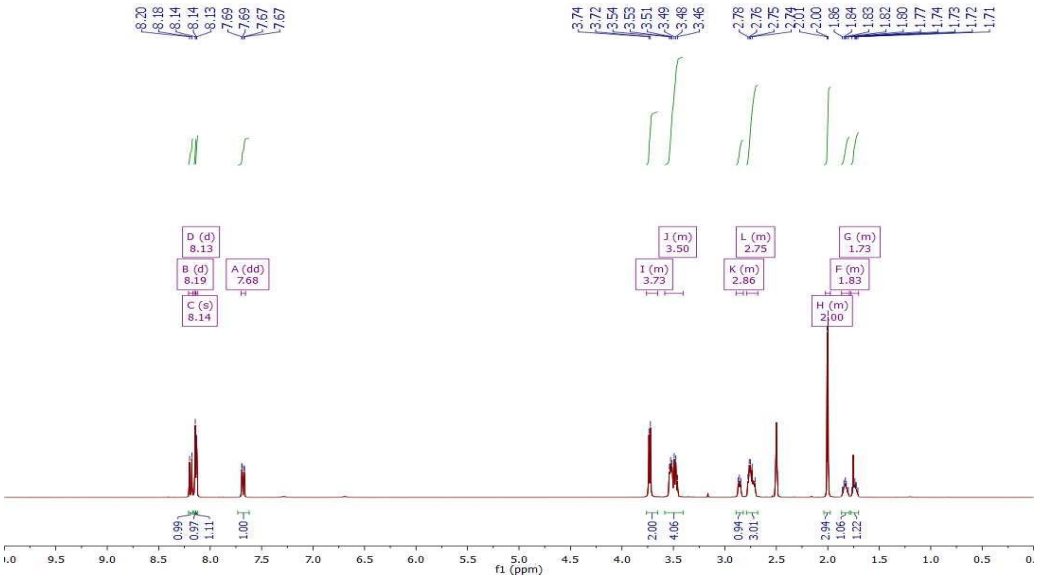

^{13}C NMR spectrum (101 MHz, DMSO)

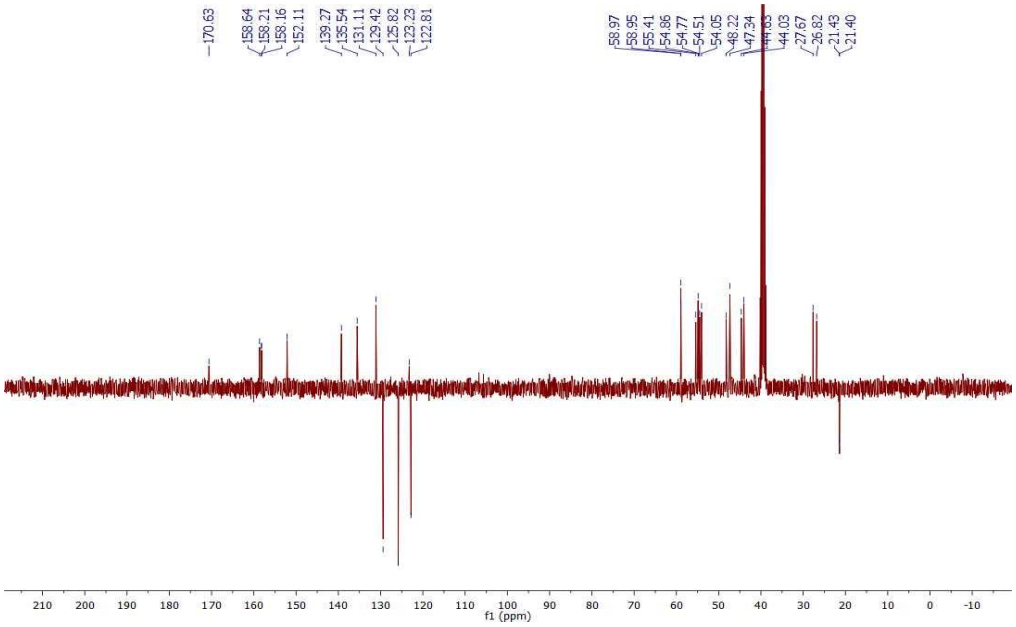

LC-MS (ES + APCI)

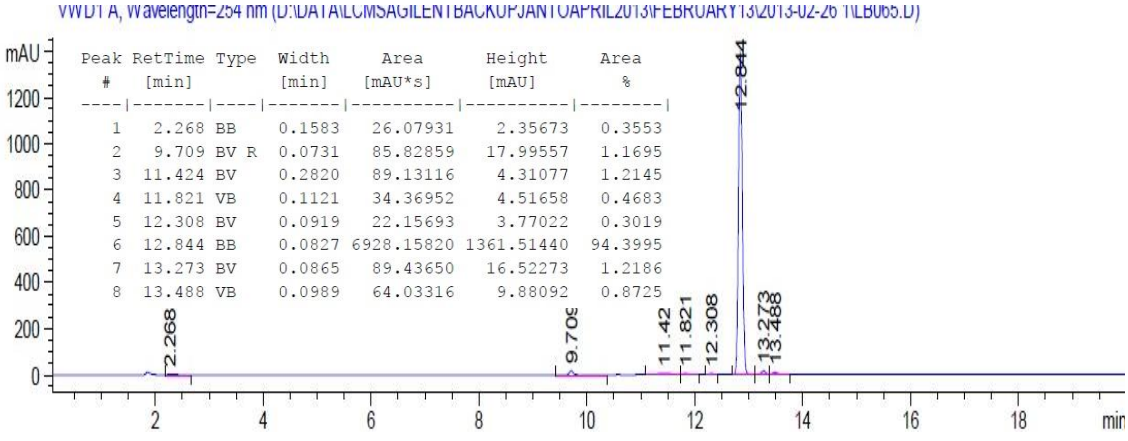

8-Chloro-2-(((2-hydroxyethyl)amino)methyl)benzo[4,5]thieno[3,2-*d*]pyrimidin-4(3*H*)-one (43f)

^{1}H NMR spectrum (500 MHz, DMSO)

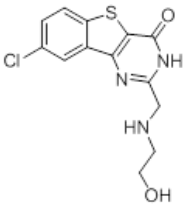

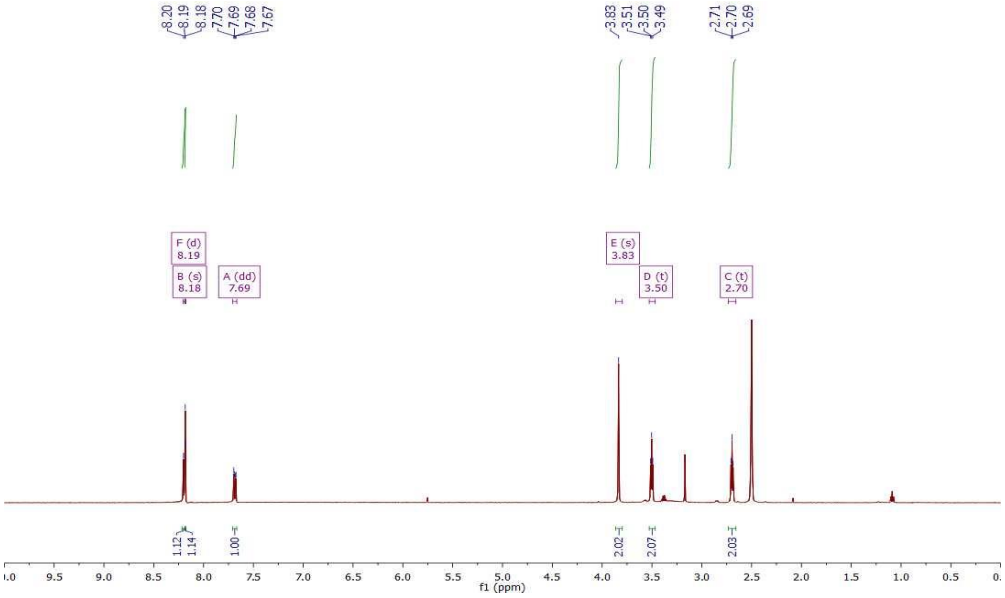

^{13}C NMR spectrum (126 MHz, DMSO)

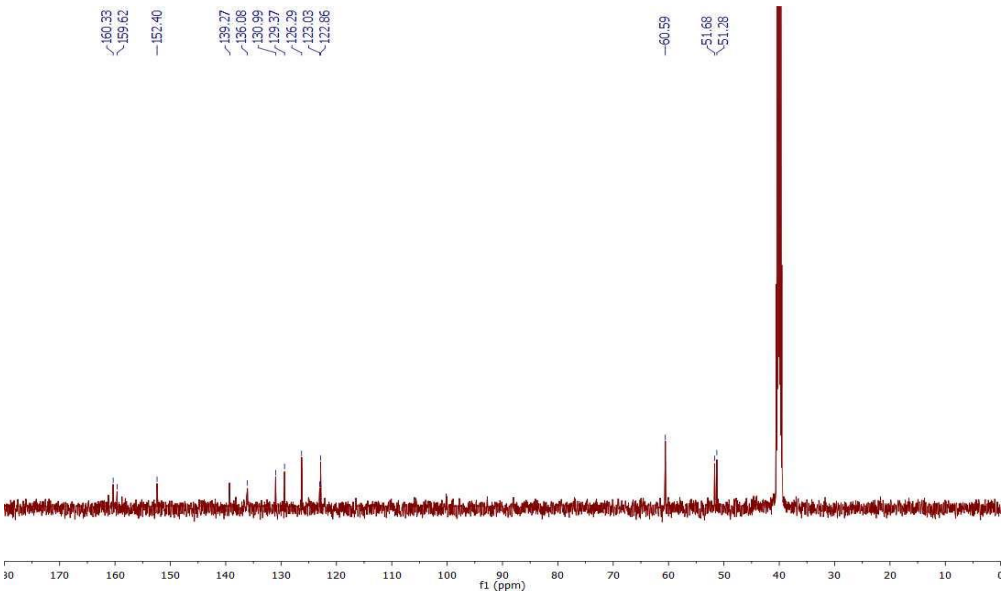

LC-MS (ES + APCI)

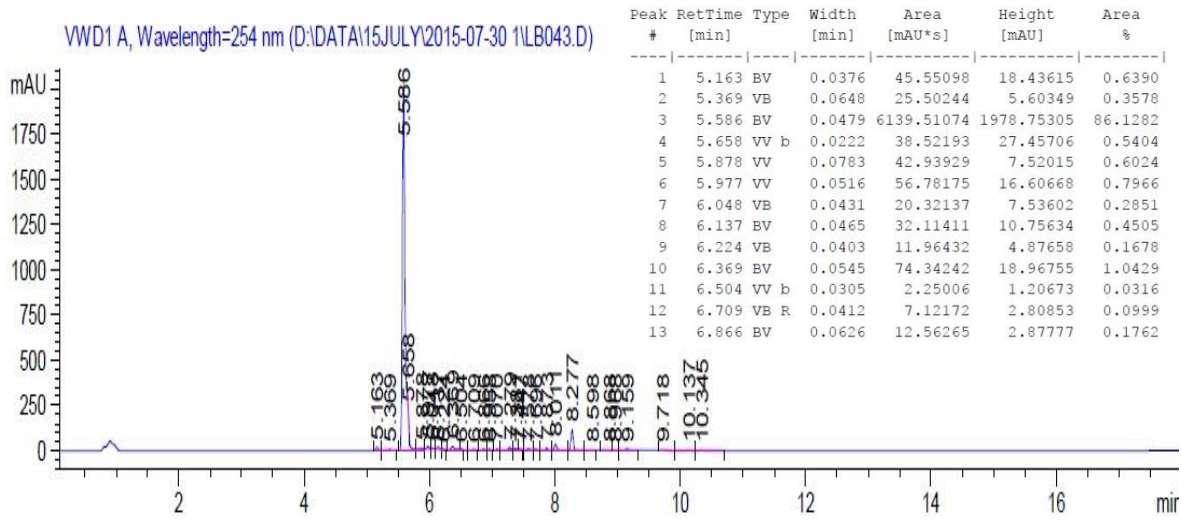

Peak #	RetTime [min]	Type	Width [min]	Area [mAU*s]	Height [mAU]	Area %
1	5.163	BV	0.0376	45.55098	18.43615	0.6390
2	5.369	VB	0.0648	25.50244	5.60349	0.3578
3	5.586	BV	0.0479	6139.51074	1978.75305	86.1282
4	5.658	VV b	0.0222	38.52193	27.45706	0.5404
5	5.878	VV	0.0783	42.93929	7.52015	0.6024
6	5.977	VV	0.0516	56.78175	16.60668	0.7966
7	6.048	VB	0.0431	20.32137	7.53602	0.2851
8	6.137	BV	0.0465	32.11411	10.75634	0.4505
9	6.224	VB	0.0403	11.96432	4.87658	0.1678
10	6.369	BV	0.0545	74.34242	18.96755	1.0429
11	6.504	VV b	0.0305	2.25006	1.20673	0.0316
12	6.709	VB R	0.0412	7.12172	2.80853	0.0999
13	6.866	BV	0.0626	12.56265	2.87777	0.1762

8-Chloro-2-(((2-methoxyethyl)(methyl)amino)methyl)benzo[4,5]thieno[3,2-*d*]pyrimidin-4(3*H*)-one (43g)

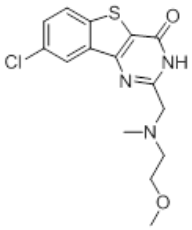

^{1}H NMR spectrum (400 MHz, DMSO)

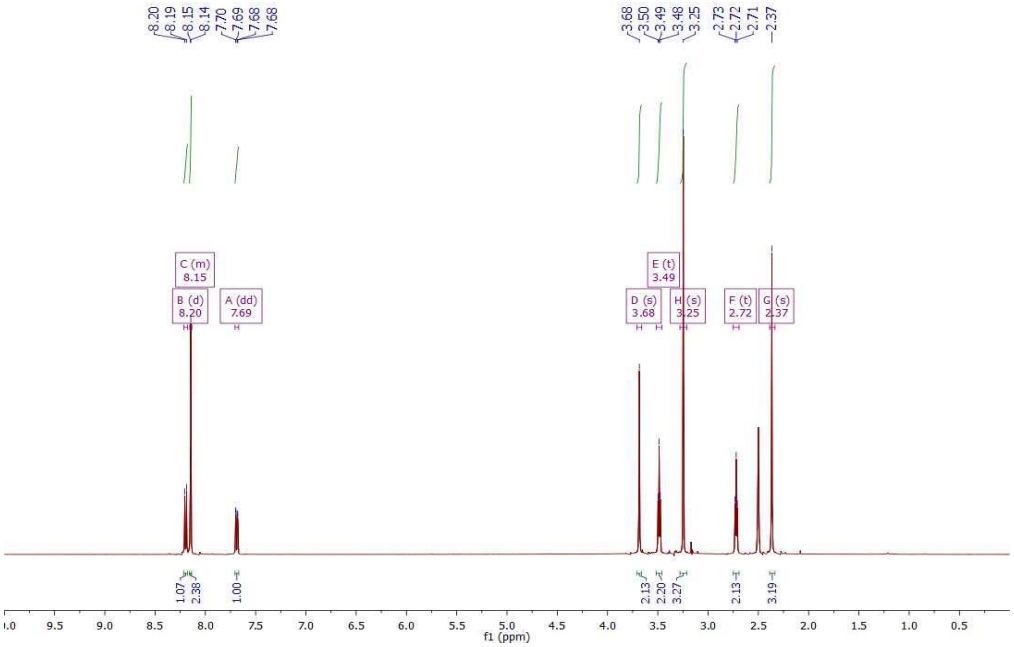

^{13}C NMR spectrum (101 MHz, DMSO)

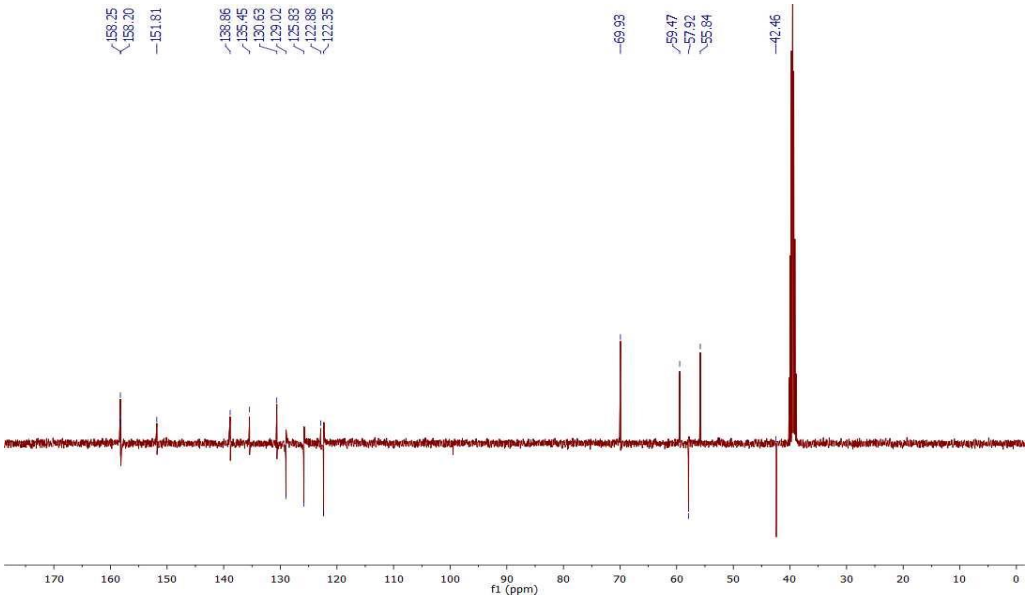

LC-MS (ES + APCI)

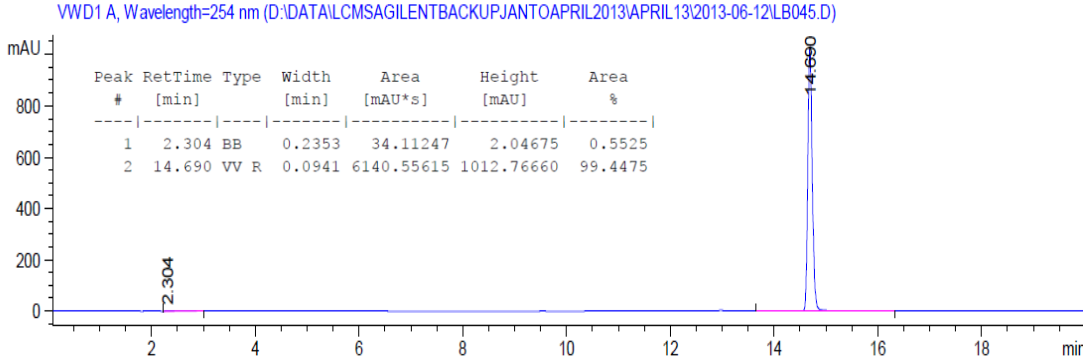

8-Chloro-2-((((1*R*,3*S*)-3-hydroxy-3-(trifluoromethyl)cyclohexyl)amino)methyl)benzo[4,5]thieno[3,2-*d*]pyrimidin-4(3*H*)-one (43h)

^{1}H NMR spectrum (400 MHz, DMSO)

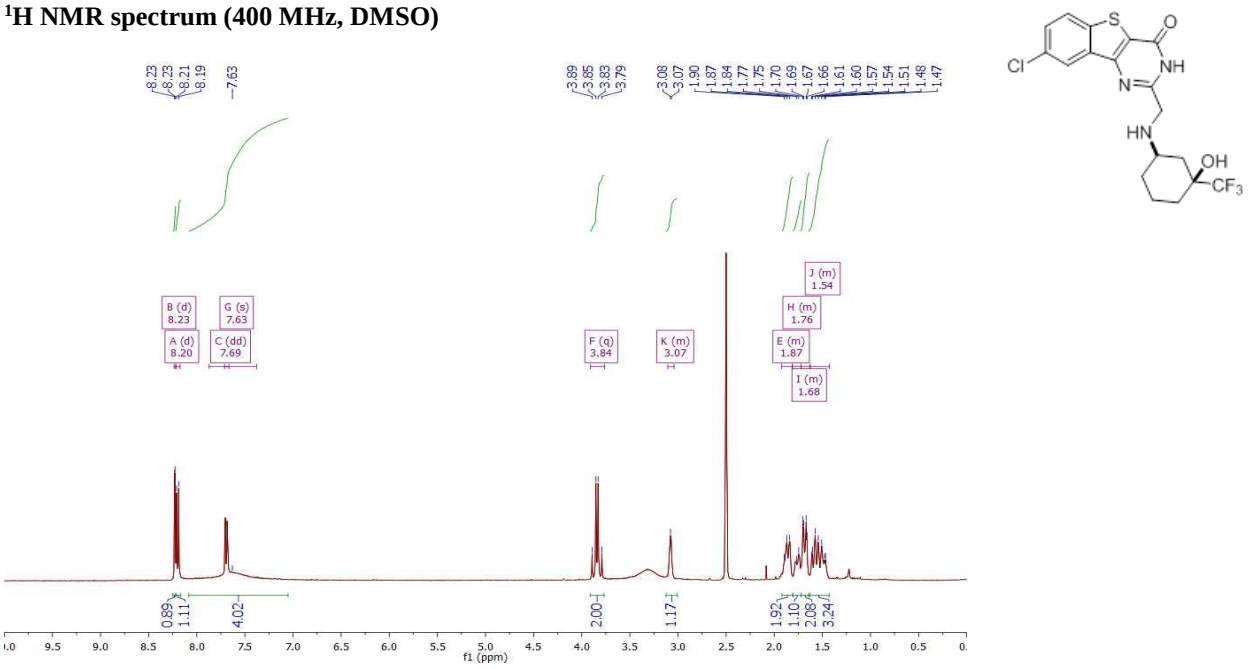

^{13}C NMR spectrum (101 MHz, DMSO)

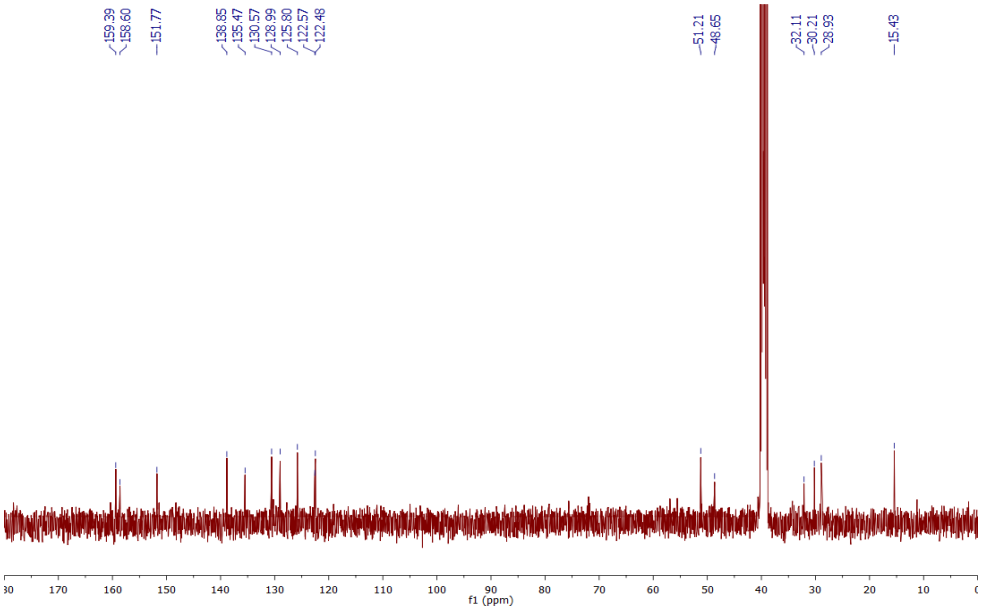

LC-MS (ES + APCI)

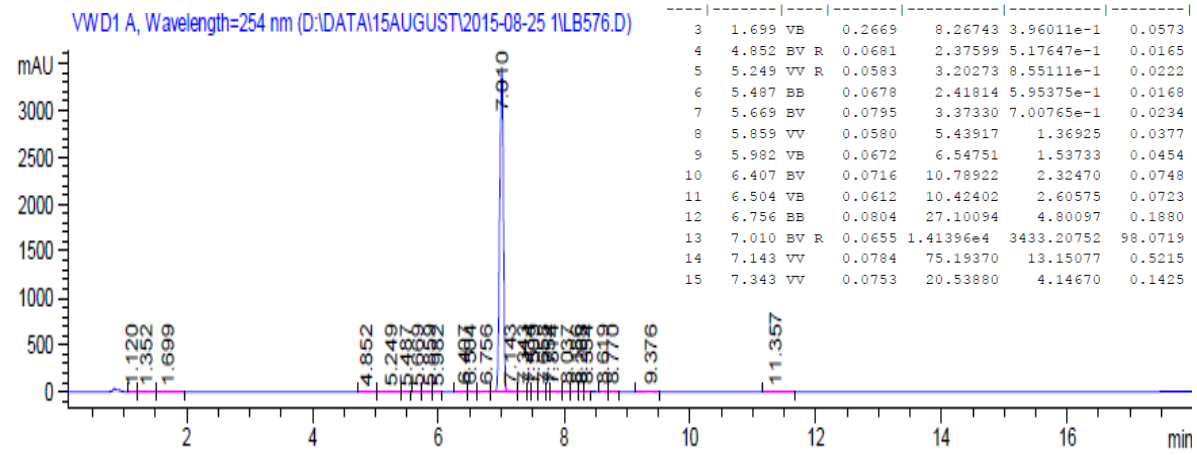

Peak #	RetTime [min]	Type	Width [min]	Area [mAU*s]	Height [mAU]	Area %
3	1.699	VB	0.2669	8.26743	3.96011e-1	0.0573
4	4.852	BV R	0.0681	2.37599	5.17647e-1	0.0165
5	5.249	VV R	0.0583	3.20273	8.55111e-1	0.0222
6	5.487	BB	0.0678	2.41814	5.95375e-1	0.0168
7	5.669	BV	0.0795	3.37330	7.00765e-1	0.0234
8	5.859	VV	0.0580	5.43917	1.36925	0.0377
9	5.982	VB	0.0672	6.54751	1.53733	0.0454
10	6.407	BV	0.0716	10.78922	2.32470	0.0748
11	6.504	VB	0.0612	10.42402	2.60575	0.0723
12	6.756	BB	0.0804	27.10094	4.80097	0.1880
13	7.010	BV R	0.0655	1.41396e4	3433.20752	98.0719
14	7.143	VV	0.0784	75.19370	13.15077	0.5215
15	7.343	VV	0.0753	20.53880	4.14670	0.1425

(*S*)-8-Chloro-2-(((1-hydroxy-3-methylbutan-2-yl)amino)methyl)benzo[4,5]thieno[3,2-*d*]pyrimidin-4(3*H*)-one (43j)

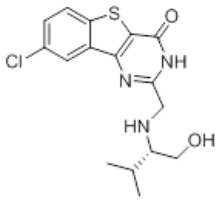

^{1}H NMR spectrum (400 MHz, DMSO)

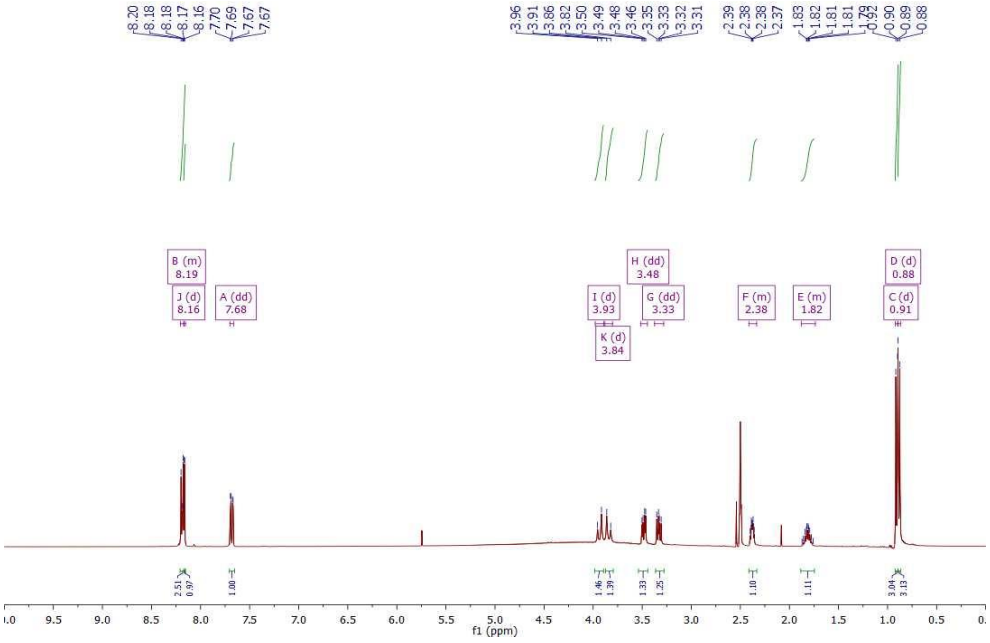

^{13}C NMR spectrum (101 MHz, DMSO)

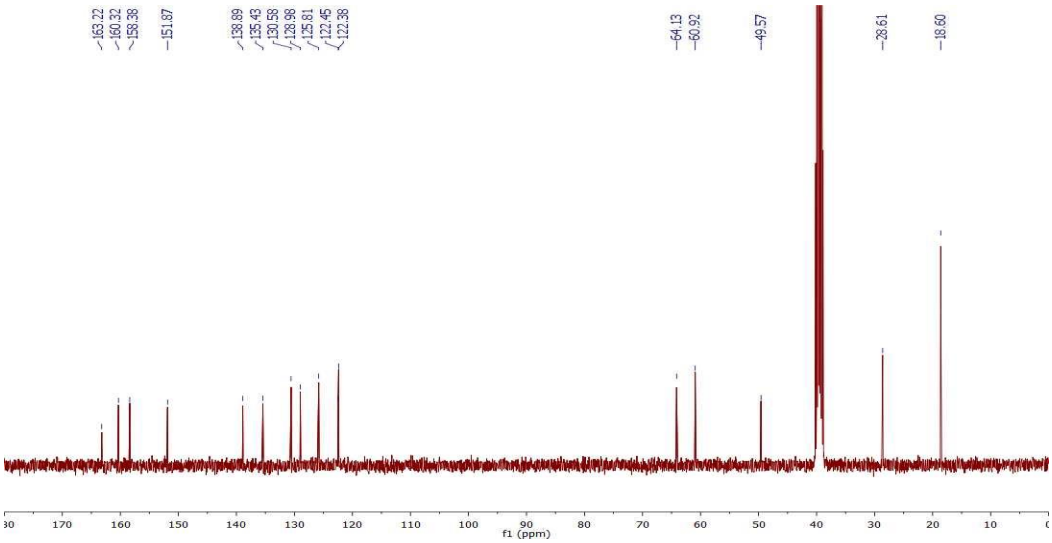

LC-MS (ES + APCI)

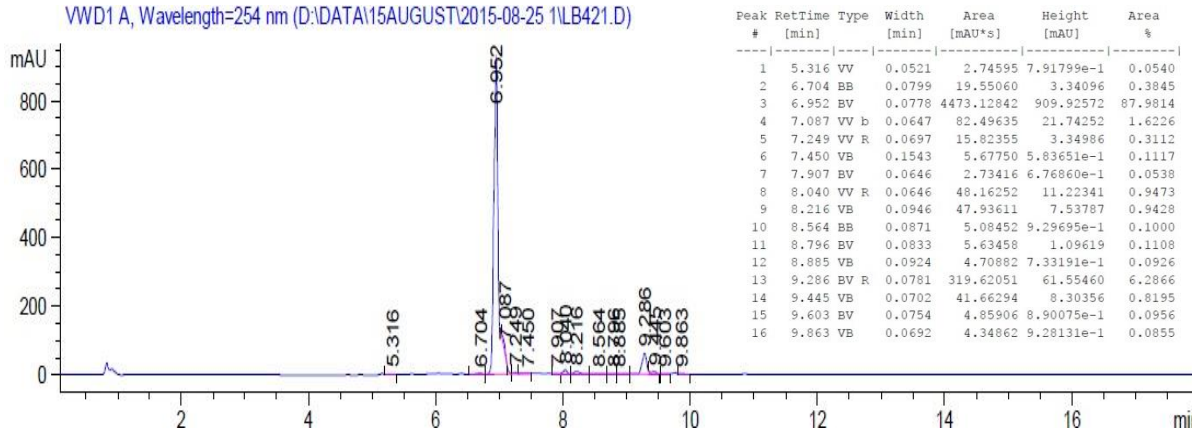

Peak #	RetTime [min]	Type	Width [min]	Area [mAU*s]	Height [mAU]	Area %
1	5.316	VV	0.0521	2.74595	7.91799e-1	0.0540
2	6.704	BB	0.0799	19.55060	3.34096	0.3845
3	6.952	BV	0.0778	4473.12842	909.92572	87.9814
4	7.087	VV b	0.0647	82.49635	21.74252	1.6226
5	7.249	VV R	0.0697	15.82355	3.34986	0.3112
6	7.450	VB	0.1543	5.67750	5.83651e-1	0.1117
7	7.907	BV	0.0646	2.73416	6.76860e-1	0.0538
8	8.040	VV R	0.0646	48.16252	11.22341	0.9473
9	8.216	VB	0.0946	47.93611	7.53787	0.9428
10	8.564	BB	0.0871	5.08452	9.29695e-1	0.1000
11	8.796	BV	0.0833	5.63458	1.09619	0.1108
12	8.885	VB	0.0924	4.70882	7.33191e-1	0.0926
13	9.286	BV R	0.0781	319.62051	61.55460	6.2866
14	9.445	VB	0.0702	41.66294	8.30356	0.8195
15	9.603	BV	0.0754	4.85906	8.90075e-1	0.0956
16	9.863	VB	0.0692	4.34862	9.28131e-1	0.0855

(*R*)-8-Chloro-2-(((1-hydroxy-3-methylbutan-2-yl)amino)methyl)benzo[4,5]thieno[3,2-*d*]pyrimidin-4(3*H*)-one (43k)

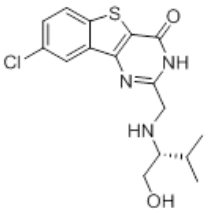

^{1}H NMR spectrum (400 MHz, DMSO)

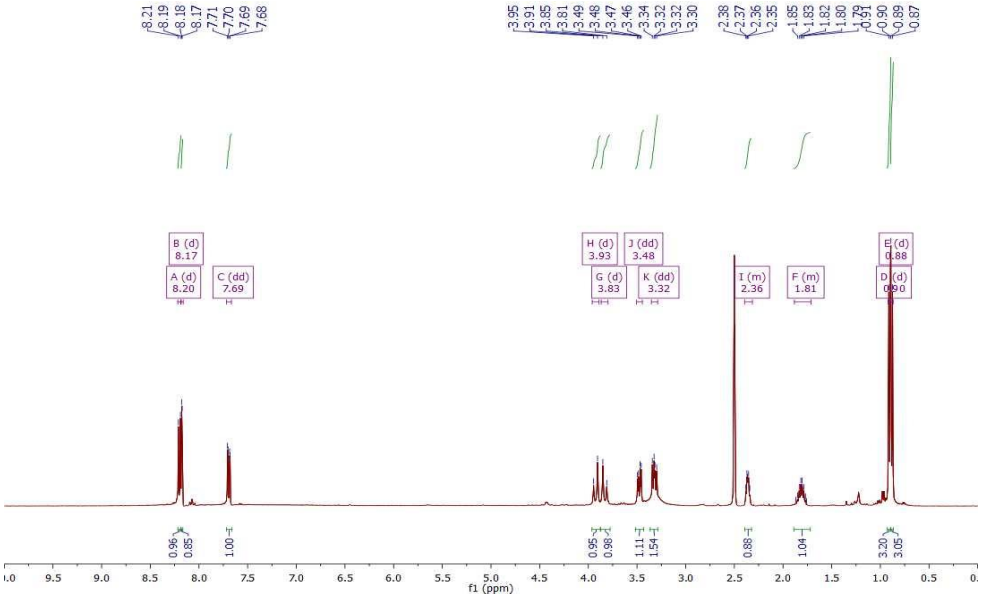

^{13}C NMR spectrum (101 MHz, DMSO)

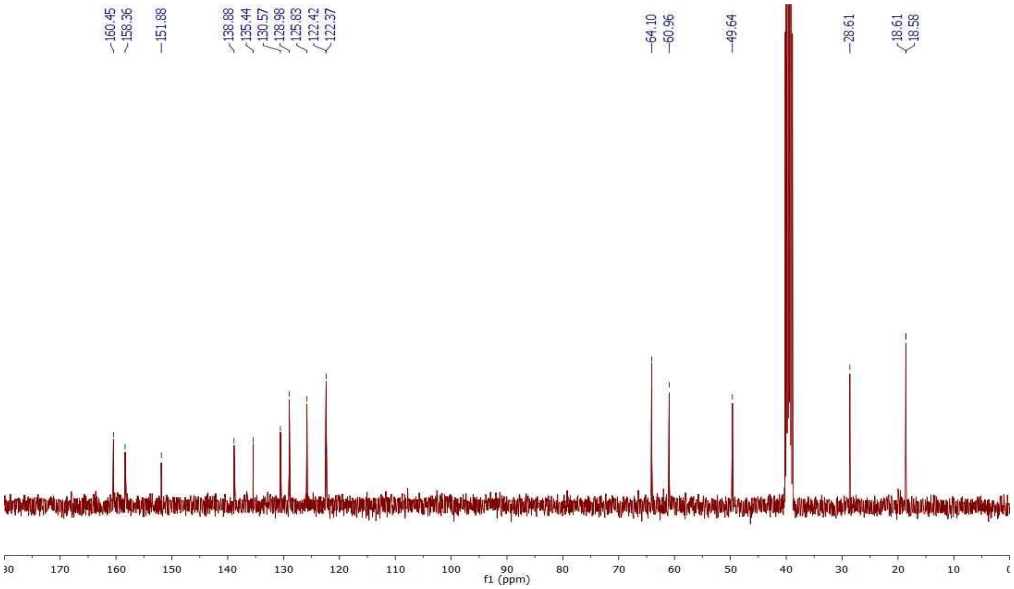

LC-MS (ES + APCI)

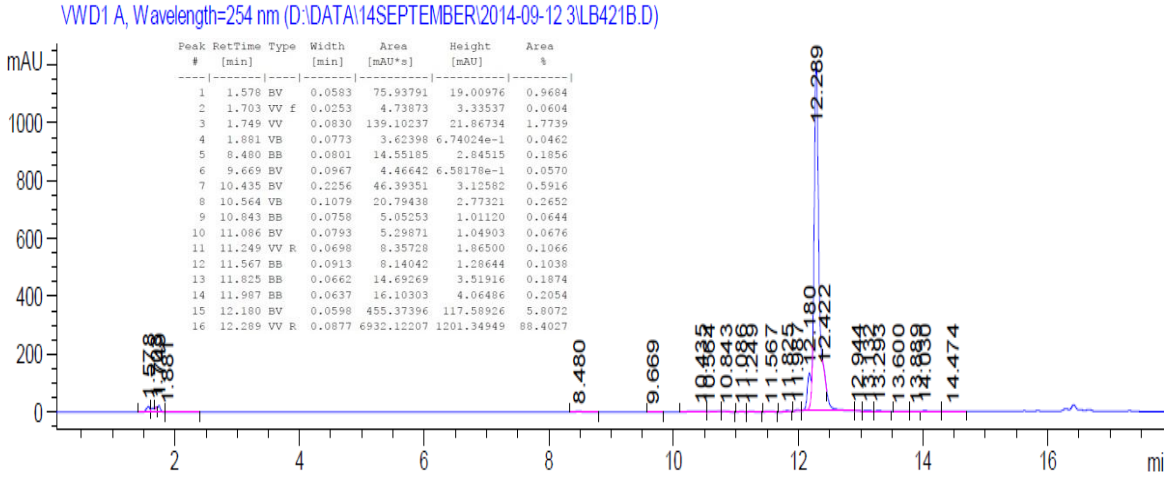

Peak #	RetTime [min]	Type	Width [min]	Area [mAU*s]	Height [mAU]	Area %
1	1.578	BV	0.0583	75.93791	19.00976	0.9684
2	1.703	VV f	0.0253	4.73873	3.33537	0.0604
3	1.749	VV	0.0830	139.10237	21.86734	1.7739
4	1.881	VB	0.0773	3.62398	6.74024e-1	0.0462
5	8.480	BB	0.0801	14.55185	2.84515	0.1856
6	9.669	BV	0.0967	4.46642	6.58178e-1	0.0570
7	10.435	BV	0.2256	46.39351	3.12582	0.5916
8	10.564	VB	0.1079	20.79438	2.77321	0.2652
9	10.843	BB	0.0758	5.05253	1.01120	0.0644
10	11.086	BV	0.0793	5.29871	1.04903	0.0676
11	11.249	VV R	0.0698	8.35728	1.86500	0.1066
12	11.567	BB	0.0913	8.14042	1.28644	0.1038
13	11.825	BB	0.0662	14.69269	3.51916	0.1874
14	11.987	BB	0.0637	16.10303	4.06486	0.2054
15	12.180	BV	0.0598	455.37396	117.58926	5.8072
16	12.289	VV R	0.0877	6932.12207	1201.34949	88.4027

8-Chloro-2-((phenylamino)methyl)benzo[4,5]thieno[3,2-*d*]pyrimidin-4(3*H*)-one (43l)

^{1}H NMR spectrum (400 MHz, DMSO)

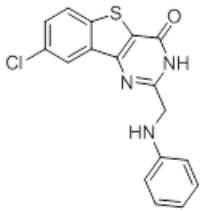

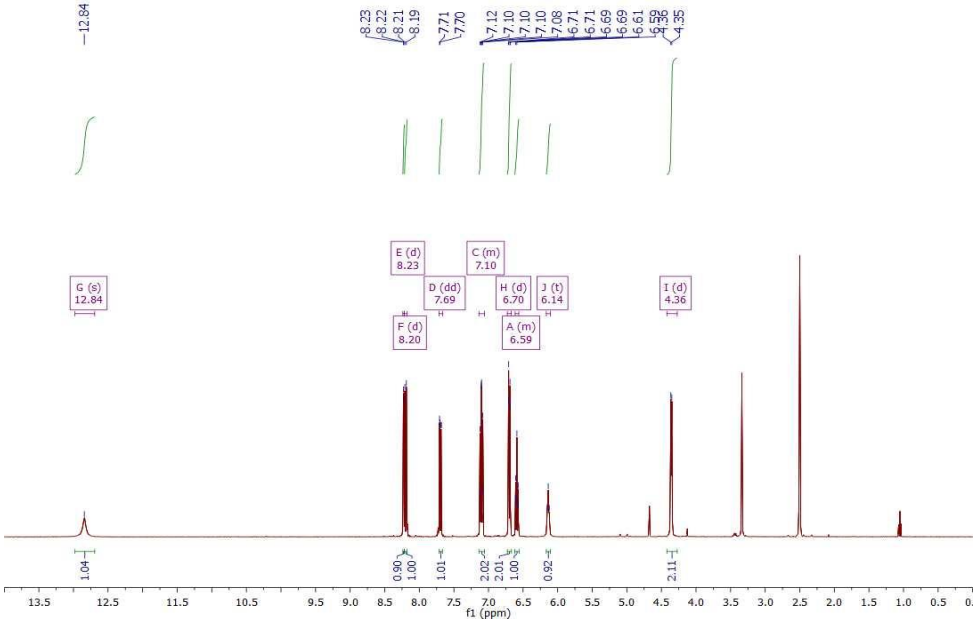

^{13}C NMR spectrum (101 MHz, DMSO)

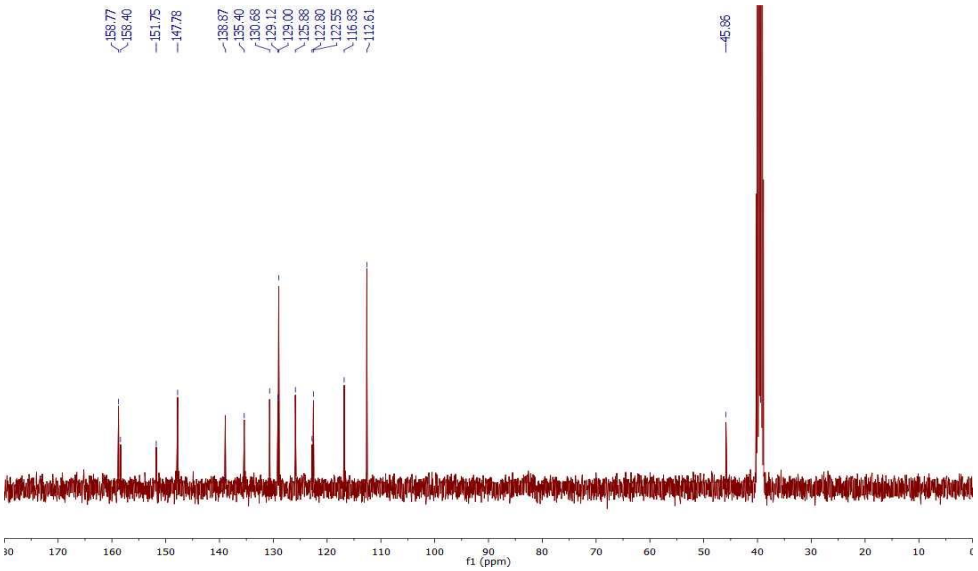

LC-MS (ES + APCI)

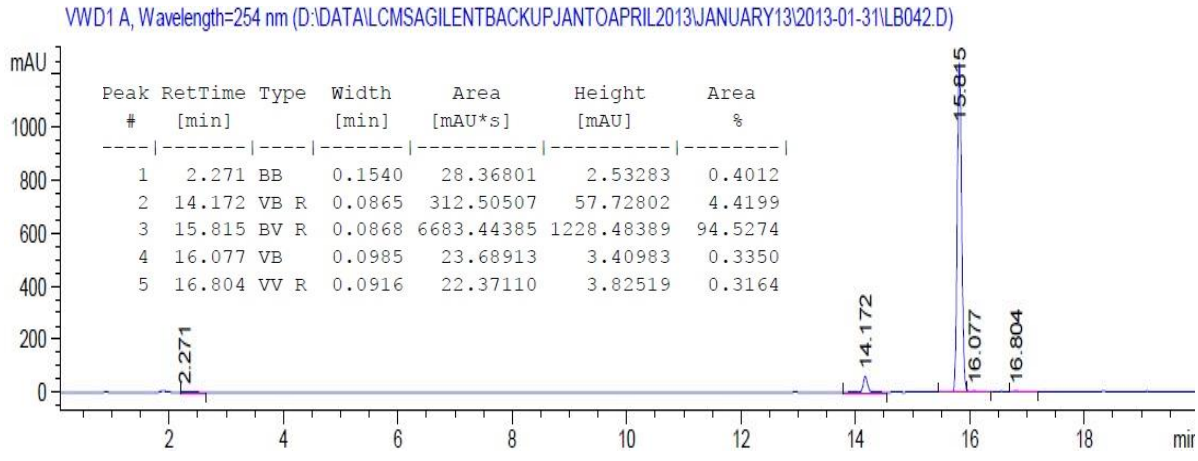

8-Chloro-2-(((4-chlorophenyl)amino)methyl)benzo[4,5]thieno[3,2-*d*]pyrimidin-4(3*H*)-one (43m)

^{1}H NMR spectrum (400 MHz, DMSO)

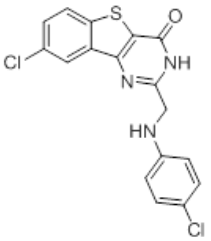

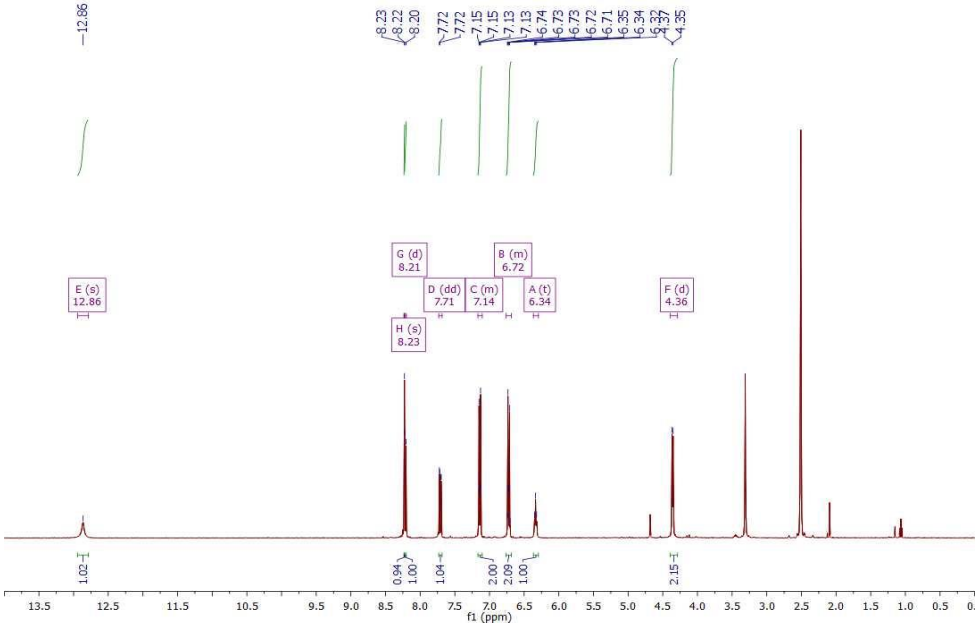

^{13}C NMR spectrum (101 MHz, DMSO)

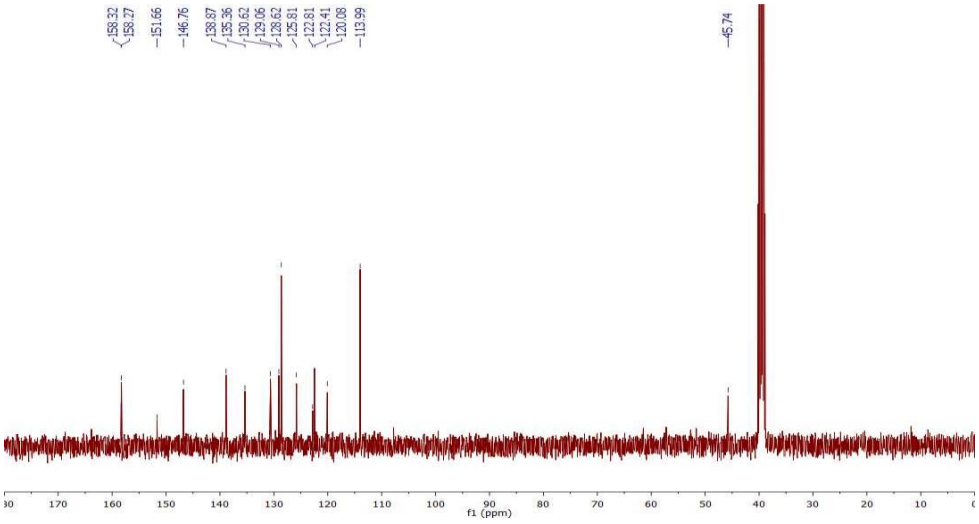

LC-MS (ES + APCI)

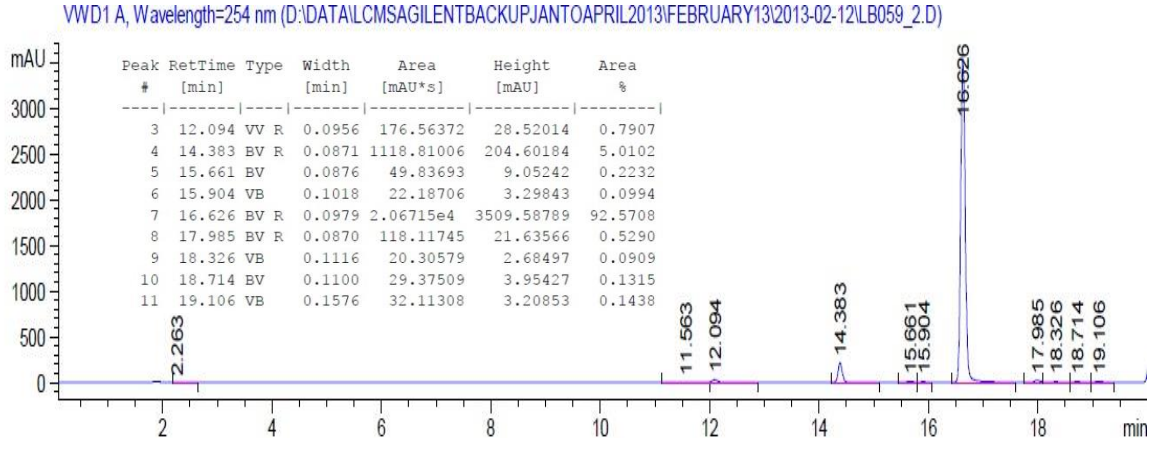

8-Chloro-2-(((3-hydroxyphenyl)amino)methyl)benzo[4,5]thieno[3,2-*d*]pyrimidin-4(*3H*)-one (43n)

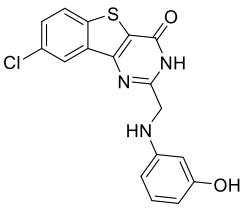

^{1}H NMR spectrum (400 MHz, DMSO)

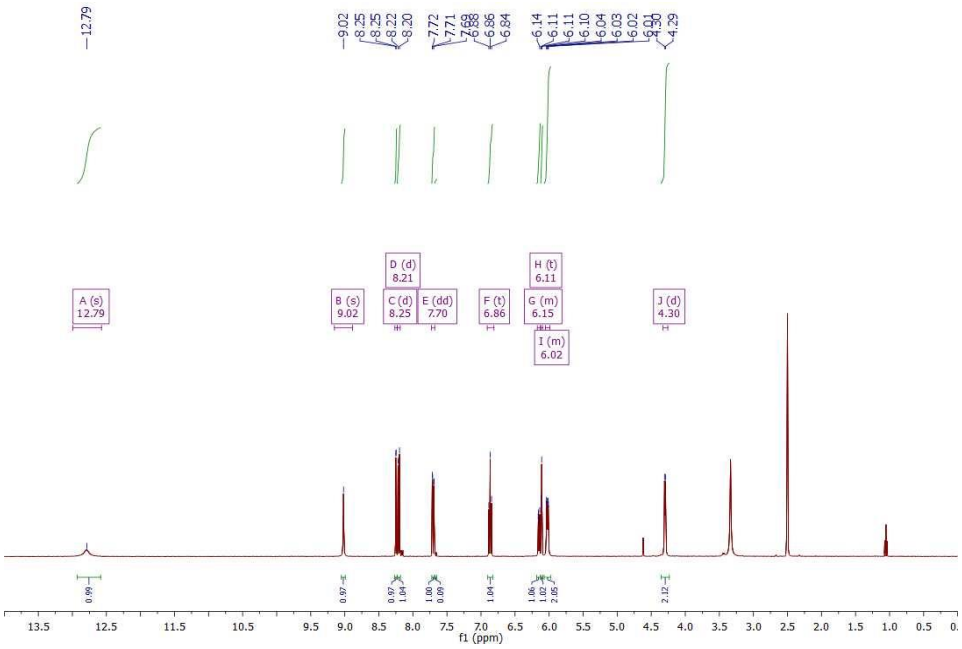

^{13}C NMR spectrum (101 MHz, DMSO)

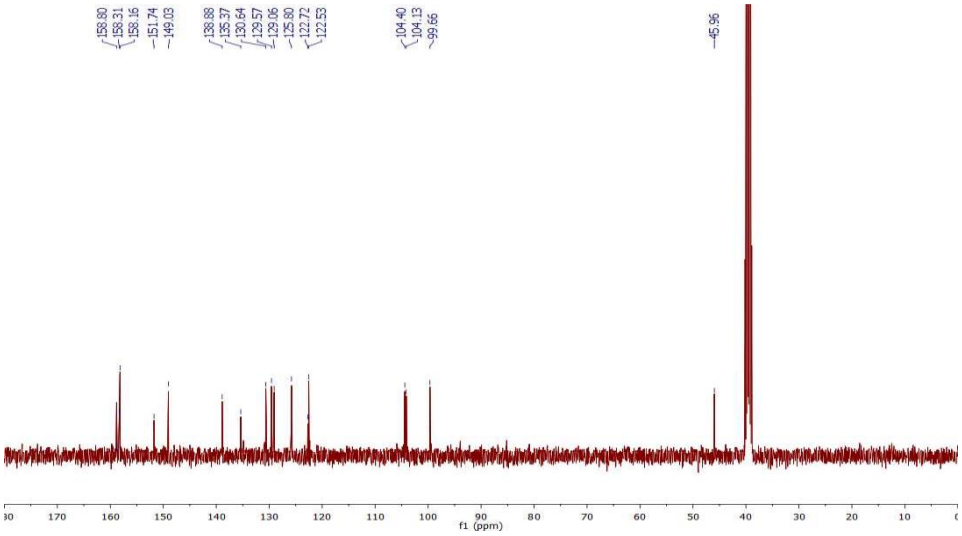

LC-MS (ES + APCI)

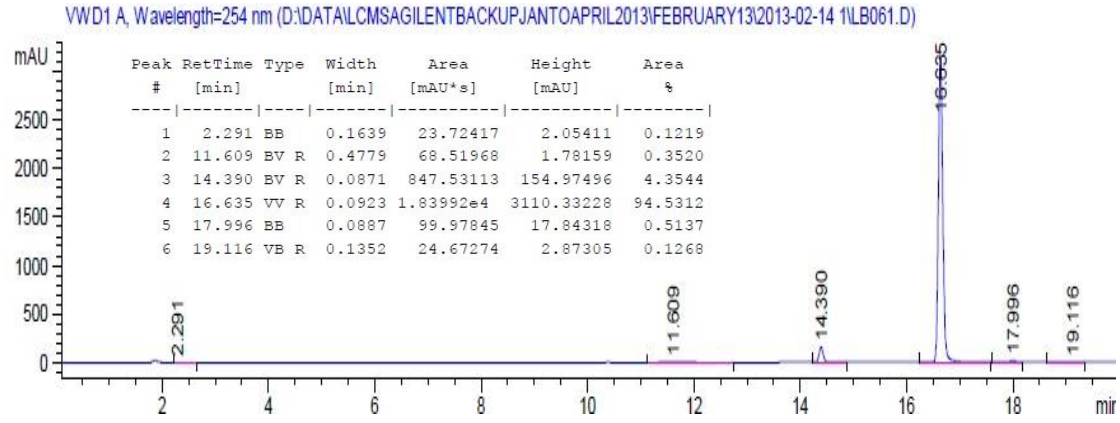

8-Chloro-2-(((3-methoxyphenyl)amino)methyl)benzo[4,5]thieno[3,2-*d*]pyrimidin-4(3*H*)-one (43o)

^{1}H NMR spectrum (400 MHz, DMSO)

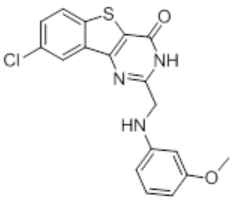

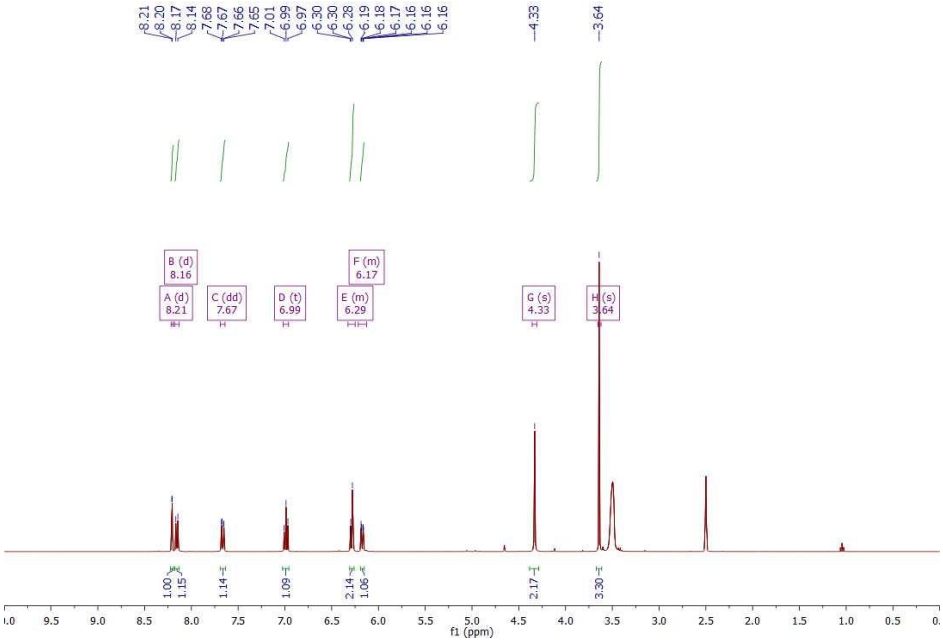

^{13}C NMR spectrum (101 MHz, DMSO)

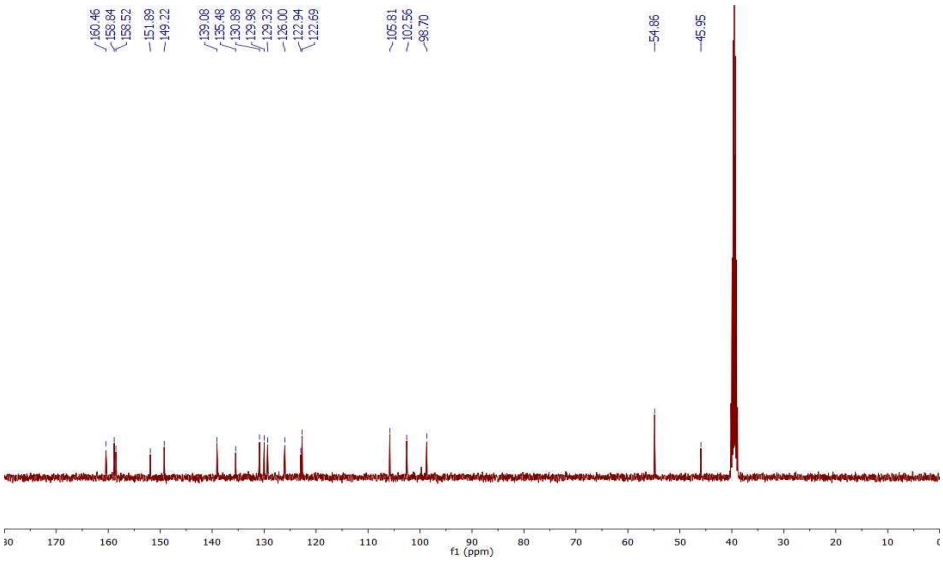

LC-MS (ES + APCI)

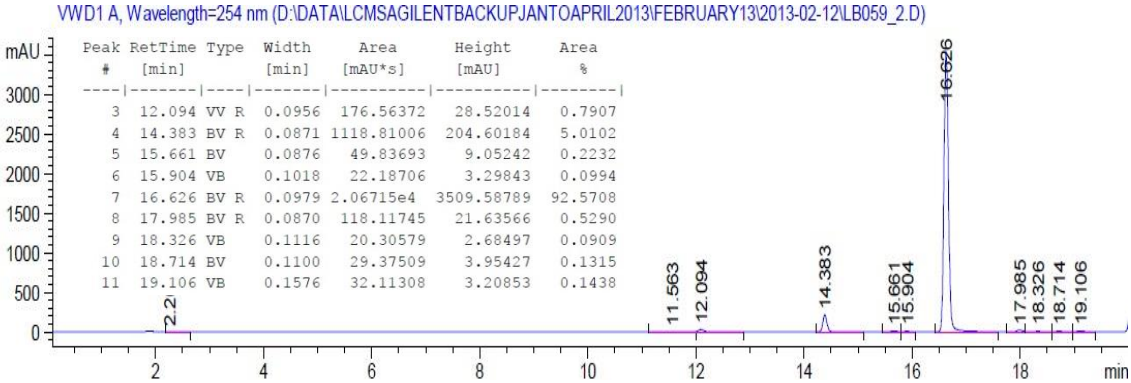

Peak #	RetTime [min]	Type	Width [min]	Area [mAU*s]	Height [mAU]	Area %
3	12.094	VV R	0.0956	176.56372	28.52014	0.7907
4	14.383	BV R	0.0871	1118.81006	204.60184	5.0102
5	15.661	BV	0.0876	49.83693	9.05242	0.2232
6	15.904	VB	0.1018	22.18706	3.29843	0.0994
7	16.626	BV R	0.0979	2.06715e4	3509.58789	92.5708
8	17.985	BV R	0.0870	118.11745	21.63566	0.5290
9	18.326	VB	0.1116	20.30579	2.68497	0.0909
10	18.714	BV	0.1100	29.37509	3.95427	0.1315
11	19.106	VB	0.1576	32.11308	3.20853	0.1438

8-Chloro-2-(((4-methoxyphenyl)amino)methyl)benzo[4,5]thieno[3,2-*d*]pyrimidin-4(*3H*)-one (43p)

^{1}H NMR spectrum (400 MHz, DMSO)

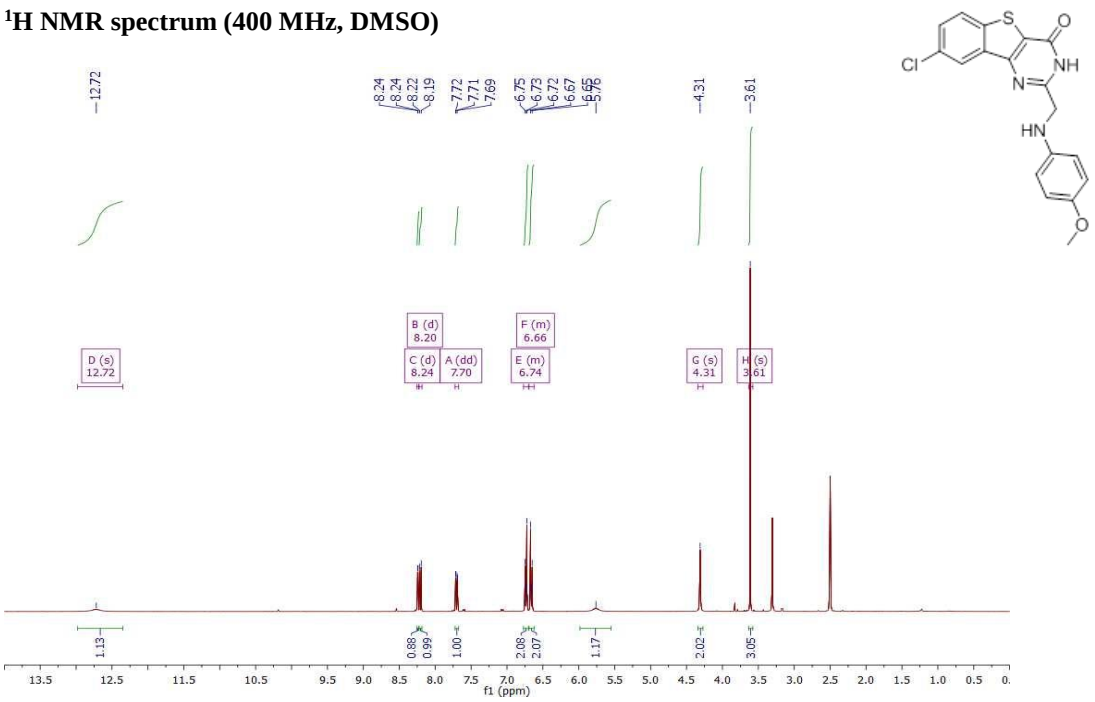

^{13}C NMR spectrum (101 MHz, DMSO)

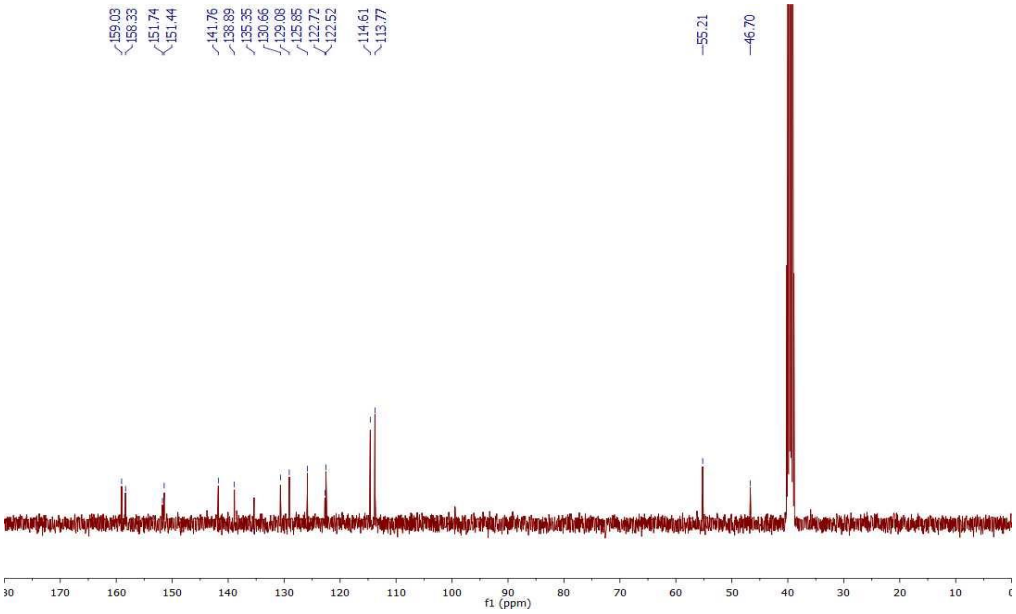

LC-MS (ES + APCI)

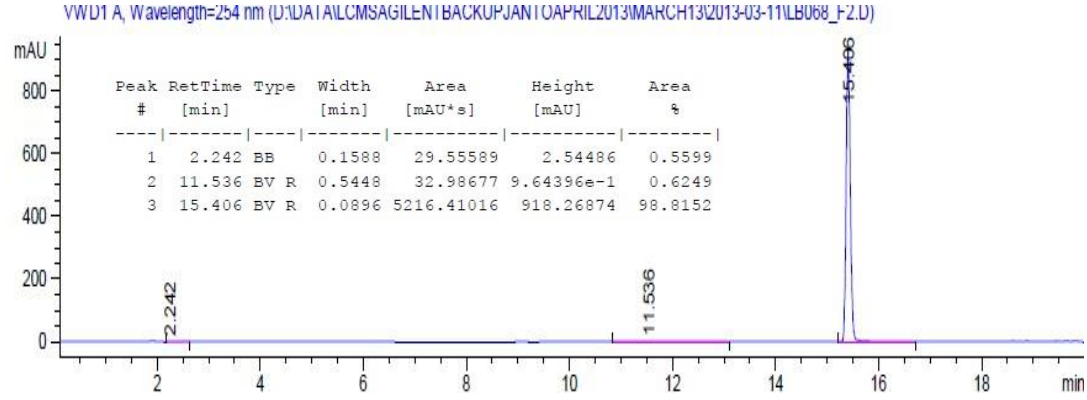

8-Chloro-2-(((3,5-dimethoxyphenyl)amino)methyl)benzo[4,5]thieno[3,2-*d*]pyrimidin-4(3*H*)-one (43q)

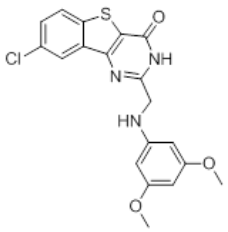

^{1}H NMR spectrum (400 MHz, DMSO)

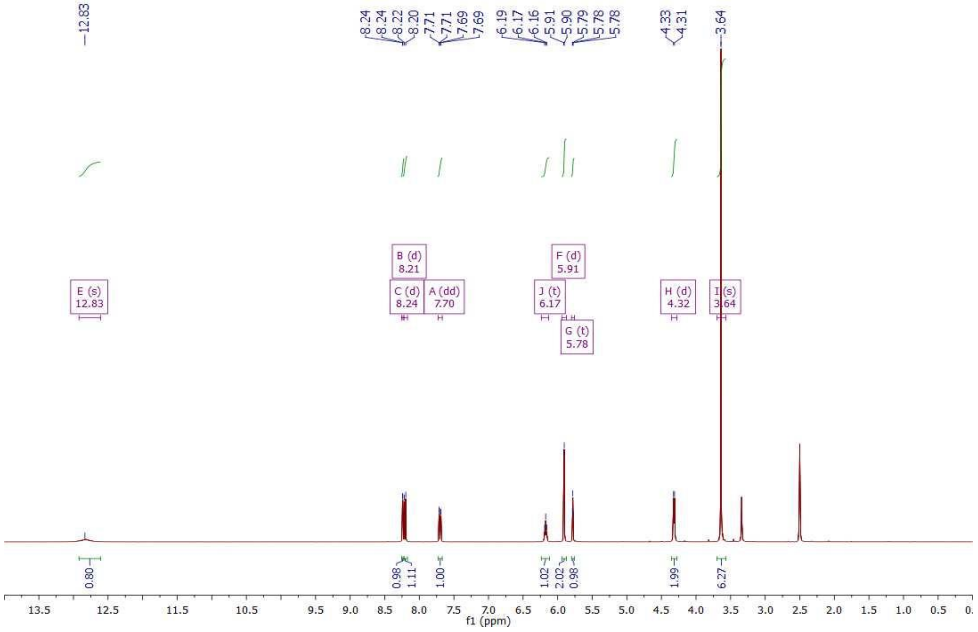

^{13}C NMR spectrum (101 MHz, DMSO)

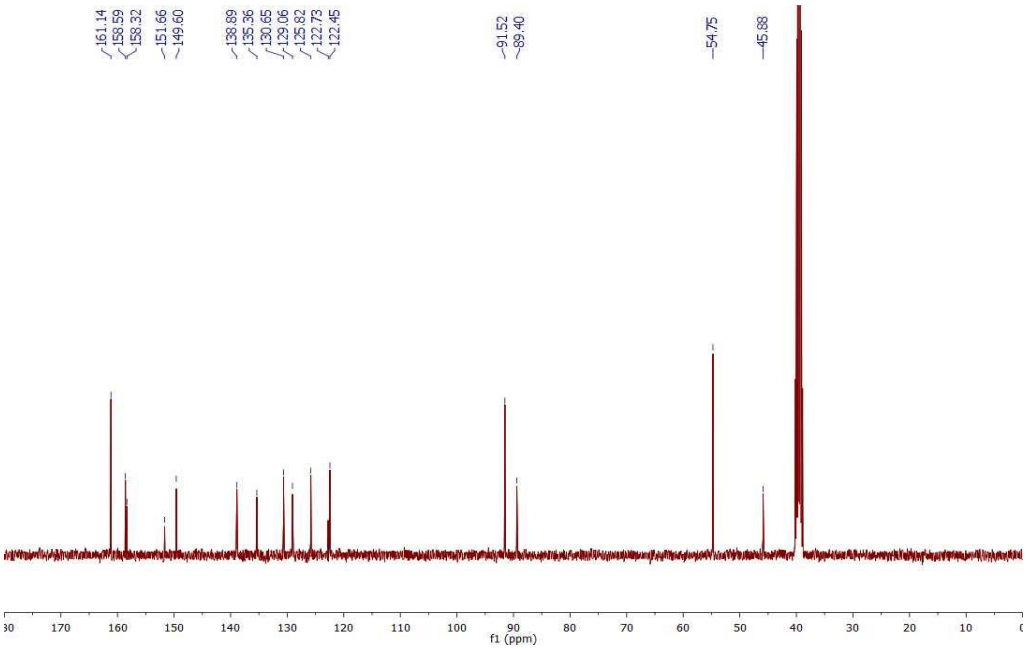

LC-MS (ES + APCI)

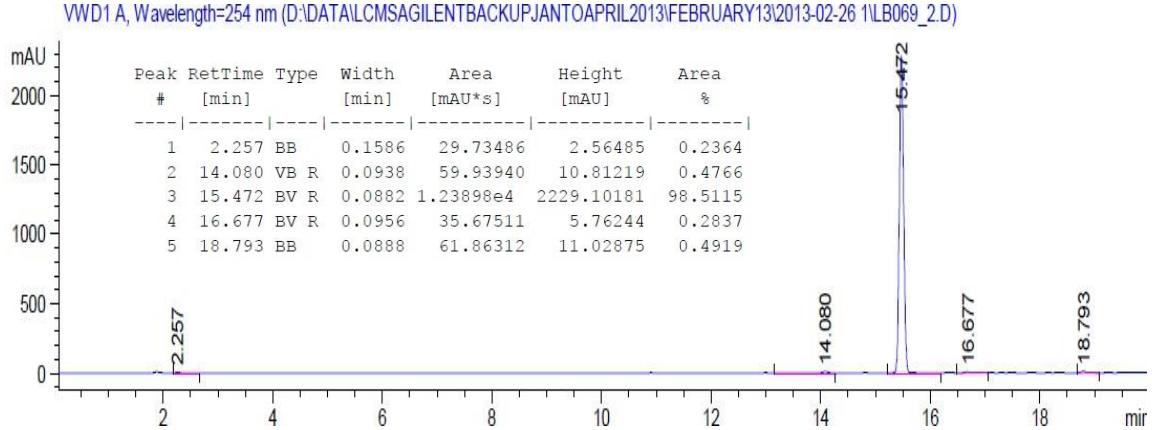

8-Chloro-2-(((4-fluorophenyl)amino)methyl)benzo[4,5]thieno[3,2-*d*]pyrimidin-4(3*H*)-one (43r)

^{1}H NMR spectrum (500 MHz, DMSO)

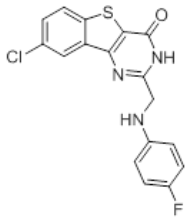

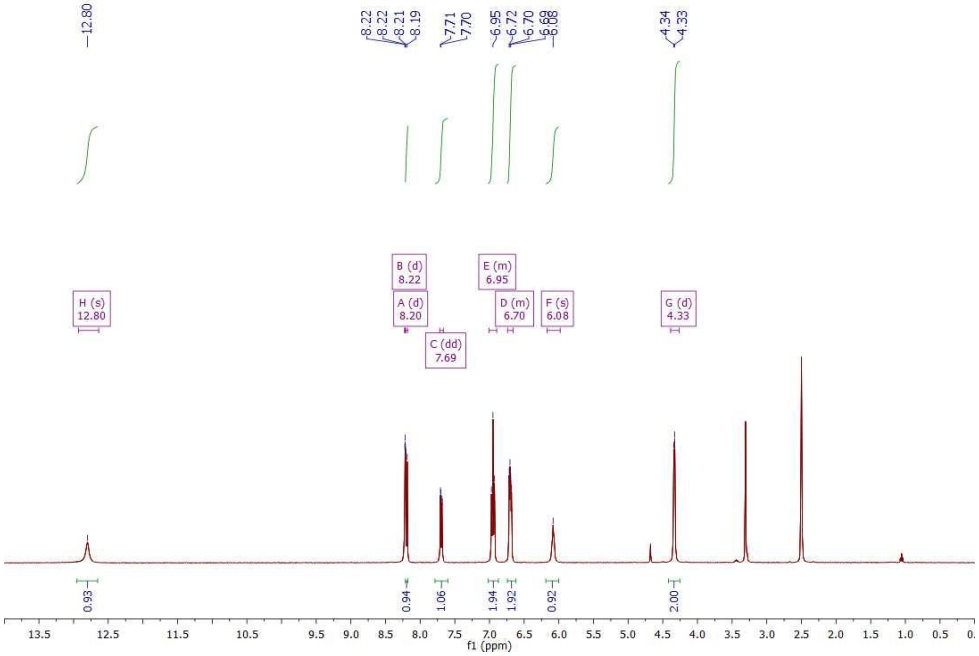

^{13}C NMR spectrum (126 MHz, DMSO)

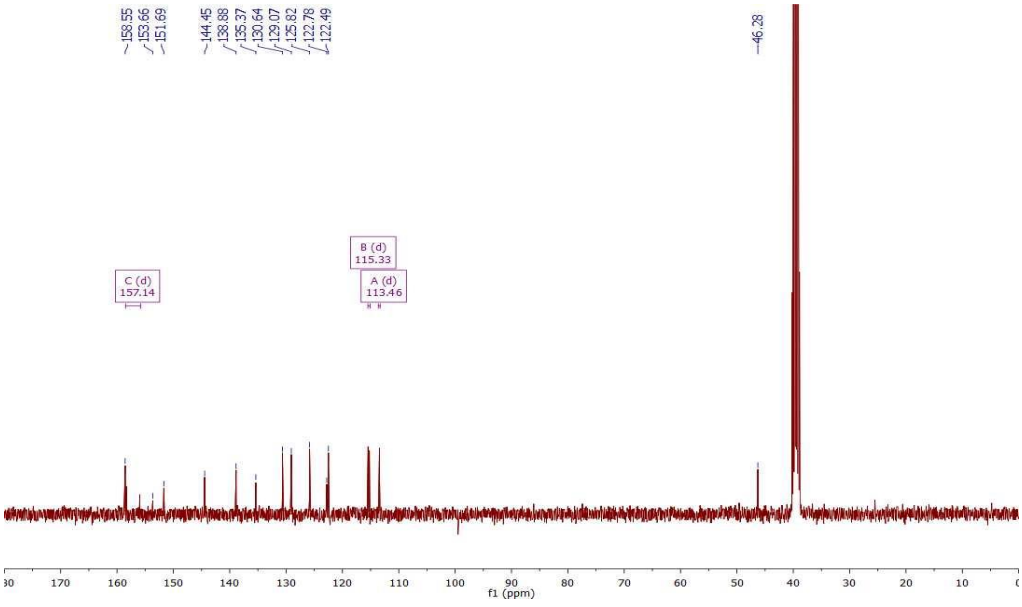

LC-MS (ES + APCI)

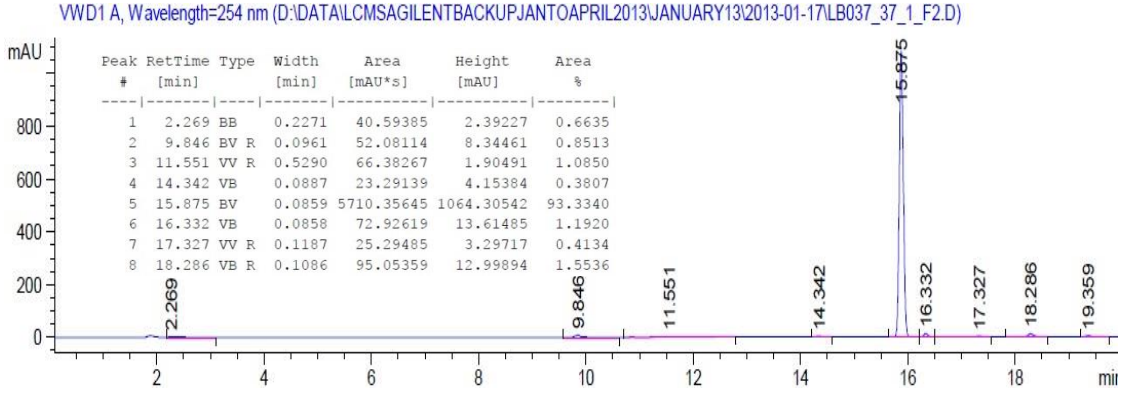

8-Chloro-2-((pyridin-2-ylamino)methyl)benzo[4,5]thieno[3,2-*d*]pyrimidin-4(*3H*)-one (43s)

^{1}H NMR spectrum (400 MHz, DMSO)

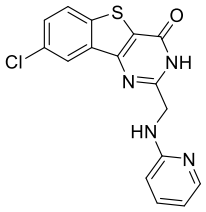

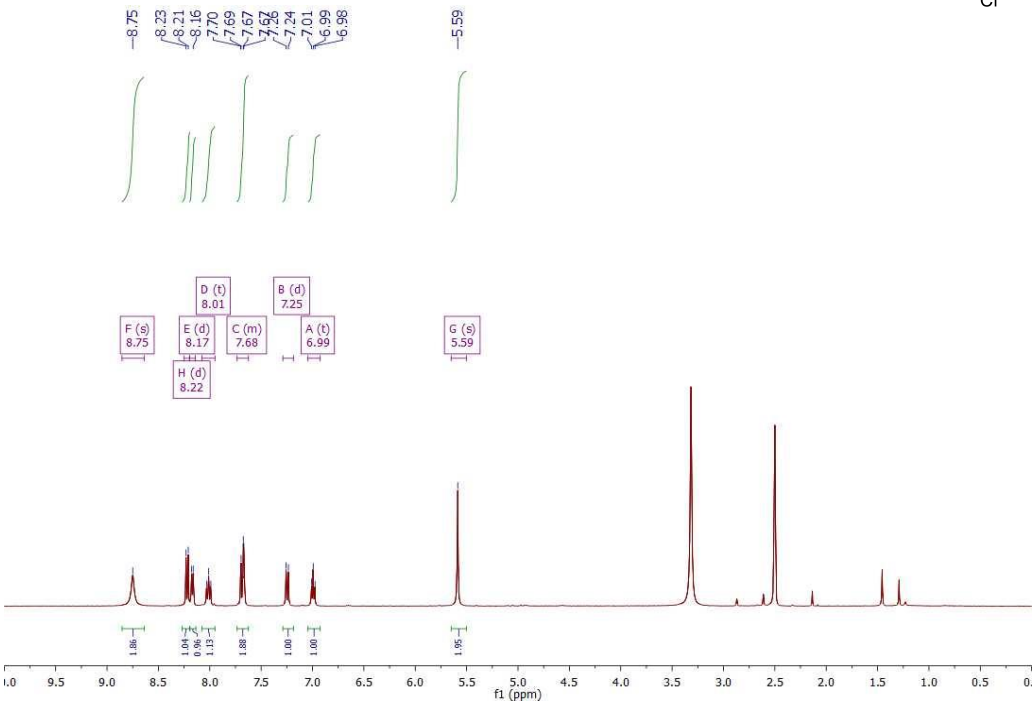

^{13}C NMR spectrum (101 MHz, DMSO)

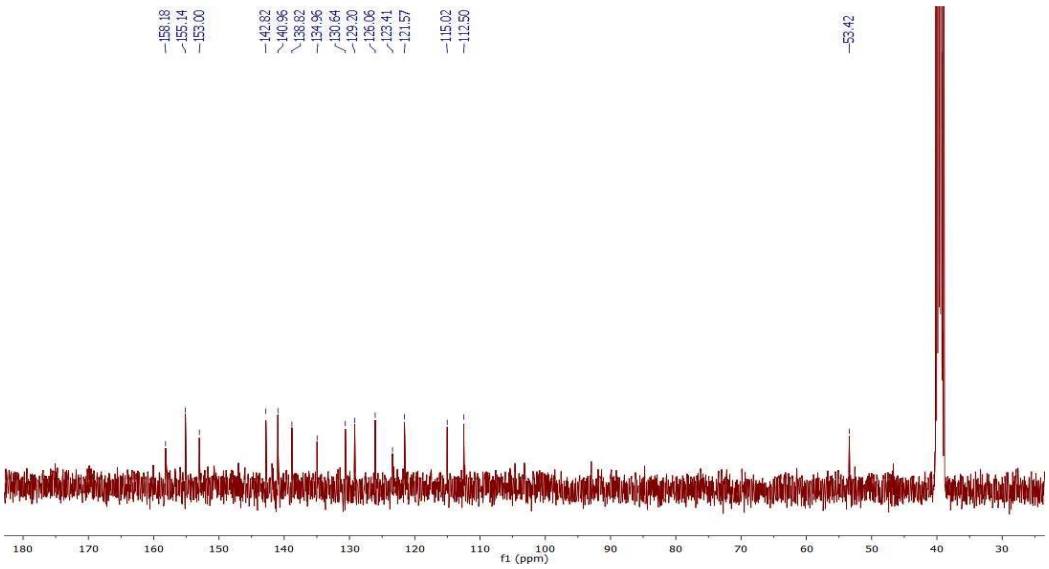

LC-MS (ES + APCI)

Peak #	RetTime [min]	Type	Width [min]	Area [mAU*s]	Height [mAU]	Area %
1	1.353	BB	0.1791	1.74075	1.53381e-1	0.0154
2	4.789	BB	0.0967	4.25466	6.04430e-1	0.0377
3	5.418	BV	0.0919	27.76925	3.89718	0.2458
4	5.522	VV f	0.0402	1125.56982	511.53317	9.9617
5	5.567	VV	0.0865	9982.41406	1556.12732	88.3476
6	5.969	VV b	0.0433	1.17755	4.34841e-1	0.0104
7	6.212	VV b	0.0491	1.59360	5.38304e-1	0.0141
8	6.387	VV b	0.1188	10.68626	1.59813	0.0946
9	6.588	VV	0.0595	15.46963	3.77614	0.1369
10	6.674	VB	0.0704	15.40547	3.05809	0.1363
11	6.841	BV	0.0759	4.50150	9.45923e-1	0.0398
12	6.938	VB	0.0489	3.26336	1.02341	0.0289
13	7.325	BV	0.0995	12.11173	1.72297	0.1072
14	7.408	VV b	0.0380	1.34280	5.94578e-1	0.0119
15	7.496	VV	0.0587	2.30816	5.72426e-1	0.0204
16	7.575	VB	0.0594	2.21693	5.77416e-1	0.0196
17	7.842	BB	0.1863	4.22564	2.82263e-1	0.0374
18	8.730	BV	0.0729	24.27967	5.11456	0.2149
19	8.814	VB	0.0570	16.87351	4.34115	0.1493
20	9.110	BV	0.2783	3.29852	1.47549e-1	0.0292

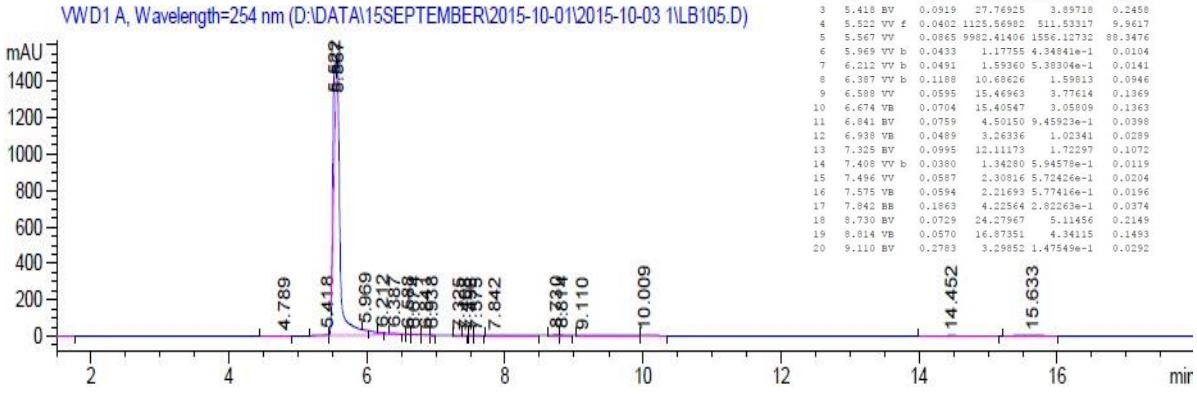

8-Chloro-2-((pyridin-3-ylamino)methyl)benzo[4,5]thieno[3,2-*d*]pyrimidin-4(*3H*)-one (43t)

^{1}H NMR spectrum (400 MHz, DMSO)

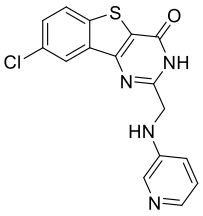

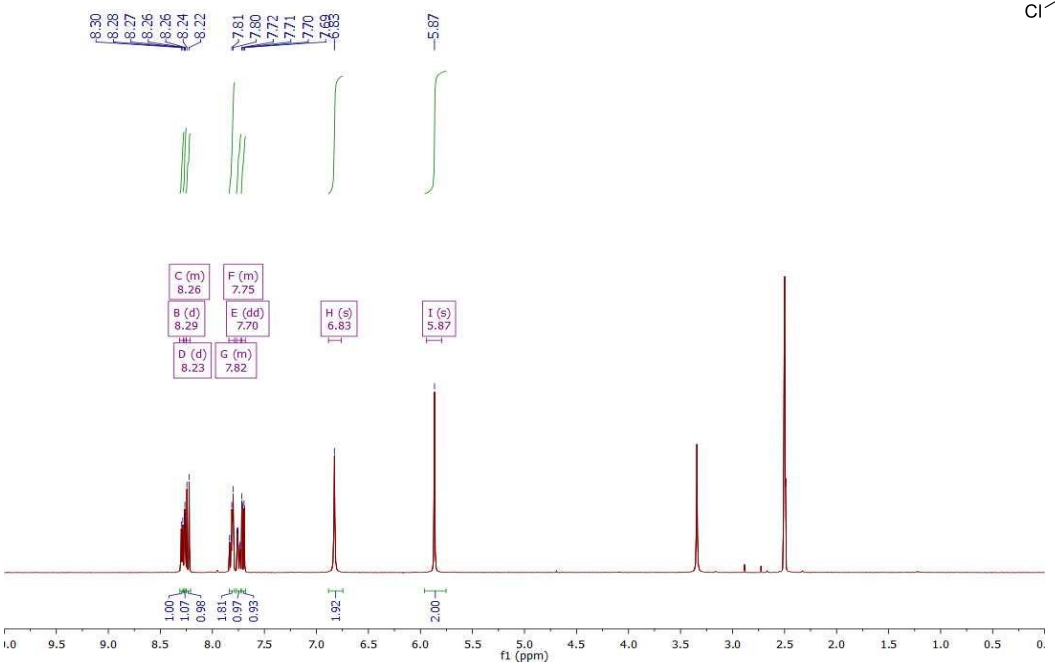

^{13}C NMR spectrum (101 MHz, DMSO)

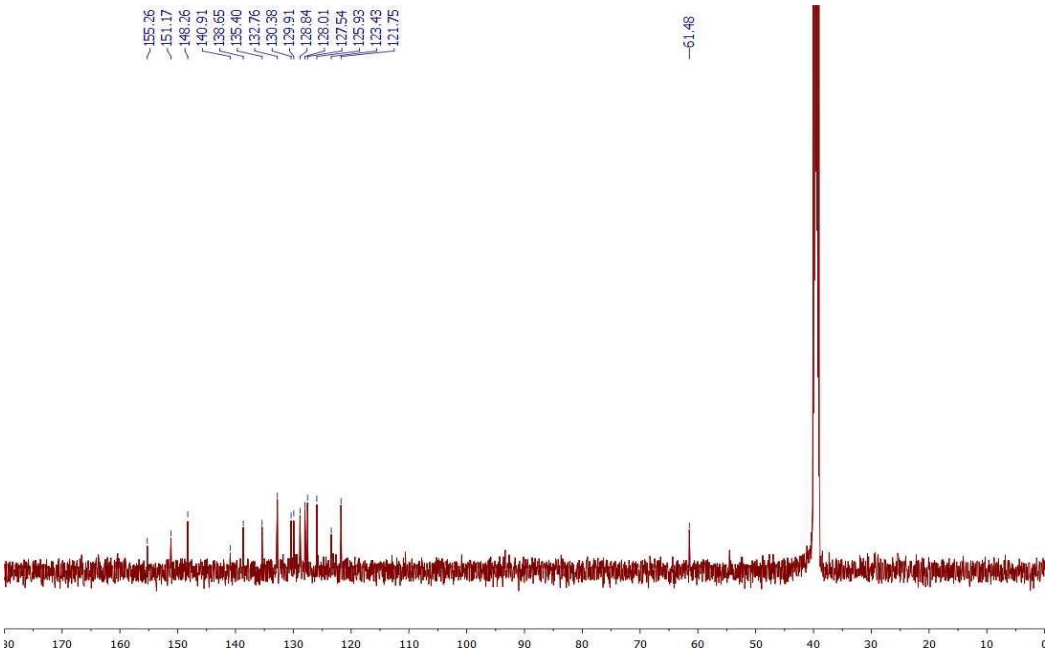

LC-MS (ES + APCI)

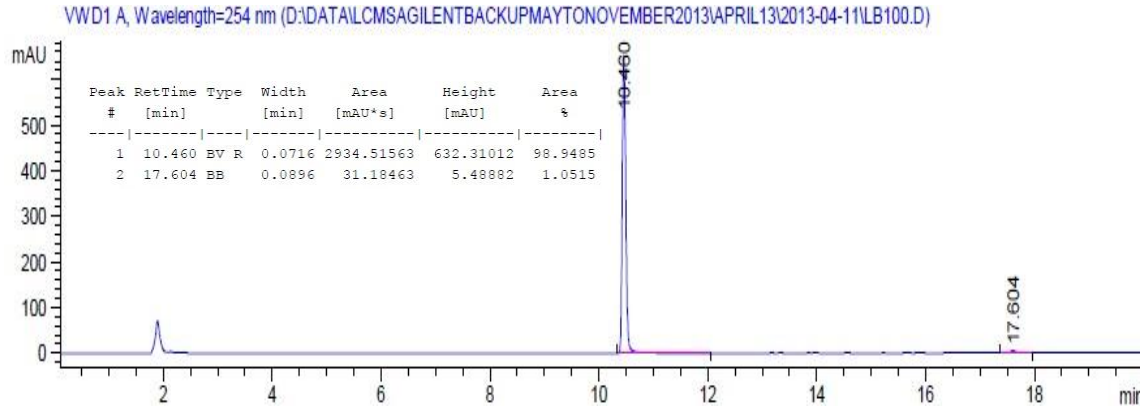

8-Chloro-2-((pyridin-4-ylamino)methyl)benzo[4,5]thieno[3,2-*d*]pyrimidin-4(*3H*)-one (43u)

^{1}H NMR spectrum (400 MHz, DMSO)

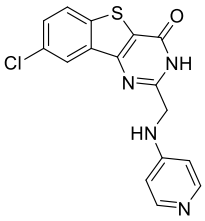

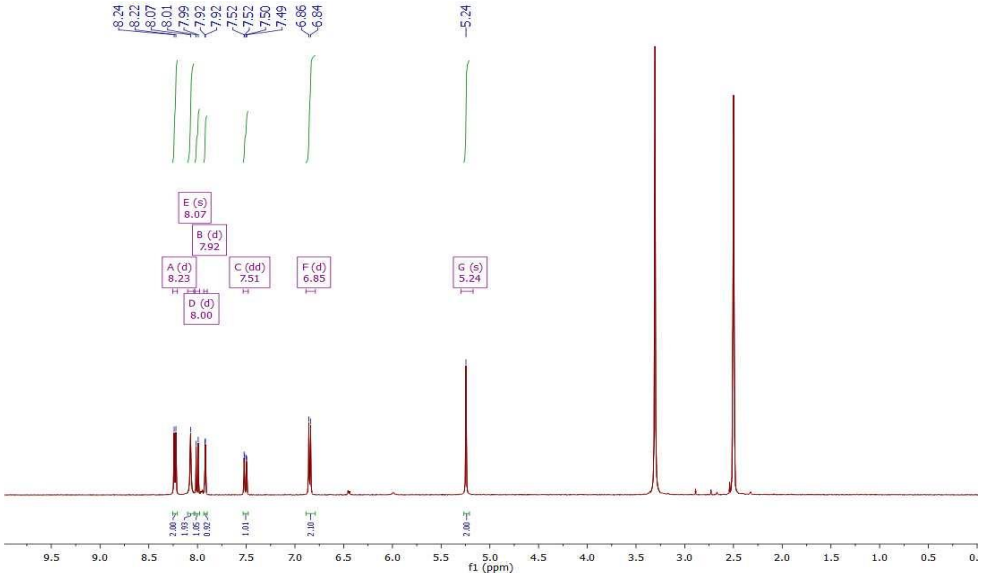

^{13}C NMR spectrum (101 MHz, DMSO/benzene)

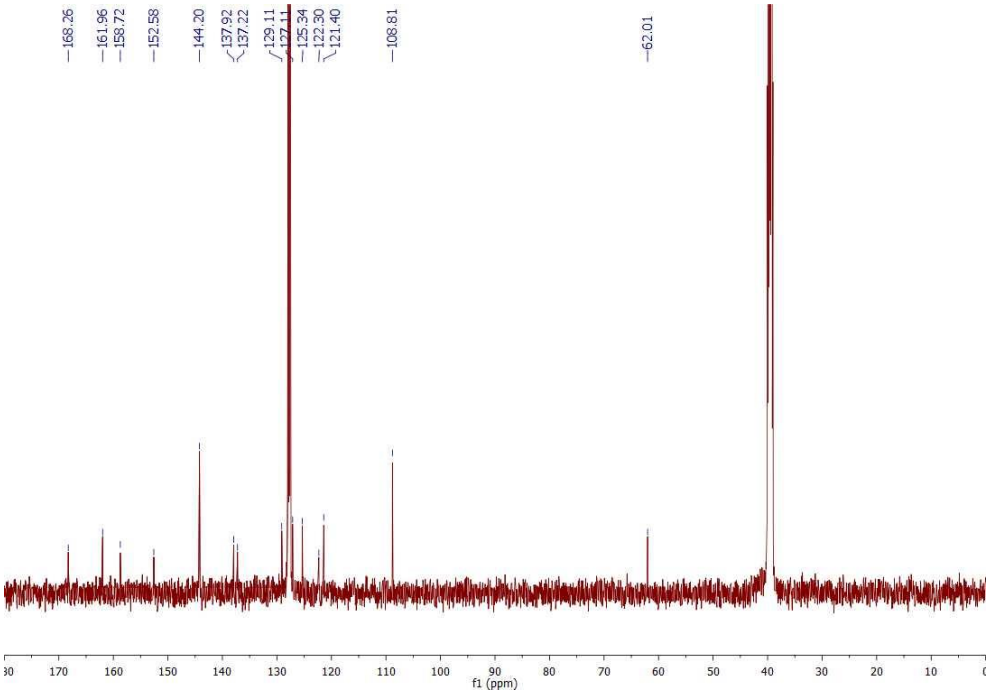

LC-MS (ES + APCI)

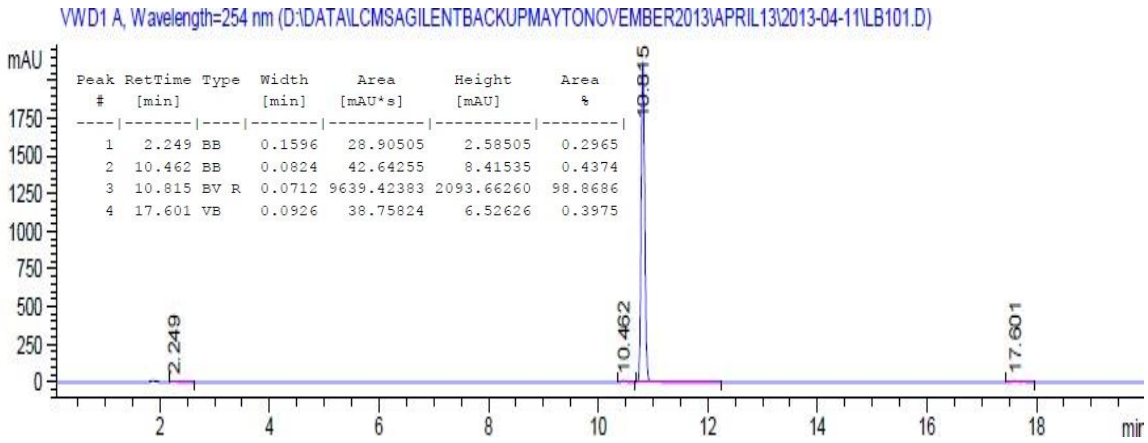

8-Bromo-2-((methylamino)methyl)benzo[4,5]thieno[3,2-*d*]pyrimidin-4(3*H*)-one (46a)

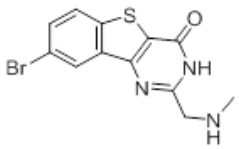

^{1}H NMR spectrum (400 MHz, DMSO)

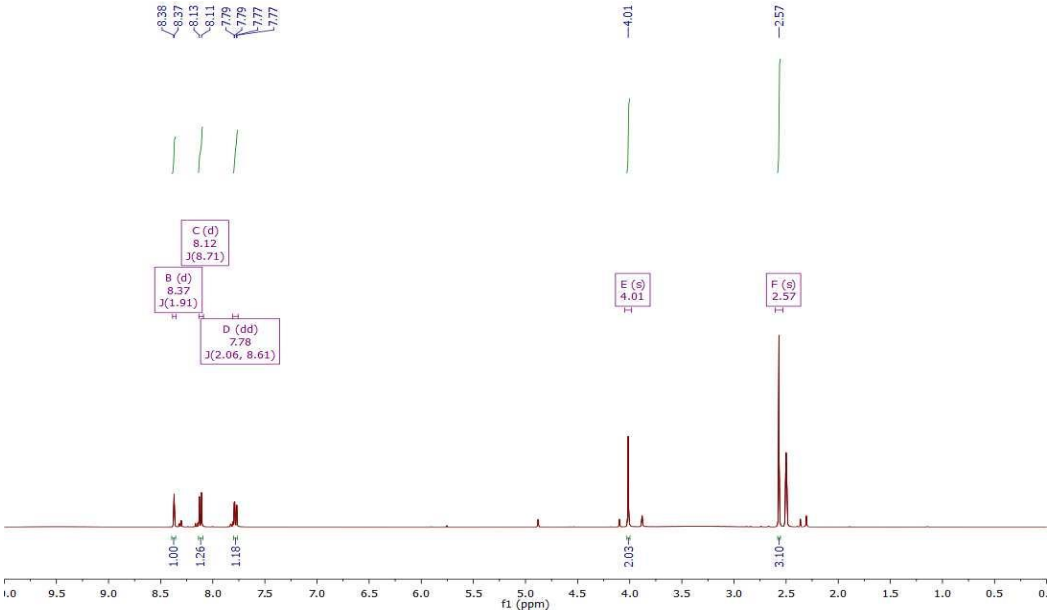

^{13}C NMR spectrum (101 MHz, DMSO)

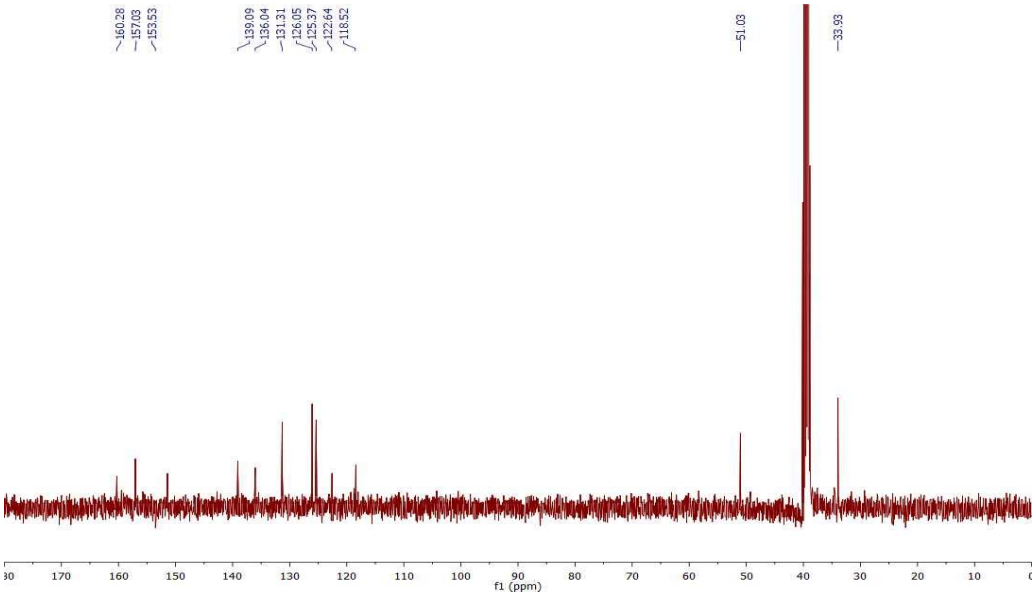

LC-MS (ES + APCI)

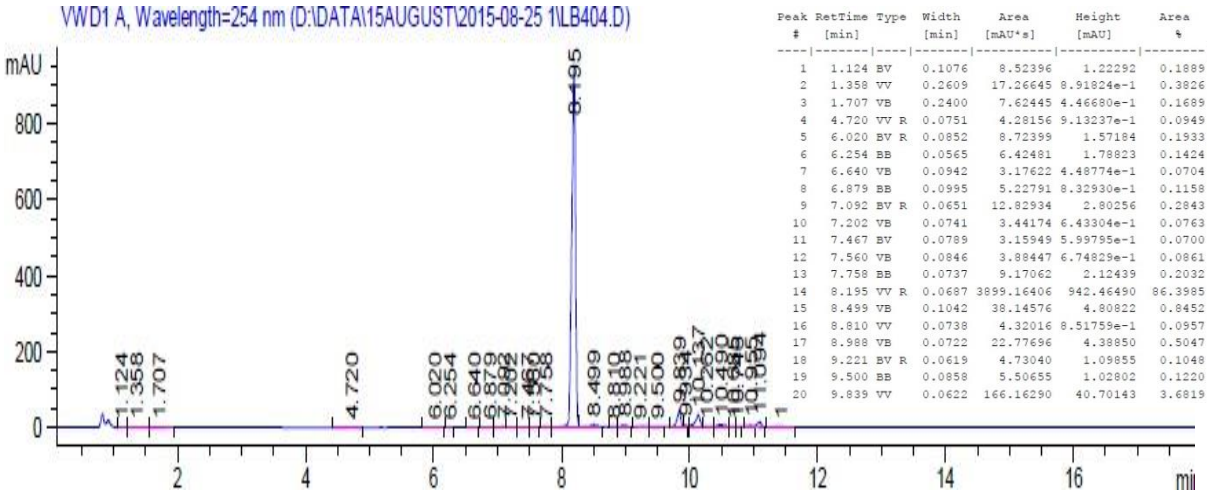

Peak #	RetTime [min]	Type	Width [min]	Area [mAU*s]	Height [mAU]	Area %
1	1.124	BV	0.1076	8.52396	1.22292	0.1889
2	1.358	VV	0.2609	17.26645	8.91824e-1	0.3826
3	1.707	VB	0.2400	7.62445	4.46680e-1	0.1689
4	4.720	VV R	0.0751	4.28156	9.13237e-1	0.0949
5	6.020	BV R	0.0852	8.72399	1.57184	0.1933
6	6.254	BB	0.0565	6.42481	1.78823	0.1424
7	6.640	VB	0.0942	3.17622	4.48774e-1	0.0704
8	6.879	BB	0.0995	5.22791	8.32930e-1	0.1158
9	7.092	BV R	0.0651	12.82934	2.80256	0.2843
10	7.202	VB	0.0741	3.44174	6.43304e-1	0.0763
11	7.467	BV	0.0789	3.15949	5.99795e-1	0.0700
12	7.560	VB	0.0846	3.88447	6.74829e-1	0.0861
13	7.758	BB	0.0737	9.17062	2.12439	0.2032
14	8.195	VV R	0.0687	3899.16406	942.46490	86.3985
15	8.499	VB	0.1042	38.14576	4.80822	0.8452
16	8.810	VV	0.0738	4.32016	8.51759e-1	0.0957
17	8.988	VB	0.0722	22.77696	4.38850	0.5047
18	9.221	BV R	0.0619	4.73040	1.09855	0.1048
19	9.500	BB	0.0858	5.50655	1.02802	0.1220
20	9.839	VV	0.0622	166.16290	40.70143	3.6819

2-((Methylamino)methyl)-8-phenylbenzo[4,5]thieno[3,2-*d*]pyrimidin-4(3*H*)-one (47a)

^{1}H NMR spectrum (400 MHz, DMSO)

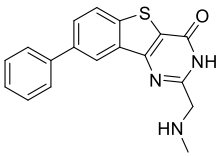

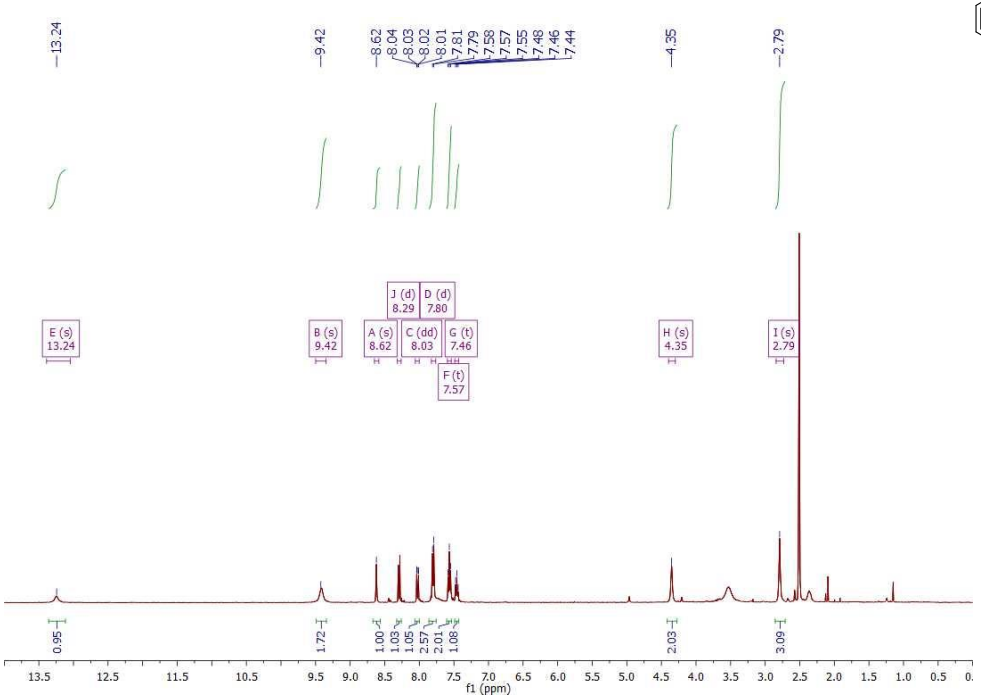

^{13}C NMR spectrum (101 MHz, DMSO)

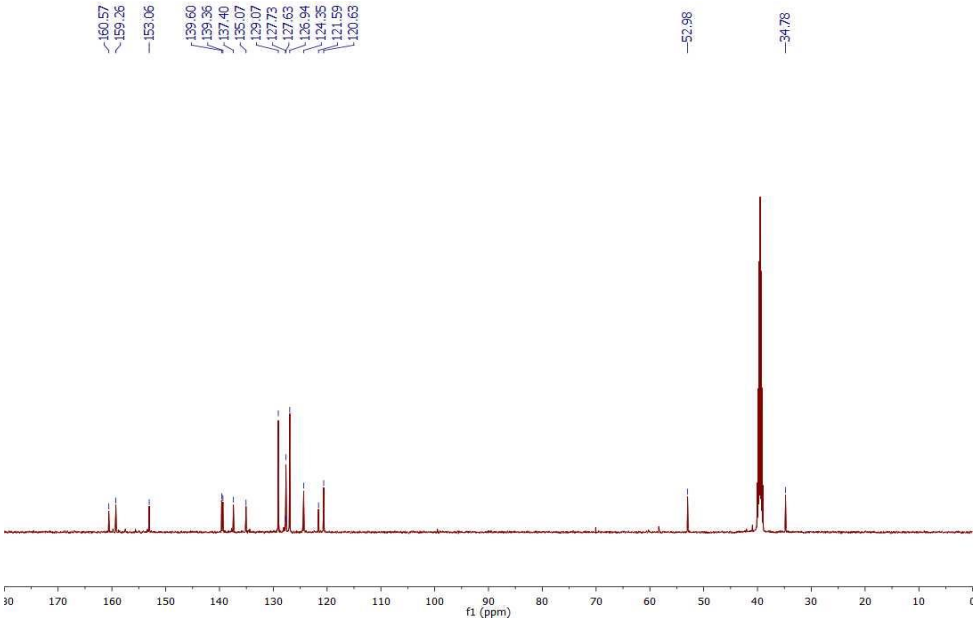

LC-MS (ES + APCI)

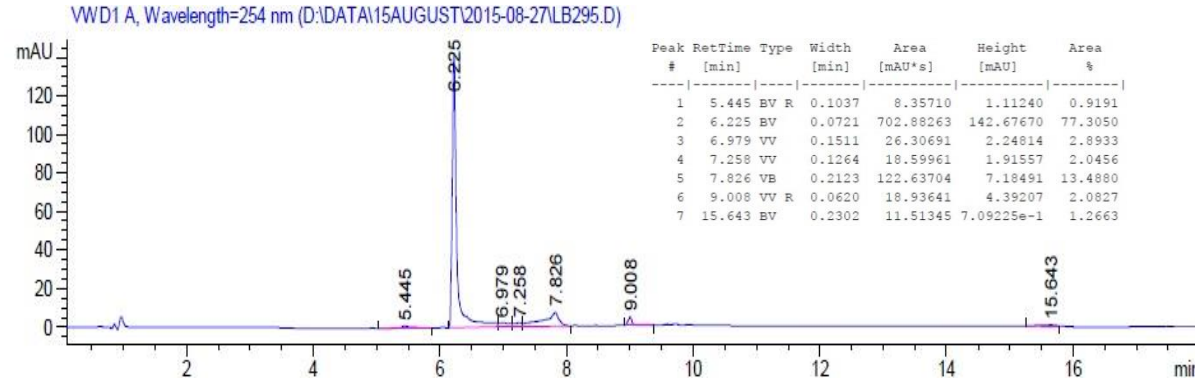

Peak #	RetTime [min]	Type	Width [min]	Area [mAU*s]	Height [mAU]	Area %
1	5.445	BV R	0.1037	8.35710	1.11240	0.9191
2	6.225	BV	0.0721	702.88263	142.67670	77.3050
3	6.979	VV	0.1511	26.30691	2.24814	2.8933
4	7.258	VV	0.1264	18.59961	1.91557	2.0456
5	7.826	VB	0.2123	122.63704	7.18491	13.4880
6	9.008	VV R	0.0620	18.93641	4.39207	2.0827
7	15.643	BV	0.2302	11.51345	7.09225e-1	1.2663

2-((Methylamino)methyl)-8-nitrobenzo[4,5]thieno[3,2-*d*]pyrimidin-4(3*H*)-one (48a)

^{1}H NMR spectrum (400 MHz, DMSO)

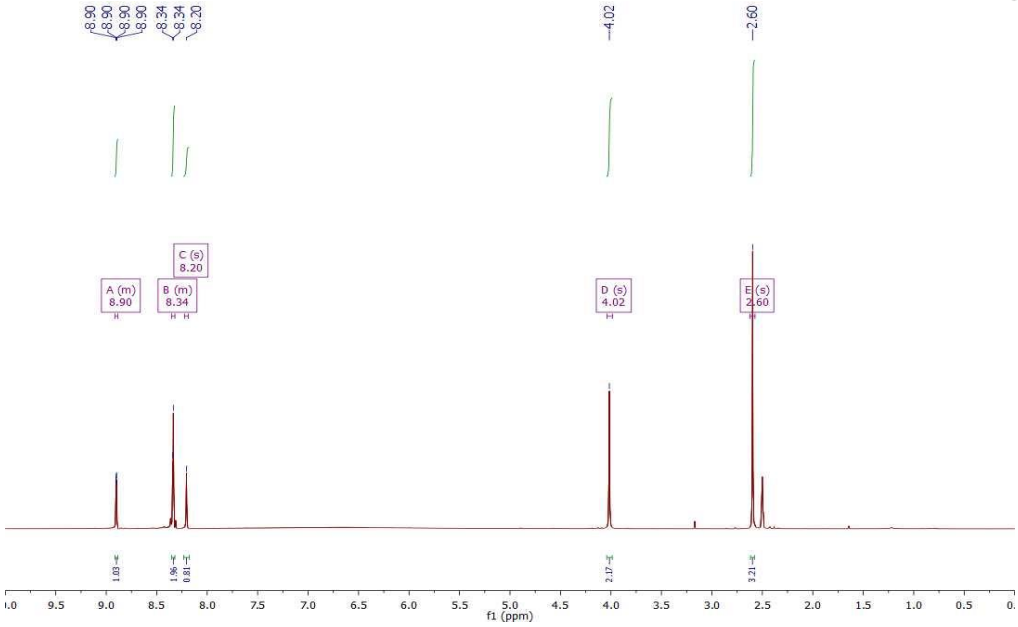

^{13}C NMR spectrum (101 MHz, DMSO)

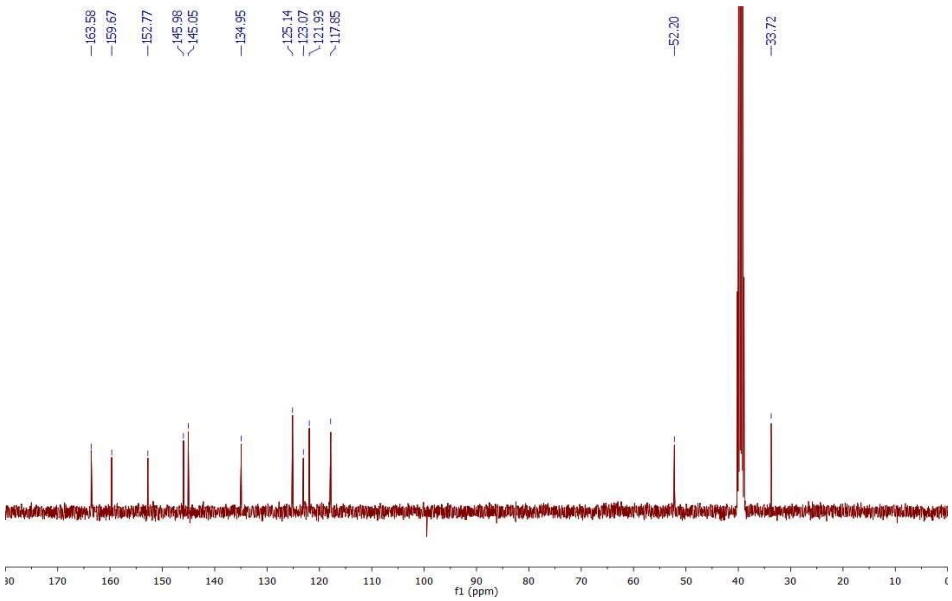

LC-MS (ES + APCI)

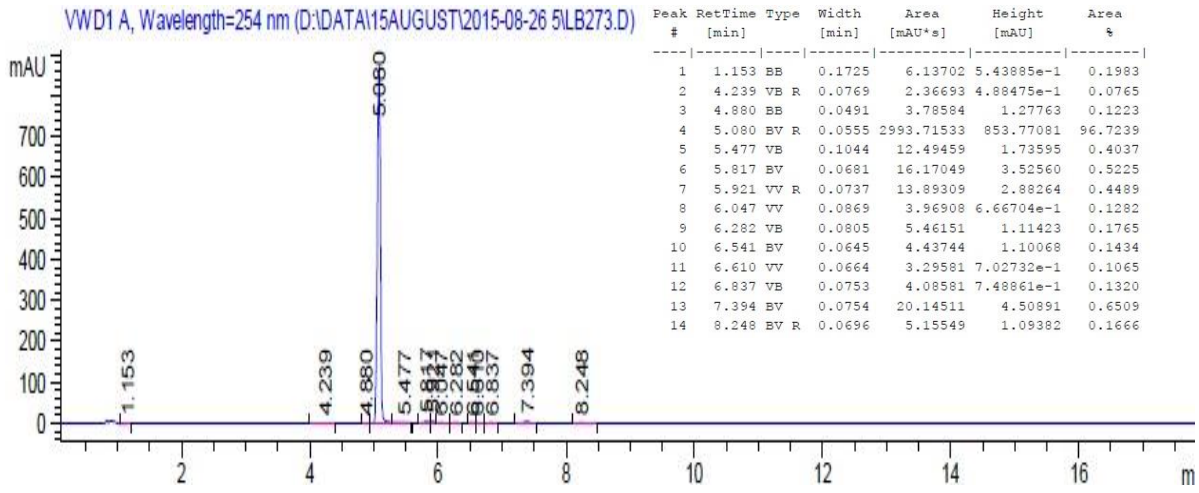

Peak #	RetTime [min]	Type	Width [min]	Area [mAU*s]	Height [mAU]	Area %
1	1.153	BB	0.1725	6.13702	5.43885e-1	0.1983
2	4.239	VB R	0.0769	2.36693	4.88475e-1	0.0765
3	4.880	BB	0.0491	3.78584	1.27763	0.1223
4	5.080	BV R	0.0555	2993.71533	853.77081	96.7239
5	5.477	VB	0.1044	12.49459	1.73595	0.4037
6	5.817	BV	0.0681	16.17049	3.52560	0.5225
7	5.921	VV R	0.0737	13.89309	2.88264	0.4489
8	6.047	VV	0.0869	3.96908	6.66704e-1	0.1282
9	6.282	VB	0.0805	5.46151	1.11423	0.1765
10	6.541	BV	0.0645	4.43744	1.10068	0.1434
11	6.610	VV	0.0664	3.29581	7.02732e-1	0.1065
12	6.837	VB	0.0753	4.08581	7.48861e-1	0.1320
13	7.394	BV	0.0754	20.14511	4.50891	0.6509
14	8.248	BV R	0.0696	5.15549	1.09382	0.1666

2-((Methylamino)methyl)-8-(trifluoromethyl)benzo[4,5]thieno[3,2-*d*]pyrimidin-4(*3H*)-one (49a)

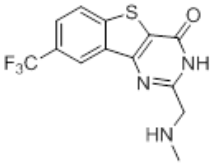

^{1}H NMR spectrum (400 MHz, DMSO)

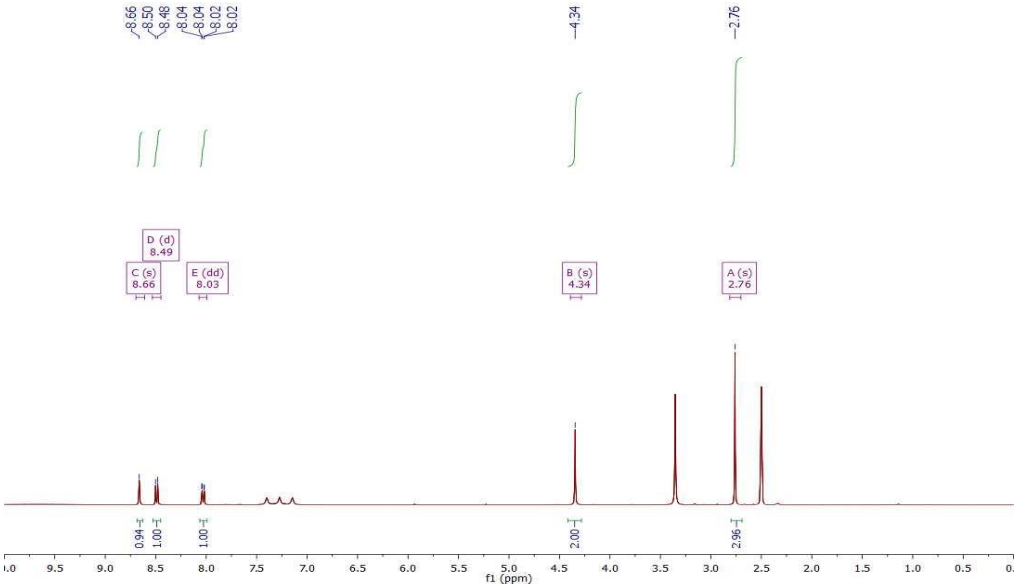

^{13}C NMR spectrum (101 MHz, DMSO)

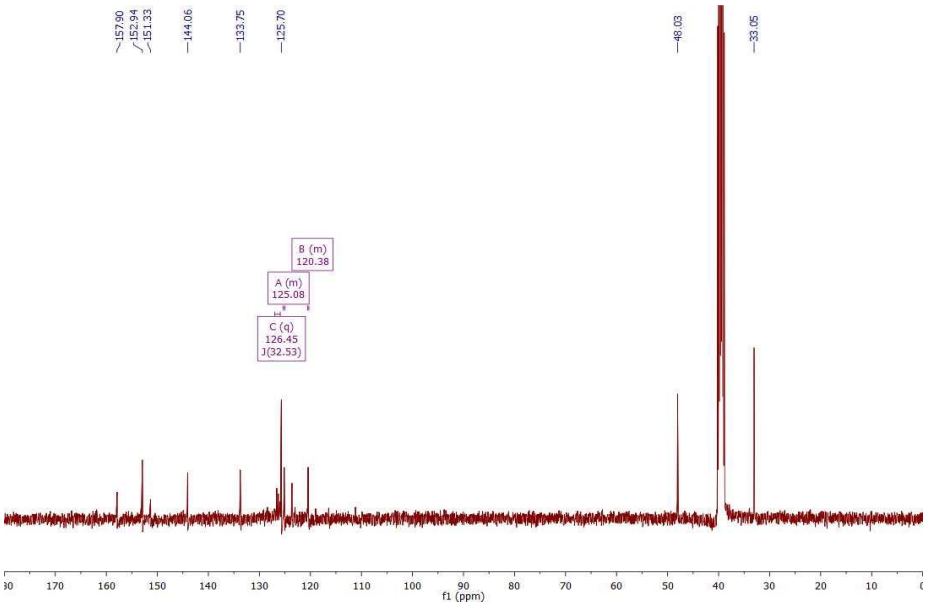

LC-MS (ES + APCI)

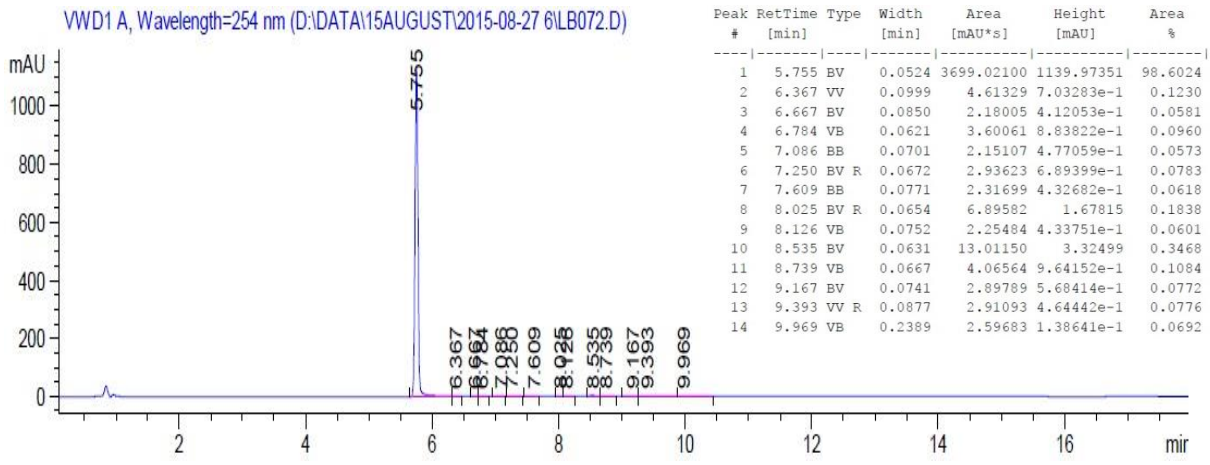

Peak #	RetTime [min]	Type	Width [min]	Area [mAU*s]	Height [mAU]	Area %
1	5.755	BV	0.0524	3699.02100	1139.97351	98.6024
2	6.367	VV	0.0999	4.61329	7.03283e-1	0.1230
3	6.667	BV	0.0850	2.18005	4.12053e-1	0.0581
4	6.784	VB	0.0621	3.60061	8.83822e-1	0.0960
5	7.086	BB	0.0701	2.15107	4.77059e-1	0.0573
6	7.250	BV R	0.0672	2.93623	6.89399e-1	0.0783
7	7.609	BB	0.0771	2.31699	4.32682e-1	0.0618
8	8.025	BV R	0.0654	6.89582	1.67815	0.1838
9	8.126	VB	0.0752	2.25484	4.33751e-1	0.0601
10	8.535	BV	0.0631	13.01150	3.32499	0.3468
11	8.739	VB	0.0667	4.06564	9.64152e-1	0.1084
12	9.167	BV	0.0741	2.89789	5.68414e-1	0.0772
13	9.393	VV R	0.0877	2.91093	4.64442e-1	0.0776
14	9.969	VB	0.2389	2.59683	1.38641e-1	0.0692

2-(Morpholinomethyl)-8-(trifluoromethyl)benzo[4,5]thieno[3,2-*d*]pyrimidin-4(*3H*)-one (49b)

^{1}H NMR spectrum (400 MHz, DMSO)

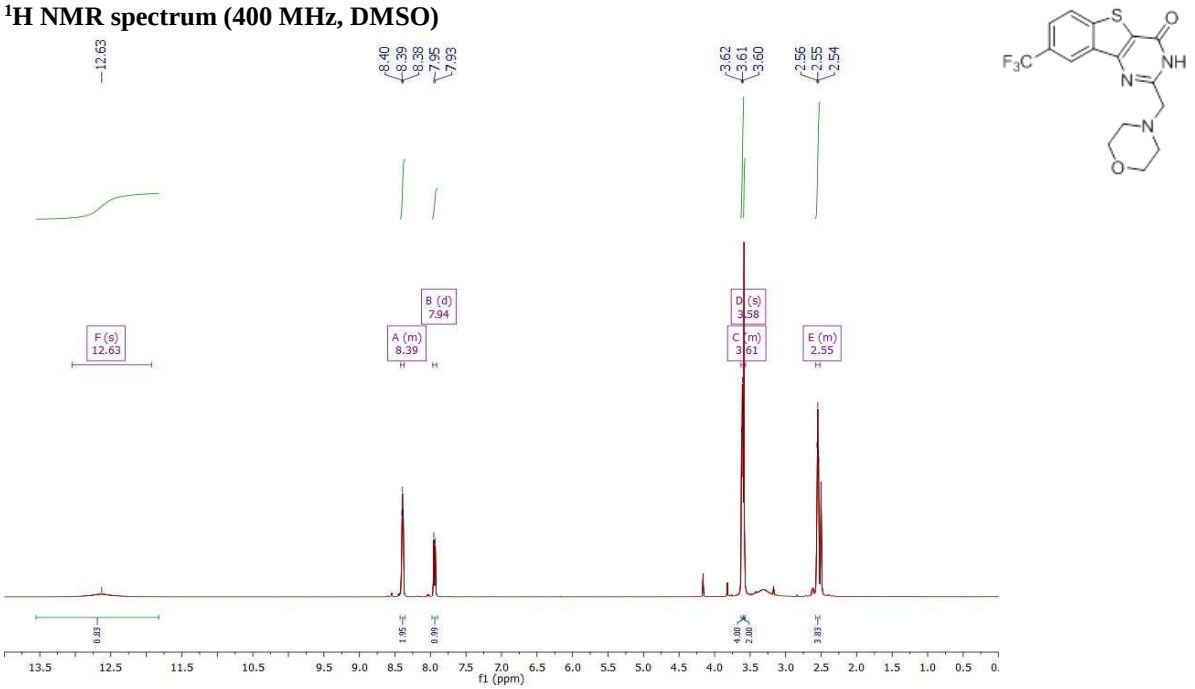

^{13}C NMR spectrum (101 MHz, DMSO)

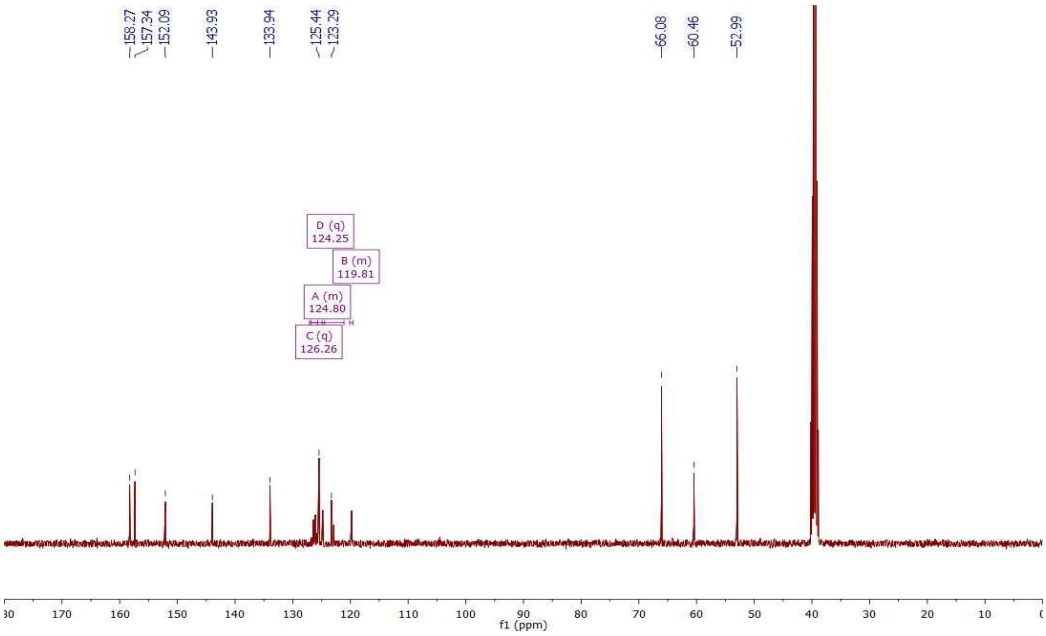

LC-MS (ES + APCI)

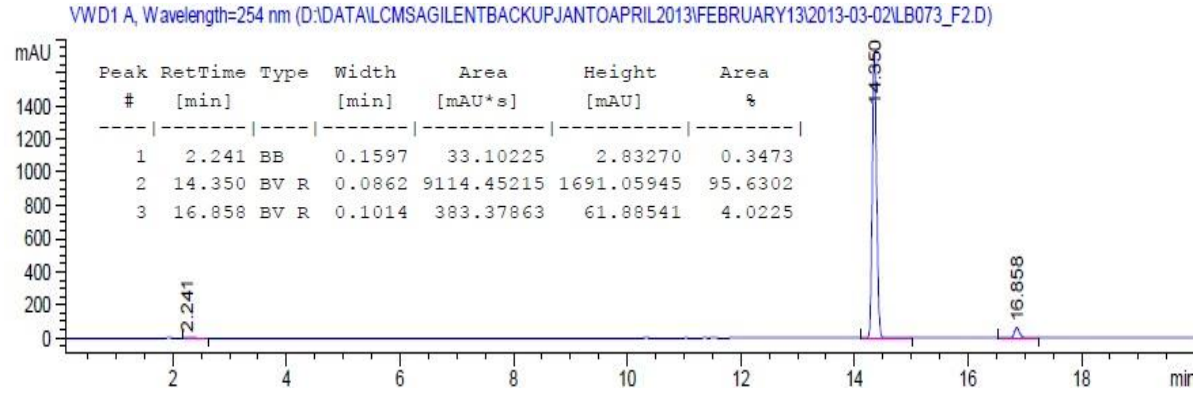

8-Nitro-2-((pyridin-3-ylamino)methyl)benzo[4,5]thieno[3,2-*d*]pyrimidin-4(3*H*)-one (48u)

^{1}H NMR spectrum (400 MHz, DMSO)

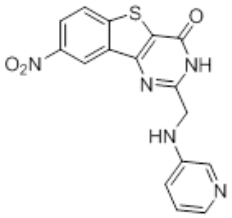

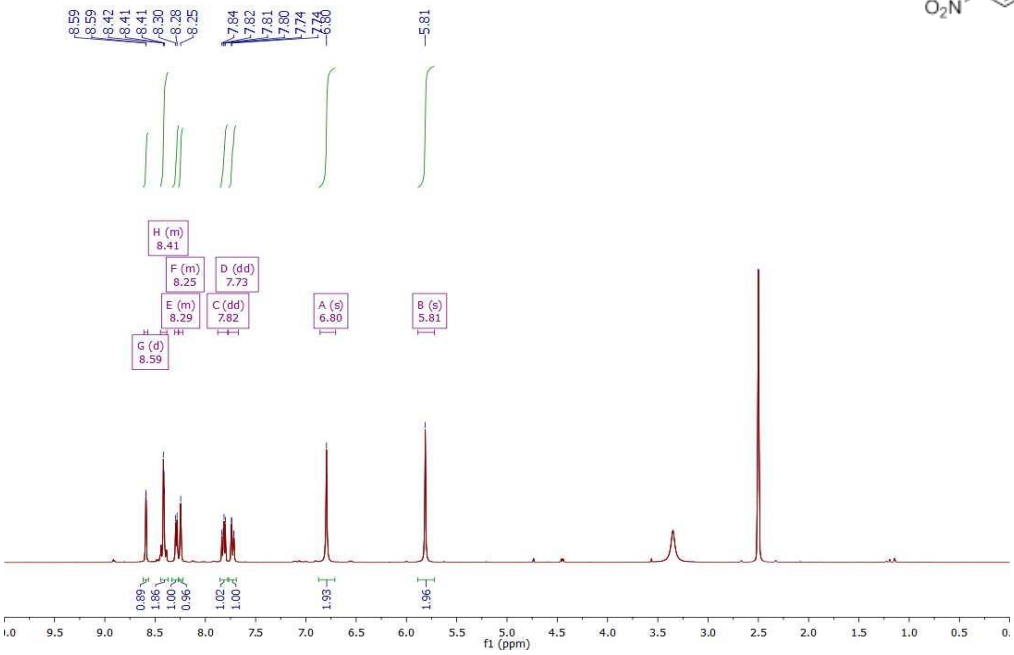

^{13}C NMR spectrum (101 MHz, DMSO)

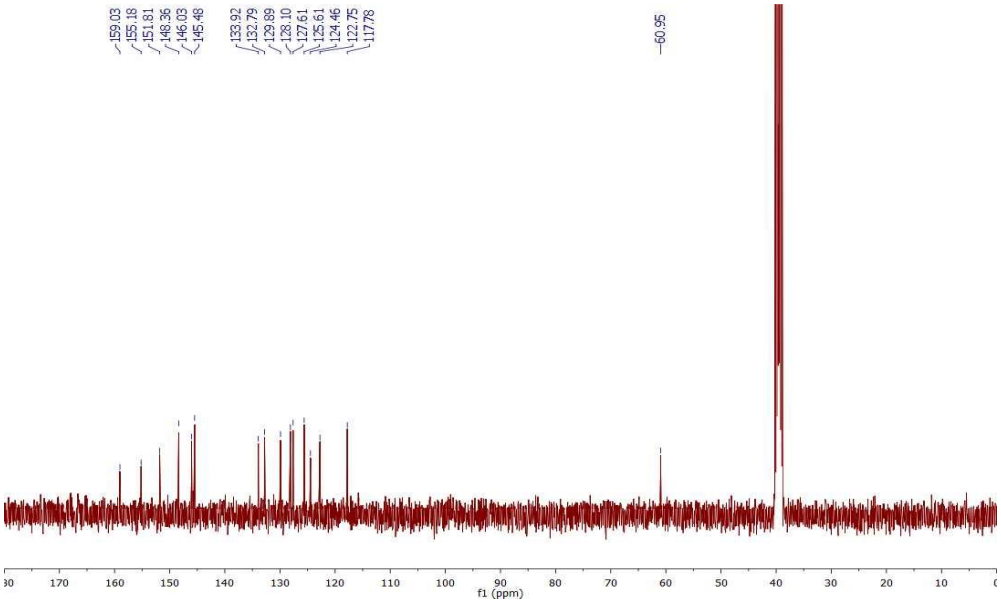

LC-MS (ES + APCI)

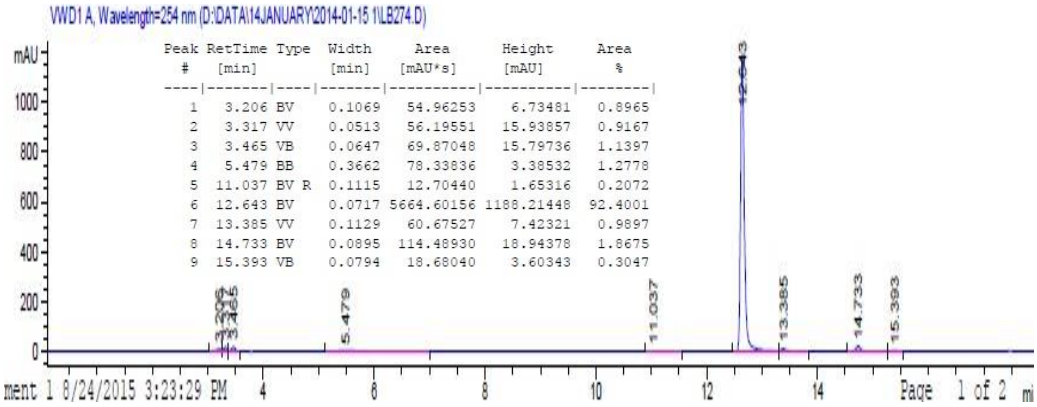

Peak #	RetTime [min]	Type	Width [min]	Area [mAU*s]	Height [mAU]	Area %
1	3.206	BV	0.1069	54.96253	6.73481	0.8965
2	3.317	VV	0.0513	56.19551	15.93857	0.9167
3	3.465	VB	0.0647	69.87048	15.79736	1.1397
4	5.479	BB	0.3662	78.33836	3.38532	1.2778
5	11.037	BV R	0.1115	12.70440	1.65316	0.2072
6	12.643	BV	0.0717	5664.60156	1188.21448	92.4001
7	13.385	VV	0.1129	60.67527	7.42321	0.9897
8	14.733	BV	0.0895	114.48930	18.94378	1.8675
9	15.393	VB	0.0794	18.68040	3.60343	0.3047

2-(((3-Hydroxyphenyl)amino)methyl)-8-nitrobenzo[4,5]thieno[3,2-*d*]pyrimidin-4(3*H*)-one (48n)

^{1}H NMR spectrum (500 MHz, DMSO)

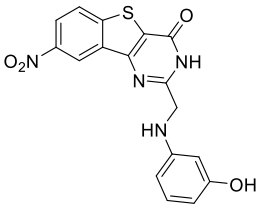

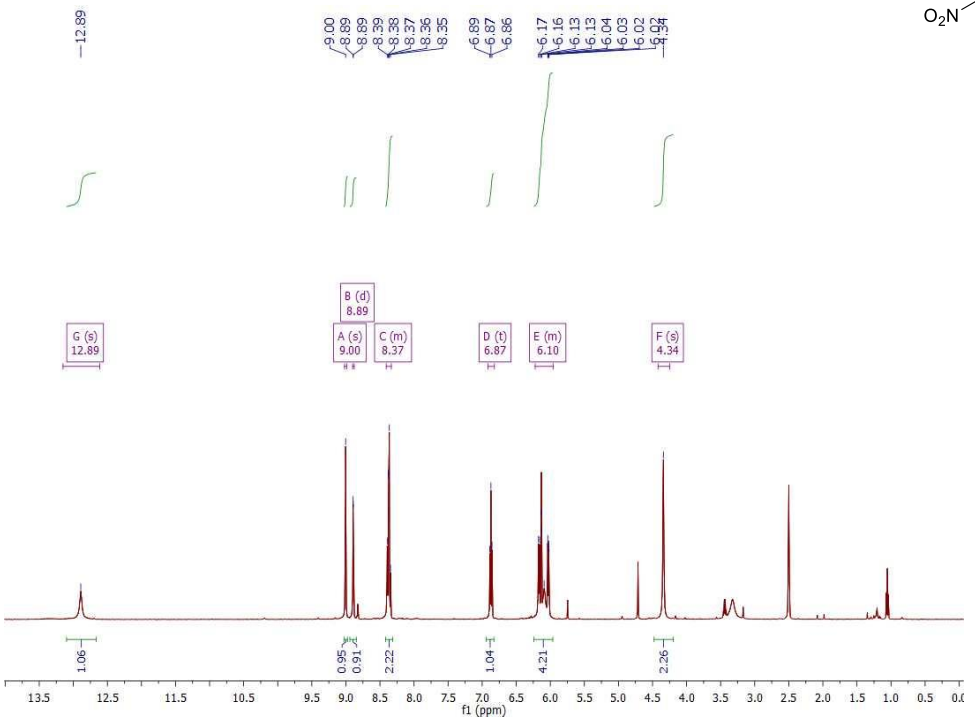

^{13}C NMR spectrum (126 MHz, DMSO)

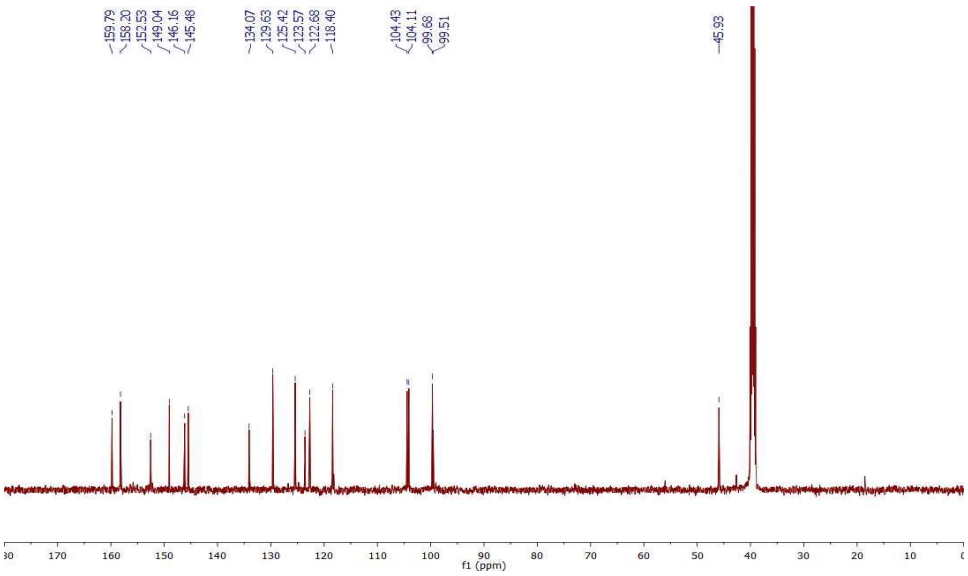

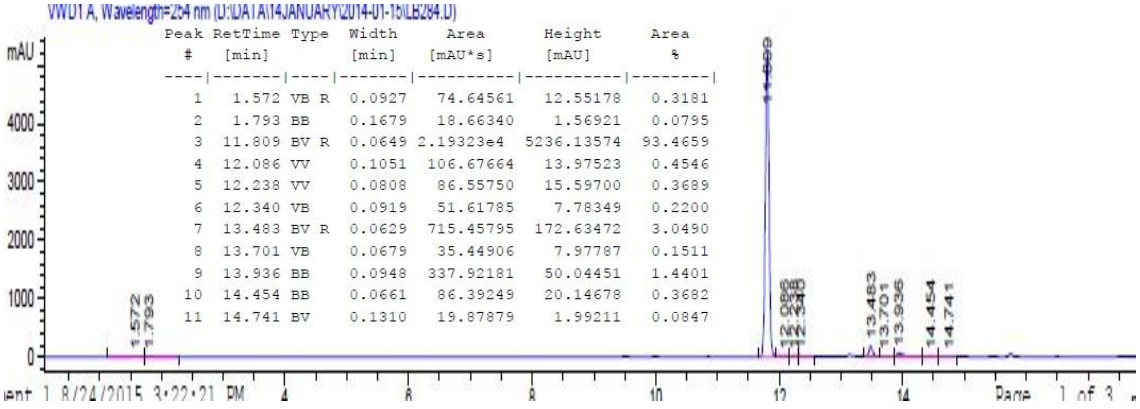

Peak #	RetTime [min]	Type	Width [min]	Area [mAU*s]	Height [mAU]	Area %
1	1.572	VB R	0.0927	74.64561	12.55178	0.3181
2	1.793	BB	0.1679	18.66340	1.56921	0.0795
3	11.809	BV R	0.0649	2.19323e4	5236.13574	93.4659
4	12.086	VV	0.1051	106.67664	13.97523	0.4546
5	12.238	VV	0.0808	86.55750	15.59700	0.3689
6	12.340	VB	0.0919	51.61785	7.78349	0.2200
7	13.483	BV R	0.0629	715.45795	172.63472	3.0490
8	13.701	VB	0.0679	35.44906	7.97787	0.1511
9	13.936	BB	0.0948	337.92181	50.04451	1.4401
10	14.454	BB	0.0661	86.39249	20.14678	0.3682
11	14.741	BV	0.1310	19.87879	1.99211	0.0847

7-Chloro-2-(morpholinomethyl)benzo[4,5]thieno[3,2-*d*]pyrimidin-4(3*H*)-one (44b)

^{1}H NMR spectrum (400 MHz, DMSO)

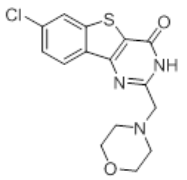

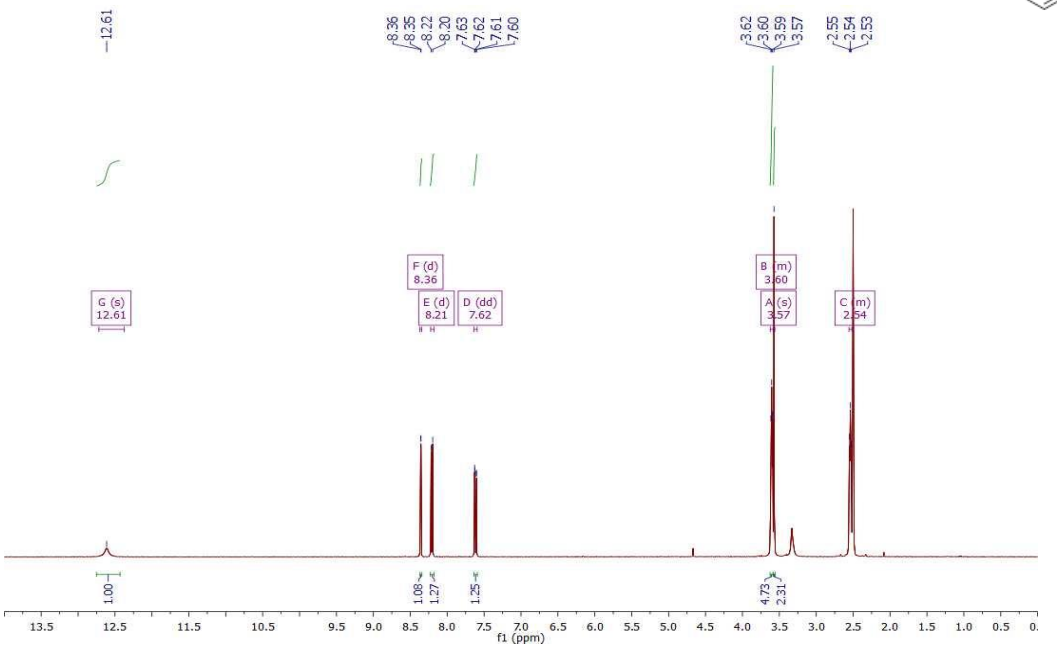

^{13}C NMR spectrum (101 MHz, DMSO)

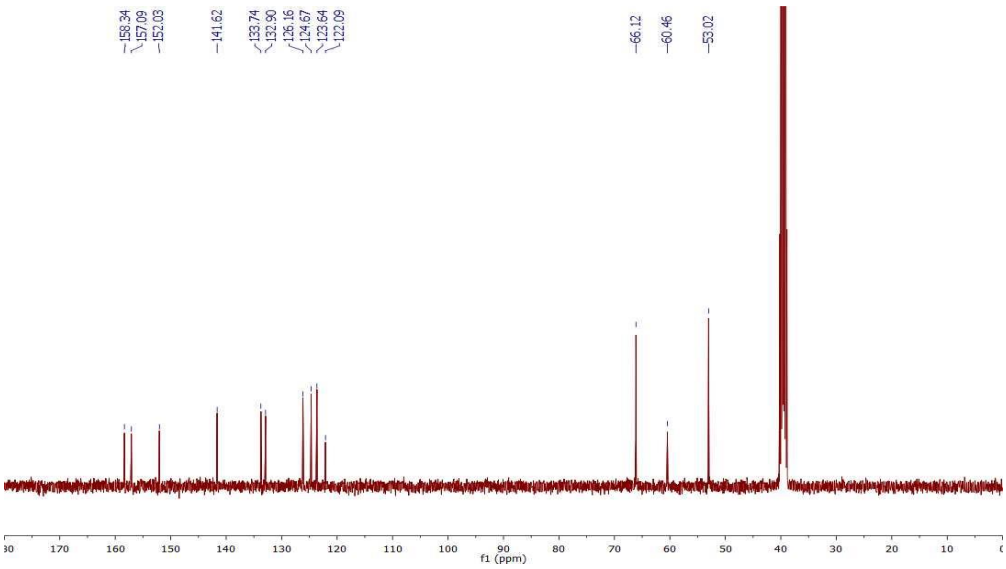

LC-MS (ES + APCI)

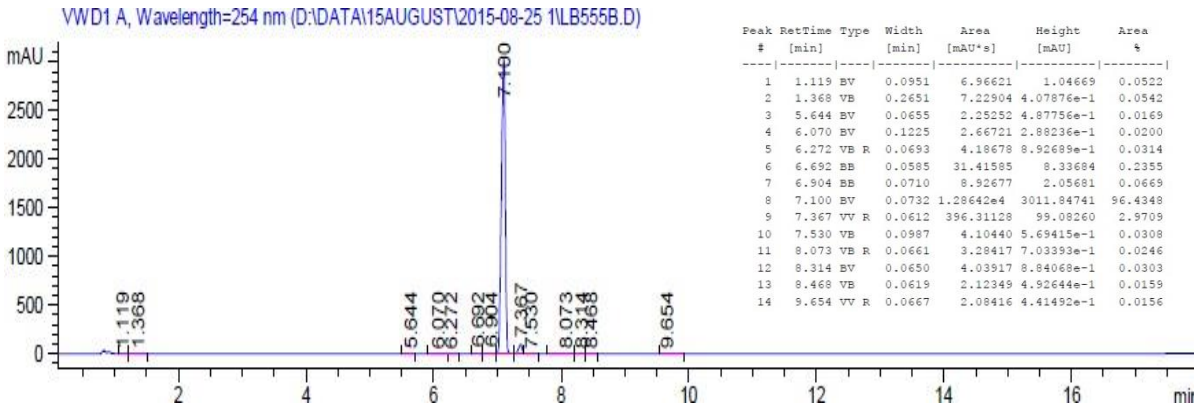

Peak #	RetTime [min]	Type	Width [min]	Area [mAU*s]	Height [mAU]	Area %
1	1.119	BV	0.0951	6.96621	1.04669	0.0522
2	1.368	VB	0.2651	7.22904	4.07876e-1	0.0542
3	5.644	BV	0.0655	2.25252	4.87756e-1	0.0169
4	6.070	BV	0.1225	2.66721	2.88236e-1	0.0200
5	6.272	VB R	0.0693	4.18678	8.92689e-1	0.0314
6	6.692	BB	0.0585	31.41585	8.33684	0.2355
7	6.904	BB	0.0710	8.92677	2.05681	0.0669
8	7.100	BV	0.0732	1.28642e4	3011.84741	96.4348
9	7.367	VV R	0.0612	396.31128	99.08260	2.9709
10	7.530	VB	0.0987	4.10440	5.69415e-1	0.0308
11	8.073	VB R	0.0661	3.28417	7.03393e-1	0.0246
12	8.314	BV	0.0650	4.03917	8.84068e-1	0.0303
13	8.468	VB	0.0619	2.12349	4.92644e-1	0.0159
14	9.654	VV R	0.0667	2.08416	4.41492e-1	0.0156

7-Chloro-2-((phenylamino)methyl)benzo[4,5]thieno[3,2-d]pyrimidin-4(3H)-one (44l)

^{1}H NMR spectrum (400 MHz, DMSO)

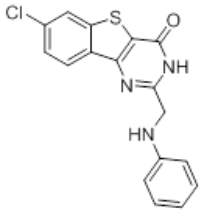

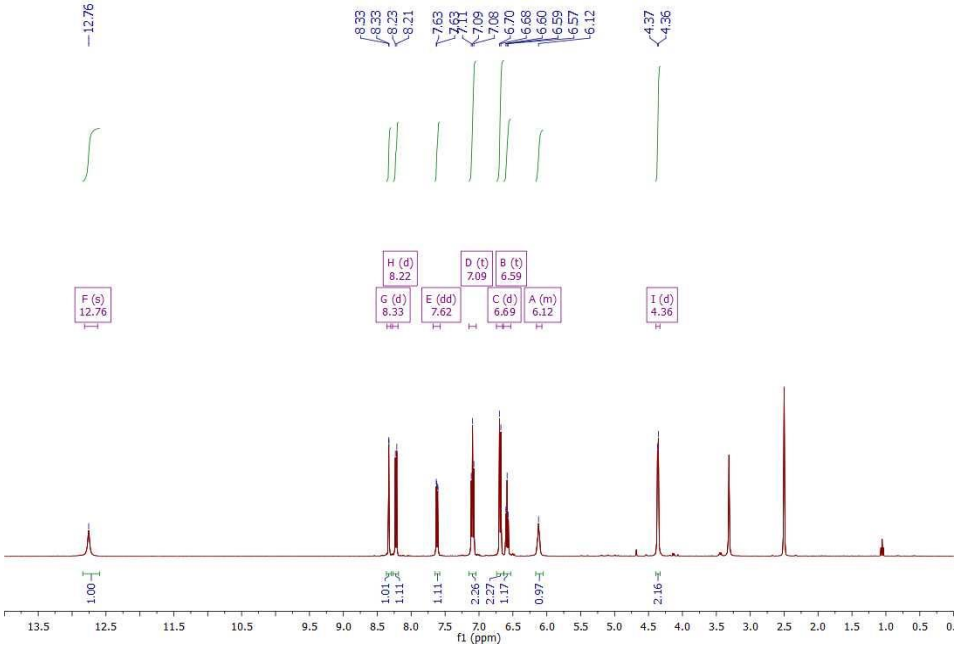

^{13}C NMR spectrum (101 MHz, DMSO)

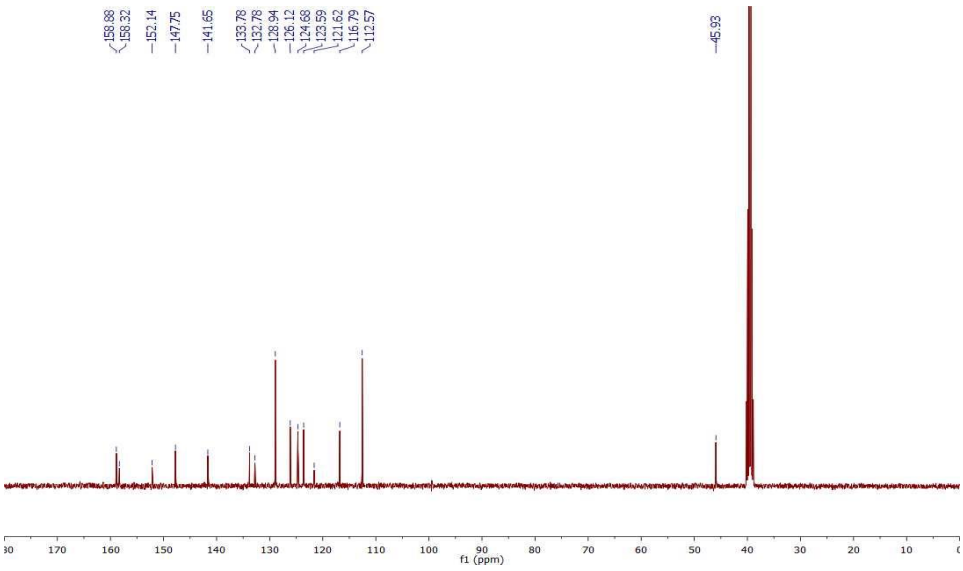

LC-MS (ES + APCI)

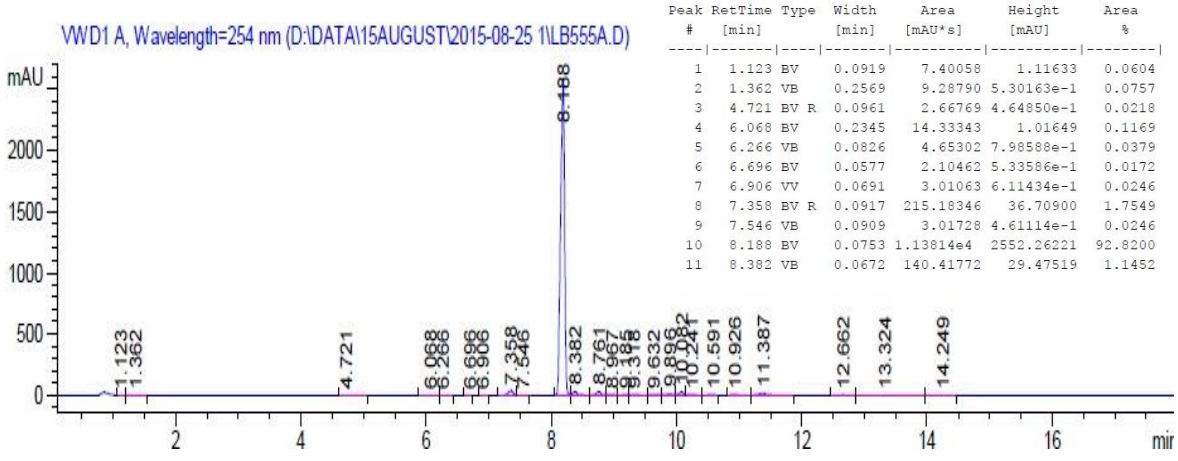

Peak #	RetTime [min]	Type	Width [min]	Area [mAU*s]	Height [mAU]	Area %
1	1.123	BV	0.0919	7.40058	1.11633	0.0604
2	1.362	VB	0.2569	9.28790	5.30163e-1	0.0757
3	4.721	BV R	0.0961	2.66769	4.64850e-1	0.0218
4	6.068	BV	0.2345	14.33343	1.01649	0.1169
5	6.266	VB	0.0826	4.65302	7.98588e-1	0.0379
6	6.696	BV	0.0577	2.10462	5.33586e-1	0.0172
7	6.906	VV	0.0691	3.01063	6.11434e-1	0.0246
8	7.358	BV R	0.0917	215.18346	36.70900	1.7549
9	7.546	VB	0.0909	3.01728	4.61114e-1	0.0246
10	8.188	BV	0.0753	1.13814e4	2552.26221	92.8200
11	8.382	VB	0.0672	140.41772	29.47519	1.1452

6-Chloro-2-(morpholinomethyl)benzo[4,5]thieno[3,2-*d*]pyrimidin-4(3*H*)-one (45b)

^{1}H NMR spectrum (400 MHz, DMSO)

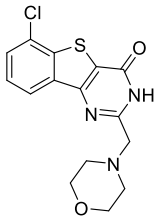

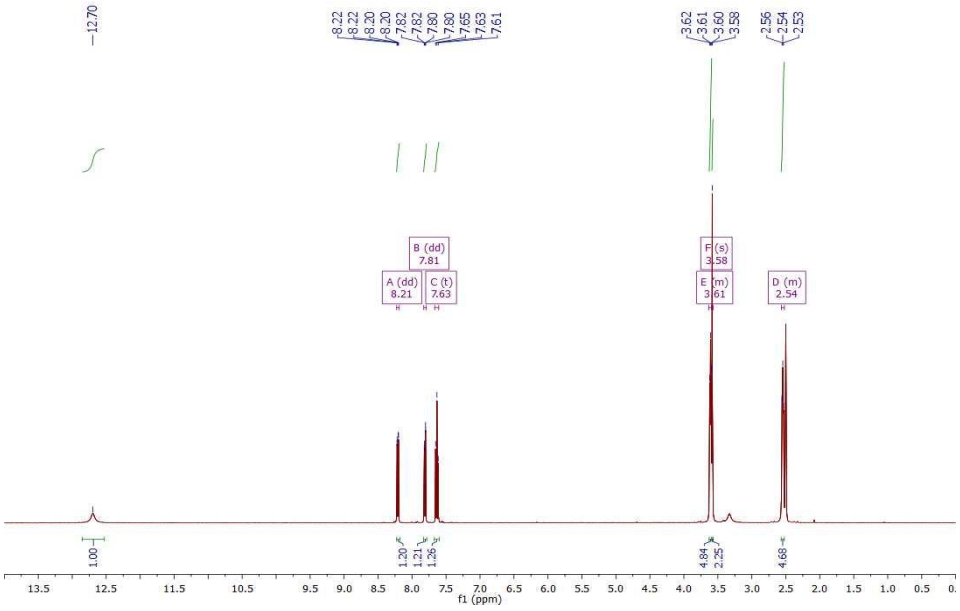

^{13}C NMR spectrum (101 MHz, DMSO)

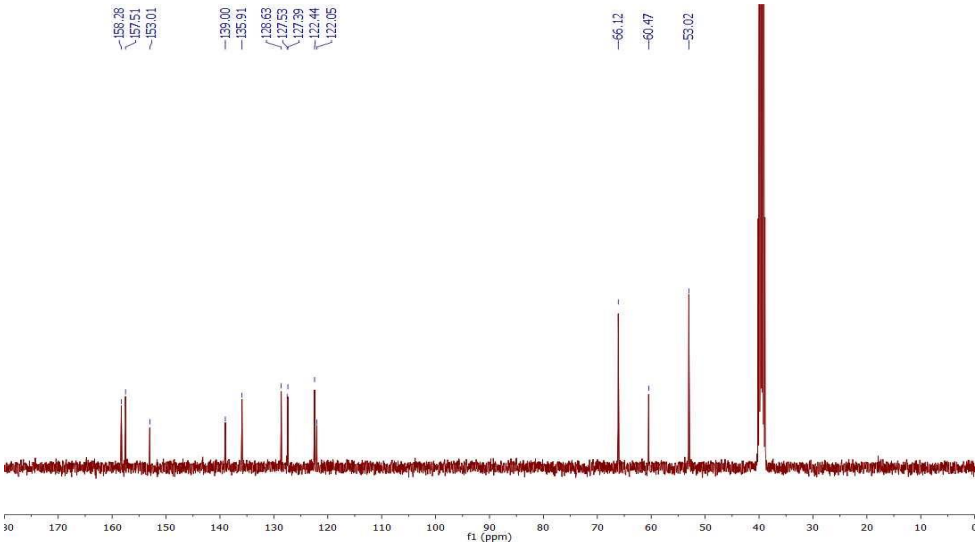

LC-MS (ES + APCI)

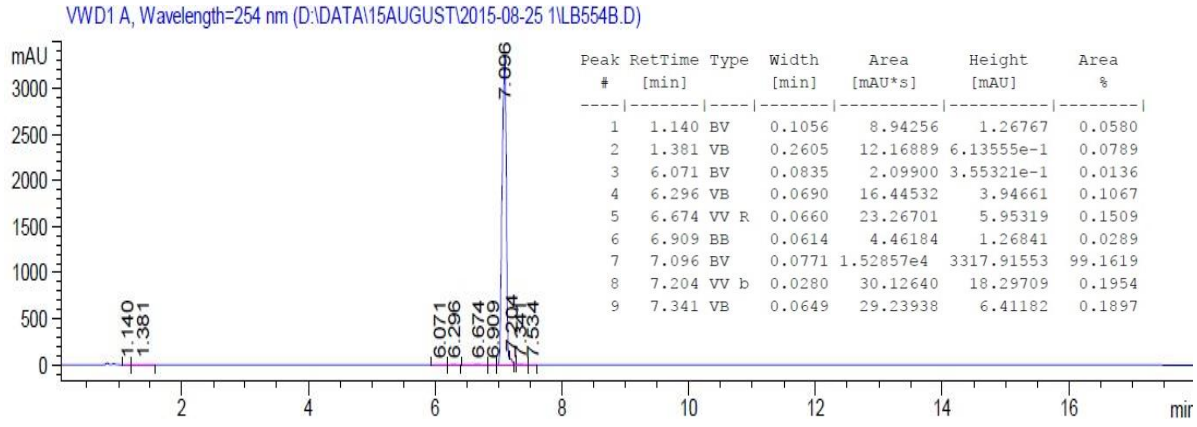

Peak #	RetTime [min]	Type	Width [min]	Area [mAU*s]	Height [mAU]	Area %
1	1.140	BV	0.1056	8.94256	1.26767	0.0580
2	1.381	VB	0.2605	12.16889	6.13555e-1	0.0789
3	6.071	BV	0.0835	2.09900	3.55321e-1	0.0136
4	6.296	VB	0.0690	16.44532	3.94661	0.1067
5	6.674	VV R	0.0660	23.26701	5.95319	0.1509
6	6.909	BB	0.0614	4.46184	1.26841	0.0289
7	7.096	BV	0.0771	1.52857e4	3317.91553	99.1619
8	7.204	VV b	0.0280	30.12640	18.29709	0.1954
9	7.341	VB	0.0649	29.23938	6.41182	0.1897

6-Chloro-2-((phenylamino)methyl)benzo[4,5]thieno[3,2-*d*]pyrimidin-4(3*H*)-one (45l)

^{1}H NMR spectrum (400 MHz, DMSO)

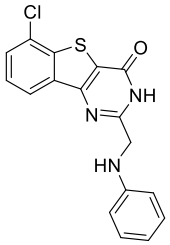

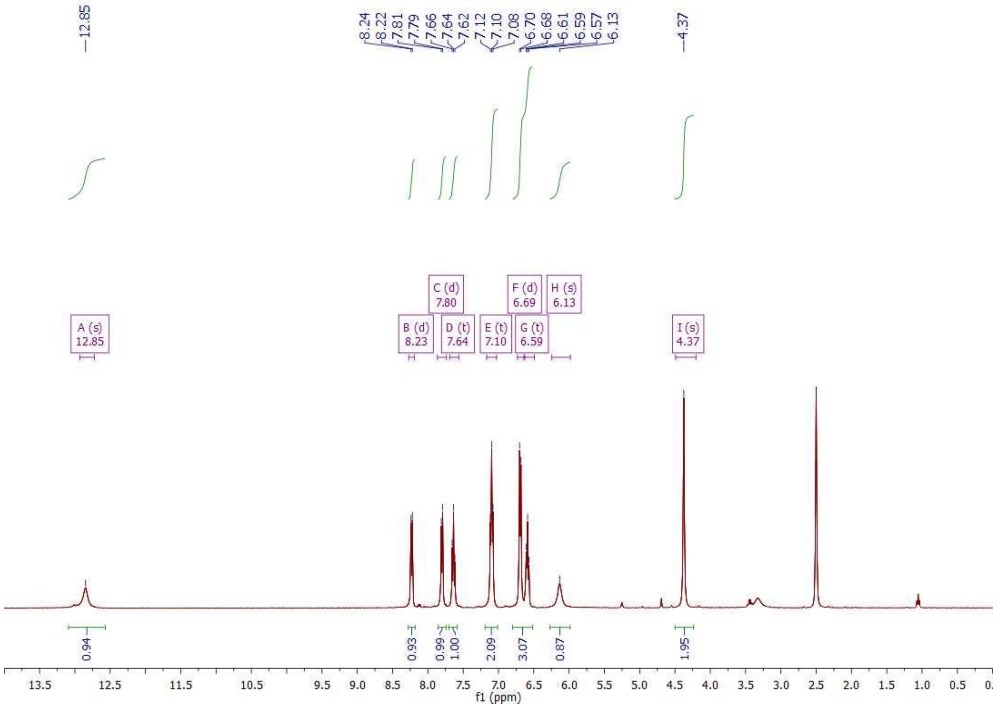

^{13}C NMR spectrum (101 MHz, DMSO)

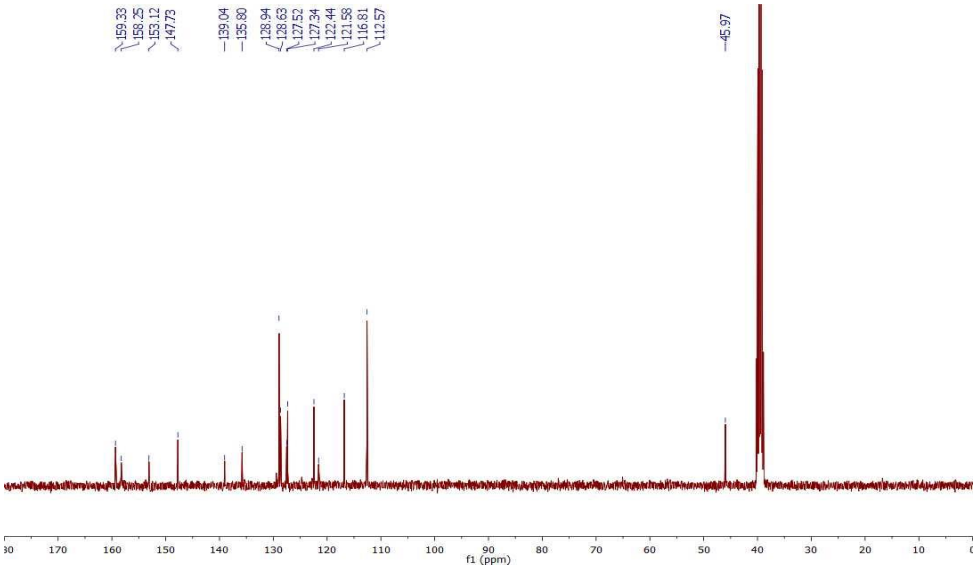

LC-MS (ES + APCI)

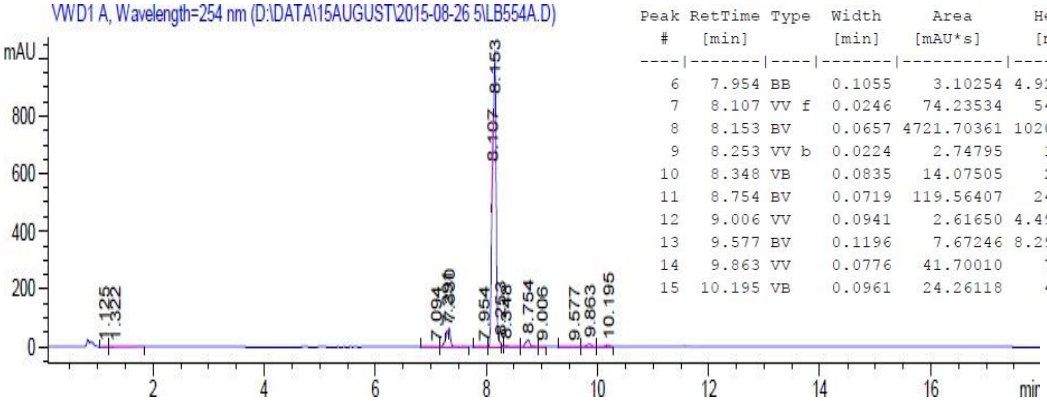

Peak #	RetTime [min]	Type	Width [min]	Area [mAU*s]	Height [mAU]	Area %
6	7.954	BB	0.1055	3.10254	4.92981e-1	0.0573
7	8.107	VV f	0.0246	74.23534	54.71333	1.3702
8	8.153	BV	0.0657	4721.70361	1020.03174	87.1508
9	8.253	VV b	0.0224	2.74795	1.93888	0.0507
10	8.348	VB	0.0835	14.07505	2.38208	0.2598
11	8.754	BV	0.0719	119.56407	24.35033	2.2069
12	9.006	VV	0.0941	2.61650	4.49657e-1	0.0483
13	9.577	BV	0.1196	7.67246	8.29054e-1	0.1416
14	9.863	VV	0.0776	41.70010	7.72393	0.7697
15	10.195	VB	0.0961	24.26118	4.05377	0.4478

6-(4-Bromophenyl)-2-cyclopropylpyrimidin-4(3*H*)-one (86)

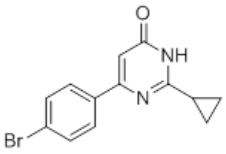

^{1}H NMR spectrum (400 MHz, DMSO)

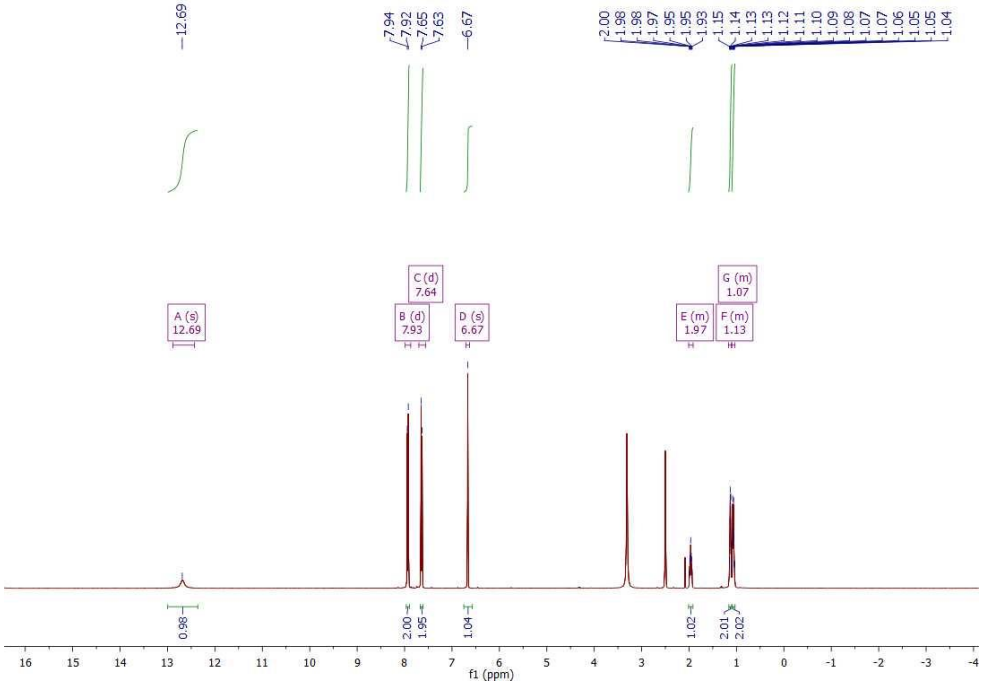

^{13}C NMR spectrum (101 MHz, DMSO)

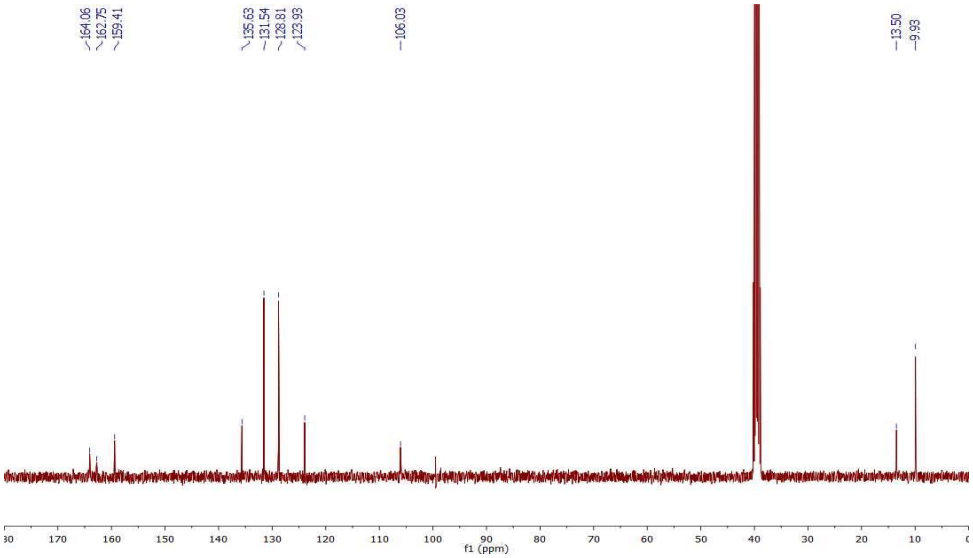

LC-MS (ES + APCI)

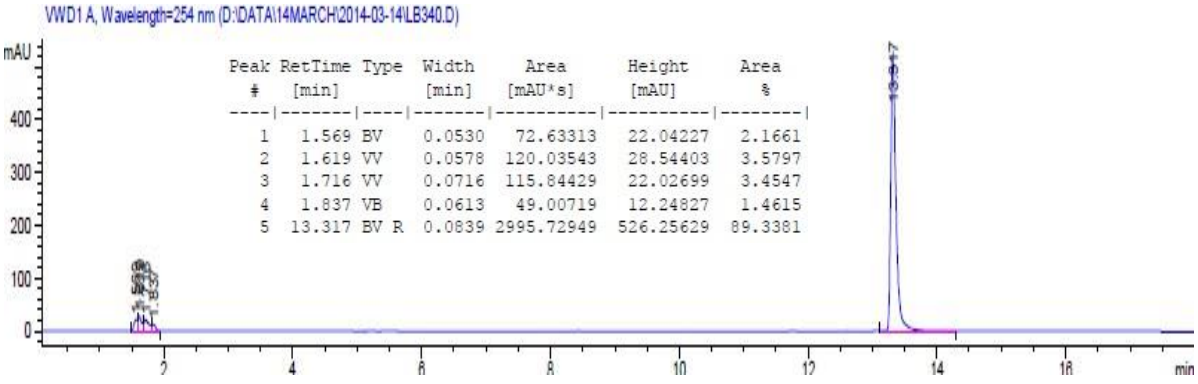

Peak #	RetTime [min]	Type	Width [min]	Area [mAU*s]	Height [mAU]	Area %
1	1.569	BV	0.0530	72.63313	22.04227	2.1661
2	1.619	VV	0.0578	120.03543	28.54403	3.5797
3	1.716	VV	0.0716	115.84429	22.02699	3.4547
4	1.837	VB	0.0613	49.00719	12.24827	1.4615
5	13.317	BV R	0.0839	2995.72949	526.25629	89.3381

6-(3-Bromophenyl)-2-cyclopropylpyrimidin-4(3*H*)-one (87)

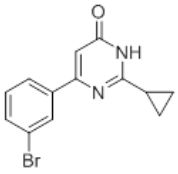

^{1}H NMR spectrum (400 MHz, DMSO)

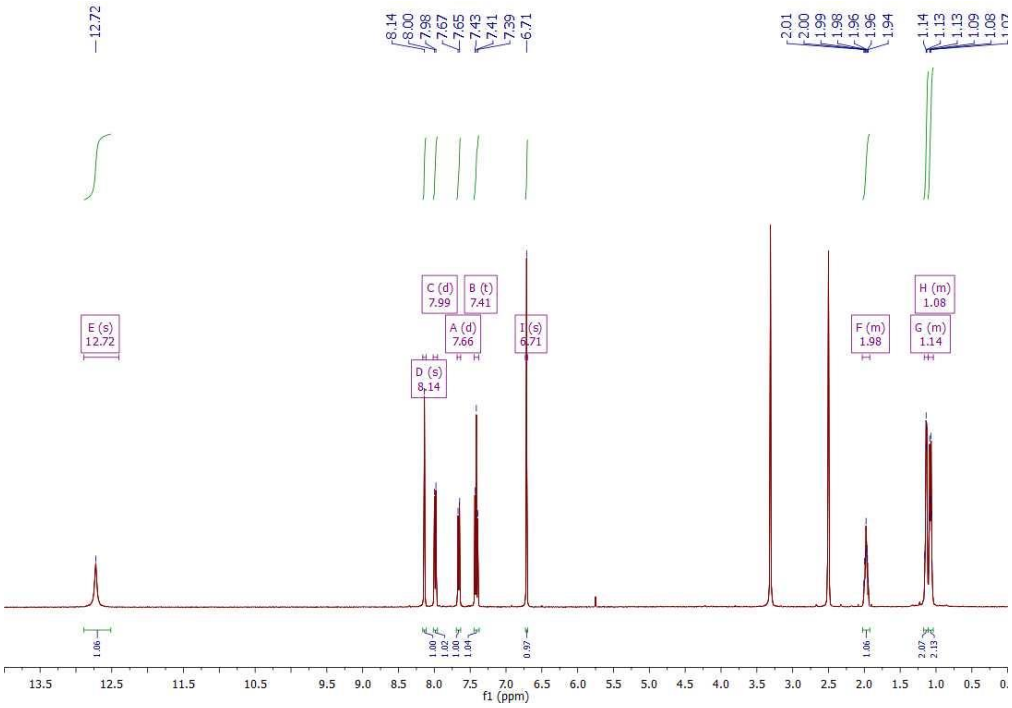

^{13}C NMR spectrum (101 MHz, DMSO)

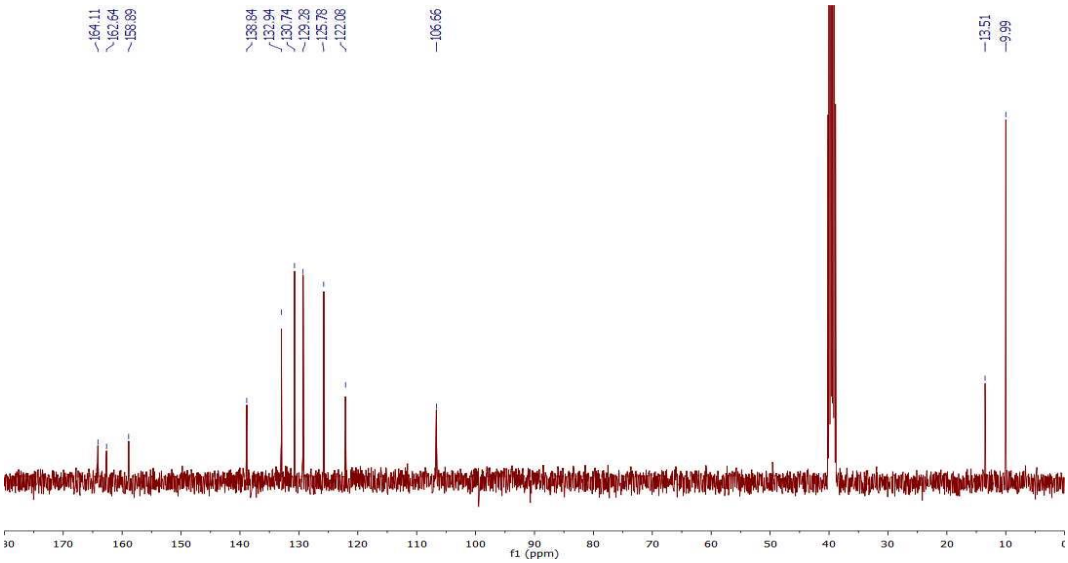

LC-MS (ES + APCI)

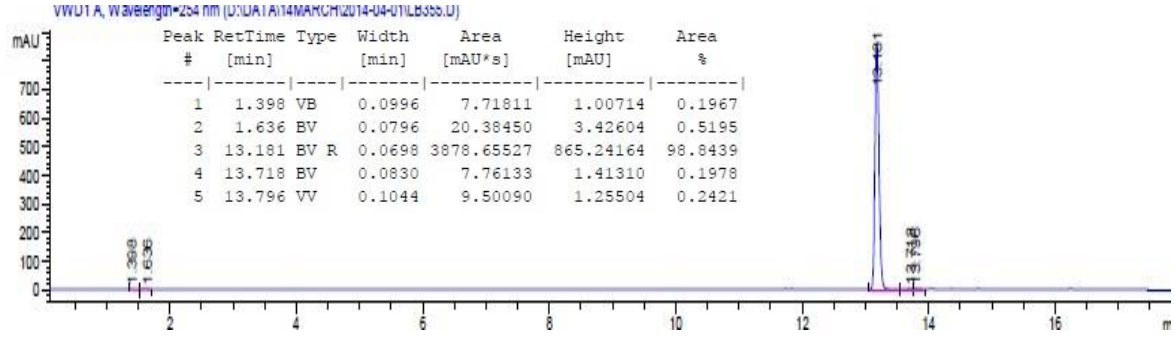

6-(4-Bromophenyl)-2-phenylpyrimidin-4(3*H*)-one (88)

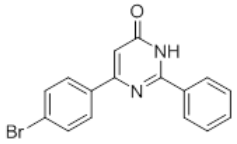

^{1}H NMR spectrum (400 MHz, DMSO)

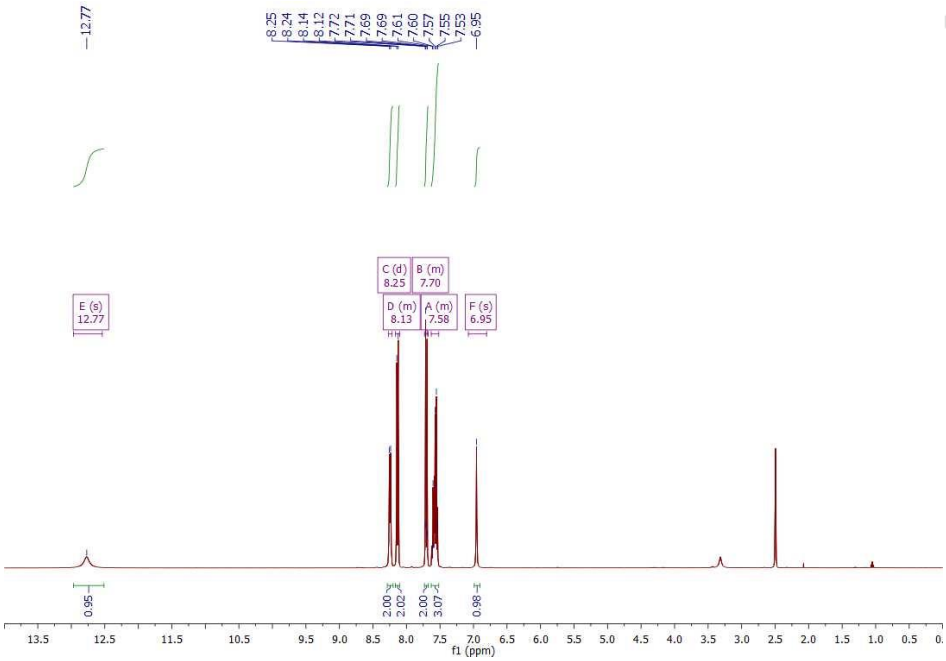

^{13}C NMR spectrum (101 MHz, DMSO)

Unable to obtain ^{13}C. Solid precipitated from NMR solvent.

LC-MS (ES + APCI)

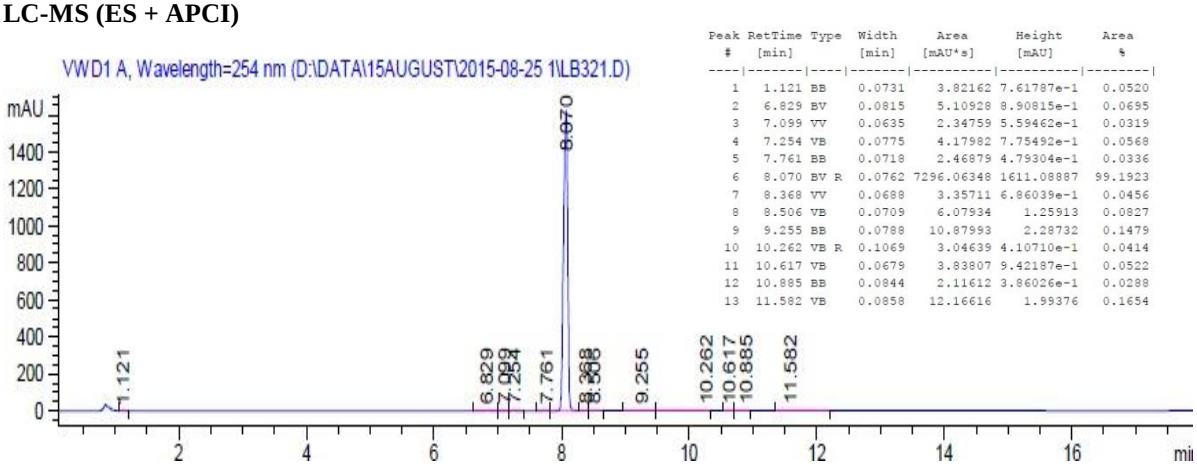

Peak #	RetTime [min]	Type	Width [min]	Area [mAU*s]	Height [mAU]	Area %
1	1.121	BB	0.0731	3.82162	7.61787e-1	0.0520
2	6.829	BV	0.0815	5.10928	8.90815e-1	0.0695
3	7.099	VV	0.0635	2.34759	5.59462e-1	0.0319
4	7.254	VB	0.0775	4.17982	7.75492e-1	0.0568
5	7.761	BB	0.0718	2.46879	4.79304e-1	0.0336
6	8.070	BV R	0.0762	7296.06348	1611.08887	99.1923
7	8.368	VV	0.0688	3.35711	6.86039e-1	0.0456
8	8.506	VB	0.0709	6.07934	1.25913	0.0827
9	9.255	BB	0.0788	10.87993	2.28732	0.1479
10	10.262	VB R	0.1069	3.04639	4.10710e-1	0.0414
11	10.617	VB	0.0679	3.83807	9.42187e-1	0.0522
12	10.885	BB	0.0844	2.11612	3.86026e-1	0.0288
13	11.582	VB	0.0858	12.16616	1.99376	0.1654

2-Cyclopropyl-6-(4-(pyrrolidin-1-yl)phenyl)pyrimidin-4(3*H*)-one (91)

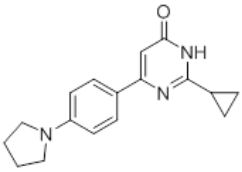

^{1}H NMR spectrum (400 MHz, DMSO)

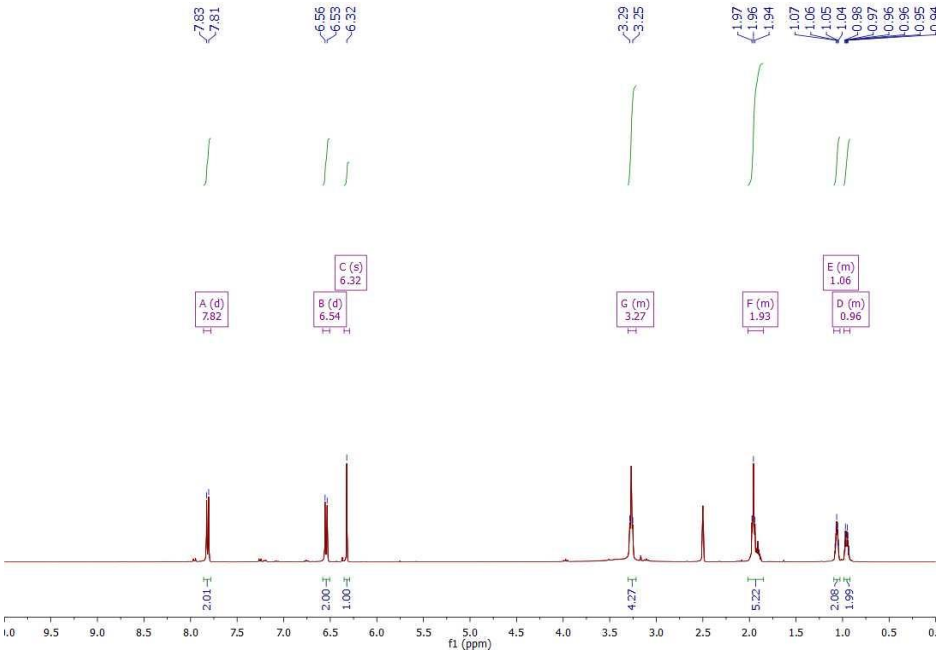

^{13}C NMR spectrum (101 MHz, DMSO)

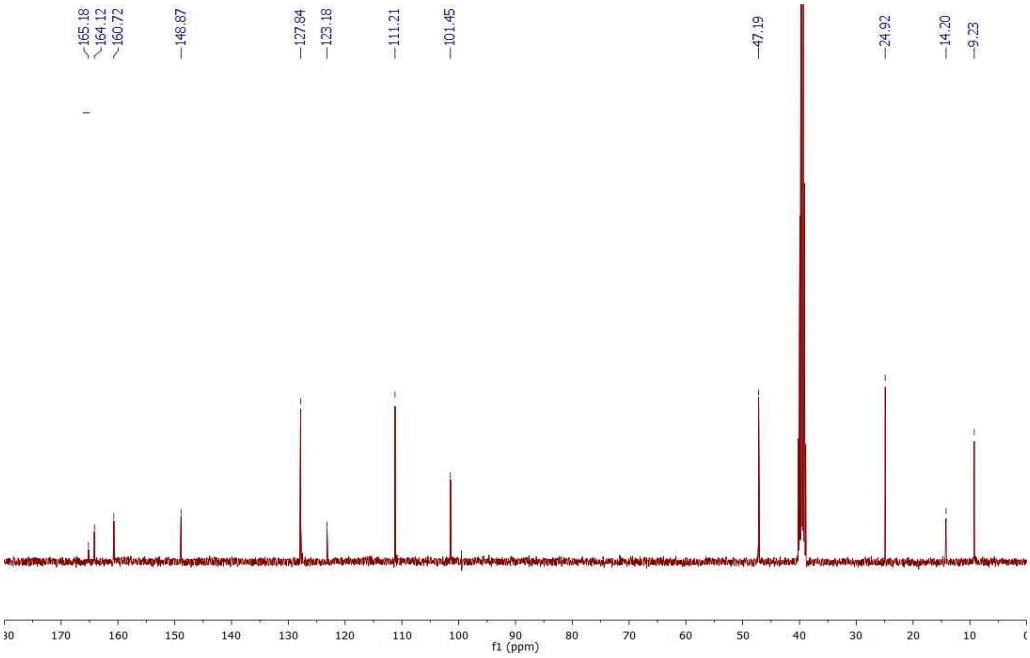

LC-MS (ES + APCI)

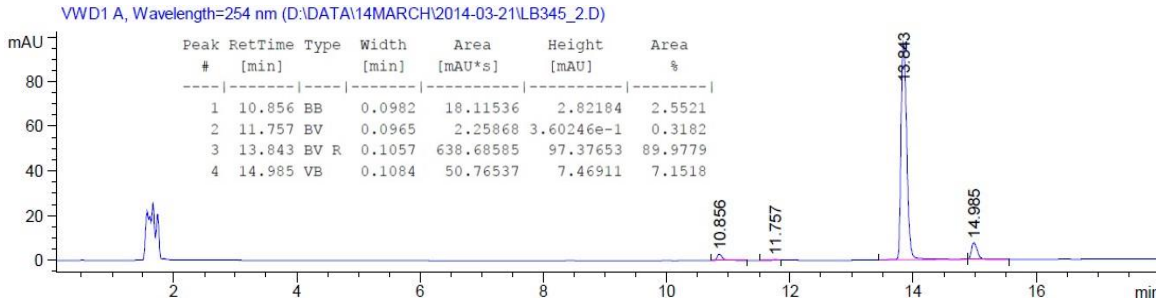

2-Cyclopropyl-6-(4-((2-(dimethylamino)ethyl)amino)phenyl)pyrimidin-4(3*H*)-one (92)

^{1}H NMR spectrum (400 MHz, DMSO)

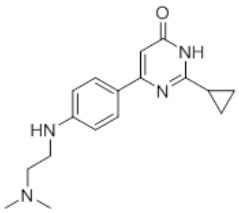

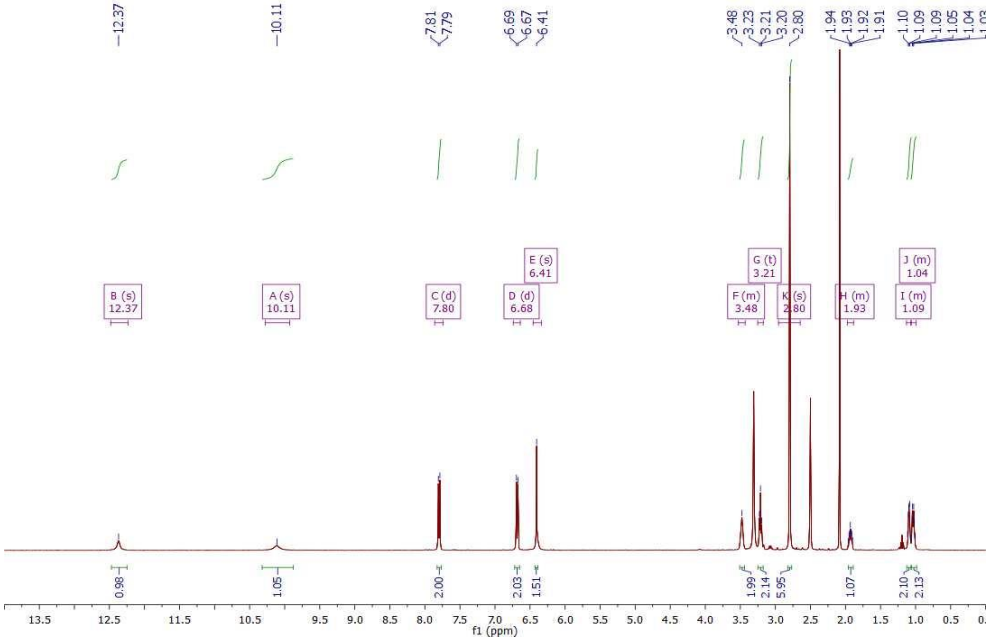

^{13}C NMR spectrum (101 MHz, DMSO)

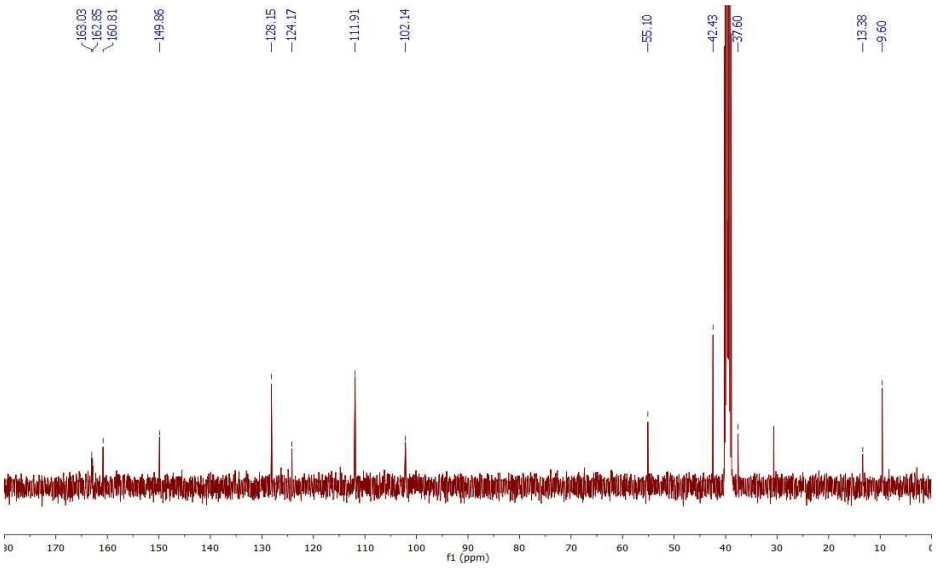

LC-MS (ES + APCI)

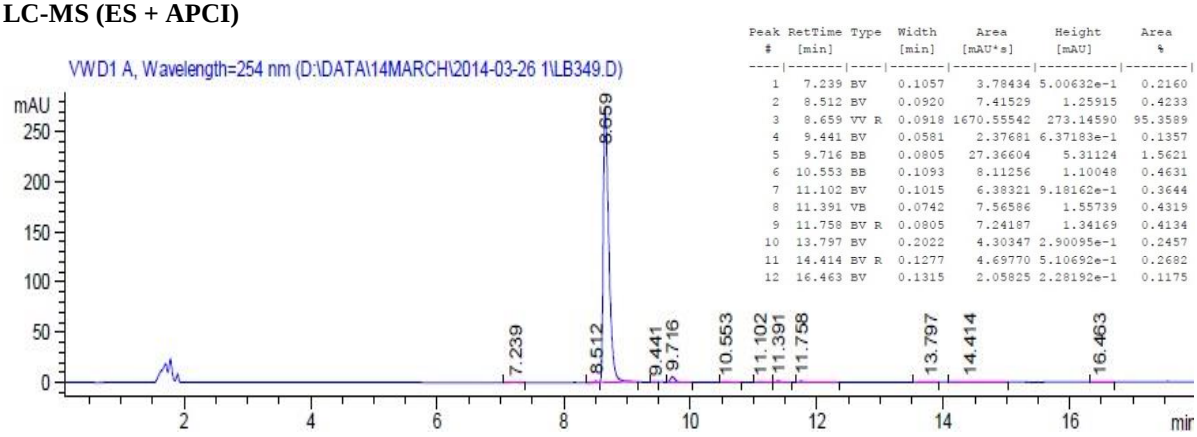

Peak #	RetTime [min]	Type	Width [min]	Area [mAU*s]	Height [mAU]	Area %
1	7.239	BV	0.1057	3.78434	5.00632e-1	0.2160
2	8.512	BV	0.0920	7.41529	1.25915	0.4233
3	8.659	VV R	0.0918	1670.55542	273.14590	95.3589
4	9.441	BV	0.0581	2.37681	6.37183e-1	0.1357
5	9.716	BB	0.0805	27.36604	5.31124	1.5621
6	10.553	BB	0.1093	8.11256	1.10048	0.4631
7	11.102	BV	0.1015	6.38321	9.18162e-1	0.3644
8	11.391	VB	0.0742	7.56586	1.55739	0.4319
9	11.758	BV R	0.0805	7.24187	1.34169	0.4134
10	13.797	BV	0.2022	4.30347	2.90095e-1	0.2457
11	14.414	BV R	0.1277	4.69770	5.10692e-1	0.2682
12	16.463	BV	0.1315	2.05825	2.28192e-1	0.1175

2-Cyclopropyl-6-(4-((2-methoxyethyl)(methyl)amino)phenyl)pyrimidin-4(3*H*)-one (93)

^{1}H NMR spectrum (400 MHz, DMSO)

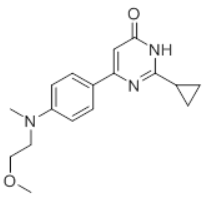

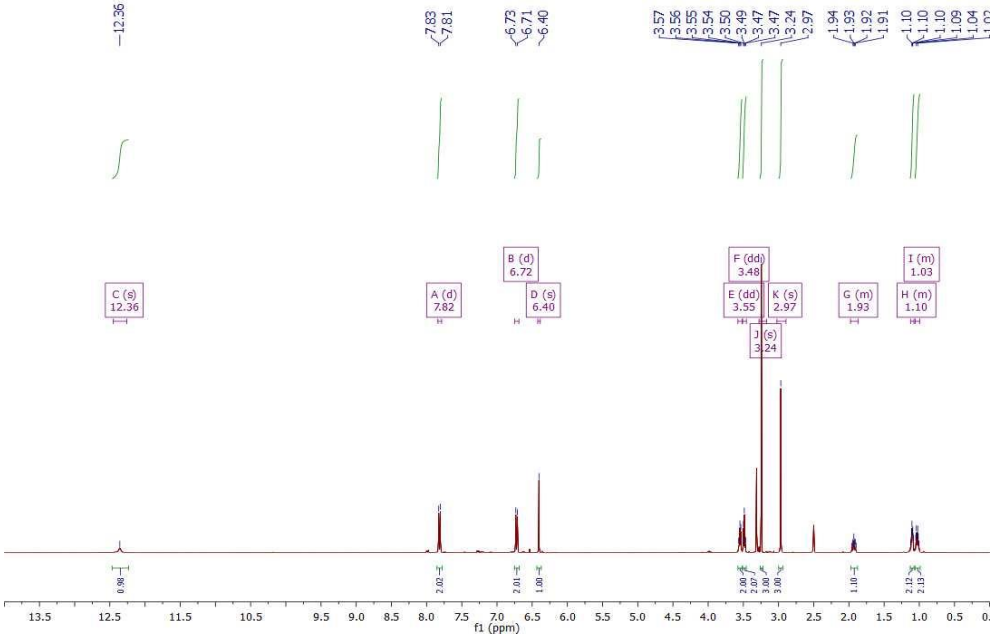

^{13}C NMR spectrum (101 MHz, DMSO)

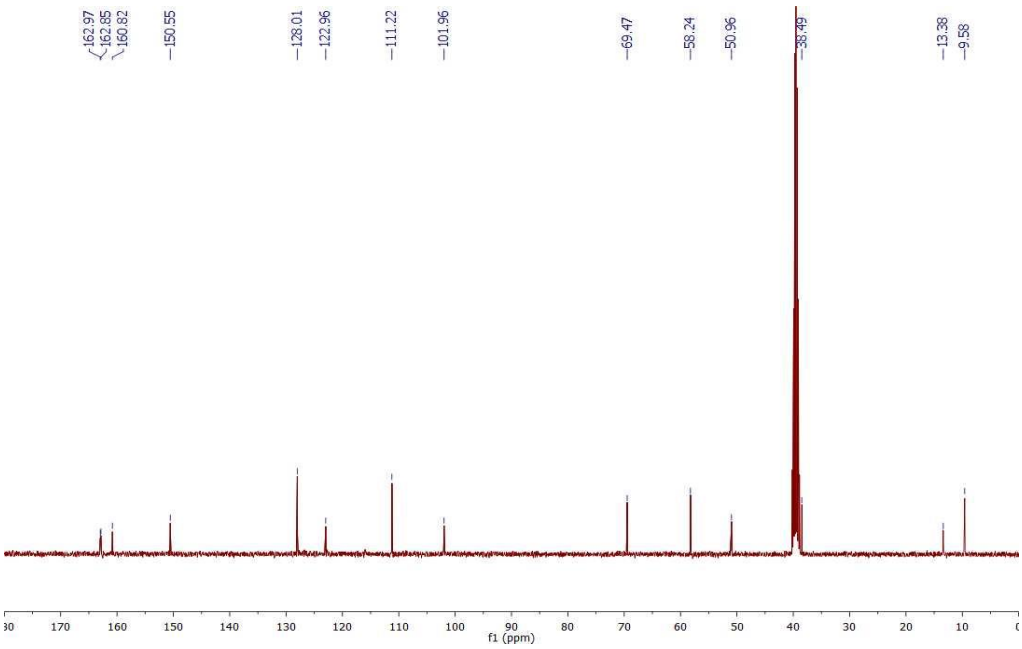

LC-MS (ES + APCI)

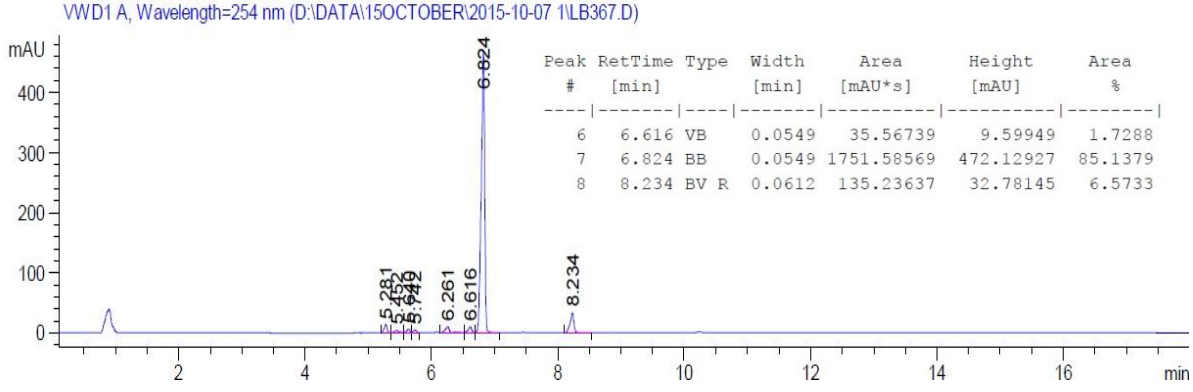

Peak #	RetTime [min]	Type	Width [min]	Area [mAU*s]	Height [mAU]	Area %
6	6.616	VB	0.0549	35.56739	9.59949	1.7288
7	6.824	BB	0.0549	1751.58569	472.12927	85.1379
8	8.234	BV R	0.0612	135.23637	32.78145	6.5733

2-Cyclopropyl-6-(3-(pyrrolidin-1-yl)phenyl)pyrimidin-4(3*H*)-one (94)

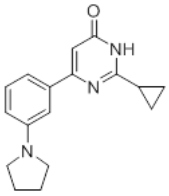

^{1}H NMR spectrum (400 MHz, DMSO)

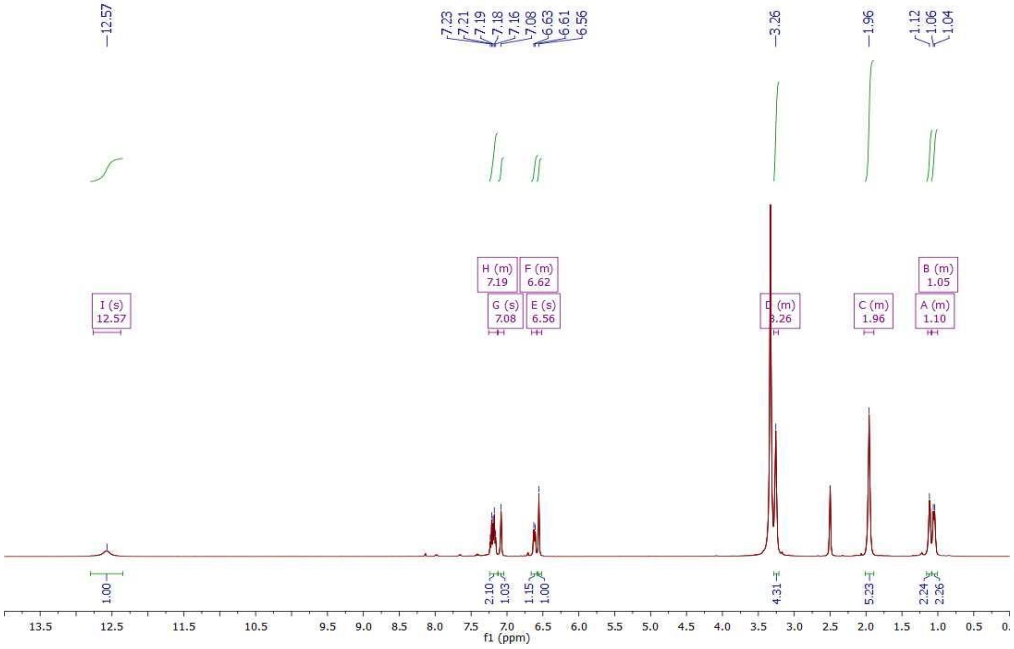

^{13}C NMR spectrum (101 MHz, DMSO)

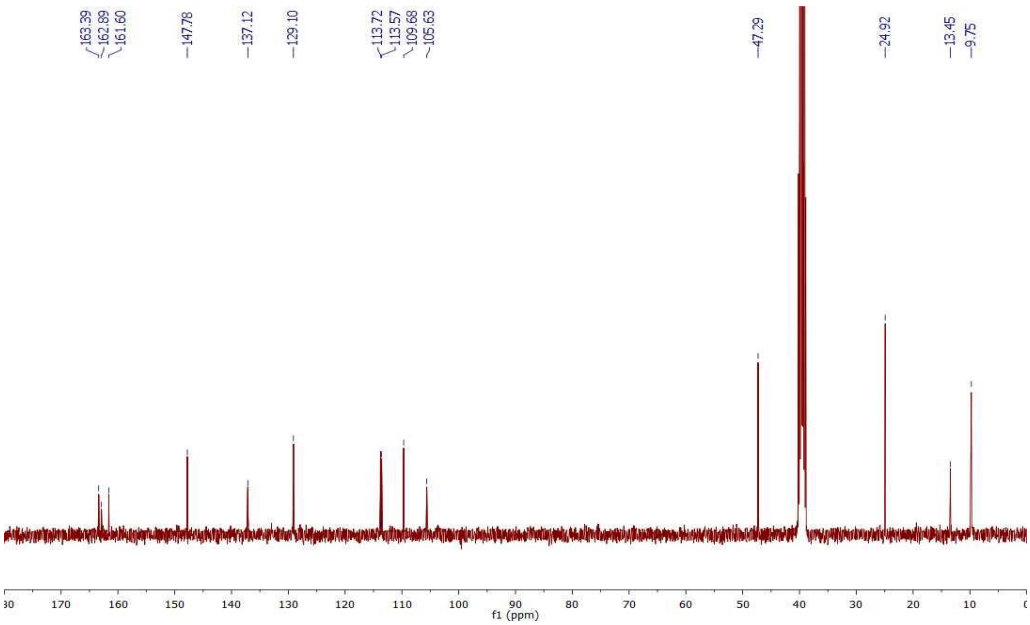

LC-MS (ES + APCI)

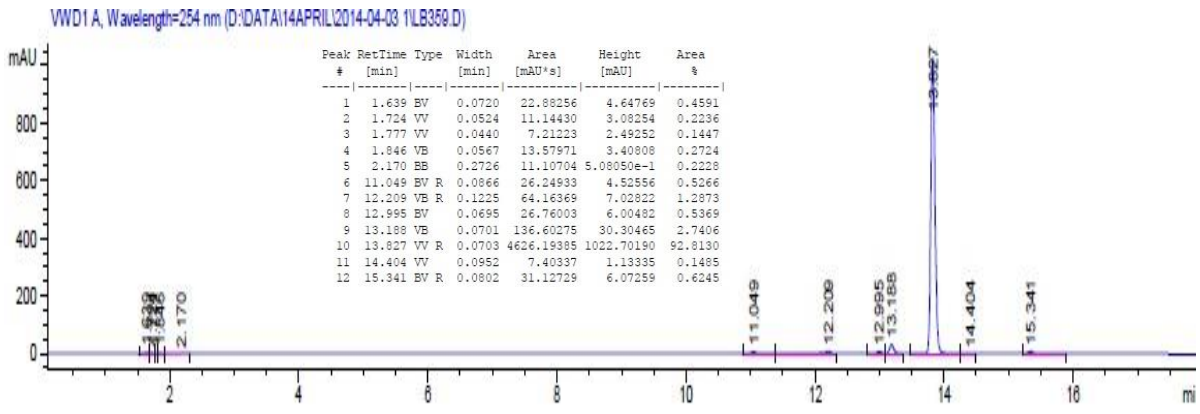

Peak #	RetTime [min]	Type	Width [min]	Area [mAU*s]	Height [mAU]	Area %
1	1.639	BV	0.0720	22.88256	4.64769	0.4591
2	1.724	VV	0.0524	11.14430	3.08254	0.2236
3	1.777	VV	0.0440	7.21223	2.49252	0.1447
4	1.846	VB	0.0567	13.57971	3.40808	0.2724
5	2.170	BB	0.2726	11.10704	5.08050e-1	0.2228
6	11.049	BV R	0.0866	26.24933	4.52556	0.5266
7	12.209	VB R	0.1225	64.16369	7.02822	1.2873
8	12.995	BV	0.0695	26.76003	6.00482	0.5369
9	13.188	VB	0.0701	136.60275	30.30465	2.7406
10	13.827	VV R	0.0703	4626.19385	1022.70190	92.8130
11	14.404	VV	0.0952	7.40337	1.13335	0.1485
12	15.341	BV R	0.0802	31.12729	6.07259	0.6245

6-(4-((2-(Dimethylamino)ethyl)(methyl)amino)phenyl)-2-phenylpyrimidin-4(3*H*)-one (95)

^{1}H NMR spectrum (400 MHz, DMSO)

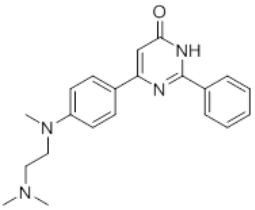

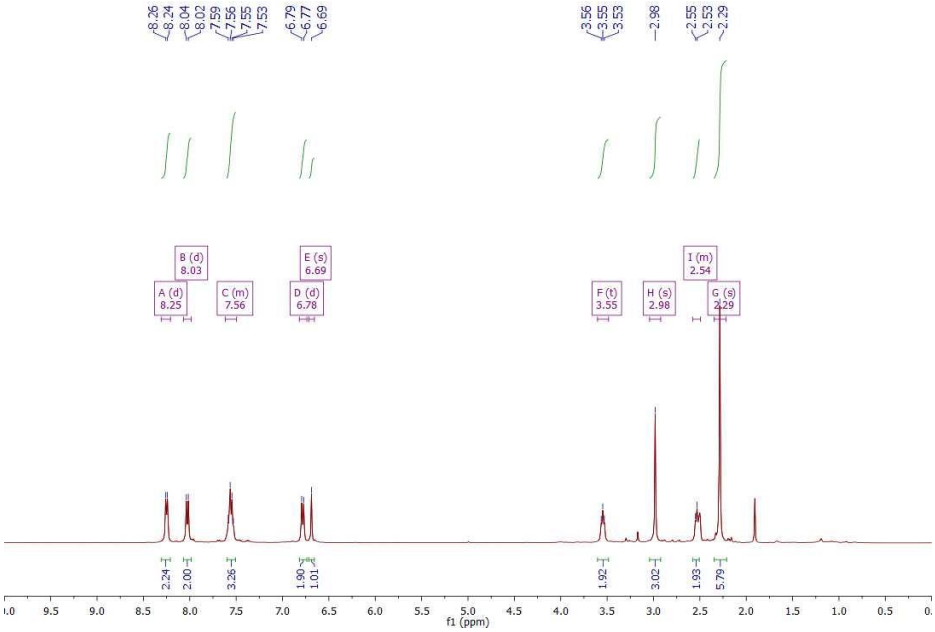

^{13}C NMR spectrum (101 MHz, DMSO)

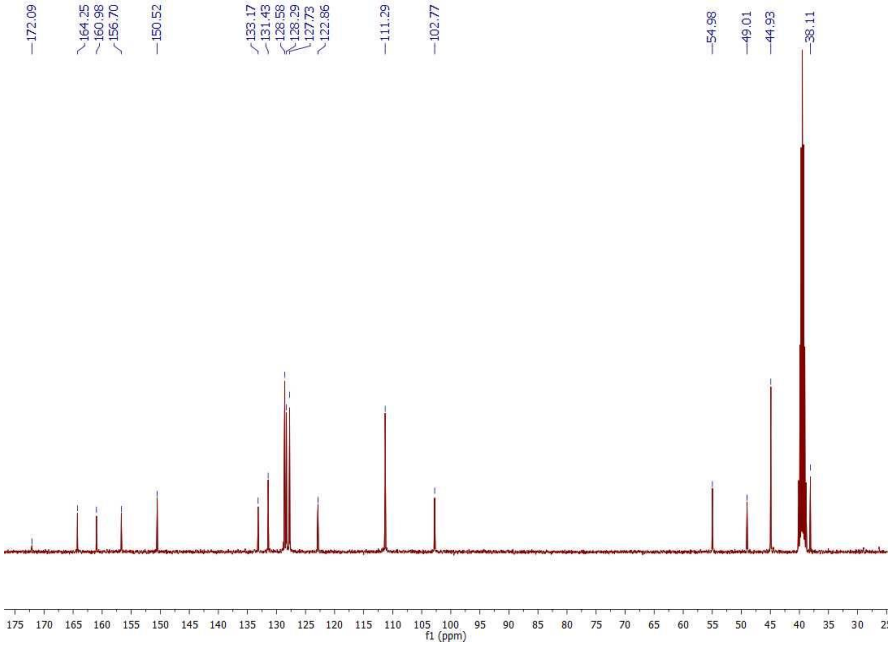

LC-MS (ES + APCI)

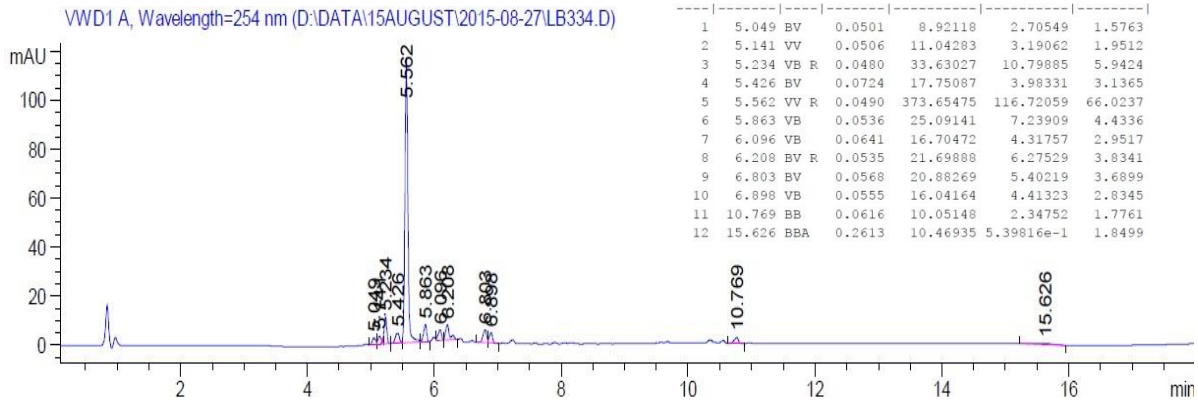

Peak #	RetTime [min]	Type	Width [min]	Area [mAU*s]	Height [mAU]	Area %
1	5.049	BV	0.0501	8.92118	2.70549	1.5763
2	5.141	VV	0.0506	11.04283	3.19062	1.9512
3	5.234	VB R	0.0480	33.63027	10.79885	5.9424
4	5.426	BV	0.0724	17.75087	3.98331	3.1365
5	5.562	VV R	0.0490	373.65475	116.72059	66.0237
6	5.863	VB	0.0536	25.09141	7.23909	4.4336
7	6.096	VB	0.0641	16.70472	4.31757	2.9517
8	6.208	BV R	0.0535	21.69888	6.27529	3.8341
9	6.803	BV	0.0568	20.88269	5.40219	3.6899
10	6.898	VB	0.0555	16.04164	4.41323	2.8345
11	10.769	BB	0.0616	10.05148	2.34752	1.7761
12	15.626	BBA	0.2613	10.46935	5.39816e-1	1.8499

2-Phenyl-6-(4-(pyrrolidin-1-yl)phenyl)pyrimidin-4(3*H*)-one (96)

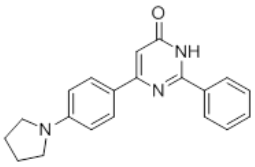

^{1}H NMR spectrum (400 MHz, DMSO)

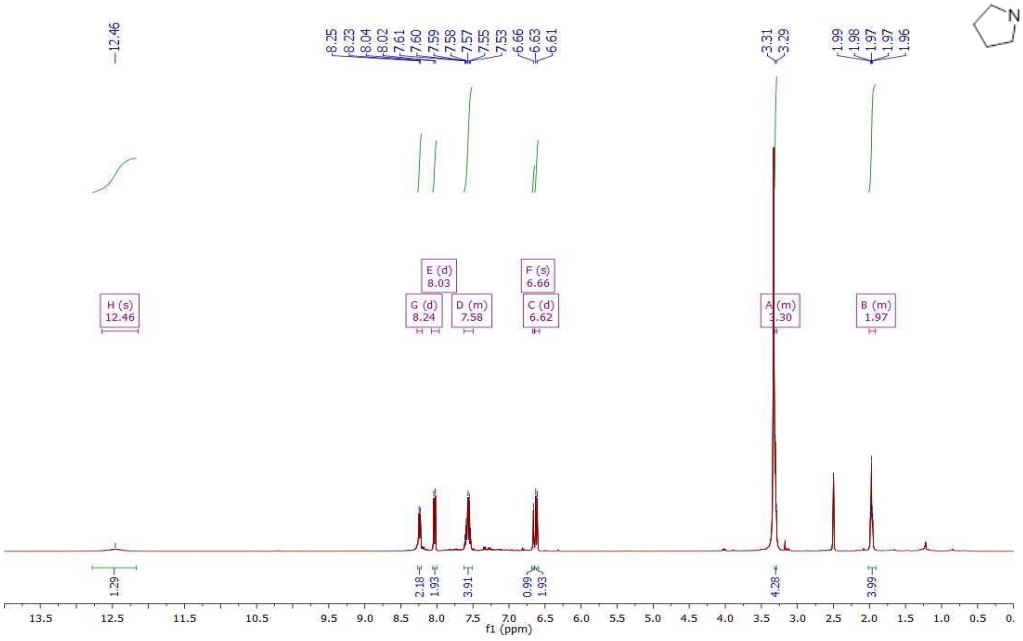

^{13}C NMR spectrum (101 MHz, DMSO)

Unable to obtain ^{13}C. Solid precipitated from NMR solvent.

LC-MS (ES + APCI)

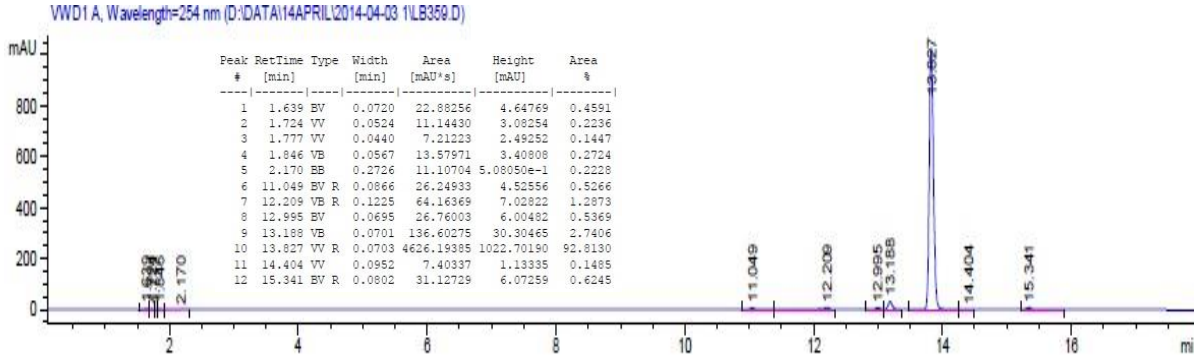

6-(4-Bromophenyl)-2-((methylamino)methyl)pyrimidin-4(3*H*)-one (97)

^{1}H NMR spectrum (400 MHz, DMSO)

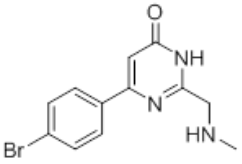

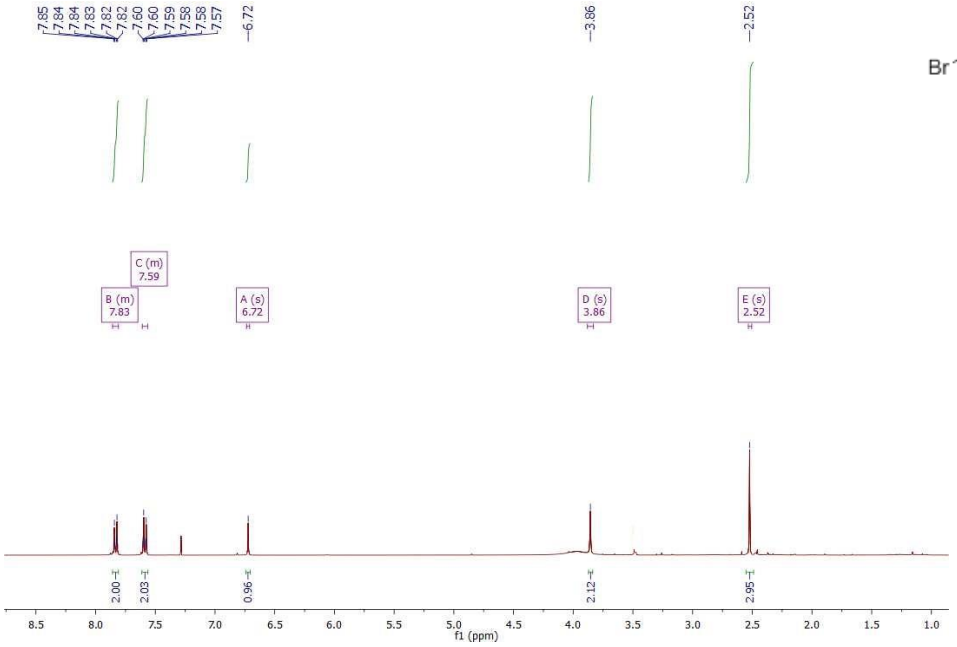

^{13}C NMR spectrum (101 MHz, DMSO)

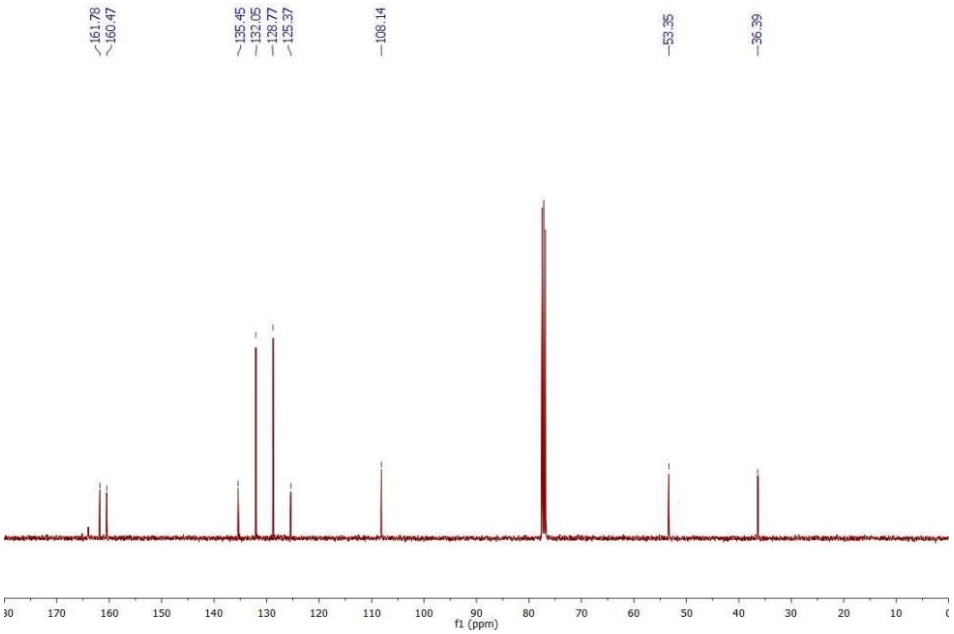

LC-MS (ES + APCI)

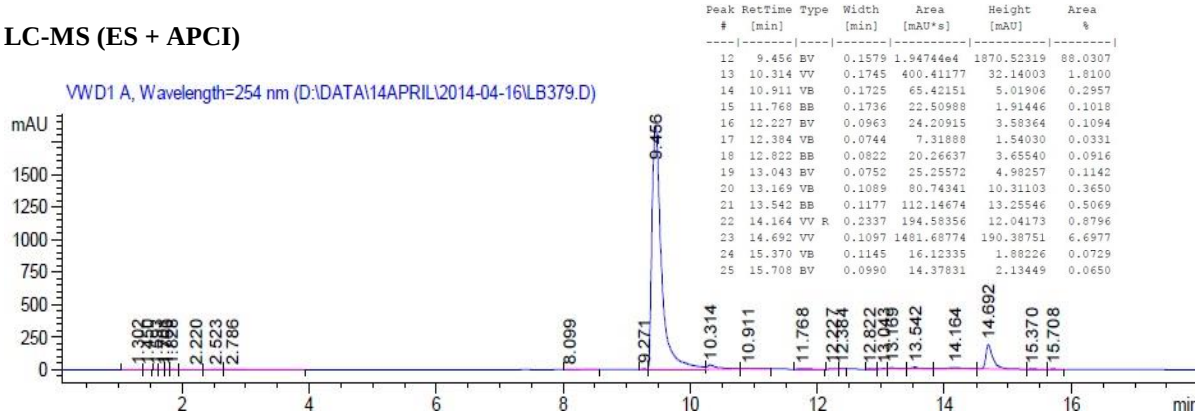

Peak #	RetTime [min]	Type	Width [min]	Area [mAU*s]	Height [mAU]	Area %
12	9.456	BV	0.1579	1.94744e4	1870.52319	88.0307
13	10.314	VV	0.1745	400.41177	32.14003	1.8100
14	10.911	VB	0.1725	65.42151	5.01906	0.2957
15	11.768	BB	0.1736	22.50988	1.91446	0.1018
16	12.227	BV	0.0963	24.20915	3.58364	0.1094
17	12.384	VB	0.0744	7.31888	1.54030	0.0331
18	12.822	BB	0.0822	20.26637	3.65540	0.0916
19	13.043	BV	0.0752	25.25572	4.98257	0.1142
20	13.169	VB	0.1089	80.74341	10.31103	0.3650
21	13.542	BB	0.1177	112.14674	13.25546	0.5069
22	14.164	VV R	0.2337	194.58356	12.04173	0.8796
23	14.692	VV	0.1097	1481.68774	190.38751	6.6977
24	15.370	VB	0.1145	16.12335	1.88226	0.0729
25	15.708	BV	0.0990	14.37831	2.13449	0.0650

6-(4-Bromophenyl)-2-(((2-hydroxyethyl)(methyl)amino)methyl)pyrimidin-4(3*H*)-one (98)

^{1}H NMR spectrum (400 MHz, DMSO)

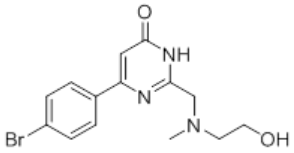

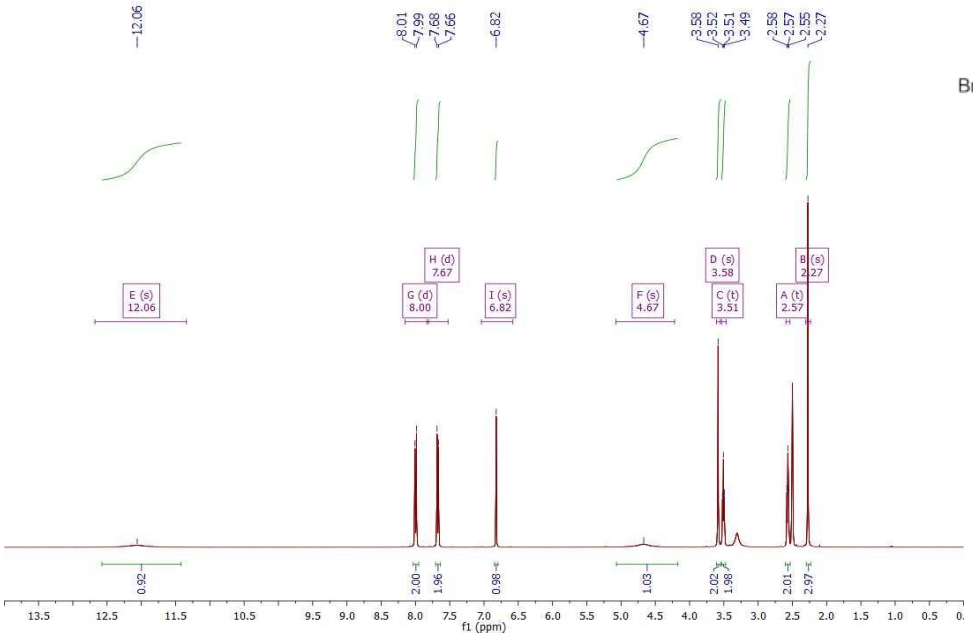

^{13}C NMR spectrum (101 MHz, DMSO)

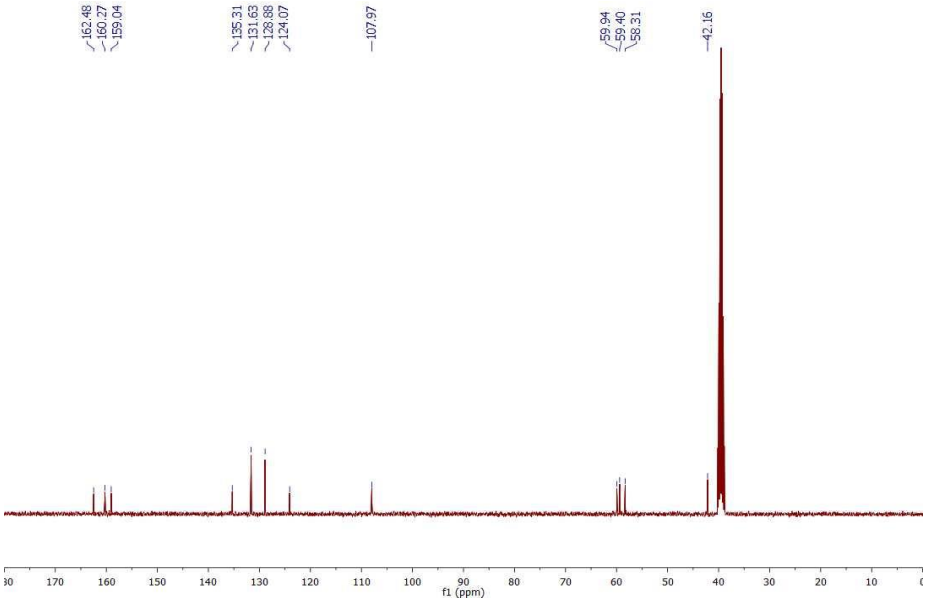

LC-MS (ES + APCI)

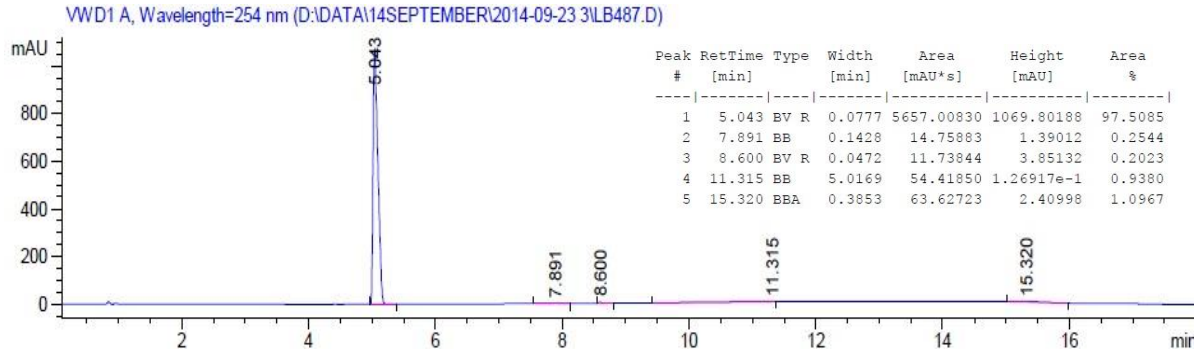

Peak #	RetTime [min]	Type	Width [min]	Area [mAU*s]	Height [mAU]	Area %
1	5.043	BV R	0.0777	5657.00830	1069.80188	97.5085
2	7.891	BB	0.1428	14.75883	1.39012	0.2544
3	8.600	BV R	0.0472	11.73844	3.85132	0.2023
4	11.315	BB	5.0169	54.41850	1.26917e-1	0.9380
5	15.320	BBA	0.3853	63.62723	2.40998	1.0967

6-(4-Bromophenyl)-2-((pyridin-4-ylamino)methyl)pyrimidin-4(3*H*)-one (99)

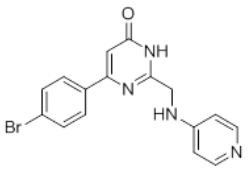

^{1}H NMR spectrum (400 MHz, DMSO)

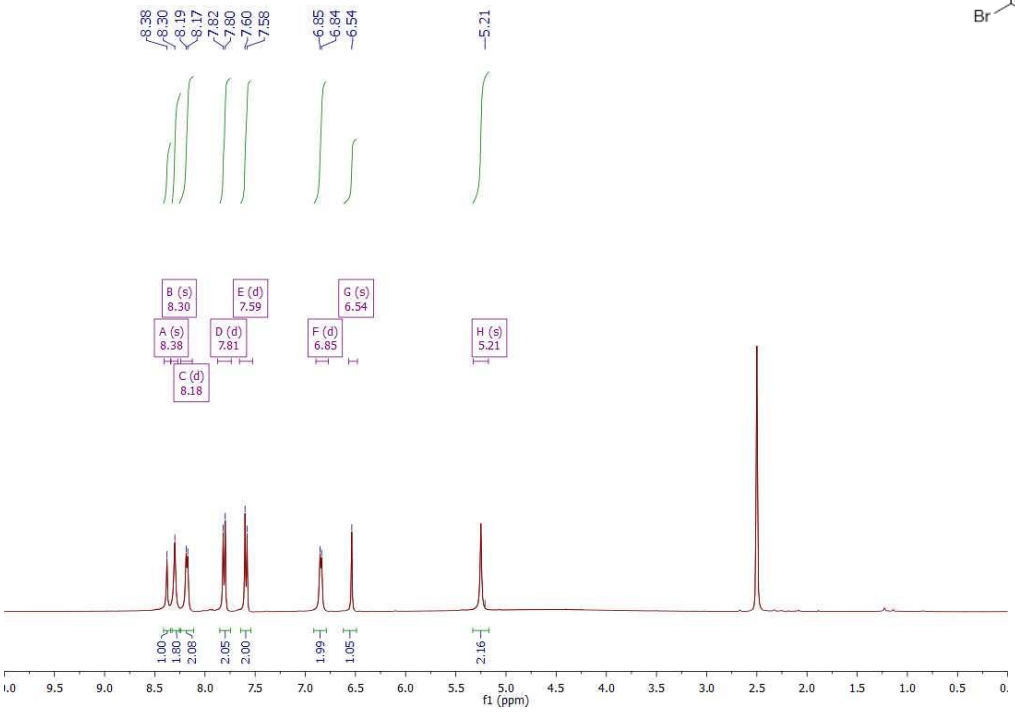

^{13}C NMR spectrum (101 MHz, DMSO)

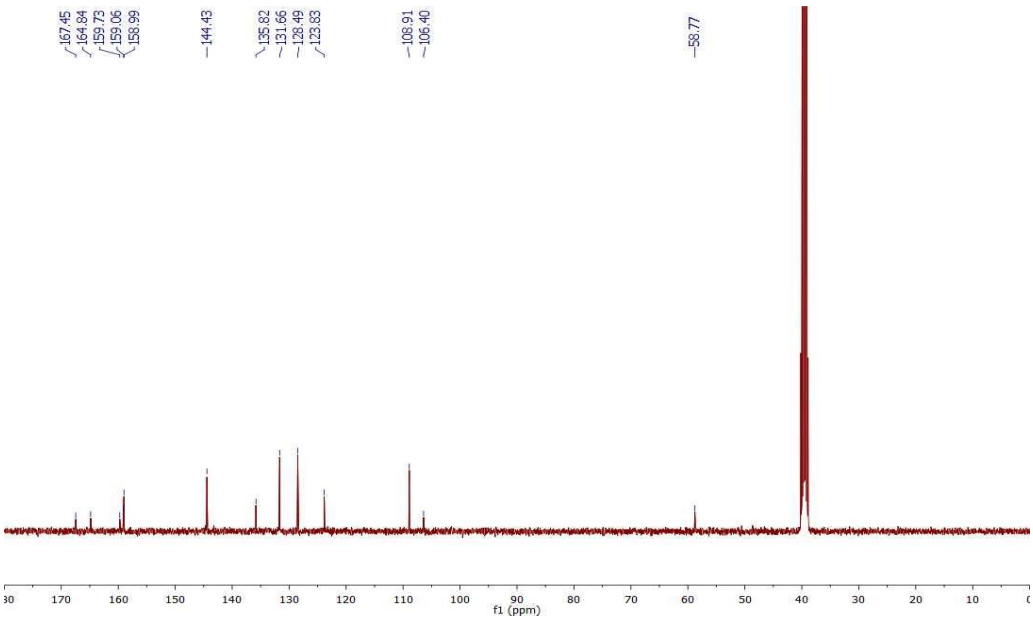

LC-MS (ES + APCI)

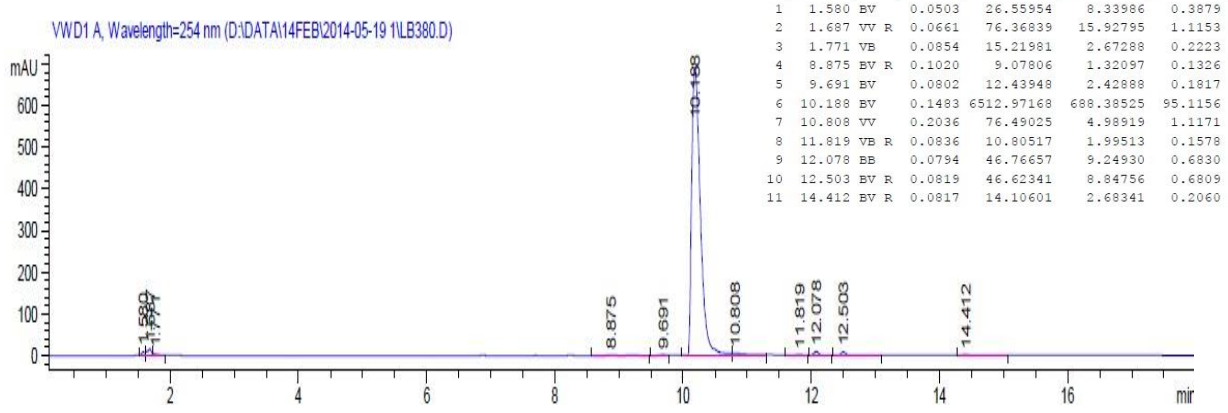

Peak #	RetTime [min]	Type	Width [min]	Area [mAU*s]	Height [mAU]	Area %
1	1.580	BV	0.0503	26.55954	8.33986	0.3879
2	1.687	VV R	0.0661	76.36839	15.92795	1.1153
3	1.771	VB	0.0854	15.21981	2.67288	0.2223
4	8.875	BV R	0.1020	9.07806	1.32097	0.1326
5	9.691	BV	0.0802	12.43948	2.42888	0.1817
6	10.188	BV	0.1483	6512.97168	688.38525	95.1156
7	10.808	VV	0.2036	76.49025	4.98919	1.1171
8	11.819	VB R	0.0836	10.80517	1.99513	0.1578
9	12.078	BB	0.0794	46.76657	9.24930	0.6830
10	12.503	BV R	0.0819	46.62341	8.84756	0.6809
11	14.412	BV R	0.0817	14.10601	2.68341	0.2060

6-(4-Bromophenyl)-2-((pyridin-3-ylamino)methyl)pyrimidin-4(3*H*)-one (100)

^{1}H NMR spectrum (500 MHz, DMSO)

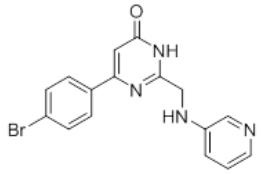

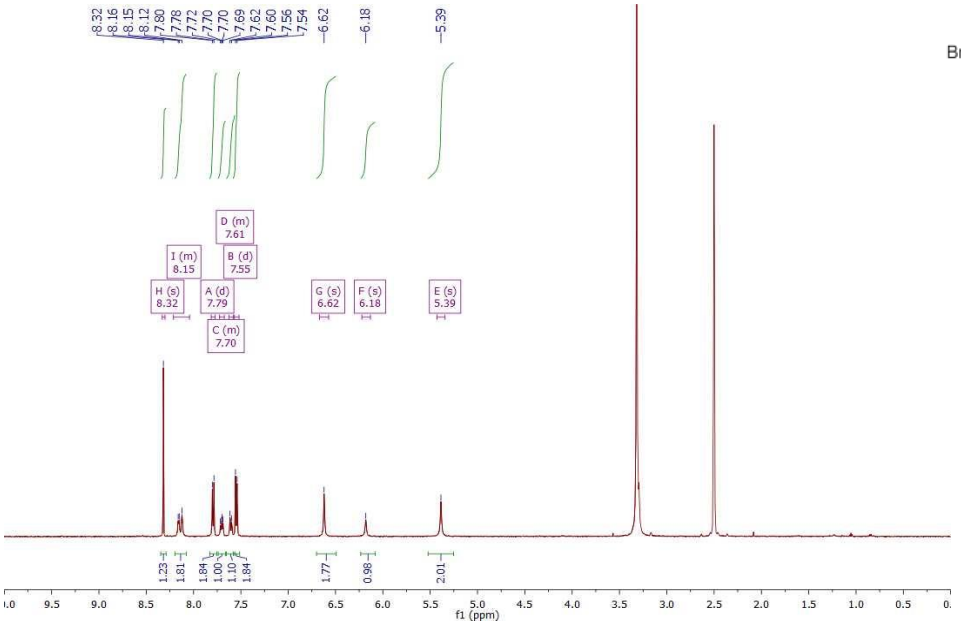

^{13}C NMR spectrum (126 MHz, DMSO)

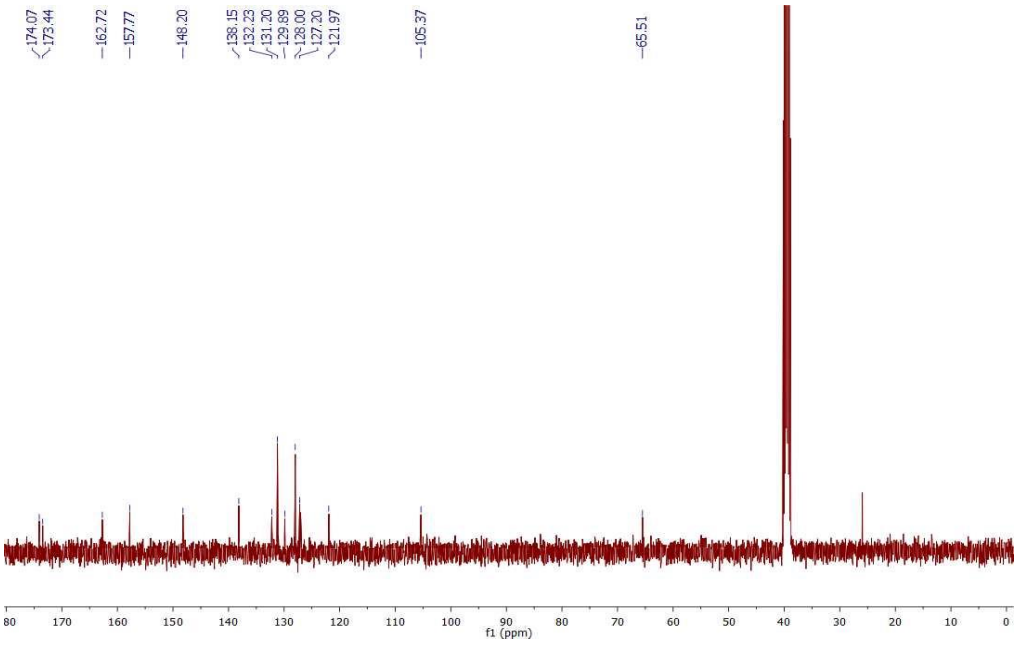

LC-MS (ES + APCI)

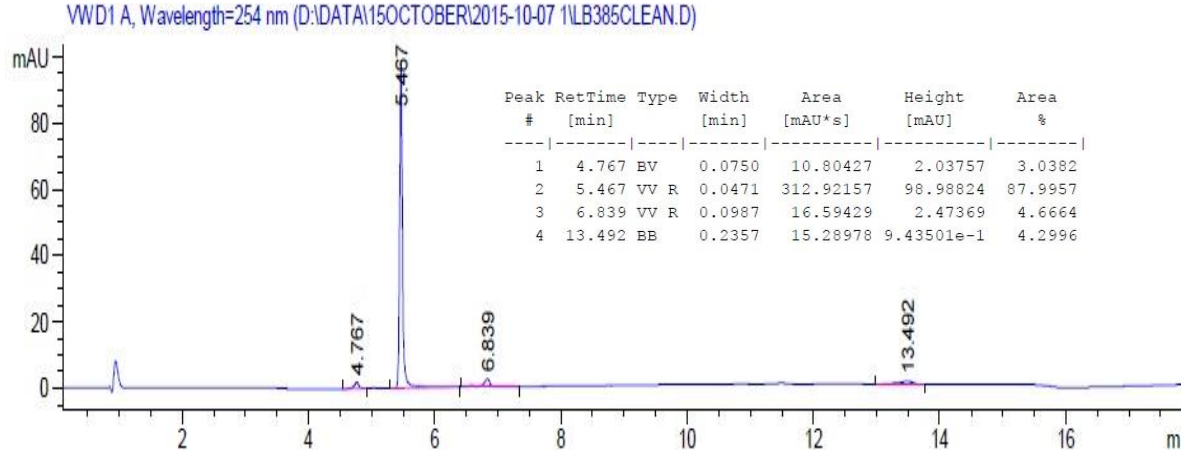

Peak #	RetTime [min]	Type	Width [min]	Area [mAU*s]	Height [mAU]	Area %
1	4.767	BV	0.0750	10.80427	2.03757	3.0382
2	5.467	VV R	0.0471	312.92157	98.98824	87.9957
3	6.839	VV R	0.0987	16.59429	2.47369	4.6664
4	13.492	BB	0.2357	15.28978	9.43501e-1	4.2996

6-(4-Bromophenyl)-2-((dimethylamino)methyl)pyrimidin-4(3*H*)-one (101)

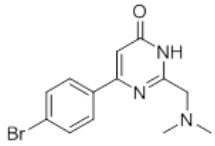

^{1}H NMR spectrum (400 MHz, DMSO)

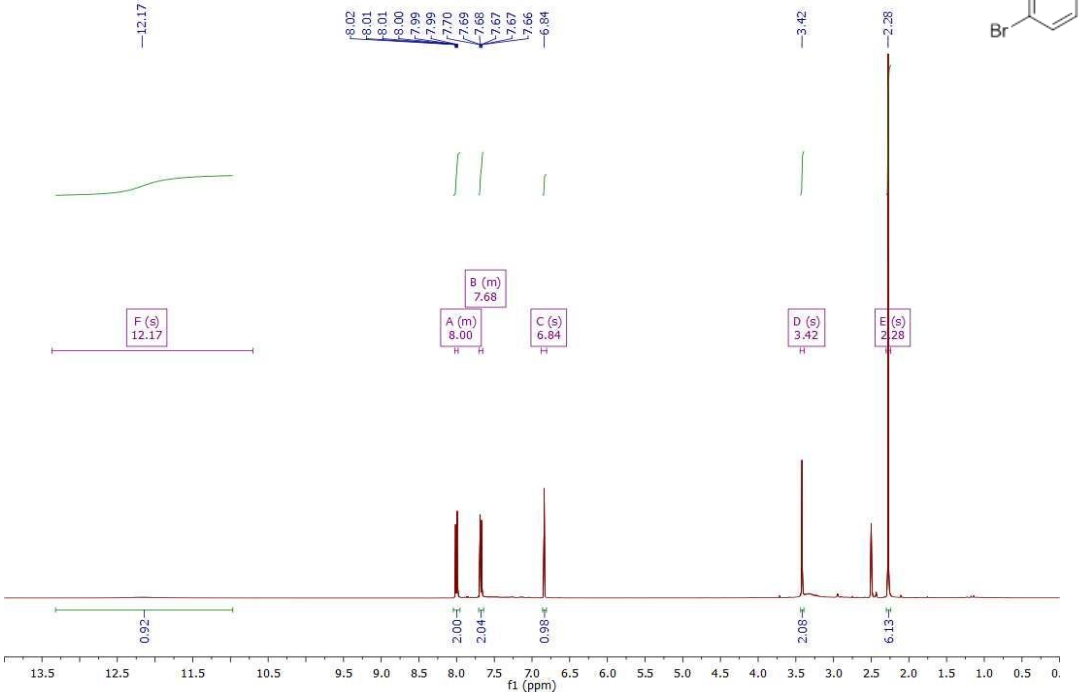

^{13}C NMR spectrum (101 MHz, DMSO)

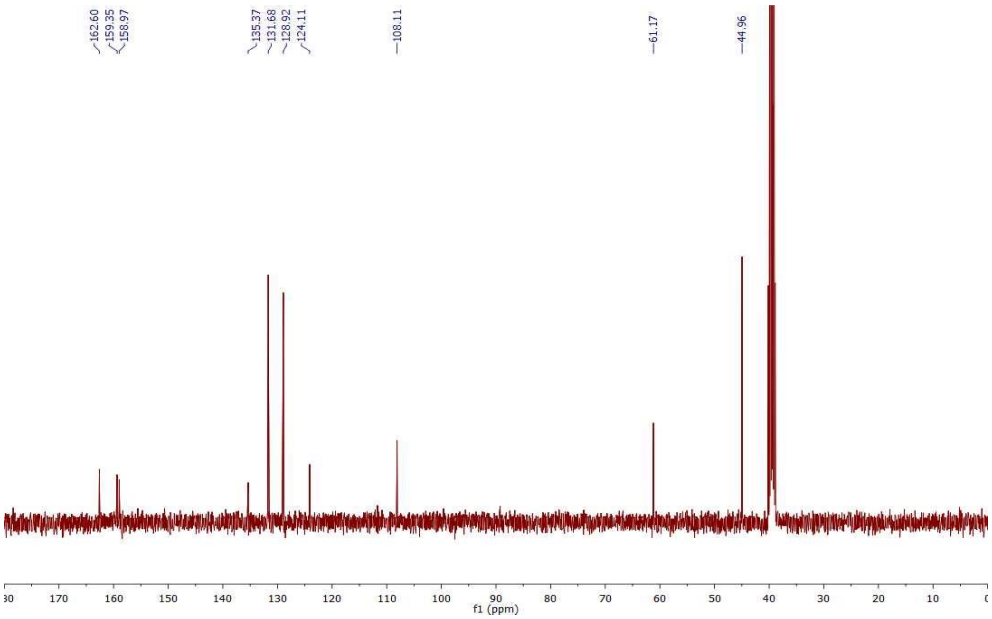

LC-MS (ES + APCI)

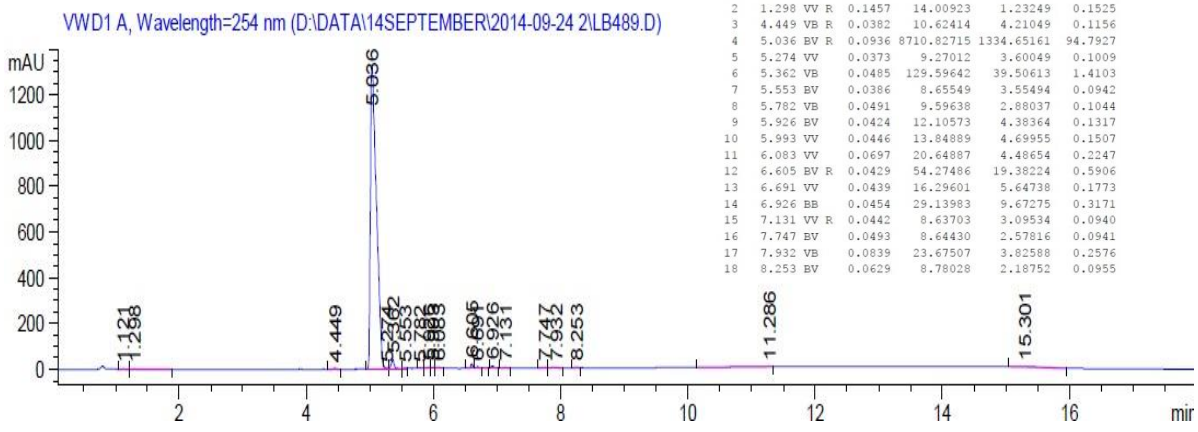

Peak #	RetTime [min]	Type	Width [min]	Area [mAU*s]	Height [mAU]	Area %
1	1.121	BV	0.0778	8.20610	1.41729	0.0893
2	1.298	VV R	0.1457	14.00923	1.23249	0.1525
3	4.449	VB R	0.0382	10.62414	4.21049	0.1156
4	5.036	BV R	0.0936	8710.82715	1334.65161	94.7927
5	5.274	VV	0.0373	9.27012	3.60049	0.1009
6	5.362	VB	0.0485	129.59642	39.50613	1.4103
7	5.553	BV	0.0386	8.65549	3.55494	0.0942
8	5.782	VB	0.0491	9.59638	2.88037	0.1044
9	5.926	BV	0.0424	12.10573	4.38364	0.1317
10	5.993	VV	0.0446	13.84889	4.69955	0.1507
11	6.083	VV	0.0697	20.64887	4.48654	0.2247
12	6.605	BV R	0.0429	54.27486	19.38224	0.5906
13	6.691	VV	0.0439	16.29601	5.64738	0.1773
14	6.926	BB	0.0454	29.13983	9.67275	0.3171
15	7.131	VV R	0.0442	8.63703	3.09534	0.0940
16	7.747	BV	0.0493	8.64430	2.57816	0.0941
17	7.932	VB	0.0839	23.67507	3.82588	0.2576
18	8.253	BV	0.0629	8.78028	2.18752	0.0955

2-(Trifluoromethyl)-7,12-dihydro-6*H*-benzo[*b*]benzo[4,5]thieno[3,2-*e*][1,4]diazepin-6-one (119)

^{1}H NMR spectrum (400 MHz, DMSO)

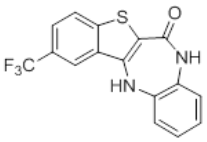

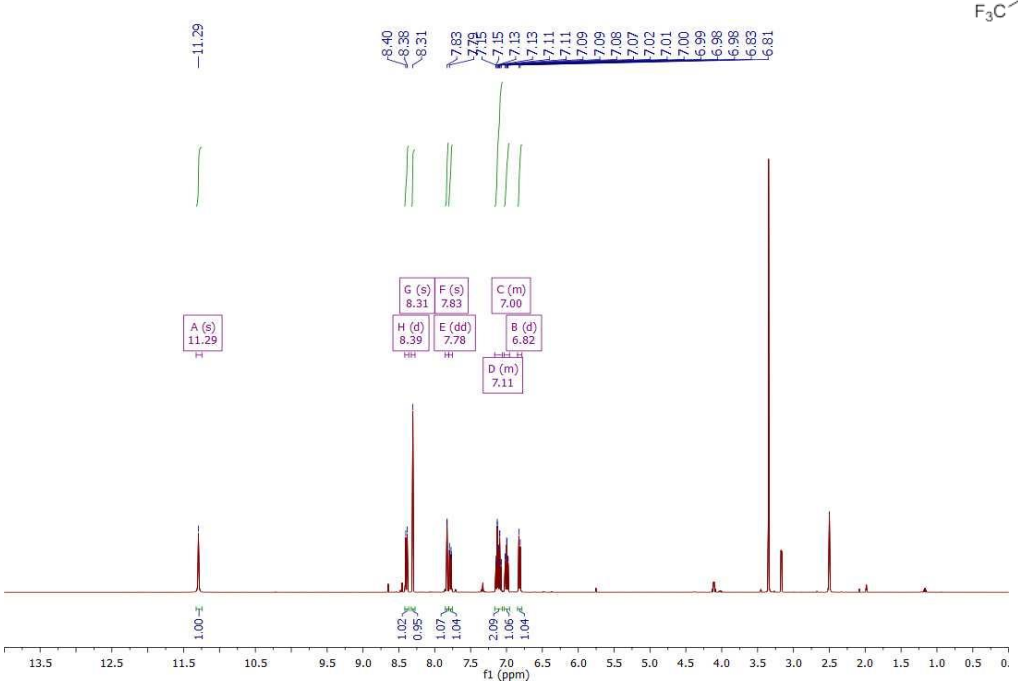

^{13}C NMR spectrum (101 MHz, DMSO)

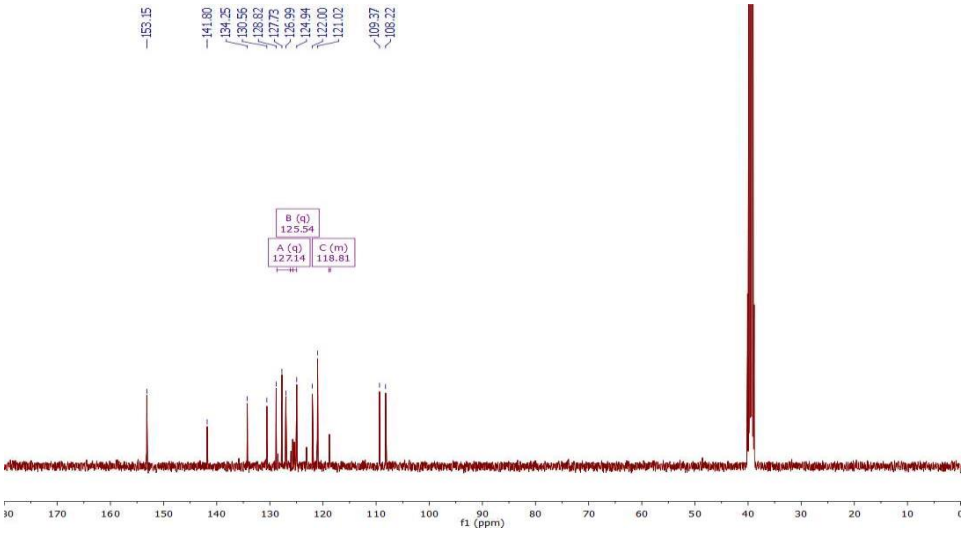

LC-MS (ES + APCI)

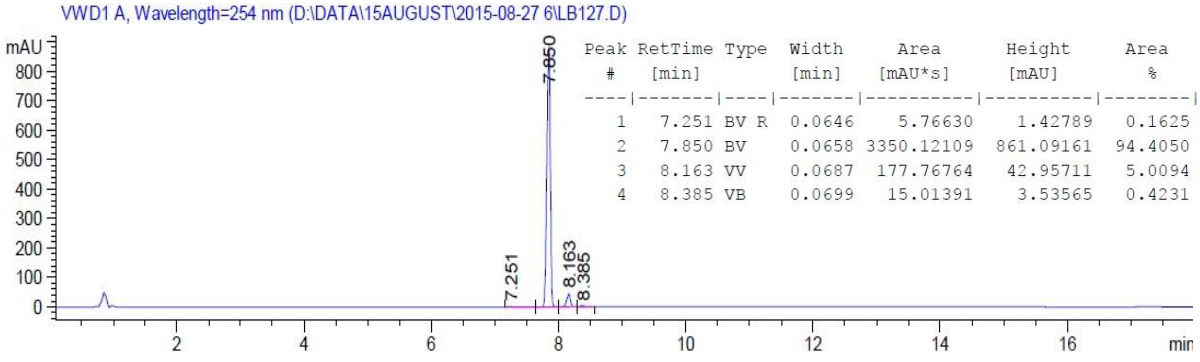

Peak #	RetTime [min]	Type	Width [min]	Area [mAU*s]	Height [mAU]	Area %
1	7.251	BV R	0.0646	5.76630	1.42789	0.1625
2	7.850	BV	0.0658	3350.12109	861.09161	94.4050
3	8.163	VV	0.0687	177.76764	42.95711	5.0094
4	8.385	VB	0.0699	15.01391	3.53565	0.4231

2-(Trifluoromethyl)-7,7a,8,9,10,11,11a,12-octahydro-6*H*-benzo[*b*]benzo[4,5]-thieno[3,2-*e*][1,4]diazepin-6-one (120)

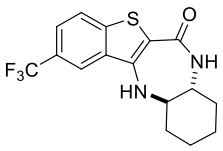

^{1}H NMR spectrum (500 MHz, DMSO)

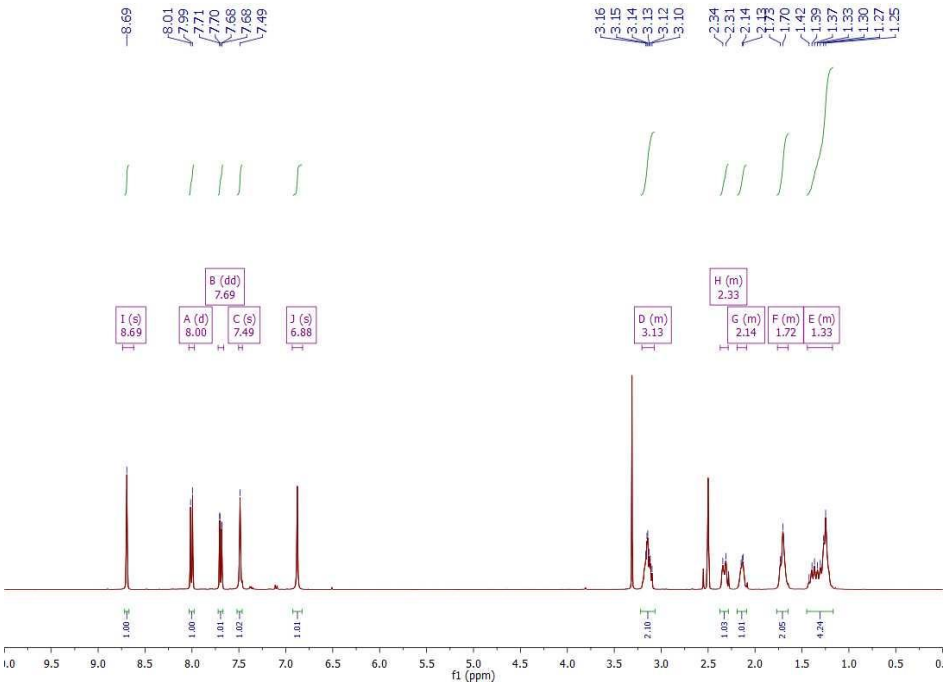

^{13}C NMR spectrum (126 MHz, DMSO)

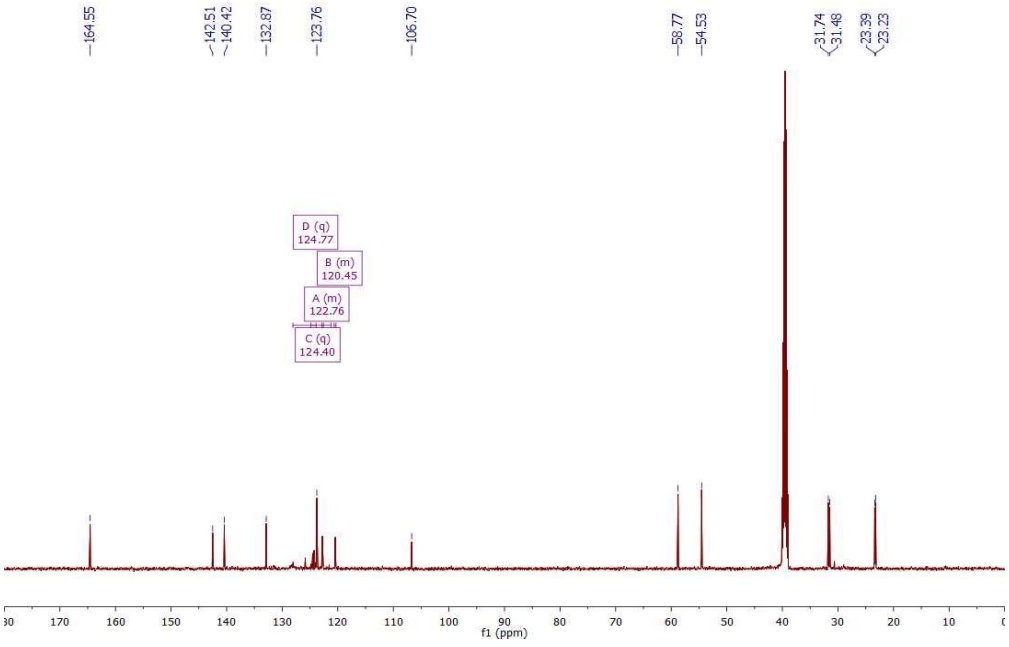

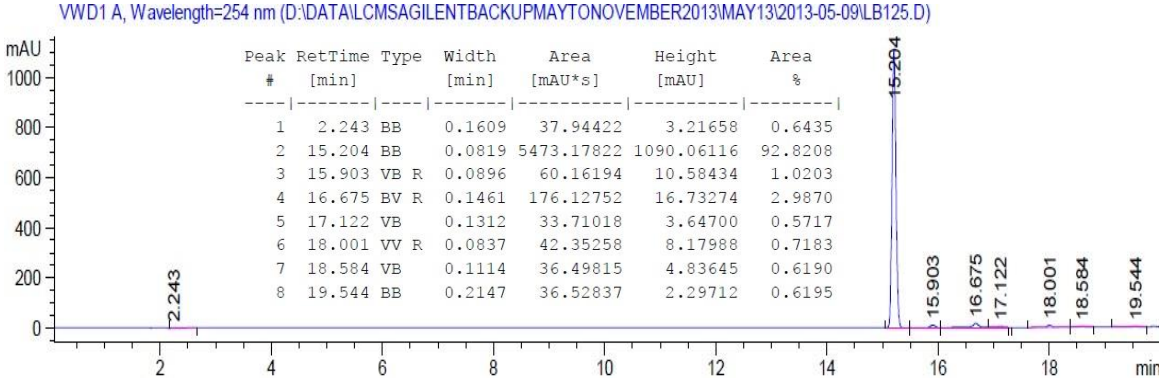

Peak #	RetTime [min]	Type	Width [min]	Area [mAU*s]	Height [mAU]	Area %
1	2.243	BB	0.1609	37.94422	3.21658	0.6435
2	15.204	BB	0.0819	5473.17822	1090.06116	92.8208
3	15.903	VB R	0.0896	60.16194	10.58434	1.0203
4	16.675	BV R	0.1461	176.12752	16.73274	2.9870
5	17.122	VB	0.1312	33.71018	3.64700	0.5717
6	18.001	VV R	0.0837	42.35258	8.17988	0.7183
7	18.584	VB	0.1114	36.49815	4.83645	0.6190
8	19.544	BB	0.2147	36.52837	2.29712	0.6195

9-(Trifluoromethyl)-1,2,3,4-tetrahydro-5*H*-benzo[4,5]thieno[3,2-*e*][1,4]diazepin-5-one (121)

^{1}H NMR spectrum (400 MHz, DMSO)

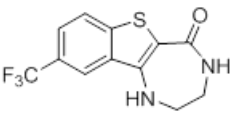

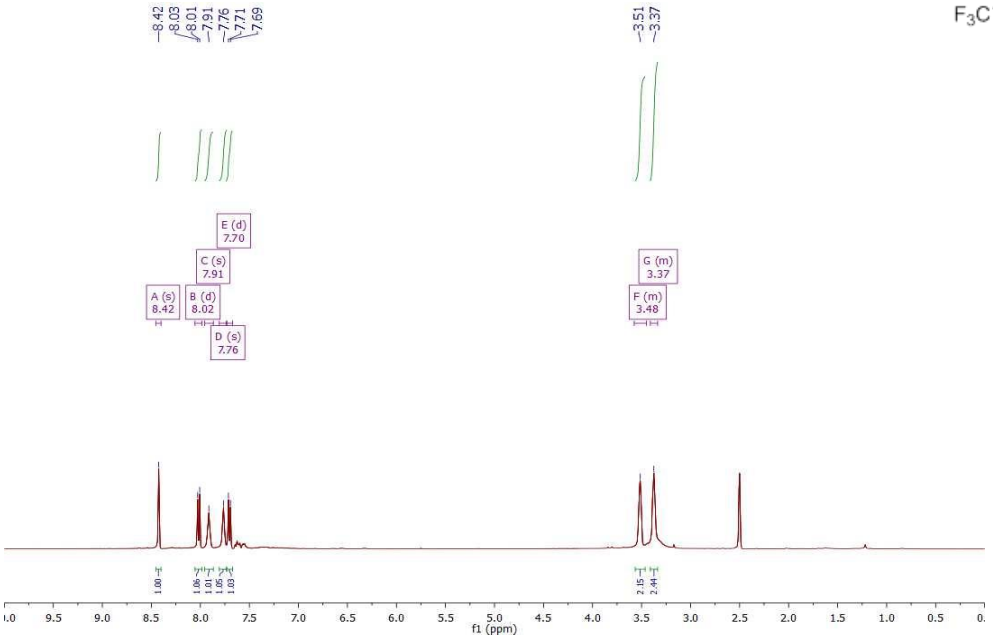

^{13}C NMR spectrum (101 MHz, DMSO)

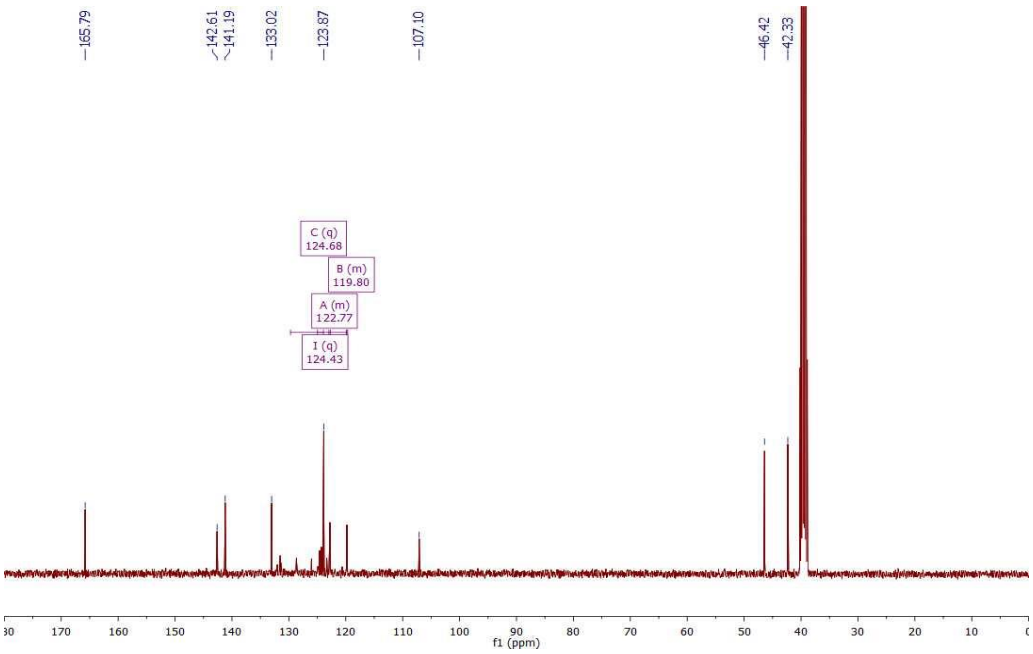

LC-MS (ES + APCI)

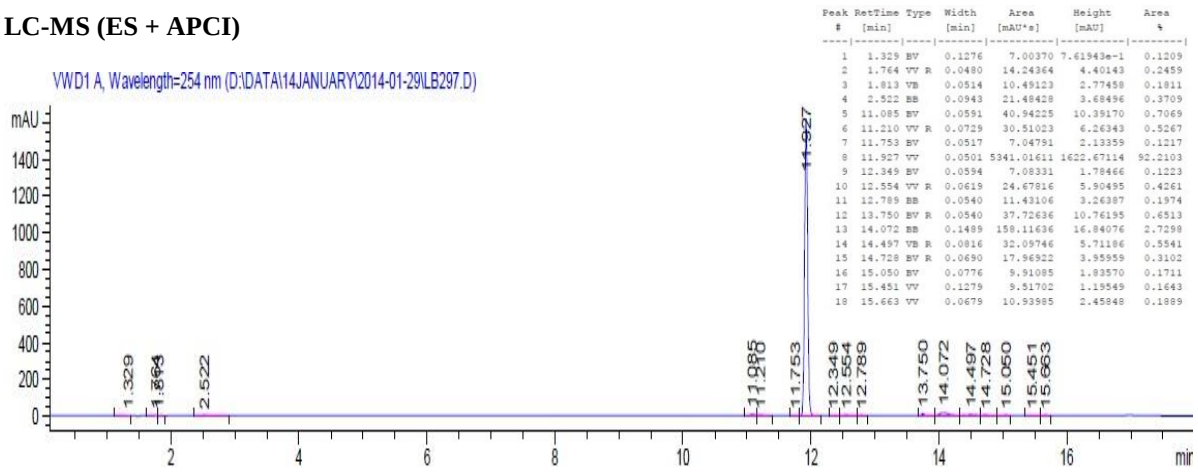

Peak #	RetTime [min]	Type	Width [min]	Area [mAU*s]	Height [mAU]	Area %
1	1.329	BV	0.1276	7.00370	7.61943e-1	0.1209
2	1.764	VV R	0.0480	14.24364	4.40143	0.2459
3	1.813	VB	0.0514	10.49123	2.77458	0.1811
4	2.522	BB	0.0943	21.48428	3.68496	0.3709
5	11.085	BV	0.0591	40.94225	10.39170	0.7069
6	11.210	VV R	0.0729	30.51023	6.26343	0.5267
7	11.753	BV	0.0517	7.04791	2.13359	0.1217
8	11.927	VV	0.0501	5341.01611	1622.67114	92.2103
9	12.349	BV	0.0594	7.08331	1.78466	0.1223
10	12.554	VV R	0.0619	24.67816	5.90495	0.4261
11	12.789	BB	0.0540	11.43106	3.26387	0.1974
12	13.750	BV R	0.0540	37.72636	10.76195	0.6513
13	14.072	BB	0.1489	158.11636	16.84076	2.7298
14	14.497	VB R	0.0816	32.05746	5.71186	0.5541
15	14.728	BV R	0.0690	17.96922	3.95959	0.3102
16	15.050	BV	0.0776	9.91085	1.83570	0.1711
17	15.451	VV	0.1279	9.51702	1.19549	0.1643
18	15.663	VV	0.0679	10.93985	2.45848	0.1889

(7a*R*,11a*R*)-2-(Trifluoromethyl)-7,7a,8,9,10,11,11a,12-octahydro-6*H* benzo[*b*]benzo[4,5]thieno[3,2-*e*][1,4]diazepin-6-one (122)

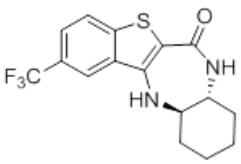

^{1}H NMR spectrum (400 MHz, DMSO)

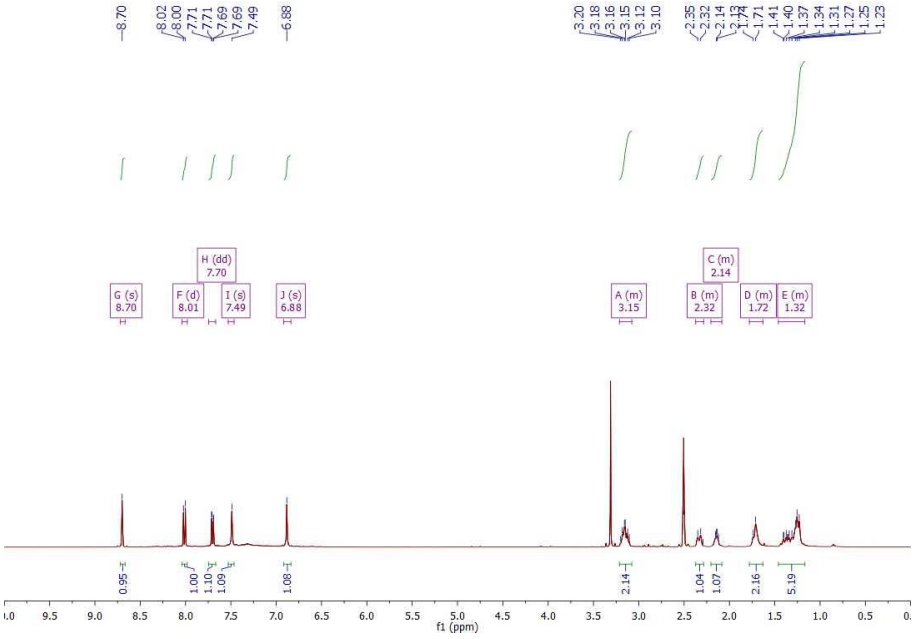

^{13}C NMR spectrum (101 MHz, DMSO)

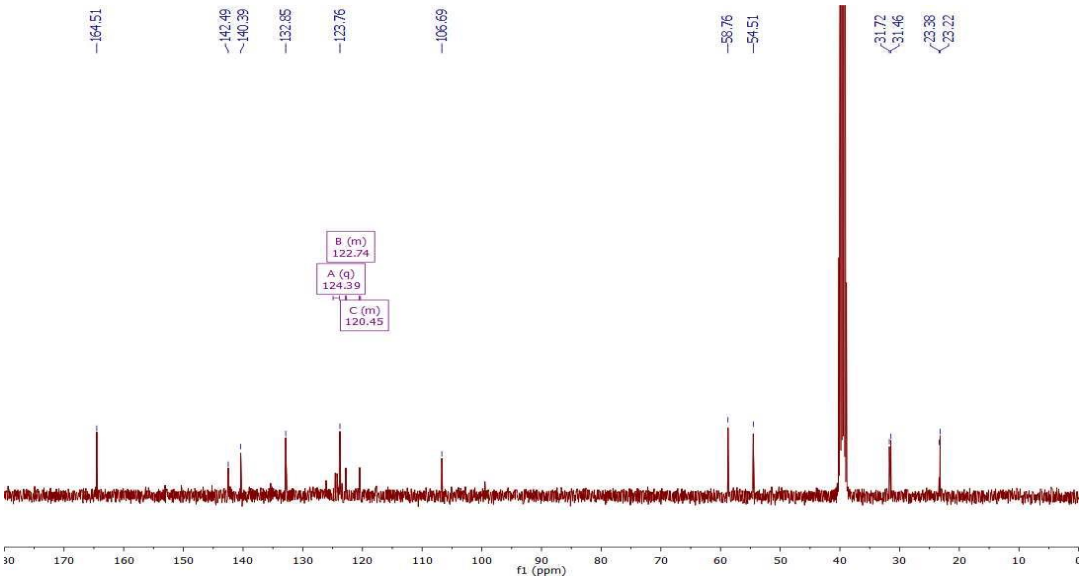

LC-MS (ES + APCI)

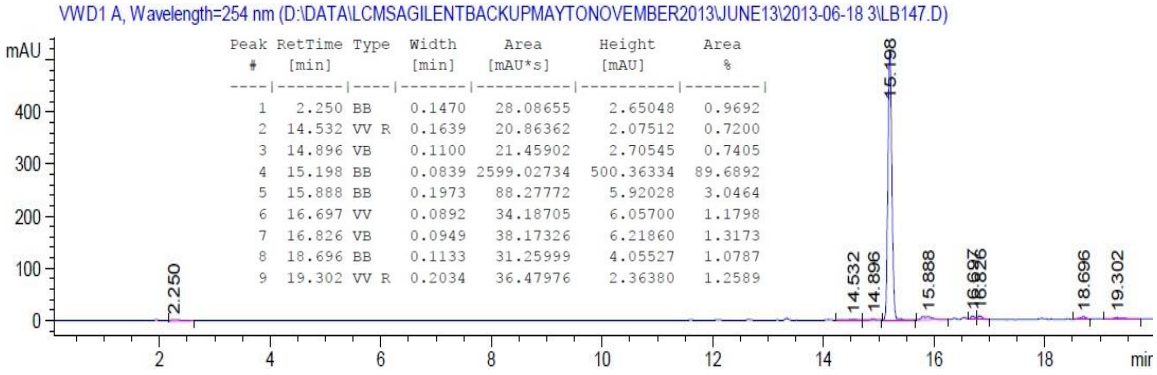

(7a*S*,11a*S*)-2-(Trifluoromethyl)-7,7a,8,9,10,11,11a,12-octahydro-6*H*-benzo[b]benzo[4,5]thieno[3,2-*e*][1,4]diazepin-6-one (123)

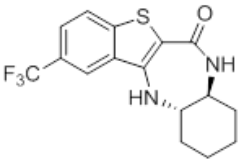

^{1}H NMR spectrum (400 MHz, DMSO)

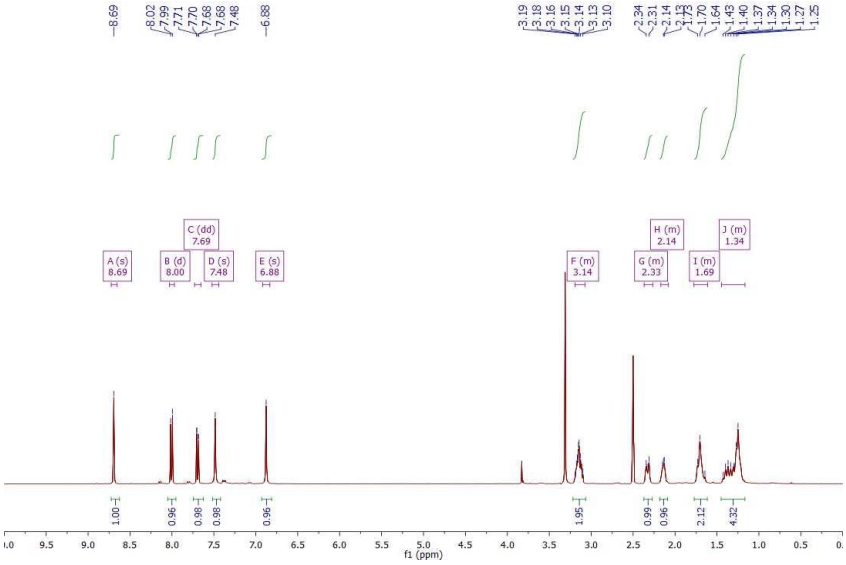

^{13}C NMR spectrum (101 MHz, DMSO)

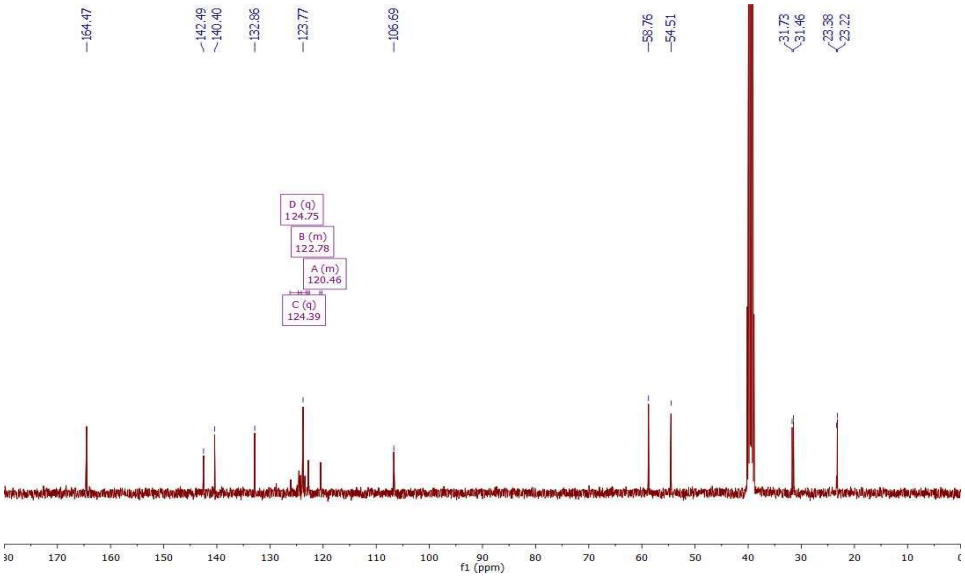

LC-MS (ES + APCI)

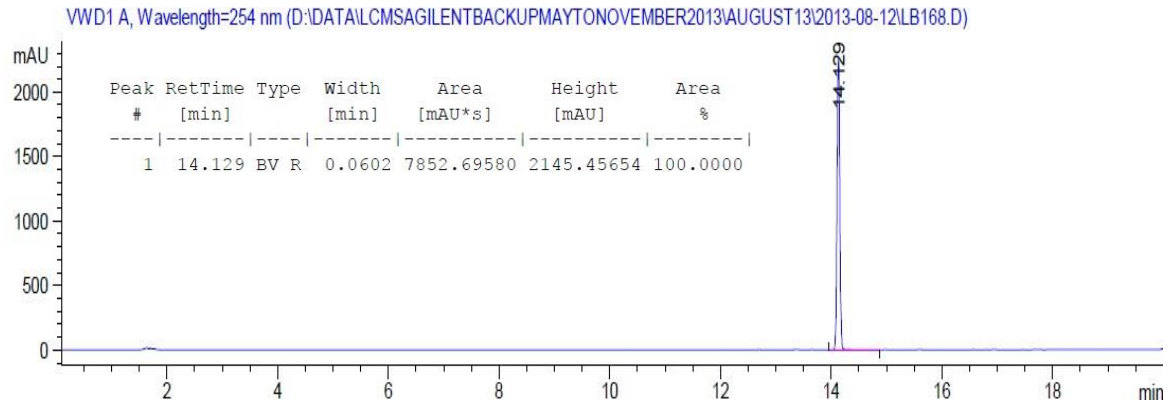

10-(Trifluoromethyl)-2,3,4,4a,12,12a-hexahydrobenzo[*b*]benzo[4,5]thieno[3,2-*e*][1,4]oxazepin-6(1*H*)-one (124)

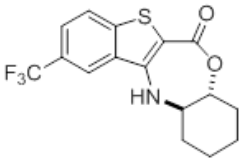

^{1}H NMR spectrum (400 MHz, DMSO)

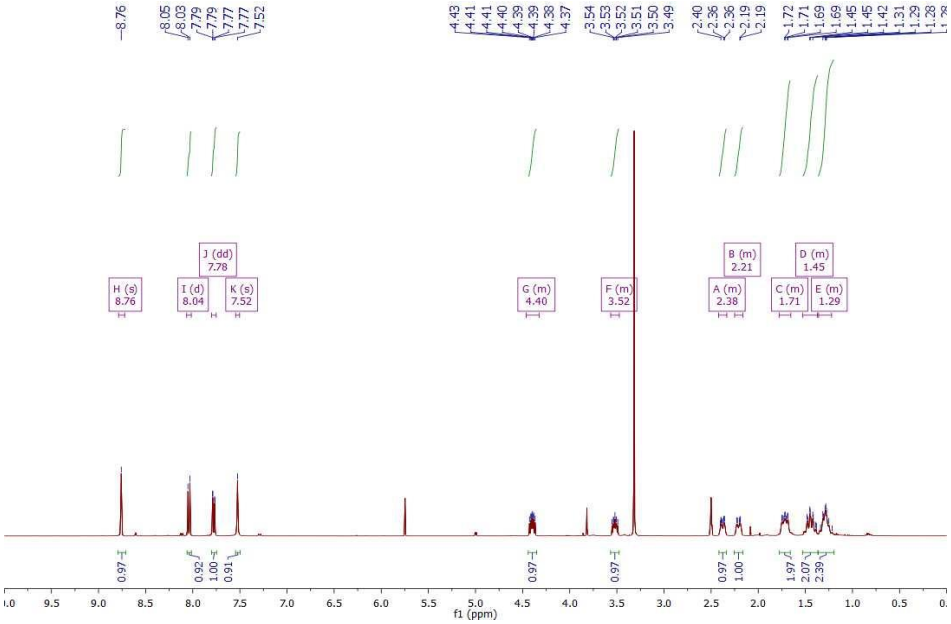

^{13}C NMR spectrum (101 MHz, DMSO)

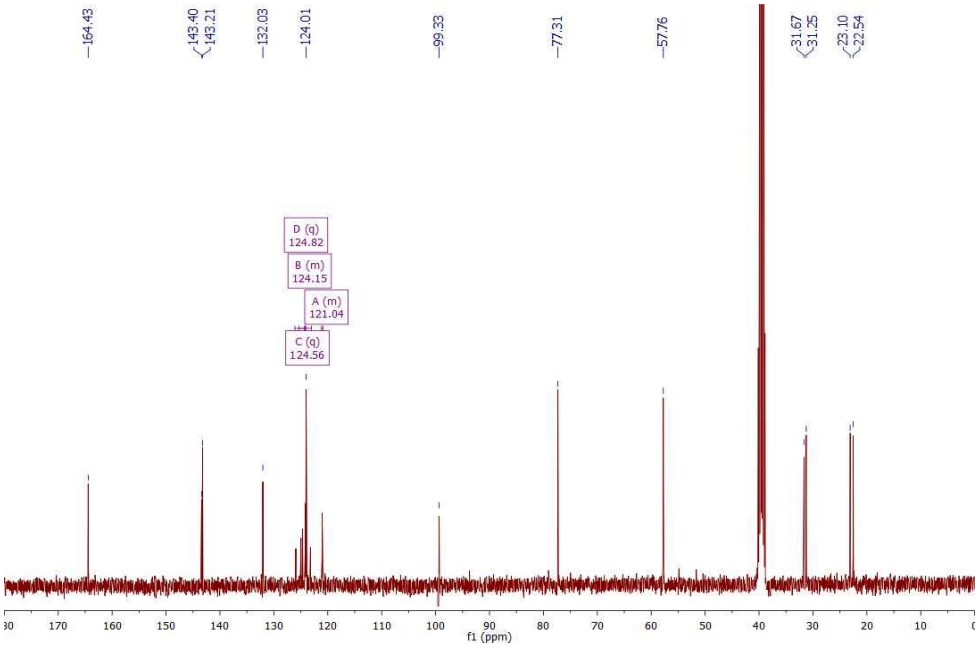

LC-MS (ES + APCI)

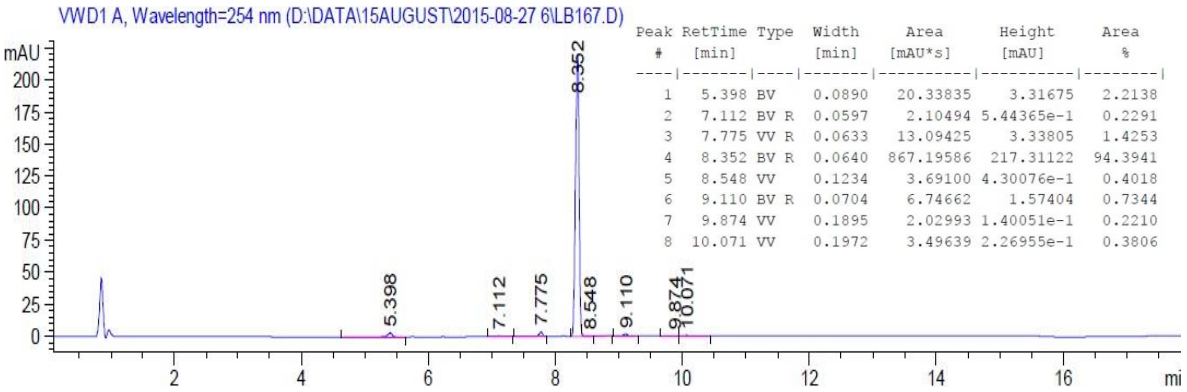

Peak #	RetTime [min]	Type	Width [min]	Area [mAU*s]	Height [mAU]	Area %
1	5.398	BV	0.0890	20.33835	3.31675	2.2138
2	7.112	BV R	0.0597	2.10494	5.44365e-1	0.2291
3	7.775	VV R	0.0633	13.09425	3.33805	1.4253
4	8.352	BV R	0.0640	867.19586	217.31122	94.3941
5	8.548	VV	0.1234	3.69100	4.30076e-1	0.4018
6	9.110	BV R	0.0704	6.74662	1.57404	0.7344
7	9.874	VV	0.1895	2.02993	1.40051e-1	0.2210
8	10.071	VV	0.1972	3.49639	2.26955e-1	0.3806

9-(Trifluoromethyl)-1,2,3,3*a*,11,11*a*-hexahydro-5*H*-benzo[4,5]thieno[3,2-e]cyclopenta[*b*][1,4]oxazepin-5-one (125)

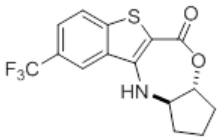

^{1}H NMR spectrum (400 MHz, DMSO)

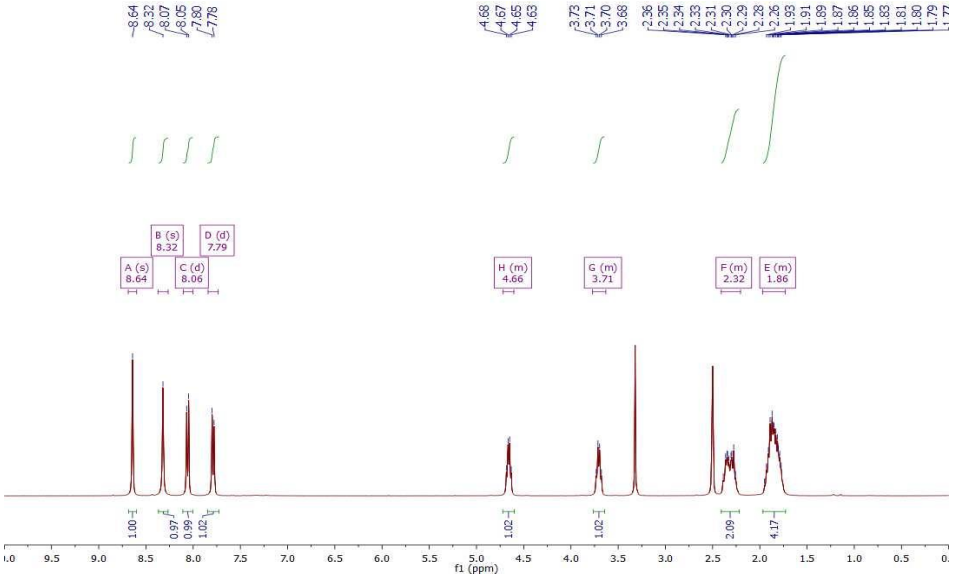

^{13}C NMR spectrum (101 MHz, DMSO)

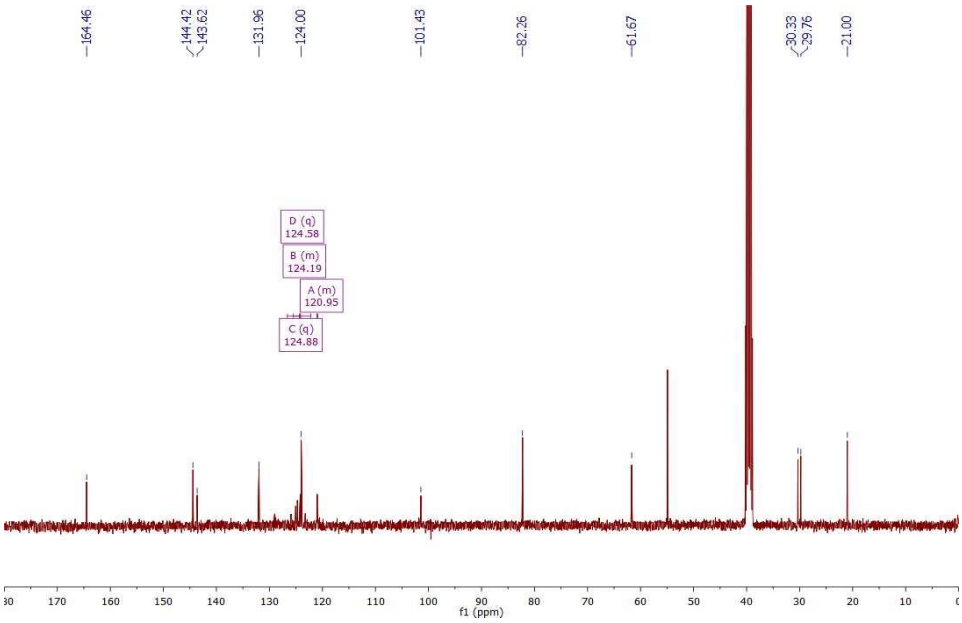

LC-MS (ES + APCI)

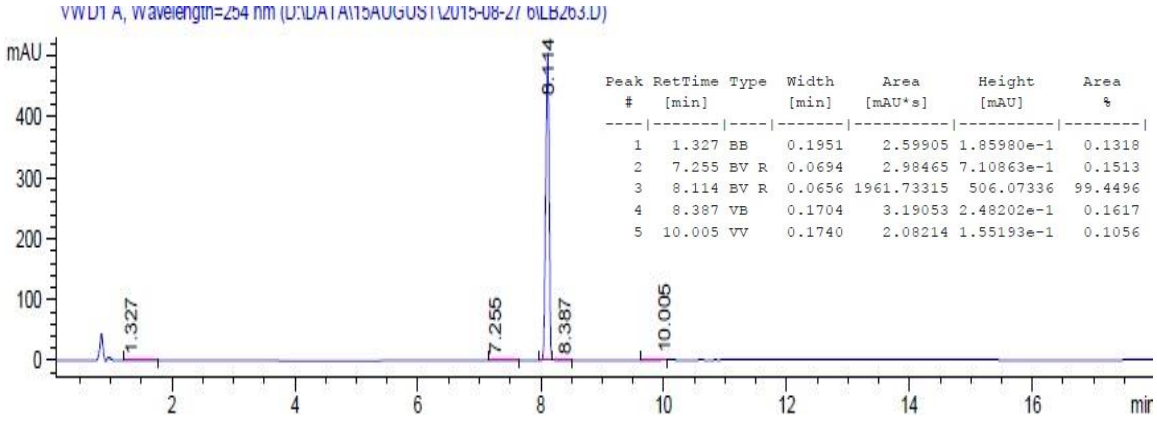

9-(Trifluoromethyl)-2,3-dihydrobenzo[4,5]thieno[3,2-*e*][1,4]oxazepin-5(1*H*)-one (126)

^{1}H NMR spectrum (400 MHz, DMSO)

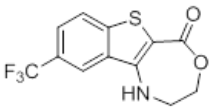

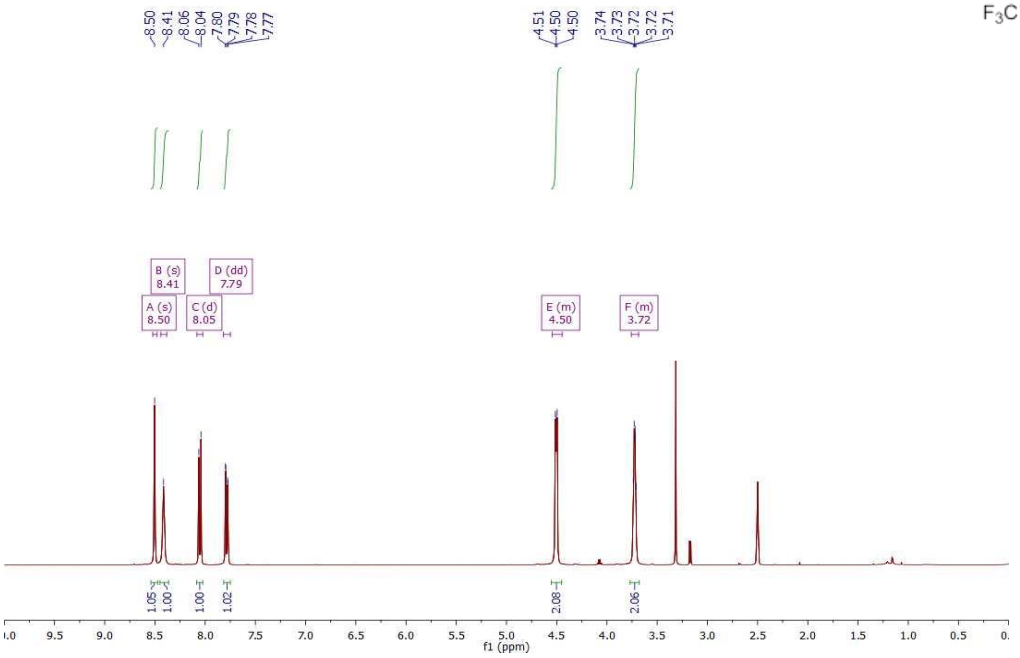

^{13}C NMR spectrum (101 MHz, DMSO)

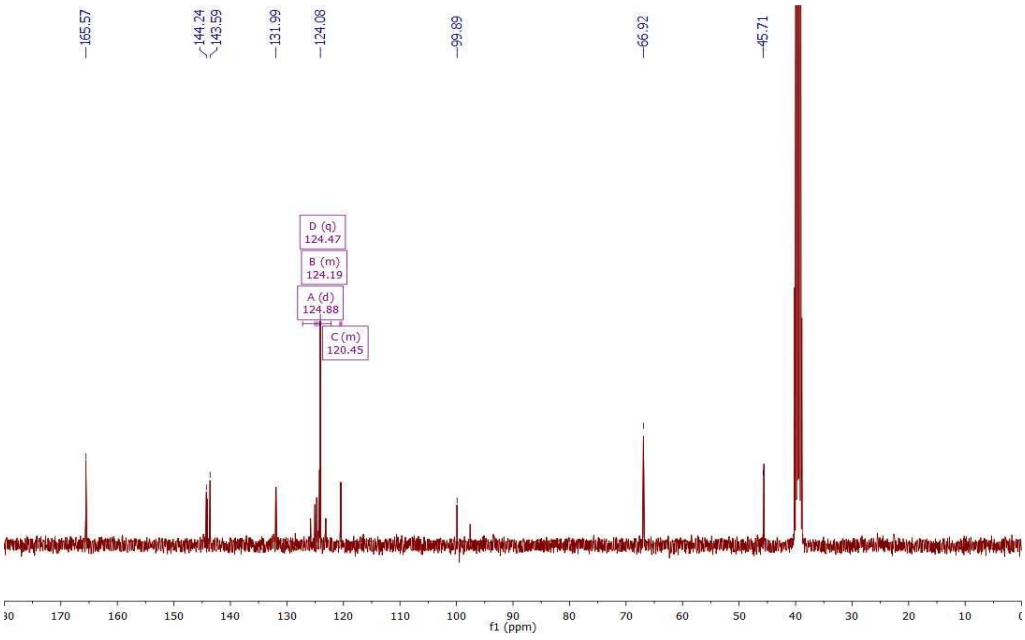

LC-MS (ES + APCI)

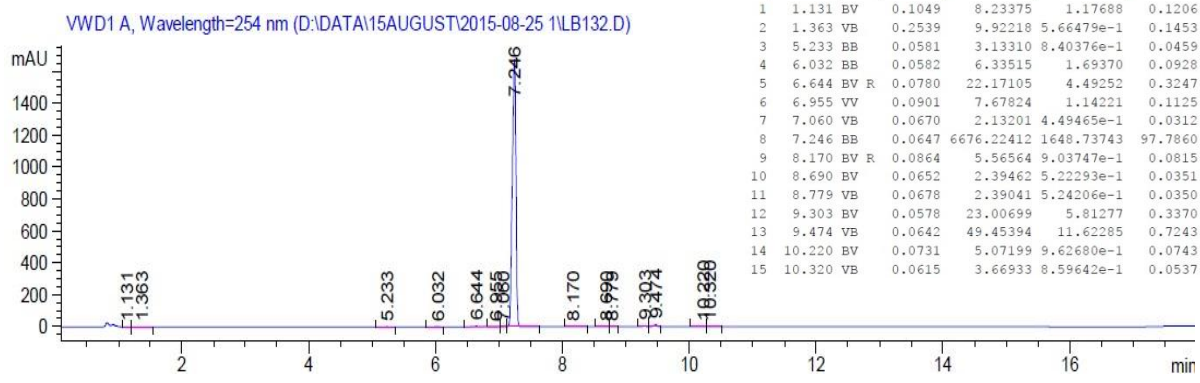

Peak #	RetTime [min]	Type	Width [min]	Area [mAU*s]	Height [mAU]	Area %
1	1.131	BV	0.1049	8.23375	1.17688	0.1206
2	1.363	VB	0.2539	9.92218	5.66479e-1	0.1453
3	5.233	BB	0.0581	3.13310	8.40376e-1	0.0459
4	6.032	BB	0.0582	6.33515	1.69370	0.0928
5	6.644	BV R	0.0780	22.17105	4.49252	0.3247
6	6.955	VV	0.0901	7.67824	1.14221	0.1125
7	7.060	VB	0.0670	2.13201	4.49465e-1	0.0312
8	7.246	BB	0.0647	6676.22412	1648.73743	97.7860
9	8.170	BV R	0.0864	5.56564	9.03747e-1	0.0815
10	8.690	BV	0.0652	2.39462	5.22293e-1	0.0351
11	8.779	VB	0.0678	2.39041	5.24206e-1	0.0350
12	9.303	BV	0.0578	23.00699	5.81277	0.3370
13	9.474	VB	0.0642	49.45394	11.62285	0.7243
14	10.220	BV	0.0731	5.07199	9.62680e-1	0.0743
15	10.320	VB	0.0615	3.66933	8.59642e-1	0.0537

1-Methyl-9-(trifluoromethyl)-2,3-dihydrobenzo[4,5]thieno[3,2-*e*][1,4]oxazepin-5(1*H*)-one (131)

^{1}H NMR spectrum (400 MHz, $CDCl_3$)

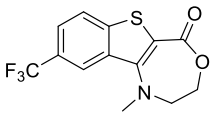

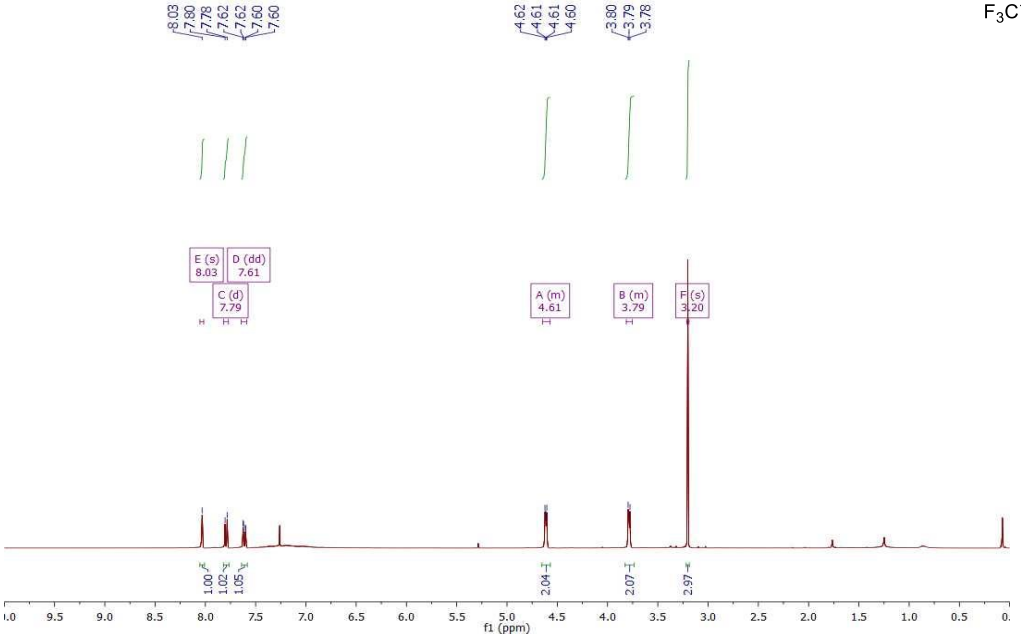

^{13}C NMR spectrum (101 MHz, $CDCl_3$)

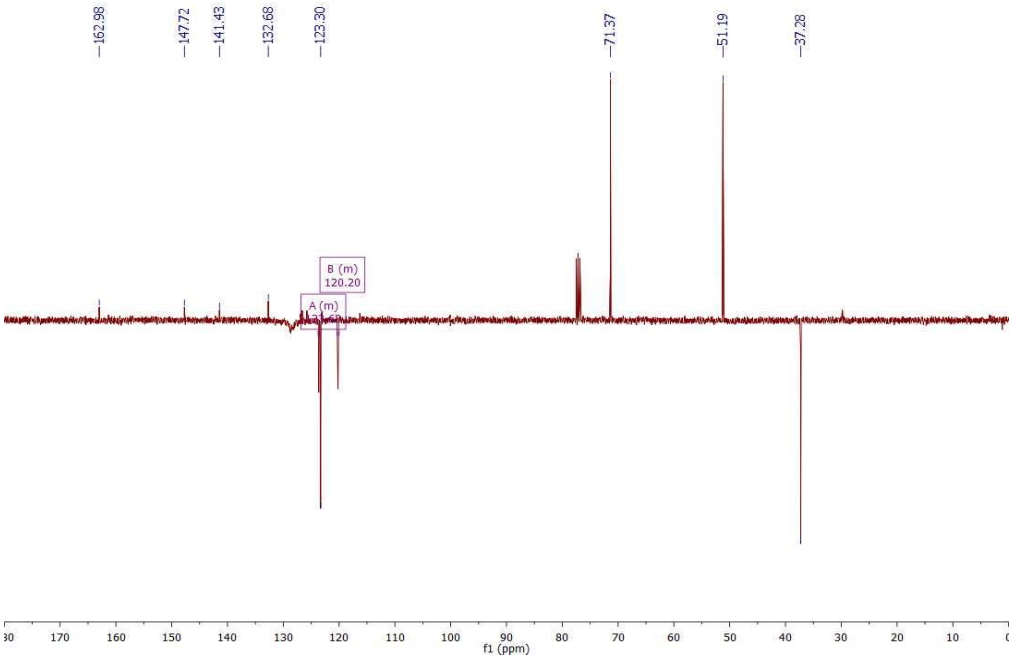

LC-MS (ES + APCI)

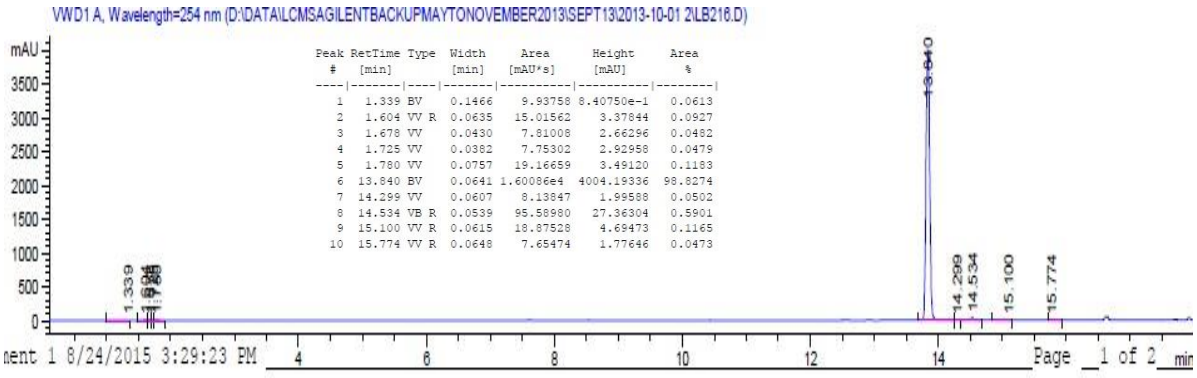

1-Ethyl-9-(trifluoromethyl)-2,3-dihydrobenzo[4,5]thieno[3,2-*e*][1,4]oxazepin-5(1*H*)-one (132)

^{1}H NMR spectrum (400 MHz, DMSO)

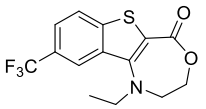

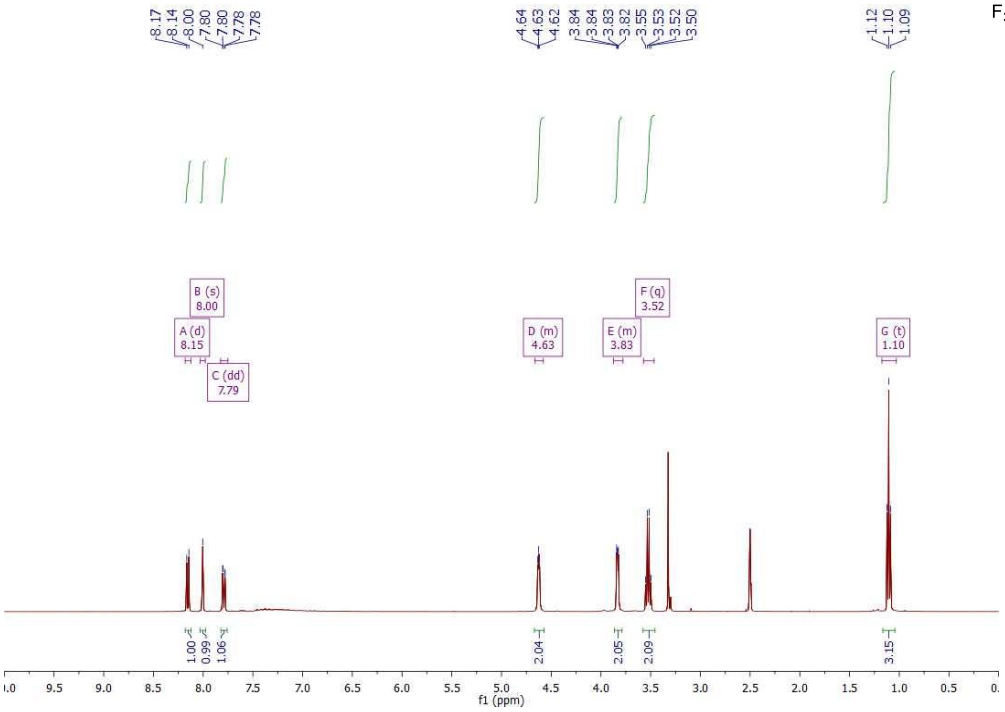

^{13}C NMR spectrum (101 MHz, DMSO)

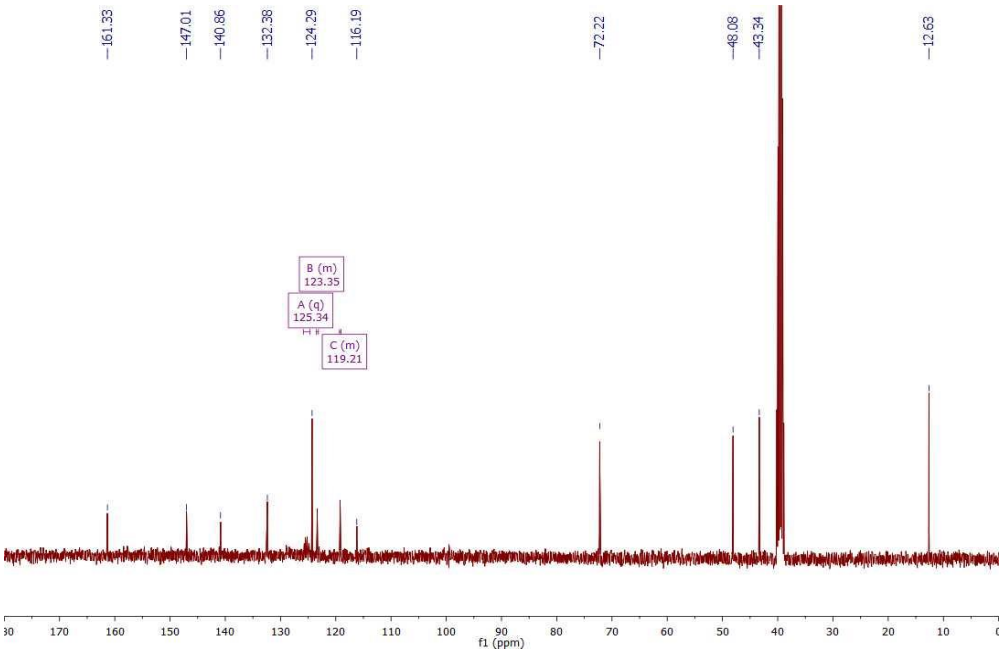

LC-MS (ES + APCI)

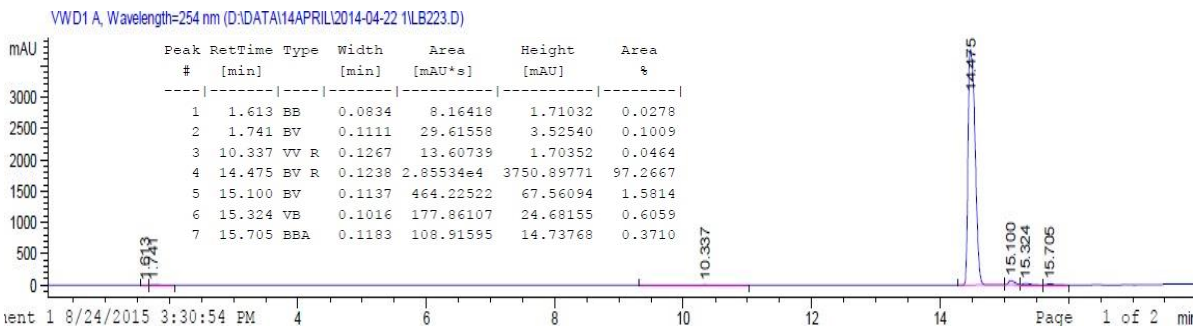

(*S*)-10-(Trifluoromethyl)-2,3,3a,4-tetrahydro-1*H*,6*H*-benzo[4,5]thieno[3,2-e]pyrrolo[2,1-*c*][1,4]oxazepin-6-one (133)

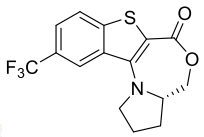

^{1}H NMR spectrum (400 MHz, DMSO)

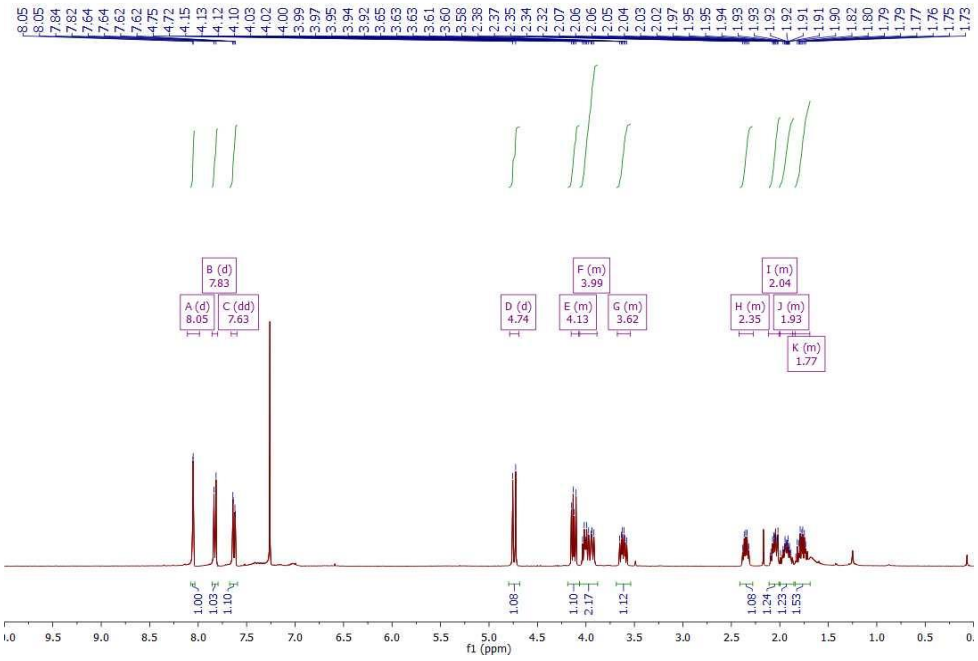

^{13}C NMR spectrum (101 MHz, DMSO)

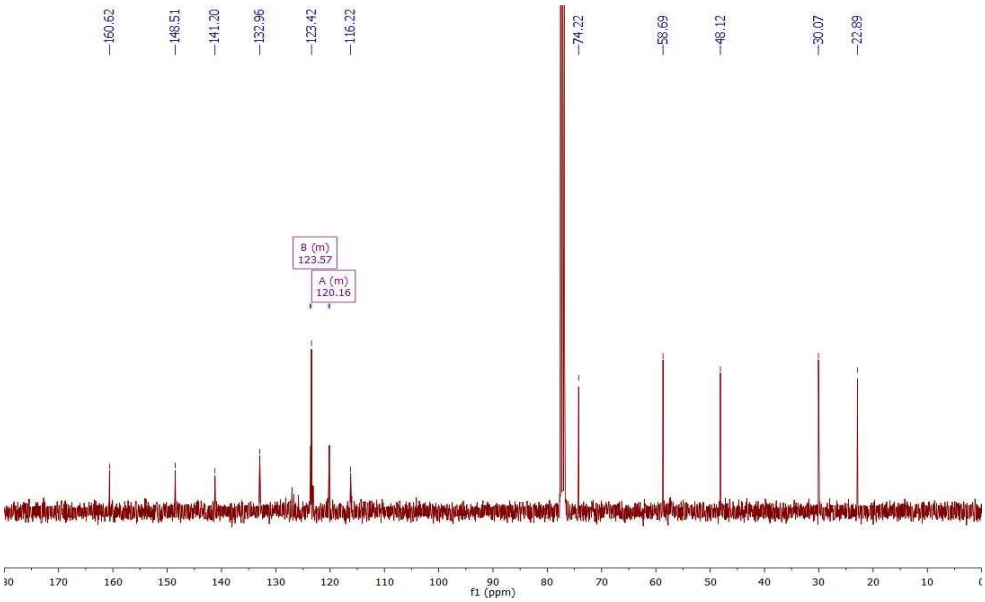

LC-MS (ES + APCI)

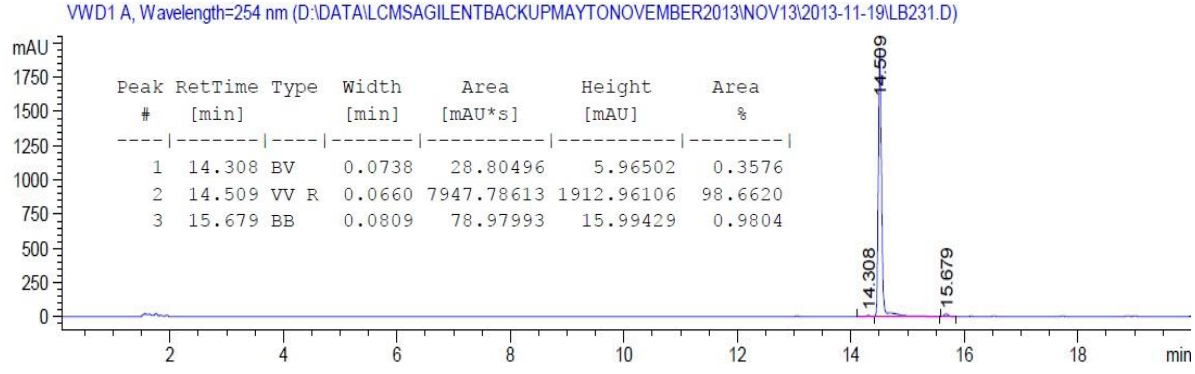

(*R*)-2-Isopropyl-9-(trifluoromethyl)-2,3-dihydrobenzo[4,5]thieno[3,2-*e*][1,4]oxazepin-5(1*H*)-one (134)

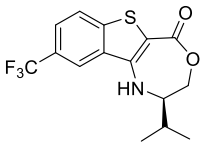

^{1}H NMR spectrum (400 MHz, DMSO)

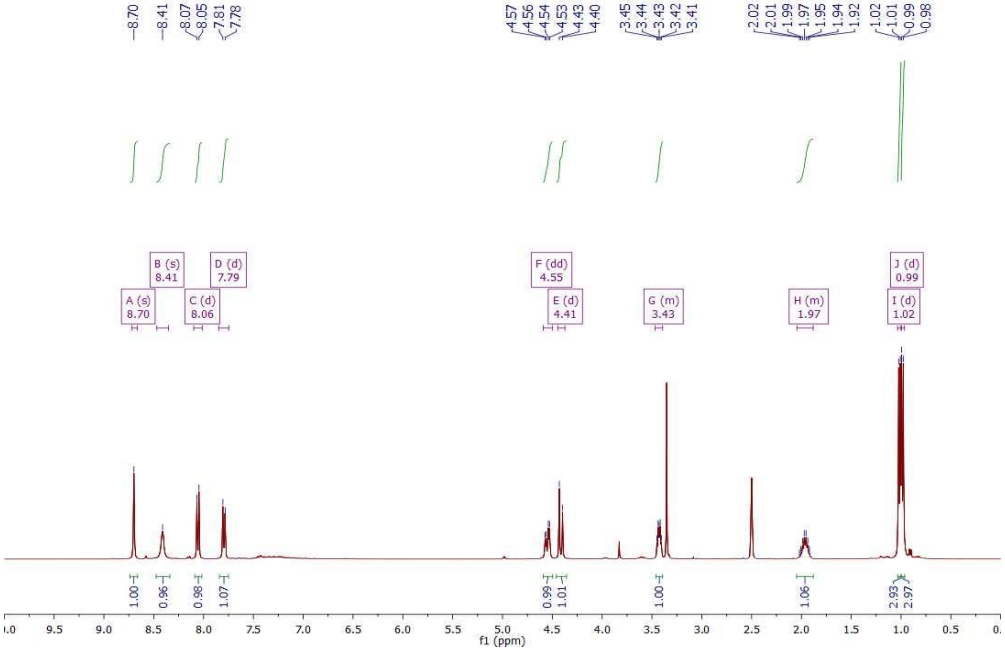

^{13}C NMR spectrum (101 MHz, DMSO)

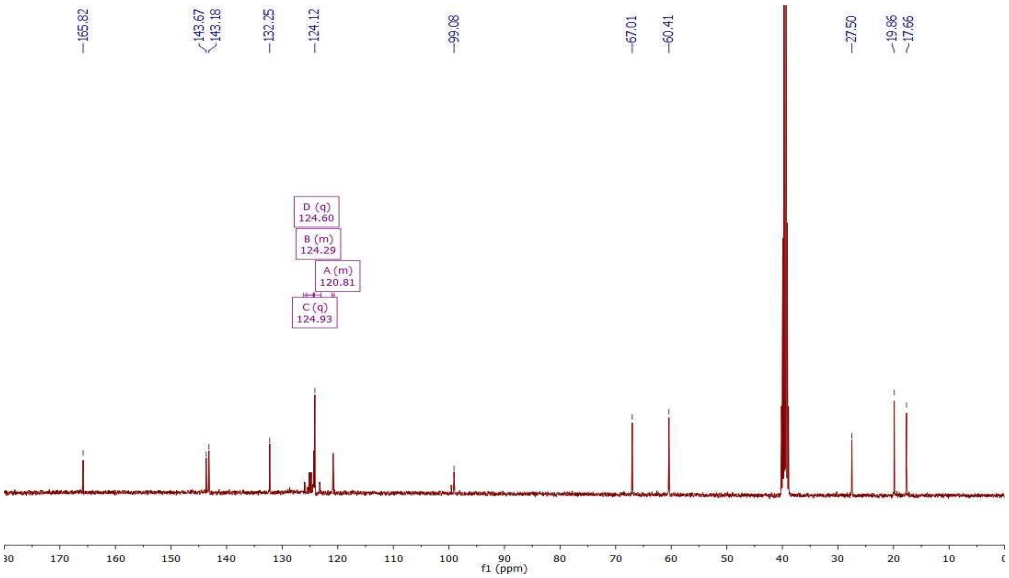

LC-MS (ES + APCI)

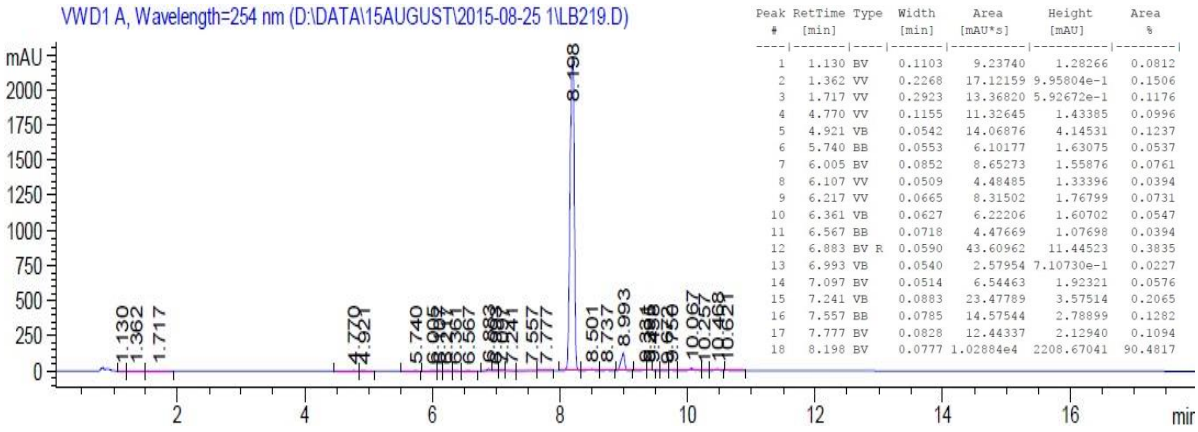

Peak #	RetTime [min]	Type	Width [min]	Area [mAU*s]	Height [mAU]	Area %
1	1.130	BV	0.1103	9.23740	1.28266	0.0812
2	1.362	VV	0.2268	17.12159	9.95804e-1	0.1506
3	1.717	VV	0.2923	13.36820	5.92672e-1	0.1176
4	4.770	VV	0.1155	11.32645	1.43385	0.0996
5	4.921	VB	0.0542	14.06876	4.14531	0.1237
6	5.740	BB	0.0553	6.10177	1.63075	0.0537
7	6.005	BV	0.0852	8.65273	1.55876	0.0761
8	6.107	VV	0.0509	4.48485	1.33396	0.0394
9	6.217	VV	0.0665	8.31502	1.76799	0.0731
10	6.361	VB	0.0627	6.22206	1.60702	0.0547
11	6.567	BB	0.0718	4.47669	1.07698	0.0394
12	6.883	BV R	0.0590	43.60962	11.44523	0.3835
13	6.993	VB	0.0540	2.57954	7.10730e-1	0.0227
14	7.097	BV	0.0514	6.54463	1.92321	0.0576
15	7.241	VB	0.0883	23.47789	3.57514	0.2065
16	7.557	BB	0.0785	14.57544	2.78899	0.1282
17	7.777	BV	0.0828	12.44337	2.12940	0.1094
18	8.198	BV	0.0777	1.02884e4	2208.67041	90.4817

(*S*)-2-Isopropyl-9-(trifluoromethyl)-2,3-dihydrobenzo[4,5]thieno[3,2-*e*][1,4]oxazepin-5(1*H*)-one (135)

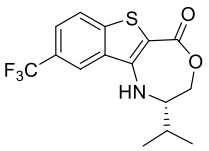

^{1}H NMR spectrum (400 MHz, DMSO)

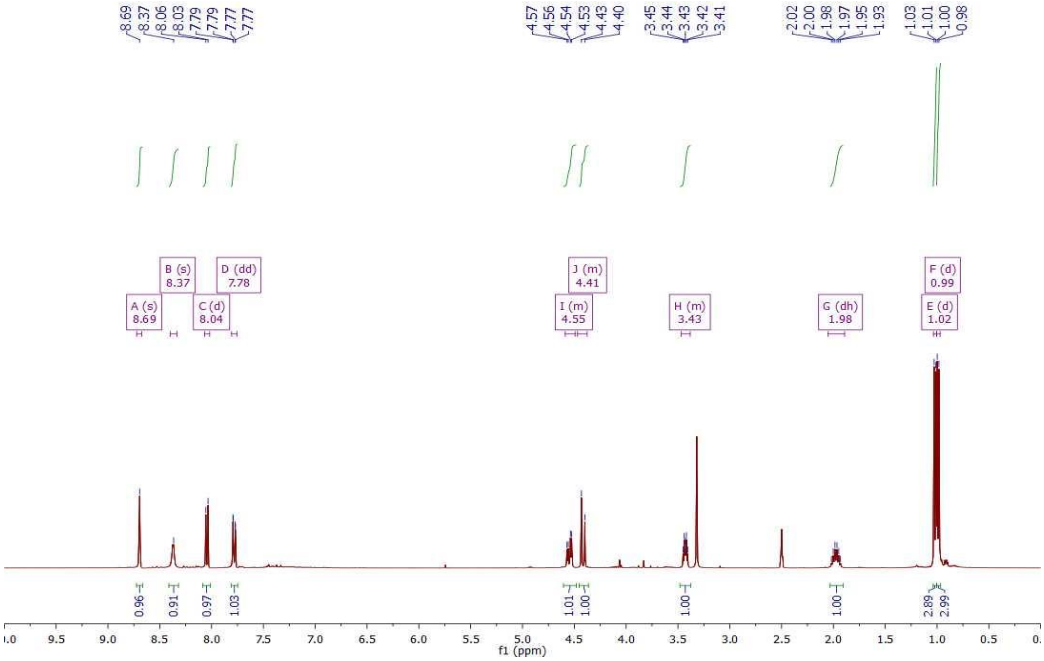

^{13}C NMR spectrum (101 MHz, DMSO)

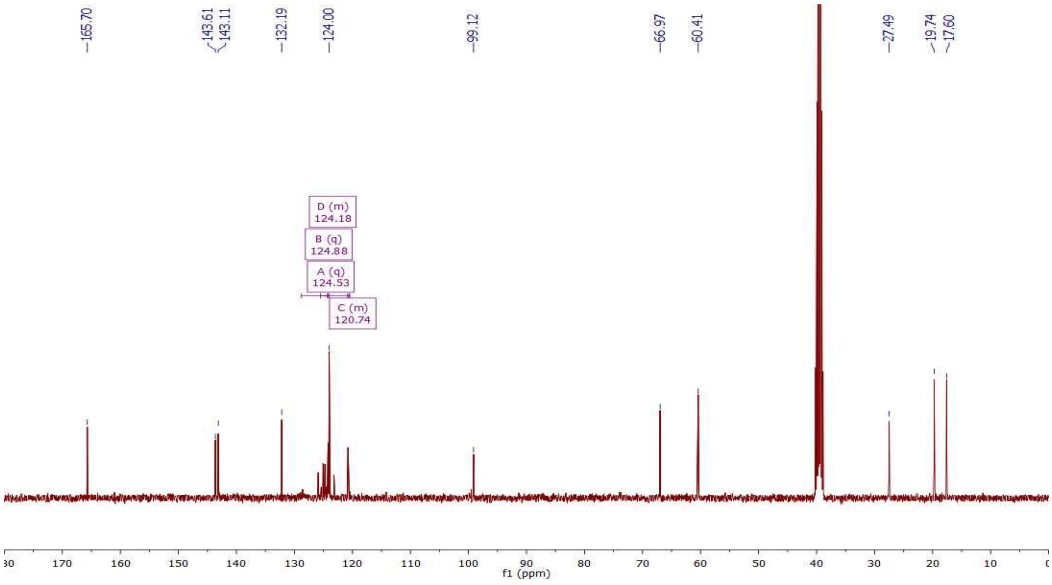

LC-MS (ES + APCI)

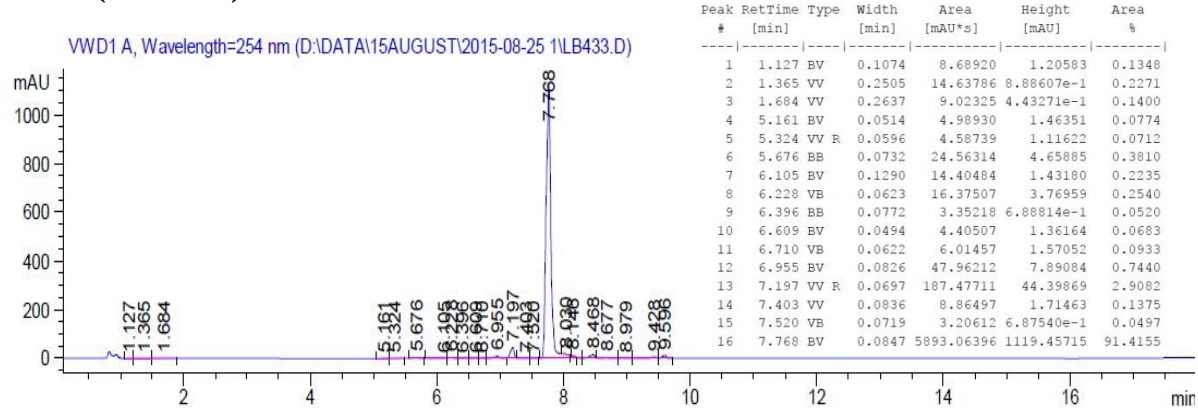

Peak #	RetTime [min]	Type	Width [min]	Area [mAU*s]	Height [mAU]	Area %
1	1.127	BV	0.1074	8.68920	1.20583	0.1348
2	1.365	VV	0.2505	14.63786	8.88607e-1	0.2271
3	1.684	VV	0.2637	9.02325	4.43271e-1	0.1400
4	5.161	BV	0.0514	4.98930	1.46351	0.0774
5	5.324	VV R	0.0596	4.58739	1.11622	0.0712
6	5.676	BB	0.0732	24.56314	4.65885	0.3810
7	6.105	BV	0.1290	14.40484	1.43180	0.2235
8	6.228	VB	0.0623	16.37507	3.76959	0.2540
9	6.396	BB	0.0772	3.35218	6.88814e-1	0.0520
10	6.609	BV	0.0494	4.40507	1.36164	0.0683
11	6.710	VB	0.0622	6.01457	1.57052	0.0933
12	6.955	BV	0.0826	47.96212	7.89084	0.7440
13	7.197	VV R	0.0697	187.47711	44.39869	2.9082
14	7.403	VV	0.0836	8.86497	1.71463	0.1375
15	7.520	VB	0.0719	3.20612	6.87540e-1	0.0497
16	7.768	BV	0.0847	5893.06396	1119.45715	91.4155

(*R*)-2-Benzyl-9-(trifluoromethyl)-2,3-dihydrobenzo[4,5]thieno[3,2-*e*][1,4]oxazepin-5(1*H*)-one (136)

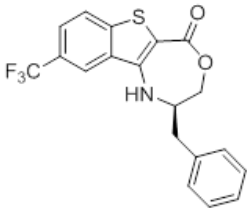

^{1}H NMR spectrum (400 MHz, DMSO)

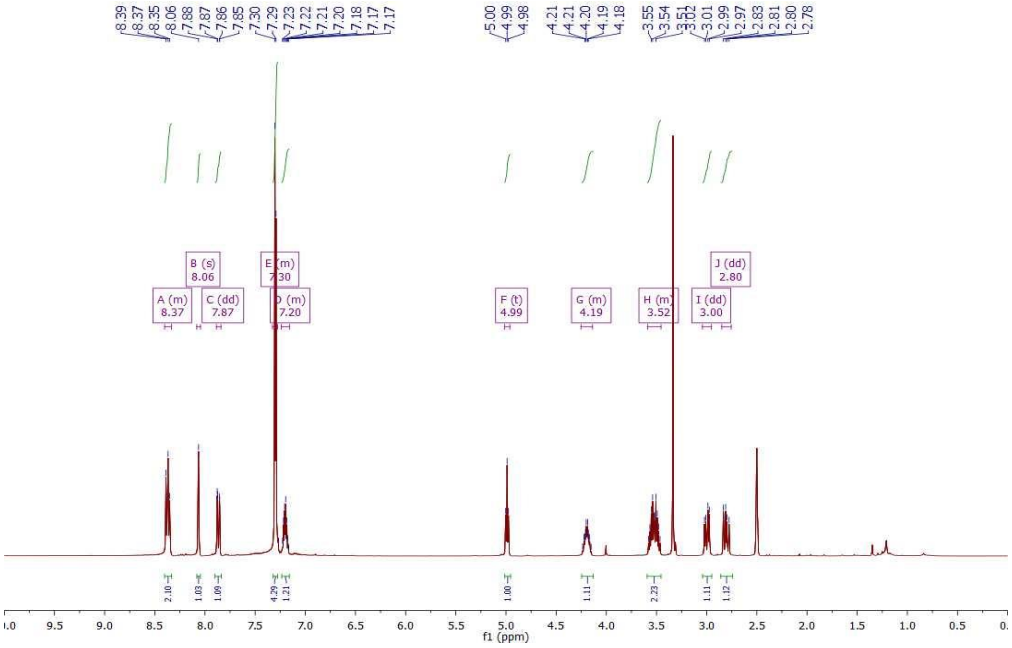

^{13}C NMR spectrum (101 MHz, DMSO)

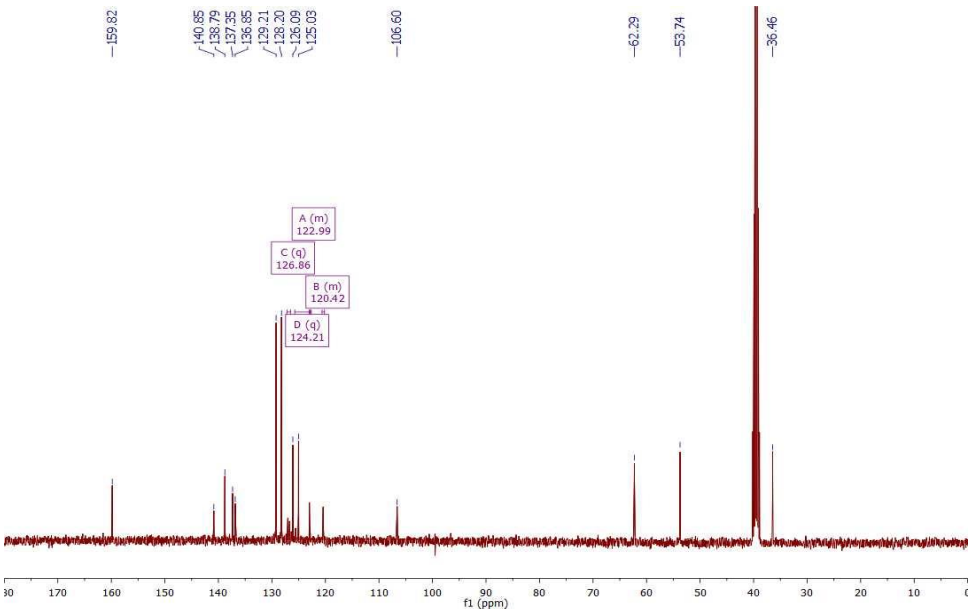

LC-MS (ES + APCI)

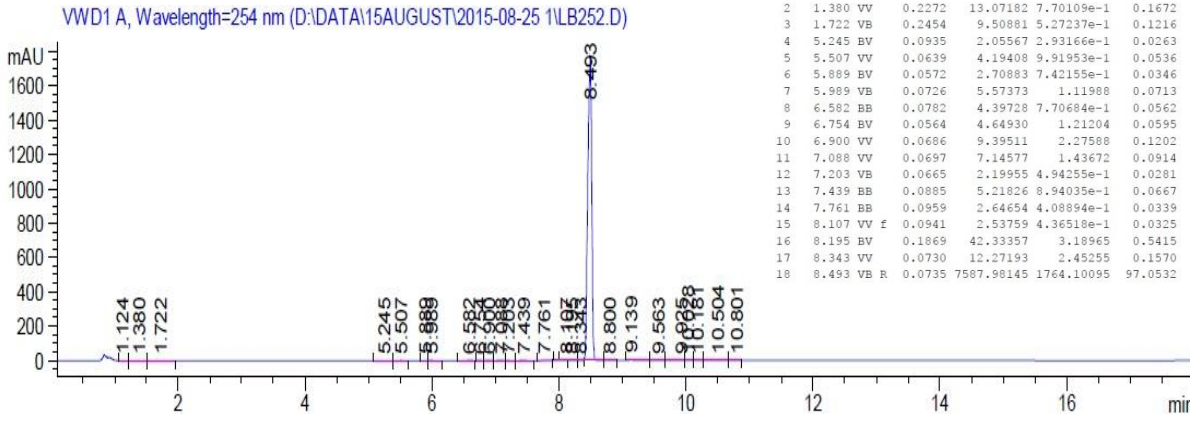

Peak #	RetTime [min]	Type	Width [min]	Area [mAU*s]	Height [mAU]	Area %
1	1.124	BV	0.1007	8.50305	1.15122	0.1088
2	1.380	VV	0.2272	13.07182	7.70109e-1	0.1672
3	1.722	VB	0.2454	9.50881	5.27237e-1	0.1216
4	5.245	BV	0.0935	2.05567	2.93166e-1	0.0263
5	5.507	VV	0.0639	4.19408	9.91953e-1	0.0536
6	5.889	BV	0.0572	2.70883	7.42155e-1	0.0346
7	5.989	VB	0.0726	5.57373	1.11988	0.0713
8	6.582	BB	0.0782	4.39728	7.70684e-1	0.0562
9	6.754	BV	0.0564	4.64930	1.21204	0.0595
10	6.900	VV	0.0686	9.39511	2.27588	0.1202
11	7.088	VV	0.0697	7.14577	1.43672	0.0914
12	7.203	VB	0.0665	2.19955	4.94255e-1	0.0281
13	7.439	BB	0.0885	5.21826	8.94035e-1	0.0667
14	7.761	BB	0.0959	2.64654	4.08894e-1	0.0339
15	8.107	VV f	0.0941	2.53759	4.36518e-1	0.0325
16	8.195	BV	0.1869	42.33357	3.18965	0.5415
17	8.343	VV	0.0730	12.27193	2.45255	0.1570
18	8.493	VB R	0.0735	7587.98145	1764.10095	97.0532

(*S*)-2-Benzyl-9-(trifluoromethyl)-2,3-dihydrobenzo[4,5]thieno[3,2-*e*][1,4]oxazepin-5(1*H*)-one (137)

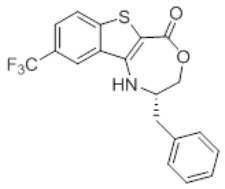

^{1}H NMR spectrum (400 MHz, DMSO)

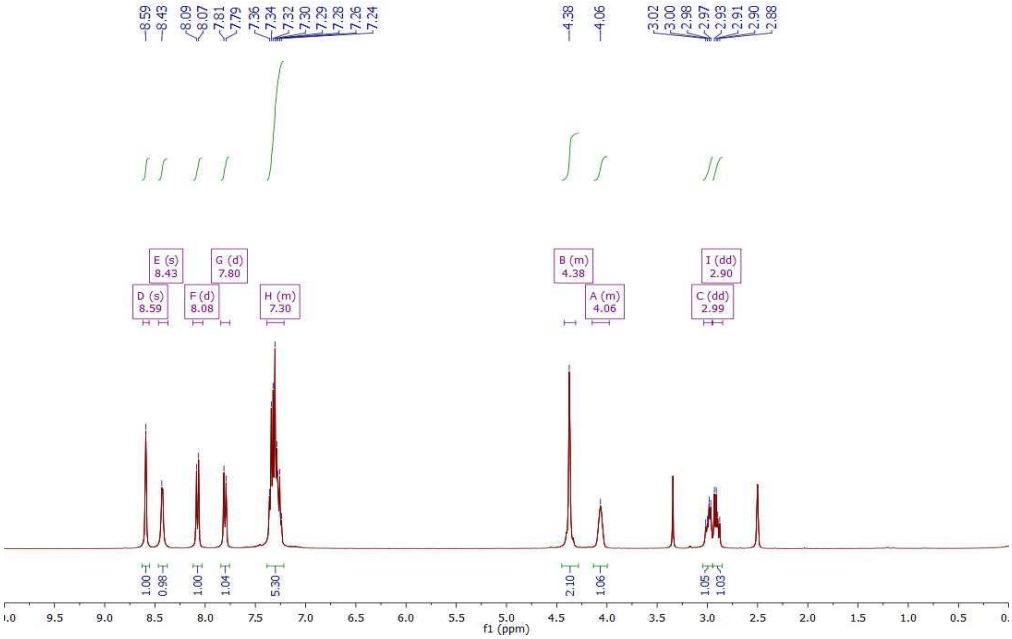

^{13}C NMR spectrum (101 MHz, DMSO)

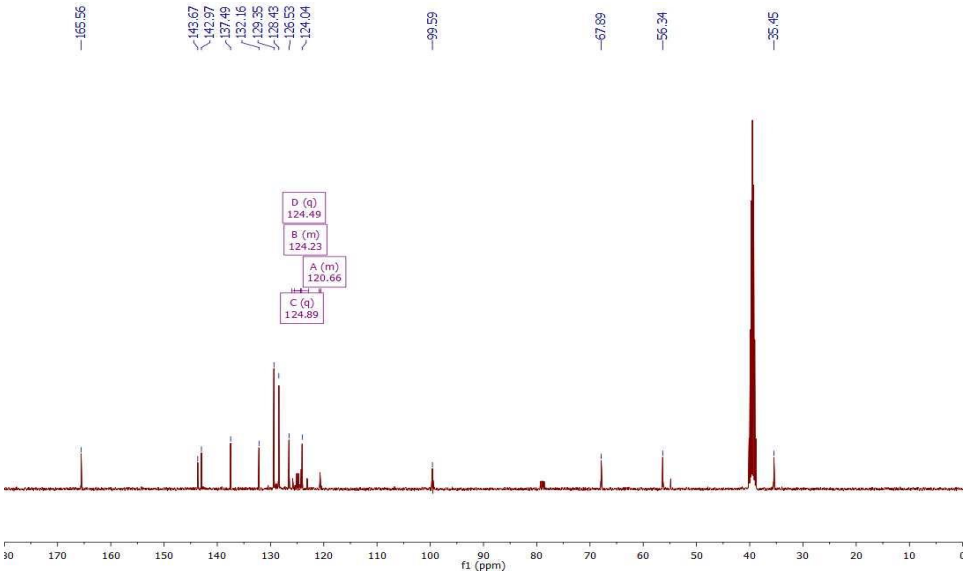

LC-MS (ES + APCI)

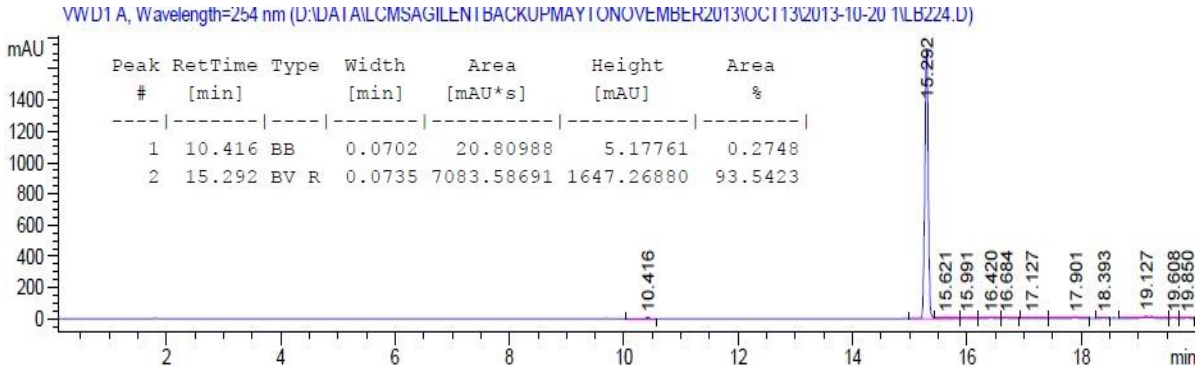

2-Chloro-7,7*a*,8,9,10,11,11*a*,12-octahydro-6*H*-benzo[*b*]benzo[4,5]thieno[3,2-*e*][1,4]diazepin-6-one (149)

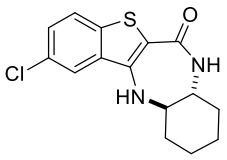

^{1}H NMR spectrum (400 MHz, DMSO)

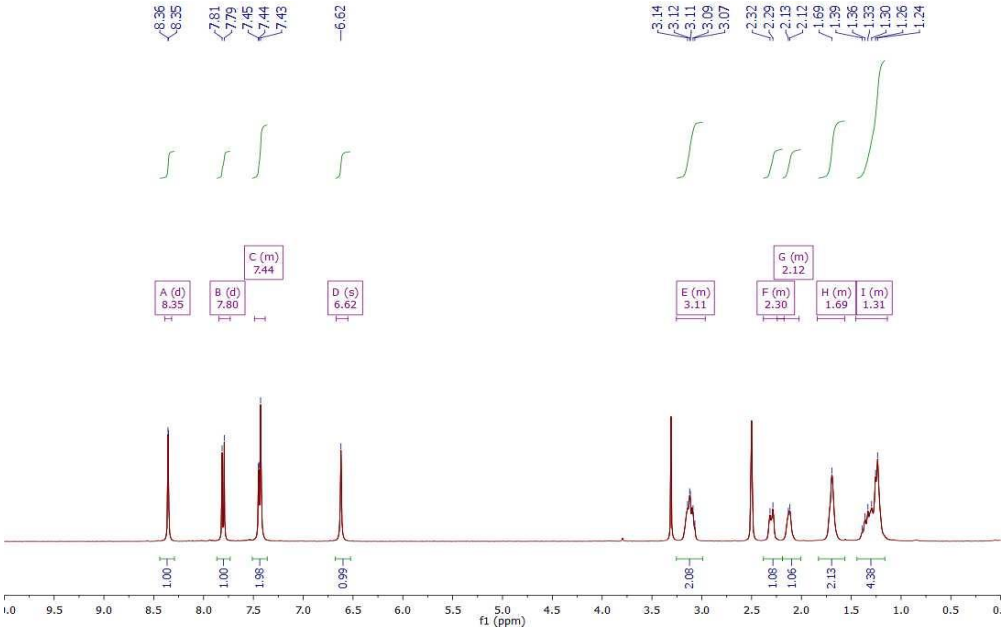

^{13}C NMR spectrum (101 MHz, DMSO)

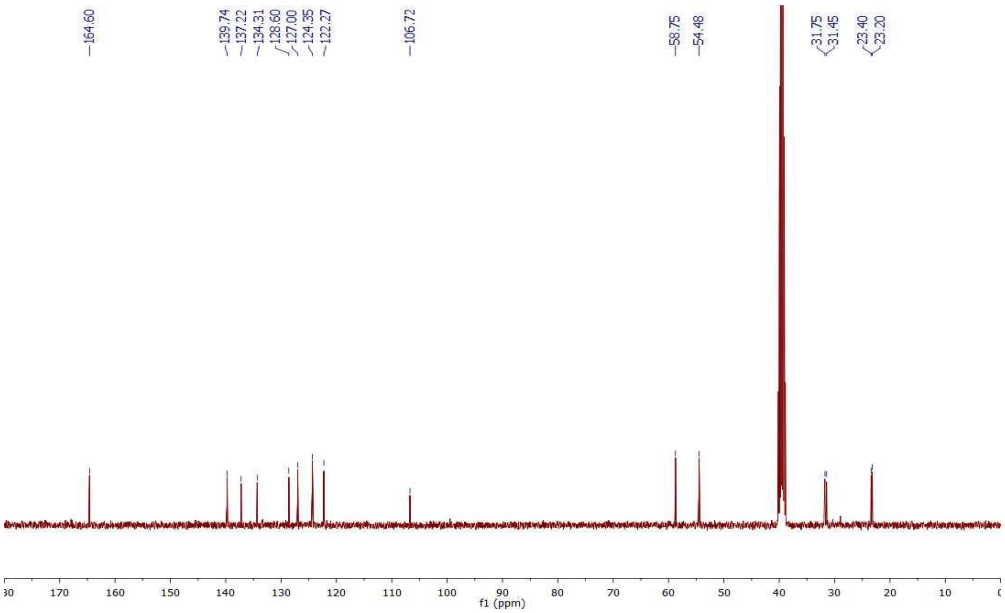

LC-MS (ES + APCI)

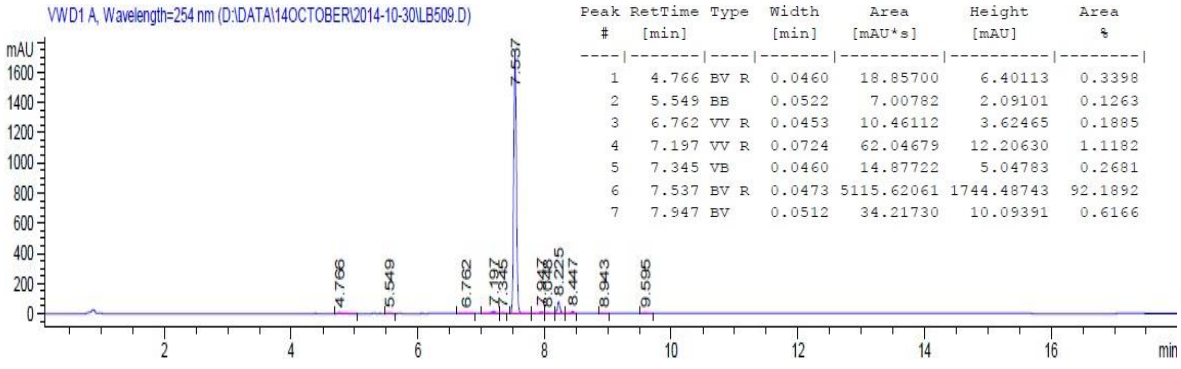

Peak #	RetTime [min]	Type	Width [min]	Area [mAU*s]	Height [mAU]	Area %
1	4.766	BV R	0.0460	18.85700	6.40113	0.3398
2	5.549	BB	0.0522	7.00782	2.09101	0.1263
3	6.762	VV R	0.0453	10.46112	3.62465	0.1885
4	7.197	VV R	0.0724	62.04679	12.20630	1.1182
5	7.345	VB	0.0460	14.87722	5.04783	0.2681
6	7.537	BV R	0.0473	5115.62061	1744.48743	92.1892
7	7.947	BV	0.0512	34.21730	10.09391	0.6166

3-Chloro-7,7*a*,8,9,10,11,11*a*,12-octahydro-6*H*-benzo[*b*]benzo[4,5]thieno[3,2-*e*][1,4]diazepin-6-one (150)

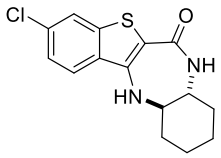

^{1}H NMR spectrum (400 MHz, DMSO)

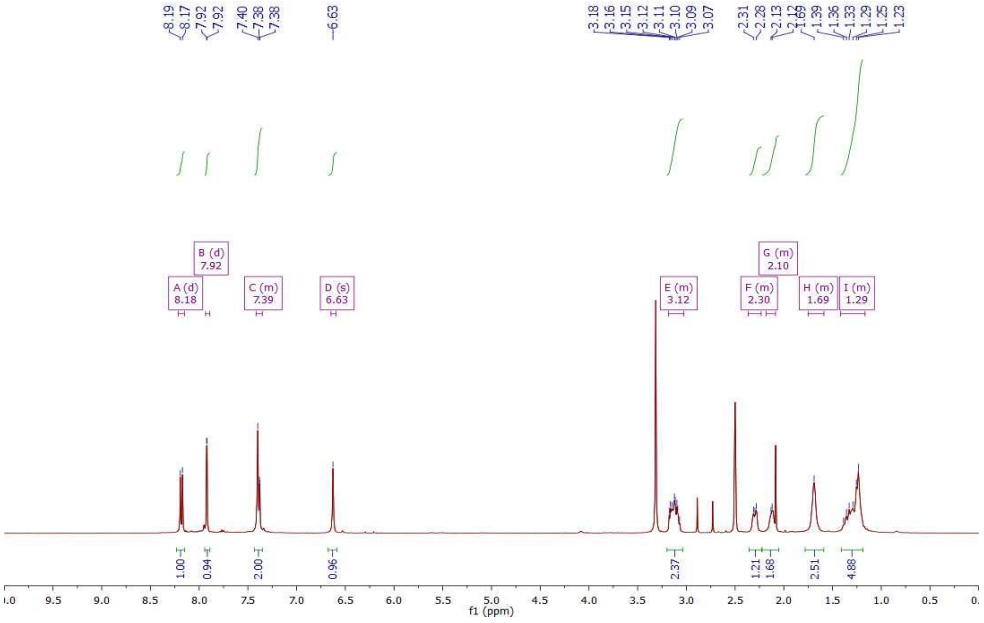

^{13}C NMR spectrum (101 MHz, DMSO)

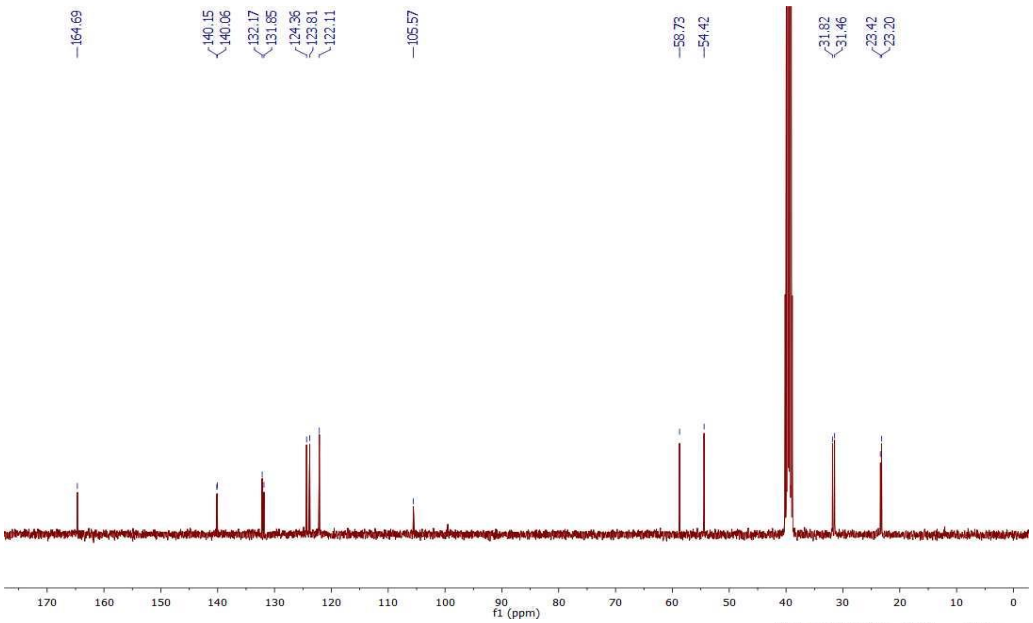

LC-MS (ES + APCI)

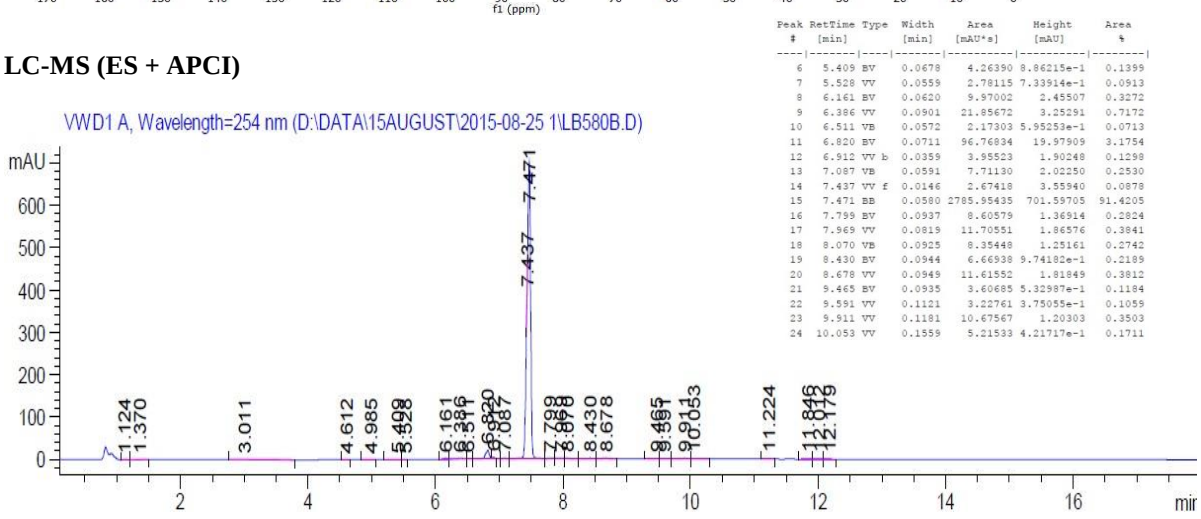

Peak #	RetTime [min]	Type	Width [min]	Area [mAU*s]	Height [mAU]	Area %
6	5.409	BV	0.0678	4.26390	8.86215e-1	0.1399
7	5.528	VV	0.0559	2.78115	7.33914e-1	0.0913
8	6.161	BV	0.0620	9.97002	2.45507	0.3272
9	6.386	VV	0.0901	21.85672	3.25291	0.7172
10	6.511	VB	0.0572	2.17303	5.95253e-1	0.0713
11	6.820	BV	0.0711	96.76834	19.97909	3.1754
12	6.912	VV b	0.0359	3.95523	1.90248	0.1298
13	7.087	VB	0.0591	7.71130	2.02250	0.2530
14	7.437	VV f	0.0146	2.67418	3.55940	0.0878
15	7.471	BB	0.0580	2785.95435	701.59705	91.4205
16	7.799	BV	0.0937	8.60579	1.36914	0.2824
17	7.969	VV	0.0819	11.70551	1.86576	0.3841
18	8.070	VB	0.0925	8.35448	1.25161	0.2742
19	8.430	BV	0.0944	6.66938	9.74182e-1	0.2189
20	8.678	VV	0.0949	11.61552	1.81849	0.3812
21	9.465	BV	0.0935	3.60685	5.32987e-1	0.1184
22	9.591	VV	0.1121	3.22761	3.75055e-1	0.1059
23	9.911	VV	0.1181	10.67567	1.20303	0.3503
24	10.053	VV	0.1559	5.21533	4.21717e-1	0.1711

4-Chloro-7,7*a*,8,9,10,11,11*a*,12-octahydro-6*H*-benzo[*b*]benzo[4,5]thieno[3,2-*e*][1,4]diazepin-6-one (151)

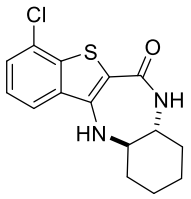

^{1}H NMR spectrum (400 MHz, DMSO)

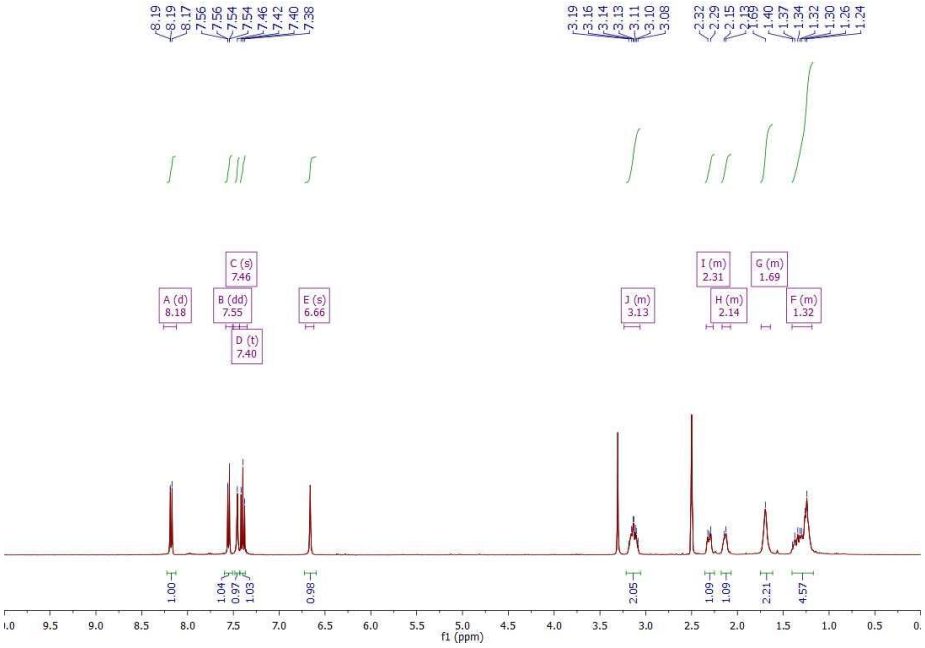

^{13}C NMR spectrum (101 MHz, DMSO)

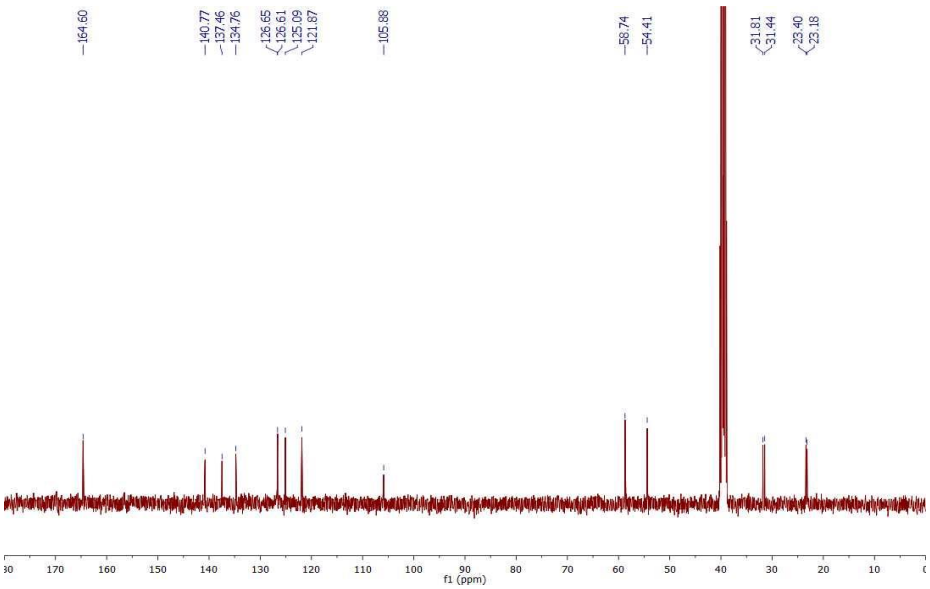

LC-MS (ES + APCI)

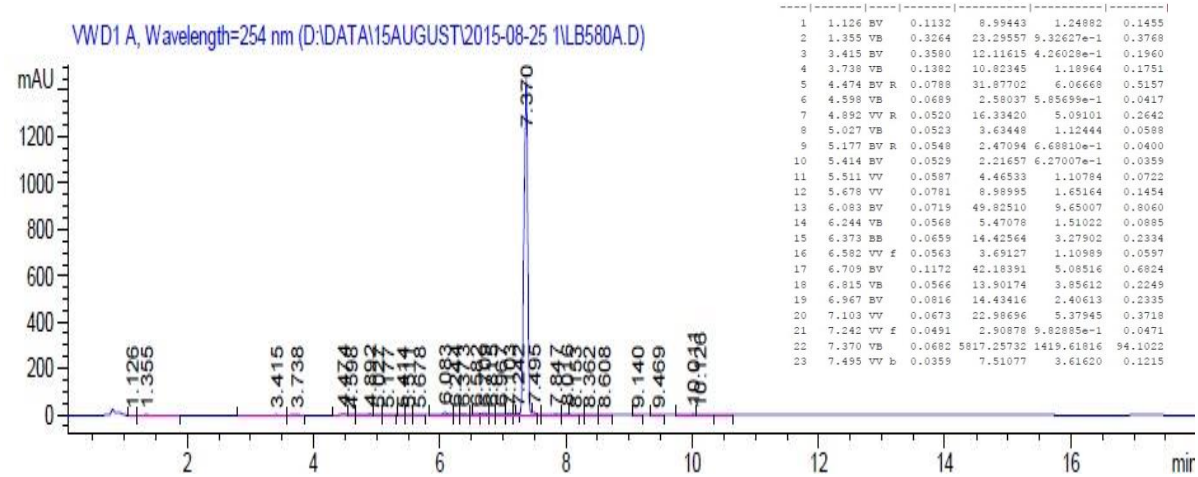

Peak #	RetTime [min]	Type	Width [min]	Area [mAU*s]	Height [mAU]	Area %
1	1.126	BV	0.1132	8.99443	1.24882	0.1455
2	1.355	VB	0.3264	23.29557	9.32627e-1	0.3768
3	3.415	BV	0.3580	12.11615	4.26028e-1	0.1960
4	3.738	VB	0.1382	10.82345	1.18964	0.1751
5	4.474	BV R	0.0788	31.87702	6.06668	0.5157
6	4.598	VB	0.0689	2.58037	5.85699e-1	0.0417
7	4.892	VV R	0.0520	16.33420	5.09101	0.2642
8	5.027	VB	0.0523	3.63448	1.12444	0.0588
9	5.177	BV R	0.0548	2.47094	6.68810e-1	0.0400
10	5.414	BV	0.0529	2.21657	6.27007e-1	0.0359
11	5.511	VV	0.0587	4.46533	1.10784	0.0722
12	5.678	VV	0.0781	8.98995	1.65164	0.1454
13	6.083	BV	0.0719	49.82510	9.65007	0.8060
14	6.244	VB	0.0568	5.47078	1.51022	0.0885
15	6.373	BB	0.0659	14.42564	3.27902	0.2334
16	6.582	VV f	0.0563	3.69127	1.10989	0.0597
17	6.709	BV	0.1172	42.18391	5.08516	0.6824
18	6.815	VB	0.0566	13.90174	3.85612	0.2249
19	6.967	BV	0.0816	14.43416	2.40613	0.2335
20	7.103	VV	0.0673	22.98696	5.37945	0.3718
21	7.242	VV f	0.0491	2.90878	9.82885e-1	0.0471
22	7.370	VB	0.0682	5817.25732	1419.61816	94.1022
23	7.495	VV b	0.0359	7.51077	3.61620	0.1215

4-Bromo-7,7*a*,8,9,10,11,11*a*,12-octahydro-6*H*-benzo[*b*]benzo[4,5]thieno[3,2-*e*][1,4]diazepin-6-one (163)

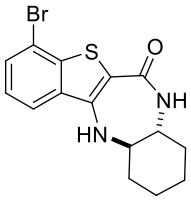

^{1}H NMR spectrum (400 MHz, DMSO)

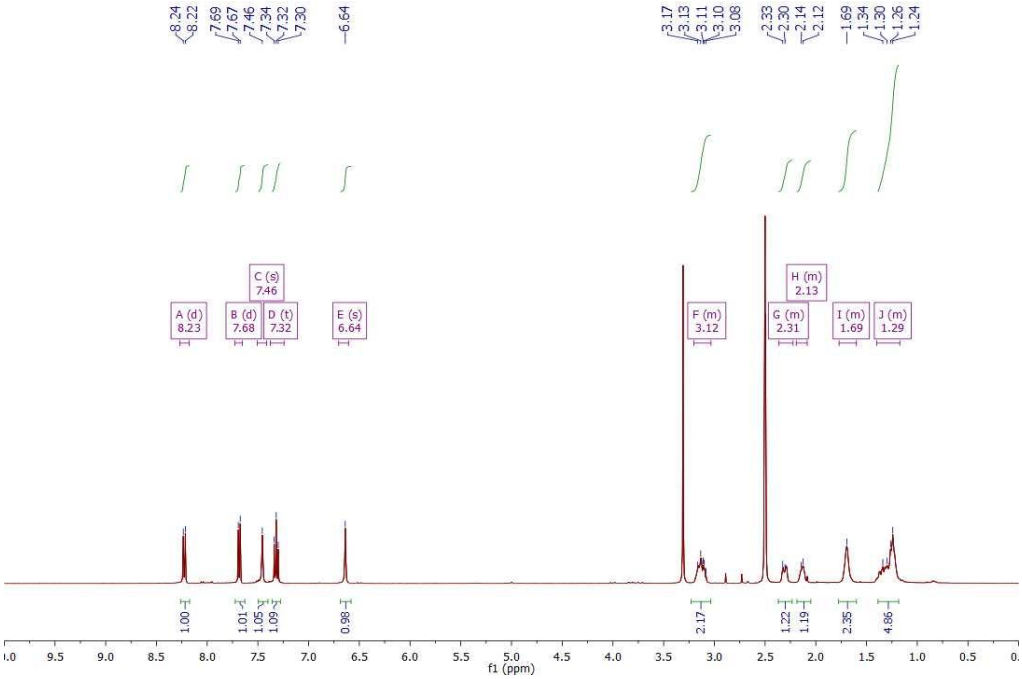

^{13}C NMR spectrum (101 MHz, DMSO)

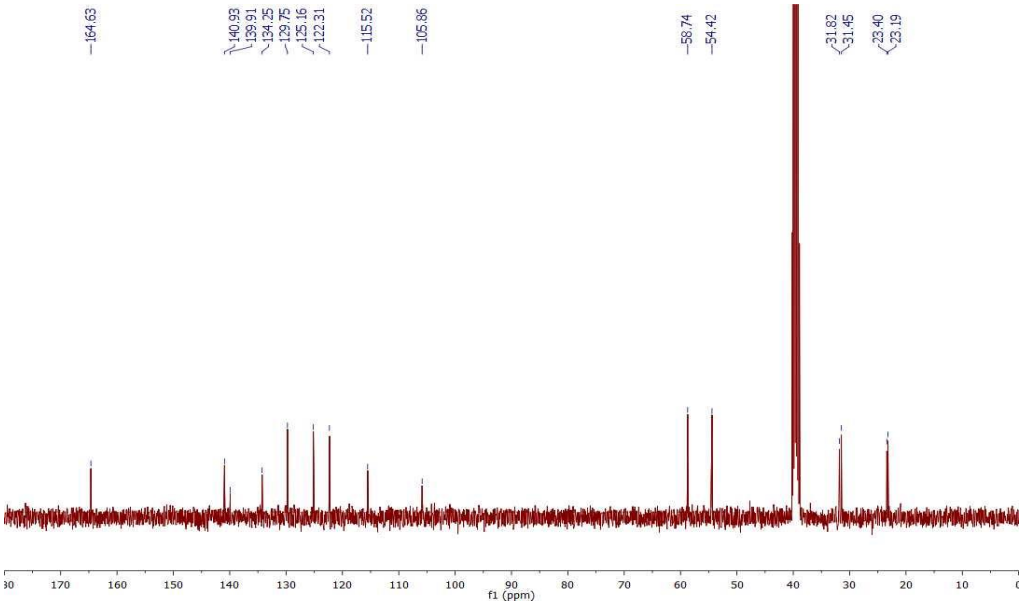

LC-MS (ES + APCI)

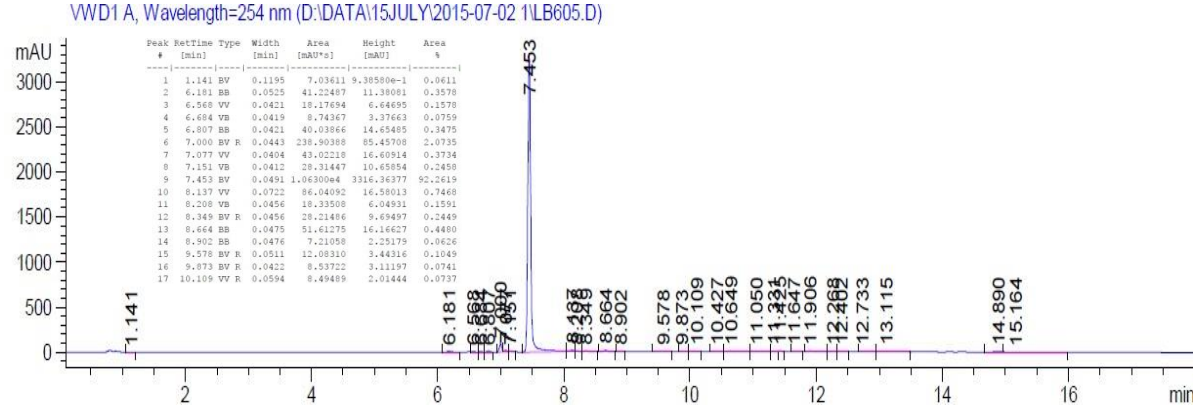

2-Nitro-7,7*a*,8,9,10,11,11*a*,12-octahydro-6*H*-benzo[*b*]benzo[4,5]thieno[3,2-*e*][1,4]diazepin-6-one (156)

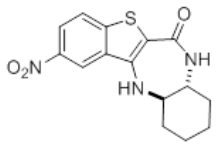

^{1}H NMR spectrum (400 MHz, DMSO)

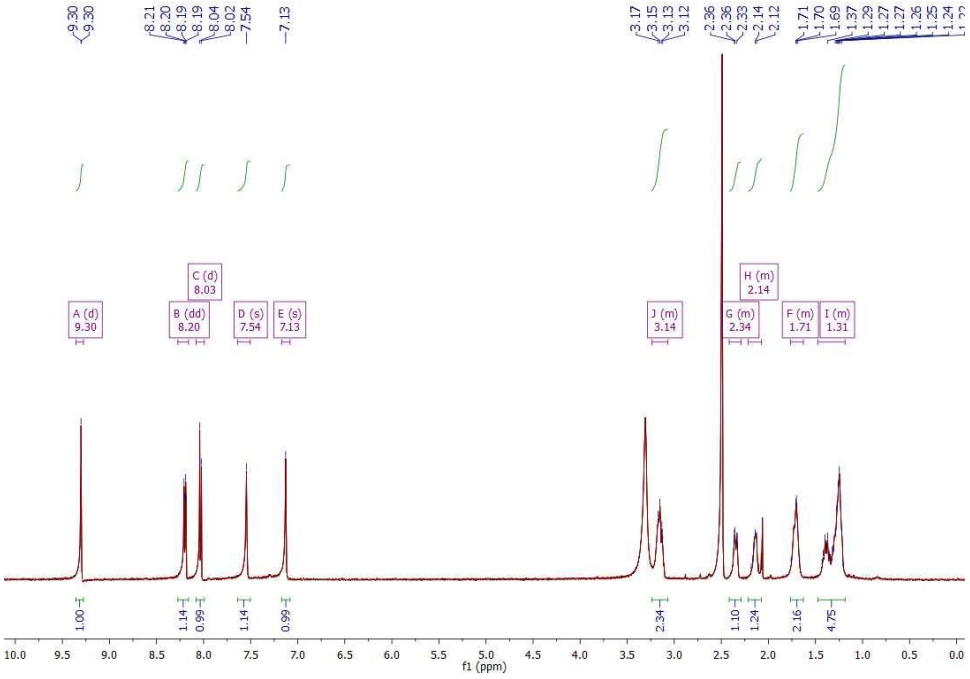

^{13}C NMR spectrum (101 MHz, DMSO)

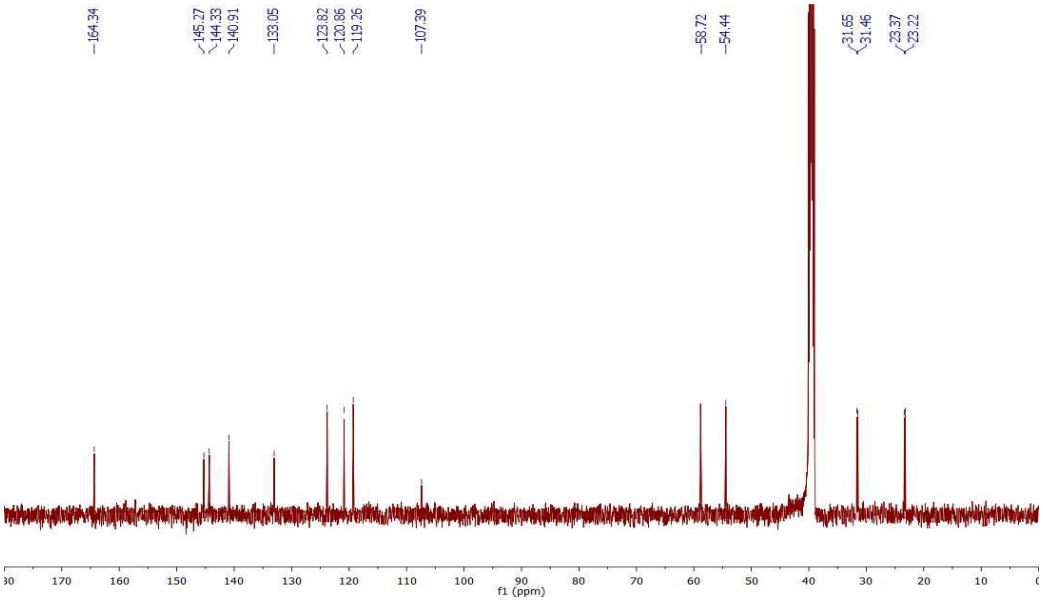

LC-MS (ES + APCI)

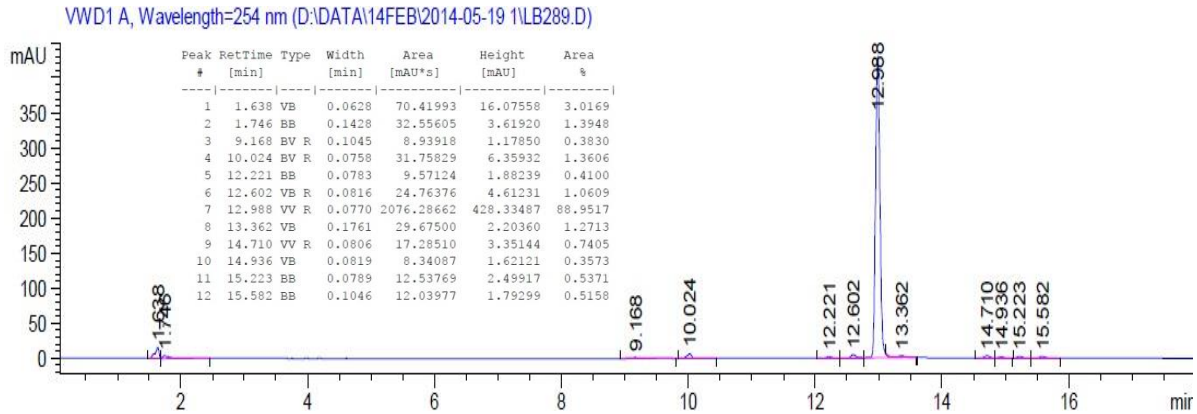

Peak #	RetTime [min]	Type	Width [min]	Area [mAU*s]	Height [mAU]	Area %
1	1.638	VB	0.0628	70.41993	16.07558	3.0169
2	1.746	BB	0.1428	32.55605	3.61920	1.3948
3	9.168	BV R	0.1045	8.93918	1.17850	0.3830
4	10.024	BV R	0.0758	31.75829	6.35932	1.3606
5	12.221	BB	0.0783	9.57124	1.88239	0.4100
6	12.602	VB R	0.0816	24.76376	4.61231	1.0609
7	12.988	VV R	0.0770	2076.28662	428.33487	88.9517
8	13.362	VB	0.1761	29.67500	2.20360	1.2713
9	14.710	VV R	0.0806	17.28510	3.35144	0.7405
10	14.936	VB	0.0819	8.34087	1.62121	0.3573
11	15.223	BB	0.0789	12.53769	2.49917	0.5371
12	15.582	BB	0.1046	12.03977	1.79299	0.5158

3-Nitro-7,7*a*,8,9,10,11,11*a*,12-octahydro-6*H*-benzo[*b*]benzo[4,5]thieno[3,2-*e*][1,4]diazepin-6-one (157)

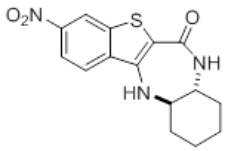

^{1}H NMR spectrum (400 MHz, DMSO)

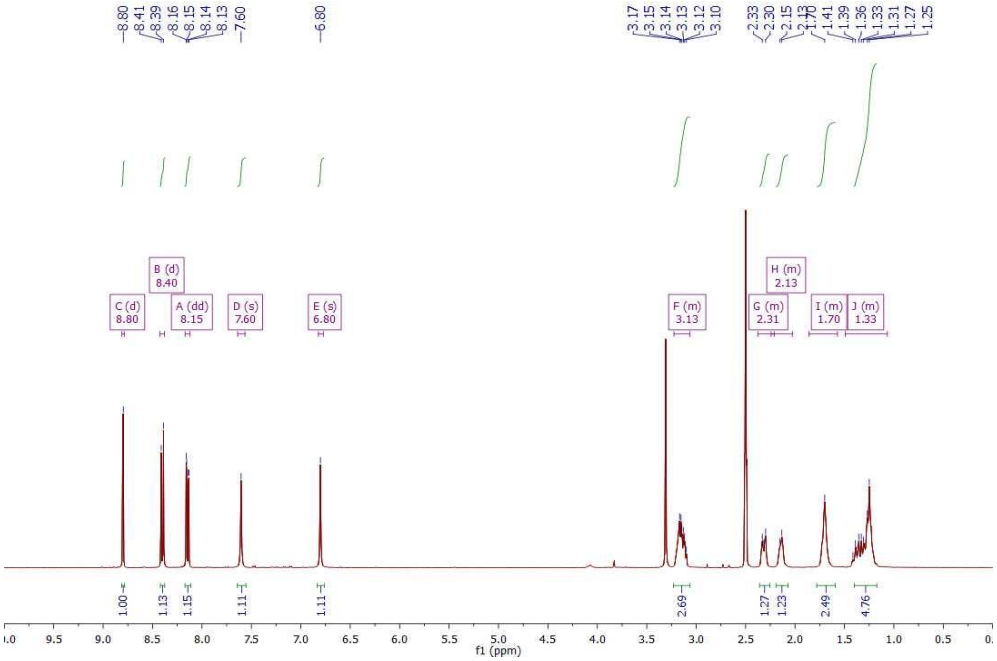

^{13}C NMR spectrum (101 MHz, DMSO)

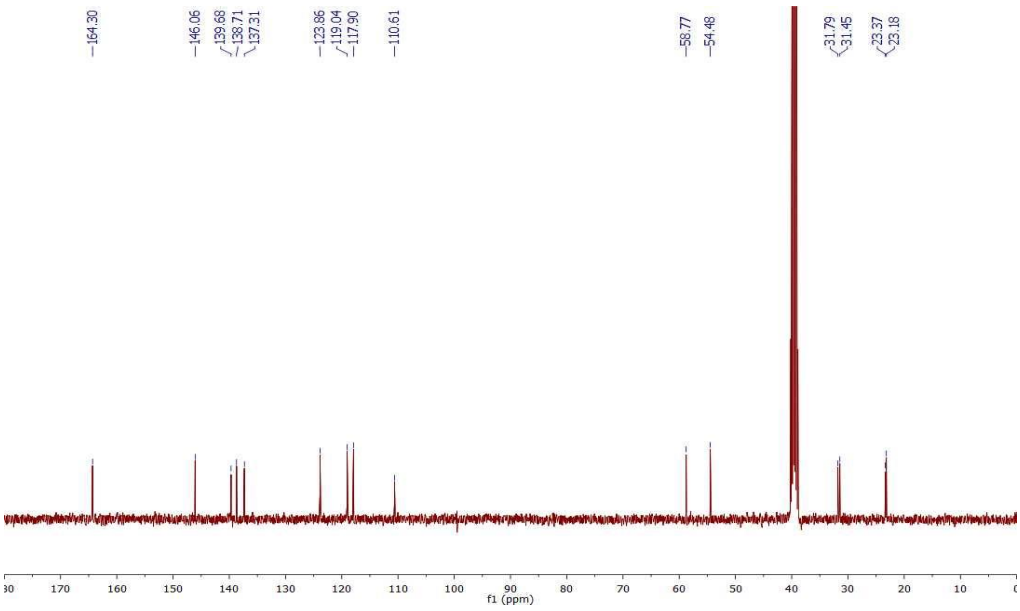

LC-MS (ES + APCI)

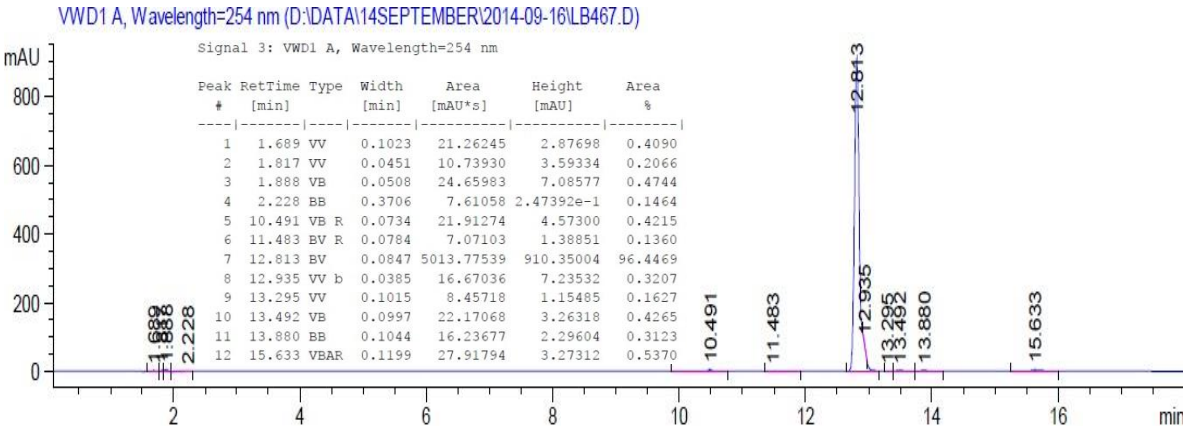

2-Amino-7,7a,8,9,10,11,11a,12-octahydro-6*H*-benzo[*b*]benzo[4,5]thieno[3,2-*e*][1,4]diazepin-6-one (158)

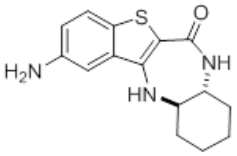

^{1}H NMR spectrum (400 MHz, DMSO)

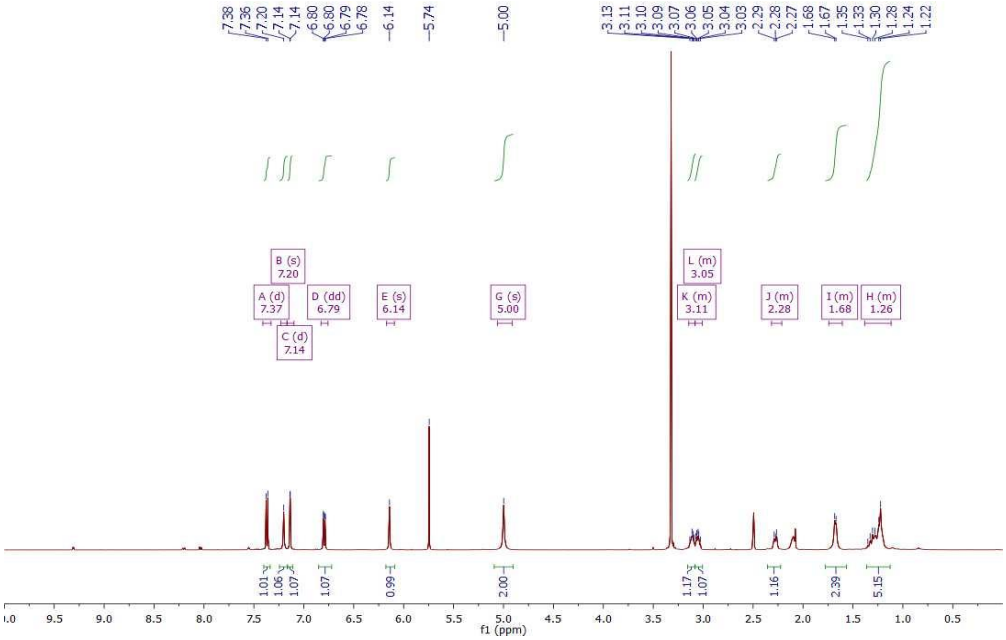

^{13}C NMR spectrum (101 MHz, DMSO)

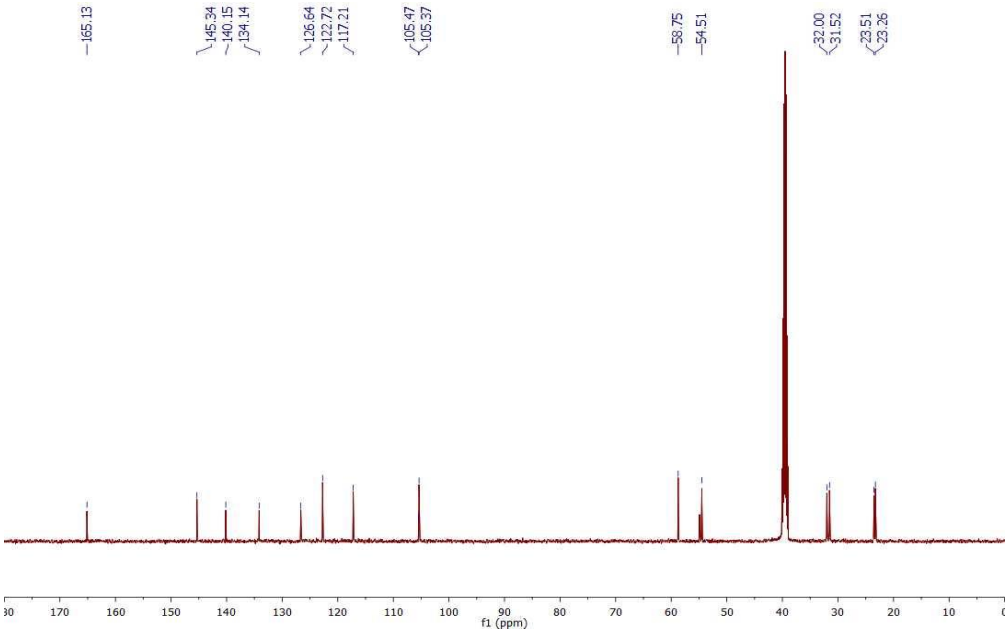

LC-MS (ES + APCI)

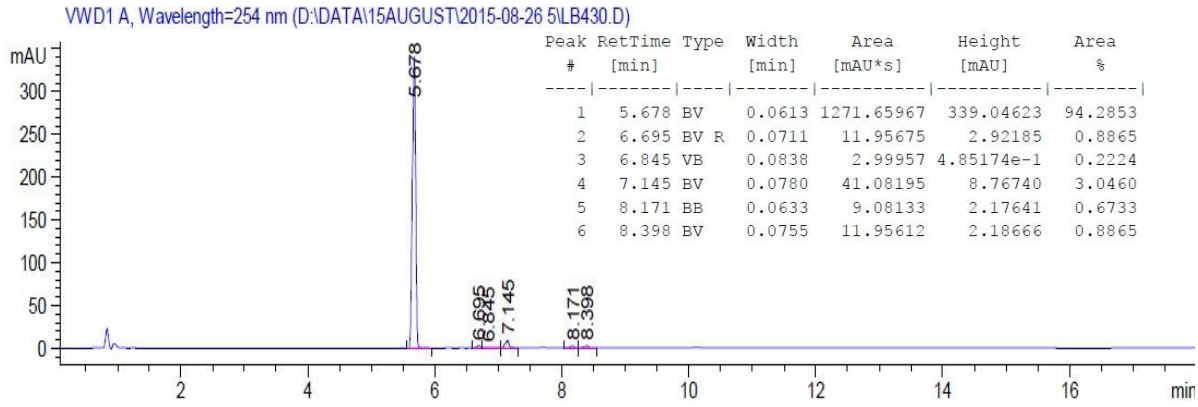

Peak #	RetTime [min]	Type	Width [min]	Area [mAU*s]	Height [mAU]	Area %
1	5.678	BV	0.0613	1271.65967	339.04623	94.2853
2	6.695	BV R	0.0711	11.95675	2.92185	0.8865
3	6.845	VB	0.0838	2.99957	4.85174e-1	0.2224
4	7.145	BV	0.0780	41.08195	8.76740	3.0460
5	8.171	BB	0.0633	9.08133	2.17641	0.6733
6	8.398	BV	0.0755	11.95612	2.18666	0.8865

3-Amino-7,7a,8,9,10,11,11a,12-octahydro-6*H*-benzo[*b*]benzo[4,5]thieno[3,2-*e*][1,4]diazepin-6-one (159)

^{1}H NMR spectrum (400 MHz, DMSO)

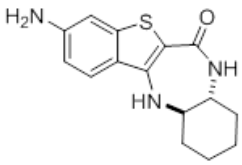

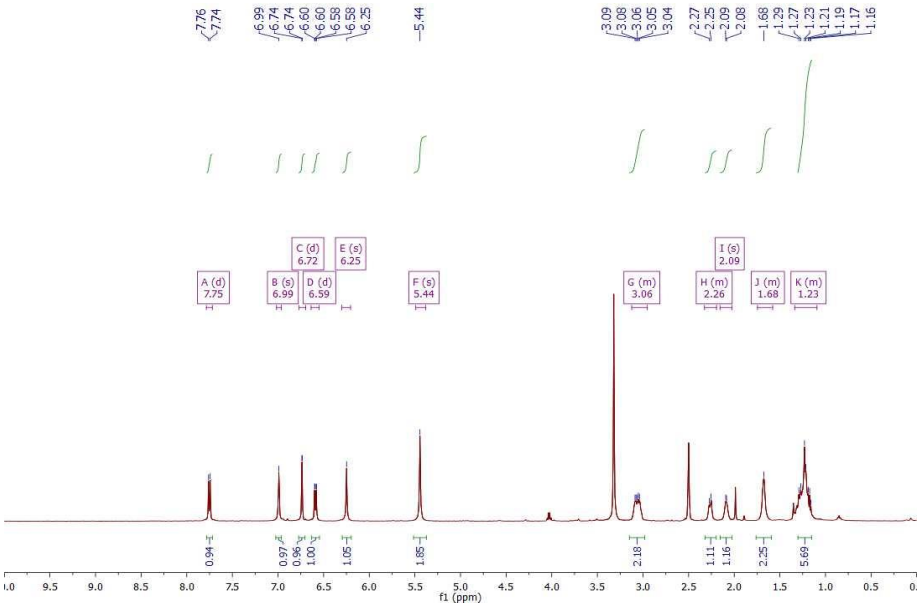

^{13}C NMR spectrum (101 MHz, DMSO)

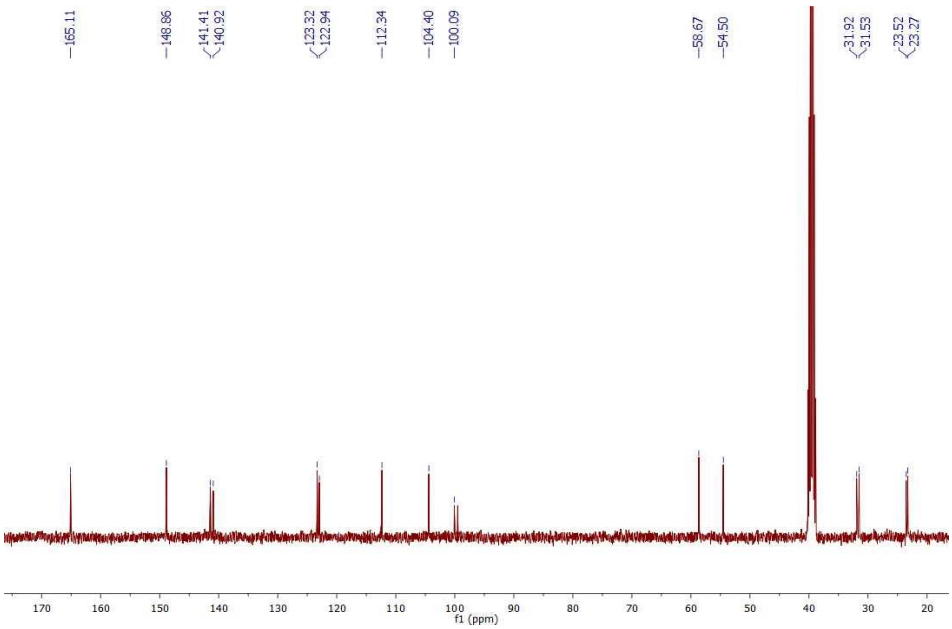

LC-MS (ES + APCI)

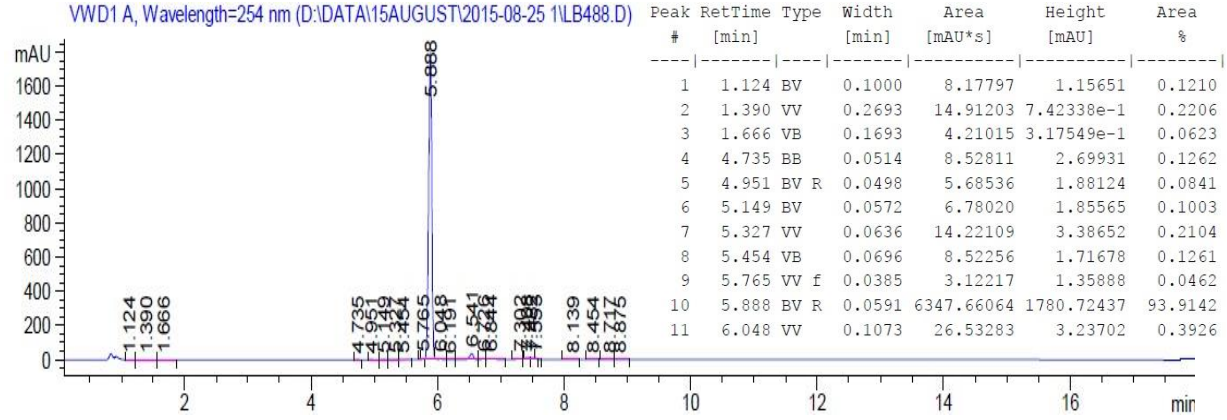

Peak #	RetTime [min]	Type	Width [min]	Area [mAU*s]	Height [mAU]	Area %
1	1.124	BV	0.1000	8.17797	1.15651	0.1210
2	1.390	VV	0.2693	14.91203	7.42338e-1	0.2206
3	1.666	VB	0.1693	4.21015	3.17549e-1	0.0623
4	4.735	BB	0.0514	8.52811	2.69931	0.1262
5	4.951	BV R	0.0498	5.68536	1.88124	0.0841
6	5.149	BV	0.0572	6.78020	1.85565	0.1003
7	5.327	VV	0.0636	14.22109	3.38652	0.2104
8	5.454	VB	0.0696	8.52256	1.71678	0.1261
9	5.765	VV f	0.0385	3.12217	1.35888	0.0462
10	5.888	BV R	0.0591	6347.66064	1780.72437	93.9142
11	6.048	VV	0.1073	26.53283	3.23702	0.3926

***N*-(6-oxo-7,7a,8,9,10,11,11*a*,12-Octahydro-6*H*-benzo[*b*]benzo[4,5]thieno[3,2-*e*][1,4]diazepin-2-yl)acetamide (161)**

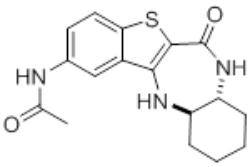

^{1}H NMR spectrum (400 MHz, DMSO)

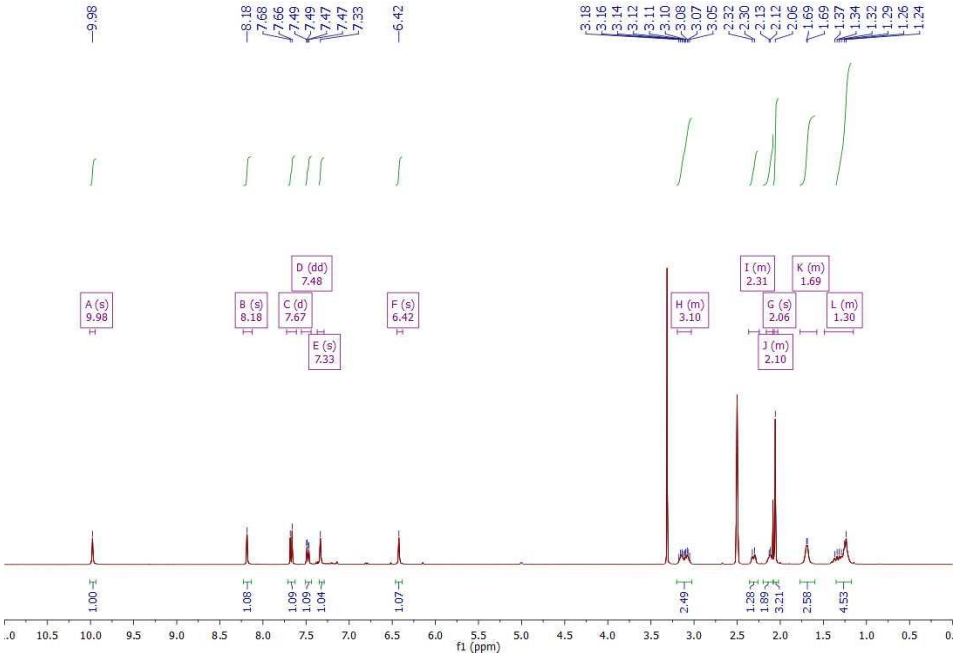

^{13}C NMR spectrum (101 MHz, DMSO)

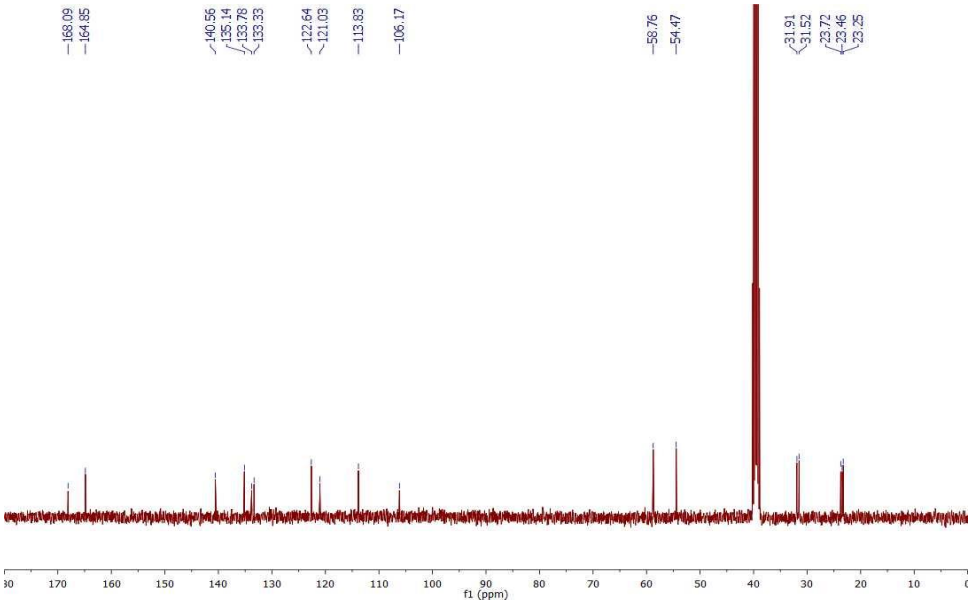

LC-MS (ES + APCI)

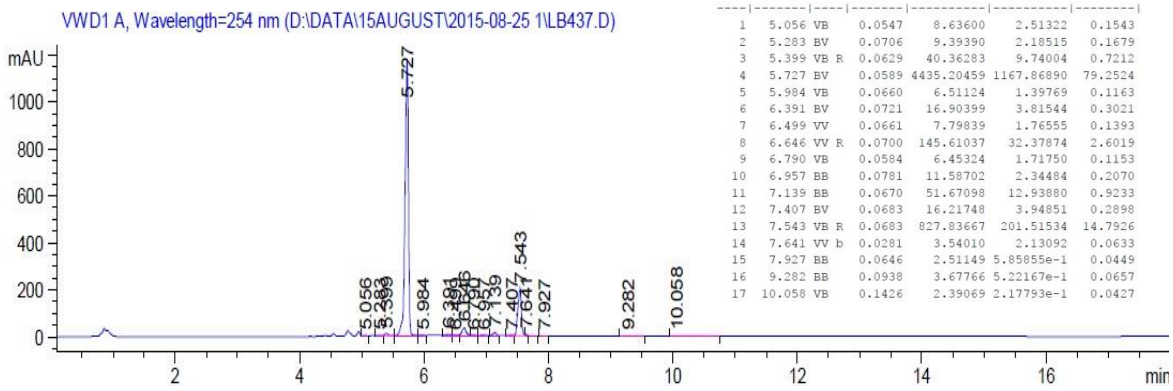

Peak #	RetTime [min]	Type	Width [min]	Area [mAU*s]	Height [mAU]	Area %
1	5.056	VB	0.0547	8.63600	2.51322	0.1543
2	5.283	BV	0.0706	9.39390	2.18515	0.1679
3	5.399	VB R	0.0629	40.36283	9.74004	0.7212
4	5.727	BV	0.0589	4435.20459	1167.86890	79.2524
5	5.984	VB	0.0660	6.51124	1.39769	0.1163
6	6.391	BV	0.0721	16.90399	3.81544	0.3021
7	6.499	VV	0.0661	7.79839	1.76555	0.1393
8	6.646	VV R	0.0700	145.61037	32.37874	2.6019
9	6.790	VB	0.0584	6.45324	1.71750	0.1153
10	6.957	BB	0.0781	11.58702	2.34484	0.2070
11	7.139	BB	0.0670	51.67098	12.93880	0.9233
12	7.407	BV	0.0683	16.21748	3.94851	0.2898
13	7.543	VB R	0.0683	827.83667	201.51534	14.7926
14	7.641	VV b	0.0281	3.54010	2.13092	0.0633
15	7.927	BB	0.0646	2.51149	5.85855e-1	0.0449
16	9.282	BB	0.0938	3.67766	5.22167e-1	0.0657
17	10.058	VB	0.1426	2.39069	2.17793e-1	0.0427

3-Methyl-*N*-(6-oxo-7,7a,8,9,10,11,11a,12-octahydro-6*H*-benzo[*b*]benzo[4,5]thieno[3,2-*e*][1,4]diazepin-2-yl)butanamide (162)

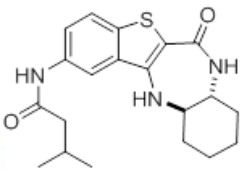

^{1}H NMR spectrum (400 MHz, DMSO)

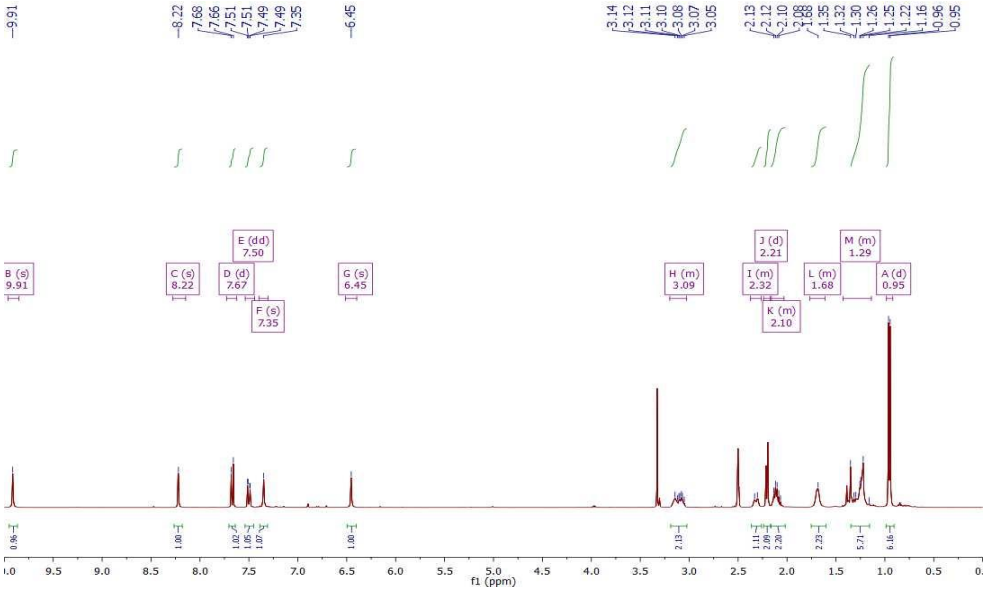

^{13}C NMR spectrum (101 MHz, DMSO)

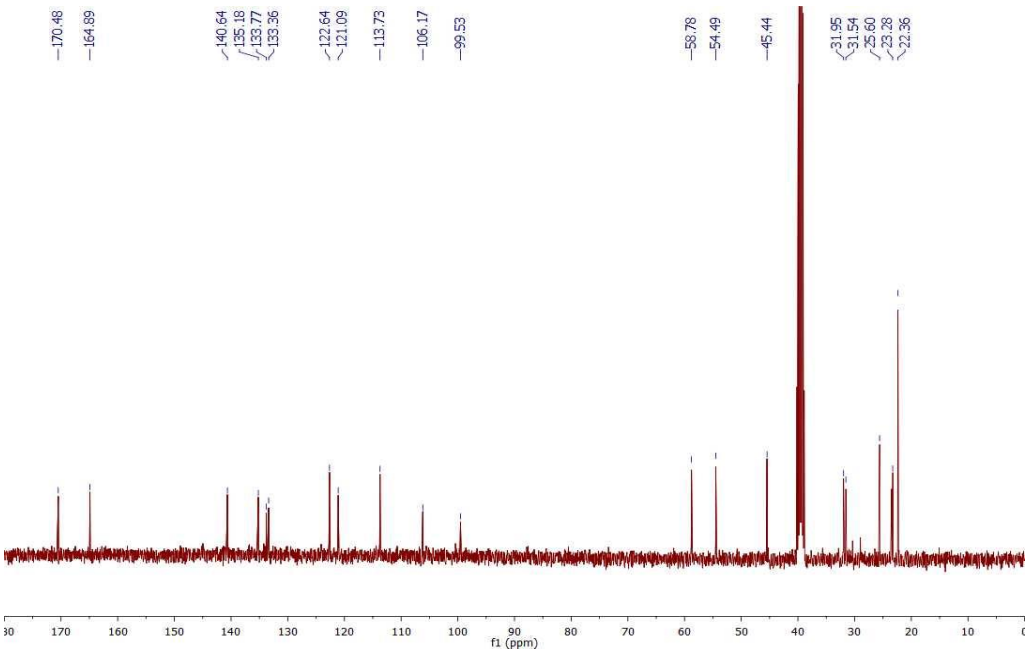

LC-MS (ES + APCI)

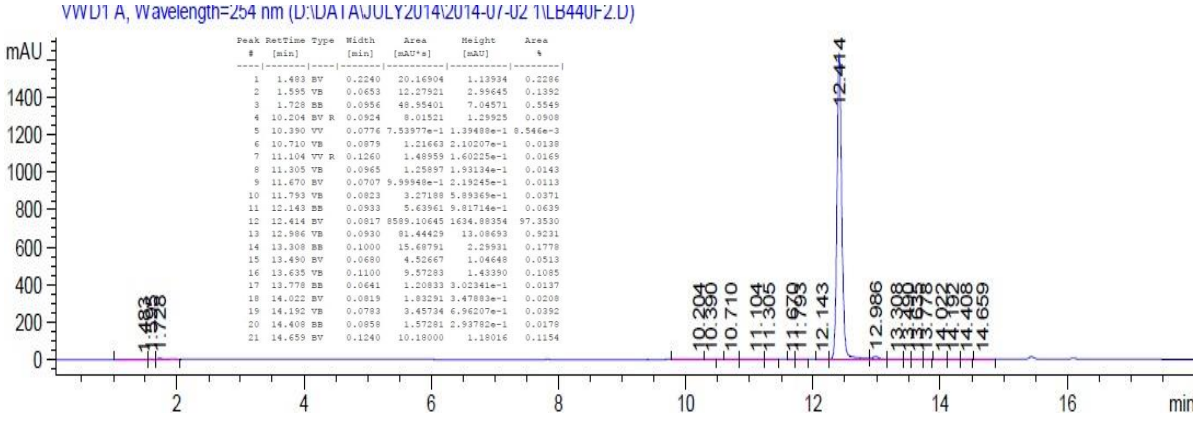

Peak #	RetTime [min]	Type	Width [min]	Area [mAU*s]	Height [mAU]	Area %
1	1.493	BV	0.2240	20.16904	1.13934	0.2286
2	1.595	VB	0.0653	12.27521	2.59645	0.1392
3	1.728	BB	0.0956	48.55401	7.04571	0.5549
4	10.204	BV R	0.0924	8.01521	1.29925	0.0908
5	10.390	VV	0.0776	7.53977e-1	1.39488e-1	8.546e-3
6	10.710	VB	0.0879	1.21663	2.10207e-1	0.0138
7	11.104	VV R	0.1260	1.48959	1.60225e-1	0.0169
8	11.305	VB	0.0965	1.25897	1.93134e-1	0.0143
9	11.670	BV	0.0707	9.99948e-1	2.19245e-1	0.0113
10	11.793	VB	0.0823	3.27188	5.89369e-1	0.0371
11	12.143	BB	0.0933	5.63961	9.81714e-1	0.0639
12	12.414	BV	0.0817	8589.10645	1634.88354	97.3530
13	12.986	VB	0.0930	81.44429	13.08693	0.9231
14	13.308	BB	0.1000	15.68791	2.25931	0.1778
15	13.490	BV	0.0680	4.52667	1.04648	0.0513
16	13.635	VB	0.1100	9.57283	1.43390	0.1085
17	13.778	BB	0.0641	1.20833	3.02341e-1	0.0137
18	14.022	BV	0.0819	1.83291	3.47883e-1	0.0208
19	14.192	VB	0.0783	3.45734	6.96207e-1	0.0392
20	14.408	BB	0.0858	1.57281	2.93782e-1	0.0178
21	14.659	BV	0.1240	10.18000	1.18016	0.1154

3-(Trifluoromethyl)-7,7*a*,8,9,10,11,11*a*,12-octahydro-6*H*-benzo[*b*]benzo[4,5]thieno[3,2-*e*][1,4]diazepin-6-one (164)

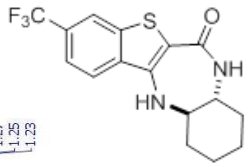

^{1}H NMR spectrum (400 MHz, DMSO)

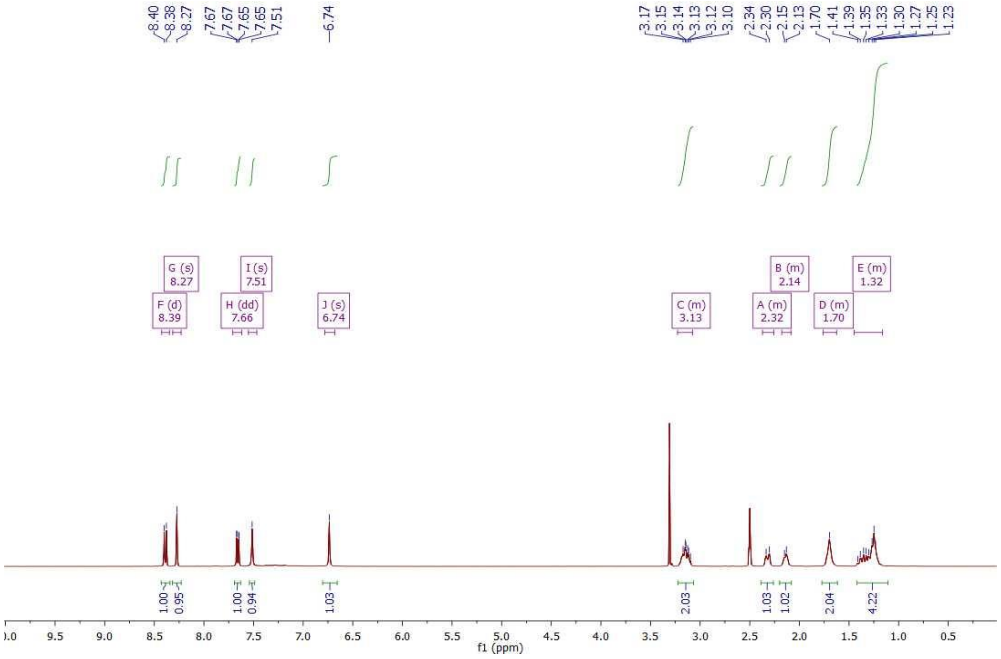

^{13}C NMR spectrum (101 MHz, DMSO)

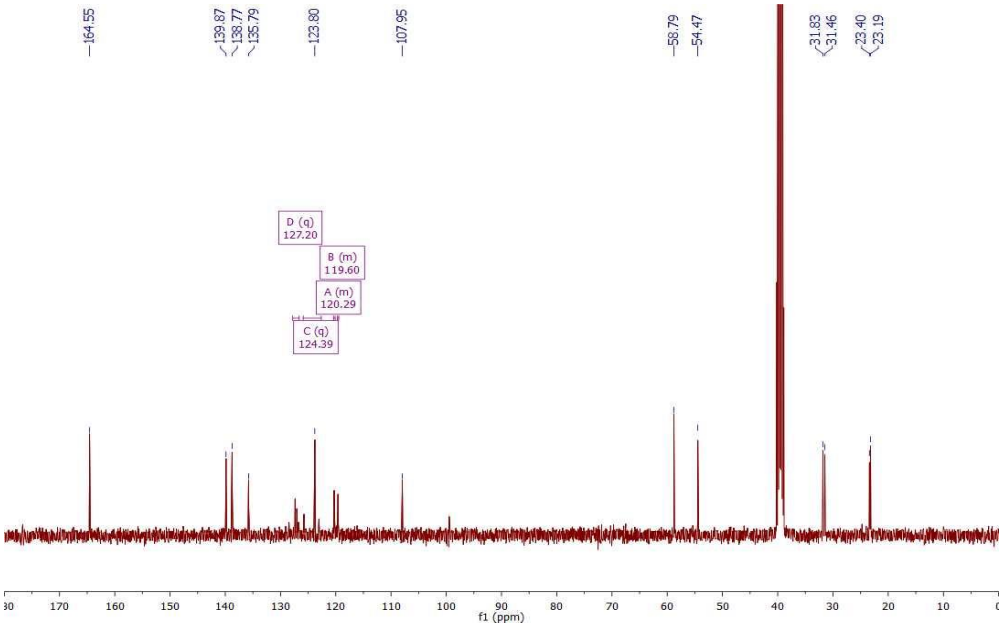

LC-MS (ES + APCI)

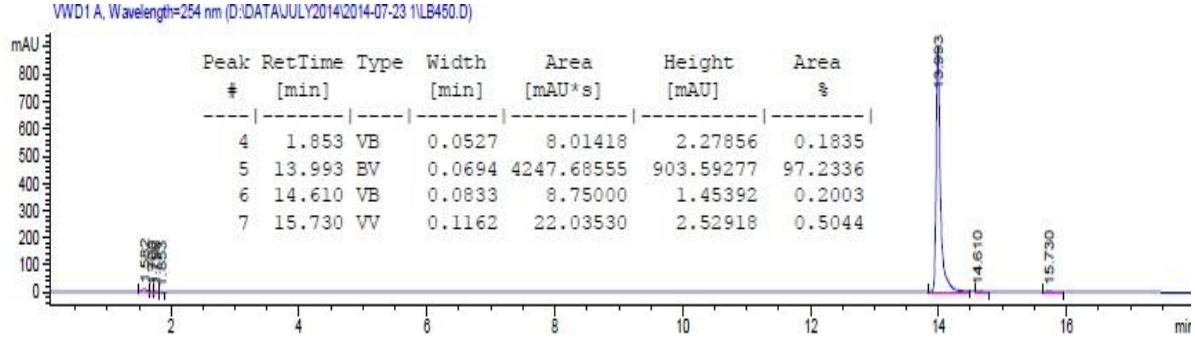

Peak #	RetTime [min]	Type	Width [min]	Area [mAU*s]	Height [mAU]	Area %
4	1.853	VB	0.0527	8.01418	2.27856	0.1835
5	13.993	BV	0.0694	4247.68555	903.59277	97.2336
6	14.610	VB	0.0833	8.75000	1.45392	0.2003
7	15.730	VV	0.1162	22.03530	2.52918	0.5044

3,3-Dimethyl-*N*-(6-oxo-7,7*a*,8,9,10,11,11*a*,12-octahydro-6*H*-benzo[*b*]benzo[4,5]thieno[3,2-*e*][1,4]diazepin-2-yl)butanamide (165)

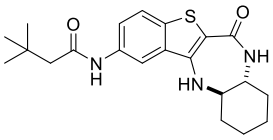

^{1}H NMR spectrum (400 MHz, DMSO)

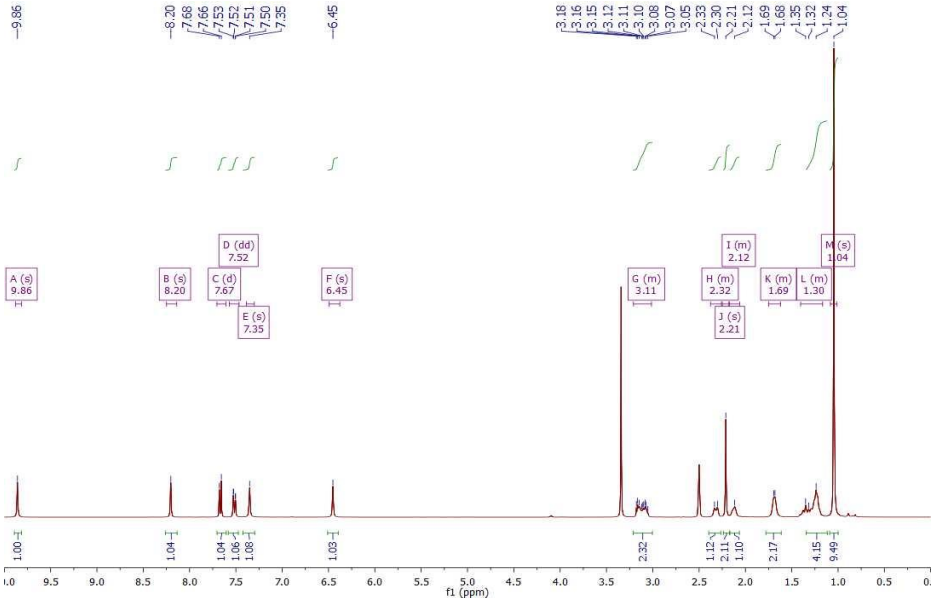

^{13}C NMR spectrum (101 MHz, DMSO)

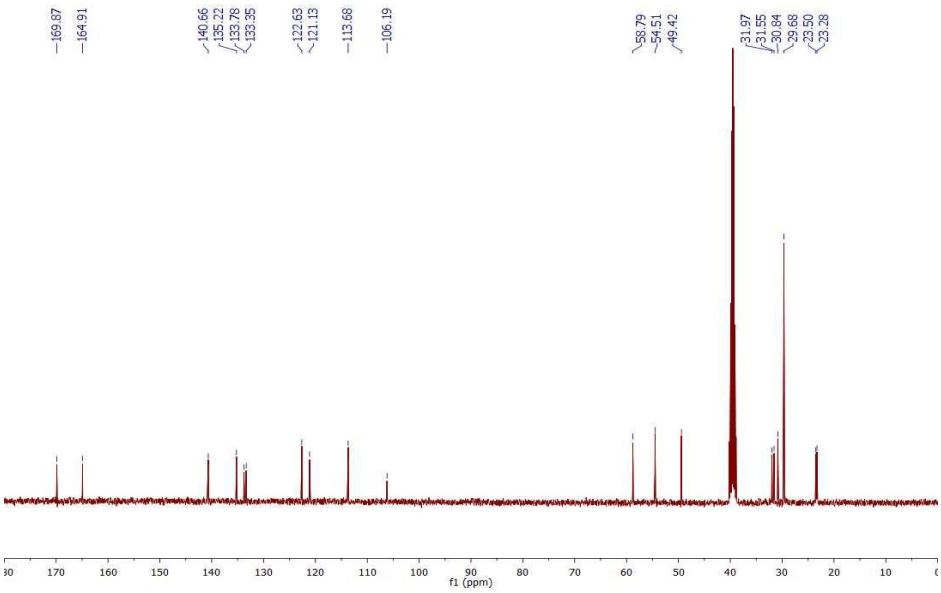

LC-MS (ES + APCI)

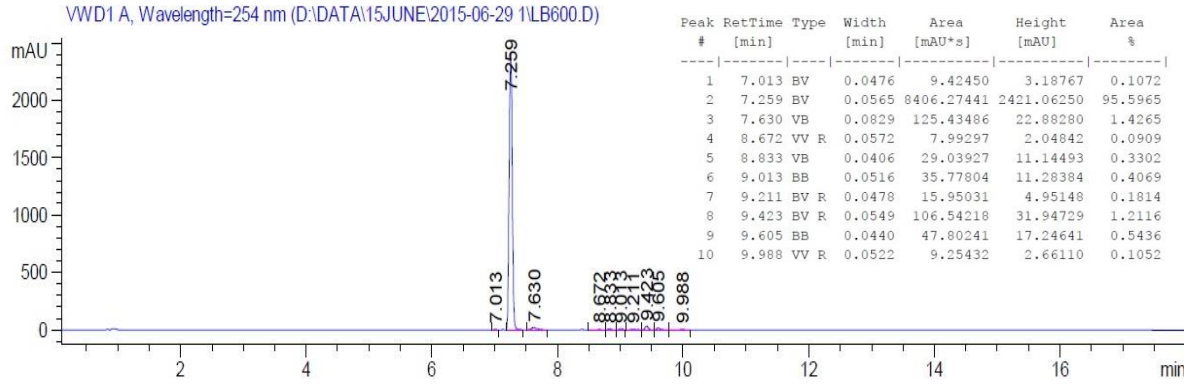

Peak #	RetTime [min]	Type	Width [min]	Area [mAU*s]	Height [mAU]	Area %
1	7.013	BV	0.0476	9.42450	3.18767	0.1072
2	7.259	BV	0.0565	8406.27441	2421.06250	95.5965
3	7.630	VB	0.0829	125.43486	22.88280	1.4265
4	8.672	VV R	0.0572	7.99297	2.04842	0.0909
5	8.833	VB	0.0406	29.03927	11.14493	0.3302
6	9.013	BB	0.0516	35.77804	11.28384	0.4069
7	9.211	BV R	0.0478	15.95031	4.95148	0.1814
8	9.423	BV R	0.0549	106.54218	31.94729	1.2116
9	9.605	BB	0.0440	47.80241	17.24641	0.5436
10	9.988	VV R	0.0522	9.25432	2.66110	0.1052

***N*-(6-oxo-7,7*a*,8,9,10,11,11*a*,12-Octahydro-6*H*-benzo[*b*]benzo[4,5]thieno[3,2-*e*][1,4]diazepin-2-yl)cyclobutanecarboxamide (166)**

^{1}H NMR spectrum (400 MHz, DMSO)

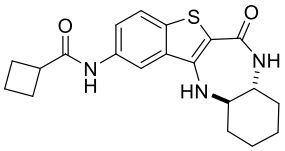

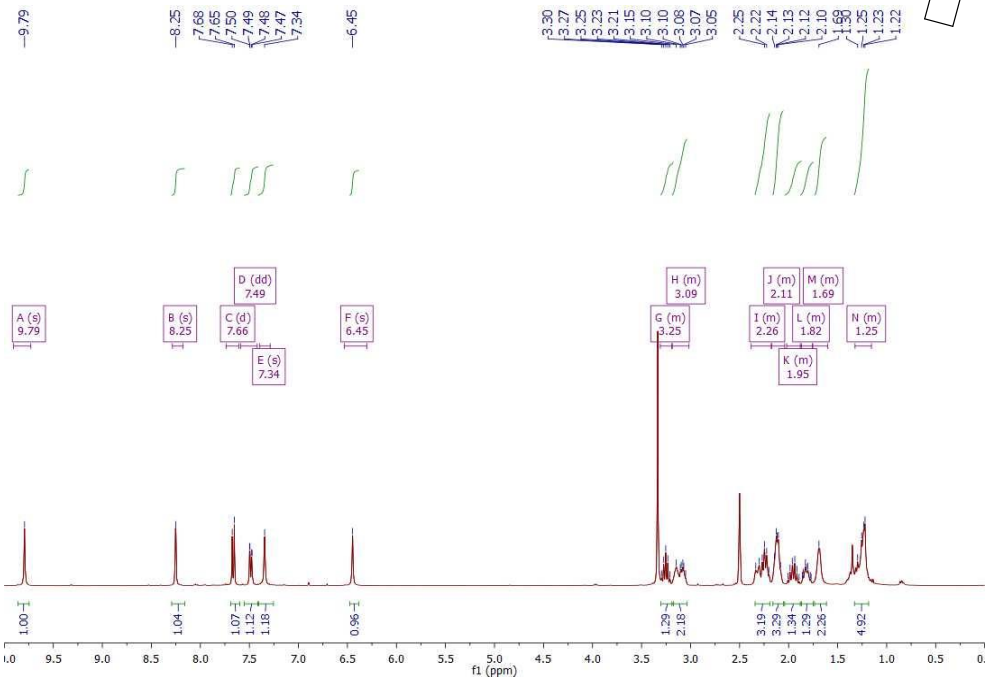

^{13}C NMR spectrum (101 MHz, DMSO)

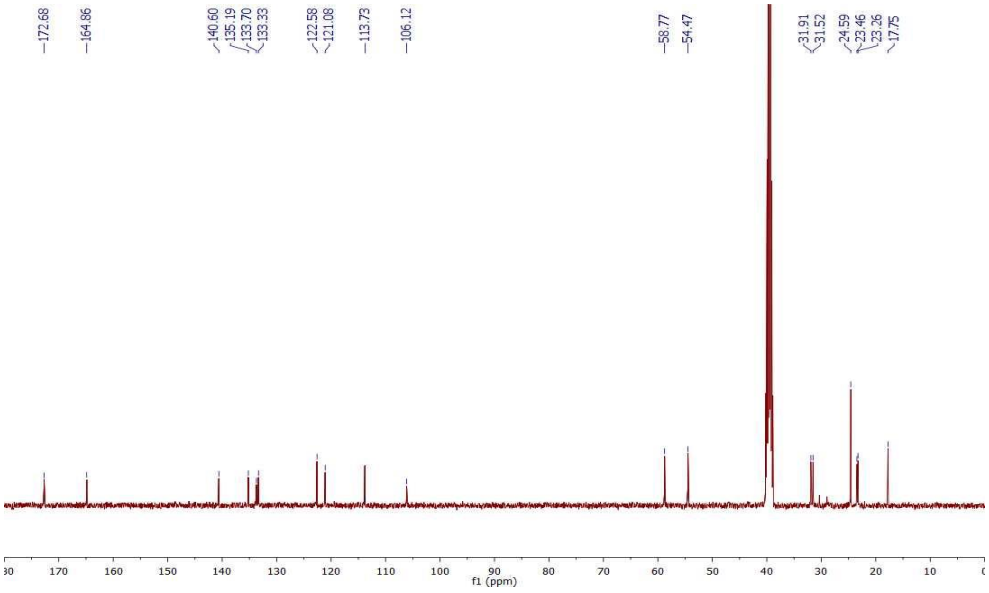

LC-MS (ES + APCI)

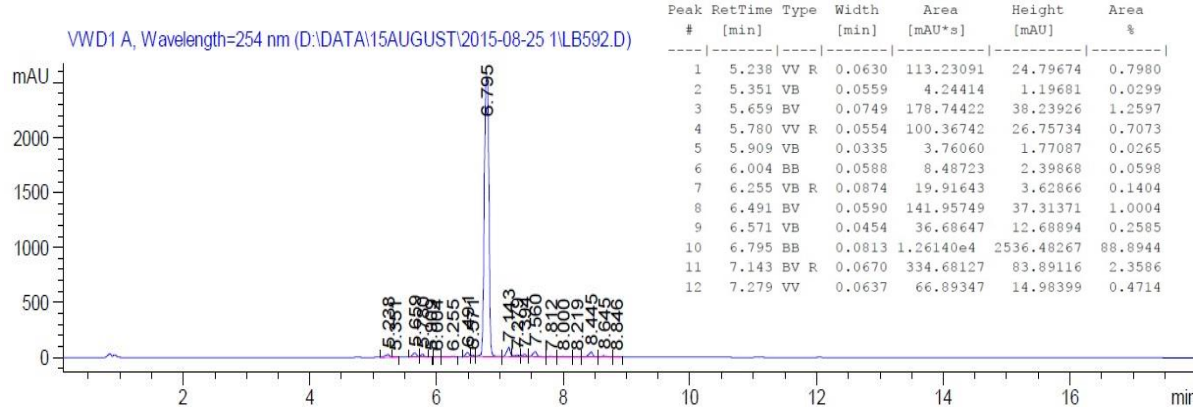

Peak #	RetTime [min]	Type	Width [min]	Area [mAU*s]	Height [mAU]	Area %
1	5.238	VV R	0.0630	113.23091	24.79674	0.7980
2	5.351	VB	0.0559	4.24414	1.19681	0.0299
3	5.659	BV	0.0749	178.74422	38.23926	1.2597
4	5.780	VV R	0.0554	100.36742	26.75734	0.7073
5	5.909	VB	0.0335	3.76060	1.77087	0.0265
6	6.004	BB	0.0588	8.48723	2.39868	0.0598
7	6.255	VB R	0.0874	19.91643	3.62866	0.1404
8	6.491	BV	0.0590	141.95749	37.31371	1.0004
9	6.571	VB	0.0454	36.68647	12.68894	0.2585
10	6.795	BB	0.0813	1.26140e4	2536.48267	88.8944
11	7.143	BV R	0.0670	334.68127	83.89116	2.3586
12	7.279	VV	0.0637	66.89347	14.98399	0.4714

***N*-(6-oxo-7,7*a*,8,9,10,11,11*a*,12-octahydro-6*H*-benzo[*b*]benzo[4,5]thieno[3,2-*e*][1,4]diazepin-2-yl)cyclopentanecarboxamide (167)**

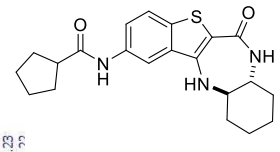

^{1}H NMR spectrum (400 MHz, DMSO)

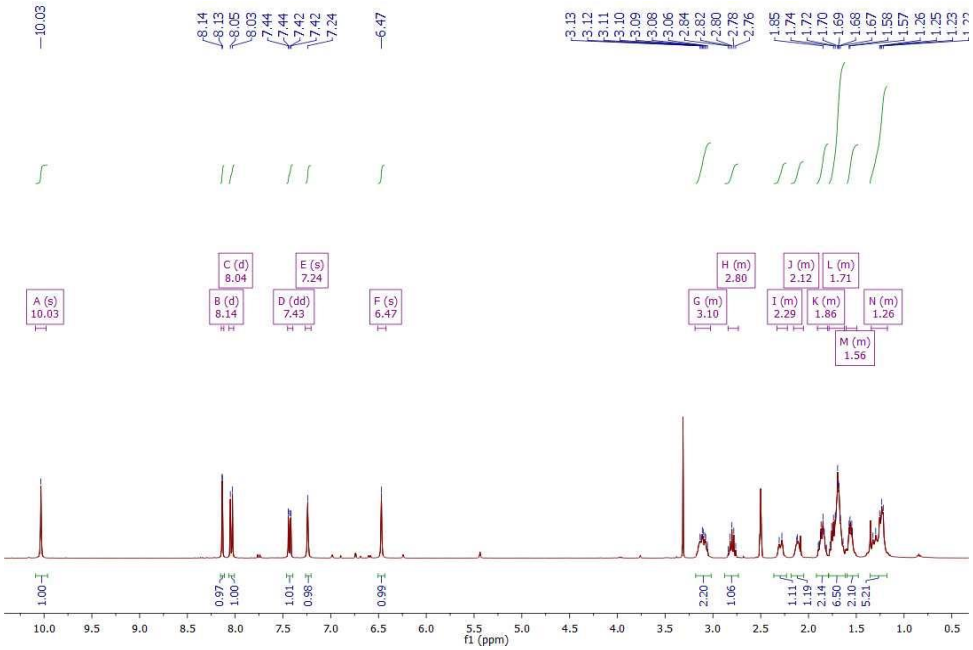

^{13}C NMR spectrum (101 MHz, DMSO)

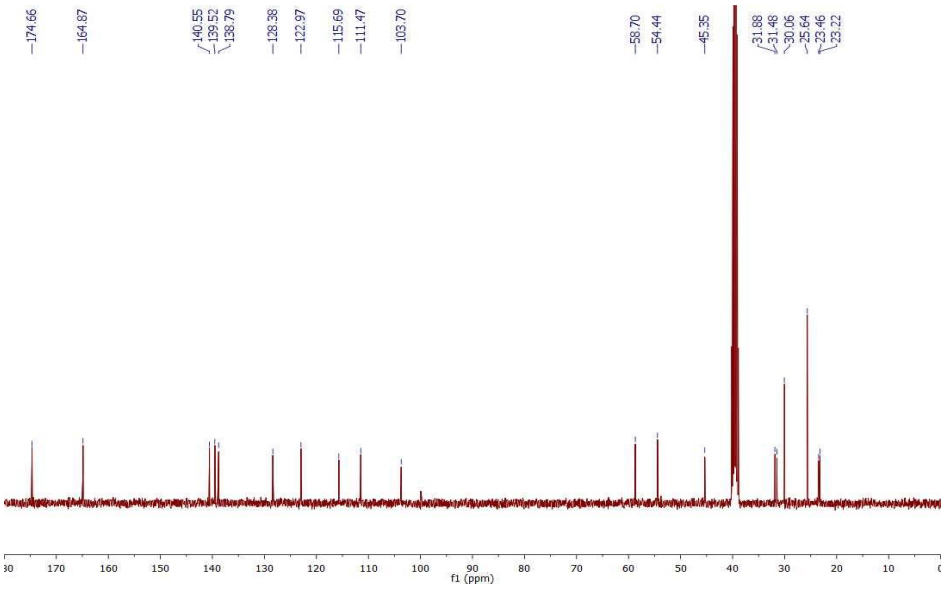

LC-MS (ES + APCI)

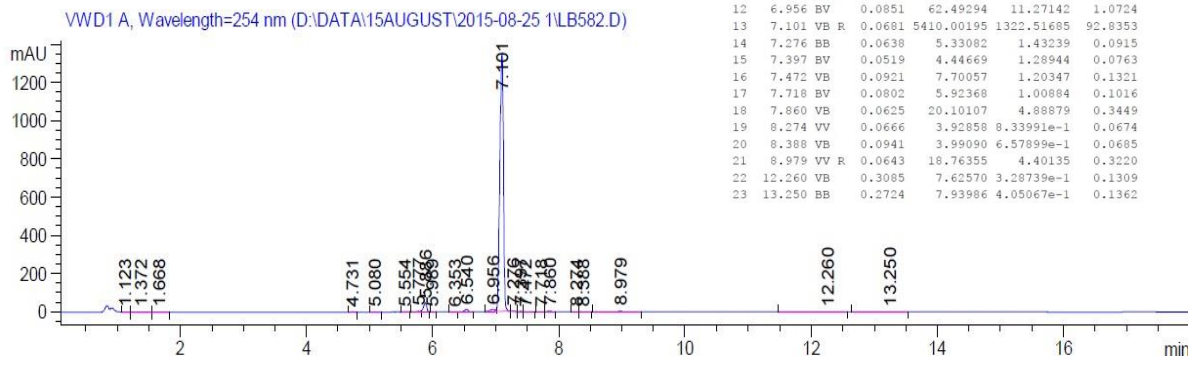

Peak #	RetTime [min]	Type	Width [min]	Area [mAU*s]	Height [mAU]	Area %
11	6.540	VB R	0.0641	51.73326	12.93658	0.8877
12	6.956	BV	0.0851	62.49294	11.27142	1.0724
13	7.101	VB R	0.0681	5410.00195	1322.51685	92.8353
14	7.276	BB	0.0638	5.33082	1.43239	0.0915
15	7.397	BV	0.0519	4.44669	1.28944	0.0763
16	7.472	VB	0.0921	7.70057	1.20347	0.1321
17	7.718	BV	0.0802	5.92368	1.00884	0.1016
18	7.860	VB	0.0625	20.10107	4.88879	0.3449
19	8.274	VV	0.0666	3.92858	8.33991e-1	0.0674
20	8.388	VB	0.0941	3.99090	6.57899e-1	0.0685
21	8.979	VV R	0.0643	18.76355	4.40135	0.3220
22	12.260	VB	0.3085	7.62570	3.28739e-1	0.1309
23	13.250	BB	0.2724	7.93986	4.05067e-1	0.1362

***N*-(6-oxo-7,7*a*,8,9,10,11,11*a*,12-Octahydro-6*H*-benzo[b]benzo[4,5]thieno[3,2-*e*][1,4]diazepin-2-yl)cyclohexanecarboxamide (168)**

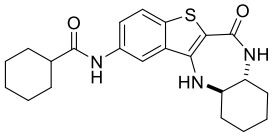

^{1}H NMR spectrum (400 MHz, DMSO)

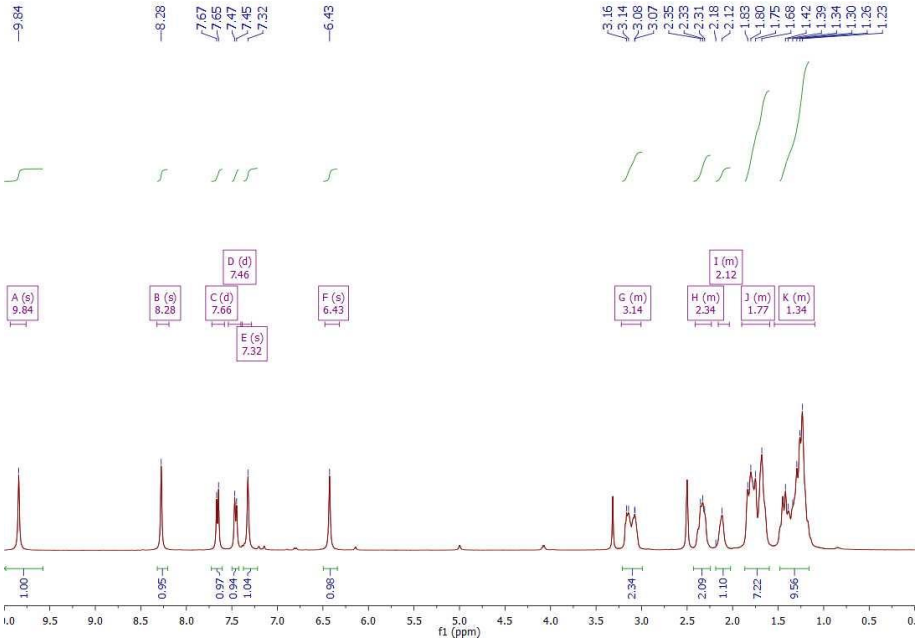

^{13}C NMR spectrum (101 MHz, DMSO)

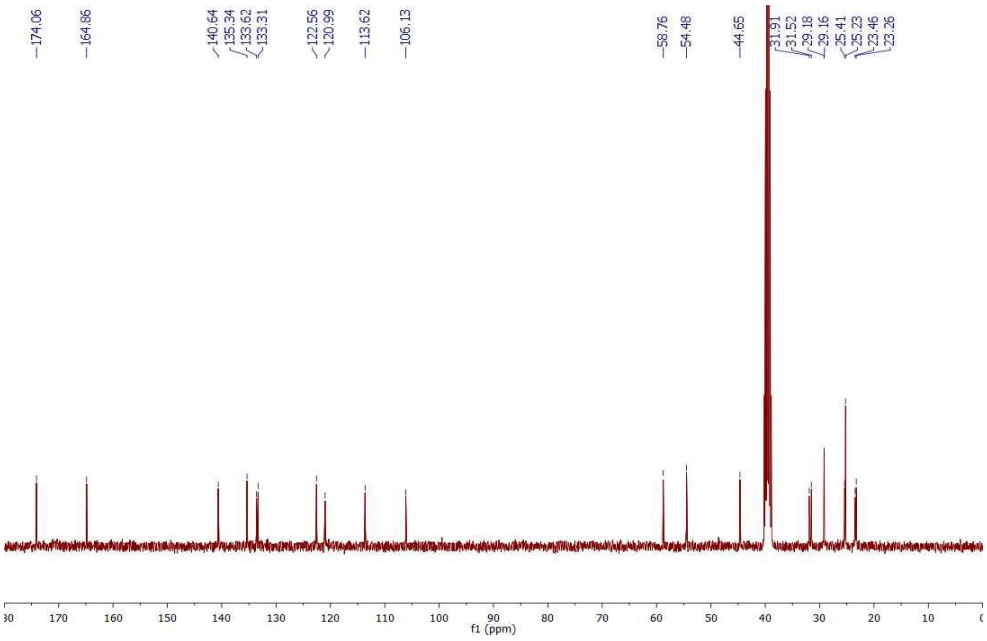

LC-MS (ES + APCI)

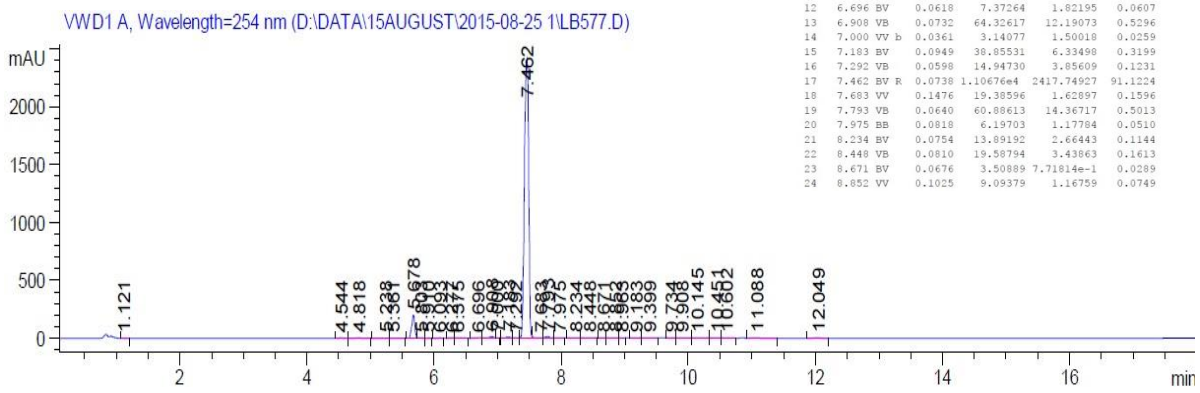

Peak #	RetTime [min]	Type	Width [min]	Area [mAU*s]	Height [mAU]	Area %
10	6.277	BV	0.0557	8.58040	2.43199	0.0706
11	6.375	VV R	0.0592	16.03192	3.93052	0.1320
12	6.696	BV	0.0618	7.37264	1.82195	0.0607
13	6.908	VB	0.0732	64.32617	12.19073	0.5296
14	7.000	VV b	0.0361	3.14077	1.50018	0.0259
15	7.183	BV	0.0949	38.85531	6.33498	0.3199
16	7.292	VB	0.0598	14.94730	3.85609	0.1231
17	7.462	BV R	0.0738	1.10676e4	2417.74927	91.1224
18	7.683	VV	0.1476	19.38596	1.62897	0.1596
19	7.793	VB	0.0640	60.88613	14.36717	0.5013
20	7.975	BB	0.0818	6.19703	1.17784	0.0510
21	8.234	BV	0.0754	13.89192	2.66443	0.1144
22	8.448	VB	0.0810	19.58794	3.43863	0.1613
23	8.671	BV	0.0676	3.50889	7.71814e-1	0.0289
24	8.852	VV	0.1025	9.09379	1.16759	0.0749

***N*-(6-oxo-7,7*a*,8,9,10,11,11*a*,12-Octahydro-6*H*-benzo[*b*]benzo[4,5]thieno[3,2-*e*][1,4]diazepin-2-yl)benzamide (169)**

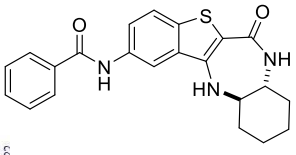

^{1}H NMR spectrum (400 MHz, DMSO)

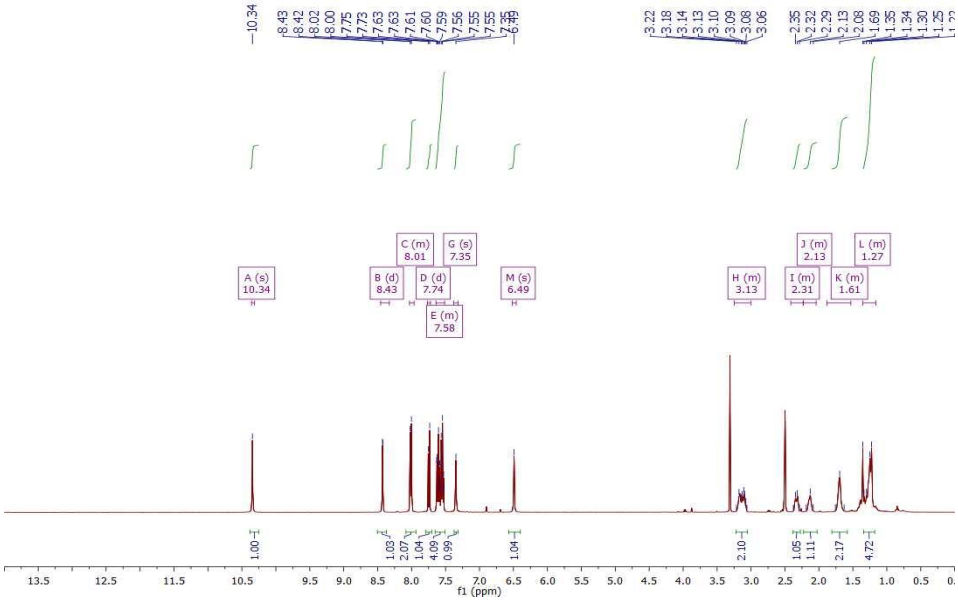

^{13}C NMR spectrum (101 MHz, DMSO)

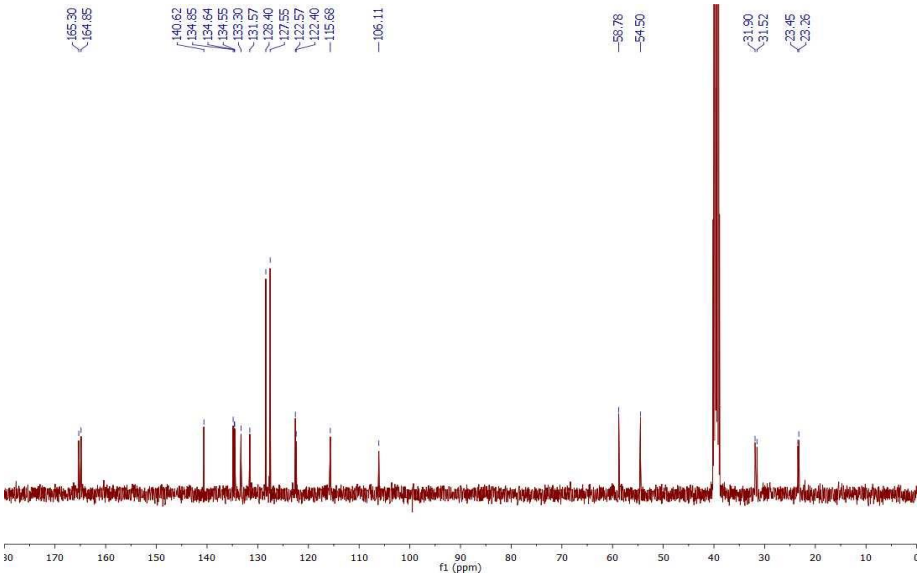

LC-MS (ES + APCI)

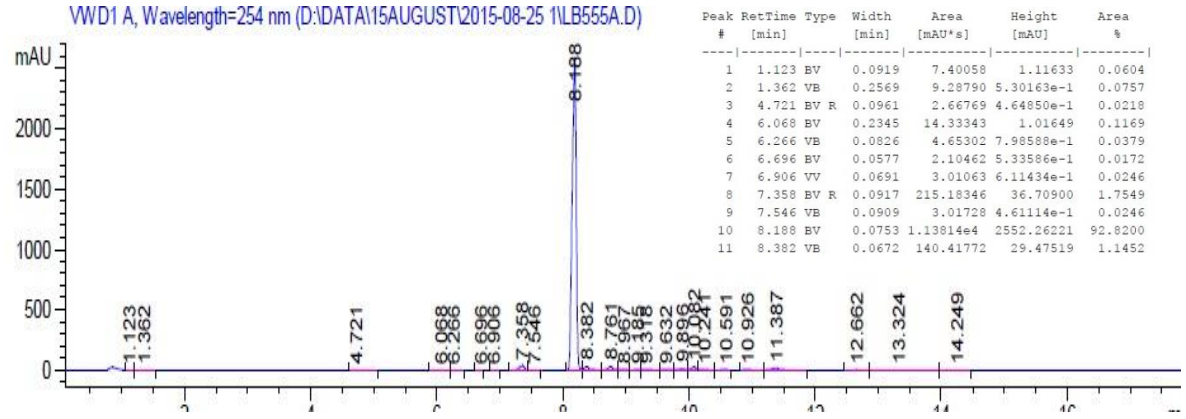

Peak #	RetTime [min]	Type	Width [min]	Area [mAU*s]	Height [mAU]	Area %
1	1.123	BV	0.0919	7.40058	1.11633	0.0604
2	1.362	VB	0.2569	9.28790	5.30163e-1	0.0757
3	4.721	BV R	0.0961	2.66769	4.64850e-1	0.0218
4	6.068	BV	0.2345	14.33343	1.01649	0.1169
5	6.266	VB	0.0826	4.65302	7.98588e-1	0.0379
6	6.696	BV	0.0577	2.10462	5.33586e-1	0.0172
7	6.906	VV	0.0691	3.01063	6.11434e-1	0.0246
8	7.358	BV R	0.0917	215.18346	36.70900	1.7549
9	7.546	VB	0.0909	3.01728	4.61114e-1	0.0246
10	8.188	BV	0.0753	1.13814e4	2552.26221	92.8200
11	8.382	VB	0.0672	140.41772	29.47519	1.1452

***N*-(6-oxo-7,7*a*,8,9,10,11,11*a*,12-Octahydro-6*H*-benzo[*b*]benzo[4,5]thieno[3,2-*e*][1,4]diazepin-2-yl)nicotinamide (170)**

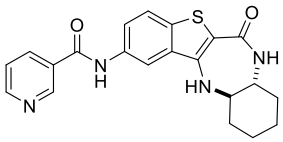

^{1}H NMR spectrum (400 MHz, DMSO)

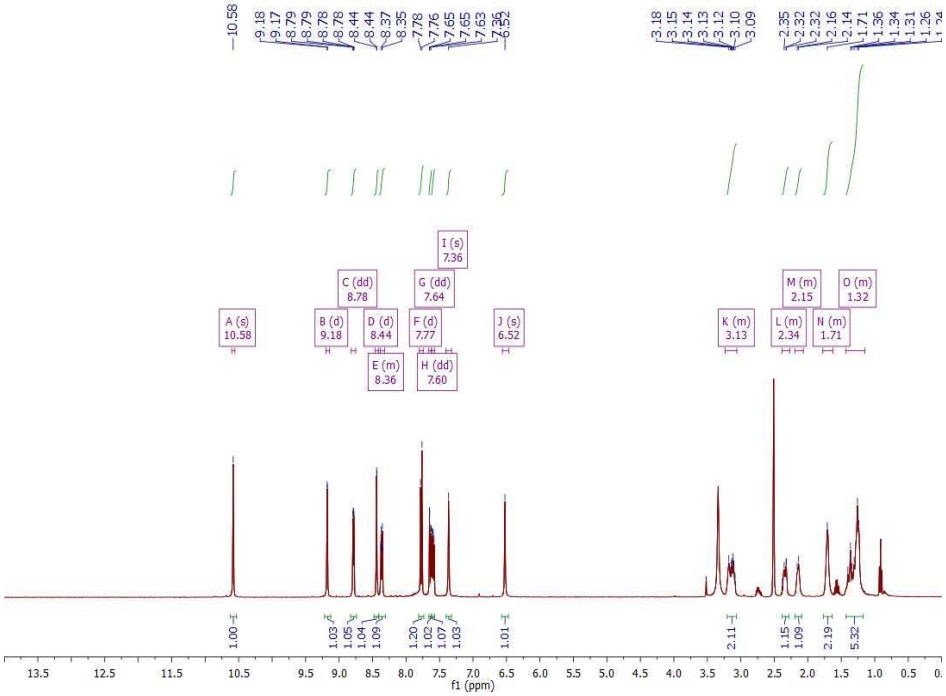

^{13}C NMR spectrum (101 MHz, DMSO)

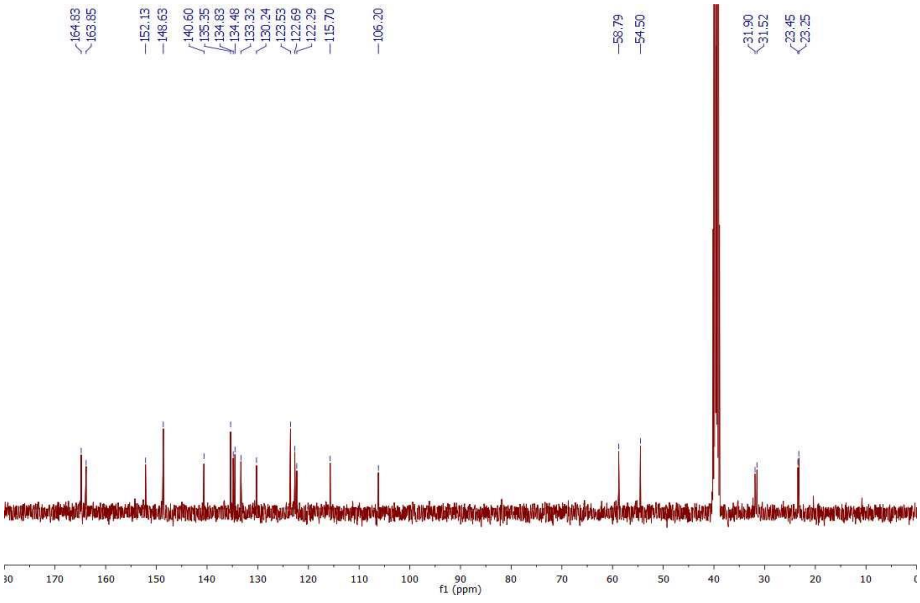

LC-MS (ES + APCI)

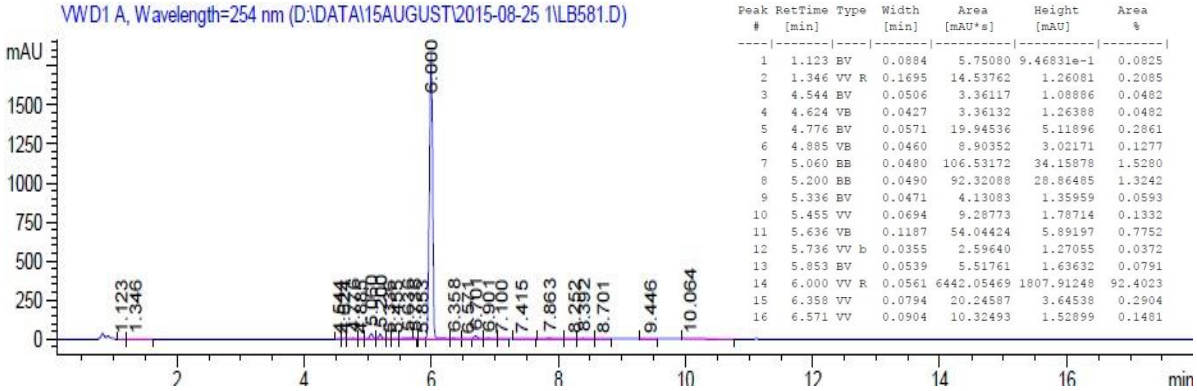

Peak #	RetTime [min]	Type	Width [min]	Area [mAU*s]	Height [mAU]	Area %
1	1.123	BV	0.0884	5.75080	9.46831e-1	0.0825
2	1.346	VV R	0.1695	14.53762	1.26081	0.2085
3	4.544	BV	0.0506	3.36117	1.08886	0.0482
4	4.624	VB	0.0427	3.36132	1.26388	0.0482
5	4.776	BV	0.0571	19.94536	5.11896	0.2861
6	4.885	VB	0.0460	8.90352	3.02171	0.1277
7	5.060	BB	0.0480	106.53172	34.15878	1.5280
8	5.200	BB	0.0490	92.32088	28.86485	1.3242
9	5.336	BV	0.0471	4.13083	1.35959	0.0593
10	5.455	VV	0.0694	9.28773	1.78714	0.1332
11	5.636	VB	0.1187	54.04424	5.89197	0.7752
12	5.736	VV b	0.0355	2.59640	1.27055	0.0372
13	5.853	BV	0.0539	5.51761	1.63632	0.0791
14	6.000	VV R	0.0561	6442.05469	1807.91248	92.4023
15	6.358	VV	0.0794	20.24587	3.64538	0.2904
16	6.571	VV	0.0904	10.32493	1.52899	0.1481

***N*-(6-oxo-7,7*a*,8,9,10,11,11*a*,12-Octahydro-6*H*-benzo[*b*]benzo[4,5]thieno[3,2-*e*][1,4]diazepin-2-yl)isonicotinamide (171)**

^{1}H NMR spectrum (400 MHz, DMSO)

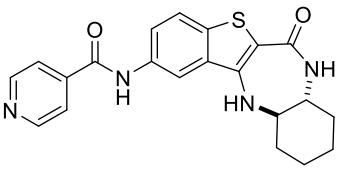

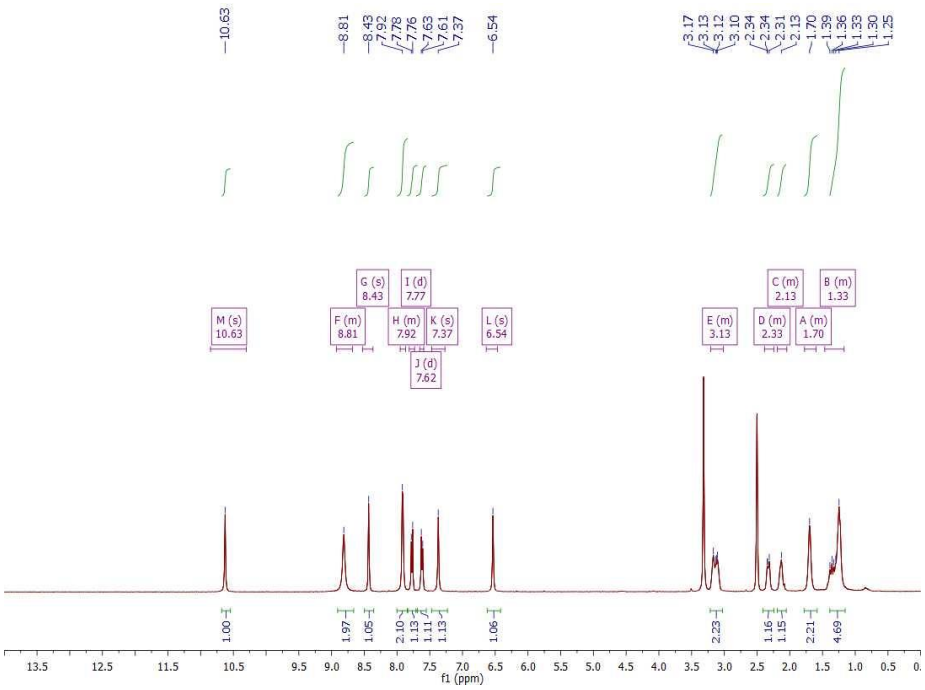

^{13}C NMR spectrum (101 MHz, DMSO)

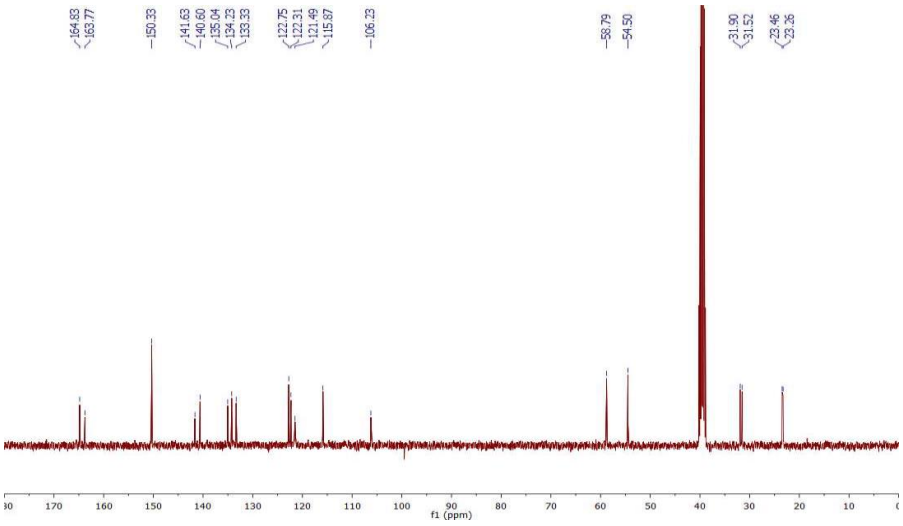

LC-MS (ES + APCI)

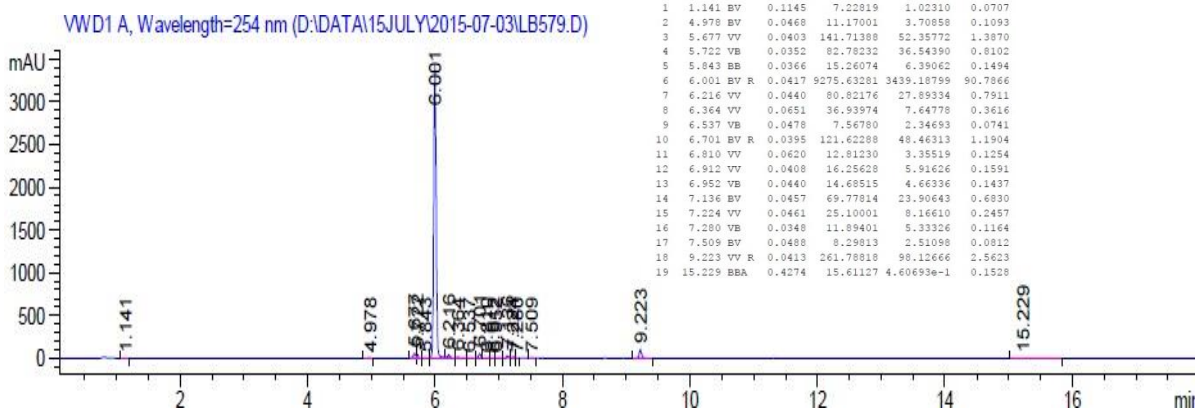

Peak #	RetTime [min]	Type	Width [min]	Area [mAU*s]	Height [mAU]	Area %
1	1.141	BV	0.1145	7.22819	1.02310	0.0707
2	4.978	BV	0.0468	11.17001	3.70858	0.1093
3	5.677	VV	0.0403	141.71388	52.35772	1.3870
4	5.722	VB	0.0352	82.78232	36.54390	0.8102
5	5.843	BB	0.0366	15.26074	6.39062	0.1494
6	6.001	BV R	0.0417	9275.63281	3439.18799	90.7866
7	6.216	VV	0.0440	80.82176	27.89334	0.7911
8	6.364	VV	0.0651	36.93974	7.64778	0.3616
9	6.537	VB	0.0478	7.56780	2.34693	0.0741
10	6.701	BV R	0.0395	121.62288	48.46313	1.1904
11	6.810	VV	0.0620	12.81230	3.35519	0.1254
12	6.912	VV	0.0408	16.25628	5.91626	0.1591
13	6.952	VB	0.0440	14.68515	4.66336	0.1437
14	7.136	BV	0.0457	69.77814	23.90643	0.6830
15	7.224	VV	0.0461	25.10001	8.16610	0.2457
16	7.280	VB	0.0348	11.89401	5.33326	0.1164
17	7.509	BV	0.0488	8.29813	2.51098	0.0812
18	9.223	VV R	0.0413	261.78818	98.12666	2.5623
19	15.229	BBA	0.4274	15.61127	4.60693e-1	0.1528

3-Chloro-*N*-(6-oxo-7,7*a*,8,9,10,11,11*a*,12-octahydro-6*H*-benzo[*b*]benzo[4,5]thieno[3,2-*e*][1,4]diazepin-2-yl)benzamide (172)

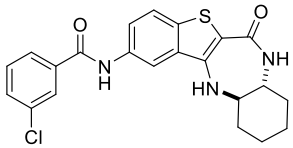

^{1}H NMR spectrum (400 MHz, DMSO)

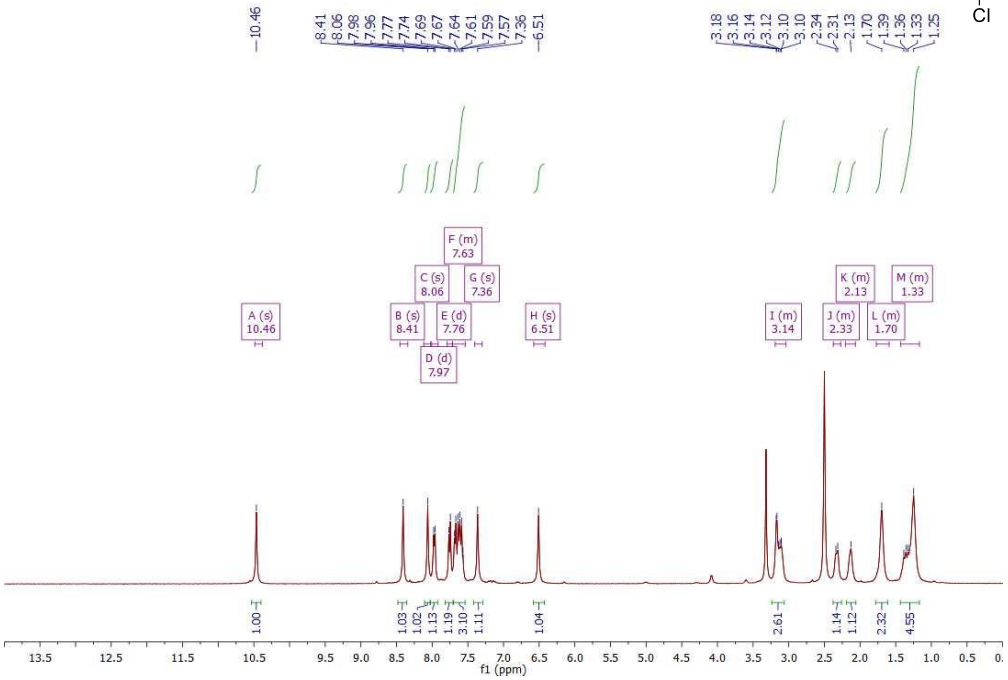

^{13}C NMR spectrum (101 MHz, DMSO)

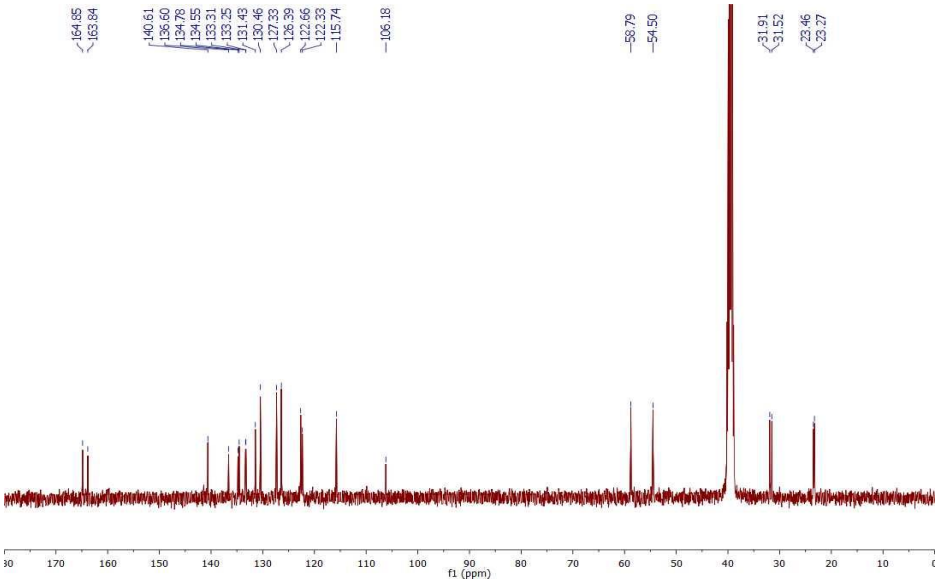

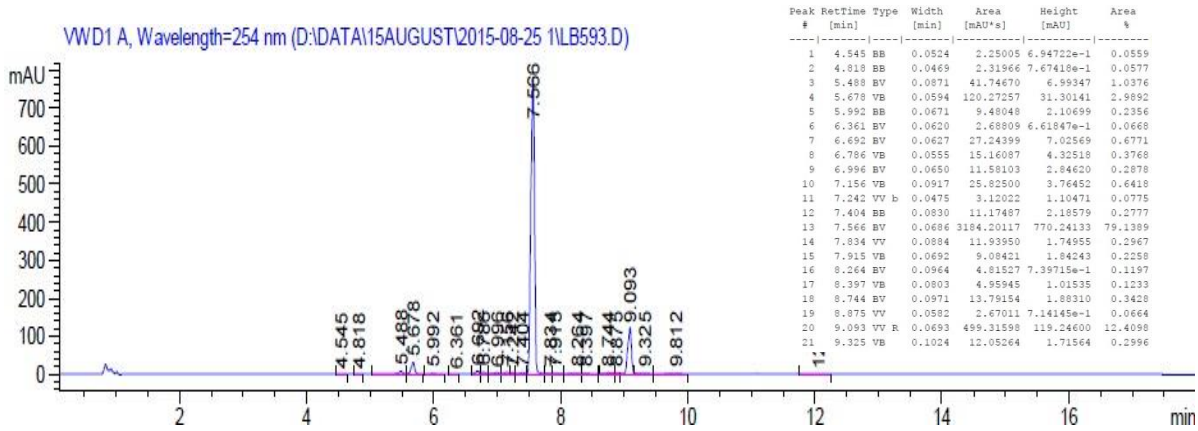

Peak #	RetTime [min]	Type	Width [min]	Area [mAU*s]	Height [mAU]	Area %
1	4.545	BB	0.0524	2.25005	6.94722e-1	0.0559
2	4.818	BB	0.0469	2.31966	7.67418e-1	0.0577
3	5.488	BV	0.0871	41.74670	6.99347	1.0376
4	5.678	VB	0.0594	120.27257	31.30141	2.9892
5	5.992	BB	0.0671	9.48048	2.10699	0.2356
6	6.361	BV	0.0620	2.68809	6.61847e-1	0.0668
7	6.692	BV	0.0627	27.24399	7.02569	0.6771
8	6.786	VB	0.0555	15.16087	4.32518	0.3768
9	6.996	BV	0.0650	11.58103	2.84620	0.2878
10	7.156	VB	0.0917	25.82500	3.76452	0.6418
11	7.242	VV b	0.0475	3.12022	1.10471	0.0775
12	7.404	BB	0.0830	11.17487	2.18579	0.2777
13	7.566	BV	0.0686	3184.20117	770.24133	79.1389
14	7.834	VV	0.0884	11.93950	1.74955	0.2967
15	7.915	VB	0.0692	9.08421	1.84243	0.2258
16	8.264	BV	0.0964	4.81527	7.39715e-1	0.1197
17	8.397	VB	0.0803	4.95945	1.01535	0.1233
18	8.744	BV	0.0971	13.79154	1.88310	0.3428
19	8.875	VV	0.0582	2.67011	7.14145e-1	0.0664
20	9.093	VV R	0.0693	499.31598	119.24600	12.4098
21	9.325	VB	0.1024	12.05264	1.71564	0.2996

4-Chloro-*N*-(-6-oxo-7,7*a*,8,9,10,11,11a,12-octahydro-6*H*-benzo[*b*]benzo[4,5]thieno[3,2-*e*][1,4]diazepin-2-yl)benzamide (173)

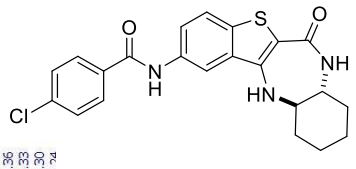

^{1}H NMR spectrum (400 MHz, DMSO)

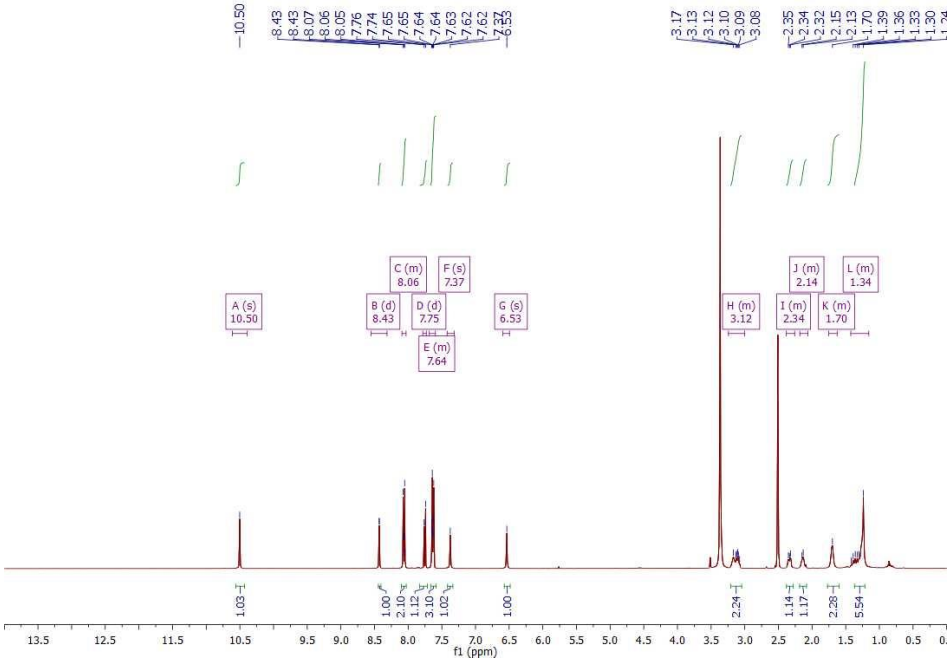

^{13}C NMR spectrum (101 MHz, DMSO)

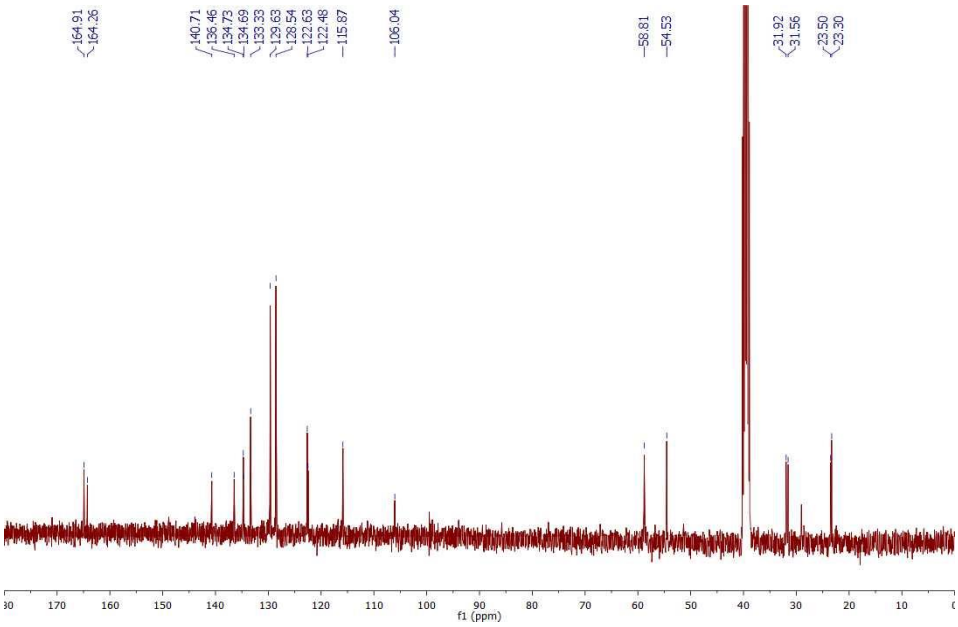

LC-MS (ES + APCI)

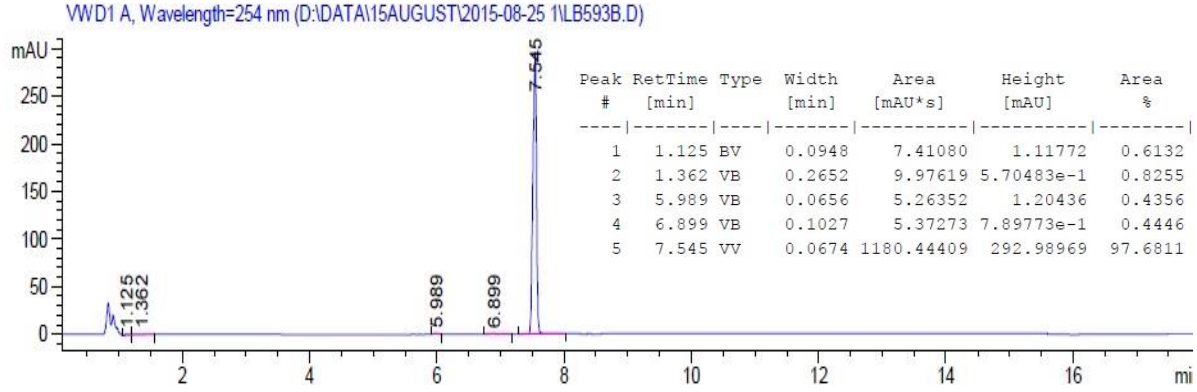

Peak #	RetTime [min]	Type	Width [min]	Area [mAU*s]	Height [mAU]	Area %
1	1.125	BV	0.0948	7.41080	1.11772	0.6132
2	1.362	VB	0.2652	9.97619	5.70483e-1	0.8255
3	5.989	VB	0.0656	5.26352	1.20436	0.4356
4	6.899	VB	0.1027	5.37273	7.89773e-1	0.4446
5	7.545	VV	0.0674	1180.44409	292.98969	97.6811

References

1. Tao, Z.-F., Hasvold, L. A., Leverson, J. D., Han, E. K., Guan, R., Johnson, E. F., Stoll, V. S., Stewart, K. D., Stamper, G., Soni, N., Bouska, J. J., Luo, Y., Sowin, T. J., Lin, N.-H., Giranda, V. S., Rosenberg, S. H. and Penning, T. D., *J. Med. Chem.*, 2009, **52**, 6621-6636.
2. www.pharma.org/files, 2009.
3. Liu, C., Constantinides, P. P. and Li, Y., *Acta Pharm. Sin. B*, 2014, **4**, 112-119.
4. Edwards, A. M., Bountra, C., Kerr, D. J. and Willson, T. M., *Nat. Chem. Biol.*, 2009, **5**, 436-440.
5. Bunnage, M. E., Chekler, E. L. P. and Jones, L. H., *Nat. Chem. Biol.*, 2013, **9**, 195-199.
6. Hughes, B., *Nat. Rev. Drug Discov.*, 2008, **7**, 631-632.
7. www.fda.gov/drugs/developmentapprovalprocess/druginnovation/ucm381263.htm.
8. Fingleton, B., *Sem. Cell. Dev. Biol.*, 2008, **19**, 61-68.
9. Pavlaki, M. and Zucker, S., *Cancer Metastasis Rev*, 2003, **22**, 177-203.
10. Weigelt, J., *EMBO Rep*, 2009, **10**, 941-945.
11. Knapp, S., Arruda, P., Blagg, J., Burley, S., Drewry, D. H., Edwards, A., Fabbro, D., Gillespie, P., Gray, N. S., Kuster, B., Lackey, K. E., Mazzafera, P., Tomkinson, N. C. O., Willson, T. M., Workman, P. and Zuercher, W. J., *Nat. Chem. Biol.*, 2013, **9**, 3-6.
12. Filmore, D., *Mod. Drug Discovery*, 2004, **7**, 25-28.
13. Wu, P., Nielsen T. E., Clausen, M. H., *Drug. Discov. Today.*, 2016, **21**, 422-439.
14. Fedorov, O., Muller, S. and Knapp, S., *Nat. Chem. Biol.*, 2010, **6**, 166-169.
15. Frye, S. V., *Nat. Chem. Biol.*, 2010, **6**, 159-161.
16. Grueneberg, D. A., Degot, S., Pearlberg, J., Li, W., Davies, J. E., Baldwin, A., Endege, W., Doench, J., Sawyer, J., Hu, Y., Boyce, F., Xian, J., Munger, K. and Harlow, E., *Proc. Natl. Acad. Sci.*, 2008, **105**, 16472-16477.
17. Bommi-Reddy, A., Almeciga, I., Sawyer, J., Geisen, C., Li, W., Harlow, E., Kaelin, W. G. and Grueneberg, D. A., *Proc. Natl. Acad. Sci.*, 2008, **105**, 16484-16489.
18. Maddika, S., Ande, S. R., Wiechec, E., Hansen, L. L., Wesselborg, S. and Los, M., *J. Cell Sci.*, 2008, **121**, 979-988.
19. Cohen, P. and Alessi, D. R., *ACS Chem. Biol.*, 2012, **8**, 96-104.
20. Steichen, J. M., Kuchinskas, M., Keshwani, M. M., Yang, J., Adams, J. A. and Taylor, S. S., *J. Biol. Chem.*, 2012, **287**, 14672-14680.
21. Liu, Y. and Gray, N. S., *Nat. Chem. Biol.*, 2006, **2**, 358-364.
22. Zhao, Z., Wu, H., Wang, L., Liu, Y., Knapp, S., Liu, Q. and Gray, N. S., *ACS Chem. Biol.*, 2014, **9**, 1230-1241.
23. Vijayan, R. S. K., He, P., Modi, V., Duong-Ly, K. C., Ma, H., Peterson, J. R., Dunbrack, R. L. and Levy, R. M., *J. Med. Chem.*, 2015, **58**, 466-479.
24. Smyth, L. and Collins, I., *J. Chem. Biol.*, 2009, **2**, 131-151.
25. Cuypers, H. T. S., G.; Quint, W.;Zijlstra, M.; Maandag, E. R.; Boelens, W.; van Wezenbeed, P.; Melief, C.; Berns, *Cell*, 1984, **37**, 141-150.
26. Theo Cuypers, H., Selten, G., Quint, W., Zijlstra, M., Maandag, E. R., Boelens, W., van Wezenbeek, P., Melief, C. and Berns, A., *Cell*, 1984, **37**, 141-150.
27. An, N., Lin, Y.-W., Mahajan, S., Kellner, J. N., Wang, Y., Li, Z., Kraft, A. S. and Kang, Y., *Stem cells*, 2013, **31**, 1202-1212.
28. Mikkers, H., Allen, J., Knipscheer, P., Romeyn, L., Hart, A., Vink, E. and Berns, A., *Nat. Genet.*, 2002, **32**, 153-159.
29. Nawijn, M. C., Alendar, A. and Berns, A., *Nat. Rev. Cancer*, 2011, **11**, 23-34.
30. Feldman, J. D., Vician, L., Crispino, M., Tocco, G., Marcheselli, V. L., Bazan, N. G., Baudry, M. and Herschman, H. R., *J. Biol. Chem.*, 1998, **273**, 16535-16543.
31. Blanco-Aparicio, C. and Carnero, A., *Biochem. Pharm*, 2013, **85**, 629-643.
32. Zippo, A., De Robertis, A., Serafini, R. and Oliviero, S., *Nat. Cell Biol.*, 2007, **9**, 932-944.
33. Zha, J., Harada, H., Yang, E., Jockel, J. and Korsmeyer, S. J., *Cell*, 1996, **87**, 619-628.
34. Peltola, K. J., Paukku, K., Aho, T. L. T., Ruuska, M., Silvennoinen, O. and Koskinen, P. J., *Blood*, 2004, **103**, 3744-3750.
35. Bachmann, M., Kosan, C., Xing, P. X., Montenarh, M., Hoffmann, I. and Möröy, T., *Int. J. Biochem. Cell Biol.*, 2006, **38**, 430-443.

36. Fox, C. J., Hammerman, P. S., Cinalli, R. M., Master, S. R., Chodosh, L. A. and Thompson, C. B., *Genes Dev.*, 2003, **17**, 1841-1854.
37. Morwick, T., *Expert Opin. Ther. Pat.*, 2010, **20**, 193-212.
38. Vertex Pharmaceuticals Inc., **US7268136B2**, 2007.
39. SuperGen Inc., **WO2008058126**, 2008.
40. Centro Nacional de Investigaciones Oncologicas (CNIO). **WI2008133952**, 2009.
41. Bullock, A. N., Debreczeni, J. É., Fedorov, O. Y., Nelson, A., Marsden, B. D. and Knapp, S., *J. Med. Chem.*, 2005, **48**, 7604-7614.
42. Pogacic, V., Bullock, A. N., Fedorov, O., Filippakopoulos, P., Gasser, C., Biondi, A., Meyer-Monard, S., Knapp, S. and Schwaller, J., *Cancer Res.*, 2007, **67**, 6916-6924.
43. Keeton, E. K., McEachern, K., Dillman, K. S., Palakurthi, S., Cao, Y., Grondine, M. R., Kaur, S., Wang, S., Chen, Y., Wu, A., Shen, M., Gibbons, F. D., Lamb, M. L., Zheng, X., Stone, R. M., DeAngelo, D. J., Platanias, L. C., Dakin, L. A., Chen, H., Lyne, P. D. and Huszar, D., *Blood*, 2013, **123**, 905-913.
44. Dakin, L. A., Block, M. H., Chen, H., Code, E., Dowling, J. E., Feng, X., Ferguson, A. D., Green, I., Hird, A. W., Howard, T., Keeton, E. K., Lamb, M. L., Lyne, P. D., Pollard, H., Read, J., Wu, A. J., Zhang, T. and Zheng, X., *Bioorg. Med. Chem. Lett.*, 2012, **22**, 4599-4604.
45. Haddach, M., Michaux, J., Schwaebe, M. K., Pierre, F., O'Brien, S. E., Borsan, C., Tran, J., Raffaele, N., Ravula, S., Drygin, D., Siddiqui-Jain, A., Darjania, L., Stansfield, R., Proffitt, C., Macalino, D., Streiner, N., Bliesath, J., Omori, M., Whitten, J. P., Anderes, K., Rice, W. G. and Ryckman, D. M., *ACS Med. Chem. Lett.*, 2011, **3**, 135-139.
46. Qian, K., Wang, L., Cywin, C. L., Farmer, B. T., Hickey, E., Homon, C., Jakes, S., Kashem, M. A., Lee, G., Leonard, S., Li, J., Magboo, R., Mao, W., Pack, E., Peng, C., Prokopowicz, A., Welzel, M., Wolak, J. and Morwick, T., *J. Med. Chem.*, 2009, **52**, 1814-1827.
47. Xiang, Y., Hirth, B., Asmussen, G., Biemann, H.-P., Bishop, K. A., Good, A., Fitzgerald, M., Gladysheva, T., Jain, A., Jancsics, K., Liu, J., Metz, M., Papoulis, A., Skerlj, R., Stepp, J. D. and Wei, R. R., *Bioorg. Med. Chem. Lett.*, 2011, **21**, 3050-3056.
48. Campaigne, E., in *Compr. Het. Chem.*, eds. R. K. Editors-in-Chief: Alan and W. R. Charles, Pergamon, Oxford, 1984, pp. 863-934.
49. Bullock, A. N., Russo, S., Amos, A., Pagano, N., Bregman, H., Debreczeni, J. É., Lee, W. H., Delft, F. v., Meggers, E. and Knapp, S., *PLoS ONE*, 2009, **4**, e7112.
50. Wang, X., Magnuson, S., Pastor, R., Fan, E., Hu, H., Tsui, V., Deng, W., Murray, J., Steffek, M., Wallweber, H., Moffat, J., Drummond, J., Chan, G., Harstad, E. and Ebens, A. J., *Bioorg. Med. Chem. Lett.*, 2013, **23**, 3149-3153.
51. Nishiguchi, G. A., Atallah, G., Bellamacina, C., Burger, M. T., Ding, Y., Feucht, P. H., Garcia, P. D., Han, W., Klivansky, L. and Lindvall, M., *Bioorg. Med. Chem. Lett.*, 2011, **21**, 6366-6369.
52. Buijsman, R., in *Chemogenomics in Drug Discovery*, Wiley-VCH Verlag GmbH & Co. KGaA, 2005, pp. 191-219.
53. Niesen, F. H., Berglund, H. and Vedadi, M., *Nat. Protoc.*, 2007, **2**, 2212-2221.
54. Schellman, J. A., *Biophys. J.*, 1997, **73**, 2960-2964.
55. Zhang, J.-H., Chung, T. D. Y. and Oldenburg, K. R., *J. Biomol. Screen.*, 1999, **4**, 67-73.
56. Berg JM, T. J., Stryer L. , in *Biochemistry. 5th edition.*, New York, 2002.
57. Lipinski, C. A., *J. Pharmacol. Toxicol. Methods*, 2000, **44**, 235-249.
58. Svennebring, A. M., *Future Med. Chem.*, 2015, **7**, 259-267.
59. Di, L., Kerns, E. H., Fan, K., McConnell, O. J. and Carter, G. T., *Eur. J. Med. Chem.*, 2003, **38**, 223-232.
60. Kansy, M., Senner, F. and Gubernator, K., *J. Med. Chem.*, 1998, **41**, 1007-1010.
61. Hubatsch, I., Ragnarsson, E. G. E. and Artursson, P., *Nat. Protoc.*, 2007, **2**, 2111-2119.
62. Koike, K., Jia, Z., Nikaido, T., Liu, Y., Zhao, Y. and Guo, D., *Org. Lett.*, 1999, **1**, 197-198.
63. Lu, P., Schrag, M. L., Slaughter, D. E., Raab, C. E., Shou, M. and Rodrigues, A. D., *Drug Metab. Dispos.*, 2003, **31**, 1352-1360.
64. Croxtall, J. and Plosker, G., *Drugs*, 2009, **69**, 339-359.
65. Bagley, M. C., Dwyer, J. E., Molina, M. D. B., Rand, A. W., Rand, H. L. and Tomkinson, N. C. O., *Org. Biomol. Chem.*, 2015, **13**, 6814-6824.
66. Beck, J. R., *J. Org. Chem.*, 1972, **37**, 3224-3226.
67. Sleebs, B. E., Levit, A., Street, I. P., Falk, H., Hammonds, T., Wong, A. C., Charles, M. D., Olson, M. F. and Baell, J. B., *Med. Chem. Comm.*, 2011, **2**, 977-981.

68. Anderson, D. R., Meyers, M. J., Kurumbail, R. G., Caspers, N., Poda, G. I., Long, S. A., Pierce, B. S., Mahoney, M. W., Mourey, R. J. and Parikh, M. D., *Bioorg. Med. Chem. Lett.*, 2009, **19**, 4882-4884.
69. Anderson, D. R., Meyers, M. J., Kurumbail, R. G., Caspers, N., Poda, G. I., Long, S. A., Pierce, B. S., Mahoney, M. W. and Mourey, R. J., *Bioorg. Med. Chem. Lett.*, 2009, **19**, 4878-4881.
70. Hagiwara, M., *BBA-Proteins Proteom.*, 2005, **1754**, 324-331.
71. Hanes, J., von der Kammer, H., Klaudiny, J. and Scheit, K. H., *J. Mol. Biol.*, 1994, **244**, 665-672.
72. Douglas, A. G. L. and Wood, M. J. A., *Brief. Funct. Genomics*, 2011, **10**, 151-164.
73. Manley, J. L. and Tacke, R., *Genes Dev.*, 1996, **10**, 1569-1579.
74. Fedorov, O., Huber, K., Eisenreich, A., Filippakopoulos, P., King, O., Bullock, A. N., Szklarczyk, D., Jensen, L. J., Fabbro, D., Trappe, J., Rauch, U., Bracher, F. and Knapp, S., *Chem. Biology*, 2011, **18**, 67-76.
75. Tsuhako, A. L., Brown, D. S., Koltun, E. S., Aay, N., Arcalas, A., Chan, V., Du, H., Engst, S., Franzini, M., Galan, A., Huang, P., Johnston, S., Kane, B., Kim, M. H., Douglas Laird, A., Lin, R., Mock, L., Ngan, I., Pack, M., Stott, G., Stout, T. J., Yu, P., Zaharia, C., Zhang, W., Zhou, P., Nuss, J. M., Kearney, P. C. and Xu, W., *Bioorg. Med. Chem. Lett.*, 2012, **22**, 3732-3738.
76. Jiang, Y., Chen, X., Zheng, Y., Xue, Z., Shu, C., Yuan, W. and Zhang, X., *Angew. Chem. Int. Ed.*, 2011, **50**, 7304-7307.
77. Carradori, S., Rotili, D., De Monte, C., Lenoci, A., D'Ascenzio, M., Rodriguez, V., Filetici, P., Miceli, M., Nebbioso, A., Altucci, L., Secci, D. and Mai, A., *Eur. J. Med. Chem.*, 2014, **80**, 569-578.
78. Surry, D. S. and Buchwald, S. L., *Chem. Sci.*, 2011, **2**, 27-50.
79. Maiti, D., Fors, B. P., Henderson, J. L., Nakamura, Y. and Buchwald, S. L., *Chem. Sci.*, 2011, **2**, 57-68.
80. Wu, G., Yin, W., Shen, H. C. and Huang, Y., *Green Chem.*, 2012, **14**, 580-585.
81. Martinez-Ariza, G., Ayaz, M., Medda, F. and Hulme, C., *J. Org. Chem.*, 2014, **79**, 5153-5162.
82. Wharton, C. J. and Wrigglesworth, R., *J. Chem. Soc., Perkin Trans. 1*, 1981, 433-436.
83. Kennedy, A. J., Mathews, T. P., Kharel, Y., Field, S. D., Moyer, M. L., East, J. E., Houck, J. D., Lynch, K. R. and Macdonald, T. L., *J. Med. Chem.*, 2011, **54**, 3524-3548.
84. Caron, S., Wei, L., Douville, J. and Ghosh, A., *J. Org. Chem.*, 2010, **75**, 945-947.
85. Kim, T. W., Yoo, B. W., Lee, J. K., Kim, J. H., Lee, K.-T., Chi, Y. H. and Lee, J. Y., *Bioorg. Med. Chem. Lett.*, 2012, **22**, 1649-1654.
86. Schaefer, F. C. and Krapcho, A. P., *J. Org. Chem.*, 1962, **27**, 1255-1258.
87. Elkins, J. M., Wang, J., Deng, X., Pattison, M. J., Arthur, J. S. C., Erazo, T., Gomez, N., Lizcano, J. M., Gray, N. S. and Knapp, S., *J. Med. Chem.*, 2013, **56**, 4413-4421.
88. Anderson, D. R., Meyers, M. J., Vernier, W. F., Mahoney, M. W., Kurumbail, R. G., Caspers, N., Poda, G. I., Schindler, J. F., Reitz, D. B. and Mourey, R. J., *J. Med. Chem.*, 2007, **50**, 2647-2654.
89. Wu, J.-P., Wang, J., Abeywardane, A., Andersen, D., Emmanuel, M., Gautschi, E., Goldberg, D. R., Kashem, M. A., Lukas, S., Mao, W., Martin, L., Morwick, T., Moss, N., Pargellis, C., Patel, U. R., Patnaude, L., Peet, G. W., Skow, D., Snow, R. J., Ward, Y., Werneburg, B. and White, A., *Bioorg. Med. Chem. Lett.*, 2007, **17**, 4664-4669.
90. Ager, D. J. and Prakash, I., *Synth. Commun.*, 1996, **26**, 3865-3868.
91. Malkov, A. V., Gouriou, L., Lloyd-Jones, G. C., Starý, I., Langer, V., Spoor, P., Vinader, V. and Kočovský, P., *Chem. Eur. J.*, 2006, **12**, 6910-6929.
92. Betschart, C. and Hegedus, L. S., *J. Am. Chem. Soc.*, 1992, **114**, 5010-5017.
93. Chen, X., Murawski, A., Patel, K., Crespi, C. and Balimane, P., *Pharm. Res.*, 2008, **25**, 1511-1520.
94. Mumenthaler, S. M., Ng, P. Y. B., Hodge, A., Bearss, D., Berk, G., Kanekal, S., Redkar, S., Taverna, P., Agus, D. B. and Jain, A., *Mol. Cancer Ther.*, 2009, **8**, 2882-2893.
95. Drygin, D., Haddach, M., Pierre, F. and Ryckman, D. M., *J. Med. Chem.*, 2012, **55**, 8199-8208.
96. Sanghera, J., Li, R. and Yan, J., *Assay Drug Dev. Technol.*, 2009, **7**, 615-622.
97. Pierce, M. M., Raman, C. S. and Nall, B. T., *Methods*, 1999, **19**, 213-221.